

Chemical Process Analysis: Chemometrics; Instrument Control; Applications in Equilibrium and Kinetic Investigations

A thesis submitted in fulfilment of the requirements for the degree of
Doctor of Philosophy
at the School of Environmental and Life Sciences, Chemistry,
University of Newcastle
by

Sarah E. Norman, B.Sc (Hons.), B.Sc (Chem.) B.Tch

January, 2008

School of Environmental and Life Sciences, Chemistry
University of Newcastle
Callaghan NSW 2308
Australia

Author's Declaration

I hereby certify that the work embodied in this Thesis is the result of original research, the greater part of which was completed subsequent to admission to candidature for the degree. This work contains no material which has been accepted for the award of any other degree or diploma in any university or other tertiary institution and, to the best of my knowledge and belief, contains no material previously published or written by another person, except where due reference has been made in the text.

I give consent to this copy of my thesis, when deposited in the University Library, being made available for loan and photocopying subject to the provisions of the Copyright Act 1968.

Signature

Sarah Norman

Acknowledgements

There are many people that I am indebted to for making my PhD experience what it has been, but I would like to single out a few who have been the key influences in this project and on this time of my life.

Firstly, my supervisors deserve the biggest thanks: to Associate Professor Marcel Maeder for his constant guidance and support through both Honours and PhD. He has taught me as much about life as about chemistry, his philosophies and insight have been an invaluable contribution to my life and to my learning; and to Professor Geoffrey Lawrance for his encouragement and endless wealth of knowledge and ideas.

I would also like to extend my gratitude to Professor Alan Williams for the unforgettable opportunity to spend three months studying in Geneva, Switzerland in 2006; and a special thanks must also go to Doctor Bobby Neuhold for his friendship, patience and for teaching me the wonders of Matlab.

Particular thanks must also go to all the other postgraduates with whom I have shared the past few years with; particularly Nichola, Jenny, Hubs, Jez, Ewen Ben, and Kate. Also I extend a huge thank you to those in the Chemistry department in Geneva; Alex, Simon, Frank, Thibaut, Oliver, Xavier and Carlos, for welcoming me there so warmly and making my experience unforgettable.

I am also indebted to my family and extended family for their love and support, especially my Mum who encouraged me the whole way, proof read and re-proof read, and who has always been, and continues to be, a huge inspiration.

And lastly, my husband Dave, who is my soul-mate and best friend and who has been on this whole journey with me. I'm looking forward to the next adventure that life takes us on!

'...the best kind of knowledge to have is that which is learned for its own sake'

Dedication

This thesis is dedicated to my family.

Table of Contents

Author's Declaration.....	iii
Acknowledgements.....	iv
Dedication.....	v
Table of Contents.....	vi
Abstract.....	xiii
List of Abbreviations and Definitions.....	xiv
Chapter 1 Introduction.....	1
1.1 Coordination Chemistry.....	3
1.2 Helices.....	4
1.2.1 Self-assembly.....	5
1.2.2 Chirality.....	7
1.3 Equilibria.....	9
1.3.1 Equilibrium Constants.....	9
1.3.2 Ionic Strength.....	11
1.3.3 Equilibria Terminology.....	14
1.3.4 Unidentate and Polydentate Ligands.....	15
1.3.5 pH Considerations.....	17
1.3.6 Relationship of Thermodynamic and Stoichiometric Constants.....	18
1.3.7 Conventions in Expressions.....	19
1.4 Kinetics.....	21
1.4.1 Reaction Rates.....	21
1.4.2 Order of a Reaction.....	22
<i>First-Order</i>	22
<i>Second-Order</i>	23
<i>Pseudo First-Order</i>	23
1.4.3 Factors Affecting the Rate of a Reaction.....	24
1.4.4 Complexation Kinetics.....	26
1.5 Chemometrics.....	26
1.5.1 Model-Based Data Fitting.....	28
1.5.2 Globalisation.....	30
1.5.3 Computational Techniques.....	32

1.6 References.....	35
Chapter 2 Programs: Data Acquisition and Analysis.....	43
2.1 Introduction.....	43
2.2 Data Acquisition	44
2.2.1 The Data.....	44
2.2.1.1 Mono-,Bi-, and Multivariate Data.....	45
2.2.2 General Techniques	48
2.2.3 Titration Experimentation	50
2.2.3.1 Overview	50
2.2.3.2 Equilibrium Investigations	52
2.2.3.3 General Experimental Procedure	54
2.2.3.4 Potentiometric Titrations.....	57
2.2.3.5 Spectrophotometric Titrations.....	59
2.2.3.6 Combined Potentiometric and Spectrophotometric Titrations.....	60
2.2.4 Kinetic Experimentation	63
2.2.4.1 Stopped-flow Acquisition - Fast Kinetics	63
2.2.4.2 Spectrophotometric Acquisition - Slow Kinetics.....	64
2.2.5 In-House Developed Software for Instrument Control	65
2.2.5.1 Titration Measurements	67
2.2.5.2 Slow Kinetic Reactions	72
2.3 Non-linear Least Squares Data Analysis	74
2.3.1 Overview	74
2.3.2 Globalisation of the Data	76
2.3.3 Model and Parameters.....	78
2.3.3.1 Spectroscopic Technique	80
2.3.3.2 Potentiometric Technique	82
2.3.4 Primary Chemical Models	83
2.3.4.1 Kinetic Analysis, Differential Equations	85
2.3.4.2 Equilibrium Studies, the Law of Mass Action	87
2.3.4.3 Non-Ideal Solutions	88
2.3.5 Fitting the Parameters	90
2.3.5.1 Computing the Calculated Data	90

2.3.5.2 The Residuals and Sum of Squares	91
2.3.6 Linear and Non-linear Parameters	92
2.3.7 Linear Parameters	93
2.3.8 Non-linear Parameters - Least-squares Fitting.....	96
2.3.8.1 Statistics of Output.....	101
2.3.8.2 χ^2 -fitting	102
2.3.8.3 Initial Estimates for Parameters	103
2.3.9 Determining the Correct Model	105
2.3.10 Published Software Packages.....	108
2.3.10.1 Package Details	102
2.3.10.2 Other Aspects of Data Fitting Programs	111
2.4 Our Data Analysis Program Design.....	114
2.4.1 User-Interface	116
2.4.2 Data Manipulation	122
2.4.2.1 Model Construction.....	122
2.4.2.2 Available Parameters	123
2.4.3 Output	124
2.5 Conclusions	125
2.5.1 Our Developed Programs.....	130
2.6 References	132
Chapter 3 Analysis of Potentiometric and Spectrophotometric Titrations with Polydentate N-donor Ligands.....	137
3.1 Introduction.....	137
3.1.1 Protonation Constants	138
3.1.2 Stability Constants	139
3.1.2.1 Defining Stability Constants	140
3.1.3 Combined Potentiometric and Spectrophotometric Titration Analysis	143
3.2 Solvent Considerations	144
3.2.1 Solvent Properties	144
3.2.2 Water-Alcohol Mixed Solvent Measurements.....	147
3.2.3 Electrode Use in Mixed Solvents.....	148
3.2.4 Ionisation Constants of Mixed Solvents	149

3.3 Experimental	150
3.3.1 Ligand Series	150
3.3.2 Analytical Solution Preparation	151
3.3.3 Titration Technique.....	153
3.4 Detailed Study of Ligand L5 (Pizda)	153
3.4.1 Determining the ‘Best’ Model	154
3.4.1.1 Protonation Model.....	155
3.4.1.2 Stability Model.....	155
3.4.2 Suggested Structures of Copper(II) – Pizda Complexes.....	166
3.5 Ligand Series Results and Discussion	169
3.5.1 Protonation Constants	169
3.5.1.1 Protonation Data Trends	172
3.5.2 Stability Constants	177
3.5.2.1 Potentiometric Titration Results	177
3.5.2.2 Spectrophotometric Titration Results	181
3.5.2.3 Stability Constant Data Trends	186
3.6 Conclusions.....	187
3.7 References.....	189
Chapter 4 Conjoint Chemometric Analysis of Equilibrium and Kinetic Data and Induced Chirality Investigations of a Helicating N-donor Ligand Interacting with Copper(II) and Nickel(II)	193
4.1 Introduction.....	193
4.1.1 Carboxamide-based Ligands.....	194
4.1.2 Helicate Formation Pathways	197
4.1.3 Induced Circular Dichroism of Racemic Helicates.....	198
4.2 Formation Pathway	198
4.2.1 Kinetic Investigation	198
4.2.1.1 Instrumentation	198
4.2.1.2 Solution Preparation.....	199
4.2.1.3 Data Analysis	201
4.2.2 Equilibrium Investigation	202
4.2.2.1 Instrumentation	202

4.2.2.2 Solution Preparation.....	202
4.2.2.3 Analytical Process.....	203
4.2.3 Conjoint Kinetic and Equilibrium Analysis.....	204
4.2.3.1 Kinetic Analysis.....	204
4.2.3.2 Equilibrium Analysis.....	207
4.2.3.3 Relationship Between Equilibrium and Rate Constants.....	209
4.2.3.4 Reaction Intermediates, $\log K_{\text{kin}} \neq \log K_{\text{eq}}$	214
4.3 Induced Chirality.....	218
4.3.1 Background.....	218
4.3.2 Circular Dichroism.....	219
4.3.3 Induced Circular Dichroism.....	220
4.3.4 PepdaH ₂ Helicity.....	223
4.3.4.1 Factors Affecting ICD Signal.....	224
4.3.5 Equilibrium of Intrinsic Induced Chirality.....	225
4.3.6 Experimental.....	227
4.3.6.1 Interaction with (-)-Tartaric Acid.....	227
4.3.6.2 Interaction with Sodium (+)-Tartrate.....	228
4.3.7 Results and Discussion.....	228
4.3.7.1 (-)-Tartaric Acid ICD Spectra.....	228
4.3.7.2 Sodium (+)-Tartrate ICD Spectra.....	230
4.3.7.3 ICD Analysis.....	232
4.4 Conclusions.....	235
4.5 References.....	238

Chapter 5 Equation Chapter 5 Section 5 Study of Nuclearity and Chirality of Complexes

Formed by a Helicating N-donor Ligand.....	243
5.1 Introduction.....	243
5.1.1 Aims of this Study.....	243
5.1.2 Overview.....	244
5.1.3 Bis(benzimidazole)-based Chelating Ligands.....	245
5.1.3.1 Basic Synthetic Process.....	245
5.1.3.2 Coordination Chemistry.....	246
5.1.3.3 Variations of the Bridging Unit.....	246

5.1.3.4 Substituted Variants	249
5.1.3.5 Applications	250
5.1.4 Stereoselectivity of ML_2 Complexes	251
5.1.4.1 Chirality	251
5.1.4.2 Theory	253
5.1.5 Previous Studies	255
5.2 Experimental	257
5.2.1 Instrumentation	257
5.2.2 Synthesis and Characterisation	257
5.2.3 Coordination Compounds	260
5.2.4 CD Spectra	261
5.2.5 CD Titrations with NaOH and HCl.....	261
5.2.6 CD Titration Technique for Determining Diastereoselectivity	262
5.2.7 ESMS Investigation of $[M(L-H)]_n$ Compounds	263
5.3 Results and Discussion	263
5.3.1 Preliminary CD and ESMS Investigations of Metal Complexes	263
<i>CD</i>	263
<i>ESMS</i>	266
5.3.2 CD Titrations	267
5.3.3 Determining Diastereoselectivity	272
5.3.4 ESMS Study.....	280
5.3.4.1 Mixed Ligand Species and Clear Resolution of Nuclearity	282
5.4 Conclusions	287
5.5 References	289
Chapter 6 Combined Glass Electrode Calibration	295
6.1 Introduction.....	295
6.1.1 The Definition of pH.....	296
6.1.2 pH Electrode Mechanism.....	296
6.2 Hydrogen Ion Activity Calibration Methods	298
6.2.1 IUPAC Recommended Methods.....	298
6.2.2.1 Primary Standard Buffer Solutions	299
6.2.2.2 Secondary Standard Buffer Solutions	302

6.2.2.3 Calibration Using Buffer Solutions.....	303
6.3 Calculating Equilibrium Constants	306
6.4 Hydrogen Ion Concentration Calibration Methods.....	308
6.4.1 Strong Acid / Strong Base Titration Calibration.....	308
6.5 Mixed and Non-aqueous Solvent Measurements.....	310
6.5.1 Standard Buffer Calibration	311
6.5.2 Alternative Calibration Techniques	312
6.5.2.1 Extrapolation.....	312
6.5.2.2 Correction Coefficients	313
6.5.3 Titration Calibration.....	314
6.5.4 Internal Concentration Calibration.....	316
6.5.5 Internal Concentration Computer Programs	318
6.6 Our Global Internal Calibration Program	320
6.6.1 Defining Parameters.....	321
6.7 Activity Approximations	325
6.8 Complex Solution Calibration Applications	327
6.8.1 pH Measurements in Beverages.....	328
6.8.1.1 Secondary Calibration.....	329
6.8.1.2 Extended Applications	336
6.8.2 Determination of the Purity of Room-Temperature Ionic Liquids	337
6.8.2.1 Synthetic Process	339
6.8.2.2 Global Analysis Method	340
6.9 Conclusions.....	347
6.10 References.....	350

Abstract

This work presents the development and application of modern data acquisition and analysis techniques for the investigations of equilibrium and kinetic reactions. The analytical technique is known as second order global analysis and a background of this relatively novel approach has been given. The theory behind and characteristics of the computer programs developed analysis as part of this research are described in Chapter Two along with descriptions of the instrumentation and programs developed for the acquisition of both potentiometric and spectrophotometric data.

Applications of the developed programs include a potentiometric and spectrophotometric study of the protonation and stability equilibria of a series of polydentate N-donor ligands, as detailed in Chapter Three. The combination of potentiometric and spectrophotometric analysis has been shown to be a powerful analytical tool.

Spectrophotometric titrations were also combined with fast stop-flow experiments in order to elucidate the complex reaction mechanisms associated with helicing ligands. The helication of the ligand 'PepdaH₂' with copper(II) and nickel(II) is examined in Chapter Four, along with discussions concerning the ability to induce chirality in the helicates from the addition of a chiral counter ion.

Investigations into chirality were further continued in Chapter Five where the stereoselectivity of a benzimidazole-based ligand was investigated with circular dichroism titrations. The synthesis and characterisation of the benzimidazole-based ligands are provided, including a study of the ability of the ligands to form higher order complexes as investigated using electrospray mass spectroscopy.

Chapter Six provides an in-depth discussion concerning the use of combined glass hydrogen selective electrodes for the determination of equilibrium constants, as this was a major focus of this research. Different calibration techniques are discussed and a description of the internal calibration technique developed is provided along with examples of the advantages of performing internal calibration of the electrode.

List of Abbreviations and Definitions

b.p.	Boiling point
Bispidinone	3,7-diazabicyclo[3.3.1]nonan-9-one
CD	Circular Dichroism
DMF	<i>N, N</i> –dimethylformamide
DMSO	Dimethyl sulphoxide
Dp-bispidinone	1,5-diphenyl-3,7-diazabicyclo[3.3.1]nonan-9-one
Dpdb-bispidinone	1,5-diphenyl-3,7-dibenzyl-3,7-diazabicyclo[3.3.1]nonan-9-one
EFA	Evolving Factor Analysis
ESMS	Electrospray Mass Spectroscopy
GA	Genetic Algorithm
¹ H n.m.r.	Proton Nuclear Magnetic Resonance
I	Molar ionic strength ($I = \frac{1}{2} \sum z^2[Z]$) of all species in solution
ICD	Induced Circular Dichroism
IR	Infra-red
K_s	Ionisation constant of a solvent
K_w	Ionisation constant of water
LJP	Liquid Junction Potential
m.p.	Melting point
NBS	National Bureau of Standards
NGL/M	Newton-Gauss-Levenberg/Marquardt
NIST	National Institute of Standards and Technology
NMI	National Metrological Institutes
PepdaH ₂	<i>N,N'</i> -bis[2-(2-pyridyl)methyl]pyridine-2,6-dicarboxamide
Piperazine	1,4-diazacyclohexane
Pizda	1-[(2''-hydroxycyclohexyl)-3'-aminopropyl]-4-[3'-aminopropyl]piperazine
Pot_Anal	Analytical Program for Potentiometric Titration Data
ProKII	Pro-Kineticist II
RLJP	Residual Liquid Junction Potential
Spec_Anal	Analytical Program for Spectrophotometric Titration Data
ssq	Sum of squared residuals

UV	Ultra-violet
x	Bold lower case characters for vectors
X	Bold upper case characters for matrices
<i>x</i>	Italic characters for scalars and chemical species
γ_z	Activity coefficient of a $\pm z$ charged species
[Z]	Molar concentration of species Z
{Z}	Activity of species Z
δ	Standard Deviation
μ	Ionic Strength (M)

Chapter 1

Introduction

The interactions of matter are a fundamental property that has been studied throughout history. Such research has resulted in discoveries that have arguably improved our quality of life and also deepened our knowledge of the world we live in and connect with everyday. The study of matter, and the reactions and changes it can undergo, are often the practical foundation on which our knowledge of the world and environment are based. As such these investigations form the basis of important decision making activities in today's society ¹.

This thesis is based on analytical chemistry, specifically chemometrics, in the area of inorganic coordination chemistry. In the specialised scientific field of analytical coordination chemistry, studies focus on gaining understandings about the composition, structure, property and reactivity of chemicals, and also about investigating the processes they undergo. For example, researchers are driven to investigate how metals and ligands[#] interact, and why particular products are observed to form, in order to further the understanding and behaviour of such interactions, which are a fundamental part of many areas of science. Such investigations were first conducted over a century ago by Alfred Werner, who is considered to have developed the basis for modern coordination chemistry, with his studies of metal-amine complexes of which $[\text{Co}(\text{NH}_3)_6\text{Cl}_3]$ won him the Nobel Prize in 1913 ². The field of coordination chemistry has been steadily developing since Werner's important discovery, with major growth seen during and after the 1950s, which was when the inaugural International Conference of Coordination Chemistry was organised by Dr Joseph Chatt. Such intensive research has led to many interesting scientific publications and important discoveries in the area of coordination chemistry ³⁻⁸.

The field of analytical chemistry is also a broad area of chemistry that has been steadily developing since the 1970s ¹. Analytical chemistry has found an important niche in the field of coordination chemistry with the investigation of solution equilibria and the rates of reactions of coordinating compounds. These investigations were greatly aided by the availability of personal computers at the beginning of the 1980s which introduced a new

[#] Ligands are Lewis bases which are capable of supplying a pair of electrons to form the bond with the metal centre which is a Lewis acid.

age for the acquisition, processing and interpretation of chemical data ⁹. Such significant improvements in technology, especially in the area of instrumentation and computer capabilities, have accelerated research and resulted in modern analytical chemistry now being dominated by instrumental analysis. This progress has led to advancements not only with regard to the reliability of the experimental data, but also with data processing, computation, and analysis. There is no doubt that the development of methods for data collection and analysis are closely related to the evolution of technology as it is clear that the computer has become an indispensable tool for modern research and development.

Generally, analytical chemistry can be divided into the study of concentrations, structures, and processes such as equilibrium and reactivity. The key themes explored for this research focused on the well-established discipline involving the determination of equilibrium and rate constants. Such investigations were conducted for a variety of ligands and transition metals in order to elucidate information not only about the properties of the species and complexes formed, but also details about the reaction paths taken and the core chemistry involved.

The thesis provides in-depth discussions on modern analytical methods and their subsequent interpretations and applications. The study includes the acquisition of experimental data from modern instruments and the related descriptions of the techniques and programs developed for such tasks. The analytical methods applied to the acquired data were also developed as part of the research and are leading in their field. The developed data acquisition and analysis techniques have been applied to a varied range of coordination chemistry reactions in order to demonstrate the complete process. The information and knowledge provided by such chemical measurements are of importance in many instances; for example, when the conclusions drawn from the experimental results are used as the basis of decision-making processes that may influence others and the future directions of related research.

The basic principles describing the research for this project are described in this chapter. The fundamental chemistry of coordination compounds is covered as such chemistry forms the basis of the majority of the investigations. A natural extension of coordination chemistry is the study of helical structures and their chirality, this is described in Section 1.2. The analytical techniques that are typically used to describe coordination and helical compounds, specifically equilibrium and kinetic investigations,

are described in Sections 1.3 and 1.4, respectively. The final section of the chapter provides a brief introduction into the field of chemometrics as a broad analytical tool applied to many types of data. Chapter 2 provides a comprehensive discussion of the particular chemometric tools developed for this research.

1.1 Coordination Chemistry

Coordination chemistry is generally described as ‘the investigation of species that are formed by the association of two or more species each being capable of an independent existence’¹⁰. From such a description it is evident that the term coordination compound covers a vast number and type of assemblies. Specifically, for this research, coordination compounds are metal complexes in which one or more metal centres are associated with one or more ligands¹¹. The study of such complexes is based on the investigation of the coordination bond that forms between the metal ions and the coordinating ligands. Due to the nature of metal-ligand interactions the coordinate bond can be often quite labile, despite its strength, making it possible for rapid rearrangements of the coordinated ligand to occur. This lability is one of the key attributes of coordination chemistry, as the structures formed are the thermodynamically most stable products.

Coordination compounds can generally be described by features such as the structural composition, the numbers and kinds of molecules involved in the compound, the constitution of the complex, the way the ligands and metals are connected, and the configuration and way the ligands are oriented relative to one another in space. Generally, there are four structural factors that underlie the arrangement of the ligand during metal complexation and these include the size, shape or geometry, connectedness or topology, and rigidity of the complexing ligand¹². The effects of size and geometry have been extensively explored by chemists.

The more subtle contributions of topology and rigidity are still areas of great interest. Such factors can effectively be explored by investigating a well chosen series of ligands; for instance, the molecular organisation of the series of nitrogen-donor polydentate ligands which was investigated in Chapter 3, using both potentiometric and spectrophotometric techniques. This work focused on the coordination chemistry of complexes with typically one metal centre, bound by the nitrogen-donor ligand. The assemblies that formed were typically 1:1 metal-ligand complexes of differing denticity, depending on the topological properties of the ligand and the pH of the solution.

Further, in Chapter 4, supramolecular structures have also been investigated which involved two and three metal ions coordinating in a helical fashion with two potentially pentadentate ligands.

As previously mentioned, analytical chemistry can be used to investigate the coordination chemistry of a compound via two main techniques. Firstly, the equilibrium constants of the coordinated species determined to exist in solution can be calculated, and secondly the rate constants and appropriate mechanisms for the formation of the species can be explored. The knowledge of either the equilibrium or rate constant is essential for understanding the process of the reaction. Sometimes equilibrium and rate constants are both determined to further aid in analysis, as described in Chapter 4.

New activity in the field of coordination chemistry has been encouraged due to many important developments that have increased the significance of determining and applying both equilibrium and rate constants. These developments have ranged from advances in macrocyclic and macrobicyclic complexes, where the equilibrium constants are a direct measure of metal ion selectivity and thermodynamic stability, to the field of bio-inorganic chemistry where it is of great significance to know the metal speciation in the environment¹³. However, a significant degree of the progress in the coordination chemistry field has been due to advancements in the computational methods used for the processing of experimental data. The development of new methods have enabled rapid and accurate determination of equilibrium and/or rate constants, and more importantly enabled the analysis of systems that have previously been considered too complex to be investigated by classical methods; for example, systems that contain multiple metal ions and numerous polydentate ligands¹³.

1.2 Helices

In coordination chemistry helices are metal-ligand complexes composed of, in their simplest architecture, two metal centres bound by one helically binding ligand. Although, the arrangement of some ligands around a single metal ion, such as three coordinated 1,10-phenanthroline ligands around a ruthenium metal centre as shown in Figure 1.1, can be seen as a helical structure. However, generally helicates are more complex, being composed of two or three ligand strands complexed to two or more metal ions^{14, 15}. The helices synthesised for our investigations led to the thermodynamically stable production of M_2L_2 and M_3L_2 helicates.

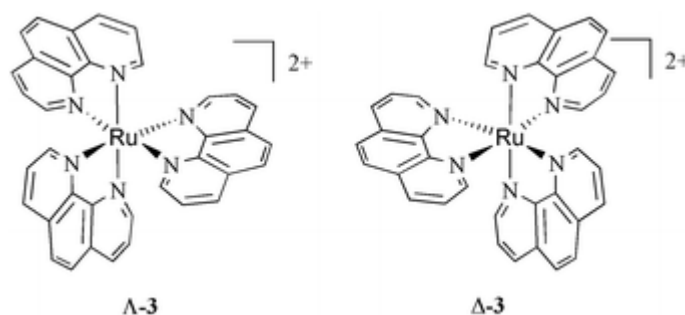


Figure 1.1: Monometallic helicate with three coordinated 1,10-phenanthroline ligands showing anticlockwise (Λ) and clockwise (Δ) helicity ¹⁶.

The structure of a helix is one that has been found to be ubiquitous in nature, such as in various biological systems, but it is also a geometric motif that has been reflected by human art and architecture, as shown in Figure 1.2 ¹⁷. It has been demonstrated that one of the most important features of helical supramolecular architectures is the simultaneous operation of several weak interactions between building blocks, such as hydrogen bonding, π - π , and metal-ligand interactions ¹⁸⁻²⁰.

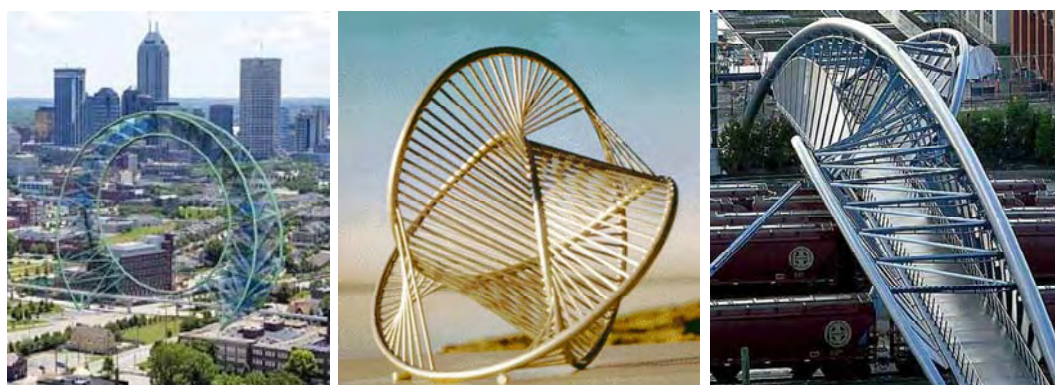


Figure 1.2: Geometric motifs of the structure of helices in art and architecture ²¹⁻²³.

1.2.1 Self-assembly

Often metal complexes, depending on the ligand and metal coordination properties, self-assemble to result in helical structures. Transition-metal helicates have played a central role in coordination chemistry for many years, resulting in the preparation of helices by self-assembly processes being a prevalent area of research ^{14, 15, 24-27}. The process of self-assembly requires the ligands to organise themselves around the metal ions, resulting in the classical intertwining structures of double or triple helices ²⁸. The synthesis of helicates, prepared via a self-assembly process, involves appropriate ligands, each having two or more binding sites, reacting with suitable metal ions to form the most thermodynamically stable product, or products if they are of comparable

stability^{14, 26, 29-31}. The specific type of helicate formed is dependant on the denticity of the ligating units and the coordination requirements of the metal ion³². Therefore, higher dentate ligands are commonly used for the synthesis of self-assembly helicates as they have the ability to wrap around two or more metal ions along the helical axis to give double or triple-stranded helical structures. Barley *et al* also demonstrated that different helicates could be synthesised depending on the coordination properties of the metal by showing that a quinquedentate ligand acted as a bidentate ligand towards the tetrahedral copper(I) metal ion, but as a terdentate donor towards pseudooctahedral copper(II)³³.

The spontaneous, self-assembling process of helicates has enabled many to be viewed as simple models of more complex natural structures³⁴. A theme of considerable interest with helical structures is not just their spontaneous formation, but also the selectivity of the organised supramolecular architectures which result from often intriguing self-assembling processes during the formation^{34, 35}. Such selectivity often mimics what has been observed to occur spontaneously in many natural systems. Lehn and co-workers³⁶ investigated pentametallic double-stranded helicates in order to determine the reaction pathways of the self-assembly process and elucidate the selectivity of helication. As a result of the investigation they reported the formation of unusual intermediates during the slow self-assembly process. Since such findings, the research into double and triple-stranded helicates has been a dominant area of interest^{28, 31, 37-40}.

Our research involved investigating the reaction pathways for the formation of helicates with different metals, in order to elucidate the respective reaction mechanisms and observe any differences resulting from the change of the metal ion. This metal-ion assisted self-assembly has been detailed in Chapter 4. The study was conducted using a polydentate nitrogen-donor ligand whose structure included three amide pyridine functional groups which are known to generate resonance stabilised dianions, which readily coordinate to metal ions. Our results led to the elucidation of the reaction mechanism for the formation of two different double stranded helical structures for two metals ions, copper(II) and nickel(II).

1.2.2 Chirality

An intrinsic property of helical systems is chirality. In synthetic supramolecular complexes chirality can be classified into several hierarchical levels. Chirality at the primary level requires optically active building blocks that result in quaternary carbon stereocentres. Ligands that are chiral on the primary level most often contain an optically active carbon centre; such chirality is denoted using *R/S* notation. Helicity may also occur in structures that have no chiral carbon as a result of the rigidity of the compound.

Molecular chirality at the primary level originates from the non-symmetric arrangement of the chemical groups that are covalently linked to the atomic centre and therefore such chirality is not easily subject to dissociation. In contrast, supramolecular chirality on the secondary level is derived from the non-symmetric arrangement of molecular components in a non-covalent ensemble^{15, 41}. Chirality on this secondary level disappears upon disassembly of the constituent components. With the secondary level of chirality the helices themselves are intrinsically chiral and assigned a *plus* (*P*) or *minus* (*M*), or alternatively Δ or Λ , depending on the handedness of the helical structure. Chirality is determined by viewing the twist direction of the propeller structure along the principal helical axis, a clockwise motion corresponds to a *P* and an anticlockwise motion to an *M* helix, as shown in Figure 1.3.

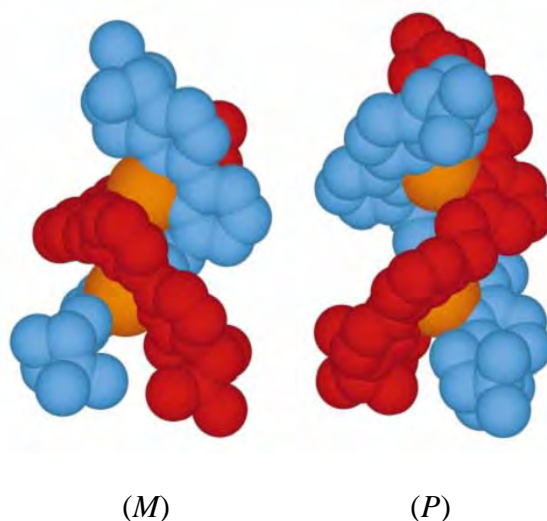


Figure 1.3: The solid state structures of the (*M*) and (*P*) structures of a helicate structure involving two metal ions and two helicating ligands⁴².

For helical structures dissociation, due to the kinetic lability of the interactions, may lead to a mixture of *P* and *M* optical isomers which results in the formation of a non-

optically active mixture known as a racemate⁴³. This is observed for the metal-directed assembly of helicates with achiral ligands, that is where there is an absence of a primary source of absolute chirality⁴². Figure 1.3 shows how complex helicity of both *P* and *M* helicates can result from the coordination process when a non-chiral ligand is used for complexation.

It has been shown, however, that if chiral helicing ligands are used in the helication process the ligands themselves can induce stereoselectivity. This means that the chiral centres of the ligands influence the chirality of the resulting helix⁴⁴⁻⁴⁷. In such instances, the resulting solution will not be a racemic mixture, but consist of an equilibrium with an excess of either *P* or *M* helicates depending on the directional influence of the chiral centre on the ligand. This has been demonstrated in Figure 1.4a, which depicts how helicity of a complex can result from chirality at the metal centre due to the chiral interaction of the ligand⁴⁸. This chirality can trigger supramolecular helicity and can be used to program the stereoselectivity of metal complex. Figure 1.4b shows how the additional of an additional chiral ligand can give a twisted geometry between two chromophoric groups in a complex, this is known as induced helicity and is discussed further in Chapter 5.

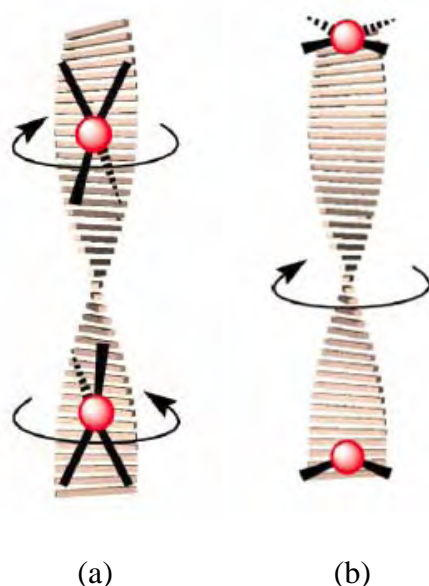


Figure 1.4: Molecular programming based on (a) complex helicity and (b) ligand chirality where the twist of the chiral ligand defines the helicity of the complex formed⁴⁸.

This research involved the investigation of both forms of chirality, that is chirality resulting from the chelation of chiral ligands with metal ions as well as the helicates formed from the interaction of non-chiral ligands with metal ions which necessarily

resulting in racemic metal-ligand complex mixtures. Chiral ligands were added to the racemic mixtures of helicates and the resulting induced chirality was also measured.

There is a tertiary level of chirality, which includes the asymmetric packing of helical coils in a liquid crystal. Such chirality is governed by chirality on the secondary level⁴⁹. Many helical structures pack together in interesting formations depending on whether the solution was comprised of racemic or pure *P* or *M* helicates. This third level of chirality was not investigated as crystal structures were not explored as part of this research.

1.3 Equilibria

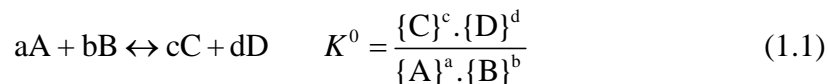
Protonation and metal complex equilibria are widely distributed in nature. The equilibrium constants of coordination compounds are what quantitatively describe the composition of both protonated and complex species that form, as well as the conditions under which they exist in solution. Knowledge of such constants has many diverse applications for modern science and industry⁵⁰. The protonation constant of a ligand provides valuable information about what state a ligand will be in at a particular pH; such knowledge is vital for many natural systems that are pH sensitive. The determination of equilibrium constants when a metal ion and a ligand are combined in solution is also beneficial as it has long been used as a measure of the success or failure of the ligand design. Further, knowledge of stability constant values can aid in achieving complexes with high thermodynamic stabilities in solution or assist with the development of ligands that can be used for selective complexation for the separation of, or discrimination between, metal ions¹³.

1.3.1 Equilibrium Constants

The equilibrium constant quantitatively and unambiguously defines the position of a given equilibrium that is determined by the values of its intensive parameters, such as pressure, temperature, and so forth. Equality of forward and backward reaction rates is a necessary condition for chemical equilibrium, which is fundamentally a single numerical value that gives information about the equilibrium position under the stated conditions.

Equilibrium constants are strictly defined by the law of mass action as the quotient of the activities of the chemical species at equilibrium, and therefore should be expressed in terms of the activities of the component ion or complexes at equilibrium in order to

have a rigorous thermodynamic meaning⁵⁰⁻⁵². For the hypothetical equilibrium in Equation (1.1) the equilibrium constant is defined as shown, where $\{A\}$ denotes the activity of the species A.



Equilibrium expressions that are defined using species activities, as shown above, are known as thermodynamic equilibrium constants and denoted as K^0 . However, it is not trivial to determine the activity of a species at equilibrium, making the determination of thermodynamic equilibrium constants difficult and impractical. As such, for convenience and reproducibility, and since concentrations are much easier to measure, equilibrium constants are generally expressed as stoichiometric constants, K_{eq} , rather than determining the impractical thermodynamic constants that are favoured by many physical chemists¹³. Hence, the majority of researchers report stoichiometric equilibrium constants. The simple relationship between concentrations and activities, as shown in Equation (1.2), demonstrates that the concentration of a species and activity are related via its activity coefficient, f .

$$\{A\} = [A] \cdot f_A \quad (1.2)$$

This relationship can be applied to the calculation of stoichiometric equilibrium constants in accordance with Equation (1.3), which are based on species equilibrium concentrations rather than the activities.

$$K^0 = K_{eq} \frac{f_C^c \cdot f_D^d}{f_A^a \cdot f_B^b} \quad \text{where} \quad K_{eq} = \frac{[C]^c \cdot [D]^d}{[A]^a \cdot [B]^b} \quad (1.3)$$

Fortunately, since measuring and determining activity coefficients is a time consuming, complicated and sometimes impossible task, concentrations almost always parallel activities in solutions where the ionic strength is held constant. Under such experimental conditions the activity coefficients are theoretically constant, although in reality the ionic strength is hardly ever perfectly constant and therefore there will be small discrepancies in the constancy of the activity coefficients. However, even though stoichiometric constants are simpler and more commonly determined than thermodynamic constants, only thermodynamic constants are constant for constant temperature and pressure and thus useful for comparisons between systems. In order for stoichiometric constants to be comparable the ionic strength of the solution has to also

be the same and constant, as well as having constant temperature and pressure. Stoichiometric constants need to be reported with information about the ionic strength conditions.

1.3.2 Ionic Strength

The use of an inert electrolyte to maintain constant ionic strength was first formally introduced in 1921⁵³, though it can be traced back to the turn of the century when Grossman⁵⁴ maintained constant ionic strength using potassium nitrate⁵⁰. These days it has become standard practise to determine equilibrium, and also rate constants, using methods for which the ionic strength is maintained, as far as possible, at a constant value by the addition of an inert salt.

Thus far, only partial standardisation has occurred across research groups with respect to common ionic strength values and the ionic medium used. Ionic strength values of 0.1, 0.5 and 1.0 appear most commonly for equilibrium investigations, but a variety of different salts can be added in order to maintain the ionic strength value. The most regularly reported salts include KNO₃, KCl, NaNO₃, NaClO₄, and NaCF₃SO₃⁵⁵. A draw-back of using an inert salt for constant ionic strength is that information is not readily available regarding the degree of interaction between the reacting species and the ions from the background medium^{51,52}. For example, in a reaction involving metal ions many anions that are added for constant ionic strength, such as ClO₄⁻ and CF₃CO₃⁻, are also weak ligands and as such react with the metal forming weak complexes, as shown below where X is the anion.



Further, it must be taken into account that rather than all free metal ions associating as hexaqua metal ions in an aqueous solvent, a combination of species may exist with varying numbers of complexed solvent and/or medium ions. Therefore, when the metal reacts with the ligand it must be remembered that the metal ion is not only solvated by the solution, but it is also complexed to the anions present from the ionic medium added, and hence equilibrium constants for complex species are in fact an average of complexations from all the different forms of the metal ion existing in solution. Consequently, such constants are not necessarily comparable if different background mediums have been used.

There are three main factors that affect the choice of which ionic medium is best to use for a particular equilibrium system. The first consideration is that the electrolyte must be inert, that is non-interfering with the equilibrium by either complexing the species of interest or by entering into redox reactions. For this reason alkaline earth metal ions are not used as part of the background medium when studying the complexation of some polydentate ligands, which form strong complexes with these cations. In such instances tetraalkylated ammonium salts are commonly used.

The second concern is that the electrolyte should not contribute to the measured physical or chemical properties. For this reason the nitrate ion is not used as part of a background medium when measuring UV absorbance.

The third consideration which influences the choice of an ionic medium is that it is necessary for the electrolyte to be sufficiently soluble in the solvent used. This factor particularly limits the choice of electrolyte for non-aqueous solutions.

When equilibrium constants are expressed using concentrations it is implied that the activity coefficients are constant because, as shown previously in Equations (1.2) and (1.3), stoichiometric constants are constant and directly proportional to thermodynamic constants when the activity coefficients are kept constant. For equilibria that involve ionic species, which includes all metal-ligand equilibria, constant ionic strength is required in order to maintain constant activity coefficients, as the activity coefficients are strongly dependent on ionic strength.

The ionic strength, I , of a solution is determined for all charged equilibrium species, i , by Equation (1.5), where m is concentration in mol L^{-1} , or strictly molality in mol kg^{-1} of solvent, and z is the magnitude of the charge of each species ⁵⁶.

$$I = \frac{1}{2} \sum m_i z_i^2 \quad (1.5)$$

Hence, it can be seen that the ionic strength is proportional to the concentration and the square of the charge on the species, and clearly the higher the charge the greater the influence the species will have on the ionic strength of the solution. It should also be noted that ionic strength is strongly pH dependant. Consider a solution with a protonated ligand species, LH^{2+} . Depending on the pH of the solution other species will be present in varying concentrations, such as LH^+ , L , and H^+ . For such a solution the equation for ionic strength would be written as combination of all ions present in

solution, as shown in Equation (1.6). Therefore, it can be seen that since a change in pH alters the concentrations of all the species present, which will result in a subsequent change in the ionic strength of the solution.

$$I = \frac{1}{2} \{ [\text{LH}^{2+}] \times (+2)^2 + [\text{LH}^+] \times (+1)^2 + [\text{L}] \times (0)^2 + [\text{H}^+] \times (+1)^2 \} \quad (1.6)$$

In order for stoichiometric constants to be directly comparable to thermodynamic constants the concentrations must be measured in a medium of relatively high ionic strength. Solutions of high ionic strength are needed to ensure that any variations in ionic strength from the changing charge of the species have the smallest effect possible on the overall ionic strength of the solution. The total ionic strength needs to be significantly greater than the change in ionic strength due to the chemical process, for example Equation (1.6). Where maintaining ionic strength is not possible, consideration needs to be given to possible activity variations.

When a high concentration of an inert electrolyte is added to the equilibrium solution as a background medium, concentrations can be directly substituted for activities. This is because the ionic strength is constant and therefore the activity coefficients may be assumed to be independent of the concentrations of the species in equilibrium, influenced only by the concentration of the electrolyte that is in large excess. The relationship between ionic strength and activity coefficients is described below where I is the ionic strength of the solution, A and B are constants with values of respectively 0.51 and 0.33 at 25°C in water, z is the charge of the species and f_i is the activity coefficient. This is an example of one of several approximations for the activity coefficient of a charged species.

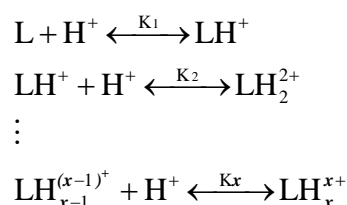
$$\log(f_i) = -\frac{Az_i\sqrt{I}}{1 + Ba\sqrt{I}} \quad (1.7)$$

Under constant ionic strength conditions, stoichiometric equilibrium constants may readily be obtained by a variety of methods. However, given the assumption of constant ionic strength, stoichiometric constants can only be reliably compared as long as they are measured under identical ionic strength conditions as well as the same temperature and pressure. This practical simplification has become standard practice amongst coordination chemists⁵⁰.

1.3.3 Equilibria Terminology

There are different terms used in coordination chemistry to denote equilibrium constants. The equilibrium constants of non-complex species, that is free ligands, are normally referred to as acidity, ionisation or protonation constants. While other terms are present in the literature, such as acid dissociation constants, hydrolysis constants, and so forth, these are less commonly used¹⁰. The equilibrium constants of complexed species characterise the stability of the complex species formed and are commonly referred to as stability, formation, or association constants.

The majority of ligands are weak bases, meaning that in aqueous solutions, as most natural systems are, most ligands exist in a number of different protonation states. For polydentate ligands the number of possible protonated ligand states can be considerable, the number of potential protonation states being depicted in Scheme 1.1. Protonation constants are usually expressed as a series of protonation steps which begin with the fully deprotonated ligand, L. The first protonation step is written as $L + H^+ \leftrightarrow LH^+$, and so forth depending on the denticity of the ligand. The relative concentrations of each individual species in any given aqueous solution are dependent on two factors: firstly the pH of the solution; and secondly the protonation constant(s) of the ligand.



Scheme 1.1: Protonation equilibria of a ligand, L. For simplicity, the unprotonated ligand is assumed to be neutral.

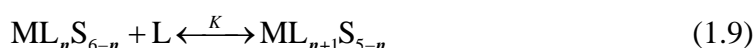
The substitution of a coordinated solvent molecule to a metal centre by a free ligand in solution is a fundamental process and the basic process for the formation of metal complexes, see Equation (1.8)⁵⁷.



Due to the numerous protonated species possible for most ligands the investigation of metal-ligand equilibria is an intricate combination of protonation and complexation equilibria, as both are necessarily coupled⁵⁸. The metal ions in solution generally interact differently with each protonated ligand species, hence many different complex species may exist simultaneously in solution.

1.3.4 Unidentate and Polydentate Ligands

The investigation of complexes formed from bi- or polydentate ligands is necessarily more complicated than the formation of simple metal-unidentate ligand complexes which are relatively straightforward, especially when only one step is involved in the complexation process. However, the complexation process for unidentate ligands does become more involved when coordinated solvent molecules are replaced by multiple ligands. The general stepwise formation of the complex ML_n can be simplified to Equation (1.9).

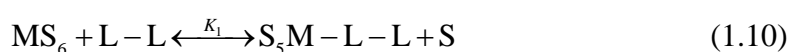


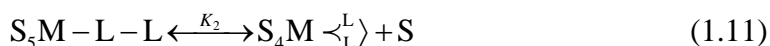
For unidentate ligands each successive replacement of a solvent molecule is less probable than the previous one and hence has a smaller equilibrium constant ⁴, that is, the stepwise formation constants lie in the order $K_1 > K_2 > K_3 \dots > K_n$, as demonstrated in Table 1.1 where n is the number of ammonia ligands attached to the metal ion. This effect is due mainly to the statistics of the substitution process, steric repulsion and hindrance, and an increase in the rate of dissociation.

n	log K
1	-2.73
2	-2.16
3	-1.83
4	-1.21
5	-1.03
6	-0.09

Table 1.1: Formation constants of ammonia complexing with nickel(II) ⁵⁹.

The replacement of solvent molecules by the donor groups of a polydentate ligand is not fundamentally different from replacement when only unidentate ligands are involved. However, the multiplicity of steps may increase the difficulty in understanding the detailed mechanism ⁶⁰. When polydentate ligands are involved in chelation the process necessarily involves several steps, for example, chelation with a flexible bidentate ligand is a two-step process. The successive steps involved in the replacement of two coordinated solvent molecules have been represented in Equations (1.10) and (1.11).





It can be seen that the replacement of a second solvated molecule is more probable with a polydentate ligand, compared with a second unidentate ligand binding. This is because for the second step of the reaction part of the ligand is already attached to the metal ion for the polydentate ligand. Therefore, the free end of the ligand is already in the vicinity of the metal ion, which consequently increases the probability that the second metal-ligand bond will form.

Another factor influencing the stability of polydentate complexes is what is known as the chelate effect. Metal chelation is the binding or complexation of a bi- or polydentate ligand. Relative to aqua complexes, for example $[M(OH_2)_6]^{2+}$, the increased stability of a chelated complex, such as the $[M(EDTA)]^{2-}$ complex shown in Figure 1.5, is called the chelate effect. If a chelate were replaced by several such unidentate ligands, the total number of molecules in the solution would decrease, whereas if several unidentate ligands were replaced by a chelate, the number of free molecules in solution consequently increases. Therefore, in general, metal complexation with polydentate ligands that form chelates lead to a much greater stability constant than results from similar unidentate ligands because of the favourable entropy for the chelation process. This means that when more coordination sites are used by fewer ligands there are more unbound molecules, resulting in a total increase in the number of molecules in solution which corresponds to an increase in entropy. Therefore, in solution, a metal-ligand system favours chelation as this leads to higher entropy.

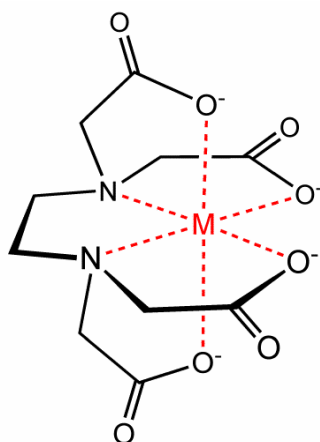
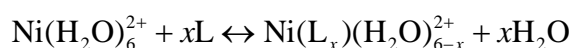


Figure 1.5: Metal-EDTA (ethylenedinitrilotetraacetic acid) chelate ⁶¹.

Table 1.2 provides the equilibrium constants for the binding of nickel(II) with four nitrogen donor ligands of increasing denticity, successively 4 NH_3 , 2 en

(ethylenediamine), 1 trien (triethylenetetramine) and 1 tetradentate "2,3,2" ligand ⁶². The measured indication of affinity increases with the chelation number of the ligand as long as exceptional strain energy is not encountered, as can be seen for the trien complex. The general trend shown in Table 1.2 clearly highlights the effect of the chelation number on the stability of the complex formed. Similar Ni-N bonds are formed in each case, yet the formation of the high-ordered chelates are distinctly more favourable due to the greater stability of chelated complexes compared with their non-chelated analogues.



L	NH ₃	en	trien	2,3,2
log β	2.73	7.30	13.8	14.6

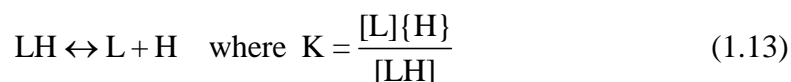
Table 1.2: The effect of chelation on the stability of complexes.

1.3.5 pH Considerations

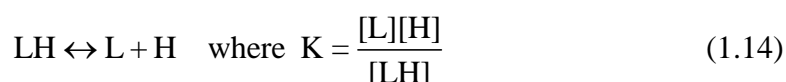
Most equilibrium investigations for ligand protonation and complexation with metals are performed using pH titrations where the pH of the solution is measured as a function of added base or acid. For pH titrations, the pH value is directly related to the measured electrochemical response of a hydrogen ion selective electrode. Strictly, pH is defined in terms of the activity of the hydrogen ion, as shown in Equation (1.12).

$$\text{pH} = -\log\{\text{H}^+\} \quad (1.12)$$

The different calibration techniques that are commonly used for hydrogen-ion electrodes have been discussed in detail in Chapter 6. Depending on the calibration technique used, the quantity measured by the electrode can be either the activity of the hydrogen ion, $\{\text{H}^+\}$, or the concentration of the hydrogen ion, $[\text{H}^+]$ ⁶³. The type of equilibrium constant determined from potentiometric titrations is dependant on whether the electrode has been calibrated by reference to solutions of known activity or known concentration. If, when determining an equilibrium constant, the electrode was calibrated to measure hydrogen ion activity the result is the determination of a mixed equilibrium constant, also known as a Brønsted constant, as shown in Equation (1.13) for a simple protonation equilibria, charges omitted for clarity.



However, if the electrode has been calibrated to measure hydrogen ion concentration the equilibrium constant would be a concentration quotient, resulting in the calculation of stoichiometric equilibrium constants, as shown in Equation (1.14) for the same protonation equilibria. For our research the pH electrode was calibrated to measure hydrogen ion concentration and therefore stoichiometric constants have been reported.



1.3.6 Relationship of Thermodynamic and Stoichiometric Constants

Due to the known relationship between thermodynamic and stoichiometric constants, that is the activity coefficient, one constant can be determined from the experimental calculation of the other. If thermodynamic constants are required, which are experimentally hard to measure, two main approaches can be followed to determine them from calculated stoichiometric constants.

The first approach is based on activity coefficients having, by definition, a value of one at low ionic strength. Hence, thermodynamic constants may be determined by a series of stoichiometric constants calculated at different ionic strengths and then extrapolated to infinite dilution in that medium. This is equivalent to a value of low ionic strength and hence $f = 1$. Such an extrapolation involves a nearly horizontal straight line and thermodynamic constants can be determined very accurately¹³. Rossotti and Rossotti⁶⁴ noted that the values of stoichiometric constants are very close to the values of true thermodynamic constants using the extrapolation technique in the various ionic mediums employed.

The second approach involves estimating the activity coefficients of each species present in the equilibrium and then calculating the activity of the species according to Equation (1.2). Such approximations remove the need for constant ionic strength as they estimate the activity coefficient of all ions present in the reaction mixture. The calculated activities can then be used to determine the thermodynamic equilibrium constant. This approximation of activity coefficients can be achieved, for example, by using one of the extended forms of the Debye-Hückel equation as previously shown in Equation (1.7)⁵¹, which is useable for approximations of ionic strengths and

concentrations up to approximately 1 M. Other approximation methods include such extensions as the Davies ⁶⁵ equation or Pitzer ⁶⁶ equations. Activity approximation methods have only recently become a viable option due to the advancement in computer systems. These advancements have greatly reduced the computational time required to incorporate the ionic strength approximations into the law of mass action, which is required in order to calculate the concentration of the species in the reaction.

1.3.7 Conventions in Expressions

Where multiple stages of protonations or complexations occur, constants can be reported in two different manners, as K values or as β values, that latter of which are known as overall constants. For example, consider an equilibrium system containing the ligand species L, LH, and LH₂, and the complex species ML, ML₂, MLH, and MLH₁ (MLOH). The difference between the equilibrium equations and equilibrium constant expressions has been represented in Table 1.3. The notation used for overall protonation constants is β_{yz} and for overall stability constants is β_{xyz} , where x is the number of metal ions, y the number of ligands, and z the number of hydrogen atoms. For K values the notation generally involves the two reactants being written as subscript and superscript letters, K^a_b , where a and b are the reacting species.

Equilibrium constants for the formation of a given species are essentially determined from the component elements; for the example in Table 1.3 that would be the ‘free’ metal, M, the deprotonated ligand, L, and the proton, H. For K equilibria, each new species is defined stepwise using constants that are comprised of the interactions of species that are already formed from the components. Hence, K equilibria are reflective of the species of the previous equilibrium, whereas overall constants are independent of previously defined equilibria. The relationship between the two forms of equilibrium constants is a straightforward mathematical function where the overall constant is calculated from the product of K constants, for example, $\beta_{LH_2} = K_{LH_2} \cdot K_{LH}$. However, stability constants are usually expressed using log values, that is either $\log \beta$ or $\log K$. Hence, the log of the overall constant is equal to the sum of the $\log K$ constants, that is, $\log \beta_{LH_2} = \log K_{LH_2} + \log K_{LH}$.

Overall Equilibrium Constants: β		Equilibrium Constants: K	
<i>Protonation:</i>			
$L + H \leftrightarrow LH$	$\beta_{11} = \frac{[LH]}{[L][H]}$	$L + H \leftrightarrow LH$	$K_L^H = \frac{[LH]}{[L][H]}$
$L + 2H \leftrightarrow LH_2$	$\beta_{12} = \frac{[LH_2]}{[L][H]^2}$	$LH + H \leftrightarrow LH_2$	$K_{LH}^H = \frac{[LH_2]}{[LH][H]}$
<i>Stability:</i>			
$M + L \leftrightarrow ML$	$\beta_{110} = \frac{[ML]}{[M][L]}$	$M + L \leftrightarrow ML$	$K_M^L = \frac{[ML]}{[M][L]}$
$M + 2L \leftrightarrow ML_2$	$\beta_{120} = \frac{[ML_2]}{[M][L]^2}$	$ML + L \leftrightarrow ML_2$	$K_{ML}^L = \frac{[ML_2]}{[ML][L]}$
$M + L + H \leftrightarrow MLH$	$\beta_{111} = \frac{[MLH]}{[M][L][H]}$	$ML + H \leftrightarrow MLH$	$K_{ML}^H = \frac{[MLH]}{[ML][H]}$
		$M + LH \leftrightarrow MLH$	$K_{LH}^M = \frac{[MLH]}{[M][LH]}$
$M + L - H \leftrightarrow MLH_{-1}$	$\beta_{11-1} = \frac{[MLH_{-1}]}{[M][L][H]^{-1}}$	$MLH_{-1} + H \leftrightarrow ML$	$K_{MLH_{-1}}^H = \frac{[ML]}{[MLH_{-1}][H]}$
or $MLOH + H \leftrightarrow ML(H_2O)$			

Table 1.3: β (overall) and K equilibrium constant expressions and equations ⁵⁰.

For computer programs that deal with equilibrium constants it is general practice to use overall constants rather than K constants as overall constants are always unique, whereas K values can be ambiguous if the ‘xyz’ notation used for overall constants is adopted, as is often the case. For example, consider the constant K_{111} which can refer to $\frac{[MLH]}{[ML].[H]}$, but can just as correctly denote $\frac{[MLH]}{[M].[LH]}$. Such ambiguity is avoided by

the using overall constant for β_{111} , which refers solely to the expression $\frac{[MLH]}{[M].[L].[H]}$.

Hence, this protocol to use overall constants was employed for our computer programs in order to avoid ambiguity with equilibrium expressions.

1.4 Kinetics

Chemical kinetics are clearly distinguishable from equilibria because thermodynamic equilibrium investigations are interested only with the initial and final states of a chemical system. The actual mechanism whereby the system is converted from one state to another, and the time required for such a conversion, are of no consequence. By contrast, the study of kinetics is fundamentally concerned with the details of the process whereby a system gets from one state to another. This is known as the mechanism of the reaction. Kinetics is also interested in the time required for the transition from one state to another, the process of which can be mathematically expressed by rate constants⁶⁷. Analytically, kinetics deals with the experimental determination of a rate law, resulting from the reaction mechanism, from which the rate constants of the chemical reaction can be derived.

The determination of parameters such as rate constants are necessary for the investigation of many complex systems as knowledge of the reaction rate constants enables comparisons between analogous reactions¹⁰, predictions of future reactions behaviour, and importantly it allows direct comparisons, for example between different ligands.

1.4.1 Reaction Rates

The determination of reaction rates by conventional methods can be generally described as the study of changing species concentrations as a function of time. The most common analytical procedures to investigate reaction rates are by physical methods, which measure some physical property of the reaction mixture that changes substantially as the reaction proceeds. Common methods include optical techniques such as polarimetry, refractometry, colorimetry, fluorimetry, circular dichroism, and spectrophotometry. Other methods also include electrical methods such as conductivity, potentiometry, and polarography. Theoretically, any property that changes sufficiently could be used to follow the course of a reaction⁶⁷. For our kinetic investigations the popular optical technique of spectrophotometry was used.

In general terms, the rate of a reaction can be described as some physical change in the reaction mixture over a measured period of time, as shown in Equation (1.15).

$$\text{rate} = \frac{\text{change in substance}}{\text{time for change to occur}} \text{ (usually in } \text{Ms}^{-1} \text{)} \quad (1.15)$$

The rate law, or rate equation, for a chemical reaction is an equation that links the reaction rate with the concentrations of reactants and parameter constants, such as rate coefficients and partial reaction orders ⁶⁸. In 1864, Peter Waage pioneered the development of chemical kinetics by formulating the law of mass action, which stated that the speed of a chemical reaction is proportional to the quantity of the reacting substances. To determine the rate equation for a particular system, the reaction rate is combined with the mass balance of the system ⁶⁹.

The rate equation is a differential equation, as shown below. Such equations can be integrated in order to obtain the integrated rate equation that links the concentrations of reactants or products with time. For the generic kinetic reaction $A + B \rightarrow C$, the law of mass action gives the rate of the reaction, shown in Equation (1.16) where k is the observed reaction rate constant and $d[C]/dt$ the rate of change in the concentration of the species C.

$$\frac{d[C]}{dt} = k[A]^x[B]^y \quad (1.16)$$

1.4.2 Order of a Reaction

For the study of kinetics it is important to relate the concentration of the species to the time of the reaction. This relationship is known as the integrated rate equation and is different for reactions of different order. In the above equation, (1.16), the exponents x and y are called reaction orders and are dependant on the reaction mechanism. The stoichiometric coefficients of a reaction and the reaction orders can be equal, but this is only the case for one step reactions, for example $aA \rightarrow \text{products}$.

First-Order

A first-order reaction is dependant on the concentration of only one reactant, which is the reaction is unimolecular, for example $aA \rightarrow \text{products}$. The rate law for a first-order reaction is shown in Equation (1.17) where k is the first order rate constant with units of time^{-1} .

$$r = -k[A] \quad (1.17)$$

Solving the mass balance of a first-order reaction results in the following differential equation where a is the stoichiometric coefficient of the species A and always equal to one.

$$-\frac{1}{a} \frac{d[A]}{dt} = k[A] \quad (1.18)$$

The integrated first-order rate law is shown in Equation (1.19). A plot of $-\ln[A]$ versus time results in a straight line with the slope equal to the reaction rate constant.

$$\ln[A] = -akt + \ln[A]_0 \quad \text{where } [A] = [A]_0 e^{-kt} \quad (1.19)$$

Second-Order

A second-order reaction depends on the concentrations of one second-order reactant, $aA \rightarrow \text{products}$, or alternatively two first-order reactants, $aA + bB \rightarrow \text{products}$. The reaction rate of both second-order reactions are shown in Equation (1.20), followed by the integrated second-order rate laws in Equations (1.21) and (1.22), respectively. For Equation (1.22) to be obtained, $[A]_0$ and $[B]_0$ must have different values.

$$r = k[A]^2 \text{ or } r = k[A][B] \quad (1.20)$$

$$\frac{1}{[A]} = kt + \frac{1}{[A]_0} \quad (1.21)$$

$$\frac{[A]}{[B]} = \frac{[A]_0}{[B]_0} e^{([A]_0 - [B]_0)kt} \quad (1.22)$$

The kinetic parameters of a complexation reaction where the order is greater than one are closely associated with both the type of metal ion present and the structural features of the ligand. The majority of complexation kinetics that are investigated have reaction orders greater than first-order.

Pseudo First-Order

Often measuring a second-order reaction rate can be problematic, for instance the concentrations of the two reactants must be followed simultaneously, or one can be measured and then the other calculated as a difference. Pseudo first-order reactions are also sometimes used to find the rate constant of a second-order reaction when one of the two components is very expensive and the other one is relatively cheap. An excess of the inexpensive reagent can be used with only a small amount of the expensive one. It is still possible to obtain the second-order rate constant by dividing the effective first-order rate constant by the concentration of the excess component.

For the reaction $aA + bB \rightarrow \text{products}$, if either concentration of the reactants remains constant as the reaction proceeds, then the reaction can be considered pseudo first-order because, in fact, it is dependant on only the concentration of one reactant. For example, if the concentration of B is in high excess and effectively remains constant then the rate constant can be approximated as shown in Equation (1.23), which is the same expression as for first-order reactions shown in Equation (1.17). Hence, the rate of the equation can be integrated in a similar way to first-order reactions. By determining k' values for many reactions with different concentrations, but always an excess, of B a plot of k' versus $[B]$ will result in the determination of k , the second order rate constant, as the slope.

$$r = k[A][B] = k'[A] \quad (1.23)$$

1.4.3 Factors Affecting the Rate of a Reaction

The most interesting aspect of the study of reaction rates is the insight it can provide into the mechanism of a reaction. Analysing the influence of different reaction conditions on the reaction rate provides useful information about the reaction mechanism and transition states of a chemical reaction. In its most detailed form a reaction mechanism describes, as a function of time, the relative arrangement of all microscopic particles whose motion is necessary for the reaction to occur⁶⁷.

There are several factors that affect the relative positions and motion of the molecules involved in a reaction, and consequently affect the rate of a specific reaction. These influences can be explained with collision theory, which states that for a reaction to occur the molecules must firstly collide, secondly have sufficient energy, and thirdly have the right geometry. These three factors which affect the reaction rate are all taken into account by the rate equation of the reaction⁷⁰. The number of reacting species, their physical state, the complexity of the reaction and other factors greatly influence the rate.

One of the most commonly investigated factors that affect the rate of a reaction is that of changing concentration. The reaction rate increases with increasing concentration, as described by the rate law and explained by collision theory and shown in Figure 1.6, which states that as the reactant concentration increases so do the frequency of collisions. In a similar way, the rate of reactions that take place in solution are also affected by the properties of the solvent as well as the ionic strength. Thus, the

interactions of the reacting molecules with the solvent or the medium used for ionic strength will directly affect the measured reaction rate. For gaseous systems, increasing the pressure has a similar effect as increasing the concentration of a solution, that is, the rate of a gaseous reaction will also increase with increased pressure. As described in Section 1.4.2, the order of the reaction controls how the change in reactant concentration or pressure will affect the reaction rate.

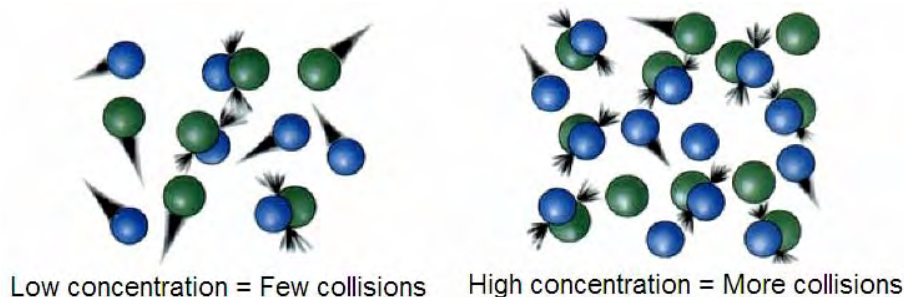


Figure 1.6: The rate of a reaction tends to increase with concentration - a phenomenon explained by collision theory ⁷¹.

Temperature is another commonly investigated parameter that affects the rate of a reaction. Usually conducting a reaction at a higher temperature delivers more energy into the system and increases the reaction rate by causing more collisions in unit time between particles, as previously explained by collision theory. However, the main reason for an increase in temperature resulting in an increase in the rate of reaction is because an increased number of colliding particles will have the necessary activation energy to result in a successful collision, that is, they will have sufficient energy to form a bond. The influence of temperature can be described by both the Arrhenius and Eyring equations, shown in Equations (1.24) and (1.25) respectively. Strictly speaking, the Arrhenius equation should only be applied to gas phase reactions ⁷², however it is often used as an approximation for solution reactions.

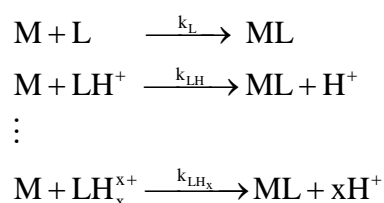
In Equations (1.24) and (1.25) k is the reaction rate constant, A is the pre-exponential factor, E_a is the activation energy, R is the universal gas constant, T is the absolute temperature, ΔH^\ddagger is the activation enthalpy of reaction, k_b is the Boltzmann constant, h is Planck's constant, and ΔS^\ddagger is the activation entropy of the reaction.

$$k = Ae^{-\frac{E_a}{RT}} \quad (1.24)$$

$$k = \frac{k_b T}{h} e^{-\frac{\Delta H^\ddagger}{RT}} \cdot e^{\frac{\Delta S^\ddagger}{R}} \quad (1.25)$$

1.4.4 Complexation Kinetics

As described earlier in Section 1.2 investigations of metal-ligand reactions often involve the inclusion of protonation equilibria of the ligand and this has been exemplified in Scheme 1.2. The differently protonated species of a ligand, LH_x , coexist in solution, and depending on the pH each species will react differently towards a given metal centre due to geometry, charge, and so forth. The resultant complex may also undergo further reactions, the rates of which may or may not be pH dependent. Consequently, complexation kinetics of systems involving protonated ligands and metal species are highly pH dependent. Furthermore, complexation of a metal ion by a protonated ligand is typically accompanied by the release of some number of protons which subsequently lowers the pH and changes the speciation. As a result, the complexation kinetics of polydentate ligands in aqueous solution is reasonably complex.



Scheme 1.2: The system of equations describing the kinetics of reaction of a metal ion, M, with a ligand, L. For clarity, charges on the metal ion and complex have been omitted.

Despite the difficulties of numerous protonation species, changing pH and differing rates of reactions with every differently protonated species, the kinetics of transition metal complexation by nitrogen-donor ligands has been extensively investigated and is consequently reasonably well understood. Such studies have furthered the understanding of a variety of different biological^{73, 74} and industrial^{75, 76} processes. The understanding of complexation kinetics has also led to discernment of fundamental concepts, such as the internal conjugate base (ICB) effect which has been used, for example, to explain the comparatively fast reaction of a number of polyamines compared to that of ammonia⁷⁷.

1.5 Chemometrics

Chemometrics is the application of mathematical or statistical methods in order to analyse chemical data. The International Chemometrics Society (ICS) provides the following definition: ‘Chemometrics is the science of relating measurements made on a chemical system or process to the state of the system via application of mathematical or

statistical methods’⁷⁸. The development of the discipline chemometrics has been strongly related to the development and use of computers in chemistry. This can be seen by the following figure which shows the significant increase in publications citing analytical techniques for data interpretation¹.

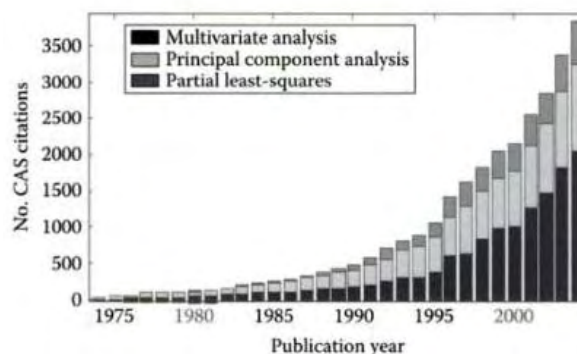


Figure 1.7: Number of publications citing multivariate, principle component, or partial least-squares analytical techniques from 1975 – 2006¹.

Analytical processes include mathematical, statistical, graphical and sometimes even symbolic or similar methods that employ formal logic to improve the understanding of chemical information. Many instrumental techniques require some form of mathematical analysis of the raw experimental data to make their results meaningful to the chemist, and as such the mathematical manipulation of experimental data is a basic operation associated with all modern instrumental analytical techniques.

Chemometrics has useful applications at any point in an analysis, from the first conception of an experiment until the data is discarded. Chemometric methods can aid in the development of techniques for the collection of good data. This includes such aspects as: the calibration, optimisation of chemical measurements and experimental procedures; signal processing; validation; the overall design of experiments, and; the significance of the analytical measurements. Most importantly, chemometric applications are focused on getting as much information as possible from the experimental data through techniques such as: statistics; pattern recognition; structure-property relationship estimations; and most importantly for this project, modelling. The aim is to extract the maximum relevant chemical information from the analytical data which leads to the subsequent development of quantitative structure activity relationships or the evaluation of analytical-chemical data⁹.

Complete analysis often involves many steps and much refining of the analytical information, using many components of the aforementioned broad array of techniques. It is in this latter area of extracting meaningful chemical information from collected data that chemometrics has become a very powerful technique offering such benefits as multivariate data reduction procedures that are now yielding chemical information from data previously not available to the analyst ⁷⁹.

Chemometric research covers a wide range of different methods that can be applied to chemistry and are also relevant in this research. Almost every aspect of chemistry can be described in a qualitative, or approximate quantitative, computational scheme. Note that the words ‘exact’ and ‘perfect’ do not appear here, as very few aspects of chemistry can be computed exactly ⁸⁰. In order to most accurately describe chemical reactions, or any science, data collection typically involves many measurements made on numerous samples. The analysis of such multivariate data has traditionally been done using one or two variables at a time. However, such approaches are inadequate compared with modern chemometric techniques. In order to discover the relationships among all samples and variables efficiently, it is advantages to process all the data simultaneously. Modern chemometrics techniques extract information from multivariate chemical data using tools of statistics and mathematics in such a way that multiple measurements can be analysed together, and additionally various parameters can also be determined robustly. The algorithms and programs that were developed as part of this research have the capacity to analyse and model a wide assortment of data types with models of varying complexity.

1.5.1 Model-Based Data Fitting

Model-based data fitting can be divided into three main components. The first, and most important, are the measured data that are waiting to be analysed. Secondly, a model needs to be proposed in order to quantitatively describe the measured data. The third aspect is the actual fitting routine that determines the most likely values for the parameters defined by the proposed model. There are many programs available for the fitting of experimental data and these computational approaches generally have many common elements. Most approaches are based on the initial proposal of a chemical model, which defines the species stoichiometries, and the analysis based on the law of mass action and mass balance equations. Minimisation usually involves some form of a least-squares fitting procedure ⁸¹.

Analytical procedures that search for a minimum can be employed to fit any data, for example the analysis of potentiometric and spectrophotometric data to some form of kinetic or equilibrium model. Generally, data fitting via such computational processes which search for a minimum consists of three steps. These include initial estimate for the unknown parameter values, the minimisation of the sum of squares (*ssq*), and examination of the minimum obtained after completion of the analysis. The first step is decisive for success of the minimisation procedure as good initial guesses are crucial for the convergence of the program. With a poor initial guess, often the minimum cannot be found at all, or the minimum obtained is a local one.

The second step describes the general process of a model-based data fitting program, that is, to fit the measured data to the parameters from the model using a sum of squares (*ssq*) procedure, which minimises the difference between the measured and calculated data. This is necessarily an iterative process and results in the determination of the parameter values that best define the data and result in a minimum *ssq*. The calculation of the *ssq* value, which is crucial for the minimisation procedure, requires the difference between the measurements, collected in a vector y , and its calculated value, collected in y_{calc} , to be determined. This difference is defined as the residual, r , as shown in Equation (1.26).

$$r = y - y_{\text{calc}} = y - f(\text{model, parameters}) \quad (1.26)$$

The sum of squares is the sum over all the squares of the individual residuals, as shown in Equation (1.27). Importantly the *ssq* value is minimised as a function of the parameters defined by the model.

$$ssq = \sum r^2 = \sum (y - y_{\text{calc}})^2 \quad (1.27)$$

The third step of the analytical procedure, examination of the minimum, is an essential step for assessing whether the procedure has converged to a reasonable result or not. It involves a physical inspection of how the measured and calculated data fit one another, ensuring that any calculated parameters have reasonable values and acceptable error estimates if available, and also assessment of the residuals to ensure that they are due only to random noise from the measurement and that no trends can be observed. Only if all these factors are satisfactory should the minimisation process be accepted and the analysis considered successful.

1.5.2 Globalisation

Proper investigation of complex processes often require the acquisition of more than one set of data, as often it is not possible to find experimental conditions which result in data that adequately define all parameters of interest from the one measurement ⁸². Traditionally each measurement, for example, spectrophotometric titrations at particular wavelengths, are analysed individually and then the average taken of all calculated constants to determine the most likely value of the parameter being investigated. With potentiometric titrations, the determination of protonation constants and stability constants from metal-ligand titrations required separate analytical processes. Fortunately, with modern chemometric techniques, it has become possible to perform what has been termed first order global analysis that enables multiple measurements to be combined in the one analytical procedure.

In first order global analysis, common parameters are linked across the series of measurements enabling the measurements to be analysed together. One example is a kinetic reaction measured at multiple wavelengths with common rate constants fitted to all kinetic traces at the individual wavelengths. There are several advantages with using multi-wavelength data compared to analysis using only a single wavelength. Benefits include determination of the pure spectra for all species and intermediates, as well as enabling the application of a wide range of model-free analyses techniques ranging from simple factor analysis, to indicate the number of species present, to sophisticated evolving factor analysis. Also the analysis is significantly more robust and there is no longer a need to determine a ‘good’ wavelength at which to perform the reaction and measurements ⁸³.

However, often the investigation of complex systems requires multiple data sets. The traditional approach for complex processes is to establish experimental conditions where only a selection of all processes occurs. Such data enable the researcher to determine a restricted number of relevant parameters. For spectrophotometric measurements it is possible to determine equilibrium, or rate constants, along with the absorption spectra of all species formed under a particular set of conditions. Subsequent experiments, using different conditions, may then facilitate the formation of additional species. The supplementary data sets can then be analysed in terms of the new parameters and data, such as new spectra, while the initial parameters are kept fixed at their previously determined values. This process can be continued over several levels.

While there is nothing dramatically wrong with such an approach, it is easy to see that error propagation of the initially fitted parameters is unavoidable. If several levels of fitting new parameter values, while holding others fixed from previous analyses, are operating, error propagation is essentially uncontrollable.

Second order global analysis of a complete set of measurements is much more straightforward and transparent than the traditional techniques that required multiple analyses of multiple measurements, followed by combining the analysis results to determine the final parameters. In general, second order global analysis involves a series of measurements often performed under different conditions such as varying the temperature, pressure or reactant concentrations, being linked together by a superimposed model that encompasses the complete series of individual measurements. For spectrophotometric measurements each experiment can be performed at multiple wavelengths.

Second order globalisation is an applicable method for the investigations of any equilibrium and/or kinetic system. It has proven to be particularly useful for spectrophotometric and potentiometric investigations where the equilibria are poorly defined and/or where data sets are rank deficient. Such problems are not readily solved if the analysis is restricted to a single measurement or a single multi-wavelength data set. Traditional approaches to overcoming deficiencies in individual measurements have included the careful choice of absolute concentrations and concentration ratios ⁸⁴ or, for spectrophotometric measurements, the addition of known spectra ⁸⁵. With second order global analysis all measurements are combined and analysis of the combined measurements proves to be much more robust, as it removes the deficiencies present in the individual measurements. It has been repeatedly proven, with both simulated and real data, that second order global analysis improves the robustness of fitting procedures, as well as enabling enhanced determination of the correct chemical model for the reaction under investigation ⁸⁶.

For the difficulty of poorly defined equilibrium and/or rate constants due to the low concentrations of some species, a set of experiments can be conducted to ensure that all species are formed to a high enough concentration in at least one of the measurements in the series. Therefore, the constants of all species will be adequately defined by analysis of the global set of data. With spectrophotometric measurements, when all species are formed to high enough concentrations, this further enables the calculation of

well defined absorption spectra whose determination would not be possible from the single linearly dependent measurements alone.

Thoughtful design of appropriate sets of measurements is essential for using the global analysis technique successfully and to its full potential. The measurements must contain different relative and absolute total concentrations of the components; for example, metal and ligand concentrations, in order to remove the linear dependence between concentration profiles and also influence the relative importance of the different species that are formed. Our research applied this second order global analysis technique in order to investigate complex systems. Hence, multiple measurements were taken for each reaction and all parameters were fitted in the one analytical process.

The second order global analysis technique can also be applied to determine such constants as the activation parameters of a reaction. For such analysis, in order to determine the temperature dependence, numerous experiments are performed at varying temperatures. Globalisation of this type, that is the process of analysing a series of measurements, has well recognised advantages^{87, 88}. Instead of fitting intermediate parameters to individual measurements, where further analysis in secondary processes is required to yield the parameters of interest, the activation parameters are directly refined as part of the second order analysis. The outcome is usually a significant reduction in the total number of parameters to be fitted which consequently results in much better defined minima⁸⁶.

1.5.3 Computational Techniques

The advent of computers has revolutionised the determination and calculation of equilibrium and rate constants from both potentiometric and spectrophotometric data. This means that systems containing many overlapping equilibria, or complicated rate mechanisms in the presence of a number of metal ions or ligands containing many functional groups, may now be easily handled. Regardless of the complexity of the system, the number of donor groups on the ligand, the number of ligands present, and the presence of one or more competing ions and the hydrogen ion, the computations can be easily handled with suitable programs¹³.

1.5.3.1 Current Computer Programs

Second order globalisation of spectrophotometric data is still relatively new to the scientific community, however global analysis of potentiometric titrations has existed

for some time, termed alternatively as a ‘batch’ analysis of a number of potentiometric titrations. Some examples of such programs are ACBA (Acid-Base titrations)⁸⁹, PHCONST⁹⁰, GLEE (GLass Electrode Evaluation)⁹¹, and PKPOT⁹². The analysis of potentiometric titration data is discussed in-depth in Chapter 6.

The most widespread programs and algorithms for determining equilibrium constants from absorbance data are LETAGROP-SPEFO⁹³, SQUAD⁹⁴⁻⁹⁸, PSEQUAD⁹⁴, HYPERQUAD⁹⁹, SPECFIT^{84, 85, 100-102}, DATAN^{81, 103-107}, and BeerOz¹⁰⁸. All these computational approaches are based on the initial proposal of a chemical equilibrium model that defines the stoichiometries of species. Calculations of the species concentrations are based on the law of mass-action and subsequent mass balance equations, and parameters are fitted using least-squares curve-fitting procedures⁸³.

Modern, user-friendly algorithms for the modelling of kinetic reactions are based on the numerical integration of the set of differential equations defined by a reaction model¹⁰⁹. Newer programs, such as ProKII¹¹⁰, simultaneously analyse many kinetic spectrophotometric measurements. ProKII is considered to be one of the most advanced programs for fitting spectrophotometric kinetic data, the program being superior to most, as it has the capability to globally fit many measurements to the one model, as well as providing many secondary options such as selecting species spectra to be coloured, non-coloured or known. ProKII fits the measured data using the appropriate rate equations and minimises the least square sum using the molecular rate constants as parameters.

For spectrophotometric analysis there are two categories of algorithms for data interpretation that can be distinguished based on the types of constraints applied. The first type was originally implemented in the program SQUAD(75)⁹⁴ and uses the constraint of non-linear thermodynamic speciation model. A non-linear least-squares method is used to optimise the absorptivity coefficients and equilibrium constants of the absorbing species. Gampp and co-workers^{84, 85, 101, 102} developed a popular program, SPECFIT/32¹⁰⁰, based on the minimisation of least-squares using the Levenberg-Marquardt method¹¹¹. SPECFIT/32 makes use of factor analysis of the data by singular value decomposition (SVD) as a powerful tool in order to determine the independent components in the data matrix used. It also utilises multi-wavelength and multivariate spectra treatment that enables a global analysis for equilibrium and kinetic systems.

1.5.3.2 Programs used for Our Research

The data analysis used for this project was performed on PCs using a non-linear least-squares regression program on published algorithms⁸⁸. The developed programs for the analysis of equilibrium in this study were performed using second order global analysis techniques for both spectrophotometric and potentiometric data. The program specifics are detailed in Chapter 2. Kinetic data was analysed using the previously described data fitting software ProKII.

Analysis of the multi-wavelength spectrophotometric titrations for equilibrium investigations was developed in-house and enabled the determination of the spectra for the intermediate and final products. The analytical method further calculated the concentration profiles for all individual species that were directly or indirectly part of the reaction. The calculations are based on the known initial concentrations of the components, for example [M], [L], and [H], the model and the appropriate equilibrium constants.

Similarly, for the in-house developed program for the analysis of potentiometric titrations, the program determines the relevant equilibrium constants from the defined model as well as the concentration profiles and also the calibration parameters of the electrode. These in-house developed programs have been described in detail in Chapter 2, Section 2.3.

1.6 References

1. Gemperline, P.; Editor, *Practical Guide to Chemometrics, Second Edition*. 2006; p 541.
2. Kauffman, G. B., *Alfred Werner, Founder of Coordination Chemistry*. Springer-Verlag: 1966.
3. Bailar, J. C., *The Chemistry of the Coordination Compounds*. Reinhold Pub. Corp.: 1956; p 834.
4. Basolo, F.; Johnson, R. C., *Coordination chemistry : the chemistry of metal complexes*. W.A. Benjamin: New York, 1964.
5. Kirschner, S., *Advances in the Chemistry of the Coordination Compounds*. Macmillan: 1961; p 682.
6. Martin, D. F.; Martin, B. B., *Coordination Compounds*. McGraw-Hill: 1964; p 108.
7. Reddy, K. H., *Bioinorganic Chemistry*. New Age Publishers: New Dehli, 2003.
8. Wilkins, R. G., Coordination chemistry. *Nature* **1951**, 167, 434-5.
9. Otto, M., *Chemometrics: Statistics and Computer Application in Analytical Chemistry*. Wiley-VCH: Weinheim, 2007; p 343.
10. Dwyer, F. P.; Mellor, D. P., *Chelating Agents and Metal Chelates*. Academic Press Inc.: London, 1964.
11. Kotz, J. C. T., P., *Chemistry and Chemical Reactivity*. 4th ed.; Saunders College Publishing: New York, 1999.
12. Busch, D. H., *Chemical Reviews* **1993**, 93, 850.
13. Martell, A. E.; Motekaitis, R. J., Potentiometry revisited: the determination of thermodynamic equilibria in complex multicomponent systems. *Coordination Chemistry Reviews* **1990**, 100, 323-61.
14. Constable, E. C., Oligopyridines as helicating ligands. *Tetrahedron* **1992**, 48, 10013-59.
15. Lehn, J. M., *Supramolecular Chemistry: Concepts and Perspectives*. 1995; p 262.
16. Sardarian, A.; Coe, B. J.; Douglas, K. T., Unusually facile syntheses of $[\text{RuII}(\text{bpy})_3]^{2+}$ (bpy = 2,2'-bipyridine) and $[\text{RuII}(\text{phen})_3]^{2+}$ (phen = 1,10-phenanthroline). *Transition Metal Chemistry* **2003**, 28, 905-907.
17. Meurer, K. P.; Voegtle, F., Helical molecules in organic chemistry. *Topics in Current Chemistry* **1985**, 127, 1-76.

18. Conn, M. M.; Rebek, J., Jr., Self-assembling capsules. *Chemical Reviews* **1997**, 97, 1647-1668.
19. Leininger, S.; Olenyuk, B.; Stang, P. J., Self-Assembly of Discrete Cyclic Nanostructures Mediated by Transition Metals. *Chemical Reviews* **2000**, 100, 853-907.
20. Mueller-Dethlefs, K.; Hobza, P., Noncovalent Interactions: A Challenge for Experiment and Theory. *Chemical Reviews* **2000**, 100, 143-167.
21. SkyscraperPage Forum.
<http://chicago.ibj.com/repository/ibj/2007/01/01/1/Img/Pc0010400.jpg>, 20/12/07
22. Amgen Helix Pedestrian Bridge. www.gkdmetailfabrics.com/horz.php4/app/35/, 20/12/07
23. Art and Geometry. www.cs.berkeley.edu/~sequin/SCULPTS/, 20/12/07
24. Caulder, D. L.; Raymond, K. N., The rational design of high symmetry coordination clusters. *Journal of the Chemical Society, Dalton Transactions: Inorganic Chemistry* **1999**, 1185-1200.
25. Lehn, J. M.; Rigault, A., Helicates. Four- and five-membered double-helix complexes of copper(I) and poly(bipyridine) ligands. *Angewandte Chemie* **1988**, 100, 1121-2.
26. Piguet, C.; Bernardinelli, G.; Hopfgartner, G., Helicates as Versatile Supramolecular Complexes. *Chemical Reviews* **1997**, 97, 2005-2062.
27. Williams, A., Helical complexes and beyond. *Chemistry--A European Journal* **1997**, 3, 15-19.
28. Lessmann, J. J.; Horrocks, W. D., Jr., Supramolecular Coordination Chemistry in Aqueous Solution: Lanthanide Ion-Induced Triple Helix Formation. *Inorganic Chemistry* **2000**, 39, 3114-3124.
29. Constable, E. C., In *Comprehensive Supramolecular Chemistry*, Lehn, J. M., Ed. Pergamon: Oxford, 1999; Vol. 9, p 213.
30. Constable, E. C., Higher oligopyridines as a structural motif in metallosupramolecular chemistry. *Progress in Inorganic Chemistry* **1994**, 42, 67-138.
31. Kramer, R. J. M., L.; Andre, de C.; Jean, F., Self-organization, structure and spontaneous racemate cleavage of a trinuclear triple helix complex formed from oligobipyridine ligands and nickel(II) ion. *Angewandte Chemie* **1993**, 105, 764-7
32. Piguet, C.; Bernardinelli, G.; Bocquet, B.; Quattropiani, A.; Williams, A. F., Self-assembly of double and triple helices controlled by metal ion stereochemical preference. *Journal of the American Chemical Society* **1992**, 114, 7440-51.

33. Barley, M.; Constable, E. C.; Corr, S. A.; McQueen, R. C. S.; Nutkins, J. C.; Ward, M. D.; Drew, M. G. B., Molecular helicity in inorganic complexes: double helical binuclear complexes of 2,2':6',2'':6'',2''':6''',2''''-quinquepyridine (L): crystal structures of $[\text{Cu}_2\text{L}_2(\text{O}_2\text{CMe})][\text{PF}_6]_3 \cdot \text{H}_2\text{O}$ and $[\text{Cu}_2\text{L}_2][\text{PF}_6]_3 \cdot 2\text{MeCN}$. *J. Chem. Soc., Dalton Trans.* **1988**, 10, 2655.
34. Lindsey, J. S., Self-assembly in synthetic routes to molecular devices. Biological principles and chemical perspectives: a review. *New Journal of Chemistry* **1991**, 15, 153-80.
35. Lehn, J. M., Perspectives in supramolecular chemistry: from molecular recognition to molecular information processing and self organization. *Angewandte Chemie* **1990**, 102, 1347-62.
36. Marquis-Rigault, A.; Dupont-Gervais, A.; Van Dorsselaer, A.; Lehn, J.-M., Investigation of the self-assembly pathway of pentanuclear helicates by electrospray mass spectrometry. *Chemistry--A European Journal* **1996**, 2, 1395-1398.
37. Constable, E. C.; Ward, M. D.; Tocher, D. A., Molecular helicity in inorganic complexes; bi- and tri-nuclear complexes of 2,2':6',2'':6'',2''':6''',2''''-sexipyridine and the crystal and molecular structure of bis(m-2,2':6',2'':6'',2''':6''',2''''-sexipyridine- $\kappa^3\text{N},\text{N}',\text{N}''$: $\kappa^3\text{N}''',\text{N}'''',\text{N}'''''$)dicadmium hexafluorophosphate acetonitrile. *Journal of the Chemical Society, Dalton Transactions* **1991**, 1675-83.
38. Potts, K. T.; Keshavarz-K, M.; Tham, F. S.; Raiford, K. A. G.; Arana, C.; Abruna, H. D., Di-, tri-, and tetrametallic double-stranded helical complexes derived from alkylthio-substituted septipyridines: synthesis, structure, and redox properties. *Inorganic Chemistry* **1993**, 32, 5477-84.
39. Serr, B. R.; Andersen, K. A.; Elliott, C. M.; Anderson, O. P., A triply-bridged dinuclear tris(bipyridine)iron(II) complex: synthesis and electrochemical and structural studies. *Inorganic Chemistry* **1988**, 27, 4499-504.
40. Williams, A. F.; Piguet, C.; Bernardinelli, G., Synthesis and Structure of a self-assembling triply helical complex with two cobalt(II) ions. *Angewandte Chemie* **1991**, 103, 1530-2.
41. Whitesides, G. M.; Simanek, E. E.; Mathias, J. P.; Seto, C. T.; Chin, D.; Mammen, M.; Gordon, D. M., Noncovalent Synthesis: Using Physical-Organic Chemistry To Make Aggregates. *Accounts of Chemical Research* **1995**, 28, 37-44.
42. Baum, G.; Constable, E.; Fenske, D.; Housecroft, C.; Kulke, T., Stereoselective double-helicate assembly from chiral 2,2':6',2'':6'',2''':6''',2''''-quaterpyridines and tetrahedral metal centers. *Chemistry--A European Journal* **1999**, 5, 1862-1873.
43. Purrello, R., Supramolecular chemistry: Lasting chiral memory. *Nature materials* **2003**, 2, 216-7.

44. Stang, P. J.; Olenyuk, B., Directed self-assembly of chiral, optically active macrocyclic tetranuclear molecular squares. *Angewandte Chemie, International Edition in English* **1996**, 35, 732-6.
45. Zarges, W.; Hall, J.; Lehn, J.-M.; Bolm, C., Helicity induction in helicate self-organization from chiral tris(bipyridine) ligand strands. *Helvetica Chimica Acta* **1991**, 74, 1843-52.
46. Libman, J.; Tor, Y.; Shanzer, A., Helical ferric ion binders. *Journal of the American Chemical Society* **1987**, 109, 5880-1.
47. Constable, E. C.; Kulke, T.; Neuburger, M.; Zehnder, M., Diastereoselective formation of P and M dicopper(I) double helicates with chiral 2,2':6',2''-terpyridines. *Chemical Communications* **1997**, 489-490.
48. Miyake, H.; Tsukube, H., Helix Architecture and Helicity Switching via Dynamic Metal Coordination Chemistry. *Supramolecular Chemistry* **2005**, 17, 53-59.
49. Yeh, R. M.; Ziegler, M.; Johnson, D. W.; Terpin, A. J.; Raymond, K. N., Imposition of Chirality in a Dinuclear Triple-Stranded Helicate by Ion Pair Formation. *Inorganic Chemistry* **2001**, 40, 2216-2217.
50. Martell, A. E. M., R.J., *Determination and Use of Stability Constants*. VCH: Weinheim, 1988.
51. Rossotti, F. J. C.; Rossotti, H., *The determination of stability constants, and other equilibrium constants in solution*. McGraw-Hill: New York, 1961.
52. Beck, M. T.; Nagypál, I., *Chemistry of complex equilibria*. Halsted Press: New York, 1990.
53. Lewis, G. N.; Randall, M., The activity coefficient of strong electrolytes. *Journal of the American Chemical Society* **1921**, 43, 1112-54.
54. Grossman, H., Complex salts of mercury sulphocyanate. *Zeitschrift fuer Anorganische Chemie* **1905**, 43, 356.
55. Martell, A. E. S., R. M., *Critical stability constants*. Plenum Press: New York, 1974.
56. Bates, R. G., *Determination of pH; theory and practice*. Wiley: New York, 1973.
57. Wilkins, R. G., *Acc. Chem. Res.* **1981**, 3, 408.
58. Albert, A.; Sergeant, E. P., *The Determination of Ionisation Constants. A Laboratory Manual*. 3rd ed.; Chapman and Hall: London, 1984.
59. Martell, A. E.; Smith, R. M., NIST Critically Selected Stability of Metal Complexes, Database 46 Version 6.0. In NIST Standard Referenced Data: 2001.

60. Wilkins, R. G., *Kinetics and Mechanism of Reactions of Transition Metal Complexes*. 2 ed.; VCH Publishers, Inc.: New York, 1991.
61. Wikipedia® Chelation. http://en.wikipedia.org/wiki/Chelate_effect, 13/9/07.
62. Busch, D. H., The complete coordination chemistry - one practitioner's perspective. *Chemical Reviews* **1993**, 93, 847-60.
63. Sigel, H.; Zuberbuehler, A. D.; Yamauchi, O., Comments on potentiometric pH titrations and the relationship between pH-meter reading and hydrogen ion concentration. *Analytica Chimica Acta* **1991**, 255, 63-72.
64. Rossotti, F. J. C.; Rossotti, H. S.; Whewell, R. J., Use of electronic computing techniques in the calculation of stability constants. *Journal of Inorganic and Nuclear Chemistry* **1971**, 33, 2051-65.
65. Davies, C. W., *Ion Association*. Butterworths: London, 1962.
66. Grenthe, I.; Wanner, H. *Guidelines for the extrapolation to zero ionic strength*; Issy-les-Moulineaux, France, 2000; p 35.
67. Moore, J. W.; Pearson, R. G., *Kinetics and Mechanism*. 3rd ed.; John Wiley and Sons, Inc.: Canada, 1981.
68. Whitten, K. W.; Davis, R. E.; Peck, M. L., *General Chemistry with Qualitative Analysis*. 5th ed.; Saunders College Publishing: 1996; p 1151.
69. Connors, K. A., *Chemical Kinetics, the study of reaction rates in solution*. VCH Publishers: 1991.
70. Wright, M. R., *An Introduction to Chemical Kinetics*. John Wiley and Sons Ltd.: West Sussex, 2004.
71. Wikipedia® Chemical kinetics. http://en.wikipedia.org/wiki/Chemical_kinetics (23/07/07),
72. Keusch, P. Eyring Equation. http://www.uni-regensburg.de/Fakultaeten/nat_Fak_IV/Organische_Chemie/Didaktik/Keusch/eyr-e.htm (9/7/07),
73. Burgermeister, W.; Winkler-Oswatitsch, R., Complex formation of monovalent cations with biofunctional ligands. *Topics in Current Chemistry* **1977**, 69, 91-196.
74. Buckingham, D. A.; Clark, C. R.; Webley, W. S., A rapid porphyrin metalation. *Journal of the Chemical Society, Chemical Communications* **1981**, 192-4.

75. Madeyski, C. M.; Michael, J. P.; Hancock, R. D., N,N',N'',N'''-Tetrakis(2-hydroxyethyl)cyclam a nitrogen-donor macrocycle with rapid metalation reactions. *Inorganic Chemistry* **1984**, 23, 1487-9.
76. Louvet, V.; Appriou, P.; Handel, H., 1,4,8,11-Tetraazacyclotetradecane grafted onto polymer: preparation and use in the extraction of copper, nickel, and cobalt dications. *Tetrahedron Letters* **1982**, 23, 2445-8.
77. Martell, A. E., *Coordination Chemistry*. Van Nostrand Reinhold: New York, 1971-1978.
78. ICS, I. C. S. Chemometrics. <http://en.wikipedia.org/wiki/Chemometrics> (21/6/2007),
79. Haswell, S. J., *Practical Guide to Chemometrics*. Marcel Dekker, Inc.: New York, New York, 1992.
80. Young, D., Introduction to Computational Chemistry. *Chemistry in Australia* **1998**, 11, 5.
81. Ghasemi, J.; Niazi, A.; Kubista, M.; Elbergali, A., Spectrophotometric determination of acidity constants of 4-(2-pyridylazo)resorcinol in binary methanol-water mixtures. *Analytica Chimica Acta* **2002**, 455, 335-342.
82. Dyson, R.; Maeder, M.; Neuhold, Y.-M.; Puxty, G., Analyses of three-way data from equilibrium and kinetic investigations. *Analytica Chimica Acta* **2003**, 490, 99-108.
83. Meloun, M.; Bordovska, S.; Syrový, T.; Vrana, A., Tutorial on a chemical model building by least-squares non-linear regression of multiwavelength spectrophotometric pH-titration data. *Analytica Chimica Acta* **2006**, 580, 107-121.
84. Gampp, H.; Maeder, M.; Meyer, C. J.; Zuberbuehler, A. D., Calculation of equilibrium constants from multiwavelength spectroscopic data - II SPECFIT: two user-friendly programs in BASIC and standard FORTRAN 77. *Talanta* **1985**, 32, 251-64.
85. Gampp, H.; Maeder, M.; Meyer, C. J.; Zuberbuehler, A. D., Calculation of equilibrium constants from multiwavelength spectroscopic data - I. Mathematical considerations. *Talanta* **1985**, 32, 95-101.
86. Bugnon, P.; Chottard, J.-C.; Jestin, J.-L.; Jung, B.; Laurenczy, G.; Maeder, M.; Merbach, A. E.; Zuberbuehler, A. D., Second-order globalization for the determination of activation parameters in kinetics. *Analytica Chimica Acta* **1994**, 298, 193-201.
87. Gampp, H., Investigation of solution kinetics of transition-metal complexes by EPR spectroscopy. *Inorganic Chemistry* **1984**, 23, 3645-9.
88. Maeder, M.; Zuberbuehler, A. D., Nonlinear least-squares fitting of multivariate absorption data. *Analytical Chemistry* **1990**, 62, 2220-4.

89. Arena, G.; Rizzarelli, E.; Sammartano, S.; Rigano, C., A nonlinear least-squares approach to the refinement of all parameters involved in acid-base titrations. *Talanta* **1979**, 26, 1-14.
90. Baeza, J. J.; Ramis, G.; Mongay, C., A program for the simultaneous potentiometric determination of protonation constants and electrode calibration parameters. *Journal of Chemometrics* **1988**, 3, 223-9.
91. Gans, P.; O'Sullivan, B., GLEE, a new computer program for glass electrode calibration. *Talanta* **2000**, 51, 33-37.
92. Barbosa, J.; Barron, D.; Beltran, J. L.; Sanz-Nebot, V., PKPOT, a program for the potentiometric study of ionic equilibria in aqueous and non-aqueous media. *Analytica Chimica Acta* **1995**, 317, 75-81.
93. Sillen, L. G.; Warnqvist, B., Equilibrium constants and model testing from spectrophotometric data using LETAGROP. *Acta Chemica Scandinavica* **1968**, 22, 3032-4.
94. Leggett, D. J. E., *Computational Methods for the Determination of Formation Constants*. Plenum: New York, 1985.
95. Leggett, D. J.; McBryde, W. A. E., General computer program for the computation of stability constants from absorbance data. *Analytical Chemistry* **1975**, 47, 1065-70.
96. Leggett, D. J., Numerical analysis of multicomponent spectra. *Analytical Chemistry* **1977**, 49, 276-81.
97. Leggett, D. J.; Kelly, S. L.; Shiue, L. R.; Wu, Y. T.; Chang, D.; Kadish, K. M., A computational approach to the spectrophotometric determination of stability constants. II. Application to metalloporphyrin-axial ligand interactions in nonaqueous solvents. *Talanta* **1983**, 30, 579-86.
98. Meloun, M.; Javurek, M.; Havel, J., Multiparametric curve fitting. Part X. A structural classification of programs for analyzing multicomponent spectra and their use in equilibrium-model determination. *Talanta* **1986**, 33, 513-24.
99. Gans, P.; Sabatini, A.; Vacca, A., Investigation of equilibria in solution. Determination of equilibrium constants with HYPERQUAD suite of programs. *Talanta* **1996**, 43, 1739-1753.
100. Associates, S. S. S. SPECFIT/32™ Global Analysis System for Windows. <http://www.bio-logic.info/rapid-kinetics/specfit.html> (16/10/06),
101. Gampp, H.; Maeder, M.; Meyer, C. J.; Zuberbuehler, A. D., Calculation of equilibrium constants from multiwavelength spectroscopic data. III. Model-free analysis of spectrophotometric and ESR titrations. *Talanta* **1985**, 32, 1133-9.

102. Gampp, H.; Maeder, M.; Meyer, C. J.; Zuberbuehler, A. D., Calculation of equilibrium constants from multiwavelength spectroscopic data - IV. Model-free least-squares refinement by use of evolving factor analysis. *Talanta* **1986**, 33, 943-51.
103. Scarminio, I.; Kubista, M., Analysis of correlated spectral data. *Analytical Chemistry* **1993**, 65, 409-16.
104. Kubista, M.; Sjoeback, R.; Nygren, J., Quantitative spectral analysis of multicomponent equilibria. *Analytica Chimica Acta* **1995**, 302, 121-5.
105. Nygren, J.; Elbergali, A.; Kubista, M., Unambiguous Characterization of a Single Test Sample by Fluorescence Spectroscopy and Solvent Extraction without Use of Standards. *Analytical Chemistry* **1998**, 70, 4841-4846.
106. Antonov, L.; Gergov, G.; Petrov, V.; Kubista, M.; Nygren, J., UV-Vis spectroscopic and chemometric study on the aggregation of ionic dyes in water. *Talanta* **1999**, 49, 99-106.
107. Nygren, J.; Andrade, J. M.; Kubista, M., Characterization of a single sample by combining thermodynamic and spectroscopic information in spectral analysis. *Analytical Chemistry* **1996**, 68, 1706-10.
108. Brugger, J., BeerOz, a set of Matlab routines for the quantitative interpretation of spectrophotometric measurements of metal speciation in solution. *Computers & Geosciences* **2007**, 33, 248-261.
109. Press, W. H.; Lannery, B. P.; Teukolsky, S. A.; Vetterling, W. T., *Numerical Recipes*. Cambridge University Press: Cambridge ; New York, 1993.
110. ProKII <http://www.photophysics.com/prokii.php>
111. Marquardt, D. W., An algorithm for least-squares estimation of nonlinear parameters. *Journal of Applied Mathematics* **1963**, 11, 431-441.

Chapter 2

Programs: Data Acquisition and Analysis

2.1 Introduction

It is the purpose of any experiment to provide information that leads to the development of related questions that then need to be answered. Good experimental design will enable the answers to be obtained with the minimum effort. In general, an experiment is used to investigate the effect of changing one or more of the conditions defining the experimental system. This effect is presented as a suitable response measure of the system.

A successful experiment has several prerequisites, the two most important being clearly stated objectives and an estimate of the acceptable level of experimental error in the result. For the preliminary design plan the experimenter must rely on prior knowledge of the system, past experience, and intuition in selecting the relevant factors for study ¹. In order to obtain suitable conclusions from any experiment it is necessary to identify all the factors that can affect the result and include them in the experimental design plan, with the aim of minimising the effects of the uncontrolled factors.

The experimental procedure then follows this process of planning and design. The first experimental step is to collect suitable and relevant data that describes the chemical process. This can be done using instrumentation that registers a signal due to some physical or chemical property of the reaction. There are a wide range of data types possible, for example spectral information, potentiometric information, chromatographic information, electrospray-mass spectroscopy information and so forth.

After the experimental stage, during which the required information is collected, the second step involves the data processing which is needed in order to extract useful information from the chemical process. The aim of analysing a chemical measurement is to calibrate and validate the collected data, optimise the measurement and the experimental procedures and also to extract the maximum chemical information from the analytical data ². Analysis is most commonly performed using specifically developed computer programs in order to determine the reaction parameters that describe the experiment. These are important as they quantitatively describe the chemical reaction and therefore enable conclusions and predictions to be made from the

reaction. Pertinent parameters that are often determined by researchers include equilibrium constants, rate constants, energy parameters, for example Gibbs free energy, the heat of formation, entropy and many more depending on the system being investigated.

Years of dedicated academic research have led to vast improvements in data acquisition techniques and also in the development of powerful analytical methods for numerous data types. Rapid technological advances, especially in the area of computerised instrumentation, have enabled and necessitated this phenomenal growth in analytical chemistry.

This chapter outlines the essential aspects of the complete experimental process, that is, the data collection, determination of the chemical process, and finally the data fitting methods and outcomes. It is the purpose of this chapter to describe the capabilities of modern computer-assisted methods for both data acquisition and analysis of a number of mono- and multivariate data sets of complex systems. The study focuses on potentiometric and spectrophotometric techniques for equilibrium and kinetic investigations using both commercially available and in-house developed methods to collect the data and also for the analysis. The in-house developed data acquisition processes, using completely computer controlled techniques are described in detail. This is followed by in-depth discussions of the data analysis programs that were developed using hard-modelling techniques.

2.2 Data Acquisition

2.2.1 The Data

Collecting data requires good experimental design in order to determine which measurements to perform, how many to carry out, the relevant and most suitable parameters, as well as specific considerations for the measurement type, such as both the range and increment of the wavelength. In order for data to be suitable for analysis the data are required to be collected as a function of some independent variable. Typical examples of independent variables are: time, for example time since the start of a reaction in a kinetic investigation; or the amount of added reagent, for example the amount of base added during a titration. Independent variables can also be experimental parameters, such as the temperature, pressure, or any other variable that can be

manipulated by the experimenter. However, these independent variable types were not investigated in our research.

All modern instruments produce digital data, which is essential as digital data are required in order to apply modern data fitting programs. Analogue data, such as a chromatogram or a spectrum on chart paper are outdated forms of data acquisition and not compatible with data analysis programs. If such data are acquired, and need to be analysed, they must be digitised in some way. This can be done either manually or via computerised analysis of scanned images of the analogue data. Digital data provides several advantages over the use of analogue data. For example, digital data are less prone to electric interferences and also less noise sensitive as noise arises only from round-off errors due to finite representation of the digits of a number³. However, most importantly, digital data are compatible with digital computers.

2.2.1.1 Mono-, Bi-, and Multivariate Data

The first step in data analysis is to convert the raw data into a computer-compatible form. Normally, the raw data are arranged in the form of a table, typically a data matrix as shown in Scheme 2.1. When using matrix-based notation it is useful to differentiate between matrices, vectors, scalars and indices by applying typographical conventions. Hence, matrices are denoted in boldface capitol characters (**A**), vectors in boldface lowercase (**a**), and scalars in lowercase italic characters (*a*), and for indices lowercase characters are used (*a*).

$$\begin{array}{ccccc}
 x_{11} & x_{12} & x_{13} & \dots & x_{1N} \\
 x_{21} & x_{22} & x_{23} & \dots & x_{2N} \\
 \vdots & \vdots & \vdots & & \\
 x_{M1} & x_{M2} & x_{M3} & \dots & x_{MN}
 \end{array}$$

Scheme 2.1: Representation of a general data matrix.

Data acquisition can result in three types of data, namely monovariate, bivariate or multivariate data, and it is useful to distinguish between these types.

Monovariate data are a simple series of measurements taken as a function of the independent variable. Typical examples include the signal of a flame ionisation detector in gas chromatography, the refractive index or absorption measurements at one wavelength of the eluting solution in HPLC or in a kinetic investigation, and pH measurements in the very common potentiometric technique. The latter was one of the

techniques applied in our research. For monivariate data the matrix depicted in Scheme 2.1 is comprised of only one column, with the row number being equal to the number of experimental data points.

Bivariate data are measurements taken as a function of two independent variables, for example absorption spectra taken by a diode array detector in liquid chromatography where the independent variables are chromatographic time and wavelength. By far the most common measuring technique that delivers bivariate data, and a technique that was also applied in our research, is absorption spectroscopy in the UV-Vis region of the electromagnetic spectrum. Absorption measurements in the NIR and mid-IR are of the same nature but less commonly acquired. Other alternatives include NMR and EPR spectroscopies or electrochemical data such as polarograms or voltamograms. The structure of bivariate data in the examples above, lend themselves to be arranged using very elegant matrix notation, as shown in Scheme 2.1. Matrix notation has distinct advantages, such as being a compact notation that can be smartly implemented into the appropriate code of matrix based computer languages that are used for data analysis theory development. The matrix-based program Matlab was the language of choice for our programming.

In general, the data collected for our investigations were monivariate data from potentiometric investigations or bivariate data from spectrophotometric acquisitions, as represented respectively in Figure 2.1. Even though spectrophotometric data can be considered as monivariate when measured at only one wavelength, our investigations were performed at multiple wavelengths and therefore classified as bivariate measurements. Both types of data shown in Figure 2.1 were collected and applied to either equilibrium or kinetic studies.

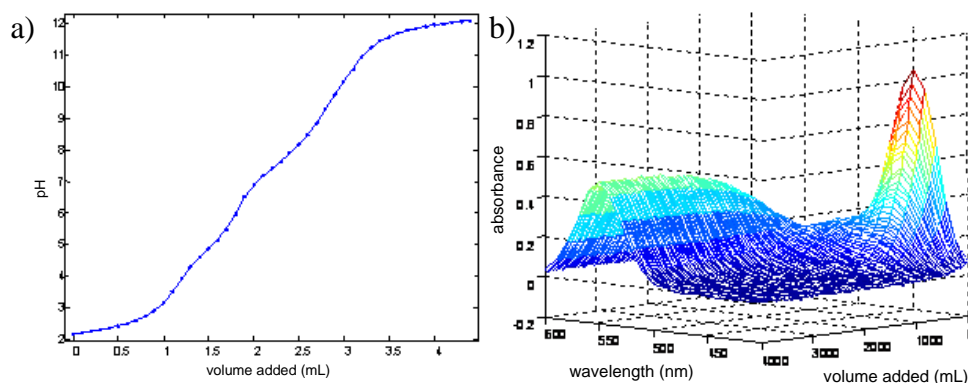
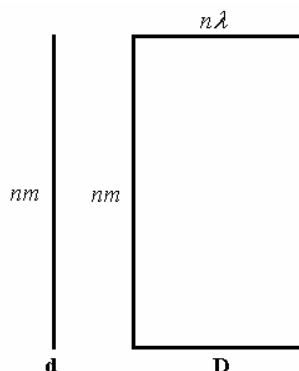


Figure 2.1: (a) Monivariate data set, for example a potentiometric titration; (b) Bivariate data set, for example a series of absorption spectra measured as a function of time.

It is most convenient to arrange monovariate and bivariate data as rows of a data matrix **D**, as depicted in Scheme 2.2. For measurements that are monovariate, such as the pH measurement represented in Figure 2.1a), or absorbance data as in Figure 2.1b), but measured at only one wavelength, the matrix **D** is reduced to a column vector **d**.



Scheme 2.2: Graphical representation of data collected during a measurement, both monovariate, **d** and bivariate, **D**; nm represents the number of additions in a titration or the number of time increments in a kinetic study, and $n\lambda$ represents the number of wavelengths used for the bivariate measurement.

Multivariate data consist of individual measurements that are acquired as a function of more than two variables, for example, kinetics measured at many wavelengths as well as a function of temperature, pH, concentrations and so forth of the reacting solutions. Often it is possible to re-arrange multivariate data to have the same structure as bivariate data. While this is not crucial, it allows the structure of matrix based software to be maintained. There is no reason to further distinguish between ter- and higher variate data, the reason being that matrix notation is directly applicable to bivariate data only and there is no equivalent notation for higher variate structures.

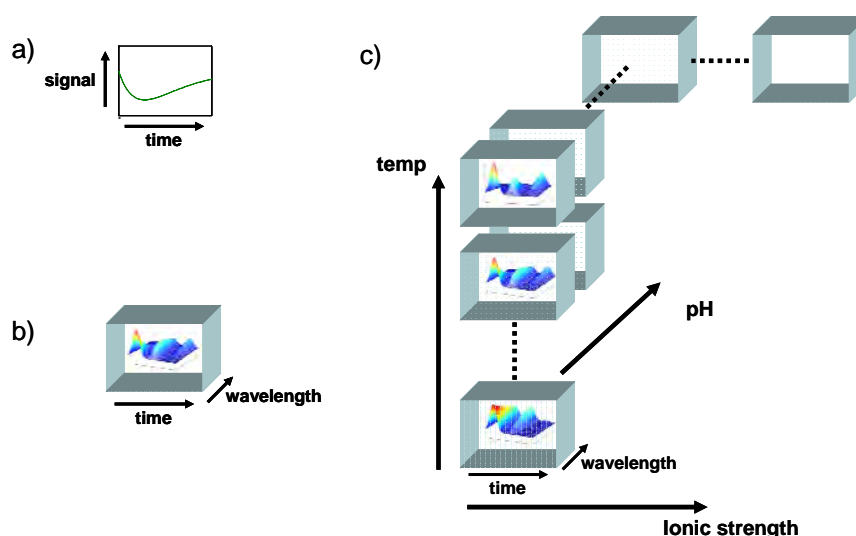


Figure 2.2: Examples of a) monovariate; b) bivariate and; c) multivariate data.

An important property of measured data is the fact they are never perfect. Quantitative analytical measurements are always subject to some degree of error and real data are always corrupted to some extent by different types of experimental problems. No matter how much care is taken, or how stringent the precautions followed to minimise the effects of gross errors from sample contamination or systematic errors from poor instrument calibration, random errors will always exist. The unavoidable errors contained in digitised data are relatively benign as only a limited number of decimal places can be measured. Similarly, additional noise of a random character introduced by the instrument does not seriously hamper the analysis, unless of course the noise level is large in comparison with the signal.

In practise this means that although a quantitative measure of any variable, be it mass, concentration, absorbance value and so on, may be assumed to approximate the unknown true value, it is unlikely to be exactly equal to it. As more samples are analysed, or more measurements are repeated, then a pattern to the inherent scatter of the data will emerge. In the absence of any bias or systematic error the results should be evenly distributed about the true value. Other problems such as baseline drift, incorrect concentrations in the solutions used and so forth, are much more difficult to deal with, and reduce consistency across the complete data set.

Repeated measurements of the same variable on similar samples will not only highlight any discrepancies between the observed results and the true value, but also show the differences between the measurements themselves. This variability between repeated measurements can be attributed to the presence of random errors associated with the measurements process, for example instrument generated noise, as well as the natural, random variation in any sample's characteristics and composition ⁴. However, any errors identified between repeated measurements that are systematic, or clearly not due to errors of a random nature, need to be identified and rectified in order for repeated measurements to be analysed successfully.

2.2.2 General Techniques

The process of data collection has been intensely discussed in the literature and several automatic data acquisition systems have been described ^[5, 6]. For this research we predominately used in-house developed techniques for the acquisition of equilibrium data, but employed the commercially available Applied Photophysics – SpectraKinetic

Workstation v4.56.4 for the collection of fast kinetic data. The basics of both equilibrium and kinetic data acquisition processes are described in order to establish a background for our in-house developed procedures. Both equilibrium and kinetic data are measured as a function of an independent variable, however in general the experimentation required for kinetic studies are not as complex and are conceptually much simpler compared to that required for equilibrium investigations⁵⁻⁷.

For kinetic experiments, the reaction is initiated by the mixing of two or more reactants and subsequently recording the change in signal, mono- or multi-variate, as a function of time. The mixing process can be carried out manually for kinetically slow reactions, for example, the process may involve two reactant solutions that are mixed in a cuvette which is then placed in the spectrophotometer, followed by initiation of the scan. Such manual manipulations enable spectra to be recorded within approximately 10 seconds of the initial mixing. However, many reactions that are investigated have very rapid kinetics where the reaction easily reaches completion within 10 seconds. For these faster reactions stopped-flow instruments replace manual mixing by pneumatically or stepper-motor driven syringes. In such experiments measurements can begin after about 1 millisecond, this start time being limited by the mixing dead-time which is a function of the hydrodynamics of the solutions being investigated.

The most well-established technique for equilibrium studies is to collect data by means of titrations. In general terms a titration involves a series of solutions measured for some physical property at varying component concentrations. The number of measurements is dependant on the type and purpose of the titration and can range from five up to greater than a hundred measurements in the series. Typical measurements include recording the pH or absorption spectra of the titrate solution. Techniques involving measuring the pH are known as potentiometric titrations, these are convenient and used most commonly due to the simplicity of the equipment and minimal time requirements⁸. Measurement of the absorption of the titrate solution, at one or many wavelengths, is performed using spectrophotometric techniques which are considered to be one of the most powerful methods for investigating solution equilibria. In order to more completely describe a chemical reaction it is also possible to acquire multiple types of data, for example to record both the pH and spectra of a solution in the one titration.

2.2.3 Titration Experimentation

2.2.3.1 Overview

The most common application for a titration is to determine the unknown concentration of the analyte, for instance titrations are used to standardise base or acid solutions so the solutions can then be used accurately in further experiments. Such acid-base titrations are one of the oldest tools in analytical chemistry. The general technique for such a titration is depicted in Figure 2.3 and involves a measured volume of solution A, into which solution B is added in small portions until sufficient has been added to reach the end-point or equivalence point. The completion of the titration is identified by some sort of physical indication, such as a colour change of an added indicator or one of the equilibrium species. Calculations can then be performed using the accurately known concentration of one of the solutions, along with the two known volumes, in order to determine the unknown concentration of the other solution.

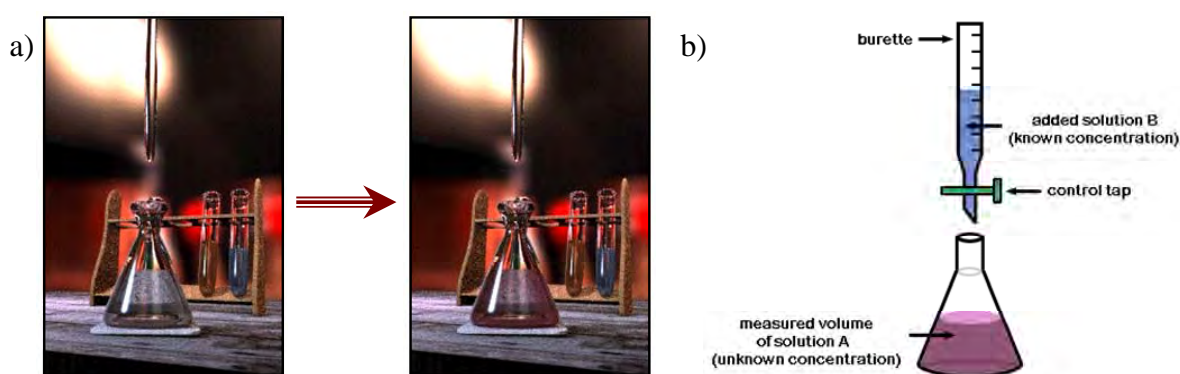


Figure 2.3: Traditional titrations for end-point detection; a) demonstrates the colour change of an indicator from clear to pink ⁹; b) depicts simplified titration equipment ¹⁰.

Modern titrations now utilise computerised instrumentation in which the classical burette is substituted by a computer controlled system such as stepper syringe or the commercially available Metrohm Dosimat automatic burette. The measurement itself has also been computerised, making the entire titration method automatic rather than a time-consuming manual method as described in Figure 2.3. A generalised modern titration set-up is depicted in Figure 2.4. Using modern instrumentation for the titration measurement has led to the investigation of many other types of problems using titrations other than the tradition end-point detection. For this project titrations were not performed to determine the initial component concentrations, for example the initial concentrations of the metal or ligand, as these were generally already known.

The focus of titrations for this project was, instead, for the quantitative analysis of solution equilibria, which is considered to be one of the most important applications of titrations aside from concentration determination. The titrations that were performed were analysed in order to determine what species existed in the solution and the value of their corresponding equilibrium constants. The determination of the equilibrium constant of each species is an important experimental parameter as it enables the calculation of the changing concentration of each species over the duration of the titration or under any other conditions. For spectrophotometric titrations a secondary step can also be employed as part of the analysis of the titration data that enables the spectra of molar absorptivities of absorbing species to be calculated. The molar absorptivities have the clear advantage of delivering structural information about intermediate species present during the titration.

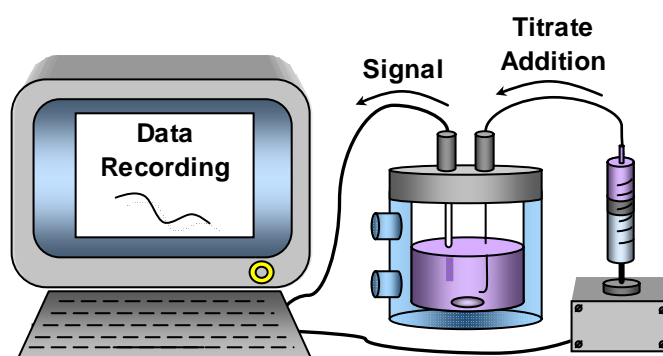


Figure 2.4 : Schematic of a simplified computer controlled titration system. The addition volume from the burette and the recording of a signal is entirely computer controlled.

The investigation of solution equilibria can be made by a variety of titration methods, for example potentiometric methods using pH titrations, electrical methods such as conductometric titrations, spectroscopic methods using spectrophotometric or circular dichroism titrations, and so forth ⁶. In order to investigate equilibria some physical property of the solution is measured after each volume addition, for example in our studies the pH, absorbance spectrum, or both pH and absorbance were measured. However, for these titrations the process is not concluded once an endpoint has been detected, but when the maximum/minimum pH has been reached, or when the spectral changes have been completed.

Classically, titrations for equilibrium investigations were conducted by some sort of fully manual batch method, involving the preparation of a series of solutions that contained different total concentrations of the components that were interacting with

each other to form the equilibrium species. Such experiments often involved the preparation of perhaps 30 solutions by hand. Each solution then required individual measurement, often needing to be transferred individually into the instrument, for example a spectrophotometer cuvette, for measurement ¹¹. In its favour, no dilution effects existed because solutions were pre-prepared in volumetric flasks, however there are a number of negative factors associated with using the batch method ⁶. For instance, pre-preparing numerous solutions for the titration, followed by the manual transfer for measurement, is a very time consuming and error prone technique, as well as being uneconomical on sample quantity and highly liable to CO₂ or other contamination during the lengthy handling process. It is clear to see that modern methods utilising fully automatic computer controlled titrations are clearly superior. Such titrations involve the same basic technique that has been classically used for end point detection titrations, that is the addition of small known volumes of solution B to the starting measured volume of solution A.

Automated, computer controlled methods have many distinct advantages, such as the avoidance of labour intensive tasks and enhanced precision as the additions of solution B are performed more accurately by computer controlled instrumentation than otherwise could be done. There is no concern with the dilution effects from the addition of solution B as the dilutions are straightforwardly accounted for in the computational analysis. Nevertheless, while a titration is a time consuming measurement, automation does convert an experiment that would have taken a day or more to a measurement that may take a couple of hours, therefore enabling two or three to be performed in a day. However, more importantly than the time saving considerations, is the fact that automation has replaced manual labour by the use of computer controlled systems which are not only cheaper but are also more efficient and less error prone.

2.2.3.2 Equilibrium Investigations

In a titration controlled displacement of a chemical equilibrium occurs through the addition of titrant, and there are several techniques currently used to perform such titrations ^[18, 19]. This research utilised automatic, computer controlled titration systems with automatic burettes and automatic recording of a physical property of the solutions, either the electrode signal in potentiometric titrations or absorbance in spectrophotometric titrations. The general experimental set-up for our titration systems involved a computer, running in-house software, which controlled the burette and also

monitored the signal. The in-house developed software is discussed in more detail in Section 2.2.5.

Potentiometric titrations are useful when the equilibrium is sensitive to changes in pH, as is generally the case in aqueous solutions. For such investigations the titration often involves the addition of a base solution, commonly sodium hydroxide, to an acidified solution of the substrate. When protonation equilibria are investigated the acidified solution contains the protonated form of the acid-conjugate base couple. In a metal-ligand complexation study, the acidified solution contains the protonated ligand and the free metal.

While potentiometric titrations may be considered as one of the most accurate methods for the evaluation of complex equilibrium constants ¹² they require aqueous solutions and pH-sensitive equilibria, and do not provide structural information such as the sites of protonation or complexation. For this type of information NMR or absorbance spectroscopic methods are required ¹³. There are advantages in using spectrophotometric titrations from the qualitative point of view. In contrast to potentiometric titrations, where only equilibrium constants are produced, spectrophotometric titrations also yield additional spectral information about the absorbing species that are formed during the titration. Knowledge of the molar absorption spectra of absorbing species not only provides a useful tool for structural analysis of the compounds but may also be used to identify species, and can also be applied as a discriminating tool in assessing the adequacy of the proposed model ¹⁴.

In order to perform spectrophotometric studies, which are probably the most commonly used quantitative technique used in chemistry, it is necessary that one or more of the species absorb light at a particular wavelength. For metal-ligand complexation investigations in aprotic solvents the ligand solution is added to the metal solution, or vice versa. Importantly, spectrophotometric studies can also be performed as described for potentiometric studies, which is in aqueous solutions with the titration being either acid, base, the protonated ligand or the free metal.

The measurement in a spectrophotometric titration produces absorbance data which are a collection of spectra as a function of pH in protic solvents, or in aprotic solvents a function of the metal-ligand ratio ⁸. The wavelength range is selected such that every species makes a significant contribution to the absorbance sometime during the titration. For analysis, minimal information is obtained in regions where there are great spectral

over-laps or where the molar absorptivities of two or more species are linearly dependant. Therefore, it is best to collect spectra at wavelengths where the molar absorptivities of the species differ greatly or alternatively to use a large number of wavelengths spaced at equal intervals. However, with modern spectrophotometers and computers the possibility of collecting bivariate data is readily available, for example a diode array spectrophotometer delivers the complete absorption spectrum of a solution at each particular point in titration. Therefore, it is of no disadvantage to measure a large wavelength range as earlier considerations with issues such as storage space for the measurement are no longer relevant. Most analytical programs can also deal with large wavelength ranges as well, making it most beneficial to the scientist to measure as large a wavelength range as is feasible for the measurement, then analyse the entire spectrum to yield the maximum amount of information possible.

Spectrophotometric determinations are also useful for the determination of the position of equilibrium when potentiometry cannot be employed. An example of such situations are at the extremes of high and low pH where potentiometric measurements are not sensitive to the equilibria being measured¹² and also where insoluble species are formed at concentrations typical for potentiometric techniques, such as metal hydroxides or polymeric species¹³. However, if the spectrophotometric technique is applied, certain intrinsic limitations need to be taken into account. The absorbance in a measurement should be in the range of 0.1 to 1.0 and, depending on the molar absorptivities of the species being investigated, this may require concentrations that are significantly lower than that used for a potentiometric investigation and association reactions are not favoured at low concentrations. Therefore, if dilute solutions are needed for the spectrophotometric measurements the species formed may be present in different relative quantities than those detected at the higher metal-ligand concentrations that are used for potentiometric investigations. Furthermore, it has been reported by some researchers that the errors associated with the formation constants calculated from spectrophotometric data generally tend to be larger than those obtained from potentiometry¹⁵.

2.2.3.3 General Experimental Procedure

The sequence of events for a standard titration involved three key steps that are repeated *nm* amount of times: (1) addition of reagent through the burette; (2) mixing and waiting for the establishment of the equilibrium; and (3) acquisition of the data.

Burette Systems

For the first step in the titration process, the addition of the reagent, two burette systems were available: a commercial Metrohm Dosimat, and an in-house designed stepper driven syringe system. Titrations could be performed by the addition of the titrant from either of the two available burettes depending on which was best suited for the investigation.

The Metrohm Dosimat automatic burette has a minimum volume addition size of 1.00 μL , and the titrant must be prepared in large volumes. Such titrations generally have a high consumption of materials and are consequently performed at a great expense or rapid rate of use of pure materials that have possibly been obtained from low yield syntheses ⁶. With the Dosimat burette titrant solutions are not readily switched as substantial volumes are required for flushing the dispenser unit. Alternatively, if more than one dispensing unit is available then an entire unit may be used for each different titrant solution, thus removing the need for rinsing the unit with each change of solution. This does however require numerous dispensing units and a compromise between the substantial cost of a Dosimat unit, amount of titrant used, and the time required for cleaning, has to be found. For these reasons the stepper syringe burette, depicted in Figure 2.5, can be quite useful.

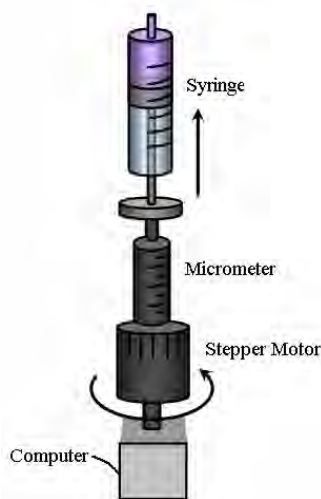


Figure 2.5 : Diagram of the stepper syringe burette developed at the University of Newcastle which adds precise, small additions in a titration.

The syringe burette was constructed at the University of Newcastle using a small stepper motor, micrometer, and a variety of glass syringes. A pulse from the computer causes the motor to move a step, rotating the micrometer, and pushing the plunger of the

syringe to deliver an exact small volume of solution. The syringe burette can add very small volumes of solution and the volume added from a rotation of the micrometer must be determined experimentally for each syringe size used. For the 2.0 mL syringe used, the minimum addition volume was 0.429 μL , the 5.0 mL syringe was 0.847 μL , and the 10.0 mL syringe added a minimum of 1.707 μL . The stepper system is convenient for switching between titrant solutions as minimal rinsing is required, therefore making it useful when only small volumes of titrant solution can be prepared. A number of titrations can readily be performed with a total prepared volume of titrant of only 2 to 5 mL, compared to a minimum volume of at least 20 mL required to use the Dosimat system. The choice between which system to use is strongly influenced by the smallest quantity of solid which can accurately be weighed for the preparation of the required solutions.

Acquisition of the Data

The external instruments in the automated systems implemented at the University of Newcastle were interfaced to the computer via a NIST A/D-D/A board. In commercial set-ups this would usually be incorporated into the computer, however, for this research it was done via an external A/D board. The systems fall into three main categories, the simplest set-up being for potentiometric titrations which simply requires the pH electrode being inserted into a thermostated titration vessel in order to take the measurement. This set-up is detailed in Section 2.2.3.4 and is shown in Figure 2.6. The potentiometric system has the potential to be easily extended to include absorbance measurements with the addition of fibre optic devices into the titration vessel.

The next system is for spectrophotometric measurements and involves an internal titration system which means the titration is performed inside the spectrophotometer as the titrant is added into the cuvette, as shown in Figure 2.7 in Section 2.2.3.5.

The cell compartment of the spectrophotometer can also be altered in order to accommodate an electrode for combined potentiometric and spectrophotometric titrations as detailed in Section 2.2.3.6, Figure 2.8. The capability to perform simultaneous spectrophotometric and potentiometric titrations is, at least for some equilibria, a strong advantage.

Combined titrations can also be carried out via a joint internal/external system. The titration can be performed externally in the thermostated titration vessel, where the pH

can be easily measured by placing the electrode in the vessel, similar to the first system. The solution is pumped from the titration vessel through a flow cell in the spectrophotometer by a device such as a peristaltic pump¹⁶ where the spectra can also be recorded at each step in the titration. This system is depicted in Figure 2.9. These available set-ups will be detailed in the following sections, along with discussions about the advantages and disadvantages of using each system^{6, 17}.

2.2.3.4 Potentiometric Titrations

Figure 2.6 shows a schematic representation of a computer controlled potentiometric pH titration. Titrations using this set-up were carried out under nitrogen atmosphere and thermostated at 25.0 ± 0.1 °C using an external water bath. Solution concentrations were generally in the range 1×10^{-3} M to 1×10^{-2} M depending on the metal-ligand ratio and quantity of ligand available for analysis. Equilibrium pH values were measured after every incremental addition of NaOH to the experimental solution.

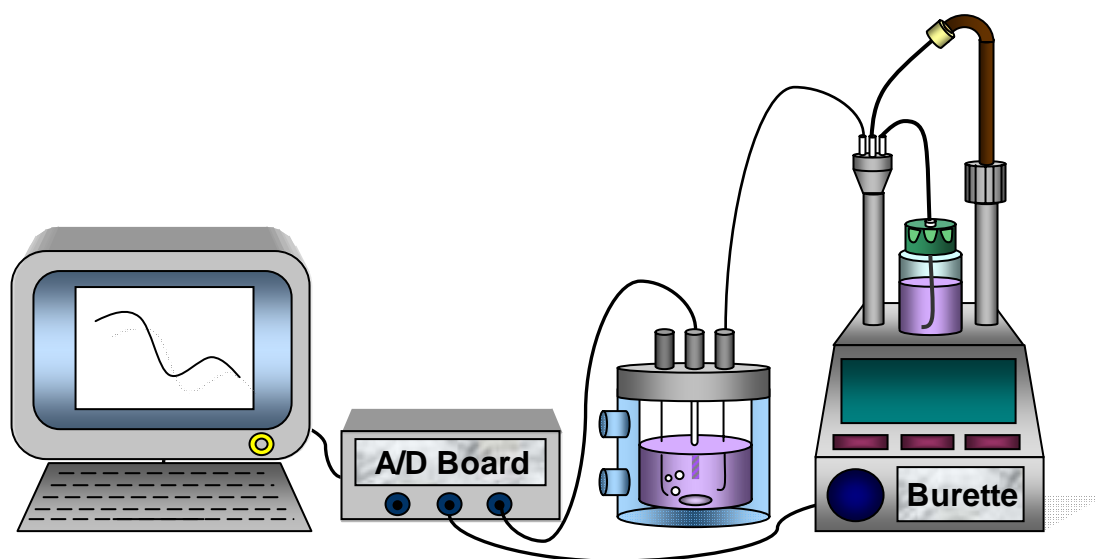


Figure 2.6: Automated potentiometric titration set-up.

The pH electrode used was a slim, 125mm Metrohm 6.0234.100 micro pH glass electrode with the internal solution changed from a saturated KCl solution to 3M NaCl in order to prevent precipitation with the ligands and metal ions that were investigated. A Metrohm 665 Dosimat automatic burette with 1 mL dispenser unit added the titrant solution, or alternatively the syringe burette was used if smaller volumes of prepared solution were necessitated. The electrode was connected to the computer via a National Instruments NI-DAQ 7 board that amplified and translated the electrode signal to a mV signal that could then be recorded by the computer.

For the potentiometric external titration system the titration was performed in the thermostatted Metrohm titration vessel, with the pH electrode, burette and nitrogen purge being inserted through the standard taper openings of the titration vessel lid. Volumes required for a titration ranged from 2 to 20 mL, depending on the titration vessel size used. A magnetic stirrer underneath the titration vessel constantly stirred for the duration of the titration.

In order to take the electrode reading after each addition of titrant it was required to determine whether or not the signal was steady, that is whether equilibrium had been established after the addition. To assess whether equilibrium had been reached the computer rapidly recorded 100 voltage readings in a one second period. The average mV value over the second is calculated and this process is continued for a one minute period, and then the overall average of the minute is taken. The entire process is then repeated for another minute period and the overall average again taken. If the determined averages from the two periods are within 0.1 mV of each other the electrode reading is considered stable and the last average value is recorded as the reading. If the stable criteria was not met, that is if there is greater than 0.1 mV difference between the two one minute periods, then the process is repeated for another minute and the average mV reading calculated again. This sequence is repeated until two successive minute periods are within 0.1 mV of each other. The timeout is after 10 sets, that is 10 minutes, after which the mV reading is assumed to be constant and the last average taken as the mV reading for that step of the titration.

As previously stated, the potentiometric titration set-up can be easily modified to include a fibre optic device, thus removing the need of a spectrophotometer which is required for the internal method discussed in Section 2.2.3.5, as the absorbance measurement is taken directly in the location of the fibre optic device. Advantages of this modification compared with the internal method include the flexibility of being able to use any titration vessel, hence a large range of solution volumes, and also the path length can more readily be varied. Disadvantages of employing fibre optic devices are that the probe is costly and very fragile, less light passes through the light path resulting in higher noise to signal ratios, and measurements are restricted to single beam mode only. There were no fibre optic devices available at the University of Newcastle so this option, even though being theoretically possible and easy to adapt, was not pursued.

2.2.3.5 Spectrophotometric Titrations

The spectrophotometric titration system constructed at the University of Newcastle consisted of a computer interfaced to an Analytica Jena Specord 210 spectrophotometer with a thermostated cell compartment using an external water bath, a Metrohm 665 Dosimat automatic burette with 1 mL dispenser unit or a syringe burette, and a computer controlled stirrer.

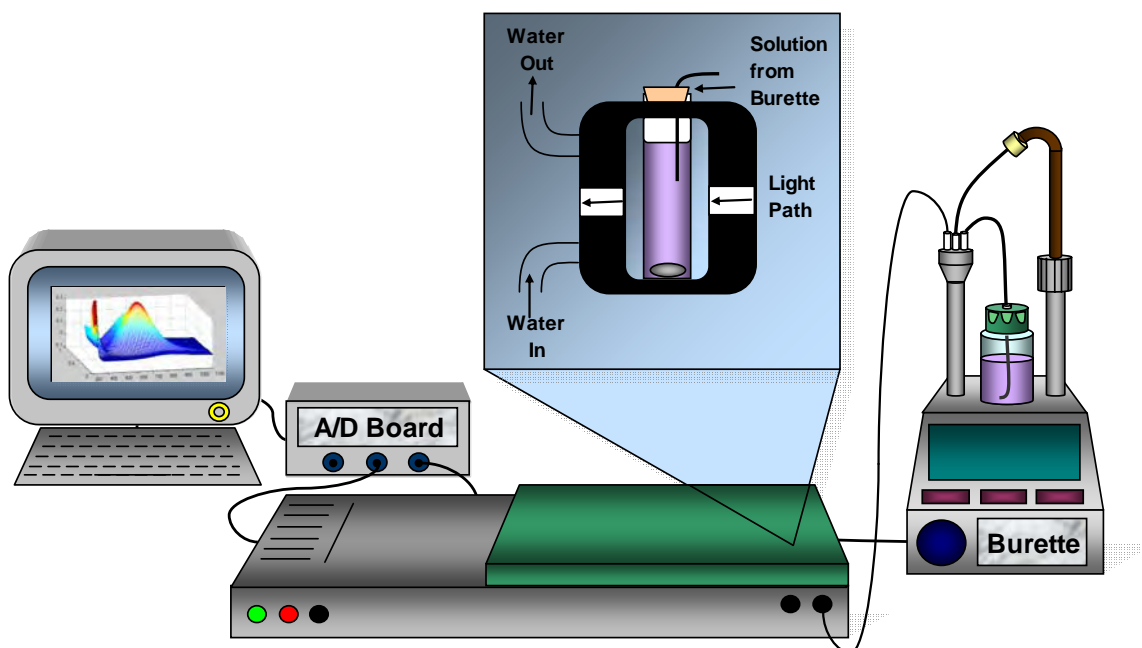


Figure 2.7: Automated spectrophotometric titration set-up.

Figure 2.7 represents the spectrophotometric titration set-up using the Dosimat burette, with the titrant being delivered directly into the cuvette inside the spectrophotometer. The solution was stirred at all times during the titration except while the spectrum was being measured. A minimum initial volume of 1.5 mL was required for the spectrophotometer cuvette, with a maximum volume limit of approximately 3.0 mL. The minimum volume requirement was determined by the liquid level needed for the entire beam to pass wholly through the solution. Spectrophotometric investigations for this research were performed using a 1.0 cm quartz cell, thermostated at 25.0 ± 0.1 °C. The spectra were scanned after every incremental addition of titrant to the cuvette with a wait-time of 80 seconds, which enabled adequate mixing of the titrant and the establishment of equilibrium. If systems with slower equilibriums were investigated the wait-time could be adjusted accordingly.

Problems with the internal method can occur because diffusion through the burette tip is difficult to avoid¹⁷ and this is particularly troublesome due to the small volumes used in

cuvettes. Evaporation of the solvent and CO₂ contamination are further complications resulting from the use of very small volumes. In addition, gas bubbles have a tendency to accumulate on the cuvette walls. However, despite such problems, this method has been reported to experience a high level of reproducibility^{18, 19}, and this was also observed for our experiments.

The internal spectrophotometric titration method used for our investigations involved no manipulation of the cuvette during the titration, meaning consistency of the spectra from one scan to the next were much improved over manual titration methods. However, the method did involve extracting the cuvette between titration sets to remove the completed titration solution and for cleaning. This had the potential to introduce baseline differences between titration sets, and such phenomena have been observed in second order global analysis. The affect can be accounted for by either applying baseline corrections or fitting individual absorptivities to a global model as is detailed further in Section 2.3.

2.2.3.6 Combined Potentiometric and Spectrophotometric Titrations

Internal System

The above spectrophotometric titration system was further adapted to incorporate an electrode which enabled both potentiometric and spectrophotometric titrations to be performed together. This set-up is shown in Figure 2.8. In order to achieve this adaptation in the sample compartment adaptation of the commercial Analytic Jena Specord 210 spectrophotometer was required. The method involved the titration being performed inside the cuvette, the lid of the cuvette having holes created to fit the pH electrode, the burette tubing and tubing for nitrogen flow to remove any carbon dioxide from the solution. The cell compartment also had to be altered in order to incorporate the pH electrode into the cell solution without interference to the light path. Having the pH electrode inserted into the top of the cuvette also meant that the sample compartment lid could not be completely shut. To exclude stray light, shaped metal replacement lid sections, cardboard and black cloth were used to completely cover the sample compartment.

Introduction of the electrode into the cuvette also subsequently changed the volumes of solutions required. The initial volume had to ensure that the membrane of the electrode was covered, but also that the electrode itself was not inserted too into the cuvette far as

to interfering with the beam. The minimum required volume in the cuvette was approximately 1 mL, with the maximum volume reduced typically to around 1.5 to 2.5 mL for the 1.0 cm quartz cell used for these investigations. A precision microburette, for our studies the stepper syringe burette, was necessary for the addition of the very small titrant volumes required for such titrations.

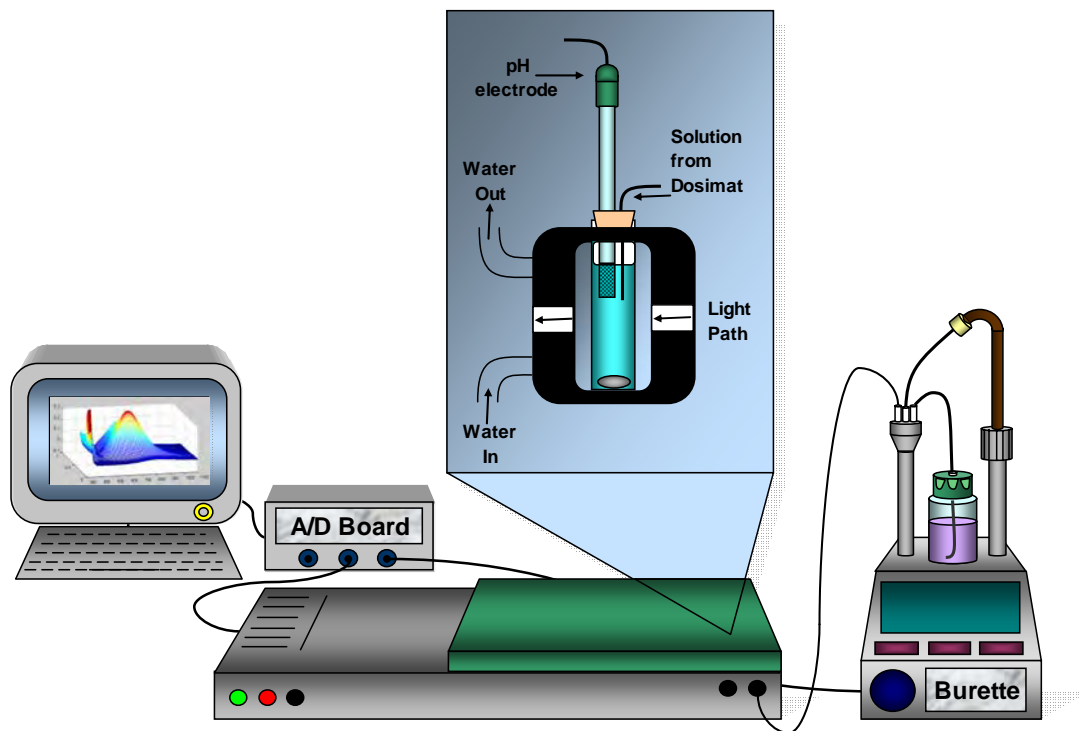


Figure 2.8: Automated combined spectrophotometric and potentiometric titration set-up, internal system.

External System

The external spectrophotometric flow-cell titration system is depicted in Figure 2.9. It consisted of a computer interfaced with the Analytic Jena Specord 210 spectrophotometer, an Ismatec MS-1 Reglo 6/160 pump, a slim, 125mm Metrohm 6.0234.100 micro pH glass electrode, a Metrohm Dosimat 665 automatic burette, or the stepper syringe burette, and an external water bath which thermostated both the Metrohm titration vessel and the spectrophotometer sample compartment at $25.0 \pm 0.1^\circ\text{C}$.

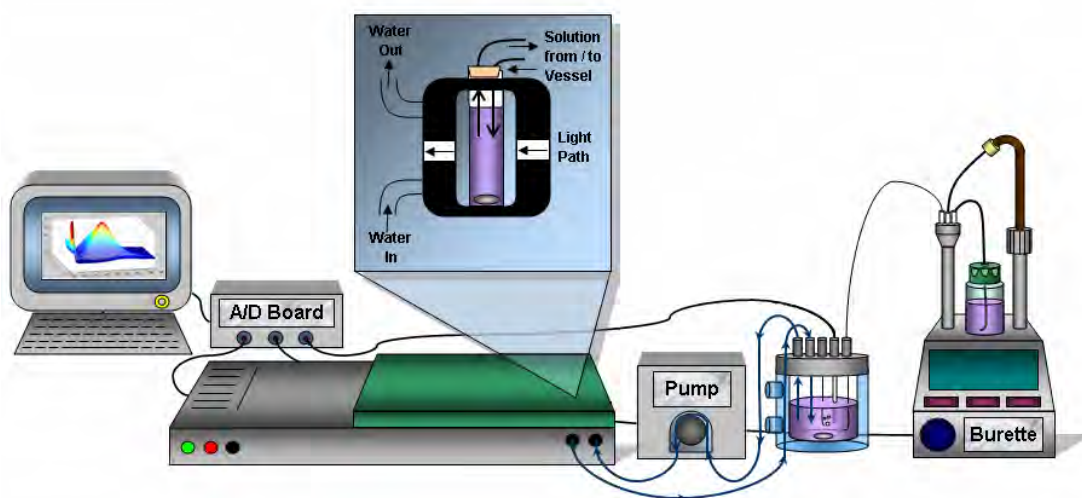


Figure 2.9: Automated combined spectrophotometric and potentiometric titration set-up, external system.

The minimum initial volume required in the titration vessel was approximately 20 mL, with the maximum total volume limited only by titration vessel size. The minimum volume was determined by the liquid level required to cover the salt bridge of the pH electrode, after pumping had filled the tubing with the starting solution. The pH electrode, burette tubing and nitrogen purge tubing were inserted through the standard taper openings of the titration vessel lid. A magnetic stirrer in the base of the titration vessel constantly stirred for the duration of the titration.

The peristaltic pump was switched on and off automatically from the computer. Pumping of the titration solution was performed at all times during the titration except while the spectrum was being measured. In the internal system the magnetic stirrer was switched on and off inside the spectrophotometer to mix the solution, while with the external system the magnetic stirrer inside the spectrophotometer is not used and instead the computer switches on and off the peristaltic pump.

After measurement of the baseline spectrum, which usually consists of the ligand solution, the metal solution or metal salt is added to the titration vessel and allowed to fully mix before being pumped through the tubing and cuvette. Pumping is continued for at least 10 minutes to ensure that any ligand solution in the tubing and cuvette are adequately mixed with the added metal.

With the combined external system a longer delay time is required for mixing and pumping to obtain solution homogeneity after titrant addition. Approximately three times the volume of solution contained in the titration vessel needs to be pumped around the system. Erroneous values can result if air bubbles form and are circulated around

the system. Also, the tubing must be of a suitable material to avoid the adsorption of titration materials onto tubing walls. With this method, however, CO₂ contamination is better controlled than for the internal system, and small amounts of evaporation have little effect.

2.2.4 Kinetic Experimentation

2.2.4.1 Stopped-flow Acquisition - Fast Kinetics

The kinetic investigations of fast complex formation were carried out with an Applied Photophysics stopped-flow spectrophotometer DX-17MV equipped with a temperature controlled optical cell, path length of 1.0 cm, and interfaced to an Acorn computer. This was the only system for which the commercially available software was used rather than developing our own system.

In the stopped-flow reactions performed for this project the kinetics of a reaction was followed until equilibrium after an initial physical mixing, which was performed within approximately 5 ms. The stopped-flow system at the University of Newcastle operated by rapidly mixing two reactant solutions, then the subsequent spectral changes are monitored. A schematic of the system is detailed in Figure 2.10. The system injects reactants from two separate reservoir syringes into the mixing cell. The effluent then fills the third syringe which, when filled to a certain volume, triggers the plunger to hit the backstop, stopping the flow in the whole system and starting the measurement²⁰. The kinetic data generated are presented as absorbance versus time data. The absorbance changes observed are directly proportional to the concentration changes of the reactant and products^{5, 21}.

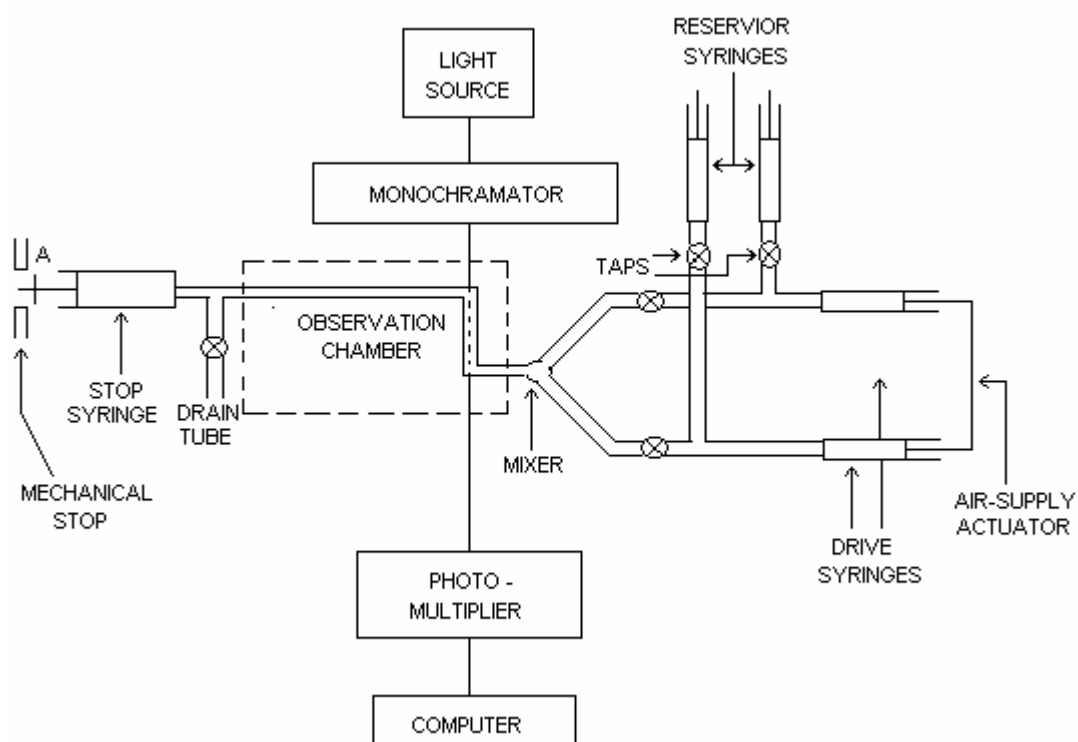


Figure 2.10: Block diagram of stopped-flow apparatus²².

2.2.4.2 Spectrophotometric Acquisition - Slow Kinetics

The spectrophotometric system depicted in Figure 2.11 is essentially the same as for the system previously described for spectrophotometric titrations, see Section 2.2.3.5. The key difference from the titration system is however that there is no burette system attached and measurements are taken as a function of time rather than of titrant addition. For these slow kinetic measurements the two reagent solutions were manually mixed together and placed in the cuvette in the spectrophotometer before initiating the data acquisition.

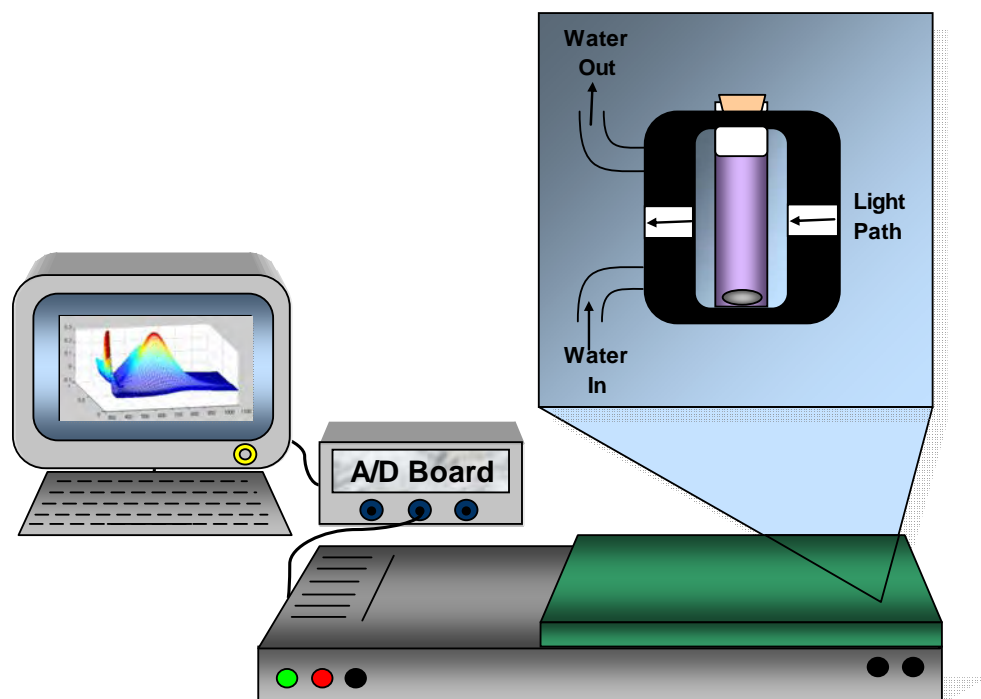


Figure 2.11: Automated spectrophotometric system for kinetic investigations.

2.2.5 In-House Developed Software for Instrument Control

The data acquisition programs were developed using an Excel-Matlab link, details of the link between the two applications are discussed in Section 2.4. The set-up requires the user to enter the experimental parameters into an Excel user-interface, while the instruments are controlled by the matrix-based computer program language Matlab via a digital/analogue I/O port. The programs for each titration system mainly differ only in the type of data recorded, the general data acquisition procedures remain the same irrespective of the actual data type.

The appropriate Excel file for each measurement type is opened from a Matlab Graphical User Interface (GUI), depicted in Figure 2.12, and the measurement itself is also initiated from the GUI. The user-interfaces for each system were designed in the well-known Microsoft application Excel and are shown from Figure 2.14 through to Figure 2.18. Once the measurement has been initiated the Matlab GUI displays the progress of the experiment. For potentiometric titrations the electrode signals are displayed as the measurement progresses which not only has the benefit of enabling the user observe the titration as it develops, but it also aids in identifying whether the electrode is operating correctly or is unstable. For spectrophotometric measurements the individual spectra are displayed as they are measured along with another plot that shows the total spectrum over the titration. For combined titrations both the electrode

signal and spectra are displayed in the GUI. Slow-kinetic reactions have a similar display to the spectrophotometric titration GUI in that individual spectra are displayed as they are measured along with another plot showing the series of spectra over all time intervals so the progression of the reaction can easily be followed.

For each measurement the recorded signal after each addition or time increment is not only displayed in the Matlab GUI but is also outputted to the Excel workbook where the user entered the specific parameters for the experiment. The benefit of this output is that the user can begin data manipulation in Excel while the measurement is still running. This can assist in identifying any problems during the measurement or, for instance, if the measurement can be stopped early. Further, having the data outputted into Excel after each measurement has the benefit of providing the added insurance that if the experiment fails, for example from a black-out or equipment failure, as the data up to that point in the experiment will be saved in the Excel file and not lost as otherwise would have been the case. The user needs to configure the computer to automatically save the Excel file every two or three minutes to ensure that if the entire computer crashes that the data in Excel can still be recovered.

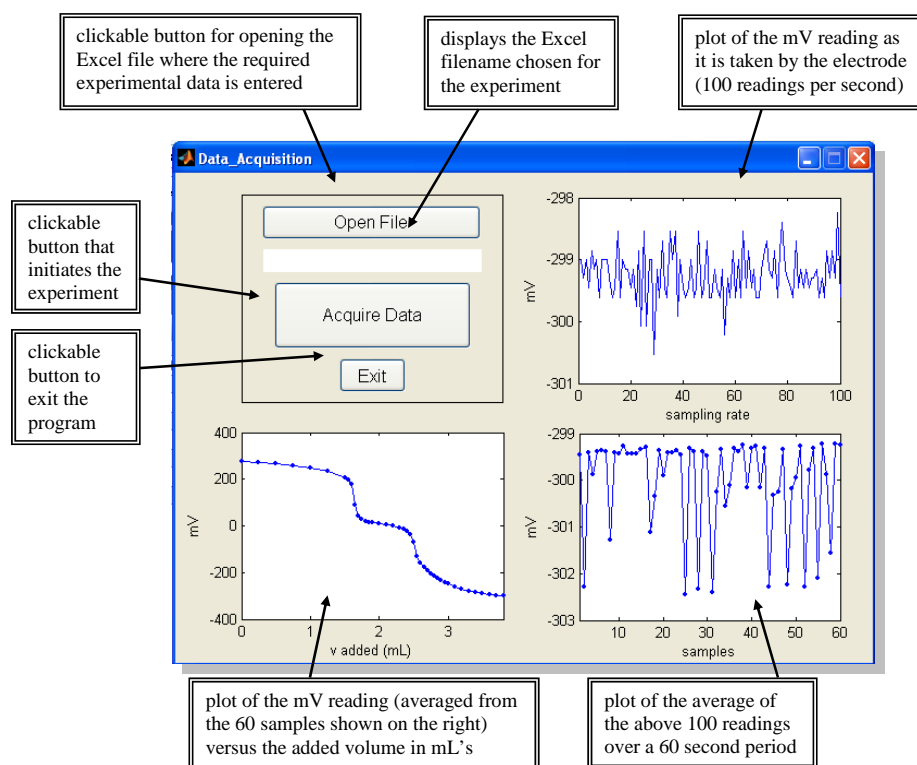


Figure 2.12: Screen shot of the Matlab GUI for potentiometric titration measurements.

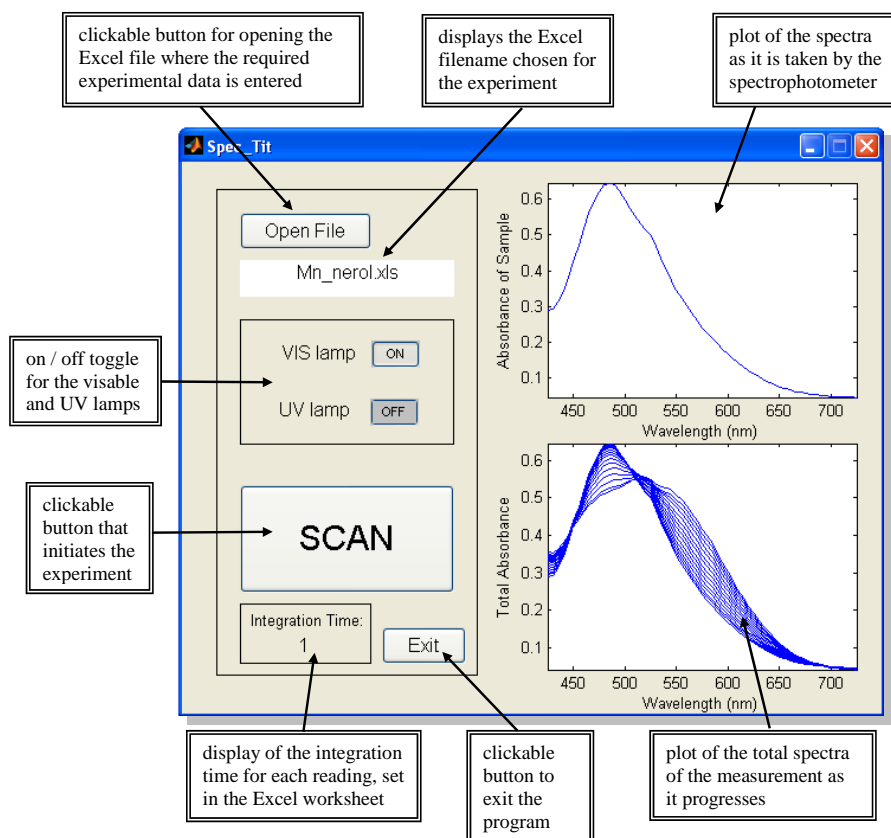
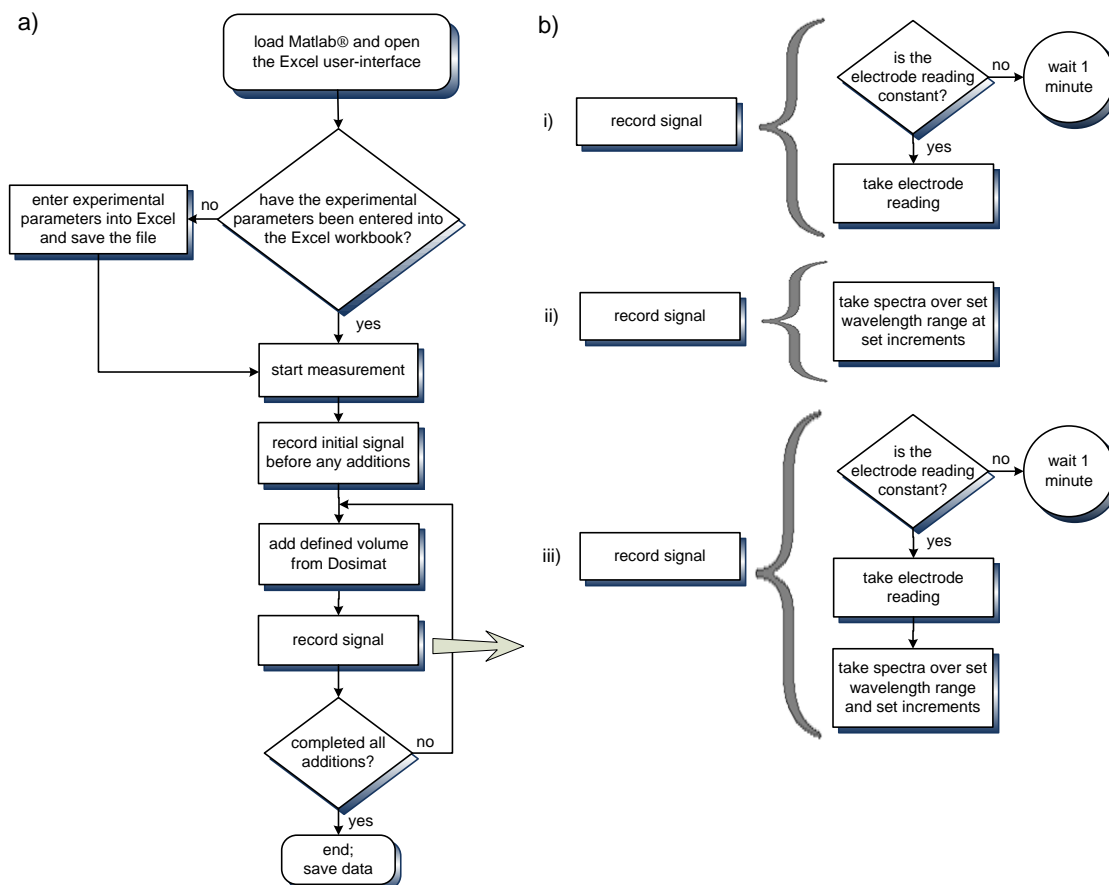


Figure 2.13: Screen shot of the Matlab GUI for spectrophotometric titration measurements.

2.2.5.1 Titration Measurements

Process Description

The titration set-up at the University of Newcastle enabled three different types of titrations to be performed. The computer programs that were developed to control the automatic systems are outlined in a general flow diagram shown in Scheme 2.3a) describing the basic titration process. Scheme 2.3b) details the specific data recording process for each acquisition type. The same flow diagram can be applied to all acquisition processes, that is potentiometric, spectrophotometric and combined titrations.



Scheme 2.3: a) Flow diagram for general data acquisition; b) Specific data recording process (i) details for recording the electrode signal for potentiometric titrations; (ii) details for recording spectra for spectrophotometric titrations; (iii) details for recording both electrode signal and spectrum for combined titrations.

Each data acquisition process requires the user to firstly open the appropriate Matlab GUI, the Excel user-interface is then opened from the GUI and the parameters for the measurement are entered. Obviously, each experiment requires different parameters depending on the measurement type and its specifics. Most parameters are of a common type for all measurements, such as the initial component concentrations, the initial volume in the titration vessel or cuvette, and also the addition vector consisting of the specific volume of each addition to be added in each step of the titration. Additionally, the wavelength range, increment and integration time need to be supplied for spectrophotometric and combined titrations. The dimensions of the acquired data are limited only for spectrophotometric measurements as a result of Excel's specification of a maximum 256 columns for each workbook. Therefore the number of wavelengths measured must be limited to a maximum of 256.

The addition vector required for each titration can vary and contain different sized additions, for example the titration may begin with 50 μL addition volumes, change to 20 μL , then 5 μL , followed by larger volume additions, such as 50 μL again, at the end of the titration. The volume increments and the number of additions that are to be made must be specified prior to the titration as they are then used to regulate burette addition. These volume increments are used together with the initial reagent volume and component concentrations in order to calculate the total concentrations at each point in the titration, taking into account the dilution after each addition.

For titrations using the Dosimat the plunger size needs to be specified as the computer program must pause while the burette refills, otherwise the computer continues to prompt the Dosimat to make additions while the refilling of the burette is occurring and consequently such additions will not be made, therefore making the added titration volume incorrect. At the University of Newcastle only 1 mL Dosimats were available so the plunger value remained unchanged at 1 mL for all measurements, however 5 and 10 mL burettes are also available and therefore this precaution was included in the program in case such Dosimats were acquired in the future. For the stepper syringe system three syringe sizes were calibrated for use, namely 1, 5, and 10 mL. The syringe size must be specified for each measurement as the minimal volume entered with each turn of the micrometer differs for each syringe. The minimal volume differences for each syringe can be seen in the user-interface diagram depicted in Figure 2.17.

User-Interfaces for Data Acquisition

The Excel user-interface for each experiment is opened from the Matlab GUI. The different user-interfaces for equilibrium investigations are shown below. The user is required to enter the appropriate information into the 'Solution Information' box and also compose the addition vector, V_{added} , for each measurement. After the measurement is initiated from the Matlab GUI the data is outputted to the predefined columns in the workbook, that is the mV and δmV columns for potentiometric titrations. For spectrophotometric titrations the spectra are outputted into a second worksheet in the workbook in order to maximise the number of available columns, that is 256, for the acquired spectrum.

For the data acquisition user-interfaces the ■ coloured cells required data entry from the user, ■ coloured cells being the automatically calculated data, that is the total

concentration of the components showing the dilution as the titration progresses, and the ■ coloured cells being the data outputted from the experiment.

The benefit of having the data stored in Excel is that data is easily transferable into any format required for the numerous analytical programs that are available. The analysis programs that were developed for our analysis required the data to be in Excel, therefore collecting the data directly in Excel simplified any data transfers that were necessary.

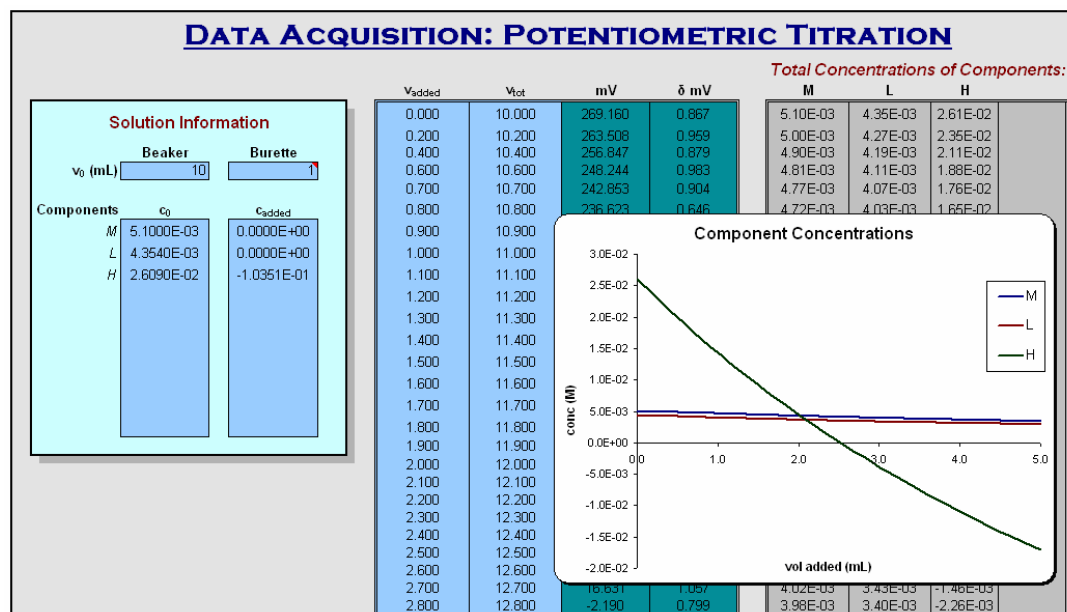


Figure 2.14: Screen shot of the Excel workbook for potentiometric titration data acquisition.

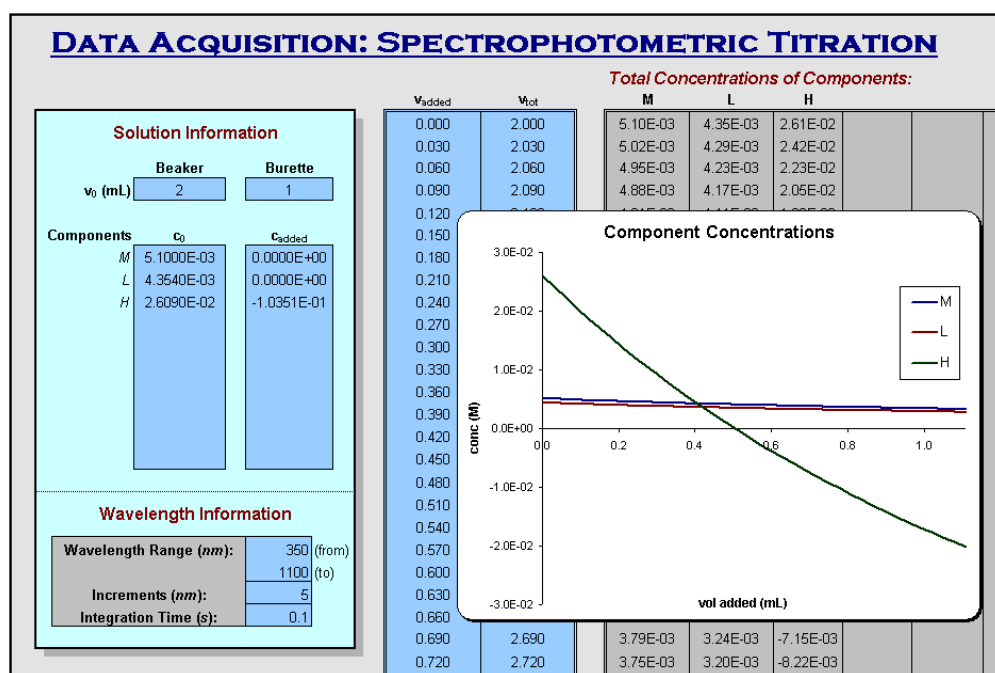


Figure 2.15: Screen shot of the Excel workbook for spectrophotometric titration data acquisition. The acquired spectra are collected in a second worksheet in the workbook.

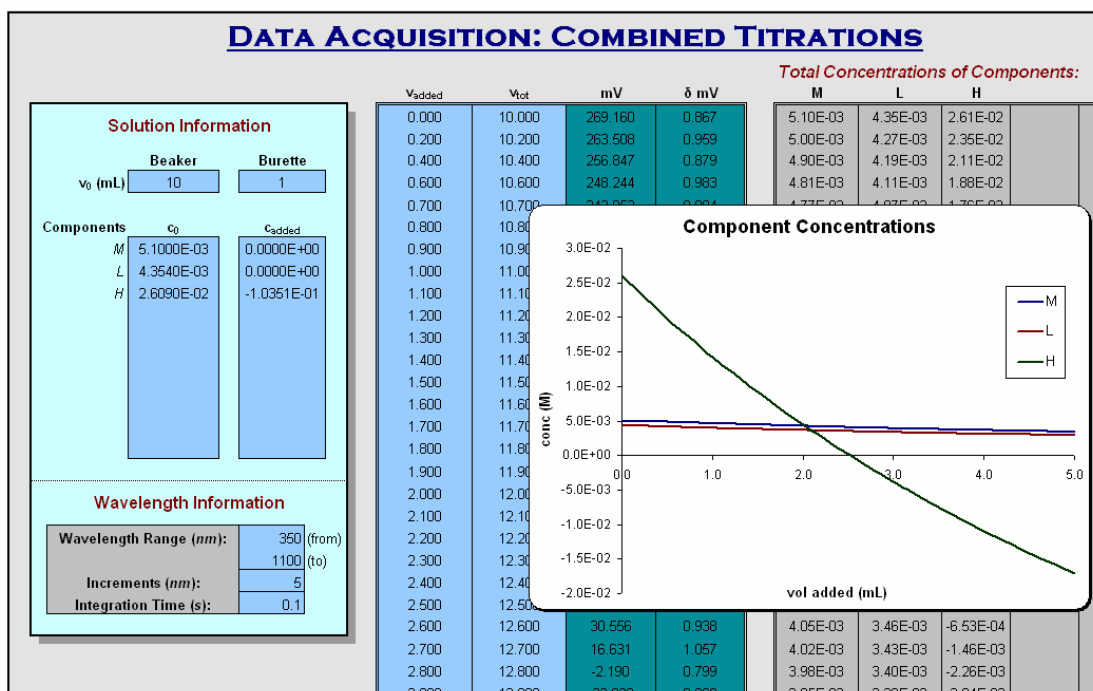


Figure 2.16: Screen shot of the Excel workbook for combined potentiometric and spectrophotometric titration data acquisition. The acquired spectra are collected in a second worksheet in the workbook.

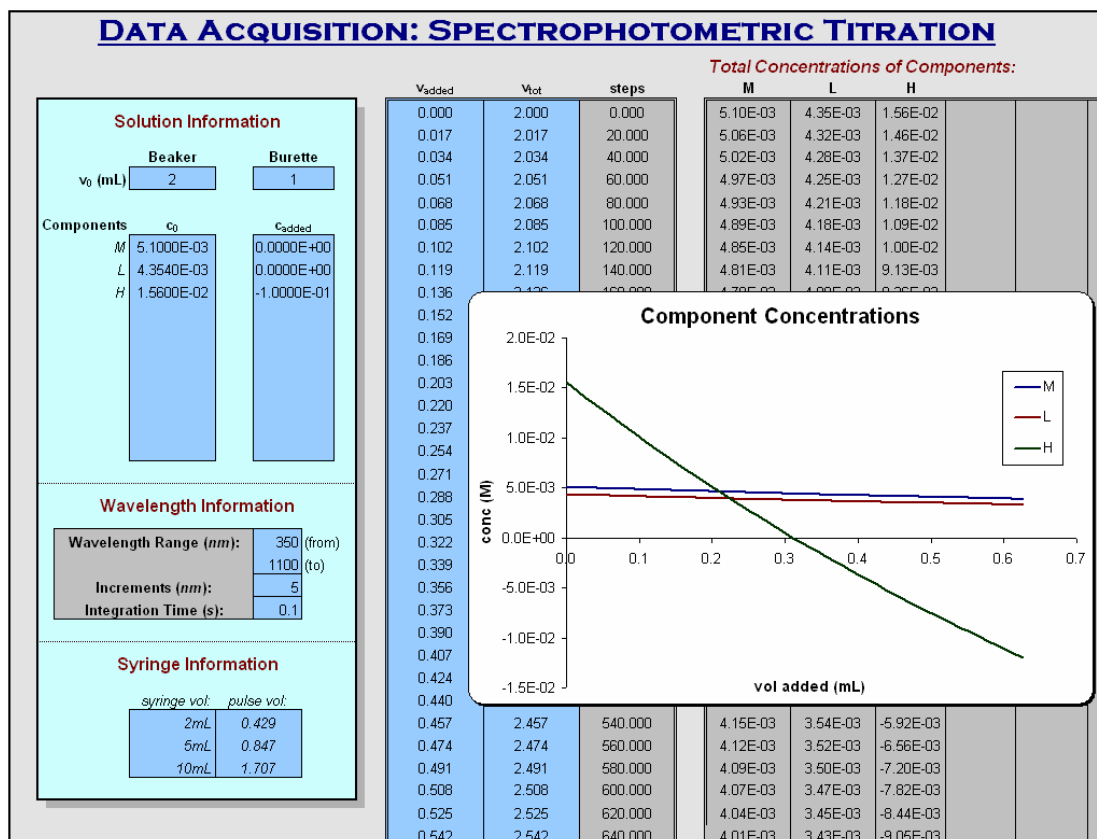


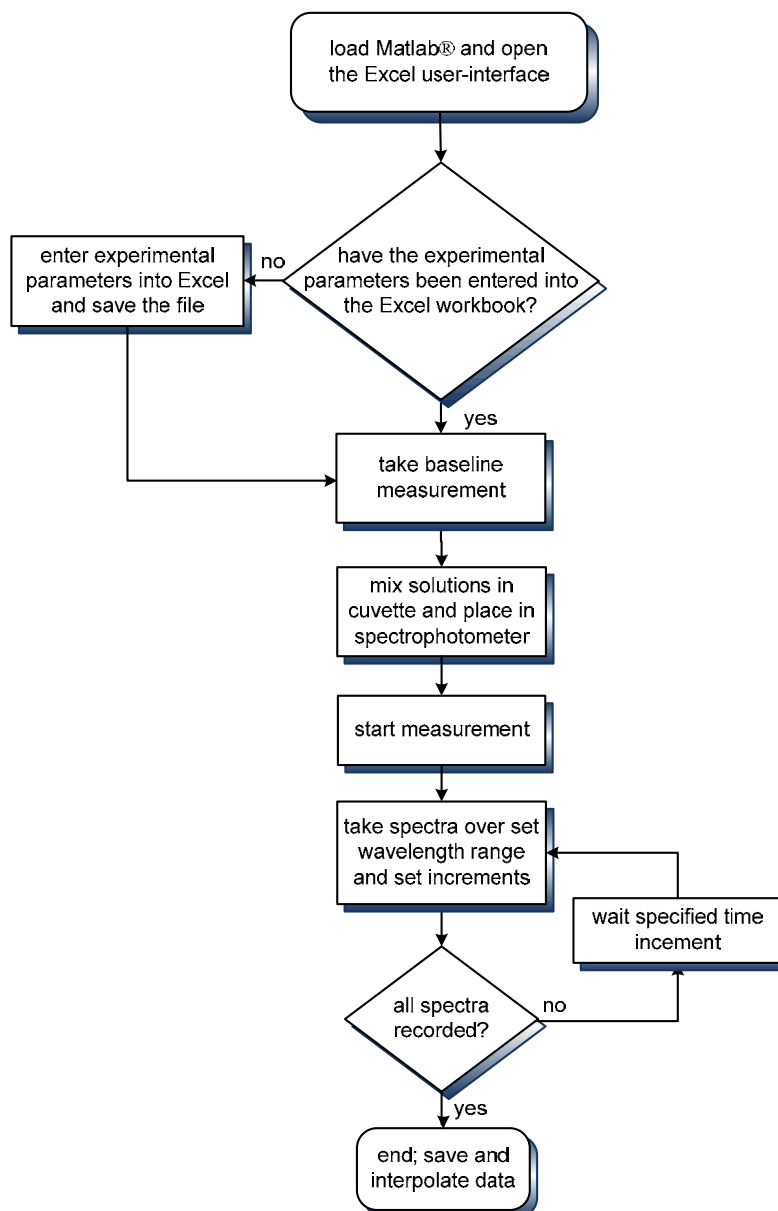
Figure 2.17: Screen shot of the Excel workbook for spectrophotometric titration data acquisition using the stepper syringe instead of the Dosimat. The acquired spectra are collected in a second worksheet in the workbook.

2.2.5.2 Slow Kinetic Reactions

Process Description

For slow kinetic investigations the user is required to specify the wavelength range, increment, and integration time, along with a time vector detailing the time intervals between each measurement. The time vector is similar to the addition vector required for titrations in that the increment between each measurement is variable, as is the total number of measurements taken. For example, the measurement may begin taking scans every minute for the first hour, then every two minutes for the next half an hour followed by scans every five or ten minutes till the reaction is complete.

The data is interpolated at the completion of the measurement to account for the limitation that the entire spectrum is not measured instantaneously. If a large wavelength range, high number of increments, or long integration time were specified each spectral measurement may require time periods greater than 30 seconds, thus the start time of the kinetic trace can be significantly different from the end time. In such cases interpolation to a common time of the data for one spectrum is essential before any data analysis can be performed.



Scheme 2.4: Flow diagram for the acquisition of slow kinetic data.

User-Interface for Data Acquisition

The data required from the user before beginning a slow kinetic measurement is similar to spectrophotometric titrations except no concentration value is needed from the burette as there is no burette system. The initial volume in the cuvette and the reagent concentrations are still required along with a time vector and the wavelength range, increment and integration time. Similarly as with the previous data acquisition user-interfaces, the ■ coloured cells required data entry from the user with the ■ coloured cells being the automatically calculated data, that is, the spectra that are outputted into a second worksheet as with all spectrophotometric experiments.

DATA ACQUISITION: KINETICS

Solution Information		time (mins)
Beaker		0.000
v_0 (mL)	2	1.000
Components		2.000
	c_0	3.000
M	5.1000E-03	4.000
L	4.3540E-03	5.000
H	2.6090E-02	6.000
Wavelength Information		7.000
		8.000
		9.000
		10.000
		11.000
		12.000
		13.000
		14.000
		15.000
		16.000
Wavelength Range (nm):		17.000
Increments (nm):		18.000
Integration Time (s):		19.000
350 (from)		20.000
1100 (to)		21.000
5		22.000
0.1		23.000
		24.000

Figure 2.18: Screen shot of the Excel workbook for spectrophotometric slow kinetic data acquisition. The acquired spectra at each time interval are collected in a second worksheet in the workbook.

2.3 Non-linear Least Squares Data Analysis

2.3.1 Overview

Although modern instrumentation and data acquisition techniques have enabled an increased amount of data to be delivered in a shorter amount of time, computer-assisted analysis is limited by intelligence and by the availability of programs that have the required logic tool applications²³. Since the mid-1960's, the rapid advancement of computer capabilities have promoted the importance of the development of modern analytical programs to evaluate data. Many papers have been published which detail techniques to determine the parameters involved with the analysis of potentiometric titration data, such as the end-point, liquid junction and standard potentials, analytical concentrations of the reagents, protonation and equilibrium constants and so forth. For examples of these see Section 2.3.10.

In data analysis the aim is to try to extract useful information from a set of measured data. The objective of model based analysis is to obtain from the measurement the basic parameters of the process, that is, the rate constants in kinetics and the equilibrium constants in equilibrium investigations and the determination of the correct model. Determining such constants is of great value as it makes it possible to predict what the chemical behaviour may be under different, yet unexplored, conditions. It also enables comparisons with other systems that can result in the elucidation of useful information such as trends in particular systems, and can also aid in the explanation of interesting or unexpected results.

There exists already an enormous number of published rate and equilibrium constants, and with ardent current research in this field of chemistry, the number is constantly increasing. Depending on the nature of the data that has been collected, additional information may be extracted along with the determination of particular constants. For example, if absorption spectra are acquired as part of the data acquisition process it is also possible to determine the molar absorptivity spectra of all absorbing species, even if they only exist as transitory minor species. Resolving such spectra is a great advantage as it can enable the structural analysis of species, which is not easily achieved otherwise²⁴.

The two analytical techniques developed in this research in order to determine equilibrium solution processes and reaction rate constants were based on the nonlinear least-squares fitting of parameters to a chemical model that described the collected data. Equilibrium and kinetic data can generally be described quantitatively by a chemical model based on the law of mass action. In such instances the parameters of interest, such as the equilibrium and rate constants, can be determined by model-based analysis of the appropriate data sets. The computations developed for the numerical analysis of the equilibrium and kinetic processes obviously had differences. There are, however, several aspects of the two types of data analysis are essentially identical, for example the calculation residuals and the minimisation of the sum of squares, which are discussed in detail in Section 2.3.5.

The data analysis developed can be classed as ‘hard modelling’ analysis, the alternative being ‘soft modelling’ analysis where, for example, data sets are decomposed into concentration profiles and absorption spectra without the use of a chemical model. Hard modelling analysis has significant advantages when compared to soft modelling

methods²⁵. Model free methods lack the framework provided by the proposed chemical model used in hard modelling methods and are therefore significantly less robust. Hard modelling involves minimisation of the squared differences between the measured and calculated data, the latter being determined from the model and relevant parameters. This process can be described by the general equation shown below, where **D** represents the measured data, *p* are the parameters of the system and model is the hypothesised model that defines the chemical process.

$$ssq = f(\mathbf{D}, p, \text{model}) \quad (2.1)$$

There are three distinct components that describe hard modelling analytical methods. The first and most important is the measured data that are to be analysed. Secondly, a model has to be provided that enables the chosen parameters to be fitted to the data. The third aspect is the fitting routine which determines the most likely values for the parameters, for example, the rate constant values that are valid for the particular model²⁴. These three components are discussed in more detail in the following sections.

2.3.2 Globalisation of the Data

Some commonly used data acquisition techniques have been thoroughly discussed previously in Section 2.2. Data are the central component of any data analysis and as such it is important to understand the structure of the data that has been acquired to be used in the analysis. In modern analysis techniques globalisation of the data has been established, the basic concept of global analysis has been previously introduced in Chapter 1.6.1. The technique is re-examined here to highlight the importance of the structure of data and to ensure that the analysis is robust, resulting in the extraction of the maximum amount chemical data possible from each measurement. The example of multivariate spectroscopic data has been used to describe globalisation, but the concepts can be easily applied to other types of data, such as the electrode response in potentiometric measurements.

For bivariate spectroscopic measurements first order global analysis of all data at all wavelengths has substantial advantages such as increased robustness of the analysis, better definition of the parameters, improved statistical analysis and circumventing the necessity of hand-picking 'good' wavelengths. The task of fitting the large number of parameters required for first order global analysis of bivariate data may seem

tremendous as such analysis requires the determination of the rate constants from numerous wavelengths measurements, with different initial concentrations for each measurement. However, appropriate algorithms are well established and nowadays the fitting of bivariate data is standard, while, unfortunately, still not embraced by all researchers. The methodologies required for the appropriate analysis of bivariate data are discussed later in this chapter.

The global analysis of a series of multivariate data, also known as second order global analysis, is relatively novel and not many examples have been published. The approach of analysing each bivariate data set of a multivariate experiment individually, followed by secondary analysis of the individual results, is still the norm. Analogous to the global analysis of bivariate data the scientific community will need some additional time to generally adapt to the improved methodology of second order global analysis. However, it must be recognised that due to modern techniques it is now as simple to perform principle component analysis or to calibrate a multicomponent system as it was to previously calculate the standard deviation. Evaluating data and extracting the information locked within it is a task that is ever changing as the sophistication and capabilities of modern instrumentation increase. This power must change the way chemists look at data. For example, a multivariate approach to data analysis offers access to information that until recently was invisible to the casual observer¹.

The example of applying second order global analysis in order to determine the activation parameters in kinetic investigations is used here to illustrate the basic principle. The general concept of globalisation is represented in Figure 2.19. The determination of activation energies in kinetics requires measuring the kinetics of a given reaction at several temperatures. Traditionally, the data were fitted individually at each temperature, resulting in a series of rate constants determined at each different measured temperature. Then, in a secondary analysis process, the temperature dependence of the rate constants were analysed in terms of the Arrhenius or the Eyring equation, fitting the activation parameters to the previously determined rate constants. Second order global analysis fits the complete data set in one process, fitting directly the activation parameters. Advantages are similar to those seen with first order global analysis, for instance improved robustness, simpler statistics, and general time savings.

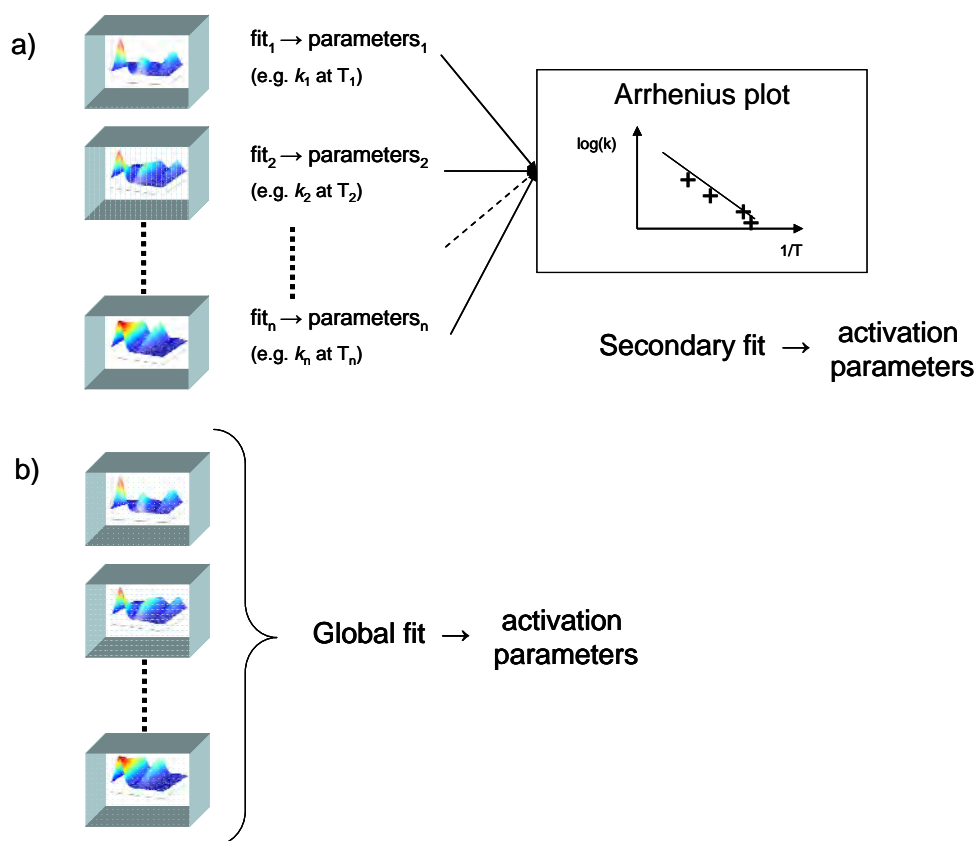


Figure 2.19: Scheme representing a) the traditional analysis of the temperature dependence of a reaction; b) global analysis of data.

2.3.3 Model and Parameters

The second important aspect of data fitting after the collection of that data is the model and its parameters. There are two levels of modelling and it is vital to clearly distinguish between them. There is the primary model that is a chemical model that quantitatively describes the chemical process under investigation. Generally this model defines the concentrations of the interacting species as a function of the independent variable. However, because concentrations are very rarely measured directly a secondary model is required which relates the concentrations of the components to the actual measurements. For example, a typical secondary model is Beer Lambert's law that relates concentrations to the absorption of a solution at a particular wavelength via the molar absorptivities of all absorbing species. Similar laws govern other types of measurements, for example, potentiometry in pH measurements.

Both primary and secondary models are defined by separate types of parameters. The primary chemical model is typically defined by rate or equilibrium constants that define the concentrations as a function of the independent variable, that is, the reaction time or

added reagent. However, it is important to note that many additional numerical values are required for the computation of the concentrations. As an example, the initial concentrations of the reacting components are required in kinetics, or total concentrations of the components in equilibrium studies. Some of these additional parameters are easy to deal with, and for certain cases they can be fitted together with the traditional parameters. However, they can also be difficult to handle and therefore the experimental design has to be carefully planned to avoid intricate problems. In theory, kinetic analyses can be used for quantitative concentration determination, however strong correlations prevent accurate estimations of the concentrations. The number of parameters that quantitatively describe the primary chemical model typically ranges from a few up to ten or twenty.

The secondary model directly relates concentrations to the measurement. A model type that often used is of the kind encountered in UV-Vis spectroscopy where the molar absorptivities of all absorbing species in the reaction define the overall measured absorption. The number of parameters required for the secondary model is typically hundreds to thousands for bi- or multivariate data. Usually, the parameters defining the primary model describing the concentrations are non-linear parameters while those that relate the concentrations to the measurements, such as the molar absorptivities, are linear parameters. As will be discussed later, it is often imperative to distinguish between linear and non-linear parameters.

To further clarify the above concepts, consider a kinetic example, the commonly referred to reaction $X \rightarrow Y \rightarrow Z$.

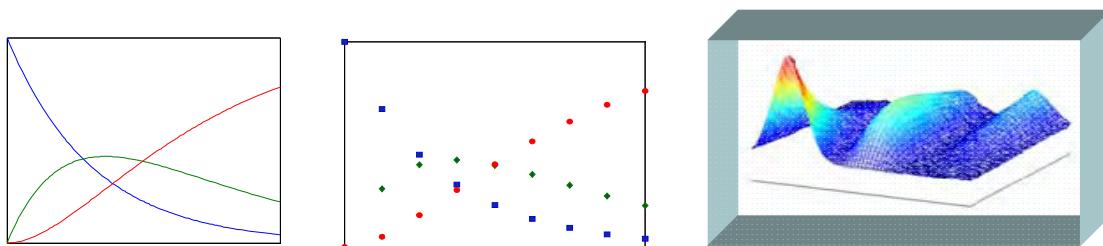


Figure 2.20: Plots showing (a) continuous concentration profiles; (b) discrete concentrations as determined, for example by chromatography; (c) multiwavelength absorption measurements.

Figure 2.20 (a) represents the true concentration profiles of the reacting species as a function of the reaction time as defined by the appropriate set of differential equations. Note that such data are never obtainable experimentally. Part (b) of the figure displays the realistic and experimentally achievable result of a series of concentration profiles,

for example as determined from chromatographic analyses of samples taken during a reaction. The concentration profiles are represented by a set of discrete and not perfect concentrations. The model that describes such a data set consists of a set of differential equations, quantitatively defined by the initial concentrations and rate constants.

2.3.3.1 Spectroscopic Technique

UV-Vis spectroscopy is the most common technique used for kinetic investigations, but alternatives such as NMR or IR spectroscopy are also possible. The technique is also commonly used for equilibrium investigations, the specifics of which are discussed in the next section, as spectroscopy is considered to be the best tool with which to determine pK values especially at low concentrations, provided that the compound possesses pH-dependant UV absorption due to the presence of a chromophore in proximity to the ionisable group²⁶. Figure 2.20(c) represents the absorption spectrum of the reacting solution, measured as a function of time. This data set can be described by the same differential equations and parameters as the data shown in part (b) of the figure.

The raw data for each measurement consists of a matrix the absorption spectra measured as a function of the reaction time, the independent variables being the reaction times at which the data are acquired and the initial concentrations of the reactants. A few assumptions have to be made with regards to the spectra of the components, for example that spectra are constant, that is, independent of variable conditions such as temperature or composition of the reaction solution.

Spectrophotometric methods depend on the fact that when complex formation takes place, the absorption of the new species formed may be considerably different from that of the reactants. This approximation should be valid for most electronic transitions. Further, a linear absorption response is assumed. These prerequisites are based on the theory that Beer-Lambert's Law is valid, which is the governing relationship between concentrations and the measured absorption data. The concentration and absorbance of a solution containing a single chemical species are related by the molar absorptivity of the species, such that the measured absorbance is proportional to the concentration and the path length, as represented by Figure 2.21. The path length is generally constant and equal to 1.0 cm and so can be ignored, which leaves the absorbance proportional to the

species concentration. Fundamentally, the constant of proportionality, that is the molar absorptivity ϵ , is always the same for a given species at a given wavelength.

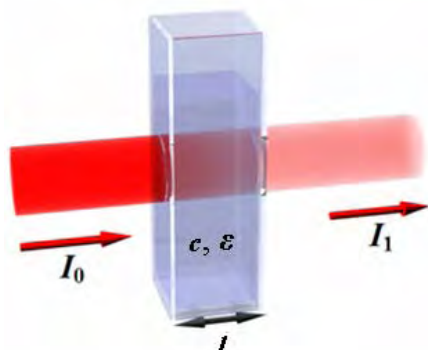


Figure 2.21: Diagram demonstrating Beer-Lambert absorption of a beam of light as it travels through a cuvette of size l containing solution of concentration c and molar absorptivity ϵ ²⁷.

This relation between absorption and concentration is a simple scalar operation. For the example of only one solution containing one absorbing species at a single wavelength, the absorbance is obviously equal to $c \times \epsilon$. Since absorbances are additive if multiple species exist together in solution, Beer-Lambert's law becomes the vector product of the concentrations of the absorbing species and their absorptivities in one solution at a given wavelength. The concept can be further extended to describe the total absorbance of many solutions containing many absorbing species, and measured at many wavelengths, that is the absorbances of multiple constituents, **D**, at the same wavelength are additive as shown in Equation (2.2).

$$\mathbf{D} = c_1 \times \epsilon_1 + c_2 \times \epsilon_2 + \dots + c_n \times \epsilon_n = \mathbf{c} \cdot \mathbf{a} \quad (2.2)$$

This measured absorbance can be extended to a spectrum, which is more than one wavelength, for numerous absorbing species. Such a relationship describing the total absorbance can be expressed in an elegant matrix notation as described by Equation (2.3).

$$\mathbf{D} = \mathbf{CA} + \mathbf{R} \quad (2.3)$$

The matrix **D** contains the measured absorbances of the solution, the rows are a function of wavelength and the columns are a function of reaction time. If ns spectra are acquired at nl wavelengths the dimensions of **D** are $ns \times nl$. According to Beer-Lambert's law the measured absorption spectra, **D**, can be decomposed into the product of a concentration matrix **C** times a matrix of molar absorptivities **A**. The matrix **C**

contains as columns the concentration profiles of the reacting species, in this example that is the concentrations of $[X]$, $[Y]$ and $[Z]$ as a function of the reaction time.

The dimensions of \mathbf{C} are $ns \times nc$ where nc is the number of coloured species, in this example nc is equal to three. The matrix \mathbf{A} contains row-wise the corresponding molar absorption spectra of the three species, its dimensions being $nc \times nl$. Due to noise and the related imperfections of any real measurement, the decomposition does not represent \mathbf{D} perfectly, the matrix \mathbf{R} of residuals being the difference²⁸. The matrix equation can be written as shown below in Scheme 2.5.

$$\begin{array}{c} nl \\ \boxed{\mathbf{D}} \\ ns \end{array} = \begin{array}{c} nc \\ \boxed{\mathbf{C}} \end{array} \times \begin{array}{c} nl \\ \boxed{\mathbf{A}} \\ nc \end{array} + \begin{array}{c} nl \\ \boxed{\mathbf{R}} \\ ns \end{array}$$

Scheme 2.5: Decomposition of spectra \mathbf{D} into corresponding concentration and absorptivity matrices.

The matrix \mathbf{R} is representative of the experimental noise associated with any real measurement.

2.3.3.2 Potentiometric Technique

As an alternative to spectroscopy, electrochemical analyses are also commonly used. Most important are potentiometric pH measurements for equilibrium studies, these types of measurements were applied to our research by using a hydrogen ion selective electrode. However, any ion or metal specific electrode can be used to gather measurements for the process under investigation.

Titration generally serve two different purposes, namely quantitative analyses in analytical chemistry and additionally for the determination of equilibrium constants. These two objectives require only marginally different experimentation and very minor adaptation of data analysis software. The first titration is the most widespread application of equilibrium studies in analytical chemistry. It is where titrations are used for the quantitative analyses of one or more components and involves the determination of the concentration of an acid or a base with the determination of the equivalence or end-point being the main objective^{29,30}. However, with modern digital technology it is no longer necessary to use equivalence points as the basis of a titration. It is enough to determine the consumption of the titrant at suitable pH intervals and use chemometrics to analyse the data. Numerical analysis of the complete titration curve, that is data fitting with these concentrations as parameters, rather than using a specialised method for the detection of the endpoint, is more reliable and certainly more instructive.

For the second class of titrations, the determination of equilibrium constants, controlled displacement of a chemical equilibrium occurs through the addition of titrant. In most instances, the titrant is a strong base or acid and the measurement produces a recordable signal such as pH or, as previously discussed, absorbance data. In potentiometric pH measurements the data is gathered as a series of pH values as a function of a component concentration, such as the amount of base or acid added.

The relationship between the concentration of the protons and the measured potential of the pH-electrode is of the form


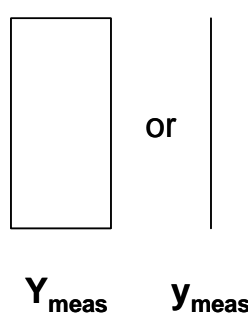

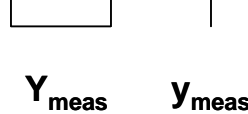
$$E = E_{const} + s \log[H^+] \quad (2.4)$$

In such data sets, the concentrations of the protons, $[H^+]$, are defined by the primary chemical model and they form one of the concentration profiles or column of the matrix **C**. The parameters E_{const} and s are essentially the electrode calibration parameters that can be determined independently or fitted as part of the measurement. For further discussions regarding the electrode parameter calibration parameters refer to Chapter 6.

2.3.4 Primary Chemical Models

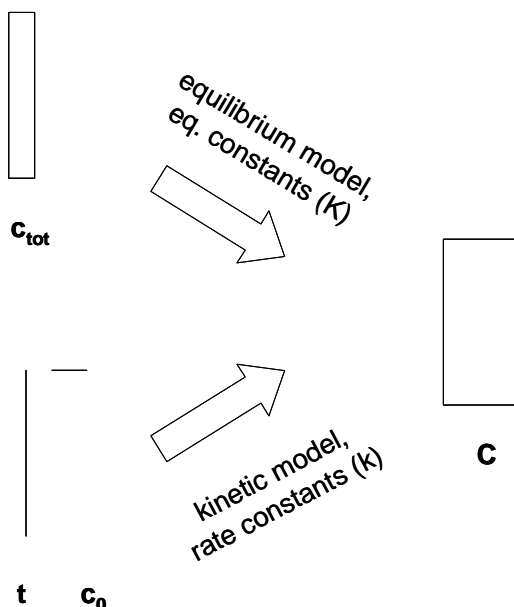
The primary chemical model essentially defines the concentrations of the reacting species as a function of the progress of the chemical process. The core of model-based data fitting is the computation of the concentration profiles of all interacting species. The actual computation of these concentrations is naturally strongly dependent on the type of process being analysed. While there are a large number of processes investigated by chemists, it is possible to group most into a few classes. The most important of these classes includes equilibrium studies and kinetic analysis which were both studied in our investigations.

As you would expect, the variables are different for both of these studies. In an equilibrium investigation the independent variable is typically the volume of added reagent with the dependent variable being the pH reading or spectrum measured as a function of the reagent addition. In kinetics the independent variable is the reaction time and the dependant variable is the absorption readings acquired as a function of time. These variables are represented graphically in Scheme 2.6.

	Independent variables, experimental conditions	Dependent variables, measured data
Kinetic study:		
Equilibrium study:		

Scheme 2.6: Graphical representation of the sets of independent and dependant variables for kinetic and equilibrium studies.

The main difference between software dealing with equilibrium and kinetic investigations is the computation of the concentration matrix that is based on the independent variables of the measurement and defined by the primary chemical model. For both equilibrium and kinetic investigations establishing the relationship between the computed concentrations and the actual measurement is identical. It does, however, depend on the type of data that are collected, that is either spectrophotometric or potentiometric data. Hence, the algorithms required to compute the concentration profiles are different for each type of investigation as they are based on the independent variables defined by the type of experiment. The calculation of the concentration profile is shown graphically in Scheme 2.7. These concentration profiles, together with the primary chemical model, allow the concentration of all species in the reaction to be determined.



Scheme 2.7: The independent variables and the parameters are required for the computation of the matrix **C** of concentration profiles.

2.3.4.1 Kinetic Analysis, Differential Equations

Kinetic processes can be defined by a set of differential equations of variable complexity. In traditional kinetics all starting materials are mixed at time zero and the progress of the reaction is then monitored by any appropriate technique, commonly spectroscopy. Usually a reaction is comprised of two to three reactants, however, there is no theoretical limit to the complexity of reactions investigated and thus no limit to the number of initial concentrations.

For simple kinetic cases the differential equations are relatively straightforward. However, few sets of differential equations representing chemical reactions can be integrated analytically and most require numerical integration. In order to demonstrate how the primary chemical model can be analysed we consider the earlier example as it is a simple kinetic process that allows analytical integration.



The set of differential equations, ODEs, for this reaction scheme are:

$$\begin{aligned}\frac{d[X]}{dt} &= -k_1 [X], \\ \frac{d[Y]}{dt} &= k_1 [X] - k_2 [Y], \\ \frac{d[Z]}{dt} &= k_2 [Y]\end{aligned}\tag{2.6}$$

The integration of the above ordinary system of differential equations (ODEs) results in the following equations for species concentrations.

$$\begin{aligned}[X] &= [X]_0 e^{-k_1 t}, \\ [Y] &= [X]_0 \frac{k_1}{k_2 - k_1} (e^{-k_1 t} - e^{-k_2 t}) \quad ([Y]_0, [Z]_0 = 0, k_1 \neq k_2) \\ [Z] &= [X]_0 - [X] - [Y]\end{aligned}\tag{2.7}$$

The concentration profiles that were previously shown in Figure 2.20 were computed using Equation (2.7).

Any reaction scheme comprised of only first order reactions can be integrated explicitly. The concentration profiles are then always linear combinations of exponential functions with observed rate constants that are functions of the actual first order rate constant. Unfortunately, often the relationship is not unique thus making it impossible to uniquely determine the chemical rate constants from the observed exponentials. In the above example, it is not generally possible to uniquely assign the two observed rate constants to the real ones.

Most reaction mechanisms result in sets of ODEs for which there is no explicit solution. For such cases it is mandatory that the concentration profiles are computed based on the numerical integration of the ODEs which define the reaction mechanism in combination with the measured data and the non-linear parameters, that is, the rate constants²⁵. The numerical integration process involves approximations of the concentrations based on the differential equations defined by the proposed mechanism, and fortunately this is always possible^[30, 35, 36].

It is beyond the scope of this chapter to introduce the numerical methods for numerical integration of ODEs, suffice it to say that there is a wide range of reliable and fast algorithms available. The appropriate choice of numerical integration routine is dependant on the nature of the reaction scheme of the kinetic system. It is important to refer to suitable manuals in order to determine which solver is best suited to the analysis

and select an appropriate algorithm. For 'normal' reactions the standard Runge-Kutta type algorithms with automatic step size control are most appropriate. However, for more complicated kinetic processes other solvers are required as the Runge-Kutta would have excruciatingly long computation times. For examples of other algorithms the Matlab manuals have in-depth information on available numerical integration routines.

It is important to reiterate that the kinetic modelling results in the concentration profiles of all reacting species, computed as a function of reaction time. In the language of Equation (2.3) we compute the matrix **C** that contains, as columns, the concentration profiles of the reacting species. Additional relevant information such as temperature, total initial concentrations, times of measurement of the spectra and amount of added reagent are also part of the experimental parameters.

2.3.4.2 Equilibrium Studies, the Law of Mass Action

Probably the second most important application of model-based data fitting is the analysis of chemical equilibria, the determination of the number and nature of the species formed between a set of interacting components and their equilibrium constants.

Most examples of equilibria can be seen as the formation of complexes between Lewis acids and Lewis bases, more specifically they may include protonation equilibria, and/or the formation of coordination compounds between metal ions and ligands. In aqueous solutions complex formation equilibria are almost always coupled to protonation equilibria as ligands can interact with metal ions as well as protons, as both are Lewis acids.

The nomenclature in equilibrium studies is well established and concise. The basic compounds interacting with each other are called the components and the resulting molecules or complexes are called the species. The interactions are quantitatively described by the law of mass action. The implementation of the law of mass action to equilibrium studies is demonstrated here with an example, the interaction between the three components; copper(II) M^{2+} , protons H^+ , and the ligand ethylenediamine L. The list of potential species formed is long and includes the protonated forms of the ligand, LH^+ and LH_2^{2+} , a series of complexes ML^{2+} , ML_2^{2+} , and ML_3^{2+} , as well as potentially several protonated or deprotonated complexes such as MLH^{3+} . Each equilibria can be defined by the law of mass action. For the example of the species MLH^{3+} application of the law of mass action results in:

$$\beta_{111} = \frac{[MLH^{3+}]}{[M^{2+}][L][H^+]} \quad (2.8)$$

In general terms such an equation can be written for each species formed from the components. In the equation below the first scalar m defines the number of metals, the second l the number of ligands, and the third h the number of protons in the species mlh .

$$mM^{2+} + lL + hH^+ \xrightleftharpoons{\beta_{mlh}} M_m L_l H_h^{(2m+h)+}$$

$$\beta_{mlh} = \frac{[M_m L_l H_h^{(2m+h)+}]}{[M^{2+}]^m [L]^l [H^+]^h} \quad (2.9)$$

For each species formed equations of the type (2.8) and (2.9) can be written. In addition, there are equations for the total concentrations of all components, remembering that all species concentrations must be positive. The method that is generally used to calculate the species concentrations is the well-established Newton-Raphson technique which is based on application of this law of mass action ^[7, 14, 19, 33, 34].

$$\begin{aligned} [M]_{tot} &= \sum m[M_m L_l H_h] = \sum m\beta_{mlh}[M]^m [L]^l [H]^h \\ [L]_{tot} &= \sum l[M_m L_l H_h] = \sum l\beta_{mlh}[M]^m [L]^l [H]^h \\ [H]_{tot} &= \sum h[M_m L_l H_h] = \sum h\beta_{mlh}[M]^m [L]^l [H]^h \end{aligned} \quad (2.10)$$

Altogether there are as many equations as there are species, given that components are species as well. It can be shown that for such systems of equations there is exactly one physically possible solution, which is of course the mathematical solution realised in the actual solution ²⁸.

2.3.4.3 Non-Ideal Situations

The law of mass action as used in equilibrium studies, or the set of differential equations in kinetics, are only strictly valid for ideal situations, that is, isothermal, zero- or at least constant ionic strength, constant pH in kinetics, and so forth. In the research laboratory such conditions can essentially be maintained, but in industrial situations such control is usually not possible. Recent developments attempt to model such inconsistencies and thus allow the model-based analysis of such non-ideal data sets.

It is relatively straightforward to model changing temperatures ³¹. All that is required is to define the rate constants in Equation (2.6) as a function of the temperature. In

engineering the Arrhenius Equation (2.11) is used, whereas in more fundamental scientific investigations the Eyring Equation (2.12) is applied instead.

$$k = Ae^{\frac{E_a}{RT}} \quad (2.11)$$

$$k = \frac{k'T}{h} e^{\frac{\Delta H^\ddagger - T\Delta S^\ddagger}{RT}} \quad (2.12)$$

In the above equations, A is a pre-exponential factor, R the molar gas constant, k' the Boltzmann constant, h Planck's constant, T the temperature in Kelvin, E_a the activation energy, ΔH^\ddagger the activation enthalpy and ΔS^\ddagger the activation entropy.

Non-constant ionic strength is another difficulty that traditionally has been circumvented by the addition of an excess concentration of an inert salt to the reaction solutions. This reduces ionic strength fluctuations, however, the introduction of such salts can cause interferences. It is routine to do this in academic research, but not feasible in industrial situations. The computational remedy here is to replace the concentrations in Equation (2.6) or (2.8) with the activities of the species. Activity coefficients mainly depend on the ionic strength and there are several approximations that can be applied. The simple ones are adequate for low concentrations, also low ionic strength, however, at high concentrations the approximations are poorer, even if more complex equations are used for the approximation. The standard Debye-Hückel equation is given by Equation (2.13) where z is the absolute value of the charge of the particular species, a is its effective radius, including the closely bound solvent molecules, μ is the ionic strength and A and B are constants with values of respectively 0.51 and 0.33 at 25°C in water.

$$\log(\gamma) = -\frac{Az\sqrt{\mu}}{1 + Ba\sqrt{\mu}} \quad (2.13)$$

Implementation of activities into the ODEs is relatively straightforward, however implementation into equilibrium calculations are more difficult and require additional iterative loops as concentrations, ionic strength and activity coefficients are always coupled.

Similar to the addition of inert salts to maintain ionic strength, the addition of buffers is done to maintain constant pH of a solution for kinetic investigations. As with the salts, buffers also can interfere with the actual reaction under investigation, therefore ideally

reactions should be performed with no buffers are added. The principal reason for the addition of buffers is due to the computational difficulties that arise from the pH varying during the process. Recent developments attempt at incorporating protonation equilibria into the ODEs. This is achieved by taking into account the changes in pH throughout the measurement, due to the shifting protonation equilibria, and incorporating knowledge of the pH into the numerical integration of the differential equations that describe the reaction. Hence, the pH can vary throughout the measurement, removing the need for buffers³².

In general, modern modelling software attempts to incorporate non-ideal situations into the computations, thus avoiding external control of the temperature, ionic strength, pH and so forth. This is useful in academic investigations as it simplifies experimentation. It is essential for the analysis of industrial processes where control of the external factors is not possible and often not even temperature control is sufficient. While most of the above corrections are based on approximations and thus are not perfect, these approximate calculations are usually preferable to either ignoring the changes altogether, or to the experimental difficulties encountered with external control.

2.3.5 Fitting the Parameters

2.3.5.1 Computing the Calculated Data

Measured data, \mathbf{D}_{meas} , as distinguished from theoretically perfect data, are always corrupted by experimental errors, for example instrumental noise as previously mentioned. The true data are never known, but the idea of data fitting is to find a calculated set of data, \mathbf{D}_{calc} , which resembles the measured data as closely as possible. This calculated data set is defined by a model, that is both the primary chemical model and the secondary model that defines the type of measurement and the collection of required parameters.

Any variables that are required to compute \mathbf{D}_{calc} , of which \mathbf{d}_{calc} is just a special monovariate case, are parameters that can potentially be fitted. Traditional parameters include the rate constants in a kinetic study and equilibrium constants in an equilibrium study. There are also less obvious parameters that can be fitted, for example the initial concentrations of the reagents in the investigation, the calibration parameters of the electrode for potentiometric experiments, and also the molar absorptivities of the different species in a spectrophotometric investigation. In fact, for spectrophotometric

measurements the complete matrix of absorptivities is comprised of unknown parameters. Calculation of the dependant variable, that is the calculated data, can be written in a generalised way, indicating that the model and its associated parameters are what completely define the calculated data.

$$\mathbf{D}_{\text{calc}} = f(\text{parameters}, \text{model}) \quad (2.14)$$

The list of potential parameters can be long and care must be taken when fitting many of them. The longer the list of parameters, the more difficult the fit, and the more likely there will be strong correlations. If badly defined or strongly correlating parameters are fitted the resulting optimised parameters will be very poorly defined. This is apparent to some extent from the error margins, but not all fitting techniques supply them and in these cases the problem can easily remain unnoticed.

2.3.5.2 The Residuals and Sum of Squares

As previously defined in Equation (2.3) and depicted in Scheme 2.4 the difference between the measured and calculated data is known as the residuals \mathbf{R} .

$$\mathbf{D}_{\text{meas}} = \mathbf{D}_{\text{calc}} + \mathbf{R} \quad (2.15)$$

In very broad terms, the task of the fitting algorithm is to determine, for a given model, those hopefully unique values for the parameters for which the re-calculated measurements \mathbf{D}_{calc} match, as close as possible, the measured data. The expression 'as close as possible' requires attention as there are different options available to define the quality of the fit. An example of a possible definition is the sum over the absolute values of all elements of \mathbf{R} , another is the minimisation of the largest element of \mathbf{R} . For several reasons, including statistical and computational rationales, it is best to minimise the sum over all the squares, *ssq*, of the elements of the residual matrix \mathbf{R} . The *ssq* difference between the experimental and calculated values provides a direct measure of the accuracy of the calculations over the whole range of the experiment. It can also be indicative of the stability of the calculated constants and other relevant parameters for the representation of the complex system under investigation, however even if a *ssq* value is small parameters may still be poorly defined and individual error estimates should also be taken into consideration. The calculation of the *ssq* is the almost universally accepted measure of the similarity between data sets.

$$\mathbf{R} = \mathbf{D}_{\text{meas}} - \mathbf{D}_{\text{calc}} \quad (2.16)$$

$$\text{quality of fit} = ssq = \sum_{\text{all } i} R_i^2 \quad (2.17)$$

The statistical reasons for the minimisation of ssq being the most common approach for determining the quality of fit between the measured and calculated data are that for normally distributed noise, the minimisation of ssq results in the most likely outcome^{33, 34}. More importantly, ssq based algorithms can be written very efficiently and thus are much faster than any of the alternatives. Even though data are not always arranged in an efficient rectangular array or a matrix, Figure 2.2 indicates that any number of experimental data, arranged in any way, can be used for the analysis. In any instance the summation in Equation (2.17) has to be done over all elements of a generalised array of residuals. For the analytical method developed in our research all data and residuals were arranged as simple matrices for the calculation of ssq .

Combining Equations (2.16) and (2.17) clearly demonstrates that ssq is a function of the parameters, and of course of the model and the data themselves. The model, together with the parameters, allows the computation of \mathbf{D}_{calc} , its difference to \mathbf{D}_{meas} defining the residuals \mathbf{R} . It is obvious that the smaller the number of parameters, then the easier the task of fitting them must be.

The task of the fitting procedure is, for a given model, to determine that set of parameters for which the fit is optimal, that is results in a minimal ssq value. If the proposed model adequately represents the data, the residuals should form a random pattern with the residual mean equal to zero and the standard deviation of residuals being near to experimental noise. The determination of the actual correct model for a given process is a completely different issue and a much more difficult task.

2.3.6 Linear and Non-linear Parameters

The distinction between the primary chemical model and the secondary model which relates the concentrations to the measured signal, and the differences between the parameters that define the two models, have been previously discussed in Section 2.3.3. In summary, the primary chemical model firstly requires parameters for the quantitative description of the concentrations, that is the matrix \mathbf{C} , and the secondary model requires the kind of parameters as those collected in the matrix \mathbf{A} , which are the molar absorptivities for the case of absorption spectroscopy, see Equation (2.3), or in other instances parameters of a similar kind.

Both spectroscopic and potentiometric data can be modelled by both non-linear and linear parameters. The parameters describing the primary chemical model are usually a few non-linear parameters. They are collected in a vector \mathbf{p} as shown in Equation (2.18). Alternatively, the parameters that relate the concentrations to the measurement, that is the parameters that define the secondary model, are numerous and usually linear parameters. In the case of multiwavelength spectroscopic measurements, the absorption spectra of coloured species, that is the matrix \mathbf{A} of molar absorptivities, are linear parameters. In potentiometric measurements the linear parameters are the calibration parameters of the electrode, as previously expressed in Equation (2.4).

$$\mathbf{D}_{\text{calc}} = \mathbf{C}(\mathbf{p})\mathbf{A} + \mathbf{R} \quad (2.18)$$

Non-linear parameters, those collected in the vector \mathbf{p} , require an iterative algorithm that begins with initial guesses and converges towards the optimal solution in a reasonable amount of iterations and time³⁵. However, the often numerous linear parameters can instead be 'fitted' using explicit equations, and can therefore be effectively eliminated from the iterative process required for the refinement of the non-linear parameters. It is crucial to deal with the two parameter types separately, that is iteratively refining only the non-linear parameters while explicitly calculating the linear ones.

Models that include Linear and Non-linear Parameters

As previously stated many models are defined by a combination of non-linear and linear parameters and these parameters must be treated separately. For any set of non-linear parameters, the primary chemical model is used to calculate the concentration profiles, the matrix \mathbf{C} , as demonstrated earlier. The corresponding linear parameters are computed explicitly using Equation (2.23), the calculation of which is explained in the following section. Depending on the size of the matrix \mathbf{A} of linear parameters, the number of parameters to be fitted iteratively can be dramatically reduced by elimination of these linear ones. This leaves the computation of the non-linear parameters, and therefore the computation of ssq is a function of the non-linear parameters \mathbf{p} only as the linear parameters have effectively been eliminated.

2.3.7 Linear Parameters

It is possible to develop the equations required for the least-squares fitting of linear parameters geometrically. Due to the limitation of the human imagination to three dimensions the model is restricted accordingly. Hence, the fitting is applied to

monivariate data, for example spectrophotometric measurements at only one wavelength. The example is also restricted to a two-component system, which means the matrix \mathbf{C} has only two columns. In such a case the matrices \mathbf{D}_{meas} , \mathbf{D}_{calc} , \mathbf{R} and \mathbf{A} from Equation (2.18) are reduced to column vectors \mathbf{d}_{meas} , \mathbf{d}_{calc} , \mathbf{r} and \mathbf{a} of appropriate length.

$$\mathbf{d}_{\text{meas}} = \mathbf{d}_{\text{calc}} + \mathbf{r} = \mathbf{C}\mathbf{a} + \mathbf{r} \quad (2.19)$$

The concept could also be developed using potentiometric measurements and the corresponding equations, however it is more instructive to discuss spectroscopic data as the theory can then be extended to multivariate considerations, whereas potentiometry is only monivariate.

In the above equation the design matrix \mathbf{C} has two columns and \mathbf{a} is a two element column vector whose values have to be fitted, these are the two linear parameters. The situation is represented in Figure 2.22.

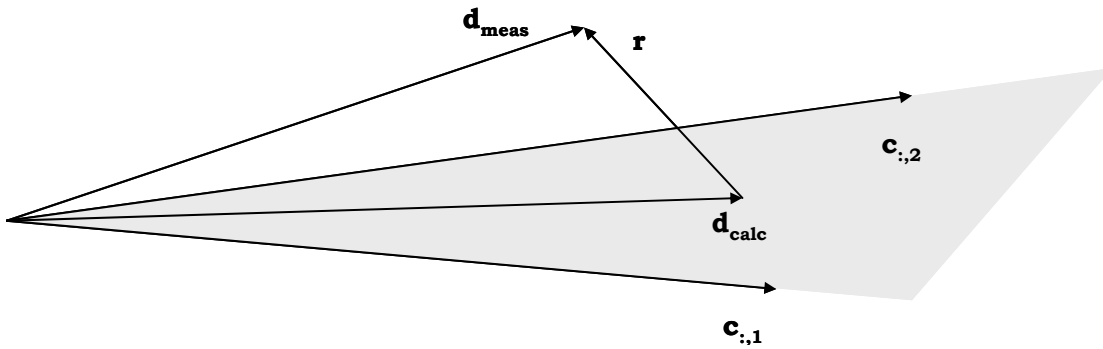


Figure 2.22: Diagram describing the residual calculation, \mathbf{r} , resulting from the difference between the measured data, \mathbf{d}_{meas} , and the data calculated, \mathbf{d}_{calc} , from the two shown parameters.

The calculated vector $\mathbf{d}_{\text{calc}} = \mathbf{C}\mathbf{a}$ is a linear combination of the column vectors of the matrix \mathbf{C} . Any value of \mathbf{d}_{calc} is located somewhere on the plane defined by the two column vectors $\mathbf{c}_{:,1}$ and $\mathbf{c}_{:,2}$. This plane is indicated in the figure by the grey shading. As ssq is the square of the length of the residual vector \mathbf{r} , the question of data fitting can be posed as: which point on the grey \mathbf{C} -plane is closest to \mathbf{d}_{meas} ? Obviously the best point on that plane, that is the optimal \mathbf{d}_{calc} vector, can be found directly under the measurement vector, \mathbf{d}_{meas} . More precisely, the residual vector \mathbf{r} must be perpendicular to the plane \mathbf{C} , thus the product $\mathbf{C}^t\mathbf{r} = 0$. This concept can be expanded in the following matrix equations:

$$\begin{aligned} \mathbf{C}^t \mathbf{r} &= \mathbf{C}^t (\mathbf{d}_{\text{meas}} - \mathbf{C} \mathbf{a}) = 0 \\ \mathbf{C}^t \mathbf{d}_{\text{meas}} &= \mathbf{C}^t \mathbf{C} \mathbf{a} \\ \mathbf{a} &= (\mathbf{C}^t \mathbf{C})^{-1} \mathbf{C}^t \mathbf{d}_{\text{meas}} \end{aligned} \quad (2.20)$$

The least-squares estimate for the linear parameter vector \mathbf{a} can therefore be computed explicitly by a simple matrix equation.

The matrix $(\mathbf{C}^t \mathbf{C})^{-1} \mathbf{C}^t$ is known as the pseudo-inverse of \mathbf{C} , and for convenience is also written as \mathbf{C}^+ . While the pseudo-inverse can be calculated as $\mathbf{C}^+ = (\mathbf{C}^t \mathbf{C})^{-1} \mathbf{C}^t$, this is numerically not advisable and there are several preferable algorithms that can be used for the calculation. Matlab has developed its own highly elegant notation for the computation of the pseudo-inverse as shown in Equation (2.21). The algorithm used for this line of code in Matlab is superior to $(\mathbf{C}^t \mathbf{C})^{-1} \mathbf{C}^t$ calculations.

$$\mathbf{a} = \mathbf{C} \backslash \mathbf{d}_{\text{meas}} \quad (2.21)$$

For multiwavelength data, Equation (2.19) is straightforwardly expanded to a matrix equation:

$$\mathbf{D}_{\text{meas}} = \mathbf{D}_{\text{calc}} + \mathbf{R} = \mathbf{C} \mathbf{A} + \mathbf{R} \quad (2.22)$$

The least squares estimate for the matrix \mathbf{A} for the given matrices \mathbf{D}_{meas} and \mathbf{C} is computed by the same pseudo-inverse of \mathbf{C} :

$$\begin{aligned} \mathbf{A} &= (\mathbf{C}^t \mathbf{C})^{-1} \mathbf{C}^t \mathbf{D}_{\text{meas}} = \mathbf{C}^+ \mathbf{D}_{\text{meas}} \\ \text{or in Matlab} \\ \mathbf{A} &= \mathbf{C} \backslash \mathbf{D}_{\text{meas}} \end{aligned} \quad (2.23)$$

Alternatively, if \mathbf{D}_{meas} and \mathbf{A} are given, then Equation (2.24) can be rearranged to result in the explicit equation that calculates the least-squares estimate of the best matrix \mathbf{C} . However, the programs developed at the University of Newcastle were intended to determine \mathbf{A} and so this option was not implemented, although theoretically it would be a simple modification.

$$\begin{aligned} \mathbf{C} &= \mathbf{D}_{\text{meas}} \mathbf{A}^t (\mathbf{A} \mathbf{A}^t)^{-1} = \mathbf{D}_{\text{meas}} \mathbf{A}^+ \\ \text{or in Matlab} \\ \mathbf{C} &= \mathbf{D}_{\text{meas}} / \mathbf{A} \end{aligned} \quad (2.24)$$

Any least-squares problem that can be formulated in such a matrix equation can be resolved explicitly by either of the two Equations (2.23) or (2.24). As an example

polynomial fits of any degree can be formulated in such a way. The popular Savitzky-Golay filter for data smoothing and interpolation is probably the most relevant application of polynomial fitting in chemistry²⁸.

2.3.8 Non-linear Parameters - Least-squares Fitting

The algorithms for the least-squares fitting of non-linear parameters are necessarily iterative processes^{34, 36}, and there are several algorithms available for such a task. The equations governing the commonly used Newton-Gauss algorithm are based on a truncated Taylor series expansion of the sum of squares as a function of the parameters. The basics of the algorithm are demonstrated in a graphical representation shown in Figure 2.23, essentially starting from an initial set of estimated values for the parameters, the values are varied systematically until the minimal *ssq* is found.

Figure 2.23 displays the situation for a two-parameter case, p_1 and p_2 . The *ssq* is graphed as a function of both parameters, and is represented by the grey surface in the figure. The algorithm starts with initial guesses p_{10} and p_{20} for the parameters, and the corresponding $ssq(p(1,2)_0)$ is computed, the dot marker in the figure shows this point ($p_{10}, p_{20}, ssq(p(1,2)_0)$).

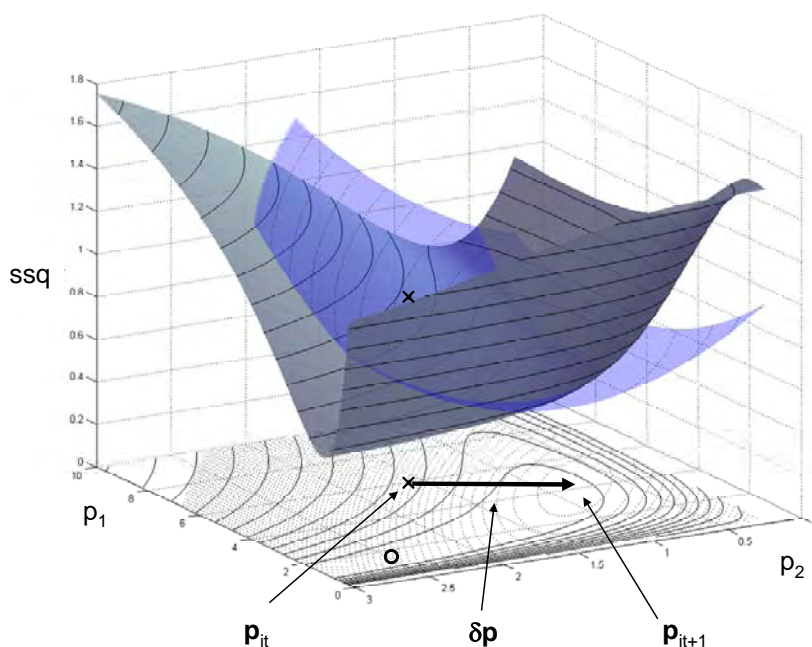


Figure 2.23: Graphical representation of the Newton-Gauss fitting procedure. The grey surface represents the *ssq* as a function of the parameters p_1 and p_2 ; the blue surface is the parabolic surface calculated at the initial parameter estimates shown by the dot marker.

The next step is the approximation of a parabolic hyper-surface to the curve at this point. This requires the computation of the first and second derivative of the curve at $(p1_0, p2_0, ssq(p(1,2)_0))$. The minimum of this parabolic hyper-surface is calculated explicitly providing the new parameter estimates, $p1_1$ and $p2_1$, hopefully closer to the best values for $p1$ and $p2$. The $ssq(p(1,2)_1)$ is then computed using the new parameter estimates $p1_1$ and $p2_1$. Then first and second derivatives and a new parabolic hyper-surface approximating the curve at $(p1_1, p2_1, ssq(p(1,2)_1))$ is calculated. In this example, the new parabola will very closely represent the true curve at the minimum. Note that the parameters $p1$ and $p2$ will both be non-linear parameters if all linear parameters have been eliminated. Linear parameters can be eliminated by computing them explicitly using Equation (2.23), allowing the ssq to be computed as a function of the non-linear parameters only, as shown below in Equation (2.25) where \mathbf{C} is the concentration profile defined by the model and non-linear parameters \mathbf{p} .

$$\begin{aligned}
 \mathbf{C} &= f(\text{model}, \mathbf{p}) \\
 \mathbf{A} &= \mathbf{C}^+ \mathbf{D}_{\text{meas}} \\
 \mathbf{R} &= \mathbf{D}_{\text{meas}} - \mathbf{C}\mathbf{A} = \mathbf{D}_{\text{meas}} - \mathbf{C}\mathbf{C}^+ \mathbf{D}_{\text{meas}} \\
 ssq &= \sum_i \sum_j R_{i,j}^2 = f(\text{model}, \mathbf{p})
 \end{aligned} \tag{2.25}$$

Closer inspection of Figure 2.23 reveals that the iterative process will converge smoothly and fast if the initial guesses $p1_0$ and $p2_0$ were chosen close to the minimum. If, however, the initial guesses were further away from the minimum, the approximated parabolic hyper-surface would be poorer, resulting in the next estimate for the parameters $p1_1$ and $p2_1$ being even further away. This means there would be no convergence and that the algorithm might ultimately collapse. The Levenberg-Marquardt addition to the algorithm addresses such situations, and will later be discussed, see Equation (2.29).

The Hessian and the Jacobian

As mentioned before in order to calculate the parabolic hyper-surface the first and second derivatives of ssq with respect to the parameters $(\frac{\partial ssq}{\partial \mathbf{p}}$ and $\frac{\partial^2 ssq}{\partial \mathbf{p}^2})$ have to be computed. The derivatives can be conveniently collected in a vector \mathbf{d} and a matrix \mathbf{H} as defined in Equations (2.26) and (2.27).

$$\mathbf{d} = \frac{\partial ssq}{\partial \mathbf{p}} = \begin{bmatrix} \frac{\partial ssq}{\partial p_1} \\ \frac{\partial ssq}{\partial p_2} \\ \vdots \\ \frac{\partial ssq}{\partial p_{np}} \end{bmatrix} \quad (2.26)$$

$$\mathbf{H} = \frac{\partial^2 ssq}{\partial \mathbf{p}^2} = \begin{bmatrix} \frac{\partial^2 ssq}{\partial p_1^2} & \frac{\partial^2 ssq}{\partial p_1 \partial p_2} & \dots & \frac{\partial^2 ssq}{\partial p_1 \partial p_{np}} \\ \frac{\partial^2 ssq}{\partial p_2 \partial p_1} & \frac{\partial^2 ssq}{\partial p_2^2} & & \frac{\partial^2 ssq}{\partial p_2 \partial p_{np}} \\ \vdots & & \ddots & \\ \frac{\partial^2 ssq}{\partial p_{np} \partial p_1} & \frac{\partial^2 ssq}{\partial p_{np} \partial p_2} & & \frac{\partial^2 ssq}{\partial p_{np} \partial p_{np}} \end{bmatrix} \quad (2.27)$$

The matrix \mathbf{H} of second derivatives is called the Hessian. The Hessian is symmetric, that is $\frac{\partial^2 ssq}{\partial p_1 \partial p_2} = \frac{\partial^2 ssq}{\partial p_2 \partial p_1}$, and so on. Thus only the upper triangular matrix has to be computed. It must be stressed again that only the nonlinear parameters are included in the parameter vector \mathbf{p} , refer to Equation (2.25) for clarification.

Using \mathbf{d} and \mathbf{H} a shift vector $\delta \mathbf{p}$ is computed as shown below in Equation (2.28)

$$\begin{aligned} \delta \mathbf{p} &= \mathbf{H}^{-1} \mathbf{d} \\ \mathbf{p}_1 &= \mathbf{p}_0 + \delta \mathbf{p} \end{aligned} \quad (2.28)$$

Referring to Figure 2.23, the shift vector $\delta \mathbf{p}$ is the value added to \mathbf{p}_0 , to result in \mathbf{p}_1 . In general terms $\delta \mathbf{p}$ is the vector that is added to the present parameter vector to result in a better estimate. The iterative process is concluded when some form of termination criterion has been met. The test for convergence is generally performed by comparing the calculated ssq with the ssq value from the previous iteration. If the difference between the two ssq values is below a certain threshold, that is if the shift in parameters has resulted in no further improvement of the ssq value, then the process is terminated and the results are reported. An alternative is to terminate when all elements of the parameter shift vector are below a certain limit.

As previously discussed the parabolic surface approximating the local response surface is not always well behaved, in these cases the shift vector points in a wrong direction and the ssq value increases from one iteration to the next. In the case of such divergence the well-proven Levenberg-Marquardt extension of the equations can be implemented^{33, 35-38}. The extension consists of a diagonal matrix containing the Marquardt parameter, mp , being added to the diagonal of the Hessian prior to its inversion. Increasing the Marquardt parameter shortens the shift vector, $\delta\mathbf{p}$, and directs it to the direction of steepest descent. In Equation (2.29) \mathbf{I} is a unity matrix of the same size as \mathbf{H} , it is multiplied by mp and added to \mathbf{H} .

$$\delta\mathbf{p} = (\mathbf{H} + mp\mathbf{I})^{-1}\mathbf{d} \quad (2.29)$$

In rare instances there are explicit equations for the computation of the first and second derivatives. However, generally there are no explicit equations and the computation of the derivatives has to be performed numerically. Equation (2.30) gives two options for the numerical approximation of the first derivative of ssq with respect to the parameter p_i . The first option requires two additional function evaluations using the original set of parameters \mathbf{p} . Two new sets of parameters are calculated, one where the i -th element of \mathbf{p} is shifted by a small amount in the positive direction, and another with the shifts being in the negative direction. This method is numerically safer than the second, simpler alternative, which requires only one additional function evaluation.

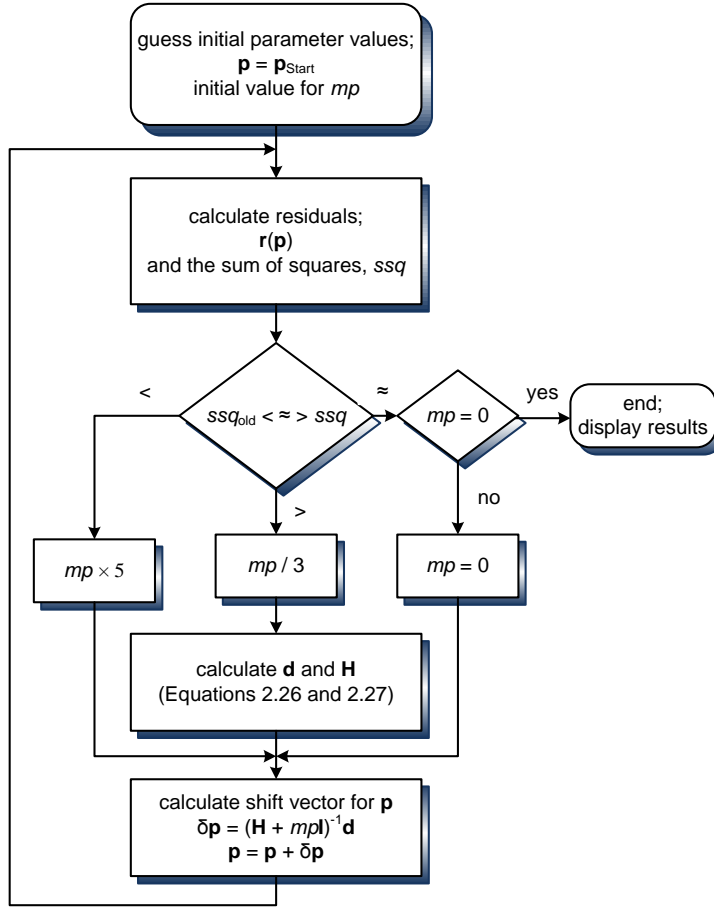
$$\frac{\delta ssq}{\delta p_i} \approx \frac{ssq(\mathbf{p} + \Delta p_i) - ssq(\mathbf{p} - \Delta p_i)}{2\Delta p_i} \approx \frac{ssq(\mathbf{p} + \Delta p_i) - ssq(\mathbf{p})}{\Delta p_i} \quad (2.30)$$

The computation of the second derivatives is numerically more demanding, they are best computed by using:

$$\frac{\delta^2 ssq}{\delta p_i \delta p_j} \approx \frac{ssq(\mathbf{p} + \Delta p_i + \Delta p_j) + ssq(\mathbf{p} - \Delta p_i - \Delta p_j) - ssq(\mathbf{p} + \Delta p_i - \Delta p_j) - ssq(\mathbf{p} - \Delta p_i + \Delta p_j)}{4\Delta p_i \Delta p_j} \quad (2.31)$$

It is straightforward to program the Equations (2.26) through to (2.31).

A flow diagram in Scheme 2.8 is provided which details the fitting procedure.



Scheme 2.8: Flow diagram for the Newton-Gauss algorithm.

A very time consuming part of the whole process is the calculation of the matrix of second derivatives. For ssq fitting it is possible to approximate the second derivatives, therefore essentially only requiring the computation of the first derivative. Instead of computing the derivatives of ssq with respect to the parameters as in Equations (2.26) and (2.27), the derivatives of the residuals \mathbf{R} with respect to the parameters are computed and collected in the so-called Jacobian, \mathbf{J} [33-35].

$$\mathbf{J} = \frac{\delta \mathbf{R}}{\delta \mathbf{p}} \quad (2.32)$$

The calculation of \mathbf{J} requires no extra effort as the all the required computations are also needed to calculate the first derivatives of ssq with respect to the parameters. As before, there are usually no explicit equations and the computation needs to be done numerically, as shown in Equation (2.33).

$$\mathbf{J} = \frac{\delta \mathbf{R}}{\delta p_i} \approx \frac{\mathbf{R}(\mathbf{p} + \Delta p_i) - \mathbf{R}(\mathbf{p} - \Delta p_i)}{2\Delta p_i} \approx \frac{\mathbf{R}(\mathbf{p} + \Delta p_i) - \mathbf{R}(\mathbf{p})}{\Delta p_i} \quad (2.33)$$

$$\mathbf{H} \cong \mathbf{J}^t \mathbf{J} \quad (2.34)$$

The vector \mathbf{d} of first derivatives are computed as

$$\mathbf{d} = \mathbf{J}^t \mathbf{R} \quad (2.35)$$

It can be shown that close to the minimum $\mathbf{J}^t \mathbf{J}$ is a good approximation for \mathbf{H} . However, away from the minimum the approximation is poor, but generally the savings in computation time outweigh the few extra iterations which may be required as a result of the approximation.

It is important to stress that the Hessian \mathbf{H} is only required to drive the iterative process towards the minimum, the location of the minimum is independent of \mathbf{H} as it is defined solely by the first derivatives \mathbf{d} which are zero at the minimum. The derivatives as computed by Equation (2.35) are correct and thus the minimum is correct irrespective of the computational method used to calculate \mathbf{H} .

The structure of the Jacobian matrix \mathbf{J} is worthwhile discussing. For bivariate data \mathbf{J} is comprised of the derivatives of the matrix \mathbf{R} with respect to a vector \mathbf{p} . This could be written as a three-dimensional array. However, it is more convenient, and enables utilisation of the matrix notation in Matlab, to rearrange the matrix of residuals \mathbf{R} into a long vector \mathbf{r} prior to computing the derivatives. \mathbf{J} can then be written as a matrix of np columns, the i -th column containing the derivatives of \mathbf{r} with respect to the i -th parameter.

It is straightforward to generalise this approach to multivariate data. Each individual data set is rearranged into a column vector and all the individual column vectors are concatenated into one very long column vector from which the matrix \mathbf{J} can then be computed.

2.3.8.1 Statistics of Output

An important strength of the Newton-Gauss fitting is the availability of error estimates for the fitted parameters. It must be kept in mind that these estimates are only correct if a series of statistical prerequisites are met, such as noise being only due to pure white and evenly distributed throughout the experiment. Ideally, repeating an experiment should result in approximately the same standard deviations for the calculated parameters. This is hardly ever the case, real data suffer from systematic errors and not

just white noise, and experiments usually do not have directly comparable standard deviation values. Nonetheless, the availability of estimates is much better than nothing.

The relevant information, σ_{p_i} , is contained in the inverse of the Hessian matrix, \mathbf{H} ³³.

The standard deviation for the i -th parameter p_i is the product of the standard deviation of the residuals σ_r and the square root of the i -th diagonal element of the inverse of the Hessian.

$$\sigma_{p_i} = \sigma_r \sqrt{\text{inv}(H)_{i,i}} \quad (2.36)$$

The standard deviation of the residuals is the square root of the sum of squares divided by the degree of freedom, which is defined as the total number of data points subtracted by the number of parameters, np , that have been optimised.

$$\sigma_r = \sqrt{\frac{ssq}{df}} \quad (2.37)$$

$$df = m - np \quad (2.38)$$

For a bivariate data set of the kind represented in Equation (2.3) df is the number of elements in \mathbf{D}_{meas} ($ns \times nl$) minus the sum of all parameters, which is the number of nonlinear parameters, that is the number of elements of \mathbf{p} , and the number of linear parameters, the elements of \mathbf{A} , which have the dimensions $nc \times nl$.

2.3.8.2 χ^2 -fitting

The calculations described so far assume homoscedastic or white noise, that is, all elements of the residuals are assumed to follow a Gaussian distribution that is constant over all measurements. This is often not the case, however the lack of detailed information about the error structure leaves no other option but to assume homoscedastic noise. While this is not perfect, the distortion of the result is often negligible.

If, however, the noise structure of the data is known it would be negligent not to use the information. Equation (2.17) is replaced with Equation (2.39). That is, instead of the sum over the squares of all residuals being calculated, the residuals are divided by the known standard deviation of the measurement at this particular point. The calculations otherwise are essentially identical.

$$\chi^2 = \sum_{all\ i} \left(\frac{R_i}{\sigma_{Y_{meas},i}} \right)^2 \quad (2.39)$$

There is one clear advantage in χ^2 -fitting, if the estimates for $\sigma_{Y_{meas}}$ are correct, the weighted residuals should be about one and the sum over all the squares should add up to the number of points. Thus, this provides a good test for the correctness of the model. If χ^2 is smaller than the number of data points there is only one conclusion, that the $\sigma_{Y_{meas}}$ have been underestimated.

2.3.8.3 Initial Estimates for Parameters

The quality of the initial guesses for the parameters is a crucial factor with data fitting. As indicated in Figure 2.23, if initial guesses are too far from the minimum the iterative process can result in catastrophic divergence. While the Levenberg-Marquardt extension often will rescue the process, there are limits to its effectiveness. If new processes are investigated it is often not clear what the mechanism might be, thus making it difficult to estimate appropriate parameters.

There are very expensive algorithms that address the problem, the extreme is to search the 'whole' parameter space in a multidimensional grid. Even for a reasonable number of parameters such attempts, while guaranteeing success, can be extremely slow and are unfeasible. Consider a problem with five parameters, each one determined at ten values, this requires 10^5 computations of *ssq*. Depending on the complexity of the model, the computation for this number of parameters might be feasible, but if the number of parameters is doubled, 10^{10} *ssq* values need to be computed, and this is out of question for any model.

For completely new investigations it can be difficult to guess sufficiently good initial values for the parameters. Any analysis should begin by performing thorough research, such as searching scientific library sources, to obtain good initial estimates and model examples for the parameters that are to be refined, for example, searching the NIST database to find protonation or equilibrium constants of analogous ligands or complexes. This information assists by providing initial estimates that are good approximations for the values of the constants under investigation. Good initial values are critical, especially when the number of unknown parameters is high, and also when there is the risk of local minima.

In addition to using known analogous values as estimates there are also computer programs available that can aid in predicting the necessary values, for example applying Genetic Algorithms, GAs³⁹⁻⁴¹. The commonly used Newton-Gauss algorithm has slow convergence far from the minimum and is not guaranteed even though convergence is quadratic and fast near the minimum. More adequate, and significantly more efficient, are the aforementioned GAs which have been developed to efficiently and elegantly search the parameter space. They robustly, and in a useful time frame, find the proximity of the global minimum. However, GAs are notoriously slow in refining parameter sets close to the minimum, therefore the combination of GAs to search the complete parameter space and provide a rough estimate to localise the vicinity of the global minimum, followed by fast Newton-Gauss algorithms to reach the exact minimum, is clearly the most advantageous method. The two algorithms complement each other ideally.

Another possibility is available for initial parameter estimates of protonation constants for organic compounds using programs that are comprised of a collection of powerful tools for making predictions of the pK_a values of any organic compound on the basis of their structural formulae⁴²⁻⁴⁴. These programs can also provide good starting points for parameter values. Additionally researchers such as May *et al*⁴⁵ have developed programs that simulate potentiometric titration data that include various types of corrections for the changes in activity, liquid junction potential and ion-selectivity of the electrode. The simulations form the basis of a library of computer programs called Equilibrium Simulation for Titration Analysis (ESTA). Such simulations can be useful for the initial estimates of real data as they enable a range of titration conditions to be investigated and altered while assessing the effect of such changes on the formation constants to be determined experimentally. Such simulations can aid the analyst in developing better models and values in order to optimise experimental formation constant.

EFA

Evolving Factor Analysis⁴⁶⁻⁴⁸ (EFA) is another powerful tool that can aid the researcher in the development of a chemical model for the analysis of spectroscopic data. It was developed as the chemometric way to monitor the evolving process of a chemical reaction. It does not provide estimates of initial parameter values, but instead determines an estimate of the number of contributing chemical species that are present

in the reaction, and at what stage in the reaction the species appear. EFA is a useful tool for processing multivariate data produced by dynamic systems. In the monitored reaction the measured spectra evolve with time or added reagent because of consumption of starting reagents during the reaction and the generation of intermediates and final products ⁴⁹. At each step in the monitored reaction EFA can be used to estimate the number of independent factors, that is, the chemical species which contribute to the overall observed spectra. Such knowledge not only informs the researcher about the number of species that form during the reaction, but also provides key information about when each species appears or disappears, if backward EFA is also applied. This can help determine what the species are, for instance if a species appears when the added metal reagent is at a 1:2 metal-ligand ratio then it is highly probable that the species formed is an ML_2 species.

2.3.9 Determining the Correct Model

When the analytical method has been chosen and implemented, and the minimisation process has terminated, diagnostic criteria need to be employed in order to determine whether the results should be accepted. This task of determining the correct model for the fitting is clearly the most difficult aspect of the complete process of data analysis. To our best knowledge there is no reasonably general and reliable algorithm that 'determines' the best model. There are several reasons for this, one of which being that there is no 'best' model. It is always possible to expand an existing model in such a way that there are more parameters, which necessarily results in a decrease in the sum of squares. The problem relating to whether or not a model should be expanded is relatively simple as statistical tools are available which allow the researcher to decide whether the improvement in the fit has been significant or not. According to Occam's razor the simplest model that adequately fits the data is the 'correct' one by definition.

Another factor that hinders determination of the correct model is that there are many processes for which the correct mechanism is simply not known. Redox reaction mechanisms often involve several very unstable intermediates, which are not observable, existing only as steady-state species. It is then very difficult to determine and verify an adequate model, and in many instances there are no clear answers to the question of the correct model.

The process of determining the correct model is in theory rather simple, but in practise can often be time-consuming and frustrating. If an incorrect hypothesis has been made with the chemical model, or the initial estimates of parameter values were too far from the minimum, the result is often divergence, cyclisation or failure of the procedure to achieve minimisation. All potential models have to be tested in some systematic way, beginning with simple models followed by models of increasing complexity. Each model is fitted and the progress of the quality of the fit is monitored. At some stage the decrease in *ssq* stops being significant and the previous model can be declared the correct one. It is difficult to ensure that no alternative models have been omitted from this trial and error process. Reliable data fitting programs make the process easier, but they do not relieve the scientist from having to understand their own research, chemical intuition is crucial in most instances. When the fitting procedure has completed the minimisation process, the following diagnostic criteria should be considered to determine whether the results should be accepted ^[38, 39].

(i) **The physical meaning of the parameters.** The physical meaning of the equilibrium or rate constants, associated molar absorptivities, and stoichiometric indices need to be examined. As a general rule for equilibrium constants the β value should neither be excessively high or low, for rate constants the reverse rate should not exceed the forward constant unless coupled to a subsequent reaction, and for absorbance data calculated absorptivities should not be negative. Additionally, the standard deviation of each parameter should be inspected. High parameter standard deviations are often caused by termination of the minimisation process before the minimum has been reached, or if the proposed model was too complex resulting in strong correlations.

(ii) **The physical meaning of the species concentrations.** There are some physical constraints that are applied to species concentrations, the most important being that the species needing to contribute to the signal above the recorded noise level, for instance with spectroscopic measurements the species contribution is dependant on the molar absorptivity meaning that the lower the absorptivity the higher concentration required to make a contribution above noise level. Furthermore, the calculated distribution of the free concentration of the basic components and the variously protonated or metalated species of the chemical model should show realistic molarities, species that do not contribute to the signal behave as numerical noise in a regression

analysis. Examining a species distribution diagram is an easy way to judge the contributions of the individual species to the total concentration.

(iii) **Parametric correlation coefficients.** Partial correlation coefficients can be determined from the calculation of what is termed the ‘curvature’ matrix. This is computed from the multiplication of the Jacobian matrix by its inverse, that is $\mathbf{J} \times \mathbf{J}'$, and these values indicate the interdependence of two parameters. Fundamentally, all of these correlation coefficients have values between -1 and +1, where zero indicates complete independence, and -1 or +1 indicates complete correlation. Two completely correlated parameters cannot be included in a chemical model because an increase or decrease of one parameter is compensated for by the other. In such an instance the parameter value of one of the correlated parameters should be ‘fixed’ and hence not involved in the minimisation process, or alternatively, if both parameter values are completely unknown and therefore fixing one is not a viable option, the complexity of the model may need to be reduced.

(iv) **Goodness-of-fit test.** This diagnosis contains the most important criteria for testing the correctness of the hypothetical chemical model proposed. To identify the most valid or the true chemical model when several possibilities have been proposed, and to establish whether or not the chemical model represents the data adequately, the residuals should be carefully analysed. That is, the difference between the measured and calculated data should be thoroughly examined and often the easiest way to investigate the overall suitability of the proposed model and calculated parameters is a visual representation of the calculated and experimental data. This enables a visual assessment of how well the calculated data agrees with what was experimentally collected. If the model represents the data adequately the residuals should be randomly distributed, as shown in Figure 2.24, as any systematic departures from randomness indicate that the model or the parameters were not satisfactory and therefore further analysis of the system would be required. Graphical representation of the residuals greatly aids the diagnosis and identification of outliers, as trends in the residuals, detection of sign change, and examination of symmetry and normality in the residuals distribution can be readily recognised visually. The residuals themselves should be randomly distributed

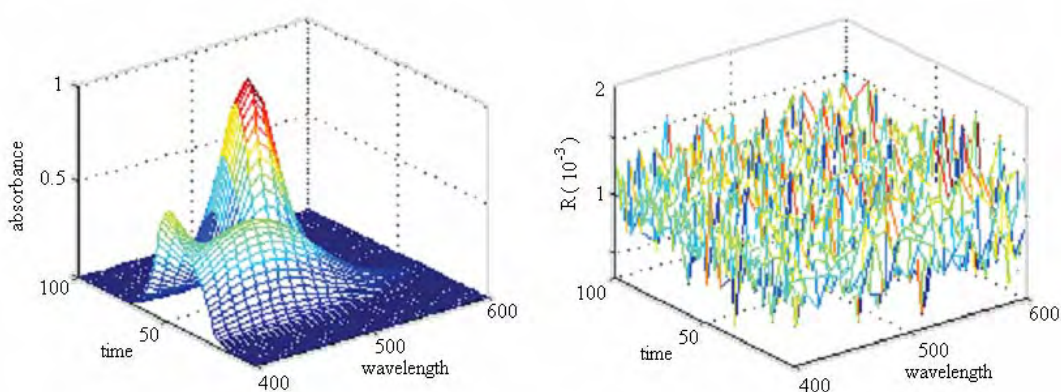


Figure 2.24: (LHS): Plot of an absorbance spectrum as a function of time; (RHS): Plot of the residuals after the measurement shown on the LHS has been analysed. It can clearly be seen that all residual values are randomly distributed and no trends can be easily identified.

(v) **The deconvolution of spectra for absorbance measurements.** Resolution of each experimental spectrum into spectra of individual species proves whether or not the experimental design has been efficient enough. If species are poorly defined, or not formed to sufficient concentrations, their spectra will be unrealistic, for example with absorptivity 100's or 1000's times greater than the other species present in the analysis. In such cases the experiment may need to be repeated under different conditions, such as increased initial concentrations, to ensure that the badly defined species form to an acceptable concentration. The measurement can then be globally analysed with the previous data. In the global analysis all species should be adequately defined. Another option if no experiment is possible to properly define all species is to use the molar absorptivity of the species, if it is known, and enter it as part of the analysis. Then the species is fixed at its known spectrum so the poorly defined species can still be used as part of the overall model.

2.3.10 Published Software Packages

Choosing the best computational strategy for analysing the data involves determining what parameters are needing to be refined, and then determining which program, either commercially available or in-house developed, will work best for that task. Currently there are many popular and competent programs available for model-based data analysis. Commercial programs that are widely available include examples such as Specfit/32™^[43, 44], Pro-Kineticist II (Pro-KII)^{32, 50}, and the well established QUAD family of programs which include MINQUAD, SUPERQUAD and HYPERQUAD^[47, 48].

There are several computer programs that have been developed specifically for the evaluation of potentiometric pH-titrations ^{36, 51}. The first example of least-squares refinement applied to an acid-base titration was with the program LETAGROP ^[50-53]. More recent programs include the program GLEE (GLass Electrode Evaluation) ⁵², which forms part of the HYPERQUAD family, MAGEC ⁴⁵ (Multiple Analysis of titration data for Glass Electrode Calibration), PHCONST ⁵³ and ACBA (Acid-Base titrations) ⁵⁴. Less widely spread are analysis packages for spectrophotometric titrations ^[8, 46, 47], but examples include the previously mentioned Specfit/32™ and also the program SQUAD(84) ^[46-50].

A comprehensive discussion of programs that have been developed for the analysis of pH titration data has been provided in Chapter 6.2.3. Further details about the other available programs will be provided below.

2.3.10.1 Package Details

SPECFIT/32 makes use of a multiwavelength and multivariate spectra treatment and enables a first-order global analysis for both equilibrium and kinetic systems. The program is based on singular value decomposition and nonlinear regression modelling using the Levenberg-Marquardt method to determine stability constants from spectrophotometric titration data and rate constants from kinetic measurements. Typically, the 3D data sets obtained from multi-wavelength spectrophotometric measurements consist of simultaneous measurements of absorbance versus wavelength as a function of an independent variable, for example time, pH, or titrant. However, the globalised fitting methodology can be adapted to virtually any type of experimental observations that respond linearly to sample concentration or mole fraction ⁵⁵. SPECFIT/32 provides a versatile, multiple document style graphical interface that includes all of the features required to display and manipulate 3D data sets. The program includes other features such as the ability to include known spectra as constraints on the fitting procedure as well as prediction of spectra for reactive intermediates or unknown products. A significant feature is the capability to simulate data for all supported chemical models, but perhaps the most important feature is that the program is easy to use.

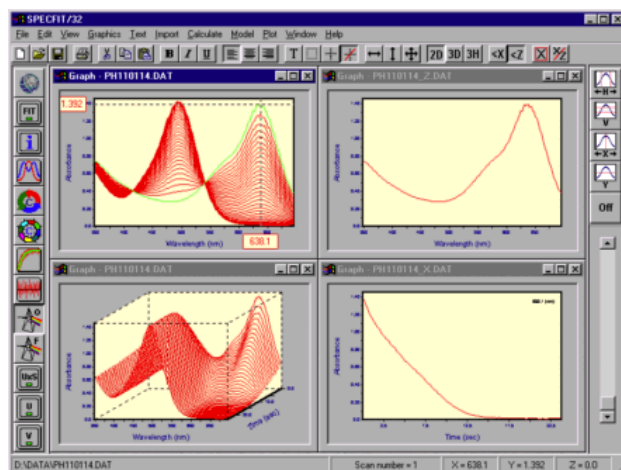


Figure 2.25: Screen shot from the Specfit/32TM interface as an example of data display ⁵⁶.

SQUAD(84) can adjust the stability constants and molar absorptivities of the absorbing species by minimising the residual-square sum function. The predicted absorbance-response surface is fitted to the given spectral data with one dimension representing the dependant variable, that is the absorbance, and the other two dimensions representing the independent variables, such as the total component concentrations or pH at each step of the titration and at each wavelength measured. The minimisation process may be done algorithmically or heuristically. The algorithm process usually finds a global minimum whereas the heuristic process depends on human control. The choice of the optimal computational strategy to use is dependant on the number of species, previous knowledge about any of the species in the chemical model, and the experimental design for changing the basic components in the equilibrium system ⁵⁷.

Pro-KII is the commercially available program that was used for the kinetic analysis performed for this research, the program was previously developed at the University of Newcastle. Pro-KII is the only commercial program that allows the global analysis of a series of measurements, that is performs secondary global analysis. The program can optimise spectrophotometric data in order to determine rate constants. It allows the incorporation of known absorption spectra for species and includes the option of declaring a particular species as uncoloured or non-absorbing in the wavelength range measured.

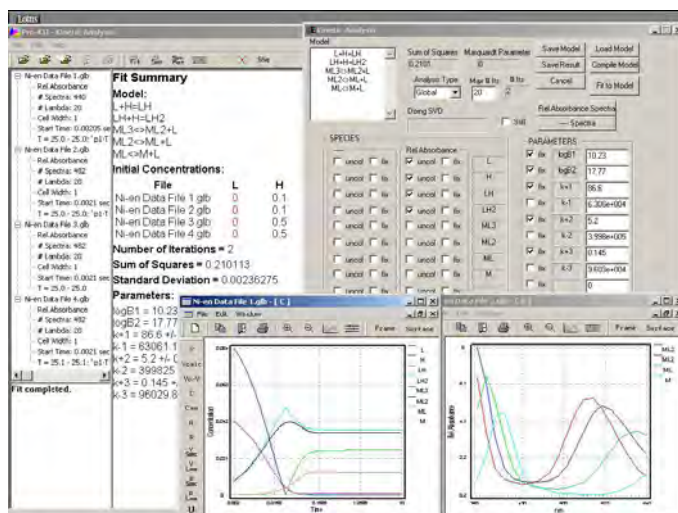


Figure 2.26: Screen shot from the Pro-KII interface ⁵⁰.

2.3.10.2 Other Aspects of Data Fitting Programs

The issues discussed so far in Section 2.3 in this chapter have been centred on the algorithms that perform nonlinear least-squares fits of different types of data sets. It has been demonstrated that substantial advances have been made since the first algorithms for simple fitting tasks were developed. The main advances that have been made recently with data fitting programs have been the globalisation of the analysis of series, or measurements and the integration of non-ideal situations into the modelling part of the fitting algorithms. The main aim of these developments have been to simplify the analysis of the data by enabling many measurements to be analysed together as one global set, and secondly to simplify the experimental procedures by enabling measurements to be non-ideal in nature. Rather than having to add buffers or excess inert salts to maintain pH and ionic strength, changes in these quantities are taken into account by the analysis software. This is particularly important for the analysis of industrial processes where often not even the temperature, and even less so pH or ionic strength, can be maintained. These significant developments have been shown to work and make data acquisition and analysis easier for the researcher.

Similar advances, aiming at improving the interaction of the software with the researcher, have also been achieved. Importantly, graphical output of any result has become straightforward for mono- and bivariate data sets. These graphs can be manipulated in many ways that facilitates comprehension and understanding of the user and eventually the reader of published results. In particular, Matlab is leading the way with an incredibly comprehensive suite of graphical options.

Key features that are universal in many current commercial programs include such characteristics as multiple document style, graphical interfaces that are versatile and include all the aspects required to display and manipulate 3D data sets. The use of computers has also made possible the development of graphical methods for displaying experimental results, such as diagrams showing the relative concentrations of individual complex species as a function of solution conditions such as pH and metal ion or ligand concentration¹².

Of similar importance is the 'friendliness' of the user-interface. While the actual computations of the data fitting do not need to be understood by the user, their interaction with the software is important. Data importing, exporting and manipulation, model development, parameter definitions and so forth are all vital considerations for the design of analytical software. These aspects need to be as user-friendly and adaptable as possible. Software for model-based analysis requires the user to propose a model for the collected data as well as provide relevant supplementary information such as initial concentration values and any known constants such as particular rate or equilibrium constants. Most important is the model-development aspect. For novel systems, where very little is known about the process, the model that should be supplied for the fitting is often unclear, hence the determination of the correct model requires constant input and manipulation from the user.

As mentioned earlier in Section 2.3.9, determination of the correct model involves the fitting of increasingly complex models until the quality of the fit as expressed by *ssq* is within the expected noise level of the data. This process can be very time consuming. At each step a new model has to be implemented and tried. Consider a kinetic investigation, for each new model proposed, the appropriate set of differential equations and the equivalent of Equation (2.6), has to be programmed. While this is not a very difficult task, it is error prone and importantly it can be very difficult to discover and correct an error in the program coding. The situation is even more difficult with equilibrium investigations where a system of non-linear equations has to be defined and coded for each potential model.

Fortunately, it is possible to write algorithms that 'translate' the chemical model as written by the chemist, for example the model for a consecutive reaction $X \rightarrow Y \rightarrow Z$, into the system of differential equations, Equation (2.6), and subsequently into the code required by the ODE solver⁵⁸. Similar parsers exist for equilibrium systems. While

these parsers are not absolutely essential, they enable the researcher to investigate the model space for a particular process in a reasonable amount of time.

Of similar importance, and closely related to the model finding process, is the convenience of the management of the parameters. For complex models and processes it can be very difficult to produce a set of initial estimates for all parameters that result in trouble free convergence. During the initial stages of the development of a set of initial guesses it is often helpful to fix a few of the parameters to reasonable values, for example such values can often be estimated from prior analysis of similar processes or previously published data. Systematic juggling of the parameters that are 'known' and those that need to be fitted is often required prior to complete analysis where all parameters are fitted. Ease of such manipulations between fixing and fitting parameters is important and tremendously facilitates the task of model finding. Programs that incorporate GAs to locate the general minimum before the minimisation procedure is initiated also aid in the analysis.

The commercially available programs listed in Section 2.3.10 are all complete packages, that is, they have specifically designed user-interfaces and graphical windows. There are obvious advantages of custom made interfaces, for example they allow limitation of the options such as tick boxes to choose between two options, yes or no, and they have predefined functions to aid with the analytical procedure. A disadvantage is that new users have to learn the syntax of the interface and also the data input/output process, both of which can be surprisingly different from program to program. Also the user is restricted to the specific predetermined outcomes of the analytical program.

Analysis programs also provide users with information such as the concentration profiles that show the change in concentration of all the reagents and intermediates associated with the reaction. Of course each individual program has their own specific features depending on the type of data analysed and the purpose of the analysis. For example, analysis programs that use spectrophotometric data may also include features such as the absorbance of each coloured species over the range of scanned wavelengths as a function of time. Also, the absorbance at a specific wavelength, or over a range of wavelengths, as a function of time is often another available feature. Modern programs also address the critical issue of speed, which is an especially important consideration for the processing of large 3D data sets. Efficient algorithms are needed, resulting in

everything from file input/output to computations and graphical outputs being notably fast.

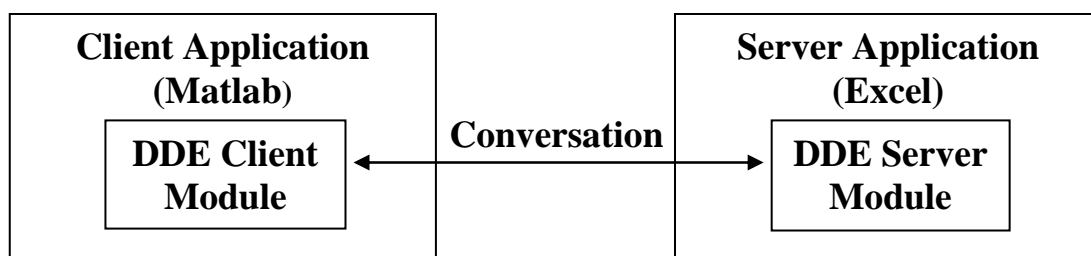
A powerful aspect that some current programs incorporate is providing a simulation tool. This enables the user to experiment with reaction models and parameters that can aid in the prediction of experimental behaviour and also with the elucidation of the sensitivity of a reaction to specific parameters. It is also a beneficial tool for familiarising users with all the features of a package without the complication or need for real data.

2.4 Our Data Analysis Program Design

Data analysis software needs to be developed in such a way that users can easily manipulate their data and the necessary parameters, while at the same time providing a powerful program to perform the required computations. The approach we used to develop our analytical programs was to use an application with which users were already familiar as the interface and couple this with a powerful operating system capable of performing the complex calculations required for modern data analysis.

We chose Microsoft Excel as the interfacing program as it is a commonly used application that most scientists are accustomed with and can manipulate at some level. Importantly, it is ideally suited for data handling processes especially where large amounts of data are involved, which is the case for spectrophotometric data acquired at multiple wavelengths. However, Excel does not have the necessary features to carry out the required data analysis, therefore a more powerful program was required in order to perform the calculations. The program we used as the computational engine was the matrix based numerical computing environment and programming language Matlab which allows easy matrix manipulation, plotting of functions and data, and implementation of algorithms. Importantly Matlab has the ability to interface with programs in other languages, Matlab functions enable it access to other Windows applications, or visa versa, Windows applications can access Matlab in a wide range of contexts. Thus, Excel was used to develop the user-interface, which provided the platform where all the data manipulation and model defining could be performed, and this interface was coupled with Matlab, which could execute the calculations required for the analysis.

The two systems were programmed to communicate with each other using dynamic data exchange (DDE) software, which establishes a conversation that is ‘live’ and requires no intermediate files or low-level, inter-process programming. For the DDE conversation a client-server relationship between the two programs is required. The application that initiates the conversation is called the client, and the application responding to the client is called the server, as shown in Scheme 2.9. For our program Matlab was used as the client with Excel acting as the server application. The link initiates a two-way access channel between the Excel workbook and the Matlab platform, therefore enabling data to be freely exchanged between the two working environments.



Scheme 2.9: Relationship between Matlab and Excel for DDE, data can be freely exchanged between the two applications once the conversation has been established.

This connection between two powerful applications enabled data pre-processing, editing, manipulation and viewing in the familiar Excel environment while accessing the computational speed, sophisticated analytical capabilities such as the extensive application toolboxes and any specifically developed programs, as well as the high-quality graphical visualisation and presentation capabilities available with Matlab. Additionally, nearly all acquired experimental data can be easily converted into a format that Excel can read, which makes this style of program very broadly applicable to any form of experimentation.

The extensible properties of both Matlab and Excel enabled easy development and updating of the programs designed for data analysis. The programs importantly allowed the incorporation of different forms of data analysis functions and techniques as well as extension of the Matlab and Excel connection to include data acquisition programs which provided us with the flexibility to acquire data under what ever conditions we decided were important for each investigation. For further discussion on the data

acquisition techniques that were developed for our research see Section 2.2 previously in this chapter.

A significant advantage with using Excel as the interface is that we were provided with virtually unlimited flexibility. Not only is data easily manipulated, Excel itself has computational abilities. Therefore the familiar analytical tools Excel provides can potentially be used to enhance the core analysis performed by Matlab. This capability can be demonstrated by a simple equilibrium investigation example. If the experiment was comprised of multiple titrations performed using dilutions of one stock solution the analyst has two options with how to proceed with setting up the analysis. The first option is that the different initial concentrations of each solution used for every measurement can be fitted as part of the analysis, that is, the analytical concentrations would be determined for each measurement along with the other experimental parameters such as the equilibrium constants. This can result in quite a large number of parameters to be optimised depending on the number of measurements performed.

Alternatively, the second option incorporates the computational abilities of Excel to easily link together the initial concentrations using the familiar '=' command in Excel along with the known dilution factors. Here only the one stock solution concentration is fitted as part of the analytical process, therefore not only reducing the number of optimised parameters, but more importantly increasing the robustness of the fit. This is just one simple demonstration of how the data can be manipulated in Excel, but the possibilities are obviously endless. By enabling such flexibility and individual interaction in Excel the Excel-Matlab link becomes a very powerful basis for any analysis program.

2.4.1 User-Interface

Two programs were developed for equilibrium analysis for this research at the University of Newcastle using the Excel-Matlab link, Pot_Anal and Spec_Anal, dealing with potentiometric and spectroscopic measurements respectively. The computational programming in Matlab was based on the previously discussed algorithms in Section 2.3. Both methods involved simultaneous, global analysis of a series of titrations, each performed under different initial conditions or concentrations, in order to determine equilibrium constants. This analytical approach has previously been termed second order global analysis⁵⁹. The first program developed analyses potentiometric

data and the second program was developed to analyse spectrophotometric data. A third program to analyse data collected from combined potentiometric and spectrophotometric titrations has also been developed, however it was not used for this research. As a result of the flexibility of Excel and elegant Matlab algorithms the programs are independent of the number of components and species in the solution and the complexity of the system.

For each interface colour coding of the cells in Excel was intended to aid with describing where specific information should be entered and alternatively what data is outputted as a result of the analysis. The □ cells require the user to enter such data as the name of the worksheet in Excel where the data is stored, the proposed model, and the actual experimental data from the measurement. The ■ cells require numerical data, for example the parameter values and component concentrations. The ■ cells contain automatically calculated data, that is cells that contain formulas, and such cells will also show the outputted data from the analysis process.

In the following screen shots of the Excel user-interfaces the greyed out box shows the template with no data entered. The zoomed in areas provide example data to illustrate the type of data belonging in each section.

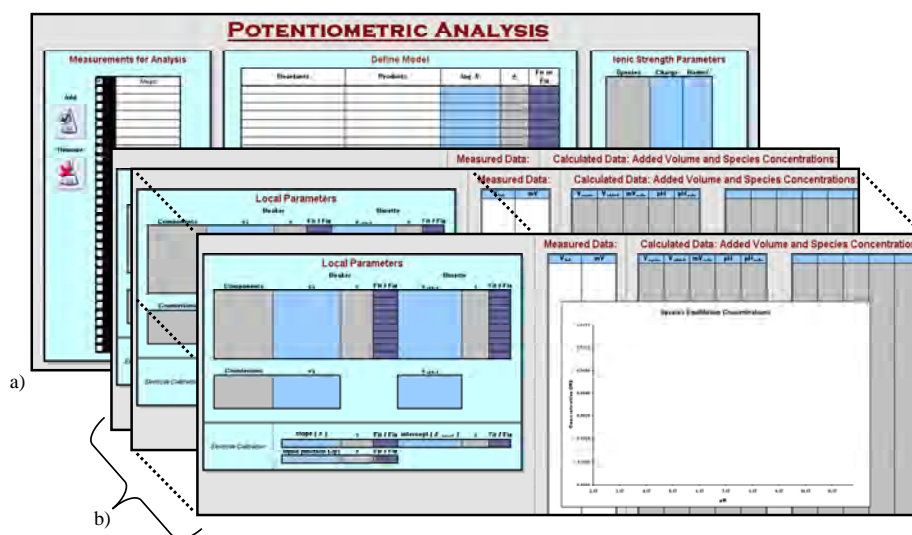


Figure 2.27: a) Main worksheet showing the Excel user-interface for potentiometric titration analysis; b) Sub-sheets in the workbook containing the specific data for each measurement.

Measurements for Analysis

Add

Meas	Value
Meas1	
Meas2	

Remove

Define Model

Reactants	Products	log K'	±	Fit or Fix
L+H	LH	8.5626884661	0.0051	fit
LH+H	LH2	6.2446951232	0.0061	fit
M+L	ML	9.1025649622	0.0140	fit
M+LH	MLH	5.2016889756	0.0151	fit

Compile

solvent	temp [°C]	mode	ε	δg	ssq
1	25	1	78.3	0.6906	56.8125

POTENTIOMETRIC ANALYSIS

Add

Meas	Value

Remove

Define Model

Reactants	Products	log K'	±	Fit or Fix

Compile

solvent	temp [°C]	mode	ε	δg	ssq
1	25	1	78.3	0.6906	56.8125

Ionic Strength Parameters

Species	Charge	Radius
M	2	12
L	0	15
H	1	9
OH	-1	3
LH	1	24
LH2	2	31
ML	2	27
MLH	3	43

Counterions

Species	Charge
Na	1
Cl	-1

Global Data

solvent	ε	
1	water	78.3
2	ethanol	24.9
3	50:50 water/EtOH	51.6
4	other	look up

mode	activity coefficient
1	1
2	$\log \gamma = \frac{-Az^2\sqrt{\mu}}{1 + \sqrt{\mu}}$
3	$\log \gamma = \frac{-Az^2\sqrt{\mu}}{1 + rB\sqrt{\mu}}$

fit parameter fitted

fix parameter not fitted

nsheets	nmeas	nfix
2	2	4

nspec	noomp	nions	nAusp
8	3	2	0

Suggested Values

parameter	Value
slope	-60
int	400
up	-19.67

Auxiliary Parameters

Name	Value	±	Fit / Fix
Limitation	0.50		fix

Figure 2.28: Detail of a) in Figure 2.27: This first worksheet is the main worksheet where the measurements for analysis are selected and global data for all titrations are entered, that is the chemical model defining the reaction, the ionic strength parameters, and also any auxiliary parameters.

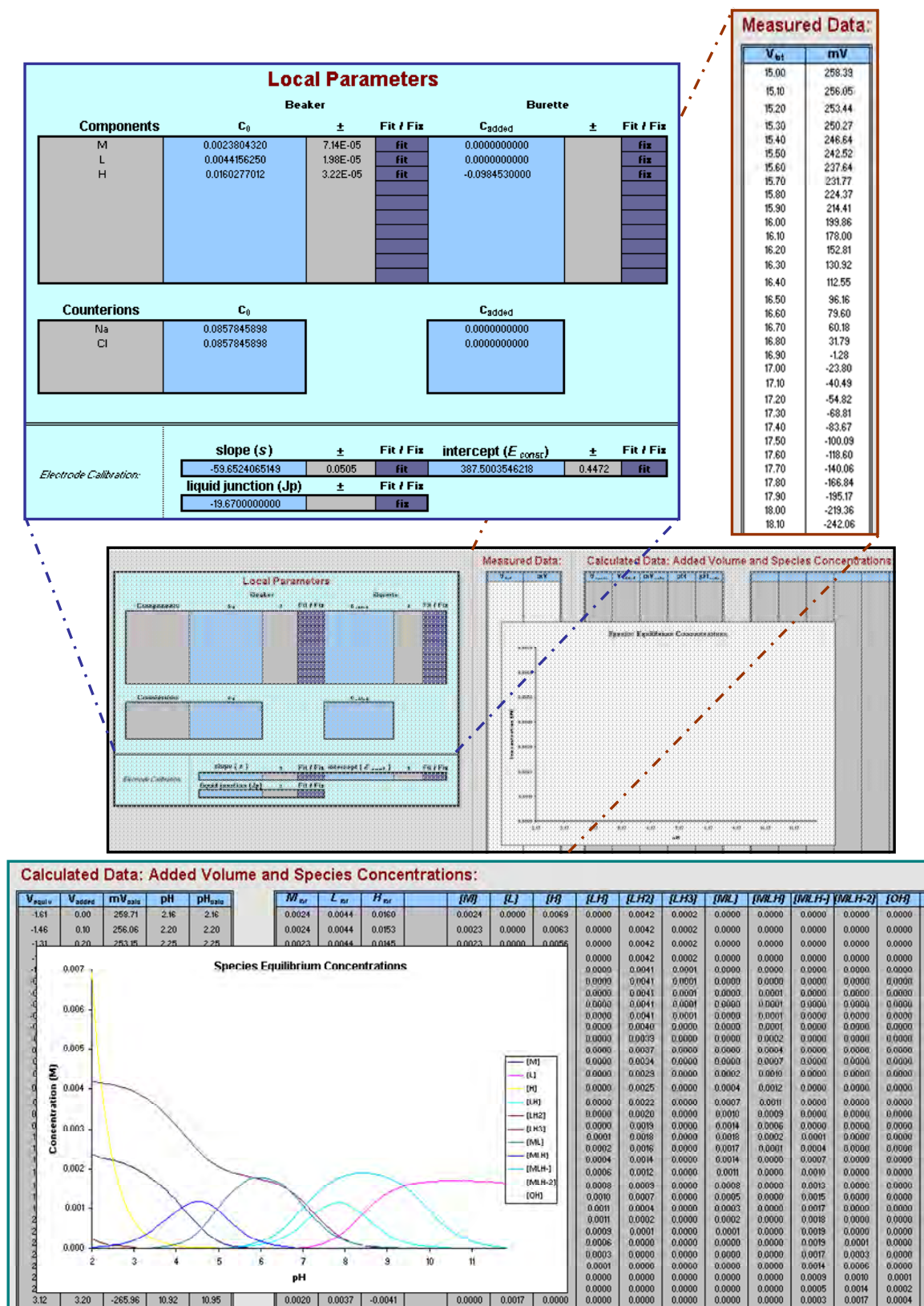


Figure 2.29: Detail of b) in Figure 2.27: The second worksheet is where the data from each titration is entered along with the specific concentrations and electrode calibration parameters for each measurement.

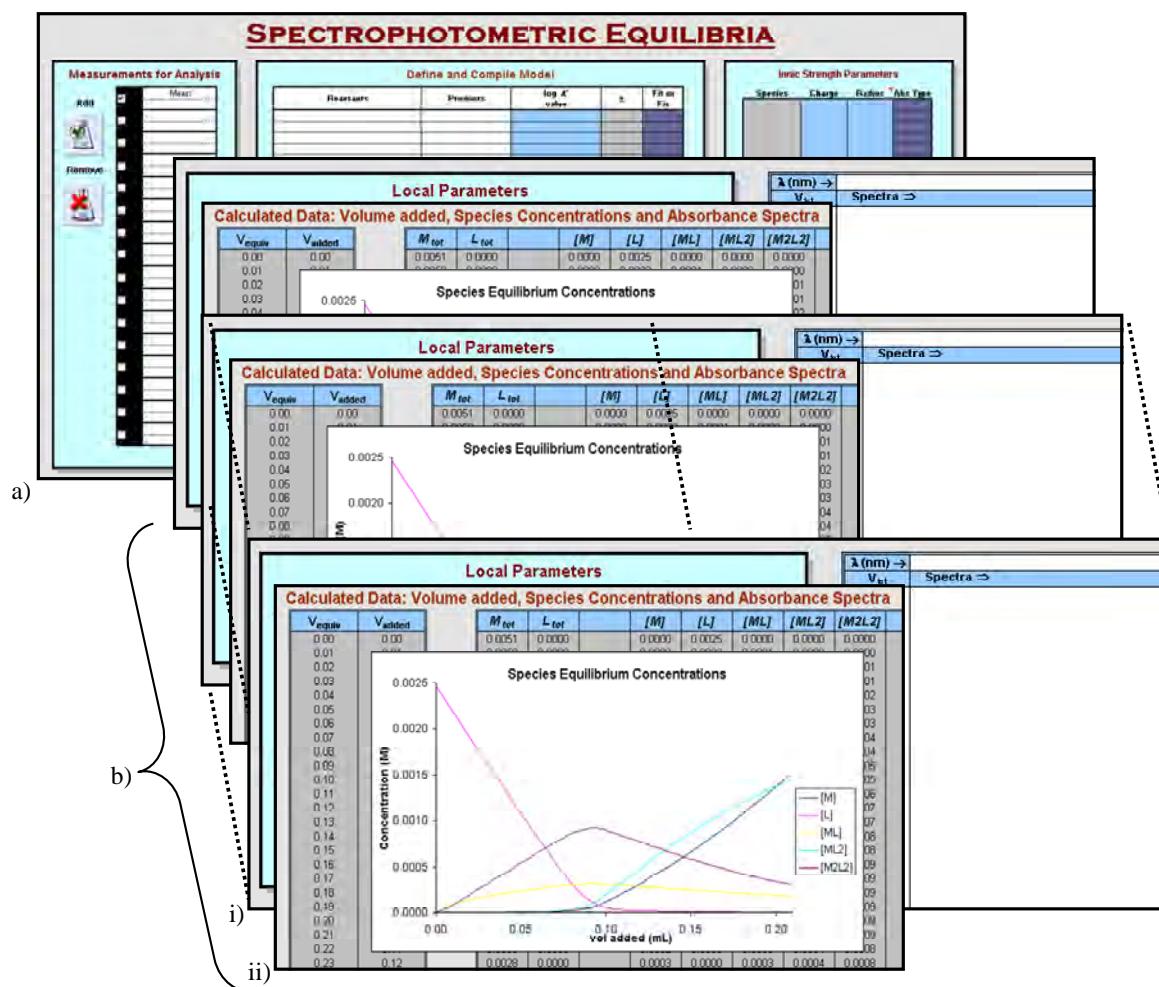


Figure 2.30: a) Main worksheet showing the Excel user-interface for spectrophotometric titration analysis; b) Sub-sheets in the workbook containing the specific data for each measurement, there are two sub-sheets required per measurement; i) for the measured data, and ii) for the calculated data.

Define and Compile Model

Reactants	Products	log K' value	±	Fit or Fix
M+L	ML	5.3403490240	0.0527	fix
M+ML	M2L	3.4903822239	0.0350	fix
M2L+L	M2L2	9.4389358489	0.0329	fix

Measurements for Analysis

Add ☒ Meas1 ☒ Calc Data1
☒ Meas2 ☒ Calc Data2
 Remove ☒

Ionic Strength Parameters

Species	Charge	Radius	Abs Type
M	2	12	known
L	0	15	non-abs
ML	2	27	coloured
M2L	4	39	coloured
M2L2	4	43	coloured

Compile

mode	temp (°C)	solvent	ε	δg	ssq
1	25	1	78.3	0.6906	56.8125

SPECTROPHOTOMETRIC EQUILIBRIA

Measurements for Analysis

Define and Compile Model

Ionic Strength Parameters

Counterions

Name	Charge
Na	1
Cl	-1

Auxiliary Parameters

Name	Value	±	Fit / Fix
ε _{water}	0.50		fix

Local Parameters

Components	Beaker	±	Fit / Fix	Burette	±	Fit / Fix
M	0.0023504120		fix	0.0000000000		fix
L	0.0000000000		fix	0.0044444357	1.98E-05	fix

Counterions

Name	Value	±	Fit / Fix
Na	0.0857945889		fix
Cl	0.0857945889		fix

Local Parameters

mode	activity coefficient
1	1
2	$\log \gamma = -A\lambda^2 \sqrt{\mu} / (1 + \sqrt{\mu})$
3	$\log \gamma = -A\lambda^2 \sqrt{\mu} / (1 + rB\sqrt{\mu})$

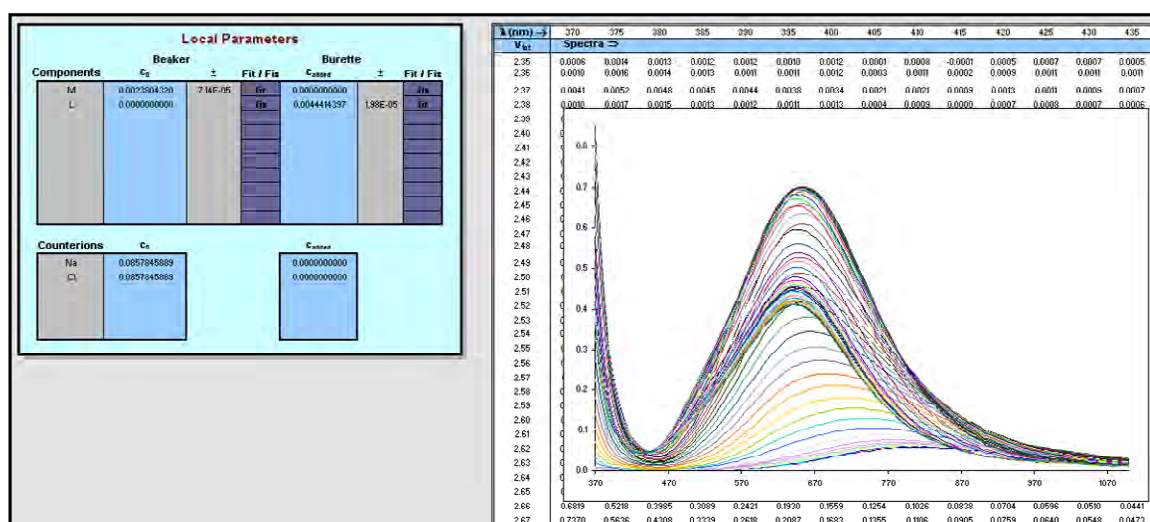
fit parameter fitted
fix parameter not fitted

noomp 2 **nspec** 5 **nions** 2

rmeas 2 **nsheets** 4 **nran** 3 **nAusp** 0

coloured species that are absorbing
non-abs species that are non-absorbing
known species spectra that are known

Figure 2.31: Detail of a) in Figure 2.30: This fist worksheet is the main worksheet where all global data for all titrations is entered, that is the model defining the reaction, the spectra type of each species, the ionic strength parameters, and also any auxiliary parameters.



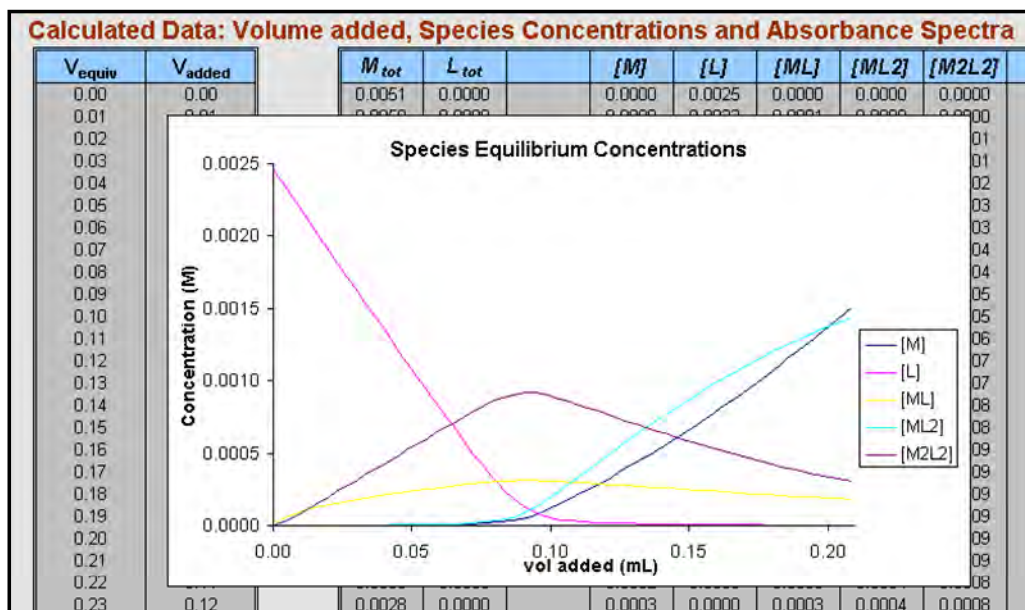


Figure 2.33: Detail of b(ii) in Figure 2.30: Example calculated data has been provided to illustrate the type of calculated data that is provided during and after the analysis of a measurement.

2.4.2 Data Manipulation

2.4.2.1 Model Construction

Strictly, the model is a description of the equilibrium species known or thought to exist coupled with the estimates for the log K values of each species. To analyse a new system, the proposed model is likely to be constructed a number of times, adding and subtracting species, altering initial guesses, and comparing the calculated results for each model until one model is seen to most acceptably and adequately fit the data.

As previously discussed, the construction of the model is an important step, requiring knowledge of the likely chemistry of the equilibrium system under study, and those closely related, so that reasonable estimates for species and equilibrium constants may be supplied. A weakness of model construction is the subjective judgments on which the model is reliant. For this reason, time spent initially in researching and building a good model may save much time later. In order help assess whether the model and initial estimates of parameters are adequate, both programs were developed with an 'update' option, which simply takes the proposed model along with the parameter estimates and returns the calculated data without any iterative fitting of the parameters. With this option the user can easily assess if their starting point has resulted in calculated data that is similar to what was measured, and hence whether the model and parameters are worth optimising. Usually, for an unknown system, the user will need to 'update' a

couple of times before finding a suitable model and parameter estimates to proceed to using the 'fit' option to begin the analysis.

2.4.2.2 Available Parameters

Both data analysis programs that were developed have some common parameters, and necessarily some specific ones depending on the data type. The common parameters that can be refined by both programs are: the equilibrium constants, the initial concentrations of the components, and any auxiliary parameters that are defined by the user. Other common parameters that are not refined by the program, but that also need to be defined, are: the species size and charge, the counterions that are present and their charge and concentrations, the solvent type, and the temperature of the reaction. Take, for example, the previously introduced reaction described on page 88. In such an equilibrium experiment, the usual parameters that are refined include the equilibrium constants, such as $\log \beta_{120}$ and $\log \beta_{111}$, and the initial concentrations, that is [M], [L], and [H]. The additional information that must be supplied as part of the analysis includes: the charge of all the species defined by the model, for example ML^{2+} and MLH^{3+} , the charge and concentration of any counterions that are present, such as ClO_4^- from the metal salt, the solvent used should be identified as solvents such as alcohols have markedly different dielectric constants compared to water, and the temperature should be recorded, most commonly 25.0°C.

For potentiometric titrations the calibration parameters of the electrode can also be refined as part of the analysis, as well as the liquid junction potential. For spectrophotometric titrations each species needs to be defined as non-absorbing, absorbing or known. Known spectra require the user to enter the absorptivity of the species for the analysis, for example the pure spectrum of the metal species in the reaction.

Each parameter that can be optimised has to be specified as one of the two options, either as 'Fix' or 'Fit'. Obviously those that are fitted are refined to their optimum value by the program. Those that are fixed are left at their original value, however, they still influence the optimisation as their values are used alongside the optimised parameters in order to calculate the data and subsequently the *ssq* value after each iteration.

Following every iterative loop in the optimisation procedure the calculated parameter values are updated in the Excel workbook. The continuous updating was implemented as it enabled the user to follow the optimisation process by observing the changing values in Excel, for example, by monitoring the relevant plots to graphically view the convergence between the measured and calculated data. However, the user must be aware that because the parameters that are fitted are updated iteratively as part of the analysis, any cell containing a fitted parameter is completely overwritten with the new parameter value following every iterative cycle. Therefore, if an equation has been entered to calculate a parameter value, and the parameter is chosen to be fitted, the equation is over-written with the parameter value after the first iteration. Consequently any functionality in that cell will be lost.

Importantly, ‘auxiliary parameters’ were introduced as part of the Excel user-interface to circumvent this problem. Any formulas corresponding to specific parameters can be entered as auxiliary parameters and chosen to be fixed, that is not optimised in the analysis, therefore enabling the functionality of the formula throughout the optimisation procedure. However, if the user wishes, auxiliary parameters can also be optimised as part of the analysis. It should be noted that any parameter specified to be a fixed parameter does not have its value updated iteratively, therefore any equations present in such parameter cells will be active throughout the analysis.

2.4.3 Output

The results of the data analysis can be displayed in varying ways depending on what the user needs to focus on. For example, the program transforms the equilibrium constant data to the desired species distribution curves of the type illustrated in Figure 2.29 and Figure 2.33, in a potentiometric titration the species concentrations can be displayed as a function of changing pH, this enables easy identification of the pH at which species is present in its maximum concentration and also the pK at which each species forms. In metal-ligand titrations the species concentrations can be displayed as the metal -ligand ratio, making it easier to identify the nuclearity of species that form.

Another example of graphs which are very useful for spectrophotometric data analysis are the forward and backward EFA⁴⁸ plots, a forward EFA plot is represented in Figure 2.34. Such plots enable identification of how many species are present in the solution and at what point they form and/or disappear. These coloured graphs and many more

can be produced in either Excel or Matlab environments and can be directly copied into a word processor documents for easy presentation and recording of results.

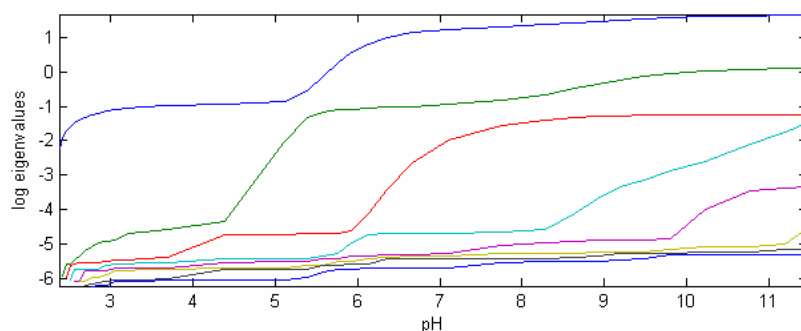


Figure 2.34: Plot representing one possible graphical output from our data analysis program for spectrophotometric data. The plot shows the log of the forward EFA plot of a spectrophotometric titration. The analyst can determine that at least five absorbing species present in the titration and can also determine the pH at which each species is seen to form.

Other useful graphs that are displayed as part of the analysis include overlaid plots of the measured and calculated data, as shown in Figure 2.35. Such plots are essential in order to determine if the model and determined parameters fit the data that was measured.

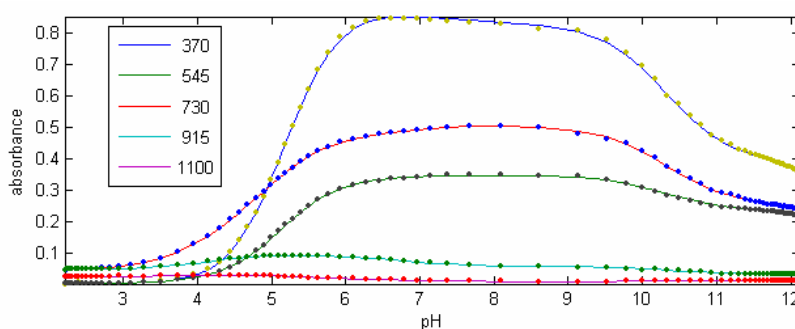


Figure 2.35: Plot showing overlaid measured (•••) and calculated (—) data for five key wavelengths after the fitting procedure has completed. It can clearly be seen that the calculated data corresponds with what was measured in the spectrophotometric titration.

2.5 Conclusions

Model-based data fitting is a powerful analytical instrument. The software available today enables robust analysis of large collections of data, based on rather complex models, to be common and often straightforward. There are a few improvements that would enhance the power of existing packages. Firstly, statistical analysis of results that goes beyond the delivery of standard deviations for the fitted parameters. While

these provide good estimates, many researchers found them of limited reliability. Secondly, the determination of the correct model is difficult and requires much input from the researcher. The model-fitting process is reasonably well advanced and usually proceeds routinely and is essentially automatic. However, in order to determine the best model the researcher has to try different alternatives and make a decision based on the statistical information given by the program and the chemical understanding available for the system under investigation.

Modern analytical techniques also introduce the possibility of the postulation of unjustified species, as well as the generation of meaningless parameters, whose purpose is merely to assist in fitting the experimental data. This can lead to serious problems as researchers can postulate the presence of species, that in fact do not exist, simply because the model and parameters converge to a minimum and the measured and calculated data still correlate. This can further result in misleading other researchers studying related systems, and the problem can be compounded as researchers justify their proposed models from previously published information, that may in fact not be accurate. Therefore, considerable care and insight into the chemical nature of the species under consideration are required to avoid the proposal of non-existent species and the calculation of meaningless equilibrium or rate constants¹².

Filella *et al*⁶⁰ address a recent problem concerning the disparate ways in which equilibrium and rate constants are now reported and published in literature, thus making it difficult to compare results from different researchers and to create a universal database. These discrepancies can be partly explained by the rapid increase in the number of computer programs available that can compute equilibrium and rate constants in recent years, for example see references [19, 48, 56, 59, 66-86]. Furthermore, many of these techniques used to calculate the equilibrium and rate constants produce significantly different answers. One reason for differing calculated constants from potentiometric data is due to how the titration parameters and other experimental parameters are calculated. The analytical concentrations and electrode calibration parameter refinement is responsible for much of the calculational diversity, especially with the development of programs that can optimise these parameters simultaneously rather than having to use estimated values for parameters. Calculated constants can also differ depending on the nature of the objective function, for example, whether the residuals are expressed in terms of electrode signal or titrate volumes and so

forth, and also what weighting of residuals have been applied. Further, variations can occur depending on whether or not corrections are made for the effects of changing ionic strength, the liquid junction potentials and/or ion selectivity of the electrode.

The following summary of recommendations for a general procedure, or checklist that should be referred to, in order to satisfactorily determine equilibrium and rate constants has been based on the outline presented by Filella *et al* ⁶⁰. The summary is a result of their extensive research and experience in the area and was presented as a response to the considerable discrepancies that were noted between values published for the same chemical systems by various authors. The purpose was to describe and justify a number of appropriate procedures that would enable valid cross-comparisons between results. In order to achieve this, the minimum amount of information that ought to be included when equilibrium and rate constants are reported is supplied.

Data Collection and Evaluation

No method or amount of data analysis can overcome faulty data. The occurrence of errors in data, such as mistaken values lying outside the researchers ordinary error distribution, that remain undetected before the data is processed by an optimising computer program is one of the most common causes of discrepancies between published sets of data. This is because the effects of many kinds of analytical errors become obscured by correlations within the system ⁴⁵. Artefacts of the least-squares calculation, known as ‘computer complexes’, arise from poor experimentation. For equilibrium investigations the nature of a titration, that is where many observations are made at highly interdependent points, exacerbates this effect. The effect can be further worsened through what has been termed the ‘linkages of systematic errors’, which can occur if interdependence exists between titrations, for example from the use of stock solutions.

Therefore, before data processing is commenced, considerable care needs to be taken to ensure that there are no gross errors in the measured data, and also that there is as much independence between experiments as possible. Ideally, the entire procedure should be replicated absolutely independently a number of times and the results shown to be satisfactorily superimposable. However, this is mostly impractical for the determination of the majority of equilibrium and rate constants. Hence, individual researchers need to assess what is a reasonable level of reproducibility and report it accordingly. The

number of measurements performed for each investigation, the number of data points for each measurement and the analytical concentrations should be reported along with the calculated equilibrium and rate constants. Also, the degree of independence between measurements, especially regarding stock solutions, and the measures taken to ensure the reproducibility of the measured data should be detailed.

Model Selection

Model selection poses a formidable problem with the characterisation of many equilibrium or kinetic systems. In essence, the difficulty is to know when an optimised equilibrium and rate constant for a proposed species reflects a genuine reaction occurring in solution, as the number of possible complex stoichiometries that can be formed by metal-ligand coordination is quite large. All equilibrium and rate constant optimisations use a pre-defined set of species, determined from the proposed model, which are supposed to exist in solution. Therefore, the calculation is undermined if the proposed model is untrue.

The inclusion of non-existent species in the least-squares analysis can often lead to spurious improvement between observed and calculated data, that is, a reduction in the *ssq* value. This is because the optimisation procedure can exploit the additional degree of freedom, refer to Equation (2.38), and therefore reduce the effect of experimental errors that are always present in real data. Hence, the question that always arises in model selection is whether or not the effect of including an additional species in the model is significant enough to establish that the species has a real existence.

The traditional approach used to determine whether a species should be included in the proposed model is to employ a variety of ‘model selection criteria’⁶¹. The principal factor is to assess whether the introduction of the new species has resulted in substantial improvement in the *ssq* value. For example, an improvement in the *ssq* value of 50% would be regarded as significant, but 10% improvement may not be. This criterion alone is obviously insufficient to determine the inclusion of species. For a minor species to be accepted as a genuine species it should also result in an improvement in internal consistency of the data, as reflected by better calculated standard deviations of calculated equilibrium and rate constants, especially with respect to improvements in the major species of the model.

Minor species should also be calculated to occur at significant concentrations over a range of points in more than one measurement. Complexes that do not reach at least 10% of the total metal concentration should always be regarded as uncertain unless the species is known to exist from other research or experimentation. In such cases either the equilibrium or rate constant should be fixed as it will be poorly defined if fitted as part of the analysis and, if spectrophotometric data is acquired, fixing the molar absorptivity of the minor species if its spectra is known would help to define it.

As a final check, the introduction of the species should result in a markedly better fit between the observed and calculated data as seen in a graphical visualisation and also the by a reduction in the aforementioned *ssq* value.

Using the traditional approach as an assessment of whether or not a species should be included in the proposed model is an inherently subjective method. Unless the criteria are applied with caution and knowledge of their limitations they can be misleading in their results. Each of the effects that can arise from the inclusion of a minor species to a model can equally arise from the removal of systematic experimental errors by the optimisation process. The implication is that species should only be selected when their effect on the data behaviour is clearly beyond any other reasonable behaviour. It then becomes preferable to exclude from the 'best model' any species that are in question. During model selection it is always better to have too few species than too many.

It cannot be overemphasised that a reaction mechanism is essentially a theory that has been devised to explain currently known experimental facts, such as the overall stoichiometry and the dependence of reaction rate and equilibrium constant on concentration, temperature, or other variables. In general such experimental facts can be interpreted in several ways, resulting in several mechanisms that are consistent with the data. Further experimentation may eliminate some of these, but even if only one mechanism remains that is in agreement with all the known facts, there is no assurance that it is unique or that new experiments will not add evidence discrediting it. As with other theories, new information can modify a reaction mechanism, rather than eliminate it completely⁶².

Ionic strength corrections

Neither corrections for changes in ionic strength, nor the choices made regarding weighting, should significantly alter the equilibrium and rate constant values obtained.

However, in practise, both produce differences which, depending on the system and the ranges over which the data has been collected, can sometimes be too large to be ignored. In traditional measurements, introducing a correction for changes in ionic strength should only have a marginal influence on the ssq value, because experimental conditions have been chosen to minimise such changes. However, even when such conditions are applied, typically the use of a high concentration of inert salt, the ionic strength must vary to some extent over the course of a measurement and it may sometimes do so markedly. Under such circumstances, or for modern experiments where the researcher can apply activity coefficient corrections in the analytical program, the chief consequence is to improve the internal consistency between data points and to ensure that all refer precisely to the same reference ionic strength. This correction can sometimes alter the equilibrium and rate constant values significantly.

Similarly, in potentiometric measurements, the use of corrections for liquid junction potentials or ion selectivity of the electrode should not be regarded as means by which equilibrium and rate constant determinations can be improved. Such corrections can be used to test the sensitivity of the results with respect to such effects so that unstable equilibrium constants can be identified.

Refinement of Values

Refinement of the equilibrium and rate constants by the simultaneous optimisation of other experimental parameters, such as the ionisation constant of the solvent and initial reagent concentrations, generally results in improved values then would be obtained otherwise. This is because the effects of unavoidable system errors, from whatever source, are at least partially adsorbed into the additional refinable parameters. This is beneficial because the latter are not relevant to the result of primary interest, namely the equilibrium and rate constant values. Thus, for the chosen model, those optimised parameters should be regarded as ‘best’, that is, the values that approximate the true values most closely.

2.5.1 Our Developed Programs

The data acquisition and analysis programs that were developed as part of this research can be considered to be some of the most modern programs available. The ease with which the data acquisition programs can be adapted to suit different experimental conditions, that are often unexpected but necessary, and the simplified user-interfaces

that are easy for new users to learn and manipulate, are key factors that influenced the design of the programs. Similarly, with the data analysis programs, one of the most important aspects of the development was to constantly ensure that the user-interfaces were as user-friendly as possible. This aspect was greatly helped as new users learnt how to use the programs and difficulties they encountered were generally rectified leading to the program being significantly improved over the few years that they were being developed.

The control of the instruments and the analytical computations were both programmed in the language Matlab which is a very suitable program as it is matrix-based and the data collected and manipulations were all matrix based for our research.

The link between Excel and Matlab proved to be a very successful design for both data acquisition and analysis. Further development of the analysis programs is currently underway as is the acquisition development, for instance, the program has been extended to perform CD titrations, see Chapter 4. Overall the programs developed have the distinct advantage that they are not only user-friendly, but are also easy to develop and improve.

2.6 References

1. Haswell, S. J., *Practical Guide to Chemometrics*. Marcel Dekker, Inc.: New York, New York, 1992.
2. Gemperline, P.; Editor, *Practical Guide to Chemometrics, Second Edition*. 2006; p 541
3. Otto, M., *Chemometrics: Statistics and Computer Application in Analytical Chemistry*. Wiley-VCH: Weinheim, 2007; p 343.
4. Adams, M. J., *Chemometrics In Analytical Spectroscopy*. 2nd ed.; Royal Society of Chemistry Cambridge, UK, 2004.
5. Espenson, J. H., *Chemical Kinetics and Reaction Mechanisms*. McGraw-Hill: New York, 1995.
6. Polster, J.; Lachmann, H., *Spectrometric Titrations: Analysis of Chemical Equilibria*. VCH Publishers: New York, NY, 1989.
7. Wilkins, R. G., *Kinetics and Mechanism of Reactions of Transition Metal Complexes*. 2 ed.; VCH Publishers, Inc.: New York, 1991.
8. Dyson, R. M.; Kaderli, S.; Lawrance, G. A.; Maeder, M.; Zuberbuhler, A. D., Second order global analysis: the evaluation of series of spectrophotometric titrations for improved determination of equilibrium constants. *Analytica Chimica Acta* **1997**, 353, (2-3), 381-393.
9. Wikipedia® Titration. <http://en.wikipedia.org/wiki/Titration> (15/06/07),
10. SparkNotes, Acid-Base Titrations. In Barnes & Noble 2006; Vol. 2007, p diagram.
11. Benesch, R. E.; Benesch, R., The acid strength of the -SH group in cysteine and related compounds. *Journal of the American Chemical Society* **1955**, 77, 5877-81.
12. Martell, A. E.; Motekaitis, R. J., Potentiometry revisited: the determination of thermodynamic equilibria in complex multicomponent systems. *Coordination Chemistry Reviews* **1990**, 100, 323-61.
13. Martell, A. E. M., R.J., *Determination and Use of Stability Constants*. VCH: Weinheim, 1988.
14. Gampp, H., Investigation of solution kinetics of transition-metal complexes by EPR spectroscopy. *Inorganic Chemistry* **1984**, 23, (22), 3645-9.
15. Araujo, C. L.; Ibanez, G. A.; Ledesma, G. N.; Escandar, G. M.; Olivieri, A. C., EPSILON: a versatile microcomputer program for the spectrophotometric data analysis of metal-ligand equilibria. *Computers & Chemistry (Oxford)* **1998**, 22, (2-3), 161-168.

16. Root, C. B., Ultraviolet spectrophotometric determination of mixtures of vanadium(IV) and vanadium(V). *Anal. Chem.* **1965**, 37, (12), 1600-1.
17. Meloun, M.; Havel, J.; Högfeltdt, E., *Computation of solution equilibria : a guide to methods in potentiometry, extraction, and spectrophotometry*. Chichester: England, 1988.
18. Lee, J. E., Jr.; Edgerton, J. H.; Kelley, M. T., Pyrohydrolytic separation and spectrophotometric titration of fluorides in radioactive samples. *Anal. Chem.* **1956**, 28, 1441-3.
19. Grabaric, B.; Piljac, I.; Filipovic, I., Numerical treatment in determining stability constants by the spectrophotometric method of corresponding solutions. *Analytical Chemistry* **1973**, 45, (11), 1932-6.
20. Dyson, R. Second Order Globalisation of Spectrophotometric Data Analysis: Theory, Instrumentation, and Application to Solution Equilibria. Doctor of Philosophy, Newcastle University, Newcastle, 1997.
21. Pilling, M. J.; Seakins, P. W., *Reaction Kinetics*. Oxford University Press Inc.: New York, 1995.
22. Gibson, Q. H.; Milnes, L., Apparatus for rapid and sensitive spectrophotometry. *The Biochemical journal* **1964**, 91, (1), 161-71.
23. Meloun, M.; Bordovska, S.; Syrovy, T.; Vrana, A., Tutorial on a chemical model building by least-squares non-linear regression of multiwavelength spectrophotometric pH-titration data. *Analytica Chimica Acta* **2006**, 580, 107-121.
24. Maeder, M.; Norman, S. E., Model Based Analysis for Kinetic and Equilibrium Investigations. *Critical reviews in analytical chemistry* **2006**, 36, 199-209.
25. Molloy, K. J.; Maeder, M.; Schumacher, M. M., Hard modeling of spectroscopic measurements. Applications in non-ideal industrial reaction systems. *Chemometrics and Intelligent Laboratory Systems* **1999**, 46, (2), 221-230.
26. Albert, A.; Sergeant, E. P., *The Determination of Ionisation Constants. A Laboratory Manual*. 3rd ed.; Chapman and Hall: London, 1984.
27. Wikipedia® Beer-Lambert Law. http://en.wikipedia.org/wiki/Beer-Lambert_law (25/9/06),
28. Maeder, M. N., Yorck-Michael, *Practical Data Analysis in Chemistry*. 1st ed.; Elsevier: Amsterdam, 2007; Vol. 26, p 326.
29. Harris, D. C., *Quantitative Chemical Analysis*. 6 ed.; Freeman, W.H.: New York, 2003.

30. Some, I. T.; Bogaerts, P.; Hanus, R.; Hanocq, M.; Dubois, J., Improved kinetic parameter estimation in pH-profile data treatment. *International journal of pharmaceutics* **2000**, 198, (1), 39-49.
31. Maeder, M.; Molloy, K. J.; Schumacher, M. M., Analysis of non-isothermal kinetic measurements. *Analytica Chimica Acta* **1997**, 337, (3), 73-81.
32. Maeder, M.; Neuhold, Y.-M.; Puxty, G.; King, P., Analysis of reactions in aqueous solution at non-constant pH: no more buffers? *Physical Chemistry Chemical Physics* **2003**, 5, (13), 2836-2841.
33. Bevington, P. R.; Robinson, D. K., *Data reduction and error analysis for the physical sciences*. 3 ed.; McGraw-Hill: Boston, 1969.
34. Press, W. H.; Lannery, B. P.; Teukolsky, S. A.; Vetterling, W. T., *Numerical Recipes*. Cambridge University Press: Cambridge ; New York, 1993.
35. Maeder, M.; Zuberbuehler, A. D., Nonlinear least-squares fitting of multivariate absorption data. *Analytical Chemistry* **1990**, 62, (20), 2220-4.
36. Gans, P., Numerical methods for data-fitting problems. *Coordination Chemistry Reviews* **1976**, 19, (2), 99-124.
37. Levenberg, K., A Method for the Solution of Certain Non-Linear Problems in Least Squares. *Quart. Appl. Math* **1944**, (2), 164-168.
38. Marquardt, D., An Algorithm for Least-Squares Estimation of Nonlinear Parameters. *SIAM J. Appl. Math* **1963**, (11), 431-441.
39. Leardi, R., Genetic algorithms in chemometrics and chemistry: a review. *Journal of Chemometrics* **2001**, 15, (7), 559-569.
40. Maeder, M.; Neuhold, Y.-M.; Puxty, G., Application of a genetic algorithm: near optimal estimation of the rate and equilibrium constants of complex reaction mechanisms. *Chemometrics and Intelligent Laboratory Systems* **2004**, 70, (2), 193-203.
41. Watkins, P.; Puxty, G., A hybrid genetic algorithm for estimating the equilibrium potential of an ion-selective electrode. *Talanta* **2006**, 68, (4), 1336-1342.
42. CompuDrug International, I. *pKalc Pallas 3.0*, Sedona, 2006.
43. Szegezdi, J.; Csizmadia, F. New Method for pK_a Estimation.
http://www.chemaxon.com/conf/New_method_for_pKa_estimation.pdf (22/10),
44. Szegezdi, J.; Csizmadia, F. Prediction of dissociation constant using microconstants.
http://www.chemaxon.com/conf/Prediction_of_dissociation_constant_using_microconstants.pdf (22/10),

45. May, P. M.; Murray, K.; Williams, D. R., The use of glass electrodes for the determination of formation constants. III. Optimisation of Titration Data: The ESTA Library of Computer Programs. *Talanta* **1988**, 35, (11), 825-830.
46. Gampp, H.; Maeder, M.; Meyer, C. J.; Zuberbuehler, A. D., Evolving factor analysis of spectrophotometric titrations: forget about the law of mass action? *Chimia* **1985**, 39, (10), 315-17.
47. Keller, H. R.; Massart, D. L., Evolving factor analysis. *Chemometrics and Intelligent Laboratory Systems* **1992**, 12, (3), 209-24.
48. Maeder, M.; Zilian, A., Evolving factor analysis, a new multivariate technique in chromatography. *Chemometrics and Intelligent Laboratory Systems* **1988**, 3, (3), 205-13.
49. Potyrailo, R. A.; Wroczynski, R. J.; Lemmon, J. P.; Flanagan, J. P.; Siclovan, O. P., Multivariate Tools for Real-Time Monitoring and Optimisation of Combinatorial Materials and Process Conditions. In *Analysis and Purification Methods in Combinatorial Chemistry*, Yan, B., Ed. John Wiley and Sons, Inc.: Hoboken, New Jersey, 2004.
50. Photophysics, A. <http://www.photophysics.com/prokii.php> (16/10/06),
51. Gaizer, F., Computer evaluation of complex equilibria. *Coordination Chemistry Reviews* **1979**, 27, (3), 195-222.
52. Gans, P.; O'Sullivan, B., GLEE, a new computer program for glass electrode calibration. *Talanta* **2000**, 51, (1), 33-37.
53. Baeza, J. J.; Ramis, G.; Mongay, C., A program for the simultaneous potentiometric determination of protonation constants and electrode calibration parameters. *Journal of Chemometrics* **1988**, 3, (Suppl. A), 223-9.
54. Arena, G.; Rizzarelli, E.; Sammartano, S.; Rigano, C., A nonlinear least-squares approach to the refinement of all parameters involved in acid-base titrations. *Talanta* **1979**, 26, (1), 1-14.
55. Scientific, H.-T. Products: SPECFIT/32T for Windows 95/98/NT4.0. <http://www.hitechsci.com/specfit32.html> (20/07/07),
56. Bio-Logic, S. Specfit/32™ <http://www.bio-logic.info/rapid-kinetics/images/specfit.gif> (12/4/07),
57. Meloun, M.; Bordovska, S.; Vrana, A., The thermodynamic dissociation constants of the anticancer drugs camptothecin, 7-ethyl-10-hydroxycamptothecin, 10-hydroxycamptothecin and 7-ethylcamptothecin by the least-squares nonlinear regression of multiwavelength spectrophotometric pH-titration data. *Anal. Chem. Acta*. **2007**, 584, 419-432.

58. Dyson, R.; Maeder, M.; Puxty, G.; Neuhold, Y.-M., Simulation of complex chemical kinetics. *Inorganic Reaction Mechanisms (Philadelphia, PA, United States)* **2003**, 5, (1), 39-46.
59. Bugnon, P.; Chottard, J.-C.; Jestin, J.-L.; Jung, B.; Laurenczy, G.; Maeder, M.; Merbach, A. E.; Zuberbuehler, A. D., Second-order globalization for the determination of activation parameters in kinetics. *Analytica Chimica Acta* **1994**, 298, (2), 193-201.
60. Filella, M.; May, P. M., Reflections on the calculation and publication of potentiometrically-determined formation constants. *Talanta* **2005**, 65, (5), 1221-1225.
61. Berthon, G.; May, P. M.; Williams, D. R., Computer simulation of metal-ion equilibria in biofluids. Part 2. Formation constants for zinc(II)-citrate-cysteinate binary and ternary complexes and improved models of low-molecular-weight zinc species in blood plasma. *Journal of the Chemical Society, Dalton Transactions: Inorganic Chemistry (1972-1999)* **1978**, (11), 1433-8.
62. Moore, J. W.; Pearson, R. G., *Kinetics and Mechanism*. 3rd ed.; John Wiley and Sons, Inc.: Canada, 1981.

Chapter 3

Analysis of Potentiometric and Spectrophotometric Titrations with Polydentate N-donor Ligands

3.1 Introduction

There are various methods for determining equilibrium constants, the most common being potentiometric and/or spectrophotometric titrations. Other techniques include nuclear magnetic resonance (NMR), electronic spin resonance (ESR), solubility, and conductance. Potentiometry has outstanding importance because it is fast, accurate and reproducible ¹. It is known as a relatively simple method that is reliable for obtaining acid dissociation constants or metal ion complex stability constants ². In this study potentiometry was used to determine protonation constants as well as the stability constants of metal-ligand complexes in solution. Spectrophotometric techniques were also applied to determine the metal-ligand complexes that formed in solution, along with the determination of the spectra of each complex identified.

The protonation constant, pK , of a ligand is a very important physio-chemical property as these constants are relevant in a wide range of applications and research areas, such as geochemistry, marine chemistry, biochemistry, pharmaceuticals, bioinorganic chemistry, analytical biochemistry, physical chemistry and analytical chemistry ³. It is of fundamental importance to accurately determine the protonation constants of many types of ligands for these various applications. In this research the newly developed in-house analytical programs, Pot_Anal and Spec_Anal, were used to determine such constants.

For many ligands it is also constructive to determine stability constants as these constitute an important auxiliary tool in qualitative and structural coordination complex analysis. Nowadays, the measurement of metal-ligand constants is often regarded as routine, a view that greatly underestimates the difficulties that are involved in determining accurate and reliable values. Interest in the formation of metal complexes has changed from the more theoretical purposes of interpreting the mechanism of formation and correlating stability constant data, to numerous applied fields ranging from the formation of complexes in biological fluids to applications such as the treatment of sewerage ⁴. Small differences in stability constant values can be of

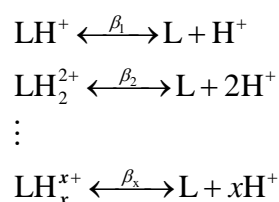
structural significance and, therefore, very accurate determinations are frequently required.

The determination of accurate protonation and stability constants is dependant on both the acquisition of high-quality data and the corresponding mathematical treatment of the data. The technique used for the experimentation in this work has already been described in Chapter 2, Section 2.2, which included in-depth discussions on the accuracy of the described methods. The analytical approach used to determine the respective equilibrium constants detailed below has also been previously discussed, see Chapter 2, Section 2.4.

Recent developments, such as the availability of high speed computers and modern solid state electronics, have facilitated equilibrium constant determination. In order to calculate protonation and stability constants knowledge of the concentration of the components in the system, for example ligands, free metals, hydrogen ions, protonated forms of ligands, hydrolysis products of metal ions, and so forth, were required. With the computer methods that are now available, it is possible to determine stability constants for one or more metal ions and ligands, together with all relevant hydrolysis and protonation constants. This provides a complete description of the solution under the conditions for which the constants apply ⁵. Such analysis is performed for the polydentate N-donor ligands in this study.

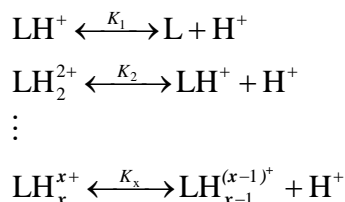
3.1.1 Protonation Constants

The protonation constant for a ligand, L, are traditionally written as dissociation expressions and can be described in two ways. Firstly, the deprotonation of a ligand can be written as overall reactions. These show the protonated species dissociating into its individual components as the products, as shown in Scheme 3.1. Equilibrium expressions written in this way result in the determination of β equilibrium constant values.



Scheme 3.1: Overall deprotonation equilibria of a ligand, L. For simplicity, the unprotonated ligand is assumed to be neutral.

The second way that deprotonation reactions are written is with the protonated species dissociating into a proton and the remaining ligand species, as shown in Scheme 3.2. Equilibrium expressions written in this way result in the determination of K equilibrium constant values.



Scheme 3.2: Deprotonation equilibria of a ligand, L. For simplicity, the unprotonated ligand is assumed to be neutral.

As with all equilibrium constants, the protonation constant, K , is defined from the concentrations of the respective species at equilibrium. Equation (3.1) depicts the protonation constant for the first protonation of the ligand shown above.

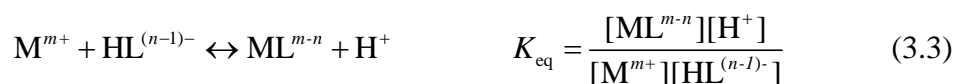
$$K_1 = \frac{[\text{L}][\text{H}^+]}{[\text{LH}^+]} \quad (3.1)$$

Protonation constants are usually quoted as $\text{p}K$ values, which are simply minus the log of the calculated K value, Equation (3.2), as K values tend to vary in many orders of magnitude. Therefore, it is easier to compare different ligands protonation constants by comparing $\text{p}K$ values as they vary over a much smaller range.

$$\text{p}K = -\log_{10}(K) \quad (3.2)$$

3.1.2 Stability Constants

Stability constants of pH dependant ligands are based primarily on the competition between hydrogen ions and metal ions for coordination sites on the ligand and involve displacement reactions analogous to Equation (3.3).



In this study the interaction of copper(II) and nickel(II) with a series of polydentate N-donor ligands was investigated. It is known that competitive binding of a metal ion to a N-donor ligand in solution drops the $\text{p}K$ values for N-H^+ ionisation by an amount related to the strength of the metal binding, in theory allowing a convenient method to determine binding constants ².

For all but the simplest systems, for example pure acid-base equilibria, it is common practice to determine equilibrium constants from a series of independent titrations with different analytical concentrations and, where applicable, different metal-ligand ratios. This technique is, in general, necessary for stepwise complexation equilibria in order to distinguish between mono-, bi-, and potentially poly-nuclear species ⁶.

3.1.2.1 Defining Stability Constants

As previously discussed there are two styles commonly used to define protonation and stability constants. Most analytical programs, including the in-house developed programs Pot_Anal and Spec_Anal, determine overall constants, $\log \beta$ values, as they are by definition less ambiguous than $\log K$ constants as discussed in Chapter 1, Section 1.3.4. However, it is often constructive to calculate $\log K$ constants from the overall constants as they are easier to compare and relate to pH. The examples given below demonstrate the typical methods applied in order to determine the relationship between $\log K$ and $\log \beta$ constants.

Consider the typical reaction of a metal ion, ligand and a hydrogen ion reacting together to produce the species MLH. Such a reaction can be written in two ways, firstly as an overall reaction, $M + L + H \leftrightarrow MLH$, and secondly as a $\log K$ reaction written as $ML + H \leftrightarrow MLH$, charges omitted for clarity. The values of the constants determined for each equation necessarily differ, as shown in the following example. Scheme 3.3 demonstrates the process followed in order to calculate the $\log K_{ML}^H$ equilibrium constant for the formation of MLH from the overall constant values acquired from the analysis.

$$\begin{aligned}
 K_{ML}^H &= \frac{[MLH]}{[ML][H]} \\
 &= \frac{\beta_{111}[M][L][H]}{[ML][H]} & \text{where } \beta_{111} &= \frac{[MLH]}{[M][L][H]} \\
 &= \frac{\beta_{111}[M][L]}{[ML]} \\
 &= \frac{\beta_{111}}{\beta_{110}} & \text{where } \beta_{110} &= \frac{[ML]}{[M][L]}
 \end{aligned}$$

Hence;

$$\log K_{ML}^H = \log \beta_{111} - \log \beta_{110}$$

Scheme 3.3: Calculation of $\log K_{ML}^H$ from overall constant values.

For example, a $\log \beta_{111}$ value of 14.586 and a $\log \beta_{110}$ value of 9.256 result in a $\log K_{ML}^H$ value of 5.330 being determined. However, the formation of the species MLH can also be written as a $\log K$ equilibrium using a different equation, that is, the reaction of a metal ion with the protonated ligand. This reaction, $M + LH \leftrightarrow MLH$, necessarily has a different equilibrium constant, $\log K_{LH}^M$, as is shown in Scheme 3.4.

$$\begin{aligned}
 K_{LH}^M &= \frac{[MLH]}{[M][LH]} \\
 &= \frac{\beta_{111}[M][L][H]}{[M][LH]} & \text{where } \beta_{111} &= \frac{[MLH]}{[M][L][H]} \\
 &= \frac{\beta_{111}[L][H]}{[LH]} \\
 &= \frac{\beta_{111}}{\beta_{011}} & \text{where } \beta_{011} &= \frac{[LH]}{[L][H]}
 \end{aligned}$$

Hence;

$$\log K_{LH}^M = \log \beta_{111} - \log \beta_{011}$$

Scheme 3.4: Calculation of $\log K_{LH}^M$ from overall constant values.

For example a $\log \beta_{111}$ value of 14.586 and a $\log \beta_{011}$ value of 8.560 result in a $\log K_{LH}^M$ value of 6.026 being determined, which is clearly a different value to that determined for the constant $\log K_{ML}^H$. Therefore, when defining the formation of a species using $\log K$ constants, it is imperative to clearly detail which process is being defined in order to prevent ambiguity concerning what reaction the $\log K$ value is representing.

The determination of $\log K$ constants from overall constants becomes more complex when deprotonated species are considered, for example MLH_1 and MLH_2 . The overall formation of MLH_1 can be written as $M + L - H \leftrightarrow MLH_1$, whereas the $\log K$ constant is, by convention, written as a protonation reaction, $MLH_1 + H \leftrightarrow ML$. The calculation of the $\log K$ constant from the overall constants is shown in Scheme 3.5.

$$\begin{aligned}
 K_{MLH_{-1}}^H &= \frac{[ML]}{[MLH_{-1}][H]} \\
 &= \frac{\beta_{110}[M][L]}{[MLH_{-1}][H]} & \text{where } \beta_{110} &= \frac{[ML]}{[M][L]} \\
 &= \frac{\beta_{110}}{\beta_{11-1}} & \text{where } \beta_{11-1} &= \frac{[MLH_{-1}]}{[M][L][H]^{-1}}
 \end{aligned}$$

Hence;

$$\log K_{MLH_{-1}}^H = \log \beta_{110} - \log \beta_{11-1}$$

Scheme 3.5: Calculation of step-wise $\log K_{MLH_{-1}}^H$ from overall constant values.

For example a $\log \beta_{110}$ value of 9.256, $\log \beta_{11-1}$ equalling 1.814, and β_{11-2} equalling -8.632, yields a resultant $\log K_{MLH_{-1}}^H$ value of 7.443. In a similar way the formation constant of $MLH_2 + H \leftrightarrow MLH_{-1}$ from the overall constant $M + L - 2H \leftrightarrow MLH_2$ can be calculated as shown in Scheme 3.6.

$$\begin{aligned}
 K_{MLH_2}^H &= \frac{[MLH_{-1}]}{[MLH_2][H]} \\
 &= \frac{\beta_{11-1}[M][L][H]^{-1}}{[MLH_2][H]} & \text{where } \beta_{11-1} &= \frac{[MLH_{-1}]}{[M][L][H]^{-1}} \\
 &= \frac{\beta_{11-1}[M][L][H]^{-2}}{[MLH_2]} \\
 &= \frac{\beta_{11-1}}{\beta_{11-2}} & \text{where } \beta_{11-2} &= \frac{[MLH_2]}{[M][L][H]^{-2}}
 \end{aligned}$$

Hence;

$$\log K_{MLH_2}^H = \log \beta_{11-1} - \log \beta_{11-2}$$

Scheme 3.6: Calculation of step-wise $\log K_{MLH_2}^H$ from overall constant values.

That is, a $\log \beta_{11-1}$ value of 1.814 and a $\log \beta_{11-2}$ value of -8.632 will result in a $\log K_{MLH_2}^H$ of 10.446. These techniques were applied in Sections 3.4 and 3.5 in order to determine the $\log K$ constants of the ligands from the $\log \beta$ constants that are determined in the analytical programs.

The analytical programs Pot_Anal and Spec_Anal provide standard deviations for the equilibrium constants that are optimised. When $\log K$ values are calculated from the determined $\log \beta$ values error propagation must be applied in order to have an error estimate of the $\log K$ constants. Error propagation is a way of combining two or more errors together to get a third. The following equation was applied in order to calculate the standard deviation of the $\log K$ values.

$$\delta(x-y) = \delta(x+y) = [(\delta x)^2 + (\delta y)^2]^{1/2} \quad (3.4)$$

3.1.3 Combined Potentiometric and Spectrophotometric Titration Analysis

As previously discussed, the analytical technique of potentiometry is considered to be one of the most accurate methods for evaluating complex equilibrium constants². For this study potentiometric titrations were performed in order to investigate two equilibria, namely protonation and metal-ligand stability, were investigated. Therefore, two types of titrations were required, the first being a titration to determine the protonation parameters of the ligand. This required the ligand to be protonated and then titrated with NaOH, the results of these titrations have been provided later in Table 3.9. The second equilibria, the interaction between a metal ion and the ligand, required the metal salt to be added to the protonated ligand solution before performing the titration with NaOH.

Spectrophotometric titrations could only be used to investigate the metal-ligand interaction as the ligand did not absorb in the visible region of the spectrum. Titrations were performed in a similar manner as for the metal-ligand potentiometric titrations and multiple titrations were performed at varying metal-ligand ratios in order to adequately define the species formed in the titration.

The use of both titration techniques to investigate a metal-ligand system enables titrations to be performed with concentrations of different orders of magnitude, depending on the molar absorptivity values of the species formed, as spectroscopic studies can generally be performed at much lower concentrations than are required for potentiometric experiments. Alternatively, potentiometric titrations can be performed at high concentrations, which would result in absorbance values greater than one if spectrophotometric titrations were used. Changing the concentration by such large factors can favour or hinder species formation, hence enabling the identification of different species from both titration techniques.

Even though potentiometric titration analysis can define metal-ligand stability constants, the analysis cannot elucidate the structure of the metal complexes formed. The inclusion of spectrophotometric studies to the potentiometric investigation of stability constants presents additional advantages from a qualitative point of view as they provide the spectra of the metal complexes. These can be informative with respect to the structure of the complexes formed and also some physical properties of the species.

Hence, with the additional spectral information provided, probable metal-ligand structures can be proposed along with the determination of the required stability constants. Further, spectrophotometric titrations are possible at the very high and low pH values at which potentiometric measurements cannot be made, which can enable the identification of species which cannot be observed in potentiometry.

For both titrations types the data were analysed globally, as described in Chapter 2, Section 2.4, and an appropriate model and subsequent equilibrium constants were then calculated. When investigating metal-ligand complex equilibria, considering both potentiometric and spectrophotometric analysis has many advantages, the most obvious being verification of the determined equilibrium constants as the values are calculated using two separate techniques.

3.2 Solvent Considerations

The application of potentiometric and/or pH dependant spectroscopic titrations for the determination of equilibrium constant values can be often hindered by poor water-solubility of samples ⁷. This was the case for the majority of ligands in the N-donor ligand series investigated for this study, as most were insoluble in pure aqueous solvents. As such, the use of mixed-solvent solutions was applied to ensure adequate solvation of all ligand in the series. A 50/50 (v/v) ethanol/water solution was chosen as this was the minimum volume of ethanol that most ligands would dissolve in at suitable concentrations. In addition, it has also been suggested that the media of organic solvents, such as alcohols, mixed with water, as well as non-aqueous media, may provide a better model for solution reactions ⁸. The effect of using mixed solvents on equilibrium constants was investigated in order to aid with the interpretation of the pK values calculated for the ligand series, and where possible compare the determined constants to literature as it has been reported that the properties of a ligand and/or metal-ligand complex are affected by the solvent type as a result of various factors such as the solvent effect, solvation power, the tendency towards forming hydrogen bonds, selective solvation, relative permittivity and the composition of the solution in the first solvation layer ⁹.

3.2.1 Solvent Properties

The properties of a solvent have a strong influence on the acid and base characteristics of a species in solution, and consequently will affect the pK values of the N-donor

ligands in this series, and also the complexes that may be formed. For example, for a given acid the pK values will vary depending on the properties of the solvent. If the basicity of the solvent is increased then the degree of dissociation of the acid consequently increases. In a similar way, solvents that have a high dielectric constant or relative permittivity, which is the preferred term for dielectric constant, also promote dissociation. Strictly speaking, permittivity is the property of a dielectric material that determines how much electrostatic energy can be stored per unit of volume when unit voltage is applied ¹⁰; refer to Table 3.1 for the values of some common solvents. Subsequently, dissociation is observed to be relatively less in solvents of low relative permittivity, and it can be seen that alcohols have low relative permittivity compared to water.

	<u>relative permittivity (ϵ)</u>
water	81.7
dimethylsulfoxide	45.0
acetonitrile	37.5
ethanol	24.3
pyridine	12.3

Table 3.1: Relative permittivities of some common solvents ¹¹.

Martell reported that solvents with low relative permittivities have a tendency to promote more complete formation of metal complexes ⁵. It has been shown that the lower relative permittivity of alcohols, such as ethanol, not only lower dissociation but also improve the association of oppositely charged ions ¹². Similar observations were also made by Gibson *et al* ¹² who noted that methanol improved the association of oppositely charged ions due to its low relative permittivity relative to water, that is 31.5 compared with 81.7 at 25 °C. The same principles that were applied to methanol can be extended to include ethanol and *n*-propanol, which are seen as more environmentally friendly than methanol, and have lower relative permittivities of 24.3 and 20.1, respectively ¹³, with permittivity falling as the alkyl chain increases in length.

The relative permittivity of mixed solvents can be approximated from Equation (3.5), where ϵ is the relative permittivity of the water and organic solvent mixture, ϵ_1 and ϵ_2 are the relative permittivities of the water and organic solvent respectively, χ_f is the

mole fraction, and the subscripts w and s refer to water and organic solvent respectively ¹⁴. Once the relative permittivity of the mixed solvent has been calculated it is then possible to determine the p*K* of a ligand measured in a mixed solvent.

$$\varepsilon = \varepsilon_1 \chi_{f(w)} + \varepsilon_2 \chi_{f(s)} \quad (3.5)$$

Many studies have shown that the equilibrium constant is related linearly to the fraction of organic solvent present in the solvent ¹⁵⁻¹⁹. For example, it has been observed that a linear relationship exists between protonation constants and the percentage of ethanol ²⁰.

For each medium the p*K* values determined in the mixed solvent can be related to p*K* values in pure aqueous medium in accordance with Equation (3.6) given by Denison and Ramsey ²¹, as well as Glikerson ²², where p*K* is the acid dissociation in the solvent mixture, p*K*₀ is the acid dissociation in pure water, *Z*₁ and *Z*₂ are the charges of the ions and *r*₁ and *r*₂ are the radii of the ions involved in the equilibrium. This equation relates the variation in p*K* that is seen in mixed solvents to the relative permittivity of the medium as calculated in Equation (3.5). Unfortunately, for our investigations the ionic radii of the ligands and metal-ligand species was not known. Hence, the p*K*₀ values were not determined for the equilibrium constants and all calculated values are reported for the 50/50 (v/v) ethanol/water solvents.

$$pK = pK_0 + \frac{0.43Ne^2}{RT} \left[\frac{Z_1 Z_2}{r_1 + r_2} \right] \frac{1}{\varepsilon} \quad (3.6)$$

According to Coetzee and Richie ²³ the calculated equilibrium constants in a mixed solvent can also be related to pure aqueous medium, p*K*₀, by the relation shown in Equation (3.7), which takes into consideration the different activities coefficients of species when the solvent is changed. In Equation (3.7) γ_m is the activity coefficient of the subscripted species in partially aqueous medium relative to that in a pure aqueous one. However, this technique could not be applied to calculate the p*K*₀ values of the ligands in this series, as the activity coefficients were not known for the species in the respective equilibrium expressions.

$$pK - pK_0 = \log \frac{\gamma_{H^+} \cdot \gamma_L}{\gamma_{LH^+}} \quad (3.7)$$

It is known that electrostatic effects of solvents operate only on the activity coefficients of charged species. Therefore, one can expect that an increase in the amount of the

organic solvent in the medium would increase the activity coefficient of all charged ions, such as LH^+ , LH_2^{2+} , and ML^{2+} ions, resulting from the change in relative permittivity of the medium. The magnitude of the electrostatic effect is inversely proportional to the radius of the ionic species, therefore the magnitude of this effect on the proton should be greater than that on the protonated forms of ligand, LH^+ and LH_2^{2+} and any metal-complexed species such as ML^{2+} . Thus, the pK value of the protonated form of the ligand is expected to increase with an increase in the proportion of the organic solvent in the medium.

Further considerations, aside from the major effect of the relative permittivity of the solvent, include the acid and base strengths and the stabilisation of different species existing in equilibrium resulting from hydrogen bonding together with any ion-solvent interactions that are present. Mohamed *et al*²⁴ examined the protonation constants of terpyridine in mixed solvents and concluded that all these factors had an influence on the pK constant value and hence were considered to play an important role in the dissociation process when mixed solvents were used²⁵.

3.2.2 Water-Alcohol Mixed Solvent Measurements

Traditionally, the method of using mixed solvents has been based on the measurement of apparent ionisation constants, denoted p_sK by many researchers. These constants are determined at different ratios of organic solvent/water mixtures, which enables the aqueous pK_0 to be obtained by extrapolation to zero % organic solvent. Takács-Novák *et al*³ investigated the accuracy of determining ionisation constants in methanol/water mixtures ranging from 16 to 65 weight percent (wt%) methanol content. The Yasuda-Shedlovsky extrapolation was employed in order to obtain the pK_0 values in zero % methanol content. According to this method a linear correlation was established from a plot of $\text{p}_sK + \log[\text{H}_2\text{O}]$ vs $a/\epsilon + b$, where $[\text{H}_2\text{O}]$ is the molar concentration of the given solvent mixture, ϵ is the relative permittivity of the mixture and a and b are the calibration parameters of the electrode, slope and intercept respectively. Aqueous pK_0 values can be obtained by using 55.5 M and 81.3, the molar concentration and relative permittivity of pure water, respectively. It was determined that for water-soluble compounds the extrapolation data were in very good agreement with pK values measured in aqueous solutions under the same conditions, the average deviation being 0.05 pH units. Also, water insoluble molecules showed acceptable accordance with spectroscopically measured or literature pK values.

As a result of their intensive studies Takács-Novák *et al* have made the following recommendations regarding mixed-solvent investigations:

1. It was recommended that electrode calibration be performed using the ‘four-parameter’ approach described in Chapter 6, Section 6.2.1.3. For such a procedure the calibration must be performed at the same constant temperature and ionic strength employed for the investigation. However, in our studies this calibration was not necessary as calibration of the electrode was performed as part of the measurement, as detailed in Chapter 6, Section 6.6.
2. The lowest possible wt% of organic solvent in which the compound dissolves should be selected, with a minimum of three measurements performed, but five or six being recommended, at different organic solvent/water mixtures in increments of 5-10%, ensuring that the highest wt% is below 70% organic solvent content. Our studies were performed at only 50/50 (v/v) ethanol/water, which corresponds to approximately 40% wt%, as we were mainly interested in trends observed within the ligand series, rather than the determination of what the equilibrium constants would be when extrapolated to zero % organic solvent content.
3. The appropriate concentration for accurate work was recommended to be between $1-5 \times 10^{-3}$ M, and the use of an inert gas atmosphere, typically nitrogen or argon, was recommended to avoid carbon dioxide absorption. This concentration range was used for our studies and nitrogen gas was bubbled through the solution before the titration and a positive nitrogen pressure was applied for the duration of the measurement.
4. Parallel measurements should be performed in order to increase the reliability of the pK determination. For our studies at least two, and often three or four, titrations were performed for each ligand and metal-ligand ratio for both potentiometric and spectrophotometric titrations.

3.2.3 Electrode Use in Mixed Solvents

Bates *et al* ²⁶ reported that the hydrogen electrode behaves satisfactorily in alcohol-water solvents, and by comparing the electrode response obtained from a hydrogen electrode with that given by a glass electrode it was shown that the response of the glass electrode was unimpaired at solvent compositions below about 90 weight % (wt%) alcohol. Bates concluded that a glass electrode is therefore able to give reproducible

values in alcohol-water solvents. Further, he reported that the potential across the junction between the alcohol-water solution and the saturated or 3.0 M aqueous solution of potassium chloride was as reproducible as the junction potential between aqueous solutions and the salt bridge. The results of this study meant that the combined glass electrode used for our potentiometric titrations could be successfully applied to the investigations in the 50/50 (v/v) ethanol/water solvent required for our equilibrium studies.

3.2.4 Ionisation Constants of Mixed Solvents

In order to investigate the equilibrium constants for the N-donor ligand series it was important to know the ionisation constant, pK_s , of the 50/50 (v/v) ethanol/water solvent mixture used for the solutions. The pK_s value of a solvent is directly related to the calculation of the hydrogen ion concentration at pH values above 7, as shown in Equation (3.8).

$$[H^+] = \frac{K_s}{[OH^-]} \quad (3.8)$$

Therefore, if an incorrect value was assumed for the ionisation of the solvent, such as the pK_s of water being used in the analysis of a titration that had been performed in a mixed solvent, the determined hydrogen ion concentrations would be systematically incorrect at a pH above 7. The ionisation constants of some common pure solvents have been provided in Table 3.2.

solvent	ionisation constant
methanol	17.20
ethanol	18.88
dimethyl formamide	29.50
acetone	32.50
dimethyl sulfoxide	33.30

Table 3.2: Ionisation constants (pK_s) of some organic solvents.

In order to determine the ionisation constant of the 50/50 (v/v) ethanol/water solvent used for this investigation numerous titrations were performed with sodium hydroxide and differing concentrations of perchloric acid in the 50/50 (v/v) ethanol/water solvent. This enabled the ionisation constant of the solvent mixture to be accurately determined.

A pK_s value of 14.685 was obtained from these titrations at 25 °C, which is in between the pK_s values of water, 13.98, and ethanol, 18.88 as would be expected.

Woolley *et al*²⁷ have also investigated the changing solvent ionisation constant for a number of different organic solvents at increasing water-solvent wt% values; a summary of the results are given in Table 3.3. A general trend was observed as the pK_s values increased with the increasing organic solvent concentration.

Ionisation Constants (pK_s) of Solvents of Differing Water – Organic Solvent Compositions									
wt% ethanol	pK_s	wt% dioxane	pK_s	wt% 1-propanol	pK_s	wt% 2-propanol	pK_s	wt% 2-methyl-2-propanol	pK_s
0.00	14.00	0.00	14.00	0.00	14.00	0.00	14.00	0.00	14.00
7.27	14.17	9.35	14.27	7.43	14.17	7.26	14.20	7.26	14.23
16.4	14.35	17.1	14.49	16.7	14.35	16.4	14.46	16.4	14.46
26.2	14.49	26.5	14.79	26.5	14.49	26.1	14.67	26.0	14.70
39.9	14.69	40.1	15.31	40.6	14.73	40.0	14.98	39.9	15.01
47.3	14.82	49.5	15.76	45.7	14.83	45.1	15.10	45.1	15.16
51.3	14.89	56.3	16.01	50.1	14.92	19.5	15.22	49.4	15.29

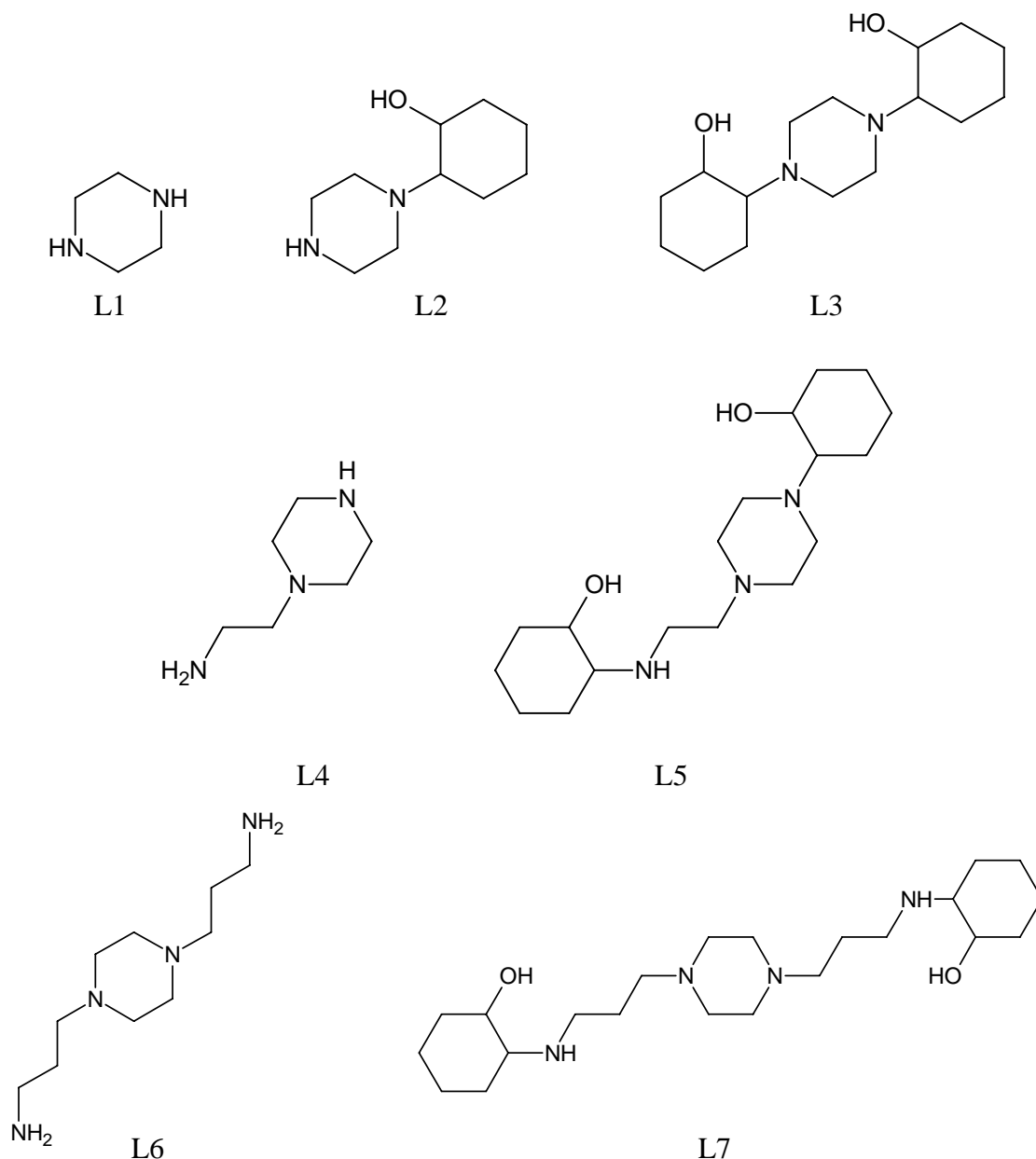
Table 3.3: Solvent ionisation constants, pK_s , for a variety of water-organic solvent mixtures at increasing organic solvent concentrations (wt%)²⁷.

The 39.9 wt% water-ethanol solvent mixture is the equivalent of the 50/50 (v/v) mixture used for the study of this series of N-donor ligands. From the table of values it can be seen that the ionisation constant of the solvent at 39.9 wt% was determined to be equal to 14.69, which is directly comparable to our calculated value which determined the pK_s to be 14.685.

3.3 Experimental

3.3.1 Ligand Series

The ligand series investigated for the study consisted of a group of seven N-donor ligands of increasing complexity, as shown in Scheme 3.7. These ligands have the same base unit, that is, the piperazine ligand numbered L1. The peripheral groups have been altered in order to investigate the effect that differing groups have on the protonation constants of the piperazine nitrogen atoms. The stability constants were also determined and compared for copper(II) and nickel(II) metal species for those ligands where metal-ligand titrations were possible.



Scheme 3.7: Series showing the numbering of the ligands used in the equilibrium study.

3.3.2 Analytical Solution Preparation

Approximate 0.1 M sodium hydroxide solutions were prepared using the appropriate volume of 50/50 (w/w) NaOH/water solution. The NaOH solution was then diluted with a 50/50 (v/v) ethanol/water solution prepared from freshly boiled water and freshly boiled ethanol, that had been flushed with nitrogen while cooling, then mixed in equal volumes once cooled. The prepared sodium hydroxide solution was also flushed with, and stored under, nitrogen. Each NaOH solution was standardised by titration with accurately prepared 0.01 M potassium hydrogen phthalate from the same 50/50 (v/v) ethanol/water solvent.

The ligand solutions were prepared at approximate concentrations of $[L] = 5 \times 10^{-3}$ M, with acid added equal to the number of hydrogen ions needed to protonate the nitrogens on the ligand plus 0.5 times the ligand concentration to ensure acid excess in the solution. For example, for L1 there are two nitrogens to be protonated, therefore the concentration of acid added was equal to 2.5 times the concentration of L1 in the solution. The added acid was HClO_4 so the anion was kept constant as the appropriate amount of solid NaClO_4 was also added to make the solutions a constant ionic strength of 0.1 M. The quantity of NaClO_4 necessarily changed when metals were introduced to the solutions. *Safety note: Although no problems were experienced in handling perchlorate compounds, these salts when combined with organic ligands are potentially explosive and should be manipulated with care and used only in small quantities*²⁸.

Titration with the transition metals copper(II) and nickel(II) were performed for all ligands; however, for ligands L2, L3 and L4 precipitation was observed for both metals. L2 precipitated before any useful data could be collected, but partial analysis could be performed for L3. For the 1:1 metal-ligand ratios a slight ligand excess was used with all solutions to try to prevent precipitation of the metal hydroxide.

Ligand	[L] (M)	$[\text{H}^+]$ (M)	$[\text{Cu}^{2+}]$ (M)	$[\text{Ni}^{2+}]$ (M)
L1	4.748×10^{-3}	1.481×10^{-2}	4.568×10^{-3}	4.493×10^{-3}
L2*	4.398×10^{-3}	8.475×10^{-3}	-	-
L3	5.211×10^{-3}	1.187×10^{-2}	4.453×10^{-3}	4.348×10^{-3}
L4	6.071×10^{-3}	2.623×10^{-2}	-	-
	8.704×10^{-3}	8.704×10^{-3}	7.234×10^{-4}	
L5	4.997×10^{-3}	1.732×10^{-2}	4.354×10^{-3}	4.339×10^{-3}
			2.229×10^{-3}	
L6	4.750×10^{-3}	2.371×10^{-2}	4.273×10^{-3}	
	8.175×10^{-3}	4.063×10^{-2}		7.557×10^{-3}
L7	4.944×10^{-3}	2.064×10^{-2}	4.532×10^{-3}	4.211×10^{-3}
	9.492×10^{-4}	4.94×10^{-3}	8.097×10^{-4}	

Table 3.4: Table detailing typical examples of the initial concentrations used for titrations. Both potentiometric and spectrophotometric titrations used similar concentrations. *Titrations showed that the starting material piperazine (L1) was still present in the L2 sample. The concentration of L2 was instead determined to be 2.483×10^{-3} M using the global analysis technique described in Chapter 2.

3.3.3 Titration Technique

Potentiometric titrations were performed as described in Chapter 2, Section 2.2.3.4 and spectrophotometric titrations were performed as described in Chapter 2, Section 2.2.3.5. All titrations were repeated at least twice to ensure reproducibility of the data.

For titrations of the ligand, the initial volume of ligand solution ranged between 3 and 20 mL, depending on the availability of the ligand and the titration vessel size. The increment size of each addition for the titration, and the total added volume of NaOH, was dependant on the concentration and volume of ligand solution, and was adjusted accordingly in order to give a final pH of approximately greater than 11 for each titration.

For complexation titrations, that is, titrations that involved a metal ion, the appropriate quantity of metal salt was added to the ligand solution prior to titration. Differing equivalents of metal were added to the ligand solution in order to investigate the complexation fully. In general, metal-ligand ratios were 0.9:1; however, for spectroscopic titrations a wider range of ratios was used. The metal-ligand solution was then titrated against 0.1 M NaOH in the same manner as for the free ligand.

Free ligand and metal-ligand data were analysed and fitted simultaneously using the program Pot_Anal for potentiometric titration data and Spec_Anal for spectrophotometric titration data. Both programs were developed in the chemistry department at The University of Newcastle and have been discussed in detail in Chapter 2, Section 2.4. For all investigations the ionisation constant of the solvent was fixed at 14.684, which had been determined experimentally from strong acid/strong base titrations in 50/50 (v/v) ethanol/water, as described in Section 3.2.4.

3.4 Detailed Study of Ligand L5 (Pizda)

The analysis of titration data is usually an involved and complicated process. In order to describe the general process followed to determine the model and subsequent equilibrium constant values of the ligands studied in this series, an in-depth study of the ligand L5, also known as Pizda, has been detailed.

Protonation constants were determined from potentiometric titration data, while the stability constants of Pizda with copper(II) were evaluated using both potentiometric and spectrophotometric titration techniques.

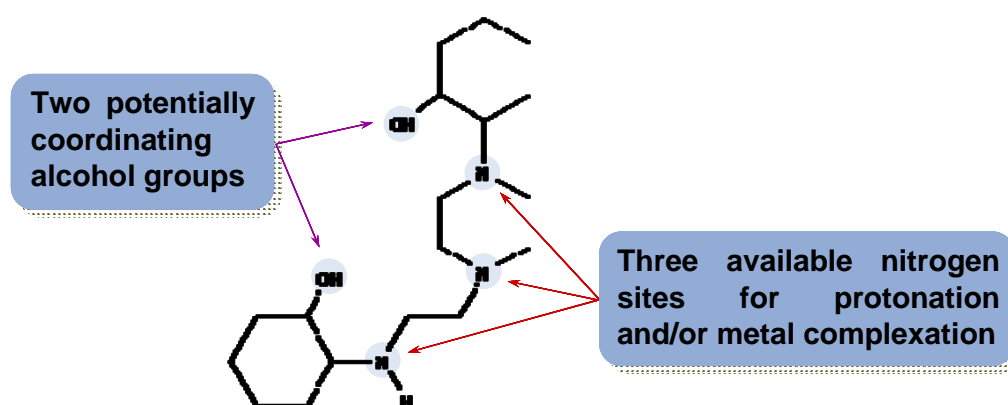


Figure 3.1: Structure of ligand L5 (Pizda) highlighting the three nitrogen sites available for protonation and the five coordination sites available for metal complexation. The ligand is shown in its neutral form.

Figure 3.1 shows the structure of Pizda with the coordination properties highlighted. There are three nitrogen atoms that can be either protonated or coordinated to a metal ion depending on the pH and the strength of the nitrogen-metal bond. The two hydroxy groups are also potentially coordinating, both as neutral groups and particularly under high enough pH conditions where they can be deprotonated.

3.4.1 Determining the 'Best' Model

As has been discussed in Chapter 2, Section 2.3.9, there is no simple way to determine the best model for a chemical reaction, as technically speaking there is no correct model. It is always possible to expand on an existing model, as an increase in the number of calculated parameters necessarily results in a decrease in the sum of squares, *ssq*. One of the key conditions is that the model that is chosen must make sense chemically and fit the data appropriately. Generally, the simplest model that adequately fits the data is the considered to be the 'correct' one. However, it should be remembered that there may be more species present than proposed in the model, they just may not be observable in the experiments that were performed.

It is an important step to verify the model that has been chosen. This involves assessing such aspects as the sum of squares, ensuring that the species distribution plots are realistic, valid equilibrium constant values have been calculated, both the chemical and physical meanings of the model are consistent and acceptable, and, where spectrophotometric data is available, also confirming that there are positive, sensible spectra for all absorbing species.

3.4.1.1 Protonation Model

The model for the protonation of Pizda was fairly simple to propose and verify as there were three nitrogens available for protonation. Hence, a model with the ligand species L , LH^+ , LH_2^{2+} , and LH_3^{3+} was fitted to the measured potentiometric data, and compared to other models this model was determined to be the best describe the data. The protonation constants of the ligand are determined as formation constants, rather than dissociation constants, as these are more consistent with the way metal complexes are defined. The data are provided in Table 3.5. The same procedure was used with the other ligands in the series, that is, the maximum number of nitrogens that could be protonated was also the best model to describe the data. The ligand protonation number ranged from two to four for the series of ligands and the protonation equilibria were modelled for all titrations.

species	$\log \beta$ value	$\log K$ value	titration
LH_3	18.528 ± 0.065	2.007 ± 0.066	
LH_2	16.520 ± 0.012	7.661 ± 0.013	
LH	8.860 ± 0.006	8.860 ± 0.006	

Table 3.5: Values of the protonation constants of the ligand Pizda and the potentiometric titration of Pizda where the • points represent the measured values, and the — shows the calculated data.

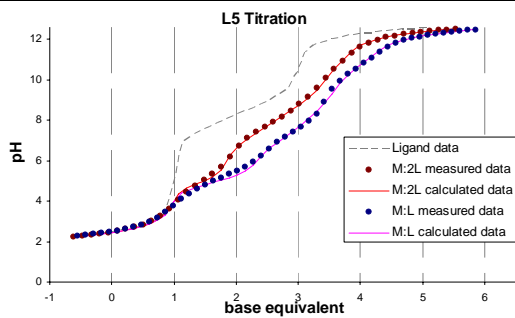
3.4.1.2 Stability Model

Verification of the model for the complexation of each ligand with copper(II) and nickel(II) was significantly more complicated and involved the proposal, testing and comparison of multiple plausible models. The determination of the best model for the reaction of ligand Pizda with copper(II) has been discussed to demonstrate the general technique. The potentiometric titration and the ligand protonation values shown in Table 3.5 were included as part of the global analysis of the copper(II) titrations.

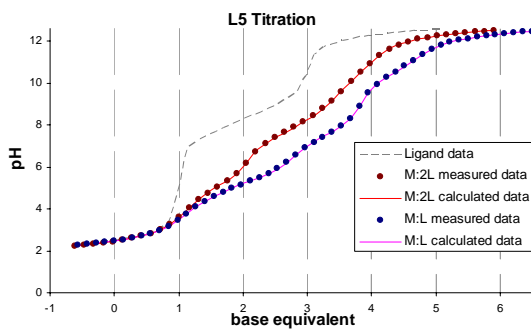
To commence the analysis, it is good technique to begin by proposing the simplest model for the metal-ligand system. The complexity of the model can then be increased until a reasonable fit is determined for the measured and calculated data and further introduction of species either results in minimal improvements in the ssq value or leads

to divergence due to the uncertainty in the proposed parameters. This process has been outlined in Scheme 3.8.

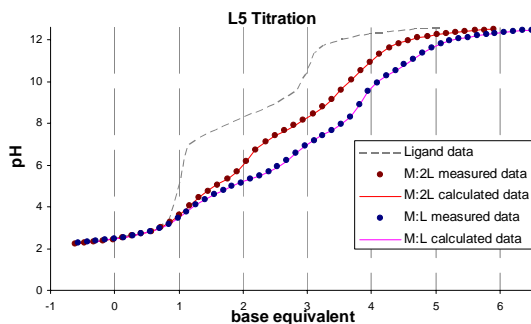
	model	$\log \beta$ value	ssq value
1)	$M + L \leftrightarrow ML$	9.231 ± 0.526	5.99×10^5
2)	$M + L \leftrightarrow ML$	9.220 ± 0.192	7.73×10^4
	$M + L - H \leftrightarrow MLH_1$	1.737 ± 0.247	
	$M + L + H \leftrightarrow MLH$	14.591 ± 0.218	6.99×10^4
3)	$M + L \leftrightarrow ML$	9.254 ± 0.197	
	$M + L - H \leftrightarrow MLH_1$	1.833 ± 0.244	
	$M + L \leftrightarrow ML$	9.187 ± 0.052	2780.36
4)	$M + L - H \leftrightarrow MLH_1$	2.414 ± 0.142	
	$M + L - 2H \leftrightarrow MLH_2$	-8.161 ± 0.142	



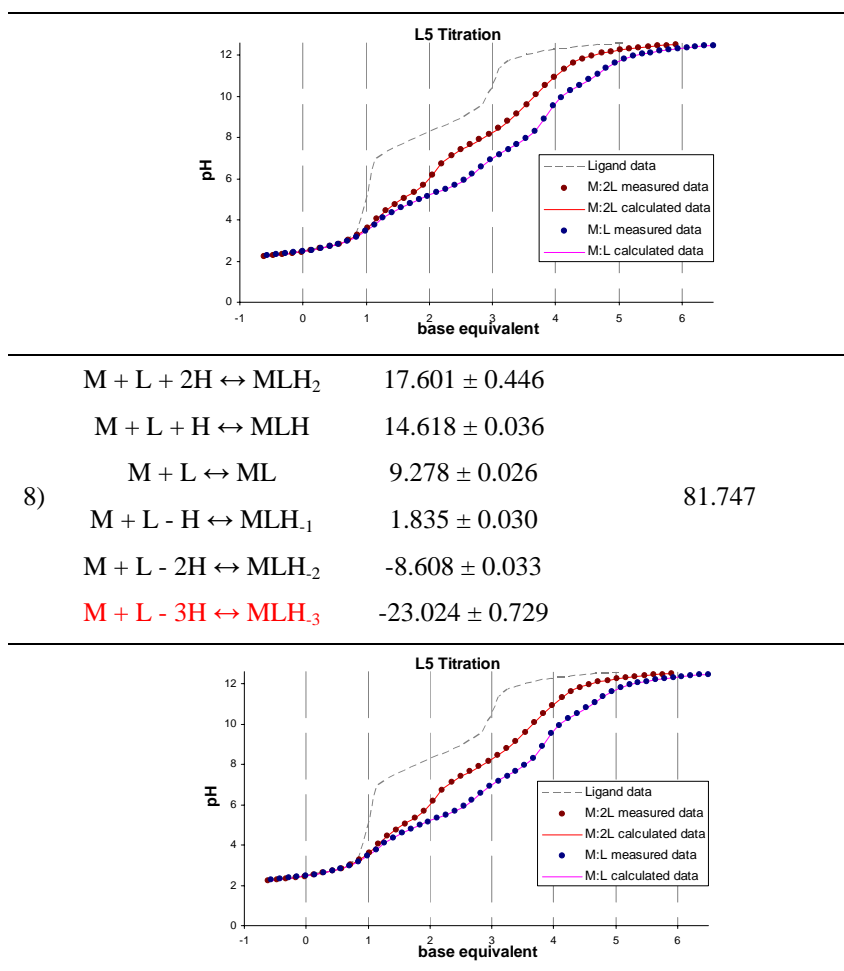
	$M + L + H \leftrightarrow MLH$	14.589 ± 0.014	
	$M + L \leftrightarrow ML$	9.256 ± 0.013	
5)	$M + L - H \leftrightarrow MLH_{-1}$	1.814 ± 0.023	82.794
	$M + L - 2H \leftrightarrow MLH_{-2}$	-8.632 ± 0.025	



	$M + L + H \leftrightarrow MLH$	14.586 ± 0.014	
	$M + L \leftrightarrow ML$	9.256 ± 0.013	
6)	$M + L - H \leftrightarrow MLH_{-1}$	1.818 ± 0.023	82.388
	$M + L - 2H \leftrightarrow MLH_{-2}$	-8.625 ± 0.027	
	$M + L - 3H \leftrightarrow MLH_{-3}$	-22.924 ± 0.544	



	$M + L + 2H \leftrightarrow MLH_2$	17.649 ± 0.421	
	$M + L + H \leftrightarrow MLH$	14.623 ± 0.034	
7)	$M + L \leftrightarrow ML$	9.280 ± 0.026	81.978
	$M + L - H \leftrightarrow MLH_{-1}$	1.834 ± 0.030	
	$M + L - 2H \leftrightarrow MLH_{-2}$	-8.611 ± 0.032	

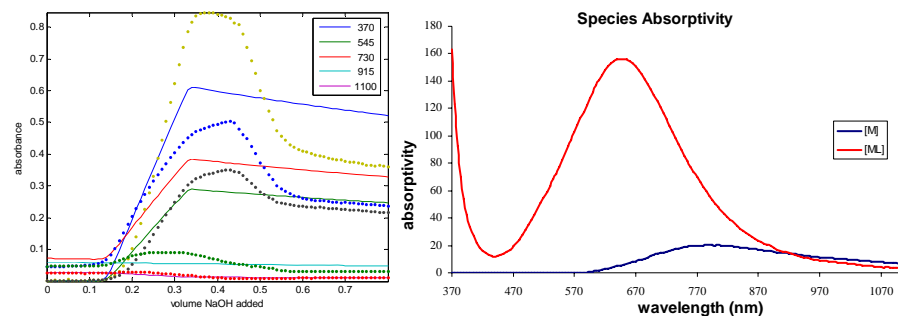


Scheme 3.8: Scheme detailing the process followed to determine the ‘best’ model for the potentiometric metal-ligand titration data. The new species in each model have been highlighted in red. From the LH column: the proposed model; the calculated equilibrium constants with their respective error estimates; the *ssq* value and; plot depicting the fit of the measured and calculated data.

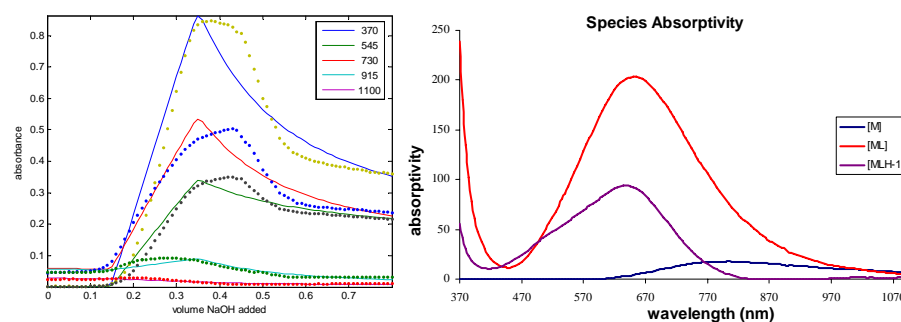
One may conclude that model 5 is sufficient as it clearly passes the ‘goodness of fit’ criteria and the introduction of additional species does not significantly improve the fit or *ssq* value. Further, the extra species have stability constants with approximately ten times larger standard deviations. However, models 5, 6, 7, and 8 all have comparable *ssq* values and therefore all need to be considered as plausible models for the interaction between Pizda and copper(II). Comparison of these models is discussed after the spectrophotometric analysis as the spectrophotometric results may aid in the determination of the best model as additional information, such as the species absorptivities, will be available.

The analysis of the spectrophotometric data has been shown in Scheme 3.9, with the same model proposal as for the potentiometric analysis. Not all models that could be fitted with the potentiometric data could be fitted in the spectrophotometric analysis.

	model	$\log \beta$ value	ssq value
1)	$M + L \leftrightarrow ML$	9.987 ± 0.215	33.218

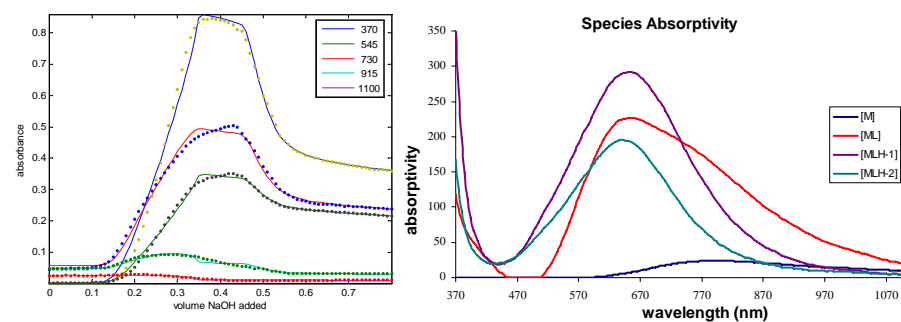


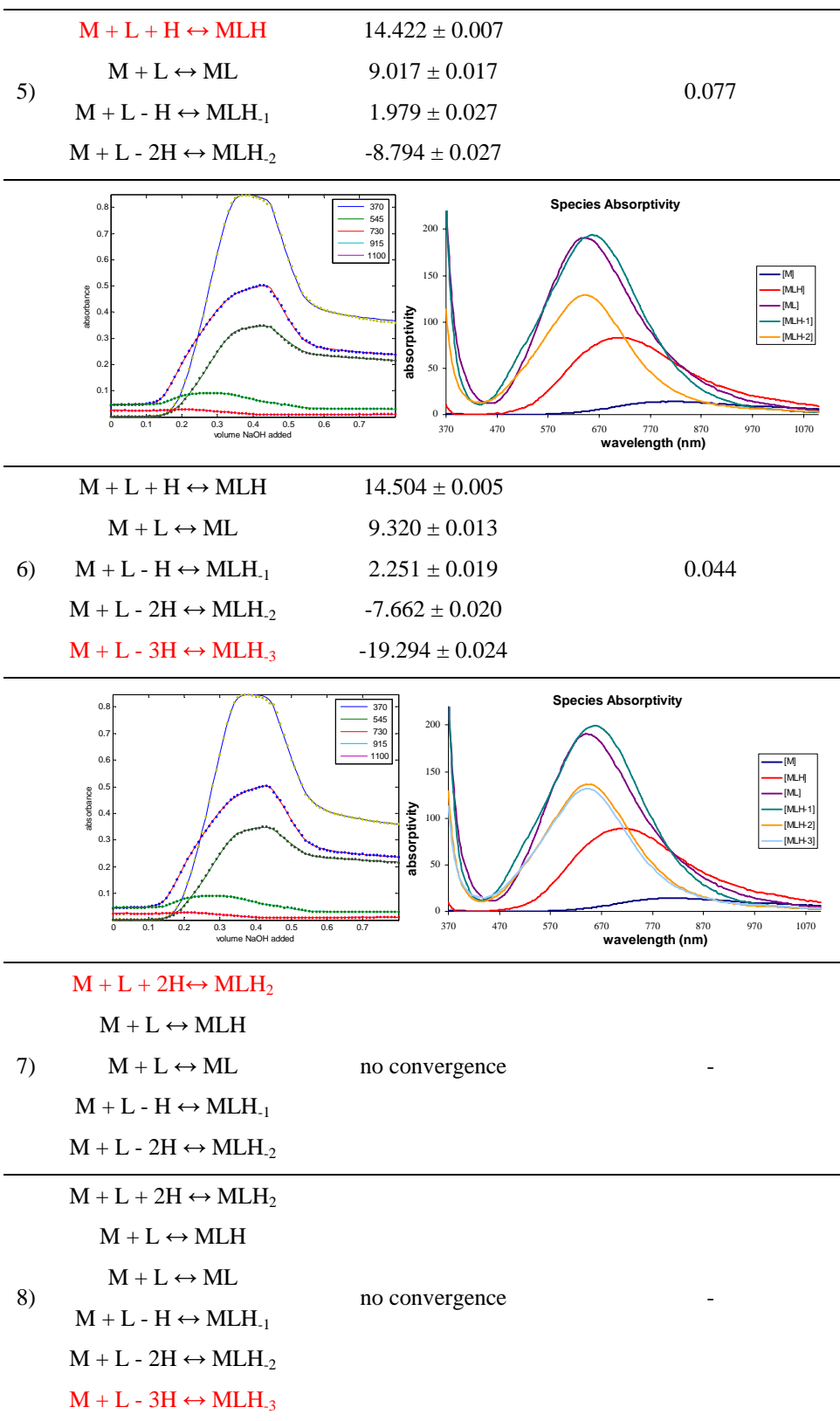
2)	$M + L \leftrightarrow ML$	5.021 ± 0.015	5.291
	$M + L - H \leftrightarrow MLH_1$	-7.412 ± 0.015	



3)	$M + L + H \leftrightarrow MLH$		-
	$M + L \leftrightarrow ML$	no convergence	
	$M + L - H \leftrightarrow MLH_1$		

4)	$M + L \leftrightarrow ML$	11.208 ± 0.027	
	$M + L - H \leftrightarrow MLH_1$	7.500 ± 0.045	0.843
	$M + L - 2H \leftrightarrow MLH_2$	-3.669 ± 0.044	





Scheme 3.9: Scheme detailing the process followed to determine the ‘best’ model for the spectrophotometric titration data. The new species in each model have been highlighted in red. From the LH column: the proposed model; the calculated equilibrium constants with their respective error estimates; the *ssq* value and; plots depicting the fit of the measured and calculated absorbance data at selected wavelengths and the absorptivity of the coloured species.

Consideration of the results from both titration types shows that model 5 had the greatest reduction in *ssq* value for both techniques. This is due to the measured and calculated data correlating well, whereas only poor fits were observed for the first four models. However, the subsequent models of increasing complexity were also fitted to both types of data, with comparable *ssq* values. The ‘best’ model is not trivial to determine as there are at least two models for each titration type for which the measured and calculated data fitted very well. Therefore, the models must be examined closely. Criteria such as realistic species distribution plots, valid and well-defined constants, and the physical meaning of the proposed species all need to be taken into account in order to determine the best model to describe the data.

A summary of the proposed models and the respective log *K* values calculated from the formation constants for each species from both types of titrations has been given in Table 3.6. This enables the stability constants to be directly compared for both types of analysis; for instance, the best correlation of values can be seen with models 5 and 6.

	model	potentiometric analysis	spectrophotometric analysis
1)	$M + L \leftrightarrow ML$	9.231 ± 0.526	9.987 ± 0.215
2)	$M + L \leftrightarrow ML$	9.220 ± 0.192	5.021 ± 0.015
	$MLH_1 + H \leftrightarrow ML$	7.483 ± 0.313	12.433 ± 0.015
3)	$ML + H \leftrightarrow MLH$	5.337 ± 0.294	-
	$M + L \leftrightarrow ML$	9.254 ± 0.197	
	$MLH_1 + H \leftrightarrow ML$	7.421 ± 0.314	
4)	$M + L \leftrightarrow ML$	9.187 ± 0.052	11.208 ± 0.027
	$MLH_1 + H \leftrightarrow ML$	6.773 ± 0.151	3.708 ± 0.052
	$MLH_2 + H \leftrightarrow MLH_1$	10.575 ± 0.142	11.169 ± 0.063
5)	$ML + H \leftrightarrow MLH$	5.333 ± 0.019	5.405 ± 0.018
	$M + L \leftrightarrow ML$	9.256 ± 0.013	9.017 ± 0.017
	$MLH_1 + H \leftrightarrow ML$	7.442 ± 0.026	7.038 ± 0.032
	$MLH_2 + H \leftrightarrow MLH_1$	10.446 ± 0.034	10.773 ± 0.027
6)	$ML + H \leftrightarrow MLH$	5.330 ± 0.019	5.184 ± 0.014
	$M + L \leftrightarrow ML$	9.256 ± 0.013	9.320 ± 0.013
	$MLH_1 + H \leftrightarrow ML$	7.438 ± 0.026	7.069 ± 0.023
	$MLH_2 + H \leftrightarrow MLH_1$	10.443 ± 0.035	9.913 ± 0.028
	$MLH_3 + H \leftrightarrow MLH_2$	14.299 ± 0.555	11.632 ± 0.031

7)	$\text{MLH} + \text{H} \leftrightarrow \text{MLH}_2$	3.026 ± 0.422	-
	$\text{ML} + \text{H} \leftrightarrow \text{MLH}$	5.343 ± 0.042	
	$\text{M} + \text{L} \leftrightarrow \text{ML}$	9.280 ± 0.026	
	$\text{MLH}_{-1} + \text{H} \leftrightarrow \text{ML}$	7.446 ± 0.040	
	$\text{MLH}_2 + \text{H} \leftrightarrow \text{MLH}_{-1}$	10.445 ± 0.044	
8)	$\text{MLH} + \text{H} \leftrightarrow \text{MLH}_2$	2.983 ± 0.467	-
	$\text{ML} + \text{H} \leftrightarrow \text{MLH}$	5.340 ± 0.043	
	$\text{M} + \text{L} \leftrightarrow \text{ML}$	9.278 ± 0.026	
	$\text{MLH}_{-1} + \text{H} \leftrightarrow \text{ML}$	7.443 ± 0.040	
	$\text{MLH}_2 + \text{H} \leftrightarrow \text{MLH}_{-1}$	10.443 ± 0.045	
	$\text{MLH}_3 + \text{H} \leftrightarrow \text{MLH}_2$	14.416 ± 0.730	

Table 3.6: Comparison of $\log K$ values of the potentiometric and spectrophotometric titration analysis for each proposed model. Similarity of values can be seen for model 5 and 6.

The formation of each species needs to be considered for each analysis in order to determine which species exist to a significant enough quantity in solution to influence the measurement and hence be well enough defined to be included in the model. Otherwise, the calculated parameter constant may be a product of the analysis, for example noise modelling, rather than a true representation of the stability of the particular species.

Consideration of the standard deviations for all species shows that the species MLH_3 is only well defined in spectrophotometric titrations. This may be because in the potentiometric titration the observed pH changes are very minimal at such high pH values, as the deprotonation occurs near the limit of the electrode at a $\text{pH} > 12$. In the potentiometric titration analysis the error estimate for the $\log \beta$ value for MLH_3 is ten times greater than the error values of other stability constants, hence it can be said that the value is not very well defined from the titration. Further, the species distribution plot, Figure 3.2a, shows that MLH_3 is not modelled to any significant concentration during the titration, as the stability constant is not well defined due to the aforementioned electrode limitations, and therefore the species is underestimated. The maximum concentration reached for MLH_3 was calculated to be 2.458×10^{-5} M, whereas other species, for example ML, formed to a maximum concentration of 1.921×10^{-3} M. Hence, only approximately 1.3% of the maximum concentration formed by the other species in the titration is formed with MLH_3 . Therefore, for the potentiometric analysis the equilibrium constants for MLH_3 cannot be considered an

accurate or valid value, and hence was not included as part of the model for the potentiometric analysis.

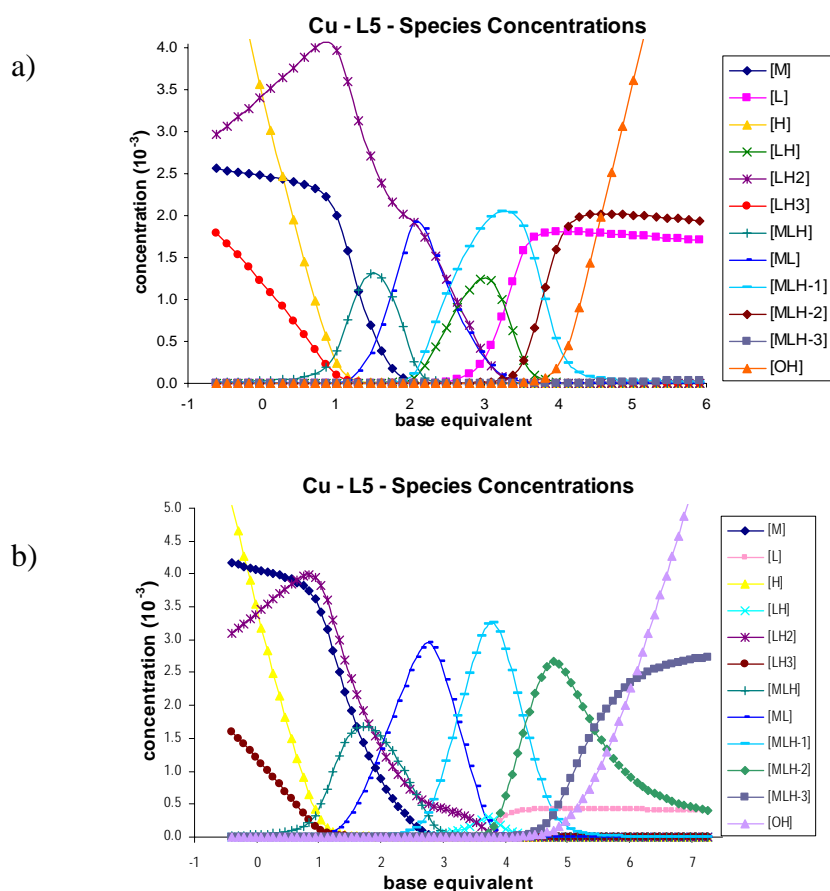


Figure 3.2: a) Potentiometric species distribution plot; b) Spectrophotometric species distribution plot for model 6.

The species distribution plot of the spectrophotometric data, Figure 3.2b, shows that in this titration model MLH_3 does form to a concentration that is directly comparable to the other species. Therefore, the MLH_3 species is adequately defined in the spectrophotometric analysis as there are no limitations of the electrode, and hence it can be included as part of the spectrophotometric model. MLH_3 provides a good demonstration that all species may not be observable in one titration type, and that a species may exist even if it cannot be modeled for a particular analysis.

The next species that was examined was MLH_2 , which was not observed in the analysis of the spectrophotometric titration data as optimisation with an MLH_2 species included in the model resulted in divergence and the calculation of completely unrealistic parameter values and species spectra. This divergence may be because the species was not formed to a significant enough concentration in the spectrophotometric titration and

therefore, unless a species has a very significant molar absorptivity, if it is present in only minute concentrations the overall spectrum will not be altered enough to adequately define the presence of that species. Hence, MLH_2 was not identifiable in the analysis.

However, MLH_2 could be included in models for the potentiometric titration data. Even so, examination of the error estimates showed that MLH_2 had an error ten times greater than the other constants, and again the species distribution plots, Figure 3.3, showed that even though MLH_2 forms at the very beginning of the titration the maximum concentration reached was only 8.952×10^{-5} M. Therefore, MLH_2 only forms to 4.7% compared with the other species. Further, from consideration of the chemistry involved for a MLH_2 species, which requires two nitrogens on the Pizda ligand to be protonated, therefore leaving only one nitrogen available for coordination to the copper(II) ion. Such a species is not expected to be very stable and hence only forms to a small extent. Therefore, due to the small percentage concentration and instability of the complex MLH_2 it was disregarded as a valid species for both potentiometric and spectrophotometric experiments.

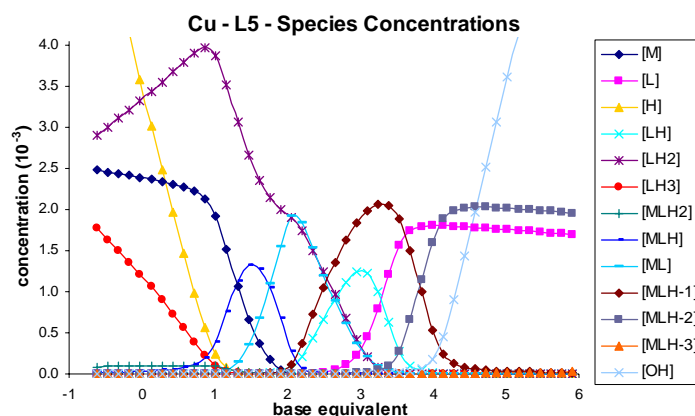


Figure 3.3: Potentiometric species distribution plot for model 8.

These considerations result in model 6 being the best model to describe the interaction of Pizda and copper(II) under the titration conditions. This model included the MLH_3 species which was observed in the spectrophotometric data, and does not include MLH_2 which was determined to be too undefined for inclusion for both titration analyses.

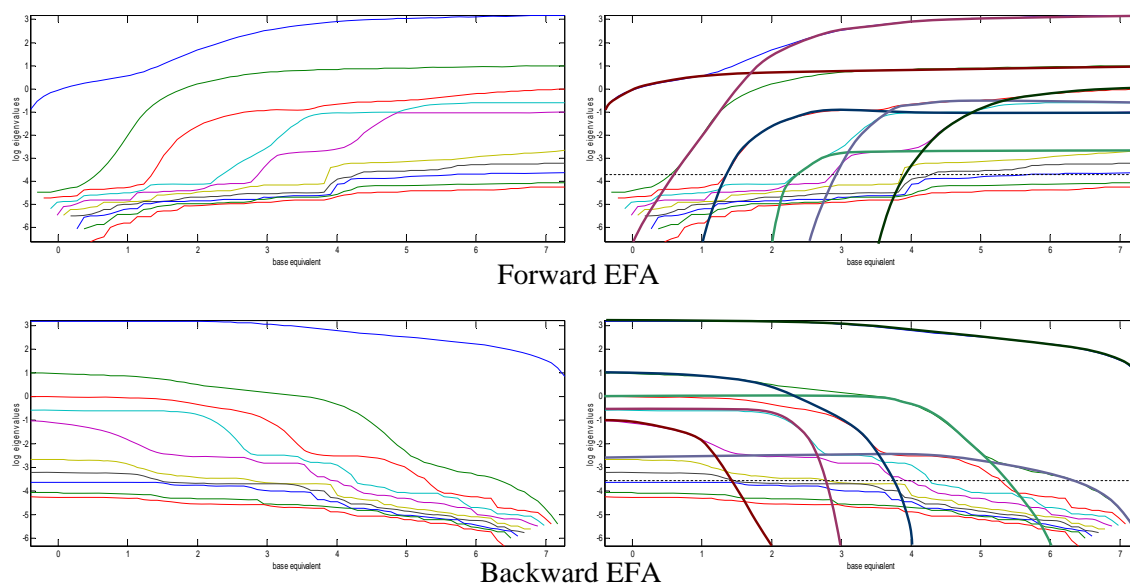


Figure 3.4: Forward and backward EFA plots for copper(II) and Pizda. The LH plots show the log of the significant eigenvalues as the titration progresses forwards and backwards respectively. The RH plots show the six major species suggested to form from examination of the EFA the plots.

As a further extension of the analysis of the spectrophotometric data eigenvector factor analysis²⁹ (EFA) was applied to help elucidate the most probable model describing the titration data. This analysis has been described in Chapter 2, Section 2.3.8.3 and the plots of the copper data, shown in Figure 3.4, clearly showed that six coloured species were present during the titration. The top left-hand figure is the forward EFA analysis, and underneath is the backward EFA analysis. The appearance of the absorbing species has been highlighted on the right-hand side with heavy coloured lines in order to illustrate the identification of the six species as each coloured line represents the formation of a new species in the titration. The six species identified in the EFA plots means that there should be six absorbing species present in the model of the spectrophotometric titration data.

As can be seen, model 6 has the species M, ML, MLH, MLH₁, MLH₂, and MLH₃ as the six absorbing species, the spectra of which are all well defined. Hence, model 6 was determined to be the ‘best’ model, as all species were formed to significant concentrations in one or both titration methods, each stability constant was well defined in the analysis with comparable error estimates, *ssq* was minimal for both methods, and consideration of the EFA plots provided the key information showing that six absorbing species needed to be present in the model.

Species	log K value
$L + H \leftrightarrow LH$	8.560 ± 0.066
$LH + H \leftrightarrow LH_2$	7.661 ± 0.013
$LH_2 + H \leftrightarrow LH_3$	2.007 ± 0.006
$ML + H \leftrightarrow MLH$	5.257 ± 0.024
$M + L \leftrightarrow ML$	9.288 ± 0.013
$MLH_{.1} + H \leftrightarrow ML$	7.163 ± 0.035
$MLH_{.2} + H \leftrightarrow MLH_{.1}$	10.178 ± 0.045
$MLH_{.3} + H \leftrightarrow MLH_{.2}$	11.632 ± 0.031

Table 3.7: Calculated average log K values for Pizda from both potentiometric and spectrophotometric techniques.

Even though models of further complexity could be fitted to the potentiometric titration data, these latter models only showed a small reduction in the ssq value which was attributed to the added degree of freedom from the extra parameters, and not because the model actually fitted the data better. Table 3.7 shows what was determined to be the final species present from the modelling and analysis. The calculated stability constants are averages from the potentiometric and spectrophotometric titration analysis, with the exception of $\log K_{MLH-3}^H$ which is only from the spectrophotometric analysis as the potentiometrically determined value for the formation of $MLH_{.3}$ was disregarded due to the aforementioned reasons. Also, the protonation constants were determined only from the potentiometric data analysis.

3.4.2 Suggested Structures of Copper(II) – Pizda Complexes

The ‘best’ model identified six absorbing species as being present, copper(II) and five metal-ligand complexes. Possible structures of the complexes are shown in Table 3.8. As can be seen for some species, there are more than one structure possible for the complex. In such cases the spectra of the species may aid in elucidating which structure is more likely to be correct, as discussed below.

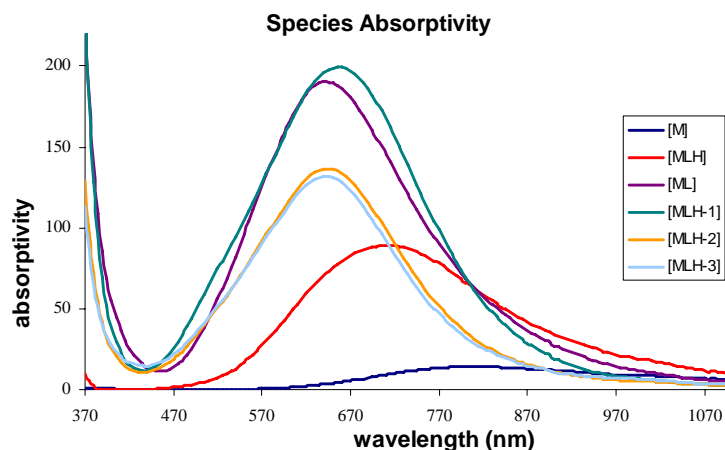


Figure 3.5: Species absorptivities determined from analysis of spectrophotometric titration data and model 6.

For the neutral ML complex, formation occurs with the neutral ligand complexing to the copper(II) centre meaning that potentially one to three nitrogens could be coordinated to the metal centre. It is assumed that the most stable neutral species would be with all three of the nitrogens coordinated and also with a water molecule occupying the fourth site to complete the preferred square-planar coordination.

The protonated ML species, MLH^+ , has two structural possibilities, that is, the protonation of either a secondary or terminal nitrogen. In order to aid in elucidating which structure was more probable for the MLH^+ species the stability constant of the ML complex with the ligand L1 was considered. For L1 $\log K_L^M$ was calculated to be 5.444, and from comparison to the similar value for Pizda, for which $\log K_{LH}^M = 5.330$, it was determined that the structure of MLH^+ for Pizda was most likely to be due to the terminal nitrogen being protonated as this would result in a structure where the copper(II) ion was coordinated to both secondary nitrogens of Pizda. This coordination is structurally analogous to the ML complex of L1 and hence may result in the comparable $\log K$ values of the complexes.

The structure of the MLH_1 species is also ambiguous as there are two hydroxy groups, and also a potentially coordinated water molecule, which can be deprotonated to result in the ' H_1 ' species. However, the structure of MLH_1 can be elucidated from the species spectra, as the MLH_1 spectra shows a shift towards higher energy, lower λ_{max} , compared with the spectra of ML. Experimental observations are that the maximum absorbance of copper(II) complexes are particularly influenced by the equatorial plane donor group. A shift in the λ_{max} of the complexes to a higher wave number is indicative

of the coordination of the deprotonated hydroxy group that is in the equatorial copper(II)/nitrogen plane. The shift in spectra of the further deprotonated MLH_2 species is towards lower energy, that is towards higher λ_{max} , which is consistent with the coordination of further anionic oxygen donors, possibly in five or six-coordinate species.

metal complex	suggested structure(s)
ML	
MLH^+	
MLH_1	
MLH_2	
MLH_3	

Table 3.8: Suggested structural diagrams of Pizda complexed with copper(II). Atoms responsible for charge change from the neutral ML complex have been highlighted; hydrogen atoms are yellow and oxygen atoms are shown in purple.

The formation of MLH_3 is dependant on the structure of the MLH_2 species. Only a small shift in spectra is observed between the two species. If the MLH_2 species was formed from the deprotonation of a hydroxy group then MLH_3 results from the deprotonation of the coordinated of a coordinated water group. Alternatively, if the formation of MLH_2 was due to the deprotonation of the coordinated water group then MLH_3 is instead formed from the deprotonated hydroxy group. In either case the final structure of the MLH_3 complex is the same. However, the similarity of the absorptivities of the MLH_2 and MLH_3 species suggests that the coordination sphere of the copper(II) centre has not been significantly altered with the formation of MLH_3 . This would be the case if the formation of MLH_3 was due to the water group being deprotonated, whereas if the axial hydroxy had been deprotonated and coordinated significant change in the coordination around the copper(II) ion should be observed. Hence, the large spectral change seen between MLH_1 and MLH_2 is likely to be a result of the hydroxy group deprotonating and coordination, and the small deviation in spectra seen from MLH_2 to MLH_3 being due to the coordinated water molecule deprotonating. Therefore, as a result of knowing the species absorptivities that are formed in the titration it is possible to propose the physical structures of each metal-ligand complex.

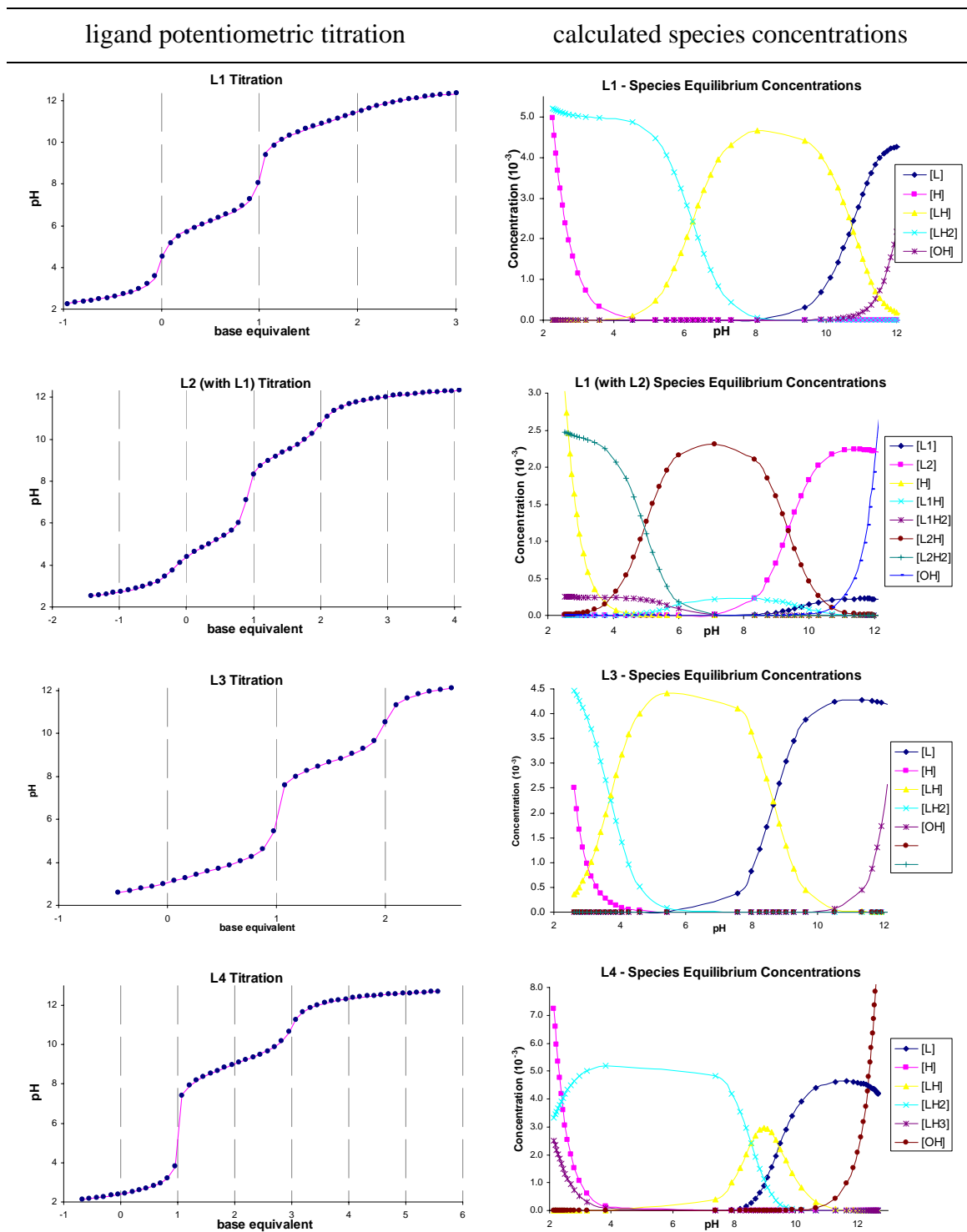
3.5 Ligand Series Results and Discussion

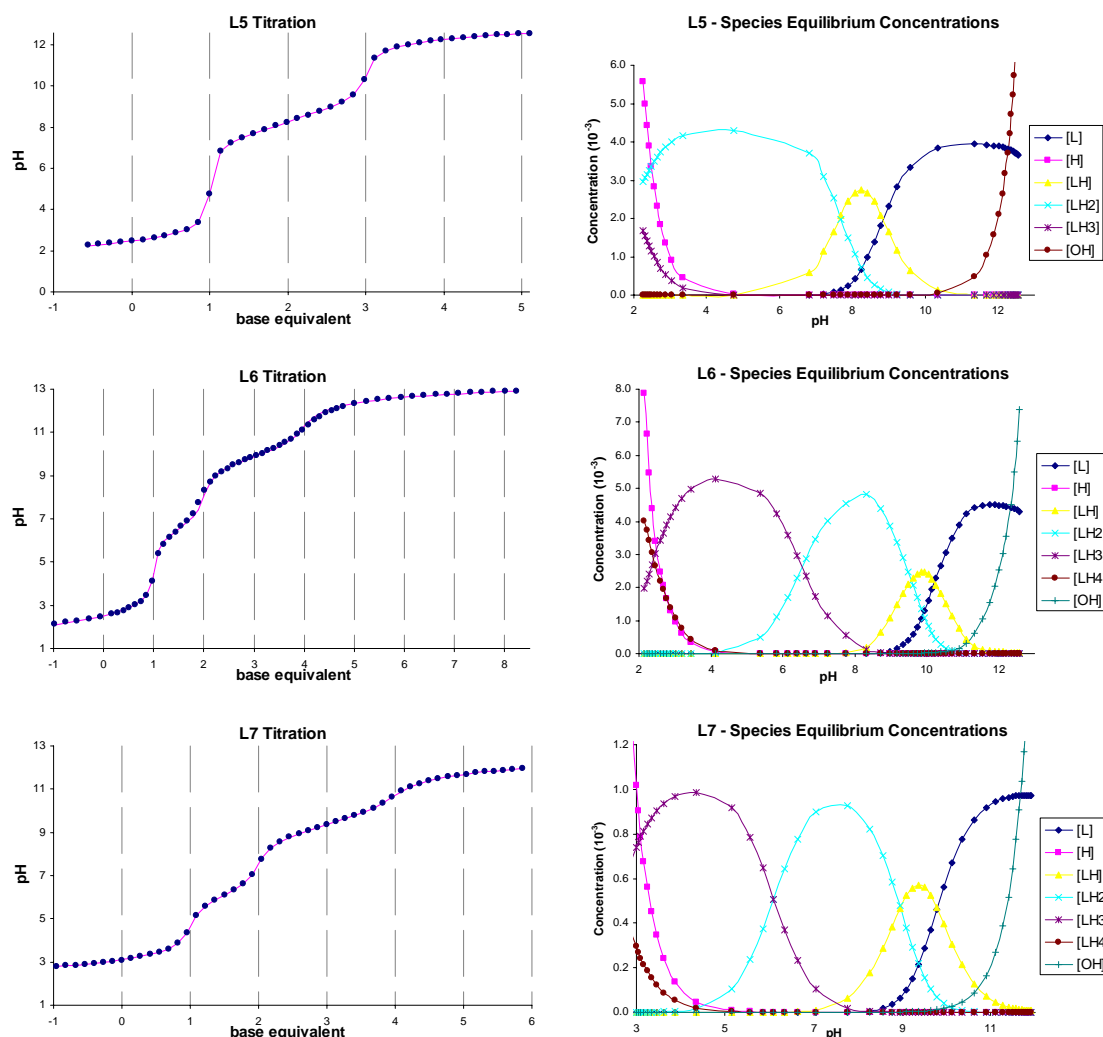
The general process described for the analysis of L5, Pizda, was applied to the analysis of both potentiometric and spectrophotometric data for all ligands in the series. The results are provided in the followed two sections, which firstly cover the determination of the protonation constants of all ligands from potentiometric titrations that are a prerequisite for the determination of stability constants. The protonation constants were not corrected to be aqueous pK_0 values as the titrations were only performed in 50/50 (v/v) ethanol/water and not over a range of ethanol percentages. The investigation of stability constants was only possible for some ligands due to precipitation issues, where possible titrations were performed using both potentiometry and spectrophotometry.

3.5.1 Protonation Constants

The potentiometric titration data for each ligand in the series is shown in Scheme 3.10, LHS. The • points represent the measured pH value for the titration and the solid line is the calculated data resulting from the analysis. The titrations have been plotted as pH versus base equivalent as this enables easy identification of the equivalent points for

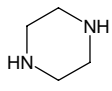
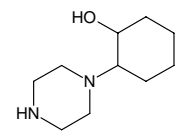
each ligand. On the right-hand side of the figure, the species concentrations over the pH range of the titration have been shown.





Scheme 3.10: (LHS) Figures of potentiometric titrations for the ligand series: • measured data, — calculated titration curve; (RHS) Figures of the changing species concentrations with increasing pH as the titration progresses.

Table 3.9 provides the calculated protonation constants for the ligand series. Both overall protonation constants, $\log \beta$ values, and calculated $\log K$ constants have been given. The process to convert the calculated $\log \beta$ values to $\log K$ values have been previously outlined in Section 3.1.2.1.

ligand	species	$\log \beta$ value	$\log K$ value
L1	 LH ₂	16.912 ± 0.026	6.226 ± 0.032
	LH	10.686 ± 0.018	10.686 ± 0.018
L2	 LH ₂	14.315 ± 0.024	4.940 ± 0.026
	LH	9.374 ± 0.010	9.374 ± 0.010

L3		LH ₂	12.358 ± 0.018	3.702 ± 0.020
		LH	8.656 ± 0.008	8.656 ± 0.008
L4		LH ₃	20.028 ± 0.060	2.014 ± 0.061
		LH ₂	18.014 ± 0.011	8.533 ± 0.013
		LH	9.482 ± 0.006	9.482 ± 0.006
L5		LH ₃	18.528 ± 0.065	2.007 ± 0.066
		LH ₂	16.520 ± 0.012	7.661 ± 0.013
		LH	8.560 ± 0.006	8.560 ± 0.006
L6		LH ₄	28.698 ± 0.155	2.413 ± 0.166
		LH ₃	26.285 ± 0.059	6.543 ± 0.069
		LH ₂	19.742 ± 0.035	9.553 ± 0.045
		LH	10.190 ± 0.028	10.190 ± 0.028
L7		LH ₄	27.436 ± 0.052	2.595 ± 0.054
		LH ₃	24.841 ± 0.013	6.100 ± 0.072
		LH ₂	18.741 ± 0.071	8.948 ± 0.086
		LH	9.793 ± 0.049	9.793 ± 0.049

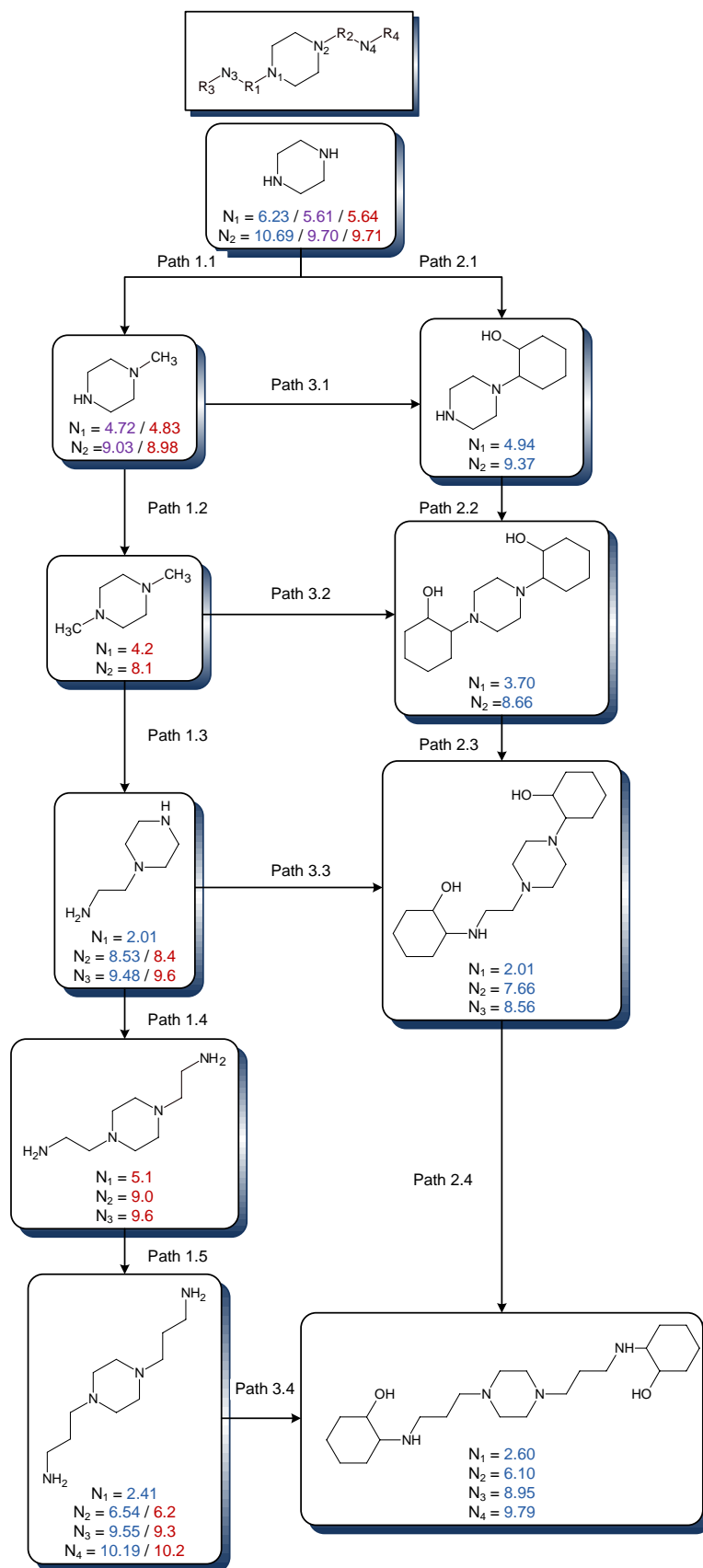
Table 3.9: Protonation constants of ligand series; log β values are determined by the Pot_Anal program and log K values have been calculated as described in Section 3.1.2.1.

3.5.1.1 Protonation Data Trends

The analysis of a series of ligands can often enable the identification of trends through comparisons of the protonation constants determined for each ligand. Scheme 3.11 shows the change in protonation constants for the ligand series, making trends easier to identify. The numbers in blue were determined experimentally in this study, the numbers in purple were determined at the University of Newcastle using the in-house developed techniques as part of Aleasia Gordon's Honours research³⁰, and the numbers in red are from the NIST³¹ database.

Both Gordon's and NIST constants were determined in aqueous solutions, whereas for this study 50/50 (v/v) ethanol/water solutions were used. It can be seen that the pK values determined by Gordon and from the NIST database are comparable for L1, whereas the constants determined in this study differ due to the different solvent used. As discussed previously in Section 3.2, it is expected that the pK values should be higher in mixed solvent solutions, which is the case for the values determined for L1. Even though direct comparison of data determined in aqueous and mixed solvents cannot be made, similar trends observed with the experimentally determined values and those quoted from Gordon and NIST support the validity of the models and the analytical procedure used for this study.

It should be noted that it is not trivial to identify which deprotonation constant applies to which nitrogen on the ligand. Therefore, the calculated constants have been assigned nitrogens as shown by the numbering system on the ligand pictured at the top of Scheme 3.11. However, it cannot be conclusively proven that, for example, the deprotonation constant quoted for N_4 physically corresponds to the N_4 nitrogen being deprotonated. NMR titrations could provide more information regarding the site of the proton, depending on whether different amine protons are differentiated and not masked by other peaks or rapidly exchanged. However, NMR investigations were not performed as part of the investigation. The numbering system is instead applied as a guide to aid with comparing respective deprotonation constants.



Scheme 3.11: Graphical representation of the protonation constants for each ligand showing the trends as the ligands become more complex. The numbers quoted in blue, purple, and red were determined for this study, Gordon's Honours thesis³⁰, and the NIST³¹ database, respectively.

Consideration of Scheme 3.11 shows that the addition of a methyl group, Path 1.1, lowered the pK of both nitrogens by 0.8 units. The addition of a subsequent methyl group, Path 1.2, further lowered the pK by 0.6 and 0.8 units for each nitrogen. Even though a methyl group is slightly electron donating and would therefore be expected to stabilise the protonated amine and increase the pK value, the introduction of one or two methyl groups instead destabilises the protonated ligand, resulting in a lowering of the pK value. This effect can be explained by considering the structural changes that occur when a methyl group is substituted for a hydrogen on a secondary nitrogen, resulting in a tertiary nitrogen, which greatly distorts the pseudo-tetrahedral geometry around the nitrogen. This distortion will destabilise the protonated nitrogen. This effect has been reported by Kilic³² in an investigation of the substituent effect on an alkylamine series in 50/50 (wt%) ethanol/water solvent, as shown in Table 3.10.

alkyl group	methyl	ethyl	propyl	butyl
ammonia	8.51 ± 0.03			
primary	9.76 ± 0.01	9.74 ± 0.01	9.76 ± 0.01	9.65 ± 0.02
secondary	9.84 ± 0.01	10.12 ± 0.02	9.89 ± 0.03	9.77 ± 0.01
tertiary	8.84 ± 0.01	9.69 ± 0.01	9.31 ± 0.01	9.36 ± 0.01

Table 3.10: pK values for alkylamine series in 50/50 (wt%) ethanol/water solvent³².

The investigation reported that the most important factor effecting the protonation constant of a compound was the structural effect. This effect can be explained by taking the electronic and sterical effects of the alkyl groups they investigated into account. As previously stated, since alkyl groups are electron donating, the replacement of the hydrogen atoms in ammonia with alkyl groups would be expected to increase the protonation constant. The pK value was seen to increase with the first and second alkyl groups, as expected due to their electron donating properties. However, the addition of the third alkyl group decreased the pK value because of the distortion and combined steric effects imposed upon introduction of the tertiary alkyl group. If there had only been electronic effects active, then the tertiary amines would have had the highest pK values. The steric effect, on the other hand, causes the pK values to decrease in contrast to the electronic effect. This order, $NH_3 < R_3N < R_2NH < RNH_2$, reported for the 50/50 (wt%) ethanol/water solvent, is identical to that found for the same series in water³³. In water there are two main opposing effects influencing the protonation of amines,

namely hydration and inductive effects. The hydration effect decreases the pK value due to a decrease in basicity with an increase in the number of alkyl substituents. Similar effects will be present in ethanol/water solvent, as this was the trend observed with our study.

The trend observed with the addition of methyl groups was further accentuated with the introduction of a cyclohexanol group to the piperazine unit, Path 2.1, as this resulted in an even greater reduction in pK of approximately 1.3 units. This is half a pK unit more than was observed with the addition of the methyl group and may be due to the cyclohexanol group being a bulkier substituent than a methyl group. Additionally, the hydroxy group may also be slightly electron withdrawing, therefore further decreasing the basicity of the nitrogen. The addition of another cyclohexanol group, Path 2.2, lowered the pK values by a further 0.7 and 1.2 units, which is again a larger reduction than seen with the methyl group, as one might expect because of the increased distortion combined with the electron withdrawing properties.

The pK values across Paths 3.1 and 3.2 cannot be directly compared due to the different solvents used for each investigation. Generally pK values determined in 50/50 (v/v) ethanol/water are greater than pK values in pure aqueous mediums. Path 3.2 shows a reduction in the pK values when substituting both methyl groups with cyclohexanol groups, hence it can be inferred that this reduction would be even greater if the cyclohexanol pK values were measured in aqueous solutions. Once again, this may be due to the increased distortion from the bulkier substituents and the electron withdrawing property of a hydroxy group.

Path 3.3 shows, from comparison of the values determined in this study, that the addition of cyclohexanol groups to both terminal nitrogens reduces the pK values of N_2 and N_3 by approximately 0.9 units. The pK of N_1 remains unchanged and it is therefore assumed that this nitrogen is the tertiary middle nitrogen of the ligand. The reduction in pK of the secondary nitrogen is expected from the previous discussion of steric influence; however, the decrease in pK that was also observed for the primary to secondary nitrogen may be due also to the bulky cyclohexanol ligand distorting the tetrahedral structure as well as the electron withdrawing effect of the hydroxy group. This effect can also be seen along Path 3.4, as a reduction in pK values is also seen when the terminal, primary nitrogens have a cyclohexanol group substituted for a hydrogen.

Comparison of the pK values of N_1 when a three carbon spacer is introduced, Path 2.4, shows an increase in value which may be attributed to the bulky and slightly electron withdrawing group cyclohexanol being separated further from the nitrogen. This would result in a decrease in distortion around the nitrogen and also a reduction in the electron withdrawing effect. In fact, the ethyl spacer is more likely to have a slight electron donating effect and therefore further increase the basicity of the nitrogen and contributing to the increase in the pK value.

Comparing the NIST calculated values in Path 1.5 shows that the pK increases in value when the chain length is increased by a carbon atom. This can be attributed to the added carbon length separating the electron withdrawing nitrogen atoms. Consequently, the effect each nitrogen has on the other will decrease, resulting in an increase in the stability of each protonated nitrogen.

Overall, the series showed that the addition of bulky substituents to the amines reduced the basicity of the nitrogen because of the destabilising effect of the distorted geometry. The results showed that this distortion has a greater influence than the electron donating properties of the methyl group. Further, if the substituted group is also an electron withdrawing group, then this has a more pronounced effect in decreasing the pK value. These trends were observed for both the NIST data and the data calculated by the in-house analysis techniques. Further, it could be seen that if the distance between interacting groups was increased the subsequent reduction in the affect they have on each other could be clearly observed by the pK trends.

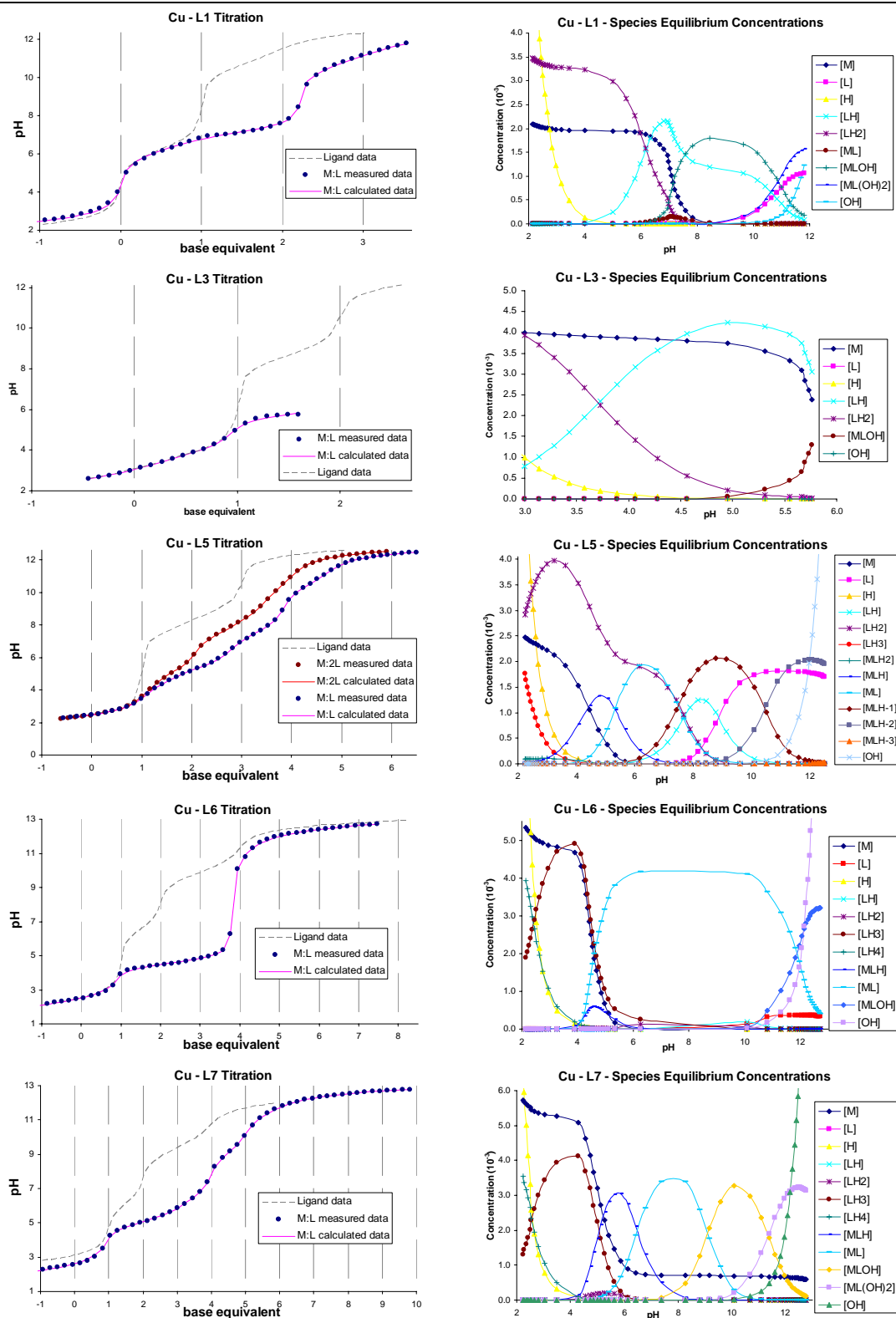
3.5.2 Stability Constants

3.5.2.1 Potentiometric Titration Results

The potentiometric metal-ligand titrations are shown for copper(II) in Scheme 3.12, and for nickel(II) in Scheme 3.13. The titration of the ligand with no metal present has been shown in the background so the difference in equivalence points due to the presence of the metal ion can easily be seen. Not all ligands in the series had usable results with copper(II) and nickel(II), as precipitation of the metal hydroxide occurred for some metal-ligand titrations. However, if a sufficient amount of the titration had progressed for analysis to be performed, the metal-ligand titration was cut off at the point where precipitation occurred in the solution before analysis of the titration data, for example L3 in Scheme 3.12.

copper - ligand potentiometric titration

calculated species concentrations



Scheme 3.12: (LHS) Figures of potentiometric titrations for the copper(II) - ligand series: — ligand titration, • measured data, — calculated titration curve; (RHS) Figures of the changing species concentrations with increasing pH as the titration progresses.

Table 3.11 provides a summary of the model that was determined to be the best model for each ligand with copper(II) along with the $\log \beta$ values and calculated $\log K$ values.

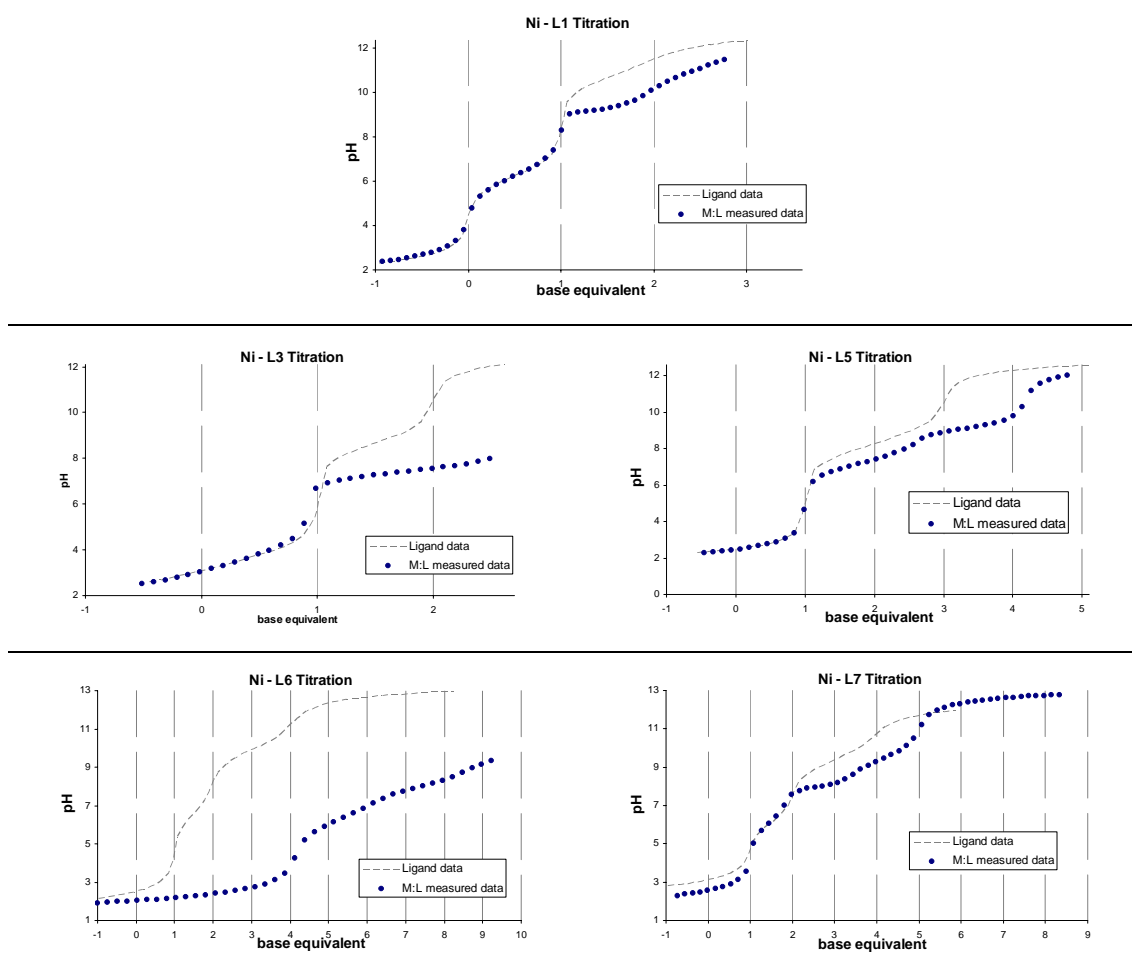
ligand	copper species	$\log \beta$ value	$\log K$ value
L1	ML	5.444 ± 0.211	5.444 ± 0.211
	MLH ₁	-0.954 ± 0.063	6.398 ± 0.220
	MLH ₂	-11.777 ± 0.130	10.823 ± 0.144
L2	-	-	-
L3	MLH ₁	-0.769 ± 0.056	-
L4	ML	5.51*	5.51
	ML ₂	14.76*	9.25
L5	MLH	14.618 ± 0.036	5.340 ± 0.044
	ML	9.278 ± 0.026	9.278 ± 0.026
	MLH ₁	1.825 ± 0.030	7.443 ± 0.040
	MLH ₂	-8.608 ± 0.033	10.443 ± 0.045
	MLH ₃	-23.024 ± 0.729	14.416 ± 0.730
L6	MLH	19.170 ± 0.099	4.110 ± 0.335
	ML	15.060 ± 0.032 13.4*	15.060 ± 0.032 13.4
	MLH ₁	3.255 ± 0.043	11.805 ± 0.054
L7	MLH	17.209 ± 0.045	6.509 ± 0.062
	ML	10.700 ± 0.061	10.700 ± 0.061
	MLH ₁	1.596 ± 0.077	9.104 ± 0.098
	MLH ₂	-9.739 ± 0.100	11.334 ± 0.126

Table 3.11: Stability constants of ligand series with copper(II); $\log \beta$ values are determined by the Pot_Anal program and $\log K$ values have been calculated as described in Section 3.1.2.1; * values are quoted from the NIST database.

With the transition metal nickel(II), all the ligands in the series resulted the precipitation of nickel(II) hydroxide during the titration. The precipitate was observed before any useful results could be obtained and hence no models of metal-ligand complexation with nickel(II) could be determined. Scheme 3.13 shows the metal-ligand titration compared

with the ligand titration. The clear kink in the curve where the two titration curves deviate is indicative of the formation of a precipitate. The fine precipitate is also visible upon passing a laser beam through the solution. The only ligand that showed some difference in titration curve before the formation of the precipitate was L6; however, the titration could still not be modelled, as a high enough pH was not achieved in order to adequately define all species present in the titration.

nickel-ligand potentiometric titration data



Scheme 3.13: Figures of potentiometric titrations for the nickel(II)-ligand series: — ligand titration, • measured metal-ligand data.

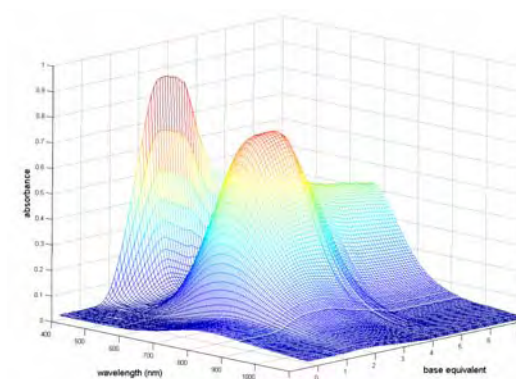
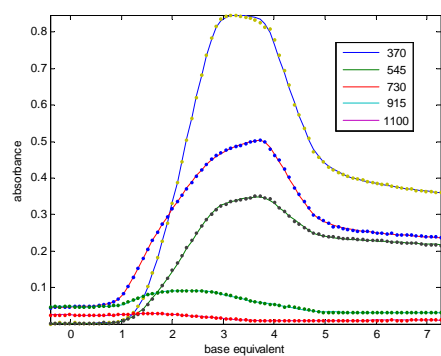
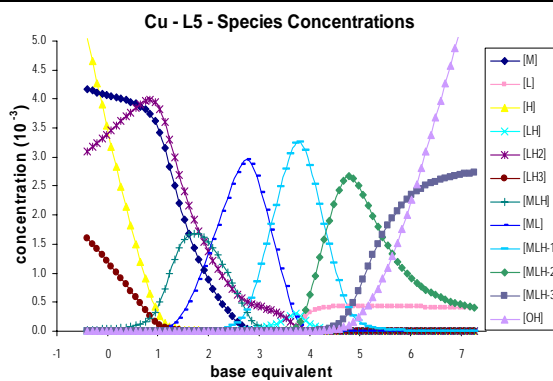
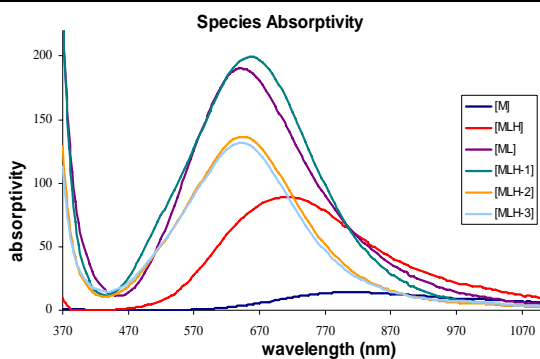
Due to the fact that precipitation prevented any useful results being obtained with nickel(II), it is hard to identify any trends in the constants from comparisons of the copper(II) and nickel(II) results. Generally, copper(II) is considered to form stronger bonds with N-donor ligands. This was observed qualitatively in this ligand series as copper(II) hydroxide precipitated in only one titration, whereas nickel(II) hydroxide was seen to form in all of the ligand titrations as the metal-ligand bond was not strong

enough to prevent the formation of the hydroxide species. From the NIST³¹ database a value of 5.4 was given for the 1:1 nickel(II)-L6 complex; this is a significantly smaller constant compared to the 13.4 stability constant quoted for copper(II). NIST also provided constants for 1:1 metal-ligand complexes for both nickel(II) and copper(II) for an analogous ligand to L6, but with one less carbon spacer in the pendant arms. For this ligand nickel(II) again had a significantly lower stability constant, 4.68, compared to copper(II) which was quoted to be 11.91. These values further support the proposition that copper(II) forms stronger coordinate bonds with N-donors.

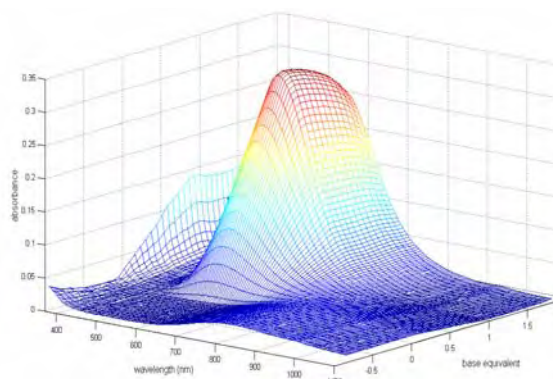
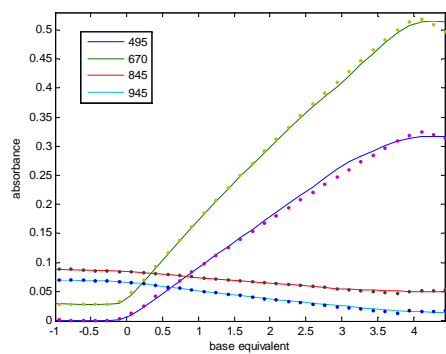
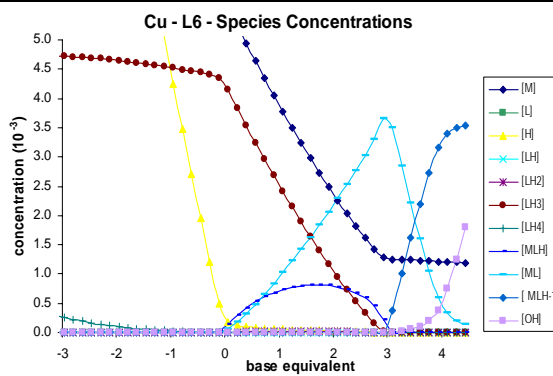
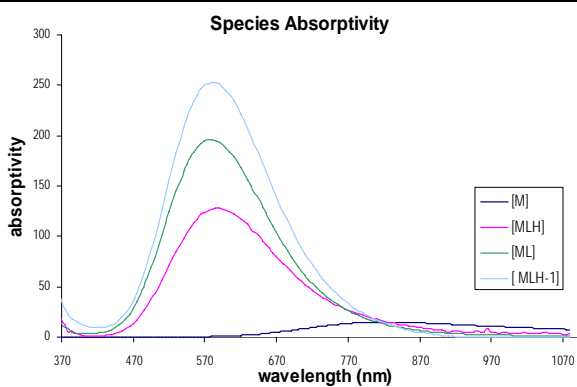
3.5.2.2 Spectrophotometric Titration Results

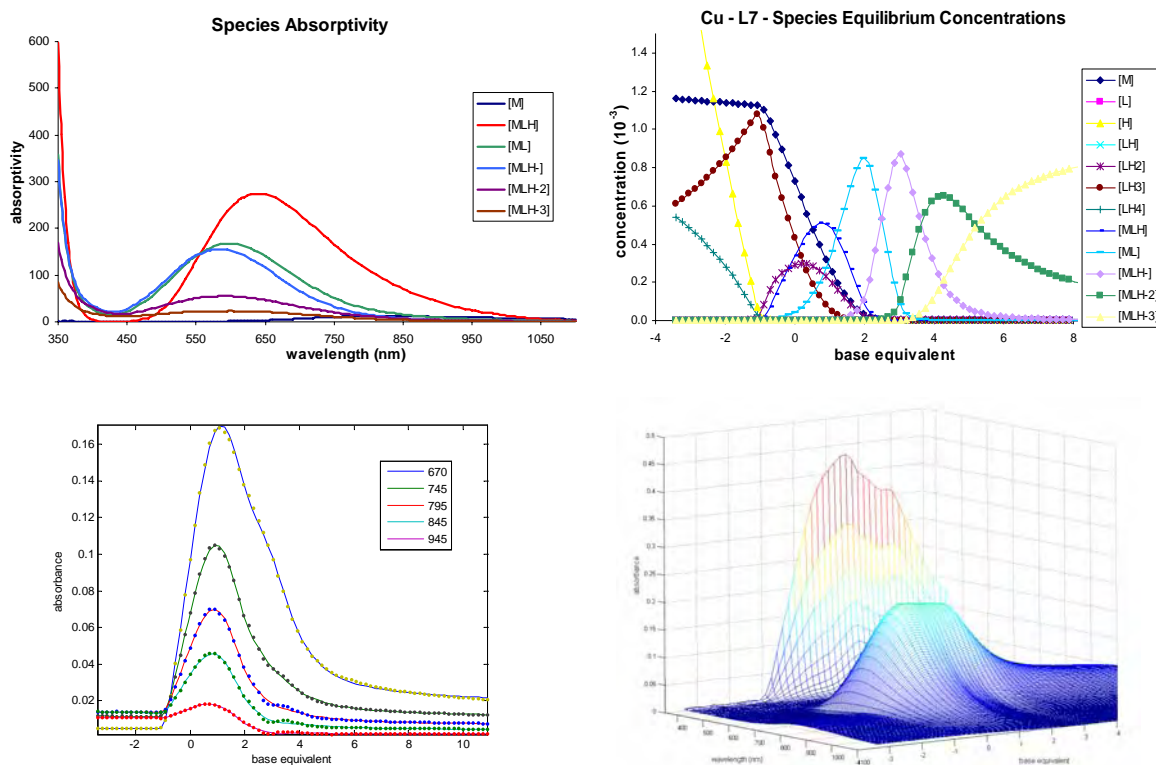
Spectrophotometric titrations were performed only with copper(II) and the last three ligands in the series, L5, L6 and L7, as all nickel(II) potentiometric titrations resulted in precipitation at some stage in the titration. Scheme 3.14 shows the results of the analysis for each ligand. The top left-hand corner shows the absorptivity of the coloured species that formed. The spectra of each absorbing species were required to be positive and of sensible shape and magnitude in order for the proposed model and/or calculated constants to be accepted. The changing species concentration with the increasing base equivalent is shown in the top right-hand corner. This clearly depicts the stages in the titration at which different species form, and also whether or not each species have formed to significant enough concentrations to be included in the model. The bottom left-hand corner shows a plot of the measured and calculated spectra in order to demonstrate the fit of the data at a selected range of wavelengths. The last plot for each ligand shows the total measured spectra from the titration; each measurement had a maximum absorbance less than one, so that Beer-Lambert's Law could be applied for the analysis.

L5



L6





Scheme 3.14 (Clockwise from top LHS for each ligand): Plot showing the absorptivity of each absorbing species in the titration; Plot of the changing species concentrations with increasing base equivalent as the titration progresses; Figure of the resulting spectra of the titration; Plot of the • measured and — calculated data at the shown selected wavelengths.

The results obtained from the analysis of the spectrophotometric data for each ligand generally led to the same model that had been determined from potentiometric analysis. The best fit model along with the $\log \beta$ and $\log K$ values have been provided in Table 3.12.

ligand	copper(II) species	$\log \beta$ value	$\log K$ value
L5	MLH	14.504 ± 0.005	5.185
	ML	9.319 ± 0.013	9.319
	MLH ₁	2.251 ± 0.019	7.068
	MLH ₂	-7.662 ± 0.020	9.913
	MLH ₃	-19.294 ± 0.024	11.632
L6	MLH	19.581 ± 0.251	4.160
	ML	15.421 ± 0.307	15.421
	MLH ₁	5.874 ± 0.331	10.547
L7	MLH	16.019 ± 0.003	6.823
	ML	9.196 ± 0.004	9.196
	MLH ₁	0.544 ± 0.008	8.652
	MLH ₂	-10.023 ± 0.016	10.567
	MLH ₃	-21.627 ± 0.020	11.604

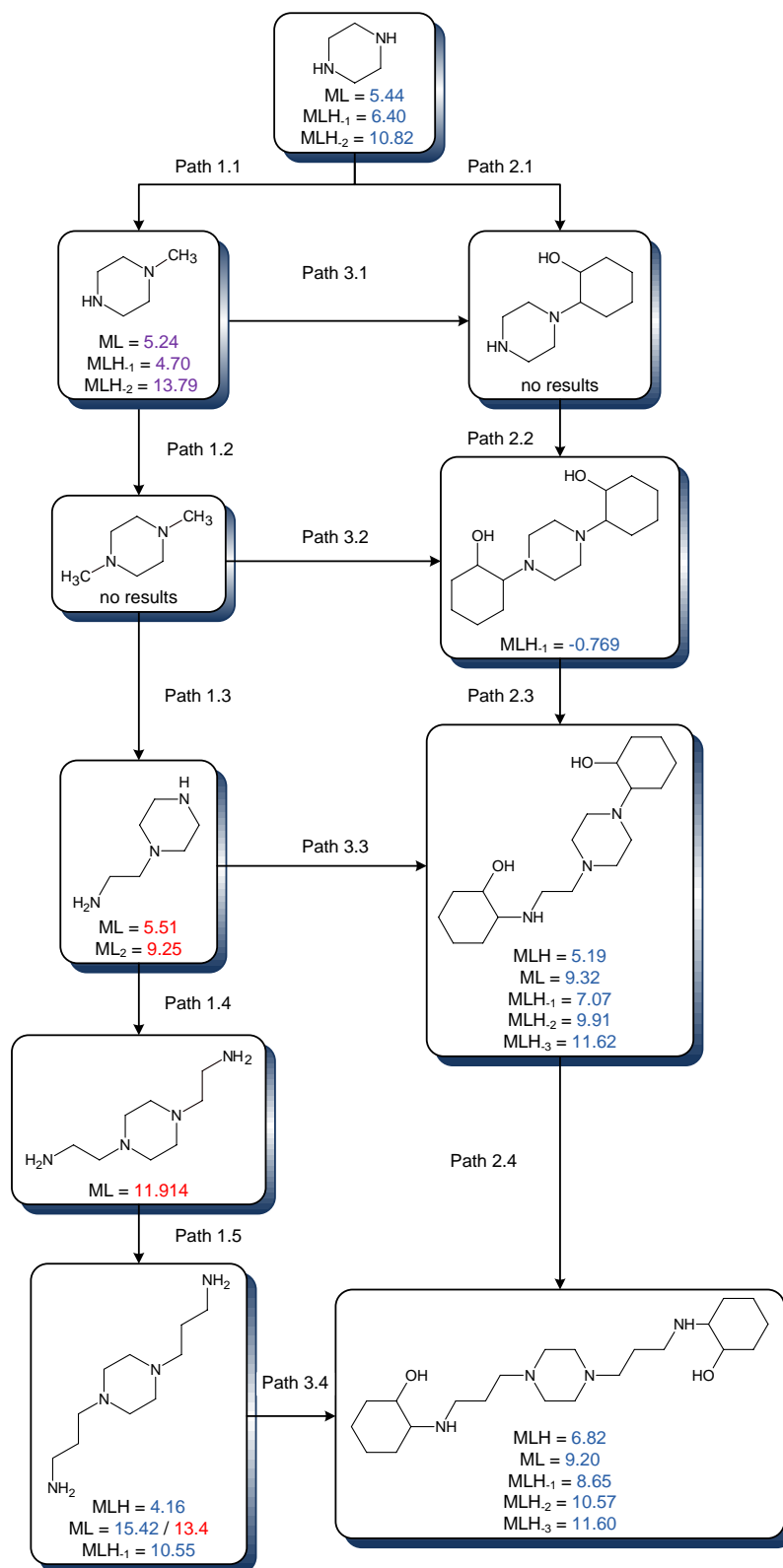
Table 3.12: Stability constants determined from spectrophotometric titrations for the ligand series with copper(II); $\log \beta$ values are determined by the Spec_Anal program and $\log K$ values have been calculated as described in Section 3.1.2.1.

The benefit of having both spectrophotometric and potentiometric data for a ligand has been discussed in depth in Section 3.1.3. Table 3.13 provides the potentiometric and spectrophotometric data for the ligand series. For the ligands where both potentiometric and spectrophotometric analysis was possible the results show that the calculated constants are directly comparable. This greatly supports both the method of analysis and also validates the determined best model.

ligand	species	log K value	
		spectrophotometric	potentiometric
L5	MLH	5.185	5.340
	ML	9.319	9.278
	MLH ₁	7.068	7.443
	MLH ₂	9.913	10.443
	MLH ₃	11.632	14.416
L6	MLH	4.160	4.110
	ML	15.421	15.060
	MLH ₁	10.547	11.805
L7	MLH	6.823	6.509
	ML	9.196	10.700
	MLH ₁	8.652	9.104
	MLH ₂	10.567	11.334
	MLH ₃	11.604	

Table 3.13: Comparison of log K values for spectrophotometric and potentiometric data analysis for copper(II).

3.5.2.3 Stability Constant Data Trends



Scheme 3.15: Graphical representation of the stability constants for each ligand showing the trend as the ligands become more complex. The numbers quoted in blue, purple, and red were determined for this study, Gordon's Honours thesis³⁰, and the NIST³¹ database, respectively.

For the stability constant data there was not enough data to enable detailed trends to be identified in the same way as for the protonation results. Even so, a few trends that could be ascertained from the stability data with copper(II), though precipitation prevented the analysis of many of the ligands. The main trend identified is for the stability constant of the formation of the complex ML. Moving along Path 1.3 shows that the stability only increases by 0.07 units with the introduction of the amine chain to the piperazine ligand; however, a noticeable increase is seen at Path 1.4 with the addition of the second pendant arm. This results in an increase of more than five pK units. This increase may be due to the second chain enabling the ligand to wrap around the copper(II) ion more completely, therefore resulting in a more stable complex. Further, introducing the carbon spacer in Path 1.5 results in a further increase of 3.5 pK units in the stability of the ML complex, which is presumably due to the added flexibility of the ligand, enabling it to wrap around the copper(II) ion more easily and to a greater extent.

Path 3.4 shows that introducing cyclohexanol groups onto the terminal nitrogens lowers the stability of the ML complex by 6.22 units. This may be due to the bulkiness of the cyclohexanol groups which can hinder the ability of the ligand to wrap around the copper(II) ion as closely as was possible without the groups attached. Overall, it can be inferred that increasing the flexibility of the chelating arms on the piperazine unit increases the stability of metal-ligand complexes providing there has not been an increase in the steric hindrance of the complex.

3.6 Conclusions

Several conclusions can be drawn from this study. First, the experiments have shown that the in-house developed computer programs, Pot_Anal and Spec_Anal, have the capability to accurately and efficiently calculate protonation and stability constants for complex systems involving many complicated equilibria. The study has also shown the validity of the methods by demonstrating that both potentiometric and spectrophotometric data analysis leads to the same equilibrium model and with the calculation of comparable stability constants for each species formed. Further, the procedure highlights the benefits of performing both potentiometric and spectrophotometric titrations for a metal-ligand investigation. The results of the analysis enabled the elucidation of some trends with regards to the change in protonation of a ligand and also the stability of some metal complexes.

This study also highlighted the common complexity that occurs when experiments cannot be performed in pure aqueous solutions, as is often the case for many ligands. The determined values in 50/50 (v/v) ethanol/water were consistent with what had been detailed in literature; that is, that a pK value generally increases in mixed solvents due most significantly to the lowered relative permittivity, although necessarily there are other factors that influence the observed change in pK . For results that had been determined in both aqueous solutions and the mixed solvent used for our investigations, an increase was observed for the pK values determined in the mixed solvent.

3.7 References

1. Albert, A.; Sergeant, E. P., *The Determination of Ionisation Constants. A Laboratory Manual*. 3rd ed.; Chapman and Hall: London, 1984.
2. Martell, A. E. M., R.J., *Determination and Use of Stability Constants*. VCH: Weinheim, 1988.
3. Takacs-Novak, K.; Box, K. J.; Avdeef, A., Potentiometric pK_a determination of water-insoluble compounds: validation study in methanol/water mixtures. *International Journal of Pharmaceutics* **1997**, 151, 235-248.
4. Nancollas, G. H.; Tomson, M. B., Guidelines for the determination of stability constants. *Pure and Applied Chemistry* **1982**, 54, 2675-92.
5. Martell, A. E.; Motekaitis, R. J., Potentiometry revisited: the determination of thermodynamic equilibria in complex multicomponent systems. *Coordination Chemistry Reviews* **1990**, 100, 323-61.
6. Dyson, R. M.; Kaderli, S.; Lawrance, G. A.; Maeder, M.; Zuberbuhler, A. D., Second order global analysis: the evaluation of series of spectrophotometric titrations for improved determination of equilibrium constants. *Analytica Chimica Acta* **1997**, 353, 381-393.
7. Michaelis, L.; Mizutani, M., The dissociation of weak electrolytes in water-alcohol solutions. *Z. physik. Chem.* **1925**, 116, 135-69.
8. Crosby, J.; Stone, R.; Lienhard, G. E., Mechanisms of thiamine-catalyzed reactions. Decarboxylation of 2-(1-carboxy-1-hydroxyethyl)-3,4-dimethylthiazolium chloride. *Journal of the American Chemical Society* **1970**, 92, 2891-900.
9. Dogan, A.; Kilic, E., Potentiometric studies on the protonation constants and solvation of some α -amino acid benzyl and tert-butyl esters in ethanol-water mixtures. *Turkish Journal of Chemistry* **2005**, 29, 41-47.
10. Definitions of Engineering Terms. <http://www.accum.com/defs.htm#p> (6/11/2007),
11. Wikipedia® Acid dissociation constant. http://en.wikipedia.org/wiki/Acid_dissociation_constant (07/08),
12. Gibson, G. T. T.; Mohamed, M. F.; Neverov, A. A.; Brown, R. S., Potentiometric Titration of Metal Ions in Ethanol. *Inorganic Chemistry* **2006**, 45, 7891-7902.
13. Harned, H. S.; Owen, B. B., *The Physical Chemistry of Electrolytic Solutions*. 3rd ed. Am. Chem. Soc. Monograph No. 137. 1958; p 803.
14. Hammam, A. M.; Ibrahim, S. A.; Abou El-Wafa, M. H.; Rageh, N. M.; Mohamad, A. A., Acidity constants of some hydroxy azopyrazolopyridines in mixed aqueous-organic solvents. *Journal of Chemical and Engineering Data* **1993**, 38, 63-6.

15. Gentile, P. S.; Cefola, M.; Celiano, A. V., Coordination compounds. VI. Determination of thermodynamic data for acetylacetone in mixed solvents. *Journal of Physical Chemistry* **1963**, 67, 1447-50.
16. Irving, H.; Rossotti, H., Relations among the stabilities of metal complexes. *Acta Chemica Scandinavica* **1956**, 10, 72-93.
17. Niazi, M. S. K.; Mollin, J., Dissociation constants of some amino acid and pyridinecarboxylic acids in ethanol-water mixtures. *Bulletin of the Chemical Society of Japan* **1987**, 60, 2605-10.
18. Panichajakul, C. C.; Woolley, E. M., Potentiometric method for determination of acid ionization constants in aqueous organic mixtures. *Analytical Chemistry* **1975**, 47, 1860-3.
19. Van Uitert, L. G.; Haas, C. G.; Fernelius, W. C.; Douglas, B. E., Coordination compounds. II. The dissociation constants of b-diketones in water-dioxane solutions. *Journal of the American Chemical Society* **1953**, 75, 455-7.
20. Kilic, E.; Koseoglu, F.; Basgut, O., Protonation constants of some pyridine derivatives in ethanol-water mixtures. *Analytica Chimica Acta* **1994**, 294, 215-20.
21. Denison, J. T.; Ramsey, J. B., Free energy, enthalpy, and entropy of dissociation of some perchlorates in ethylene chloride and ethylidene chloride. *Journal of the American Chemical Society* **1955**, 77, 2615-21.
22. Gilkerson, W. R., Application of free-volume theory to ion-pair dissociation constants. *Journal of Chemical Physics* **1956**, 25, 1199-1202.
23. Coetzee, J. F.; Ritchie, C. D.; Editors, *Solute-Solvent Interactions*. 1969; p 653
24. Mohamed, A. E.-G.; Said, A. I.; Dina, M. F.; Hammam, A. M., Medium Effect on the Acid Dissociation Constants of 2,2',6',2''-Terpyridine. *Journal of Chemical Engineering Data* **2003**, 48, 29-31.
25. Douheret, G., Liquid junction potentials and medium effects in mixed solvents (water-dipolar aprotic solvent). Application to the standardization of the glass-calomel electrodes system in these mixtures. Dielectric properties of these mixtures. *Bulletin de la Societe Chimique de France* **1968**, 3122-31.
26. Bates, R. G.; Paabo, M.; Robinson, R. A., Interpretation of pH measurements in alcohol-water solvents. *Journal of Physical Chemistry* **1963**, 67, 1833-8.
27. Hepler, L. G.; Woolley, E. M.; Hurkot, D. G., Ionization constants for water in aqueous organic mixtures. *Journal of Physical Chemistry* **1970**, 74, 3908-13.
28. Wosley, W. C., Perchlorate salts, their uses and alternatives (Safety). *Journal of Chemical Education* **1973**, 50, A335.

29. Maeder, M.; Zilian, A., Evolving factor analysis, a new multivariate technique in chromatography. *Chemometrics and Intelligent Laboratory Systems* **1988**, 3, (3), 205-13.
30. Gordon, A. Complexation of Unsymmetrical Ligands N-Ethylpiperazine and Thiomorpholine. Honours, University of Newcastle, Newcastle, 2006.
31. Martell, A. E.; Smith, R. M., NIST Critically Selected Stability of Metal Complexes, Database 46 Version 6.0. In NIST Standard Referenced Data: 2001.
32. Kilic, E.; Gokce, G.; Canel, E., The protonation constants of some aliphatic alkylamines in ethanol-water mixtures. *Turkish Journal of Chemistry* **2002**, 26, (6), 843-849.
33. Brown, H. C., Studies in stereochemistry. V. The effect of F-strain on the relative strengths of ammonia and trimethylamine. *Journal of the American Chemical Society* **1945**, 67, 374-8.

Chapter 4

Conjoint Chemometric Analysis of Equilibrium and Kinetic Data and Induced Chirality Investigations of a Helicating N-donor Ligand Interacting with Copper(II) and Nickel(II)

4.1 Introduction

The formation of helicates is a well recognised area in the field of supramolecular chemistry, and ligands that have a tendency to form helical structures when coordinated to transition metals are of intense current interest ^{1, 2}. The programmed matching of the number and spatial arrangement of donor atoms within a specific ligand with the coordination number and geometry of a metal ion has enabled researchers to prepare topologically and topographically novel species. The design of metal-ligand complexes has grown to include not only double helicates and triple helicates, but also complexes known as catenates, knots, grids, racks and ladders ³.

The broad definition of a helicate is a discrete helical supramolecular complex constituted by one or more covalent organic strands wrapped about, and coordinated to, a series of metal ions that define the helical axis ^{4, 5}. The synthetic approach to these structures has been well researched and the typical path follows a two-step process. The first step is the synthesis of a suitable organic ligand prior to the second step which involves the reaction of the synthesised ligand with suitable metal ions in order to assemble the desired helicate ⁶. The ligand synthesised for this study was a potentially pentadentate N-donor ligand and it was reacted with transition metal ions in order to investigate the formation of double-stranded helical species.

It is considered that the driving force that controls the chemical pathways for the formation of helicates is the minimisation of the intercomponent electrostatic forces ⁷⁻¹⁰. Additionally, the basic drive to form the maximum number of coordination bonds in the final helicate structure is also another contributing factor, as this contributes to minimising the free energy of complexation. This concept is often referred to as ‘the principle of maximum occupancy’ ¹¹ and influences the thermodynamically stable final helicate product in a metal-ligand reaction.

Investigating the stability of the final helicate is an important aspect of helicate formation, and this requires equilibrium investigations of the reaction. Kinetic data are

also useful as they define the rate of the helicate reaction. It is not trivial to determine the reaction pathway for the formation of helical structures and usually only one field is investigated. Equilibrium studies provide thermodynamic information about a reaction, but no kinetic information defining the formation and dissociation rates, and while the full kinetic analysis of a system provides data sufficient to define equilibrium constants, this is not routinely done. Hence, if both techniques were to be examined conjointly, the resulting suite of data may provide information pertinent to the mechanistic pathway.

Conjoint analysis of a system may be achieved by comparison of the determined parameters for each possible pathway determined from separately studied kinetic and thermodynamic methods and by then equating the reaction pathway with the best data match. To our knowledge such an approach has not been attempted previously for complex systems. Such a conjoint analysis may be considered for a range of options, for example complexation reactions where monomer and/or oligomer systems may form as these systems present a clear challenge for analysis. Section 4.2.3 details the analysis of a helical system demonstrating how this problem of complex reaction pathways can be resolved by applying a full kinetic and equilibrium study of metal helicate formation, which reveals the value of the approach applied.

4.1.1 Carboxamide-based Ligands

This study combined kinetic and equilibrium studies of the complexation of the ligand *N,N'*-bis[2-(2'-pyridyl)methyl]pyridine-2,6-dicarboxamide, earlier given the trivial name PepdaH₂ and depicted in Figure 4.1, with both copper(II) and nickel(II) metal ions. The synthesis of the potentially pentadentate ligand PepdaH₂, which contains a -NH-CO-pyridine-CO-NH- core, was previously prepared at the University of Newcastle by Mery Napitupulu¹².

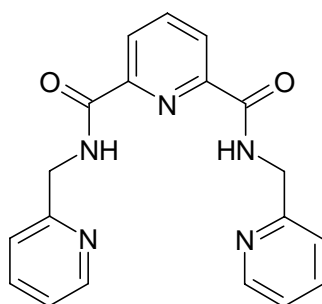


Figure 4.1: Structure of *N,N'*-bis[2-(2'-pyridyl)methyl]pyridine-2,6-dicarboxamide, also known by the trivial name PepdaH₂ and denoted Pepda²⁻ in its deprotonated form.

The synthesis and coordination properties of ligands based on 2,6-disubstituted pyridine, in particular diamides incorporating the –NH–CO–pyridine–CO–NH– core, have attracted a great deal of attention. The carboxamide [–CO–NH–] group is ubiquitous throughout nature in the primary structure of proteins and is an important construction unit for coordination chemists. Interest in pyridine carboxamides extend to potential applications as diverse as telomerase inhibitors¹³, as reagents for heavy metal selection and/or removal from water^{14–17}, as electroluminescent devices¹⁸, artificial enzymes¹⁹, catalysts for aldehyde hydrophosphonylation²⁰, and they have also been used as brightening agents for synthetic fibres²¹.

Previous research has shown that deprotonation of the two amide groups present on the PepdaH₂ ligand yields a potent dianionic ligand, Pepda^{2–}. Pepda^{2–} has been reported to exhibit a limited tendency to form some monomeric complexes with labile divalent metal ions, [M(Pepda^{2–})], but only as a minor species. Importantly, the most probable tendency is towards PepdaH₂ forming robust double helical complexes^{12, 22–24}. Alcock *et al*¹² isolated polynuclear PepdaH₂ complexes that all featured a racemic mixture of left- and right-handed double helices. It was noted that inter-ligand π -stacking appeared to be key with the formation of the robust helical complexes and as such was considered to be the stabilising factor. Alcock *et al*¹² reported that deprotonation of the amide groups led to the structural characterisation of a dinuclear double stranded copper(II) helix, [Cu₂(Pepda^{2–})₂]. Further, he also observed the formation of a trinuclear nickel(II) complex, [Ni₃(Pepda^{2–})₂(OAc)₂(MeOH)₂]. These helicates are depicted in Figure 4.2. The formation of both the copper(II) and nickel(II) helicate species were observed in our research.

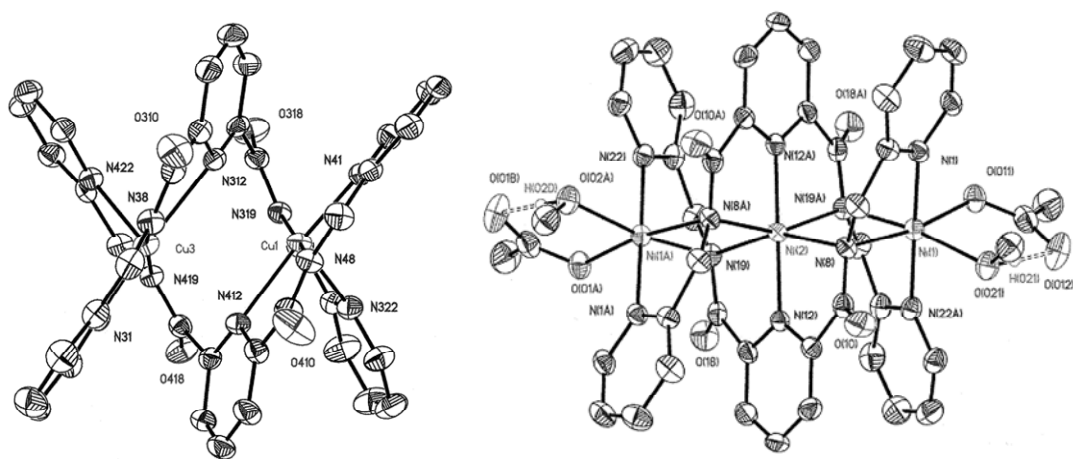


Figure 4.2: ORTEP drawings of (LHS) the helical [Cu₂(Pepda^{2–})₂] dinuclear complex; (RHS) the helical [Ni₃(Pepda^{2–})₂(acetate)₂(MeOH)₂] trinuclear complex, showing atom numbering.

Crystal structure analysis has shown that the dinuclear copper(II) complex contains two dianionic ligands coordinated to two copper(II) ions in a 5:5 coordination motif, with the two central pyridine nitrogen atoms bridging both copper(II) atoms. The crystal structure of this helicate is shown in Figure 4.3, clearly highlighting the 10-membered ring resulting from the complexation of both ligand strands. With nickel(II), the 3:2 Ni:Pepda²⁻ trinuclear complex had both ligands bound to all three metal ions, with each ligand wrapped as the separate arms of a double helix around the central metal framework and a 6:6:6 coordination motif operating with each nickel(II) atom in a distorted octahedral environment ¹².

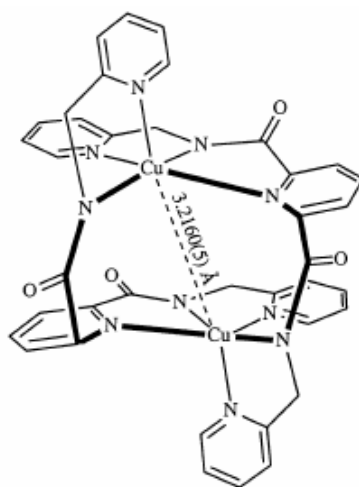


Figure 4.3: Drawing of the right-handed helicate of [Cu₂Pepda²⁻]₂ showing the ten-membered ring connecting the two copper centres (bold lines) and the Cu–Cu distance (dashed line) ²³.

Hubert *et al* ²⁵ has investigated the coordination properties of a carboxamide-based ligand that is structurally similar to PepdaH₂ with copper(II) and nickel(II). The ligand pycdien, Figure 4.4, has five potential donor sites and two pyridine carboxamide moieties, as does PepdaH₂. The formation of only 1:1 metal-ligand products were reported for copper(II), however for nickel(II) a 1:2 metal-ligand species was proposed from potentiometric titration analysis. Neither metals showed the formation of a helical structure in solution, which suggests that the pyridine group in PepdaH₂ plays a key role in the helicate formation noted with both copper(II) and nickel(II).

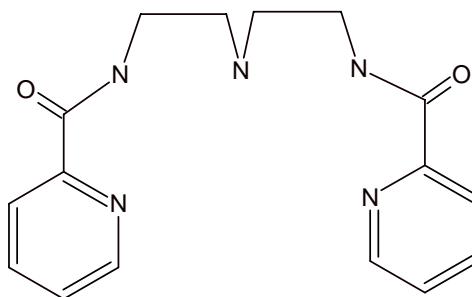


Figure 4.4: Structure of pycdien (1,7-bis(2-pyridylcarbamoyl)-1,4,7-triazaheptane) ²⁵.

Figure 4.5 shows the crystal structure of a complex of pycdien with nickel(II) that was characterised. In the solid state the formation of a M_2L_2 helicate was able to be identified, the intramolecular bonding within the two ligands strands can clearly be seen in the structure.

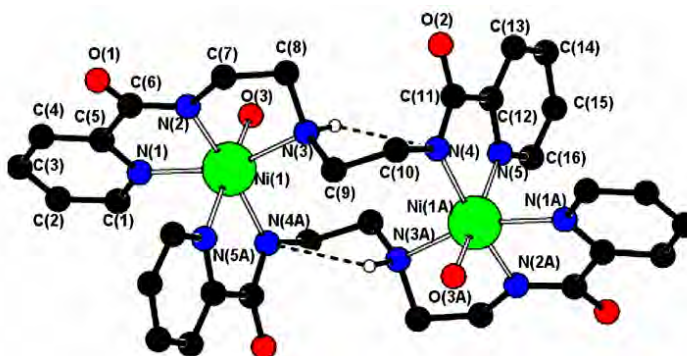


Figure 4.5: Dimeric structure of pycdien complexed to nickel(II), with the intramolecular hydrogen bonds shown ²⁵.

4.1.2 Helicate Formation Pathways

It is common practise to determine the solid state, X-ray structural data of a helicate as this facilitates characterising the self-assembling architectures. However, it is also desirable to determine data about the robustness and inertness of helicates in solution, as quantitatively expressed by the equilibrium and rate constants. Such information is essential in order to properly elucidate the assembly of such structures. In this study the kinetic data were acquired by means of stopped-flow kinetic measurements, and the equilibrium data by the use of spectrophotometric titrations.

The first quantitative study describing the self-assembly of a helicate can be attributed to Williams and co-workers ^{26, 27} who reported the formation of a triple-stranded bimetallic helicate which apparently did not involve any thermodynamic intermediate in significant amounts. This led the authors to suggest the occurrence of a strongly positive cooperative process, but no quantitative argument supports this hypothesis.

This study investigated the pathways leading to the formation of double-stranded helicates. Similarly to Williams' study, the intermediates that were determined to form were not thermodynamically stable products. However, it can be proposed that the ML intermediate species that was identified would be more stable than the intermediate M_2L , as an M_2L species requires the fixation of two cations onto a single ligand strand. The formation of such bimetallic helicates requires highly charged metal ions to be incorporated closely together, and such species are usually not the stable final product. A second ligand is often required to ensure that there is sufficient preorganisation and partial charge compensation to overcome the electrostatic repulsion before the formation of helicate can progress. The analysis of both the kinetic and equilibrium data enabled elucidation of the coordination properties, speciation, and the formation pathways for the complexes formed in solution, such as M_2L_2 and M_3L_2 helicates depending on the metal ion present.

4.1.3 Induced Circular Dichroism of Racemic Helicates

In Section 4.3 the interaction of the PepdaH₂-metal helicates with a chiral counter ion were investigated using circular dichroism (CD) techniques. The observed appearance of a CD signal with addition of the chiral reagent is due to a preferential binding of the chiral ligand to either the right, *P*, or left-handed, *M*, helical complex. These studies examined the induced chirality properties of the M_2L_2 and M_3L_2 helicates using the chiral, non-chromophore additives (-)-tartaric acid and sodium (+)-tartrate, presumably through outer-sphere interactions. Such investigations can provide insight into the equilibrium between the *P* and *M* enantiomers of a racemic helicate mixture.

4.2 Formation Pathway

4.2.1 Kinetic Investigation

4.2.1.1 Instrumentation

Kinetic investigations were carried out on an Applied Photophysics DX-17MV stopped-flow spectrophotometer equipped with a temperature controlled 1.0 cm pathlength optical cell block thermostated at 25 (\pm 0.1) °C by a water circulation bath, and interfaced to a PC. The data acquisition process has been previously described in detail in Chapter 2, Section 2.2.4. With the Applied Photophysics apparatus, kinetic traces were taken at different wavelengths between 380 and 700 nm.

4.2.1.2 Solution Preparation

The ligand PepdaH₂ used was a sample synthesised by Mery Napituputu¹², but recrystallised from ethanol. All solutions were made in 50:50 (v/v) ethanol:water mixtures and kept at constant 0.1 M ionic strength by the addition of NaClO₄. The presence of a base in the reaction mixture was required in order to deprotonate both amide groups and facilitate the coordination of the amido nitrogens to the metal ions. In this study metal acetates were used for the metal salt as the acetate ions made the reaction mixture sufficiently basic to enable the coordination of the deprotonation amido nitrogens to the metal ion.

Experiments were also performed using NaCH₃COO for ionic strength as it was proposed that the increased concentration of acetate ions to deprotonate the amide groups on the ligand may influence the rate of reaction. Comparison of the reactions with both salts for ionic strength showed similar kinetic traces; however, experiments with NaCH₃COO resulted in precipitation of metal hydroxide due to the increased basicity of the solution. Hence, it was decided that NaClO₄ was the most suitable salt for ionic strength consistency.

The measurements were performed at two ligand concentrations, with three metal-ligand ratios at each ligand concentration. Repeats were performed for all experiments to ensure consistency of the collected data. The concentrations used for a typical set of measurements are provided in Table 4.1. It should be noted that the concentration of each solution is halved when it is injected into the stopped-flow instrument as equal volumes of ligand and metal are mixed for the measurement.

M:L ratio	[L] M	[Cu(II)] M	[Ni(II)] M
1:1	2.11×10^{-3}	2.08×10^{-3}	1.91×10^{-3}
1:2		9.97×10^{-4}	1.05×10^{-3}
1:3		6.65×10^{-4}	6.43×10^{-4}
	[L] M	[Cu(II)] M	[Ni(II)] M
1:1	2.11×10^{-4}	2.08×10^{-4}	2.01×10^{-4}
1:2		1.04×10^{-4}	1.05×10^{-4}
1:3		6.65×10^{-5}	6.43×10^{-5}

Table 4.1: Typical concentrations used for stopped-flow measurements.

Ethanol Compression

Difficulties arose with the kinetic stopped-flow measurements due to the use of 50/50 (v/v) ethanol/water mixture as the solvent. It was observed that in the kinetic traces a peak repeatedly occurred at the beginning of the measurements at approximately 5 ms, see Figure 4.6, LHS. The peak was reproducible at all wavelengths for all ratios of metal(II)-PepdaH₂ injections. It was clear that the trace could not be explained with normal kinetic considerations. Injection of the 50/50 (v/v) ethanol/water solvent from both reservoir syringes into the system also resulted in the unexpected peak at 5 ms, even though no kinetics should have been observed with the injection of two identical solutions. Similar observations had previously been made when DMF was used as a solvent for a different metal-ligand system²⁸. Investigations where de-ionised water was injected from both reservoir syringes resulted in no observable spectral change, as expected since no reaction was occurring. Thus, it was concluded that the peak at 5 ms was not an instrumental problem, but that the unexpected spectral changes must in fact be due to the solvent.

The Applied Photophysics[®] technical support documentation outlined that a small pressure release artefact could sometimes be observed in the kinetic measurement. Therefore, the peak at 5 ms may be due to compression of the solvent as the system applies approximately 10 Bar of drive pressure to inject the solutions. When the pressure was released after the injection the solvent would then relax. The change in the refractive index of the ethanol/water solvent, resulting from compression and subsequent relaxation, appears as an artefact in the data trace, producing the observed pseudo-kinetic trace.

In order to prevent the change in refractive index, the drive pressure was held on for the entire measurement so that the solutions would not relax. However, experiments performed under such constant pressure conditions produced results with even greater baseline problems, as the solvent slowly relaxed over the entire measurement causing a constant shift in the baseline. In order to produce results that could be analysed, the pressure was released as normal for all measurements, and compensation made.

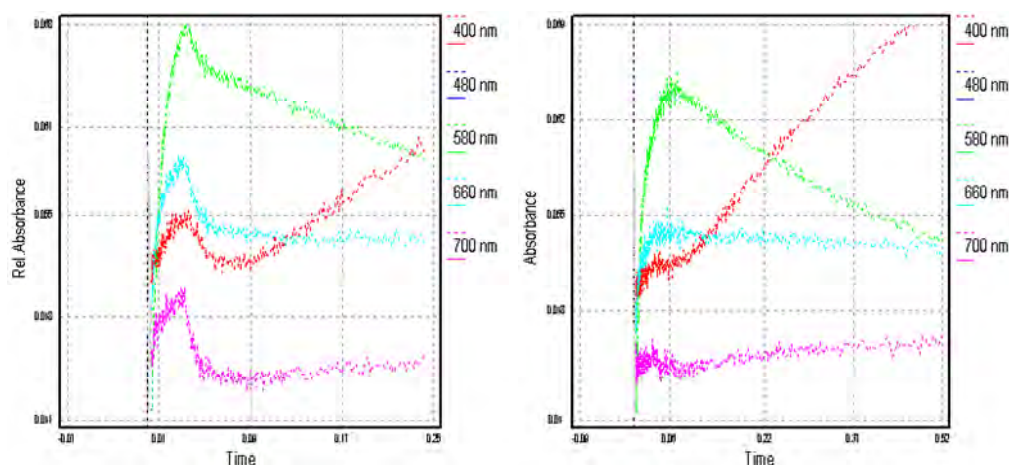


Figure 4.6: (LHS) Copper(II) kinetic traces with the pseudo-kinetic trace from the compression of the solvent present; (RHS) Kinetic trace after removal of the baseline pseudo-kinetics.

For the analysis of the kinetic nickel(II) data the reaction was sufficiently slow enough that the first part of the trace could be ignored for the analysis without any loss of significant data. However, the reaction of copper(II) and PepdaH₂ was too rapid and ignoring the section of the kinetic trace with the peak would have resulted in the loss of important data as the pseudo-kinetic trace occurred simultaneously with the fast spectral changes. Therefore, in order to correct for the peak from the solvent compression the 50/50 (v/v) ethanol/water solution was injected in the same manner as the metal-ligand experiments in order to obtain a pseudo-kinetic background. A program developed in Matlab was then used to remove the pseudo-kinetic trace of the solvent compression and hence correct the copper(II) kinetic traces. This efficiently removed the influence of the change in refractive index at all wavelengths. An example of the kinetic trace correction for copper(II) has been shown in Figure 4.6.

4.2.1.3 Data Analysis

The complexation kinetics studied herein have been analysed using the PC software Pro Kineticist II ²⁹ (ProKII) which allows the analysis of non-constant pH kinetics. This program incorporates the protonation of ligand species within the kinetic fitting algorithm. That is, at each step, it calculates the concentration of each species present, based on the pH, the acid dissociation constants and importantly the kinetic constants. ProKII also has the capacity to do multiwavelength analysis. As a result, the spectra of all the coloured species present in the reaction can be calculated. Thus, an additional constraint on the proposed model for the reaction is the determination of realistic calculated spectra for each absorbing species. The final result of such an analysis is a

more robust model than would arise from the use of traditional single wavelength analysis. In addition a Genetic Algorithm ³⁰ program was used in order to calculate reasonable initial guesses for the rate constants before optimisation.

4.2.2 Equilibrium Investigation

4.2.2.1 Instrumentation

The complexation equilibria for the copper(II) and nickel(II) systems were investigated at $25 (\pm 0.1) ^\circ\text{C}$ by spectrophotometric titrations with a Specord 210 spectrophotometer, using 1.0 cm quartz cells. The in-house developed technique for spectrophotometric titrations has been described in Chapter 2, Section 2.2.3.5. The spectra were scanned between 410 and 1100 nm at 5 nm intervals. Each series was made by using samples of constant ligand concentration with the metal ion titrated into the cell.

4.2.2.2 Solution Preparation

The titration solutions were prepared using NaClO_4 for constant ionic strength as precipitation also occurred when CH_3COONa was used due to the increased basicity of the solution. The measurements were performed at different initial concentrations in order to adequately define the species, and also with differing final metal-ligand ratios in the titrations. The concentrations used for the titrations have been provided in Table 4.2; note that metal acetates were used for the metal salts.

metal	cuvette [L] ₀ M	burette [M] ₀ M	final M:L ratio in cuvette
copper(II)	2.13×10^{-3}	3.35×10^{-2}	1.0
	1.07×10^{-3}	3.35×10^{-2}	1.2
	6.09×10^{-3}	9.80×10^{-3}	1.6
nickel(II)	1.07×10^{-3}	9.95×10^{-3}	1.0
	7.11×10^{-3}	9.95×10^{-3}	2.3
	3.55×10^{-4}	9.95×10^{-3}	2.4
	1.78×10^{-4}	9.95×10^{-3}	4.8

Table 4.2: Initial ligand and metal concentrations and the final metal-ligand ratio reached in each titration; the initial volume in the cuvette was 2 mL.

4.2.2.3 Analytical Process

The program used to analyse the spectrophotometric titration data of PepdaH₂ with both copper(II) and nickel(II) was an in-house developed program which has been previously described in Chapter 2, Section 2.3. In general, the procedure optimises parameters, such as the equilibrium constants defined by the proposed model, using non-linear least-squares minimisation of the residuals. Analysis results in fitted equilibrium constants, as well as calculated species absorptivities and species concentration values during the titration.

An initial limitation to the proposal of the reaction pathways and final products that were possible for the reaction of copper(II) and nickel(II) with PepdaH₂ was determined from evolving factor analysis (EFA) ³¹ of the spectral data from the spectrophotometric titrations. This initial data analysis enabled the number of significant coloured species to be clearly defined in the reactions. For both the copper(II) and nickel(II) reactions four absorbing species present were identified to be present, as shown in Figure 4.7.

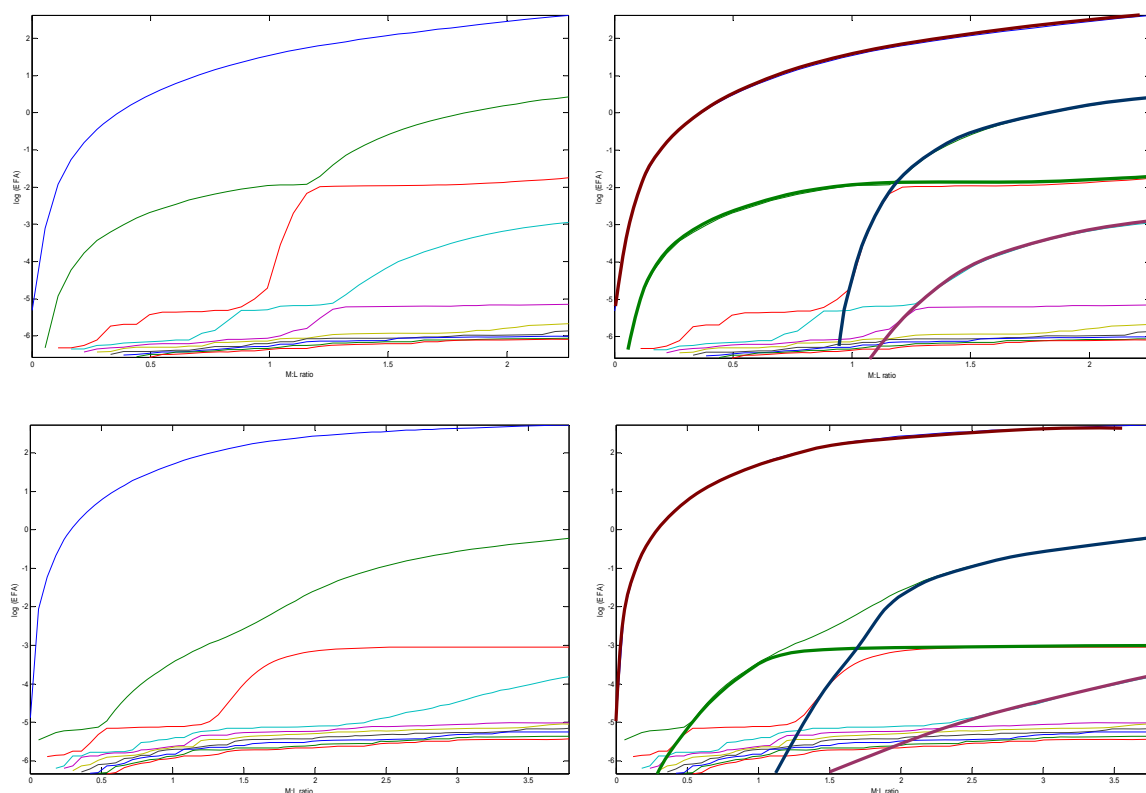
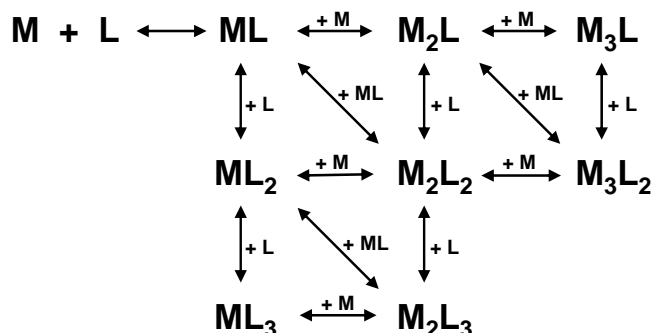


Figure 4.7: EFA plots: (top) copper(II) (bottom) nickel(II); reactions show the formation of four significant species for both metals. LHS shows the raw EFA plots while the RHS shows the four species highlighted for clarity.

4.2.3 Conjoint Kinetic and Equilibrium Analysis

The reaction of PepdaH₂ with metal ions has many possible reaction pathways and final products. Scheme 4.1 provides an outline of the general reaction scheme leading to mono-, di- or tri-metal species. Those pathways with either less than or greater than four absorbing species were considered to not be plausible reactions due to the previously discussed EFA analysis of the spectral data. Some final species were not highly probable species, for example M₃L, however the pathways forming such species were not discounted from analysis to avoid prejudgement.

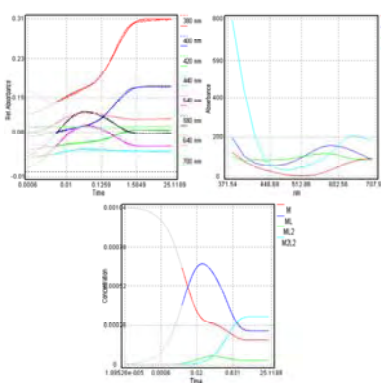


Scheme 4.1: Overall scheme showing all possible reaction pathways for PepdaH₂, L, with either copper(II) or nickel(II) metal ions, M, where dimeric or trimeric complexes result.

4.2.3.1 Kinetic Analysis

Modelling and analysis of the kinetic data resulted in only certain reaction pathways in Scheme 4.1 that adequately described the data for the copper(II) and nickel(II) reactions. The kinetic data was globally analysed using a series of data sets that encompassed a range of initial concentrations and M:L ratios. Analysis of the reaction of PepdaH₂ with copper(II) resulted in four possible competing pathways; models 1, 2, 4 and 5 as shown in Table 4.3.

copper(II) models	k_+	k_-
$ \begin{array}{c} \text{M} + \text{L} \xrightleftharpoons{+\text{M}} \text{ML} \xrightleftharpoons{+\text{M}} \text{M}_2\text{L} \xrightleftharpoons{+\text{M}} \text{M}_3\text{L} \\ \updownarrow +\text{L} \quad \swarrow +\text{ML} \quad \updownarrow +\text{L} \quad \swarrow +\text{ML} \quad \updownarrow +\text{L} \\ \text{ML}_2 \xrightleftharpoons{+\text{M}} \text{M}_2\text{L}_2 \xrightleftharpoons{+\text{M}} \text{M}_3\text{L}_2 \\ \updownarrow +\text{L} \quad \swarrow +\text{ML} \quad \updownarrow +\text{L} \\ \text{ML}_3 \xrightleftharpoons{+\text{M}} \text{M}_2\text{L}_3 \end{array} $	$ \begin{array}{l} \text{M} + \text{L} \leftrightarrow \text{ML} \\ \text{ML} + \text{L} \leftrightarrow \text{ML}_2 \\ \text{ML}_2 + \text{M} \leftrightarrow \text{M}_2\text{L}_2 \end{array} $	
1)	$7.99 \times 10^4 \pm 0.01$	7.78 ± 0.03
	$9.67 \times 10^3 \pm 0.02$	9.14 ± 0.06
	$5.23 \times 10^4 \pm 0.09$	0.58 ± 0.01
<i>ssq</i>	0.1960	



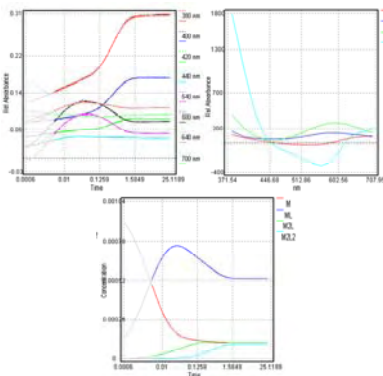
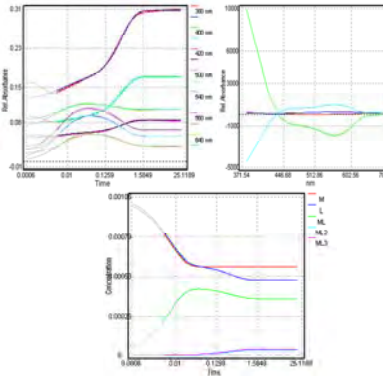
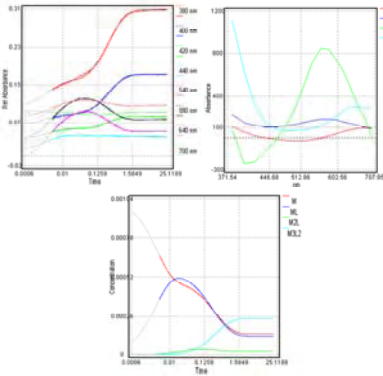
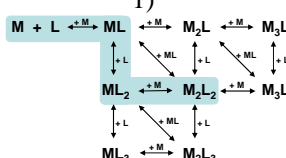
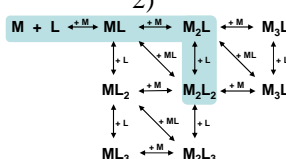
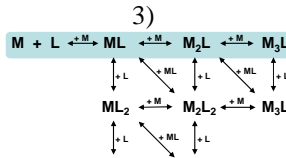
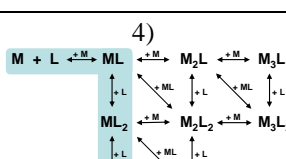
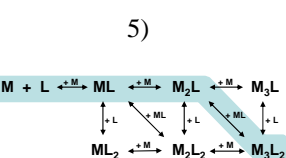
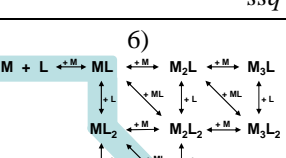
	$M + L \leftrightarrow ML$			
2)	$1.05 \times 10^5 \pm 0.02$	3.54 ± 0.05		
	$ML + M \leftrightarrow M_2L$			
	$1.28 \times 10^4 \pm 0.09$	4.04 ± 0.07		
	$M_2L + L \leftrightarrow M_2L_2$			
	$7.22 \times 10^3 \pm 0.14$	3.02 ± 0.01		
<i>ssq</i>	0.1771			
<hr/>				
3)			no convergence	
<hr/>				
	$M + L \leftrightarrow ML$			
4)	$2.98 \times 10^4 \pm 0.09$	0.13 ± 0.05		
	$ML + L \leftrightarrow ML_2$			
	$1.22 \times 10^5 \pm 0.12$	4.98 ± 0.04		
	$ML_2 + L \leftrightarrow ML_3$			
	$3.03 \times 10^4 \pm 0.19$	0.05 ± 0.01		
<i>ssq</i>	0.3552			
<hr/>				
	$M + L \leftrightarrow ML$			
5)	$2.46 \times 10^4 \pm 0.04$	181.33 ± 0.05		
	$ML + M \leftrightarrow M_2L$			
	$2.75 \times 10^5 \pm 0.02$	17.58 ± 0.10		
	$M_2L + ML \leftrightarrow M_3L_2$			
	$4.67 \times 10^4 \pm 0.12$	0.69 ± 0.09		
<i>ssq</i>	0.1251			
<hr/>				
6)			no convergence	

Table 4.3: Results for the analysis of the copper(II) stopped-flow data in terms of four species, forward (k_+) and reverse (k_-) rate constants are given for each model optimised with ProKII. The RH column shows, in a clockwise direction, the calculated and fitted data at selected wavelengths; the spectra of the absorbing species; and the species concentrations over the time of the scan.

For PepdaH_2 with nickel(II) only one reaction pathway led to convergence, that is model 5. The results of the optimisation with ProKII have been shown in Table 4.4.

nickel (II) models	k_+	k_-
1) 	No convergence	
2) 	No convergence	
3) 	no convergence	
4) 	no convergence	
5) 	$1.80 \times 10^3 \pm 0.05$ $1.15 \times 10^4 \pm 0.01$ $1.64 \times 10^4 \pm 0.02$ ssq	$9.61 \times 10^{-5} \pm 0.07$ 2.98 ± 0.10 $4.75 \times 10^{-6} \pm 0.04$ 0.5478
6) 	no convergence	

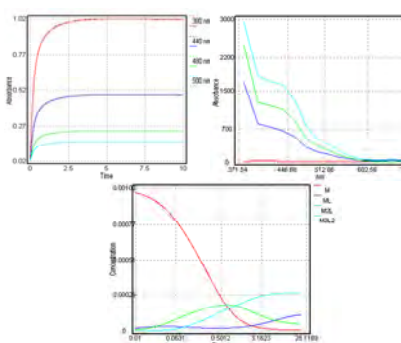


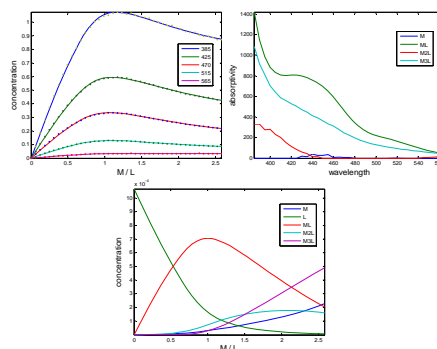
Table 4.4: Results for the analysis of the nickel(II) stopped-flow data in terms of four species, forward (k_+) and reverse (k_-) rate constants are given for each model optimised with ProKII. The RH column shows, in a clockwise direction, the calculated and fitted data at selected wavelengths; the spectra of the absorbing species; and the species concentrations over the time of the scan.

5)		no convergence
6)		no convergence

Table 4.5: Analysis results for copper(II) overall equilibrium constants ($\log \beta$) showing all models for the copper(II) spectrophotometric titration data from the proposed pathways shown in Scheme 4.2.

Table 4.6 shows the results of the nickel(II) analysis using Spec_Anal. It can be seen that models 3, 4, and 5 all led to convergence in the analysis.

nickel(II) models	$\log \beta$ Values
1)	no convergence
2)	no convergence
3)	<div> $M + L \leftrightarrow ML$ 5.142 ± 0.037 $M + L \leftrightarrow M_2L$ 8.678 ± 0.019 $M_2L + M \leftrightarrow M_3L$ 12.798 ± 0.020 ssq 0.0659 </div>



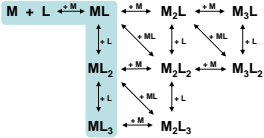
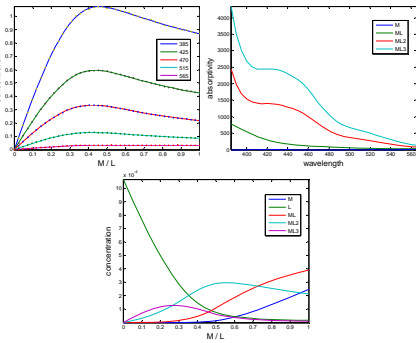
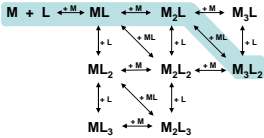
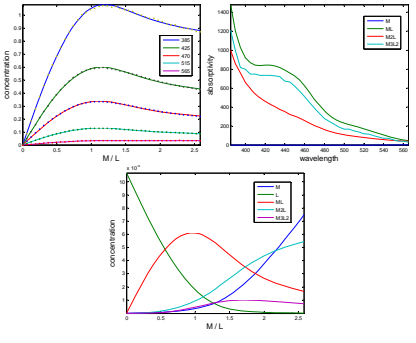
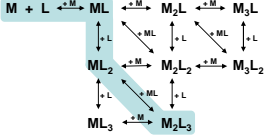
<p>4)</p> 	$M + L \leftrightarrow ML$ 5.004 ± 0.016 $ML + L \leftrightarrow ML_2$ 9.549 ± 0.015 $ML_2 + L \leftrightarrow ML_3$ 13.003 ± 0.019 $ssq \quad 0.0226$	
<p>5)</p> 	$M + L \leftrightarrow ML$ 4.979 ± 0.008 $M + L \leftrightarrow M_2L$ 8.616 ± 0.010 $M_2L + ML \leftrightarrow M_3L_2$ 16.506 ± 0.038 $ssq \quad 0.0362$	
<p>6)</p> 	<p>no convergence</p>	

Table 4.6: Analysis results for nickel(II) overall equilibrium constants ($\log \beta$) showing all models for the nickel(II) spectrophotometric titration data from the proposed pathways shown in Scheme 4.4.

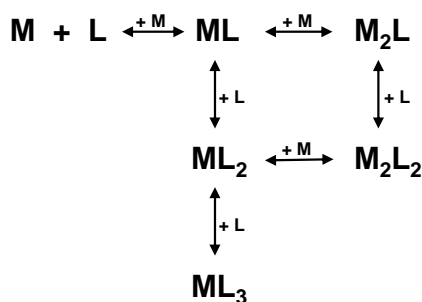
4.2.3.3 Relationship Between Equilibrium and Rate Constants

Copper(II) Analysis

From Scheme 4.1 there were three possible pathways that fitted the copper(II) data for both the kinetic and equilibrium data analysis. These have been shown schematically in Scheme 4.2 with the combined results for both analysis listed in Table 4.7. The stability constants from the kinetic rate data were determined as shown in Equation (4.1).

$$\log K_{kin} = \log\left(\frac{k_f}{k_r}\right) \quad (4.1)$$

The stability constants, $\log K$, from the overall equilibrium constants, $\log \beta$, that are determined in the Spec_Anal analysis of the titration data were calculated as previously described in Chapter 1, Section 1.3.7.



Scheme 4.2: Reaction scheme detailing the three plausible reaction pathways from the conjoint analysis for PepdaH₂, L, and copper(II), M.

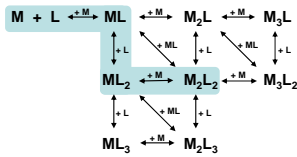
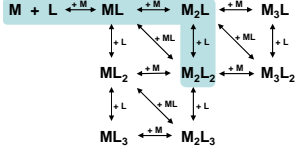
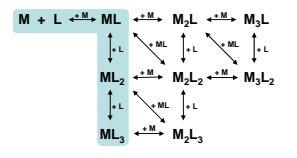
model	copper(II)	log K_{kin}	log K_{eq}
Pathway One			
	$\text{M} + \text{L} \leftrightarrow \text{ML}$	4.01 ± 0.02	7.66 ± 0.75
	$\text{ML} + \text{L} \leftrightarrow \text{ML}_2$	3.02 ± 0.02	7.77 ± 0.91
	$\text{ML}_2 + \text{L} \leftrightarrow \text{M}_2\text{L}_2$	4.96 ± 0.12	4.30 ± 0.51
	<i>ssq</i>	0.1960	0.0537
Pathway Two			
	$\text{M} + \text{L} \leftrightarrow \text{ML}$	4.47 ± 0.11	6.12 ± 0.03
	$\text{ML} + \text{M} \leftrightarrow \text{M}_2\text{L}$	3.50 ± 0.25	3.51 ± 0.05
	$\text{M}_2\text{L} + \text{L} \leftrightarrow \text{M}_2\text{L}_2$	3.38 ± 0.07	5.24 ± 0.08
	<i>ssq</i>	0.1771	0.0500
Pathway Three			
	$\text{M} + \text{L} \leftrightarrow \text{ML}$	5.36 ± 2.07	6.58 ± 0.06
	$\text{ML} + \text{L} \leftrightarrow \text{ML}_2$	4.39 ± 0.43	3.12 ± 0.06
	$\text{ML}_2 + \text{L} \leftrightarrow \text{ML}_3$	5.78 ± 1.10	3.86 ± 0.09
	<i>ssq</i>	0.3552	0.0824

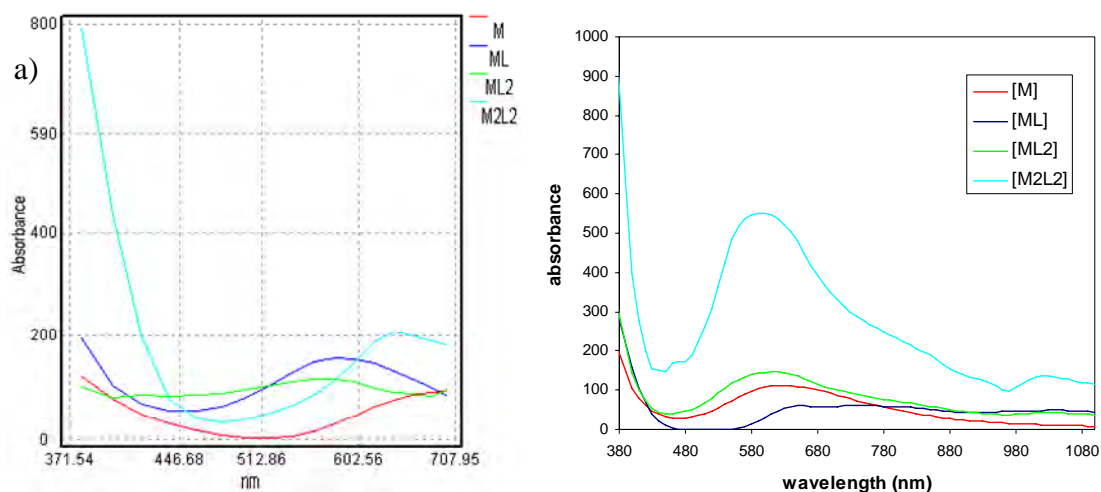
Table 4.7: Equilibrium constants for possible pathways for copper(II) complexation determined from kinetic, log K_{kin} , and equilibrium, log K_{eq} , data.

Comparison of the respective stability constants determined from both kinetic and equilibrium investigations showed that Pathway Three had significantly higher *ssq* values for both analyses and was therefore discounted as a feasible model. However, determining the most likely model between Pathway One and Two was more complicated as the *ssq* values were comparable and the M₂L₂ final species from this

pathway is also the species that had been previously defined in the solid state by crystal structure analysis ^{12, 24}, whereas the discounted Pathway Three predicted a different final species. Although solution and solid state outcomes need not equate, M_2L_2 being the final species for both Pathway One and Two is comfortably consistent.

Marlin *et al* ²³ reported that, in methanol, the $[Cu_2(Pepda^{2-})_2]$ complex displayed an absorption band with λ_{max} at 646 nm ($\epsilon = 140 \text{ M}^{-1} \text{ cm}^{-1}$) and a shoulder at 740 nm. It was also noted that the monomeric complex, $[CuPepda^{2-}]$, displayed a similar broad band with λ_{max} at 613 nm ($\epsilon = 220 \text{ M}^{-1} \text{ cm}^{-1}$) and a shoulder at 740 nm. The similarity in absorption spectra between $[CuPepda^{2-}]$ and $[Cu_2(Pepda^{2-})_2]$ was not surprising since both complexes are comprised of a similar set of donors around the copper(II) centre(s). The observed spectrum is characteristic of a tetragonally distorted copper(II) complex where the bands arise from the $d_{xz}(d_{yz}) \rightarrow d_{x^2-y^2}$ and $d_{xy} \rightarrow d_{x^2-y^2}$ transitions. The high extinction coefficient associated with the d-d transition(s) and the shoulder are both indicative of low-symmetry 5-coordinate copper complexes ³².

The kinetic and equilibrium analysis in this study resulted in a similar spectral shape to what Marlin reported for both $[CuPepda^{2-}]$ and $[Cu_2(Pepda^{2-})_2]$ products, Figure 4.8, suggesting that the analysis resulting in these products is most likely, with the bimetallic helicate as the final product. However, this conclusion does not distinguish between Pathways One and Two, as both involved the above products.



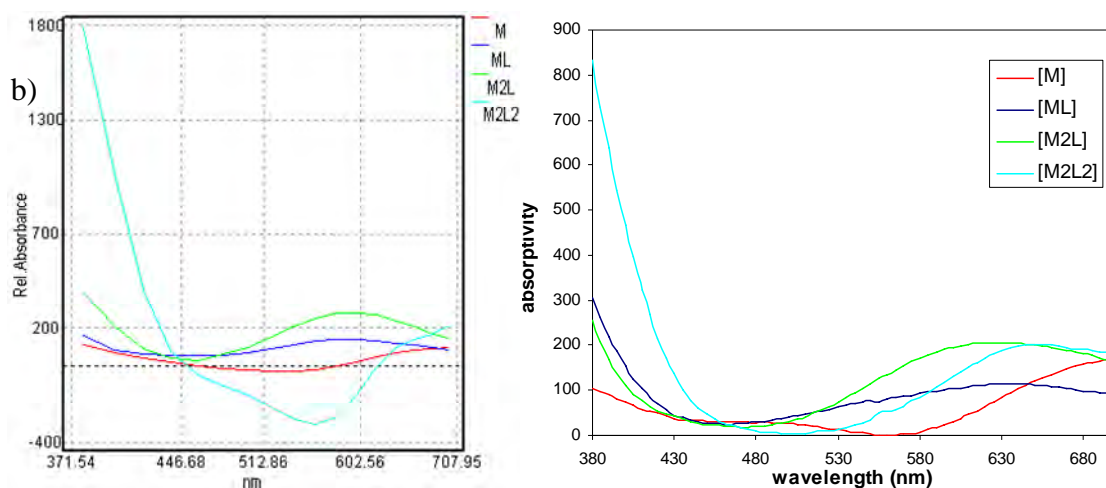
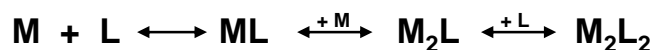


Figure 4.8: Copper(II)-PepdaH₂ species absorptivities: a) Pathway One; b) Pathway Two; (LHS) kinetic analysis; (RHS) equilibrium analysis.

In order to try to determine the best model between Pathways One and Two the species spectra were compared, as each analytical technique should result in similar calculated absorptivities for the absorbing species; as shown in Figure 4.9. Comparisons of the spectra, detailed in Table 4.8, led to the conclusion that the species in Pathway Two had the most comparable spectra and as such this reaction pathway was determined to be the most likely for copper(II)-PepdaH₂, as summarised in Scheme 4.3.



Scheme 4.3: Determined reaction pathway for PepdaH₂, L, and copper(II), M.

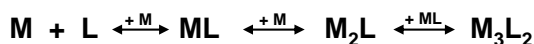
species	kinetic		equilibrium	
	λ_{\max} (nm)	ε (M ⁻¹ cm ⁻¹)	λ_{\max} (nm)	ε (M ⁻¹ cm ⁻¹)
	Pathway One			
M	>700	150 (at 700 nm)	600	100
ML	590	180	670	80
ML ₂	570	160	580	140
M ₂ L ₂	630	200	590	550
Pathway Two				
M	>700	100	>700	170
ML	590	120	630	120
M ₂ L	600	300	625	205
M ₂ L ₂	undefined		635	200

Table 4.8: Values of maximum absorptivity for each species present in Pathway's One and Two for copper(II)-PepdaH₂ kinetic and equilibrium analysis.

Nickel(II) Analysis

The single acceptable reaction pathway derived from kinetic analysis of the nickel(II) reaction, shown in Scheme 4.4, also resulted in the best fit when analysing the equilibrium data, confirming the validity of the approach. The kinetic analysis was only successful for the formation of M_3L_2 , and although the equilibrium analysis led to the formation of M_3L and ML_3 products such species are not highly probable.

The M_3L_2 final species from this pathway is also the species that had been previously defined in the solid state by crystal structure analysis ¹², whereas the discounted pathways predicted different final species. Although solution and solid state outcomes need not equate, M_3L_2 being final species for both models is again comfortably consistent. As such, from consideration of the chemical credibility of the final products, and since both the kinetic and equilibrium analysis independently resulted in the formation of M_3L_2 species, this pathway was considered to be the only plausible reaction for nickel(II) with PepdaH₂. The reaction pathway has been detailed in Scheme 4.4 and the calculated parameters for both analysis techniques are collected in Table 4.9.



Scheme 4.4: Reaction scheme showing the reaction pathway for PepdaH₂, L, and nickel(II), M.

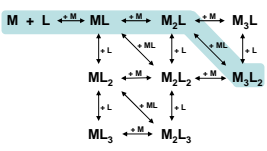
model	nickel(II)	log K_{kin}	log K_{eq}
	$M + L \leftrightarrow ML$	7.27 ± 0.21	4.98 ± 0.01
	$ML + L \leftrightarrow M_2L$	3.59 ± 0.12	3.64 ± 0.01
	$M_2L + ML \leftrightarrow M_3L_2$	9.54 ± 0.14	7.89 ± 0.04
	<i>ssq</i>	0.5478	0.0362

Table 4.9: Equilibrium constants for the reaction of nickel(II) and PepdaH₂ from both the kinetic, log K_{kin} , and equilibrium, log K_{eq} , data.

Alcock *et al* ¹² reported that, in ethanol, the $[Ni_3(Pepda^{2-})_2(acetate)_2]$ complex displayed an absorption band with λ_{max} at 204 nm ($\epsilon = 44200 \text{ M}^{-1} \text{ cm}^{-1}$), 264 nm ($\epsilon = 22400 \text{ M}^{-1} \text{ cm}^{-1}$), 304 nm ($\epsilon = 17900 \text{ M}^{-1} \text{ cm}^{-1}$), and 930 nm ($\epsilon = 45 \text{ M}^{-1} \text{ cm}^{-1}$). Unfortunately, neither kinetic or equilibrium studies were in the UV part of the spectrum, and measurements above 700 nm were not deemed important enough to include in the analysis as an absorptivity of $45 \text{ M}^{-1} \text{ cm}^{-1}$ is significantly smaller than the absorptivity in lower visible region of the spectrum. Hence, direct comparison of the reported spectra for the trinuclear nickel species cannot be made with the calculated

spectra from both kinetic and equilibrium analysis, but it can be seen that the shoulder at 370 nm is increasing in absorbance which may lead to the spectra in the UV reported by Alcock.

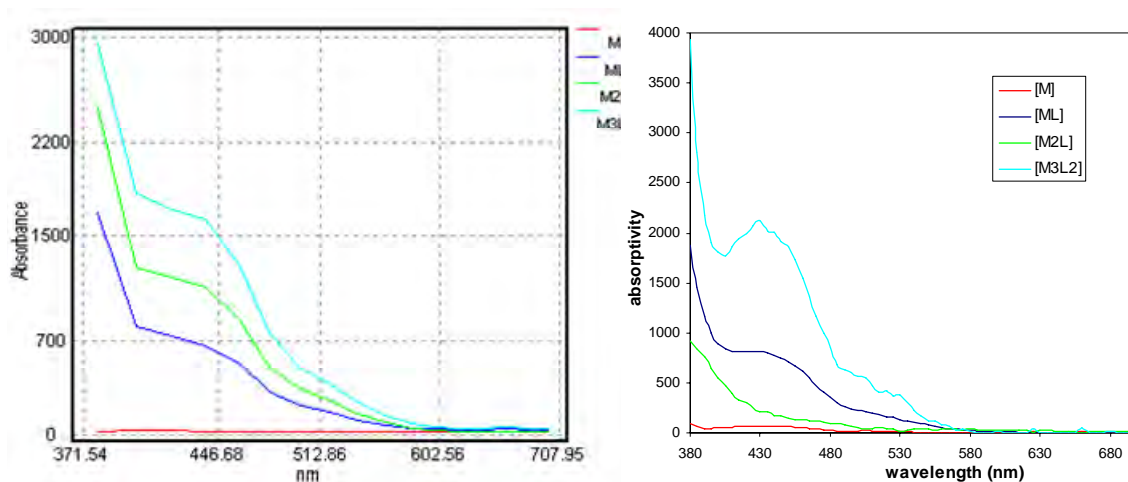


Figure 4.9: Calculated spectrum of each coloured species from nickel(II) data analysis; a) ProKII analysis of the kinetic data; b) Spec_Anal analysis of the equilibrium data.

species	kinetic		equilibrium	
	λ_{\max} (nm)	ϵ ($\text{M}^{-1} \text{cm}^{-1}$)	λ_{\max} (nm)	ϵ ($\text{M}^{-1} \text{cm}^{-1}$)
Pathway One				
M	0	0	450	50
ML	450	600	450	800
M_2L	445	1100	<380	~
M_3L_2	440	1600	430	2100

Table 4.10: Values of maximum absorptivity for each species present in the formation of the nickel(II)-PepdaH₂ helicate from kinetic and equilibrium analysis.

4.2.3.4 Reaction Intermediates, $\log K_{\text{kin}} \neq \log K_{\text{eq}}$

In order to describe the observed differences in the stability constants calculated from both rate and equilibrium data it is imperative to firstly define the concept of a steady-state species. Reactions that involve intermediate species that are present in only very, very low, and thus almost constant concentrations, are called steady-state species. If intermediate species are in a steady-state then it can be said that the intermediates are very reactive and never build up to a significant concentration throughout the reaction. Therefore, this implies that the total rate of production of intermediates is balanced by the total rate of their removal. This steady concentration over the time of the reaction

means that the rate of change of the intermediate concentration can be approximated to zero. Importantly, the rate of change of the intermediate concentration can be expressed in terms of the rates of all steps producing the intermediate and the rates of all steps removing the intermediate species³³.

For a simple reaction, such as $A \leftrightarrow B$ where there are no steady-state intermediate species, it can be said that the forward and reverse rate constants can be used to determine the equilibrium constant of the described reaction, as shown in Equation (4.2).

$$K = \frac{k_f}{k_r} \quad (4.2)$$

This concept has been detailed in Figure 4.10, left-hand side, where it can be seen that the energy defined by the forward rate and backward rate define the equilibrium constant if no intermediate species is present.

However, for more complex reactions such as $A \leftrightarrow I \leftrightarrow B$, the presence of steady-state intermediate(s) may result in the equilibrium constant of a reaction being no longer equal to the rate of the formation of a species divided by the rate of dissociation of the species. The forward rate constant is now a measure of the time taken to reach the steady-state intermediate(s), which are not the final product and cannot be detected by the experiment. Similarly, the reverse rate constant measures the dissociation of the complex to steady-state intermediate(s), and not the rate of dissociation to return to the starting reactants. In contrast, equilibrium measurements only take into account the initial and final products and are not a measure of any steady-state intermediates that may form. In these reactions the energy required to form the intermediate may be different than the energy required for the reverse formation of the intermediate. Hence, the equilibrium constant is no longer equal to the energies defined by the forward and reverse kinetic rates, as shown on the right-hand side of Figure 4.10.

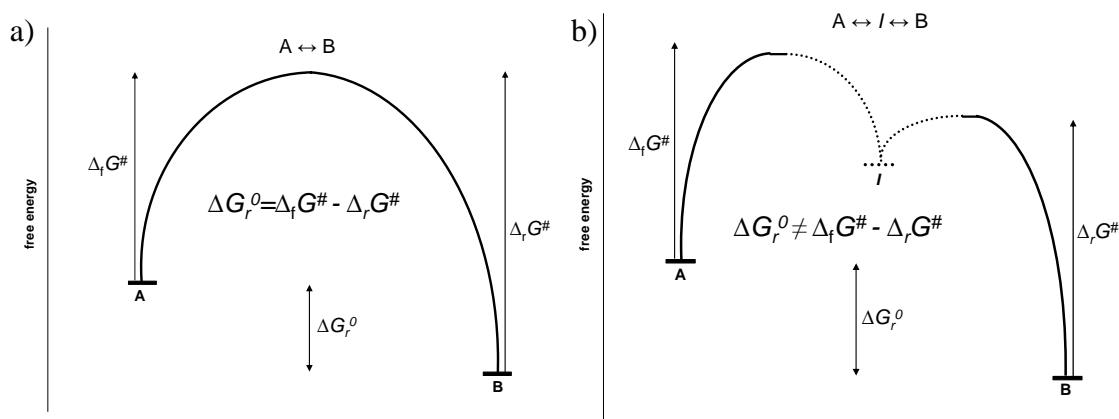


Figure 4.10: Diagram showing the free energy of the overall reaction, ΔG_r^0 , and forward and reverse reaction energies, ΔG_f^\ddagger and ΔG_r^\ddagger respectively; a) A simple $A \rightarrow B$ reaction where the energy $\Delta G_f^\ddagger - \Delta G_r^\ddagger$ is equal to ΔG_r^0 ; b) $A \rightarrow B$ via a steady-state intermediate, clearly showing that $\Delta G_f^\ddagger - \Delta G_r^\ddagger$ is no longer equal to the ΔG_r^0 .

The reaction of PepdaH₂ with metal ions can be considered to be a complex reaction, of the type $A \leftrightarrow I \leftrightarrow B$, with many potential steady-state intermediates possible for each step in the reaction pathway. Consider the reaction of PepdaH₂ with copper(II), for which the reaction pathway has been previously outlined in Scheme 4.3. The first step in the reaction requires one PepdaH₂ ligand to complex with one copper(II) ion in order to reach the thermodynamically stable product ML. In order to form the ML complex there are numerous steady-state intermediates that may form in the reaction process. For instance, a steady-state species may exist were PepdaH₂ has only two of the potential five sites coordinated to the copper(II) ion. Such a species would not be detected in the analysis of the kinetic absorbance data, even though it does exist. Hence, such steady-state species may result in discrepancies between the kinetically determined K_{kin} values and the K_{eq} values calculated from equilibrium studies.

The energy differences between the kinetic constants and equilibrium constants for the PepdaH₂ analysis have been depicted graphically in Figure 4.11. The ΔG values from equilibrium constants have been calculated in accordance with Equation (4.3), where R is the universal gas constant in J/K, and T is the absolute temperature in Kelvin³⁴.

$$\Delta G^0 = -RT \ln K \quad (4.3)$$

The ΔG^0 values from rate constants were calculated by application of the Arrhenius equation³⁵, as shown in Equation (4.4), where R is the universal gas constant in J/K, T

is the absolute temperature in Kelvin, k_B is Boltzmann constant in J/K, and h is Planck's constant in Js.

$$k = \frac{k_B T}{h} e^{-\frac{\Delta G^\ddagger}{RT}} \quad (4.4)$$

In the free energy diagrams below, the bold dashes show the G_{eq} values (referenced to a reactant free energy of zero) corresponding to the equilibrium $\log K_{eq}$ values, and the dark curved lines are the ΔG^\ddagger values ($\Delta_f G^\ddagger$ and $\Delta_r G^\ddagger$) calculated from the forward and reverse rate constant values. The dotted lines represent the unknown free energy difference for the formation of the steady-state inetermediate(s). As can be seen in the graph, the difference between the kinetic and equilibrium stability constants can be attributed to the large energy differences resulting from the presence of steady-state intermediates.

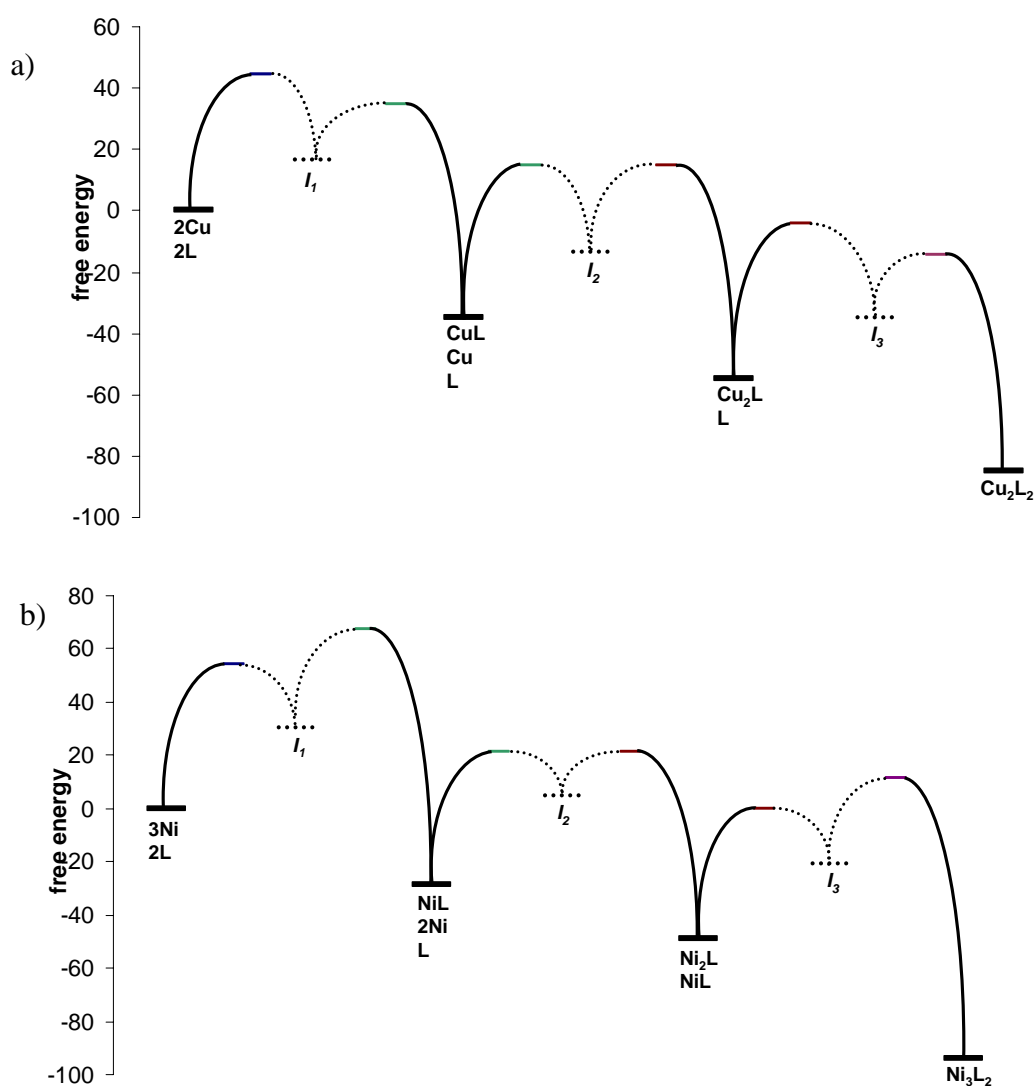


Figure 4.11: Calculated ΔG values for PepdaH₂ and a) copper(II) and b) nickel(II) from equilibrium $\log K_{eq}$ values (dark black dashes) and from kinetic $\log K_{kin}$ values (coloured dashes). The curved dark lines

are the calculated forward and reverse energy values for the kinetic reaction paths and the dotted lines show the unknown energy difference from the steady-state intermediates, I_1 , I_2 , and I_3 .

After considering that a complex reaction, such as the complexation of PepdaH_2 , may have many steady-state intermediate species, it is clearly unreasonable to expect the forward and reverse rate constants to accurately describe the equilibrium constant because the energy required to form an intermediate species will differ from the energy required to form the thermodynamically stable product as defined by the equilibrium constant. However, the study of the energies associated with the kinetic and equilibrium stability constants showed similar trends for the reaction pathway.

Even though the discrepancy between the kinetically calculated and equilibrium stability constants can be adequately explained by considering the formation of steady-state intermediates, it would still be expected that the trends in the reaction energy be consistent. Both the data shown in Table 4.7 and Table 4.9 and the above energy diagrams show that the trends in the $\log K$ values are consistent for both kinetic and equilibrium investigations for the models determined to be the most likely for the PepdaH_2 reactions with both metal ions.

4.3 Induced Chirality

4.3.1 Background

There is a growing interest in induced chirality in metal-ligand complexes that stems not only from the relevance of such studies to the chiral bias inherent to life, but also from the potential technological applications, such as the separation of optical isomers for the pharmaceutical or food industries³⁶.

In general, the majority of helical molecular assemblies reported are based on the use of achiral building blocks and therefore form non-optically active racemates. The most important feature of a helix is its chirality; that is, whether the helical structure is a right, P , or left-handed, M , helix. P and M helices are non-identical mirror images, so if either the pure P or M helicate is synthesised, or one exists in excess of the other, then the solution will show optical activity³⁷. However, metal-ligand helicates that are assembled from achiral ligands form racemic mixtures of P and M structures. Such mixtures show no optical activity, as the influence of one chiral helicate is negated by the presence of the mirror image.

The chirality of a complex, that is *P* or *M* rotation, can be influenced by interaction of external stimuli with the helical complex. The question concerning how chirality is communicated in helical structures, and whether or not such properties can be controlled through noncovalent forces in solution, is pertinent to many systems. The control of chirality using the external stimuli approach was focused upon for the investigation of the helical properties of the PepdaH₂ complexes, a graphical representation of which can be seen in Figure 4.12.

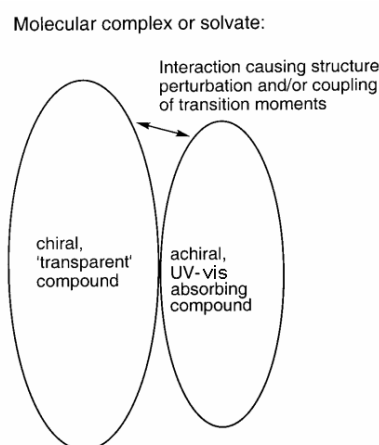


Figure 4.12: Simplified representation of the generation of induced optical activity in the visible region where the chiral compound does not absorb ³⁸.

4.3.2 Circular Dichroism

The spectroscopic technique of circular dichroism (CD) is a powerful tool that can be used to investigate chiral properties of compounds. Dichroism is a word derived from Ancient Greek meaning ‘two-colours’, because a CD-active solution has one colour when illuminated with right circular polarised light, and a different colour when illuminated with left circular polarised light ³⁹. The colour is dependant on light absorption of the particular molecule. Hence, CD is the absorptive property of optically asymmetric or chiral molecules and is a measure of the differences in the absorption of left-handed circular polarised light versus right-handed circular polarised light which arises due to structural asymmetry. The absence of a chiral structure in a system results in zero CD intensity, while a chiral structure results in a spectrum that can contain both positive and negative signals ⁴⁰. This CD spectrum is due to the interaction of the molecule with the polarised light as the electric field vector of the light traces out an elliptical path while propagating. Therefore, at a given wavelength, the measured CD

spectrum is a result of the difference in absorbance between left circularly polarised (A_L) and right circularly polarised (A_R) light, ΔA .

$$\Delta A = A_L - A_R \quad (4.5)$$

This difference in absorbance can also be expressed by applying Beer's law, as shown in Equation (4.6) where ε_L and ε_R are the molar extinction coefficients for right and left circularly polarised light, C is the molar concentration, and l is the path length in centimeters (cm).

$$\Delta A = (\varepsilon_L - \varepsilon_R)Cl \quad (4.6)$$

From this equation a definition of molar circular dichroism can be derived, as shown in Equation (4.7). This is what is usually meant by the circular dichroism of the substance; although ΔA is usually measured for historical reasons most measurements are reported in degrees of ellipticity.

$$\Delta\varepsilon = \varepsilon_L - \varepsilon_R \quad (4.7)$$

Molar circular dichroism and molar ellipticity, $[\theta]$, are readily interconverted as shown in Equation (4.8), which results in the molar ellipticity having the standard units of degrees decilitres mol⁻¹ decimeter⁻¹ ⁴¹.

$$[\theta] = 3298.2\Delta\varepsilon \quad (4.8)$$

4.3.3 Induced Circular Dichroism

Induced circular dichroism (ICD) results from a CD signal that is induced in an achiral, chromophoric molecule due to an interaction with a chiral, nonracemic counterpart. Such an interaction causes a perturbation which effects the enantiomer distribution of a racemate ³⁸. Pure chiral small molecules have been shown to either induce enantiomeric enrichment in a racemic mixture of helicates in a dynamic equilibrium, or even resolve the mixture outright by selective precipitation or crystallisation of one enantiomer ⁴².

The effects of ICD from the transfer of chiral information to achiral or dynamically racemic supramolecules and macromolecular helical systems from nonracemic guest molecules through noncovalent bonding interactions has attracted great interest in recent years ^{38, 43-45}. A diagram depicting the chirality of a helicate being changed due to external stimuli has been shown in Figure 4.13.

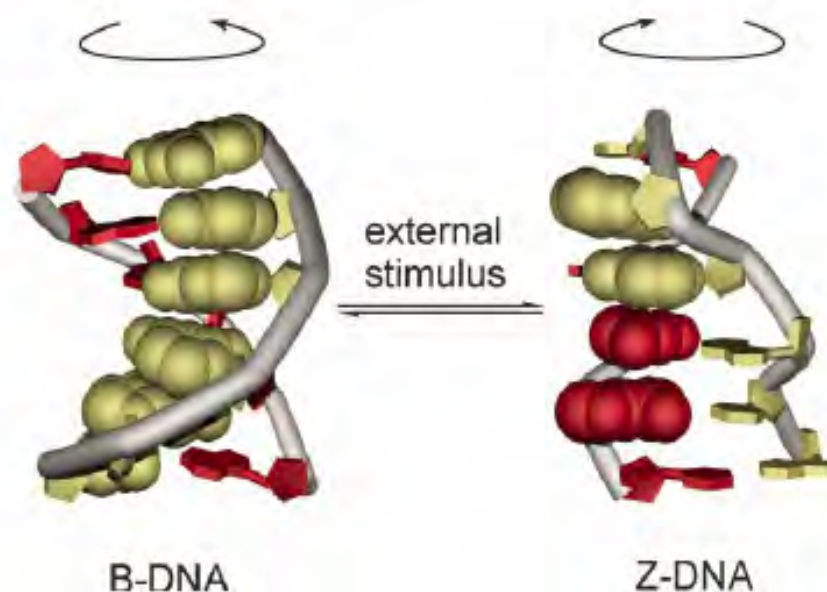
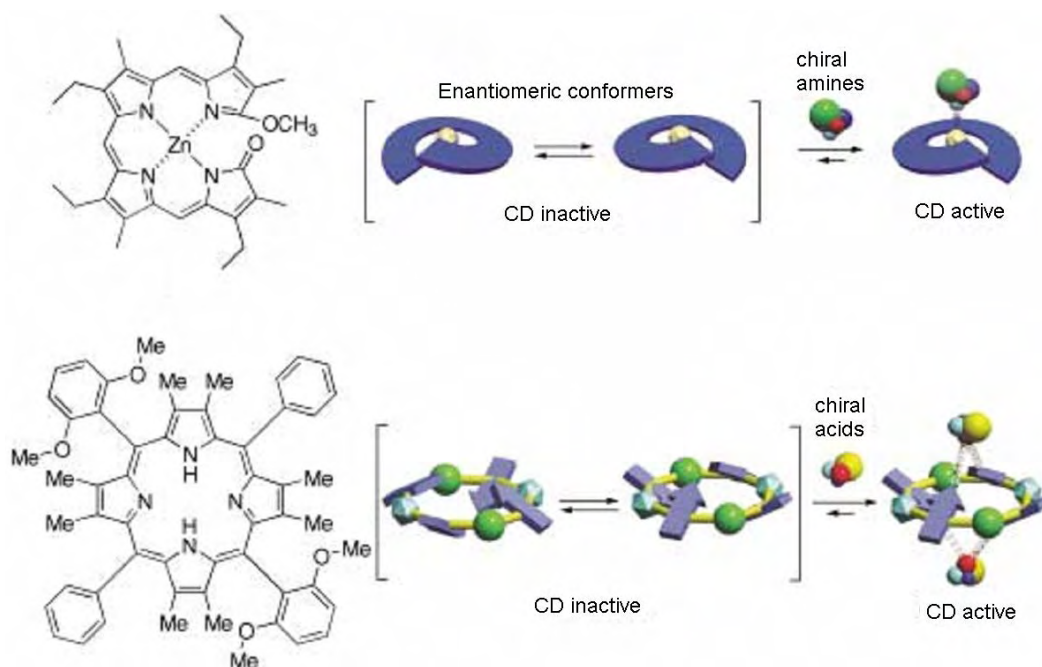


Figure 4.13: Double-helix structures of DNA d(CGCGCG) demonstrating the change in helicity due to the presence of external stimuli⁴⁶.

Figure 4.14 shows an example of some ligands that form racemic helicates upon complexation with metal ions. The complexes form CD inactive mixtures, however upon interaction with a chiral guest molecule the helicates show a preferential helicity resulting in a CD active solution.



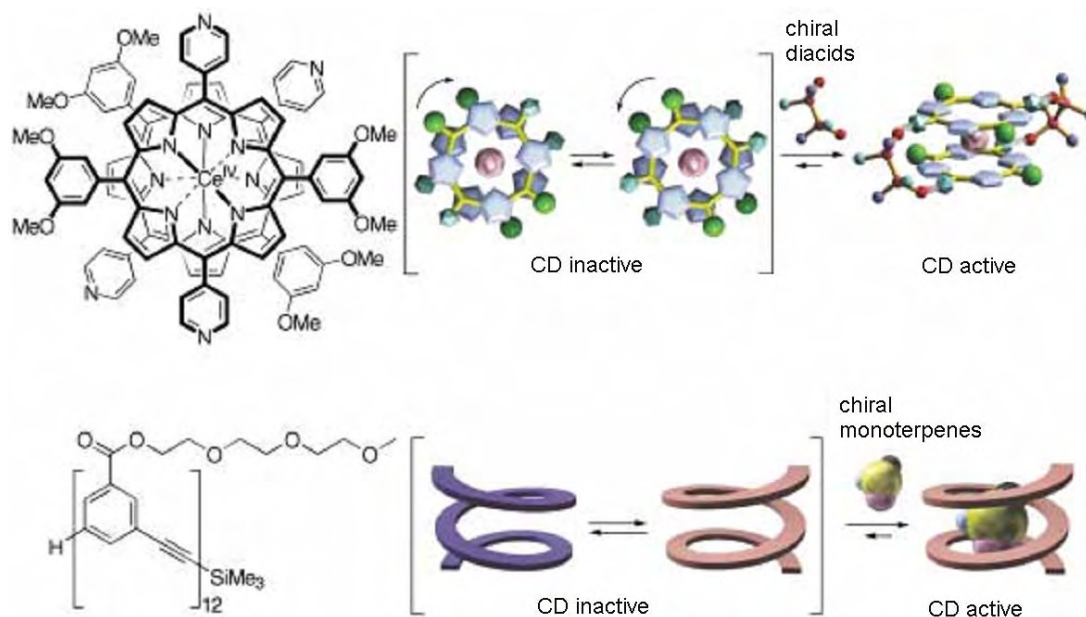


Figure 4.14: Structures of different ligands that form racemic helicates and their interactions with chiral receptor molecules and the consequent possible enantiomerisation mechanisms that occurs upon binding to chiral guests resulting in a CD active molecule ⁴⁷.

These interactions between a chiral guest molecule, and an achiral receptor molecule that is chromophoric can give rise to extrinsic ICD of the achiral counterpart, provided the latter absorbs in the UV or visible region under study and the former does not. The acquired CD spectra are specific to a particular chromophore and sensitive to the changes in the relative geometry of the chromophores. The kinetic appearance of chiroptical properties from the introduction of a chiral molecule can be indicative of the kinetics of the process of complex formation and also provide structural information about the complex itself. Thus, the CD spectra obtained are of interest as the sign of the signal can indicate the absolute configuration of the guest chiral component, as well as the orientation of the molecules relative to each other within the host-guest complex ^{38, 43-45}.

There have been a number of reports in literature in which the chirality of a supramolecular system, composed entirely of achiral components, were controlled by noncovalent contacts with independent chiral molecules ⁴⁸⁻⁵². For example, Nakashima *et al* ⁵³ have demonstrated that achiral polysilylene polymers formed asymmetric helical structures upon interaction with chiral alcohols. Although the achiral ligand itself showed no CD signal, addition of *S*-2-butanol induced a positive CD signal around 350 nm, while *R*-2-butanol showed a negative signal.

4.3.4 PepdaH₂ Helicity

Yano *et al*²⁴ have investigated the chiral properties of an analogous ligand to PepdaH₂, but intrinsically chiral due to the presence of two methyl groups that are not present on PepdaH₂. The ligand has been shown in Figure 4.15 in the *S*-chiral form.

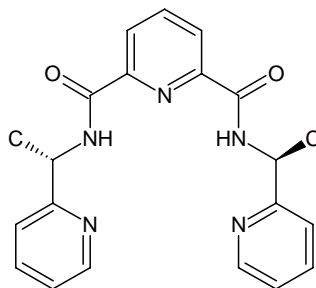


Figure 4.15: Structure of *N,N'*-bis[*S*-1-(2'-pyridyl)-ethyl]pyridine-2,6-dicarboxamide, which is analogous to the ligand PepdaH₂, but optically active due to the methyl groups that are not present in PepdaH₂.

In Yano's study, the reversible formation of the dicopper helicate, [Cu₂L₂], from H[CuBr₂LH] was controlled with the addition and removal of HBr, which protonated and deprotonated the amide nitrogens respectively. These changes were monitored by following the change in CD spectra, as shown in Figure 4.16, where it can be seen that the intensity of the helicate is enhanced in different regions compared to the monomer.

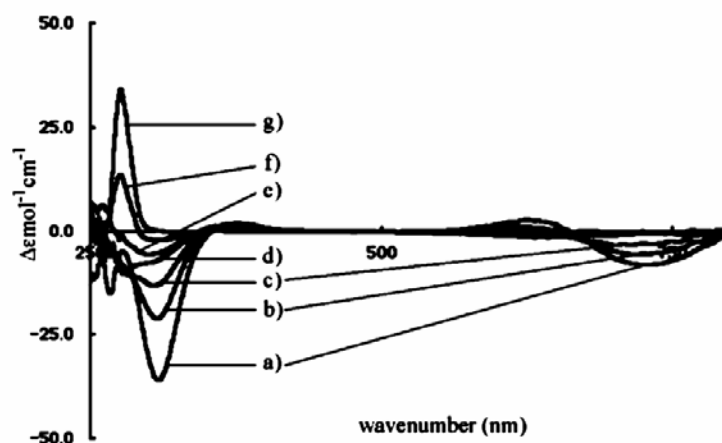


Figure 4.16: CD spectrum change of (*M*)-[Cu₂S-L₂] in methanol with addition of HBr: (a) 0, (b) 0.1, (c) 0.2, (d) 0.4, (e) 0.6, (f) 1.0, (g) 2.0 equivalents²⁴.

It was reported that treatment with CuBr₂ in the presence of triethylamine resulted in the racemic mixture of *S* and *R* ligands producing a racemic mixture of the helicates, (*M*)-[Cu₂S-L₂] and (*P*)-[Cu₂R-L₂] quantitatively. This is indicative of self-recognition during the helicate formation, just as self-recognition through hydrogen bonding is involved in the double strand formation of DNA.

PepdaH₂, however, is an achiral ligand, hence the ligands that bridge the metal centres have no inherent chirality. Therefore, due to the absence of an external stereogenic source, a racemic mixture of helicates was observed for PepdaH₂ complexes. Even though Yano's results are not associated with ICD, they demonstrate that the formation of pure (*M*) and (*P*) helicates are possible and hence induced chirality with a chiral counter ion should be possible that favours either the (*M*) or (*P*) helical structure.

In this study the change in chiroptical properties were observed from an induced influence as PepdaH₂ is an achiral and symmetric ligand and forms a racemic mixture of *P* and *M* helicates upon binding to metal ions. It was proposed that any change to the equilibrium of the racemic mixture of helical compounds formed by PepdaH₂ from the addition of an optically pure guest molecule may be observed from monitoring the spectral changes of the CD spectra. For the investigations (-)-tartaric acid was used for the preliminary experiments to induce a CD signal from the preferential coordination of one enantiomer of the PepdaH₂ helicate with the chiral acid. If the chiral counter ion, (-)-tartaric acid, interacted favourably with one enantiomer than either the *P* or *M* will be in excess resulting in an induced CD signal. Further experiments were performed with sodium (+)-tartrate as the chiral counter ion as it was hypothesised that the addition of (-)-tartaric acid may protonate the amide groups on the ligand and cause dissociation of the helical structure.

4.3.4.1 Factors Affecting ICD Signals

There are many influences that affect the ICD between a host and guest molecule. Since noncovalent interactions are the key elements of ICD, there are several external factors that can effect these interactions and consequently influence the whole chirality induction process. These include such stimuli as the temperature, phase transition, polarity, spatial orientation of the guest in relation to the host, and so forth. There are also internal factors that influence ICD, the most common being bonding strength, steric and electronic effects, and stoichiometry.

Borovkov *et al*⁵⁴ investigated some of these influences with a bisporphyrin analogue. In this study steric effects were reported to have a strong influence, along with the polarity of the solvent. These effects have been shown in Figure 4.17a where it has been shown that if the polar solvent interacts with the guest or host molecule, in such a manner that the molecule becomes bulkier, the result is that the noncovelant interaction is sterically hindered and the CD will be subsequently affected.

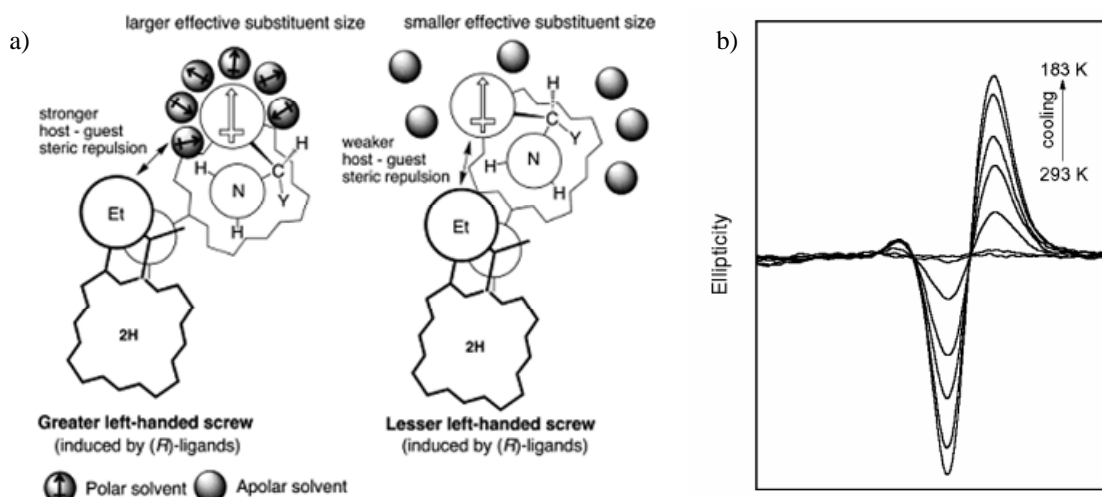


Figure 4.17: a) Schematic representation of the solvent effect on the supramolecular chirogenesis in a helical system b) the effect of temperature on the induced CD spectra of a helical system⁵⁴.

Another factor Borovkov investigated was the effect of temperature as, due to the dynamic nature of supramolecular systems, such an influence is clearly crucially important. Obviously, changing the temperature of a system has a direct effect on the binding strength of the coordination pair and thus the chirality induction in the host-guest system. It was found that a reduction in temperature resulted in enhancement of the degree of chirality induction. This was attributed to an increase in the percentage of bound ligand and therefore an increase in the degree of chiral steric interactions occurring along with the general reduction in thermal molecular motion, as shown in Figure 4.17b.

4.3.5 Equilibrium of Intrinsic Induced Chirality

Figure 4.18 provides a schematic representation of how a chiral guest molecule can alter the equilibrium between *P* and *M* helicates in a racemic chiral mixture of helicates. Usually one enantiomer will interact more favourably with the chiral guest molecule, resulting a shift in the equilibrium towards the more stable configuration, shown as the clockwise enantiomer in the figure.

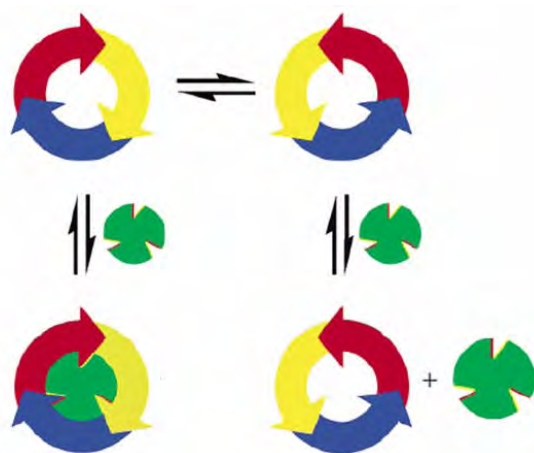
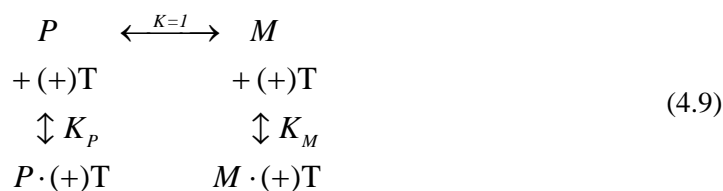


Figure 4.18: Schematic representation of racemates in dynamic equilibrium is shown as clockwise and counter-clockwise rings. The source of chiral information, represented by the green insert, interacts more favourably with the clockwise ring, driving the equilibrium toward the clockwise enantiomer⁵⁵.

In a racemic solution the equilibrium between *P* and *M* enantiomers is, by definition, equal to one because the racemic solution has equal concentrations of the *P* and *M* helicates, that is $[P]/[M] = 1$. There is also an equilibrium between the racemic mixture of the *P* and *M* helicate isomers and the free chiral ligand. This equilibrium is represented in Equation (4.9), where the chiral ligand was either (-)-tartaric acid or sodium (+)-tartrate, denoted (+)T. The equilibrium constants K_P and K_M will necessarily differ for the two chiral counter ions due to such effects as the pH changes from each reagent.



When (+)T is present, an enantiomeric excess is observed if (+)T binds more extensively and strongly to one particular chiral isomer. For the case where (+)T shows a preference towards the *P* isomer, then K_P will be greater than K_M , Equation (4.10).

$$\frac{K_P}{K_M} = \frac{[P \cdot (+)T]}{[M \cdot (+)T]} \quad (4.10)$$

For our investigations the CD of the pure *P* or *M* helicate could not be determined, therefore it was not possible to determine absolute K_P or K_M values. However, the ratio of one to the other could be calculated from the observed ICD, as discussed in Section 4.3.7.3.

4.3.6 Experimental

All solutions were prepared in 50/50 (v/v) ethanol/water solvent as PepdaH₂ was insoluble in water.

4.3.6.1 Interaction with (-)-Tartaric Acid

CD spectra were recorded on a Jasco 710 spectrometer using thermostated quartz cells of path length 1.0 cm, a step size of 0.5 nm, and at 25.0 °C at the laboratory in Geneva University.

The initial solutions for the induced chirality CD titrations were prepared as 25 mL solutions. From the equilibrium studies discussed previously in Section 4.2.3.2, a 1:1 ratio was observed to be optimum for the formation of the M₂L₂ helicate with copper(II). This ratio was also used for nickel(II); however, with nickel(II) titrations were also performed at a 2.4:1 M:L ratio, as from the equilibrium studies the 2.4:1 ratio was observed to be optimum for the formation of the M₃L₂ helix.

1.0 mL of each metal and PepdaH₂ solution was pipetted into the cuvette and then increasing equivalents of (-)-tartaric acid were added for each CD measurement. The concentration of (-)-tartaric acid was 20 times greater than the metal/PepdaH₂ concentrations in order to minimise dilution effects from the addition of the (-)-tartaric acid for the titration. It should be noted that the CD measurements performed in the Geneva University laboratory were not automated titrations, as this set-up was not available.

The concentrations for both the copper(II) and nickel(II)-PepdaH₂ titrations have been shown in Table 4.11; the initial volume in the cuvette was 2.0 mL for each measurement. A 0.02 M solution of (-)-tartaric acid was prepared and added from 0 → 1 equivalents in 0.1 equivalent increments, then from 1 → 3 equivalents in 0.5 equivalent increments, with the total added volume of (-)-tartaric acid being 0.75 mL. The final volume in the cell was 2.75 mL. The spectrum was scanned from 300 – 800 nm.

	Cu:L (1:1)	Ni:L (1:1)	Ni:L (2.4:1)
[metal] M	1.25×10^{-3}	1.31×10^{-3}	1.85×10^{-3}
[PepdaH ₂] M	1.25×10^{-3}	1.25×10^{-3}	0.74×10^{-3}

Table 4.11: Total initial concentrations for metal and PepdaH₂ for (-)-tartaric acid CD titrations.

4.3.6.2 Interaction with Sodium (+)-Tartrate

CD spectra were recorded at Newcastle University on an Applied Photophysics Chirascan using thermostated quartz cells of path length 1.0 cm, a step size of 5 nm, and at 25.0 °C.

The initial solutions for the induced chirality CD titrations were prepared as 25 mL solutions of metal-PepdaH₂ mixtures. 2 mL volumes of the metal-PepdaH₂ solutions were used for the titrations with sodium (+)-tartrate, which were fully automated. The concentrations for both the copper(II) and nickel(II)-PepdaH₂ titrations have been shown in Table 4.12. A 0.1 M solution of sodium (+)-tartrate was prepared and added from 0 → 1.5 equivalents in 0.05 equivalent increments, a total of 0.13 mL sodium (+)-tartrate was added to the cell. Additionally, the copper(II) titration was also performed to a six equivalent tartrate ion excess to determine if any interaction between the copper(II) ion and tartrate ligand could be detected. The CD spectrum was scanned from 340 – 900 nm.

	Cu:L (1:1)	Ni:L (2.4:1)
[metal] M	5.03×10^{-3}	12.30×10^{-3}
[PepdaH ₂] M	5.19×10^{-3}	5.00×10^{-3}

Table 4.12: Total initial concentrations for metal and PepdaH₂ for sodium (+)-tartrate acid CD titrations.

4.3.7 Results and Discussion

4.3.7.1 (-)-Tartaric Acid ICD Spectra

The results of the titrations with (-)-tartaric acid for both copper(II) and nickel(II) with PepdaH₂ have been shown in Figure 4.19. The copper(II)-PepdaH₂ titrations showed a significant CD signal indicating that the (-)-tartaric acid was preferentially interacting with either the *P* or *M* enantiomer. However, even at the optimum 2.4:1 M:L ratio it can be seen that the nickel(II) CD signal is approximately an order of magnitude smaller than that of the copper(II), showing insignificant induced helicity. This may be due to a weaker interaction with the chiral counter ion, resulting in a smaller ICD effect, or merely reflect an inherent weaker CD spectrum for nickel(II)-PepdaH₂ complex. It is notable, however, that the ICD for the nickel(II) system is clearly enhanced for high concentration of (-)-tartaric acid, which may indicate a weaker ion pair, or simply competition for the nickel(II) by the added component.

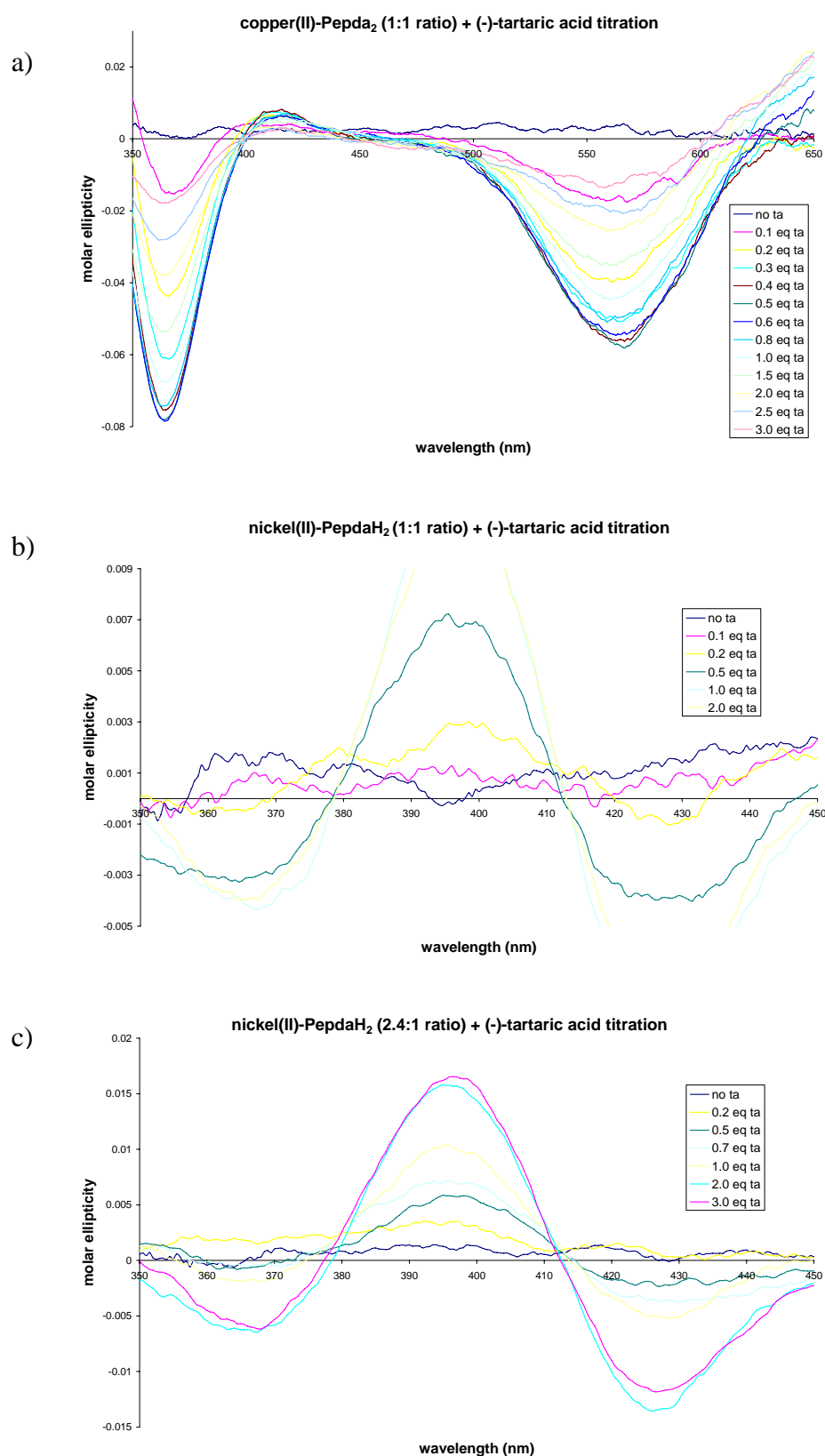
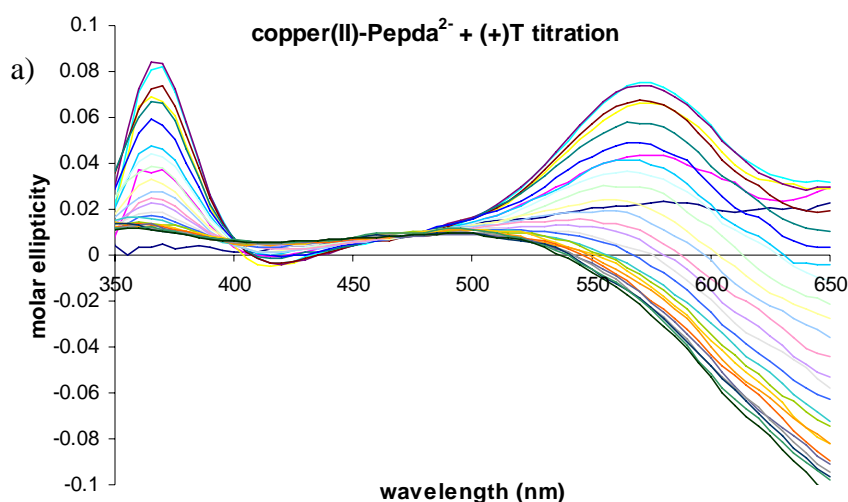


Figure 4.19: (-)-tartaric acid titrations: a) copper(II)-PepdaH₂ at a 1:1 M:L ratio; b) nickel(II)-PepdaH₂ at a 1:1 M:L ratio; c) nickel(II)-PepdaH₂ at a 2.4:1 M:L ratio.

It was initially thought that the difference of CD signal between the two metal helicates may be due to the tartaric acid causing the nickel(II) helicate to dissociate, promoted by protonation from the added acid, as it is known that nickel(II) generally forms weaker metal-nitrogen bonds than copper(II). The stronger copper(II)-nitrogen bonds limit dissociation, allowing the chiral tartaric acid to preferentially bind to one enantiomer. In order to investigate whether this explained the poor CD signal with nickel(II), Na (+)-tartrate was used instead of (-)-tartaric acid as the chiral counter ion.

4.3.7.2 Sodium (+)-tartrate ICD Spectra

Similar to the (-)-tartaric acid experiments, a 1:1 copper(II)-PepdaH₂ ratio and a 2.4:1 nickel(II)-PepdaH₂ ratio were used for the CD measurements. A 1:1 nickel(II)-PepdaH₂ ratio was not used because the previous (-)-tartaric acid results showed higher CD signal with the 2.4:1 ratio. Results with sodium (+)-tartrate, Figure 4.20, were similar to (-)-tartaric acid with copper(II), giving a clear ICD; again, the nickel(II) had a very poor signal. Compared to the previous studies, the CD signal was opposite when sodium (+)-tartrate was used as the chiral counter ion, as it is the enantiomer of (-)-tartaric acid.



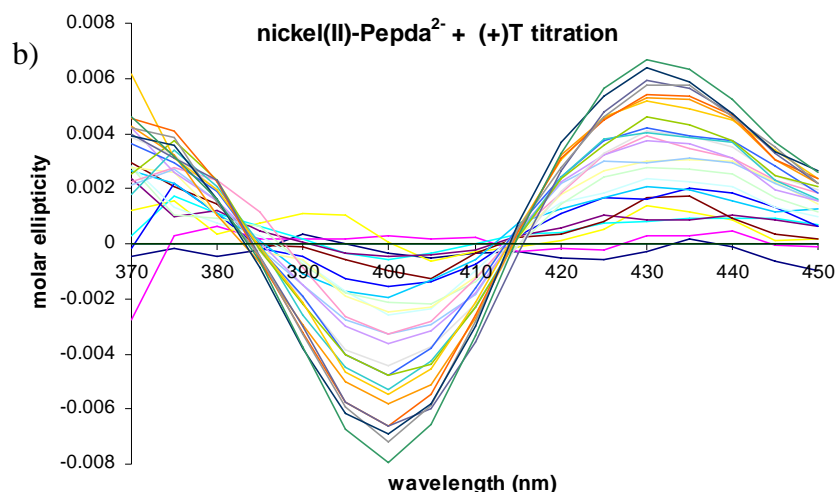


Figure 4.20: a) Cu(II)-PepdaH₂⁻ and b) Ni(II)-PepdaH₂ titration with (+)-tartrate.

The poor results with nickel were further investigated, as the theory that the previously low CD signal could be explained by the (-)-tartaric acid dissociating the helicate clearly did not apply. In these titrations no acid was being introduced to the system, but the nickel(II)-PepdaH₂ still showed a very small CD.

To investigate whether the observed CD signal was even assignable to a small induced CD and not from the (+)-tartrate interacting with free nickel(II), experiments were performed using nickel(II) chloride and titrating with the sodium (+)-tartrate solution. A comparable concentration of nickel(II) chloride was used as with the nickel(II)-PepdaH₂ solution, that is 1.296×10^{-2} M. It can be seen from comparing the nickel(II) chloride titration, Figure 4.21b), with the previous nickel(II)-PepdaH₂ titrations, Figure 4.19b) and c) and Figure 4.21a), that the CD spectrum is comparable, with peaks at 360, 400, and 425 nm, for all titrations, with the opposite signal observed in Figure 4.19 due to the addition of the enantiomer, (-)-tartaric acid ion.

The similarity of all nickel(II) titration results implied that no induced chirality was observed with the nickel-PepdaH₂ helicate; rather, the small CD spectrum was a result of the tartrate ions forming a complex with free nickel(II). This observation is further supported by the noted increase in CD signal with (-)-tartaric acid when a 2.4:1 nickel(II)-PepdaH₂ ratio was used compared to the 1:1 ratio, Figure 4.19c) and b) respectively, as the higher concentration of nickel(II) ions present in the 2.4:1 ratio solution meant that there were an increased number of metal ions that were able to be complexed by the tartrate ions and therefore produce a greater CD signal. Hence, it was hypothesised that the interaction between nickel-PepdaH₂ may be weaker than the formation of a nickel(II) tartrate complex, resulting in no induced chirality in the

helicate. A chiral additive that is unable to bind, or highly disfavoured from binding as a ligand, would seem necessary when weak complexation is present in labile systems.

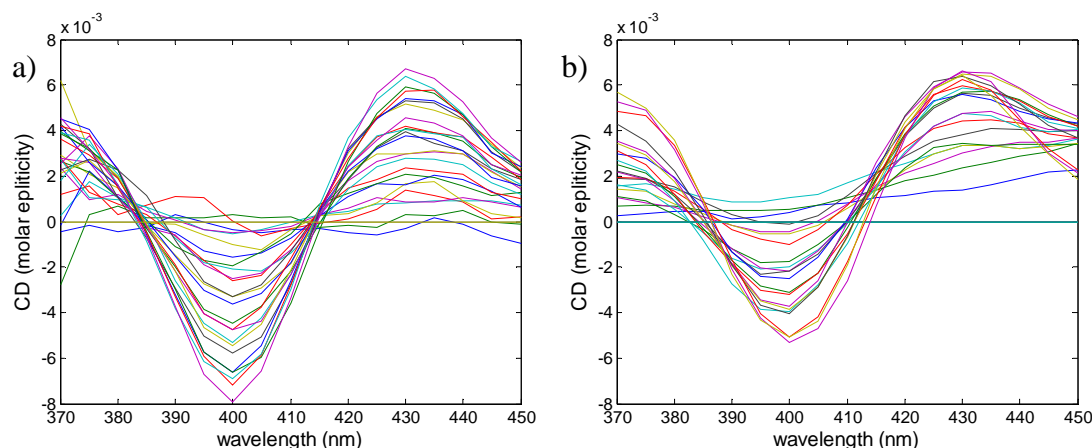


Figure 4.21: a) Ni-PepdaH₂ and b) NiCl₂ titrated with (+)-tartrate.

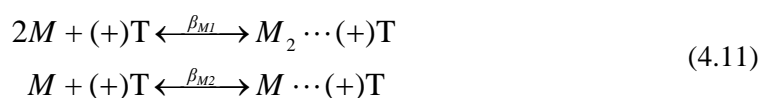
A titration with copper(II) nitrate and sodium (+)-tartrate was also performed to ensure that the CD signal in the copper(II)-PepdaH₂ titrations was not also due to copper(II) complexing the (+)-tartrate ion. These titrations showed no CD signal in the wavelength range used for the copper(II)-PepdaH₂ titrations. Both copper(II) and nickel(II) have similar stability constants for $M + L \leftrightarrow ML$ equilibrium with the tartrate ion, $\log K$ values of 2.5 and 2.6, respectively⁵⁶. Therefore, it is unusual that copper(II) shows no CD signal with the chiral tartrate ion considering it has similar stability to nickel(II), although the situation is complicated by polynuclear species having been reported for copper(II) and tartrate⁵⁷. Due to copper(II) and tartrate having negligible CD signal it was concluded that the CD signal observed in the copper(II)-PepdaH₂ titration was indeed a result of the chiral counter ion interacting favourably with one of the helicate enantiomers, resulting in a shift in the equilibrium.

4.3.7.3 ICD Analysis

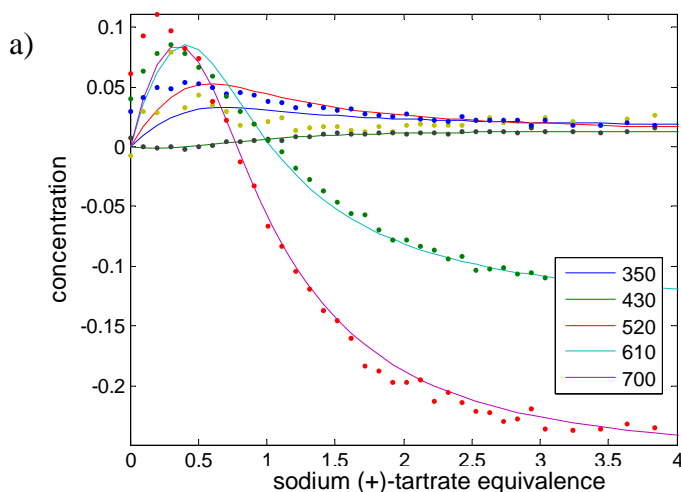
For the ICD data of copper(II)-PepdaH₂ the significant CD signal enabled some elementary analysis of the interaction of the helicate with the (+)-tartrate ion. Since the pure spectrum of neither the *P* nor *M* enantiomer was known, it could not be determined from the ICD spectrum if the equilibrium shifted towards the *P* or *M* helicate. It should be noted that the opposite ICD spectrum was observed when the (-)-tartaric acid ion was used, which clearly indicated that the copper(II)-PepdaH₂ helicate was influenced by the chirality of the guest species. Comparison of the ICD spectra with the CD spectrum reported by Yano *et al*²⁴, shown in Figure 4.16, the spectrum with no HBr added shows

that from 350 – 650 nm the spectrum has the same sign as the induced CD spectrum with copper(II)-PepdaH₂, shown in Figure 4.20a. That is, the peak at ~ 325 nm is positive, as is the peak at 590 nm, with the shoulder then becoming negative at wavelengths greater than 650 nm. Therefore, it can be inferred that the (+)-tartrate ion favours the *M* enantiomer, resulting in a shift in equilibrium towards the *M* helicate from outer-sphere interactions with the (+)-tartrate ion. Alternatively, the (-)-tartaric acid favours the formation of the *P* enantiomer as the CD signal with this counter ion is opposite to that reported by Yano, as seen in Figure 4.19.

Analysis using the in-house developed Spec_Anal program of the copper(II)-PepdaH₂ (+)-tartrate titration resulted in a model describing the formation of two induced helical species, the model is shown below.



The stability constants, $\log \beta_{M1}$ and $\log \beta_{M2}$, were determined to be 7.249 ± 0.089 and 4.067 ± 0.026 , respectively. The results in Figure 4.22 show the fit of the measured and calculated data, the concentrations of species over the titration, and the induced CD spectrum for both species.



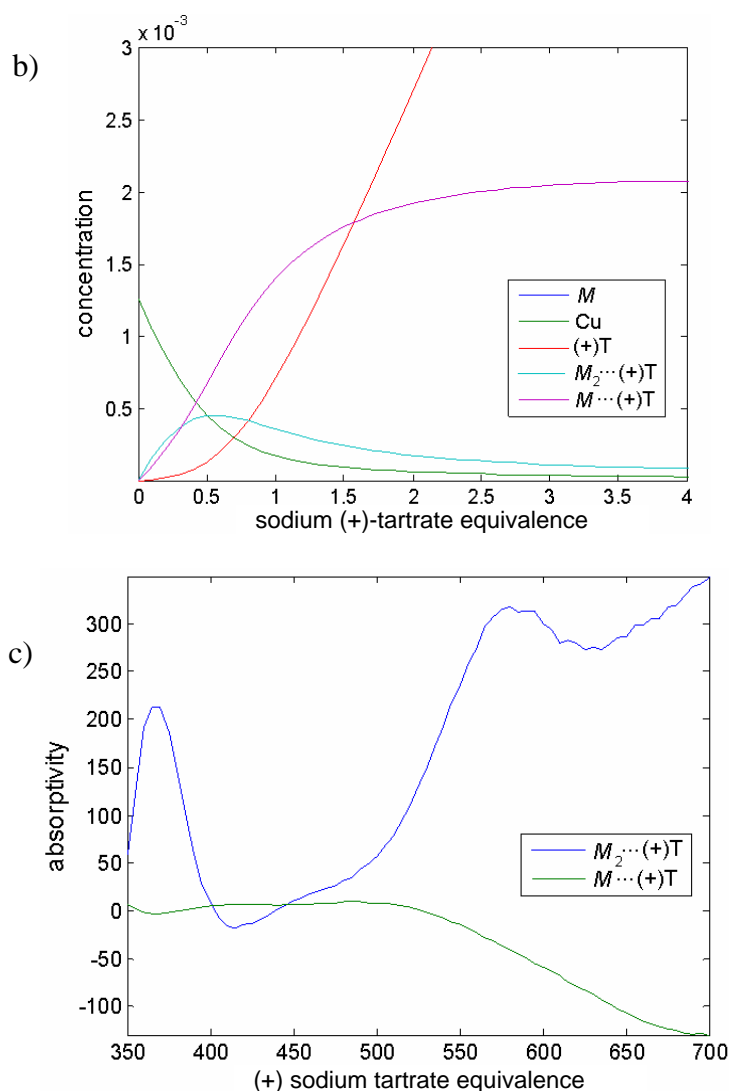


Figure 4.22: a) Figure showing the fits of the measured (•••) and calculated (—) data; b) Species concentrations profiles; c) Species CD spectrum.

This model that was fitted to the copper(II)-PepdaH₂ titration data was further supported through consideration of the EFA plots, Figure 4.23, which clearly showed that there were two species influencing the CD signal. The proposed model, with $M_2\cdots(+)\text{T}$ and $M\cdots(+)\text{T}$ forming as a result of interaction with the (+)-tartrate ion, means that there are two chiral species that influence the observed CD signal in the titration. It can be seen that a species forms at 0.5 equivalents of (+)-tartrate ion, which corresponds to the formation of the proposed $M_2\cdots(+)\text{T}$ species. The formation of an $M_2\cdots(+)\text{T}$ species is surprising. However, the maximum of the CD signal at 0.5 equivalents of (+)T is a clear indication for such a species. Further investigations are required to confirm such a species.

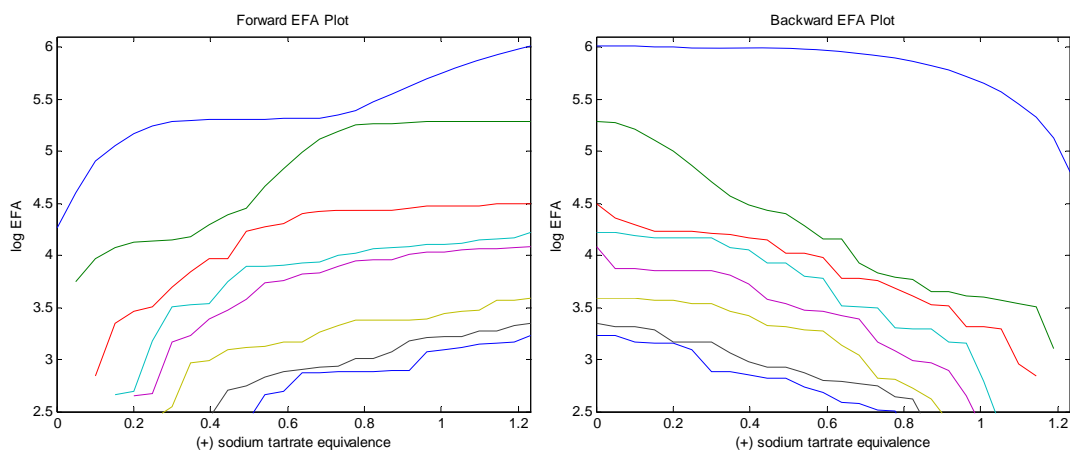


Figure 4.23: Forward (LHS) and backward (RHS) EFA plots for copper(II)-PepdaH₂ sodium (+)-tartrate titration at a 1:1 M:L ratio.

The EFA plots with nickel(II) resulted in only one species influencing the CD signal. Drawing on the nickel(II) chloride titration results, this species is considered to be the complex formed via interaction of the free nickel(II) with the tartrate ion, which means that there are no other interactions in the solution. Thus an intermediate between the helicate and chiral counter ion is not contributing, as the EFA clearly shows that only one species is optically active.

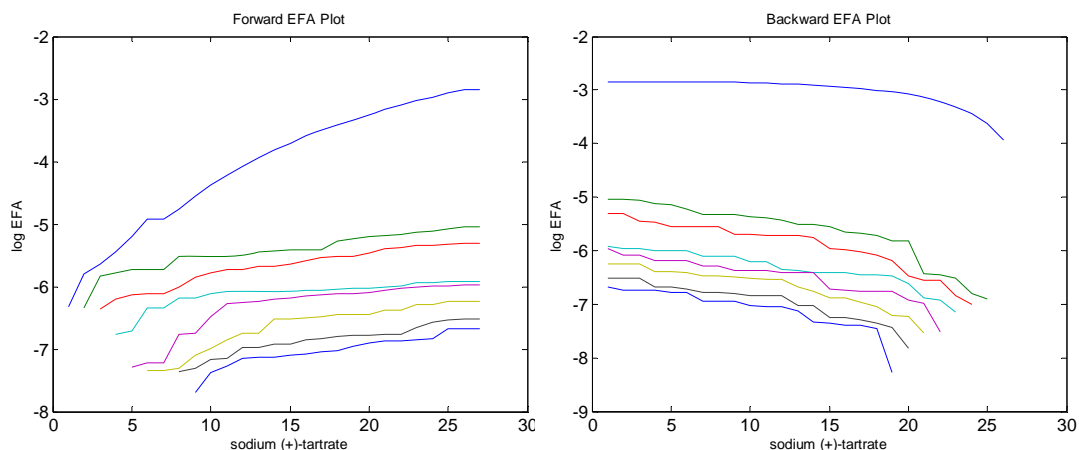


Figure 4.24: Forward (LHS) and backward (RHS) EFA plots for nickel(II)-PepdaH₂ sodium (+)-tartrate titration at a 2.4:1 M:L ratio.

4.4 Conclusions

The conjoint chemometric approach applied in the first section of this study with kinetic and equilibrium data is an approach that can be generally applicable for probing formation pathways in complex polynuclear systems such as potentially complicated oligomeric complexation reactions. The fact that both the kinetic and equilibrium data analysis separately resulted in elucidation of the same reaction pathway to model the

reaction of PepdaH₂ with copper(II) and nickel(II) validates the chosen model and legitimacy of the conjoint analysis technique and successfully shows that both techniques can compliment each other and enable greater understanding of a system then would be possible if either technique was used independently.

The approach, while defining the reaction pathway effectively, did not elucidate any details of the steps in the complexation mechanism within each stage at the molecular level. It was noted that the unknown complexity of reaction was the most likely reason for discrepancies in the calculated log *K* values for both analytical techniques. It was significant that for both the nickel(II) and copper(II) systems the formation of an M₂L species, subsequent to the ML species, was observed. This implies that chelation of the two metal ions by separate amidopyridine arms of the ligand can occur. The formation of this species facilitated the subsequent substitution reactions of the two partly aquated metal centres which led to the final products. In fact, it is logical that the two like-charged metal ions would tend to separate as much as possible, giving an extended structure likely to promote ‘wrapping’ of another ligand to form a helicate.

The circular dichroism studies with copper(II)-PepdaH₂ displayed clear chiral inducement from outer-sphere interactions, unlike the nickel(II) results which only showed the interaction of free metal ion with the tartrate ion. The nickel(II) helicate is a more complex structure than copper(II), involving three metal ions and two ligands, whereas the copper(II) complex consists of two metals and two ligands. In the nickel(II)-PepdaH₂ helicate each metal ion is bound in 4:6:4 motif by the nitrogens in the ligand, the two end nickel(II) ions are stabilised by coordinated anions such as acetate ions which are necessary for the overall neutrality of the complex. On the other hand, the copper(II) is in a robust 5:5 motif and does not require anions in order to neutralise the charge on the helicate. One reason why copper(II) helicate shows clear ICD is that it can readily reorganise geometry from the *P* to the *M* configuration, or visa versa, whereas the nickel(II) helicate may not be able to undergo such a reconfiguration as easily due to the larger number of components present in the helicate. This may result in the helicate releasing nickel(II) ion while rearranging, which can then preferentially complex the chiral counter ion, producing the weak CD signal observed for all nickel(II) titrations.

The preliminary analysis of the CD titrations with copper(II) show that there is potential to model the interactions of outer-sphere complexation of molecules using the highly

sensitive technique of CD. Specifically, the work with copper(II)-PepdaH₂ and (+)-tartrate will be further investigated to try and determine the equilibrium constants of the *P* and *M* enantiomers with the chiral guest (+)-tartrate. These investigations show great promise for future research.

4.5 References

1. Lehn, J. M., *Supramolecular Chemistry: Concepts and Perspectives*. 1995; p 262.
2. MacNicol, D. D. V., F.; Lehn, J.-M.; Atwood, J.E.D., Davies (Eds.), *Comprehensive Supramolecular Chemistry*. Pergamon: New York, 1996; Vol. 9.
3. Sauvage, J.-P.; Hosseini, M. W., *Comprehensive Supramolecular Chemistry, Volume 9: Templating, Self-Assembly, and Self-Organization*. 1996; p 664.
4. Piguet, C.; Bernardinelli, G.; Hopfgartner, G., Helicates as Versatile Supramolecular Complexes. *Chemical Reviews* **1997**, 97, 2005-2062.
5. Lehn, J. M.; Rigault, A.; Siegel, J.; Harrowfield, J.; Chevrier, B.; Moras, D., Spontaneous assembly of double-stranded helicates from oligobipyridine ligands and copper(I) cations: structure of an inorganic double helix. *Proceedings of the National Academy of Sciences of the United States of America* **1987**, 84, 2565-9.
6. Telfer, S. G.; Sato, T.; Kuroda, R., Noncovalent ligand strands for transition-metal helicates: The straightforward and stereoselective self-assembly of dinuclear double-stranded helicates using hydrogen bonding. *Angewandte Chemie, International Edition* **2004**, 43, 581-584.
7. Spasojevic, I.; Boukhalfa, H.; Stevens, R. D.; Crumbliss, A. L., Aqueous Solution Speciation of Fe(III) Complexes with Dihydroxamate Siderophores Alcaligin and Rhodotorulic Acid and Synthetic Analogues Using Electrospray Ionization Mass Spectrometry. *Inorganic Chemistry* **2001**, 40, 49-58.
8. Boukhalfa, H.; Crumbliss, A. L., Multiple-Path Dissociation Mechanism for Mono- and Dinuclear Tris(hydroxamato)iron(III) Complexes with Dihydroxamic Acid Ligands in Aqueous Solution. *Inorganic Chemistry* **2000**, 39, 4318-4331.
9. Caudle, M. T.; Cogswell, L. P., III; Crumbliss, A. L., Mechanistic Studies on the Dissociation of Mono- and Bimetallic 1:1 Ferric Dihydroxamate Complexes: Probing Structural Effects in Siderophore Dissociation Reactions. *Inorganic Chemistry* **1994**, 33, 4759-73.
10. Caudle, M. T.; Stevens, R. D.; Crumbliss, A. L., A Monomer-to-Dimer Shift in a Series of 1:1 Ferric Dihydroxamates Probed by Electrospray Mass Spectrometry. *Inorganic Chemistry* **1994**, 33, 6111-15.
11. Lehn, J.-M.; Eliseev, A. V., Dynamic combinatorial chemistry. *Science* **2001**, 291, 2331-2332.
12. Alcock, N. W.; Clarkson, G.; Glover, P. B.; Lawrance, G. A.; Moore, P.; Napitupulu, M., Complexes of 2,6-bis[N-(2'-pyridylmethyl)carbamyl]pyridine: formation of mononuclear complexes, and self-assembly of double helical dinuclear and tetranuclear copper(II) and trinuclear nickel(II) complexes. *Dalton Transactions* **2005**, 518-527.

13. Bouchard, H.; Hittinger, A. Heterocyclic diamides and related compounds as telomerase inhibitors. 2002, Patent CAN 138:24646.
14. Atwood, D. A.; Howerton, B. S.; Matlock, M. Novel multidentate sulfur-containing ligands. 2002, Patent CAN 137:67462.
15. Matlock, M. M.; Henke, K. R.; Atwood, D. A., Effectiveness of commercial reagents for heavy metal removal from water with new insights for future chelate designs. *Journal of Hazardous Materials* **2002**, 92, 129-142.
16. Chevallier, P.; Soutif, J.-C.; Brosse, J.-C.; Grote, M., Synthesis of poly(amide-ester)s from 2,6-pyridine dicarboxylic acid and ethanolamine derivatives - investigation of the polymer sorption behavior towards heavy metal ions. *Reactive & Functional Polymers* **1999**, 42, 129-146.
17. Hiratani, K.; Taguchi, K., 2,6-Bis[N-(8-quinolyl)carbamoyl]pyridine as a highly selective extractant for copper(II). *Bulletin of the Chemical Society of Japan* **1990**, 63, 3331-3.
18. Matthias, P.; Takahashi, M.; Goto, K. Preparation of polyoxadiazole derivatives for electroluminescent device. 1999, Patent CAN 131:158116.
19. Chavarot, M.; Socquet, S.; Kotera, M.; Lhomme, J., Synthesis of an adenine-pyridinaldoxime-acridine conjugate for recognition of abasic site lesions in DNA. *Tetrahedron* **1997**, 53, 13749-13756.
20. Mitchell, M. C.; Cawley, A.; Kee, T. P., Phosphono-transfer catalysis mediated by an amphoteric receptor. *Tetrahedron Letters* **1995**, 36, 287-90.
21. Maruyama, T.; Koga, J.; Kuroki, N.; Konishi, K., Study of several fluorescent brightening agents for synthetic fibers. *Kogyo Kagaku Zasshi* **1962**, 65, 1071-4.
22. Jain Sneh, L.; Bhattacharyya, P.; Milton Heather, L.; Slawin Alexandra, M. Z.; Crayston Joe, A.; Woollins, J. D., New pyridine carboxamide ligands and their complexation to copper(II). X-Ray crystal structures of mono-, di, tri- and tetranuclear copper complexes. *Dalton transaction* **2004**, 862-71.
23. Marlin, D. S.; Olmstead, M. M.; Mascharak, P. K., Structure-Spectroscopy Correlation in Distorted Five-Coordinate Cu(II) Complexes: A Case Study with a Set of Closely Related Copper Complexes of Pyridine-2,6-dicarboxamide Ligands. *Inorganic Chemistry* **2001**, 40, 7003-7008.
24. Yano, T.; Tanaka, R.; Nishioka, T.; Kinoshita, I.; Isobe, K.; Wright, L. J.; Collins, T. J., Mononuclear-dinuclear helicate interconversion of dibromo{N,N'-bis[(S)-1-2-(pyridyl)ethyl]pyridine-2,6-dicarboxamidate}copper(II) via a deprotonation-protonation process. *Chemical Communications* **2002**, 1396-1397.
25. Hubert, S.; Mohamadou, A.; Gerard, C.; Marrot, J., Equilibrium and structural studies of copper and nickel complexes with a pentadentate ligand providing amide, amine and

pyridyl nitrogen donors. Crystal structure of the dinuclear nickel(II) complex. *Inorganica Chimica Acta* **2007**, 360, 1702-1710.

26. Ruettimann, S.; Piguet, C.; Bernardinelli, G.; Bocquet, B.; Williams, A. F., Self-assembly of dinuclear helical and non-helical complexes with copper(I). *Journal of the American Chemical Society* **1992**, 114, 4230-7.
27. Williams, A. F.; Piguet, C.; Bernardinelli, G., Synthesis and Structure of a self-assembling triply helical complex with two cobalt(II) ions. *Angewandte Chemie* **1991**, 103, 1530-2.
28. Norman, S. E. Investigation into the interaction of constrained bidentate nitrogen-donor ligands with transition metal ions. *Honours Thesis*, Newcastle University, 2003.
29. ProKII <http://www.photophysics.com/prokii.php>
30. Maeder, M.; Neuhold, Y.-M.; Puxty, G., Application of a genetic algorithm: near optimal estimation of the rate and equilibrium constants of complex reaction mechanisms. *Chemometrics and Intelligent Laboratory Systems* **2004**, 70, 193-203.
31. Maeder, M.; Zilian, A., Evolving factor analysis, a new multivariate technique in chromatography. *Chemometrics and Intelligent Laboratory Systems* **1988**, 3, 205-13.
32. Belford, R. L.; Calvin, M.; Belford, G., Bonding in copper(II) chelates: solvent effects in their visible absorption spectra. *Journal of Chemical Physics* **1957**, 26, 1165-74.
33. Wright, M. R., *An Introduction to Chemical Kinetics*. John Wiley and Sons Ltd.: West Sussex, 2004.
34. Gibbs Free Energy.
<http://chemed.chem.purdue.edu/genchem/topicreview/bp/ch21/gibbs.php>
35. Wilkins, R.G., *Kinetics and Mechanisms of Reactions of Transition Metal Complexes*, 2nd ed., VCH Publishers, New York, 1991, p88.
36. Purrello, R., Supramolecular chemistry: Lasting chiral memory. *Nature materials* **2003**, 2, 216-7.
37. Huang, M.; Liu, P.; Wang, J.; Chen, Y.; Liu, Z.; Liu, Q., Synthesis structure and luminescence of a double helical coordination polymer with a semirigid ligand: L = N-(4-pyridylmethyl)benzimidazole. *Inorganic Chemistry Communications* **2006**, 9, 952-954.
38. Allenmark, S., Induced circular dichroism by chiral molecular interaction. *Chirality* **2003**, 15, 409-22.
39. Bucci, E. The Circular Dichroism Site. <http://www.imb-jena.de/ImgLibDoc/cd/tut1b.html>

40. Alliance Protein Laboratories Inc. Circular Dichroism. http://www.ap-lab.com/circular_dichroism.htm
41. Berndt, K. D. Circular dichroism spectroscopy. http://www.cryst.bbk.ac.uk/PPS2/course/section8/ss-960531_21.html (12/12/2007),
42. Yeh, R. M.; Raymond, K. N., Supramolecular Asymmetric Induction in Dinuclear Triple-Stranded Helicates. *Inorganic Chemistry* **2006**, 45, 1130-1139.
43. Canary, J. W.; Holmes, A. E.; Liu, J., Prospects for circular dichroism detection of nonracemic extraterrestrial organic molecules. *Enantiomer* **2001**, 6, 181-8.
44. Yashima, E.; Okamoto, Y., In *Circular Dichroism: Principles and Applications*, 2 ed.; Berova, N. N., K.; Woody, R.W., Ed. Wiley-VCH: New York, 2000; pp 521-546.
45. Tsukube, H.; Shinoda, S., Lanthanide Complexes in Molecular Recognition and Chirality Sensing of Biological Substrates. *Chemical Reviews* **2002**, 102, 2389-2403.
46. Miyake, H.; Tsukube, H., Helix Architecture and Helicity Switching via Dynamic Metal Coordination Chemistry. *Supramolecular Chemistry* **2005**, 17, 53-59.
47. Yashima, E.; Maeda, K.; Nishimura, T., Detection and amplification of chirality by helical polymers. *Chemistry--A European Journal* **2004**, 10, 42-51.
48. Kramer, R. J. M., L.; Andre, de C.; Jean, F., Self-organization, structure and spontaneous racemate cleavage of a trinuclear triple helix complex formed from oligobipyridine ligands and nickel(II) ion. *Angewandte Chemie* **1993**, 105, 764-7
49. Lintuluoto, J. M.; Borovkov, V. V.; Inoue, Y., Direct Determination of Absolute Configuration of Monoalcohols by Bis(magnesium Porphyrin). *Journal of the American Chemical Society* **2002**, 124, 13676-13677.
50. Oda, R.; Huc, I.; Schmutz, M.; Candau, S. J.; MacKintosh, F. C., Tuning bilayer twist using chiral counterions. *Nature* **1999**, 399, 566-569.
51. Hasenknopf, B.; Lehn, J. M., Trinuclear double helicates of iron(II) and nickel(II). Self-assembly and resolution into helical enantiomers. *Helvetica Chimica Acta* **1996**, 79, 1643-1650.
52. Suarez, M.; Branda, N.; Lehn, J. M.; Decian, A.; Fischer, J., Supramolecular chirality. Chiral hydrogen-bonded supermolecules from achiral molecular components. *Helvetica Chimica Acta* **1998**, 81, 1-13.
53. Nakashima, H.; Koe, J. R.; Torimitsu, K.; Fujiki, M., Transfer and amplification of chiral molecular information to polysilylene aggregates. *Journal of the American Chemical Society* **2001**, 123, 4847-8.

54. Borovkov, V. V.; Hembury, G. A.; Inoue, Y., Origin, Control, and Application of Supramolecular Chirogenesis in Bisporphyrin-Based Systems. *Accounts of Chemical Research* **2004**, 37, 449-459.
55. Yeh, R. M.; Ziegler, M.; Johnson, D. W.; Terpin, A. J.; Raymond, K. N., Imposition of Chirality in a Dinuclear Triple-Stranded Helicate by Ion Pair Formation. *Inorganic Chemistry* **2001**, 40, 2216-2217.
56. Martell, A. E.; Smith, R. M., NIST Critically Selected Stability of Metal Complexes, Database 46 Version 6.0. In NIST Standard Referenced Data: 2001.
57. Blomqvist, K.; Still, E. R., Solution studies of systems with polynuclear complex formation. 5. Copper(II) and cadmium(II) D-(+)-tartrate systems. *Inorganic Chemistry* **1984**, 23, 3730-3734.

Chapter 5

Study of Nuclearity and Chirality of Complexes Formed by a Helicating N-donor Ligand

5.1 Introduction

5.1.1 Aims of this Study

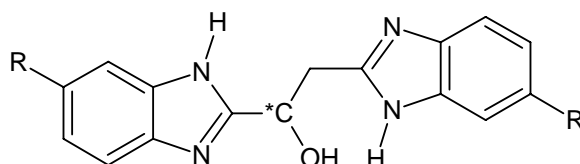
Ligands that occupy the coordination sites of transition metal ions in predictable ways play an important role in modern coordination chemistry. This is because such ligands may define both the number of reactive sites available at a metal centre and also modulate their reactivity¹⁻³. The coordination properties of ligands that bind to an octahedral metal centre in a meridional geometry have been well researched⁴⁻⁷, and are consequently fairly well understood. However, facially coordinating ligands have not been as well reported and hence deserve attention, as such ligands potentially offer different and interesting types of binding sites.

This chapter covers three main aspects of facially coordinating ligands. Firstly, a discussion focused on benzimidazole-based ligands, their history and current importance in research. Secondly, the stereoselectivity of complexes formed with chiral benzimidazole-based ligands with different metals, and thirdly the nuclearity of the metal-ligand species that can form with the reaction of benzimidazole-based ligands with transition metals using differing concentrations and conditions.

Over the last quarter of a century a variety of benzimidazole-type chelating ligands have been prepared and their coordinating behaviour studied⁸⁻¹². Isele *et al*¹³ have investigated the tridentate ligand 1,2-bis(1*H*-benzimidazol-2-yl)-1,2-ethandiol, which is structurally analogous to the ligands synthesised for this investigation. A fundamentally interesting aspect of these linear tridentate ligands is the possibility for them to bind in a meridional or a facial fashion.

Even though benzimidazole-type ligands have a fairly simple synthetic process, little has been reported concerning their chemistry. This study intended to further develop knowledge of bis(benzimidazole)-based ligand coordination chemistry by the study of two

ligands, 1,2-di(1*H*-benzo[d]imidazol-2-yl)ethanol (**L1**) and its methylated derivative 1,2-bis(6-methyl-1*H*-benzo[d]imidazol-2-yl)ethanol (**L2**), as shown in Scheme 5.1. The coordination chemistry of these ligands was investigated with the late 3d transition metals copper(II), nickel(II), and cobalt(II).

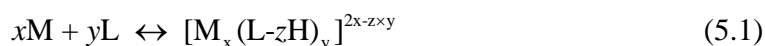


L	R
L1	H
L2	CH ₃

Scheme 5.1: Structures of the benzimidazole-based ligands **L1** and **L2** that were synthesised for this research.

*C denotes the chiral carbon in the structure.

The main aim for this project was to form $[ML_2]^{2+}$ complexes for both ligands and determine the diastereoselectivity of each metal-ligand species using circular dichroism (CD) experiments, see Section 5.3.3. The second key goal was to investigate the different complexes that formed with the ligands and the transition metal series. The general metal-ligand reaction can be described as follows:



Complexes of the specific form $[M(L-H)]_n$ were investigated also to determine if dimers, tetramers, or higher order helicates were being formed, as these had been reported for similar ligands^{13, 14}. These investigations were performed using CD combined with electrospray mass spectrometry (ESMS) techniques. Investigations of the complexes formed when a mixture of both **L1** and **L2** were reacted with the transition metals were also performed using ESMS in order to aid in identifying the nuclearity of species that were present.

5.1.2 Overview

Ligands of the bis(benzimidazole)-type with alcohol(s) present in the bridging unit have been reported to act as bidentate ligands, binding either through the two benzimidazole

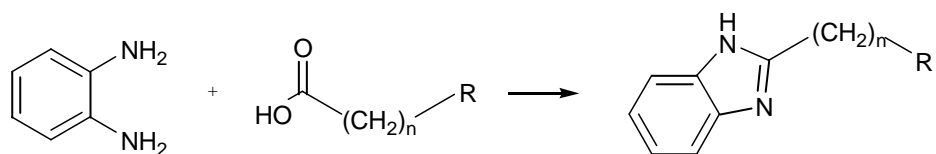
nitrogens or one benzimidazole nitrogen and the deprotonated alcohol group. However, with deprotonation of the alcohol there is also the potential for the ligands to act as tridentate chelating ligands, binding with both benzimidazole nitrogens and the deprotonated alcohol. It has been theorised that the ligands deprotonate when bridging occurs between two or more metals, this loss of the hydrogen at the alcoholic group allowing the oxygen atom to bridge between two or three metal ions. In such cases the ligands have the capability to form both monomeric and oligomeric species, such as strongly exchange coupled dimers and tetramers ¹⁵.

The potentially tridentate ligands **L1** and **L2** exist as two chiral isomers, *R*-**L** and *S*-**L**. For this work the chiral (*R*) and an achiral mixture (*R,S*) were synthesized using enantiomerically pure L- or racemic DL- malic acid respectively. The chiral (*S*) form, resulting from D-malic acid, was not synthesised as part of this study. The chirality of the ligands are an additional feature of bis(benzimidazole)-type ligands that provide an attractive prospect, for example enantioselective catalysis ¹⁶. In addition, it enabled us to investigate the chiral complexes by CD. The chirality of such ligands has been reported to be significant, especially with crystal formation ¹⁵. The studies were also aided by the fact that the only major dissimilarity between the two ligands **L1** and **L2** was the mass difference due to the additional methyl groups present on the benzene ring for **L2**. This difference in mass enabled the two ligands, and the complexes they formed, to be distinguished by their respective mass spectrums.

5.1.3 Bis(benzimidazole)-based Chelating Ligands

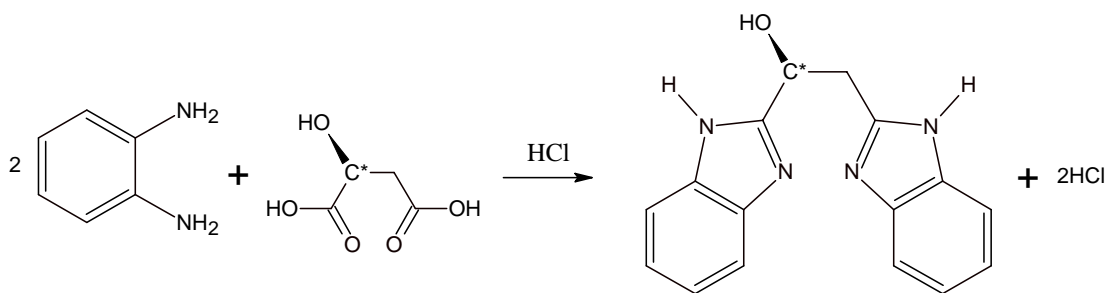
5.1.3.1 Basic Synthetic Process

As previously mentioned, the synthesis of benzimidazole-based ligands is a relatively straightforward process. The most direct method is via a ring-closure reaction of a 1,2-diaminobenzene moiety with a carboxylic acid group, as described in Scheme 5.2.



Scheme 5.2: The synthesis of a benzimidazole analogue from 1,2-diaminobenzene and a carboxylic acid where R represents various substituents.

Carboxylic acids are abundant and therefore altering the variable R of the carboxylic acid group can lead to the synthesis of widely different and interesting benzimidazole-based ligands that can act as chelating ligands. The variation of R obviously has great influence on the properties and complexes of each ligand and the synthesis of such variations is a feasible and attractive prospect¹⁷. For instance, in our research R was a 2-hydroxyethanoic acid group, resulting in the synthesis of an unsymmetrical bridging unit in the bis(benzimidazole)-based ligand, as shown in Scheme 5.3. Some of the different variations of such bis(benzimidazole) ligands, and their resulting chemistry, is discussed below.



Scheme 5.3: General reaction scheme for the synthesis of the benzimidazole-based ligands for this study.

5.1.3.2 Coordination Chemistry

Research has shown that ligands based on bis(2-benzimidazole) analogues have the ability to form supramolecular aggregates with d^{10} metal ions¹⁸. Both ligands investigated in this study, **L1** and **L2**, are, from a structural point of view, somewhat flexible, especially when compared to similar analogues such as bipyridine, due to the presence of the $-\text{CH}_2\text{-CH(OH)}-$ bridging unit between the benzimidazole moieties. If the nitrogen on each benzimidazole moiety can coordinate to a metal centre, with the deprotonated hydroxy group also potentially coordinating, then the ligands may act as μ_2 -bridging ligands. From examples of such architectures¹⁹⁻²¹ it can be demonstrated that ligands with some flexibility and little spatial hindrance are very efficient for constructing helical polymers. Thus, the coordination chemistry of the ligands **L1** and **L2** was considered to be worth exploring, as they both are moderately flexible, versatile ligands that have several potential binding modes that could potentially lead to structural varieties such as the formation of

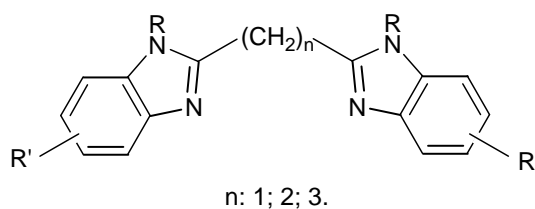
oligomeric helical structures. Such complexes potentially have interesting structural, spectroscopic, magnetic and catalytic properties.

5.1.3.3 Variations of the Bridging Unit

A variety of bis(benzimidazole)-based chelating ligands have been used in supramolecular coordination chemistry¹⁴, which is the area of interest for this research. Many different spacers, that is the $-(CH_2)_n-$ unit in Scheme 5.2 where R is a second carboxylic acid group, have been used in order to synthesise bis(benzimidazole)-based ligands with particular coordination properties. The ligands are made of two bi- or tridentate binding units, linked by the spacer or bridging unit, which can be easily varied.

Carbon Bridge

The generic structure of a bis(benzimidazole)-based ligand, represented in Scheme 5.4, is comprised of one, two or three carbon-atom spacers. Interestingly, such ligands have unusual coordination geometries when complexed with transition metals, such as copper(II). The geometry of the complex is determined to a large degree by the structure of the ligand, and the coordination chemistry of these ligands can be explained by the ligand's bidentate nature, as they coordinate through the two benzimidazole nitrogens, which can result in six-, seven- and eight-membered chelate rings depending on the length of the spacer^{22, 23}. For instance, a tetrahedral coordination is imposed when a three carbon spacer is used as the bridging unit, resulting in an eight-membered chelate ring^{10, 24}.



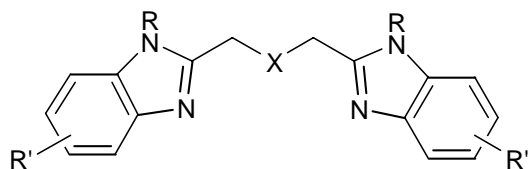
Scheme 5.4: General structure of the bis(benzimidazole)alkanes where R and R' represent various substituents.

Sulphur and Oxygen Atoms in the Bridge

The incorporation of sulphur or oxygen atoms in the linking chain of bis(benzimidazole) ligands has also been reported, as shown in Scheme 5.5. Such spacers are commonly comprised from three to eight atoms with a varying number of thioether or ether groups

present in the chain ²⁵. The coordination chemistry of ligands with a spacer length of 3 or 5 atoms, containing only one sulphur or ether group has been well documented. For instance, with dinuclear methoxo, ethoxo and propoxo-bridged complexes the bis(benzimidazole)alkane acts as the end-capping ligand, completing the basal plane of the four or five-coordinated copper(II) ion ²⁶.

In all coordination compounds with copper(II), nickel(II) and cobalt(II) the ligands are tridentate, coordinating via the two benzimidazole nitrogens and the sulphur or oxygen donor of the linking bridge ^{14, 27-29}. The steric constraints of these ligands are an important parameter as the relatively bulky ligands provide sufficient rigidity in order to control the stereochemistry of the complex.

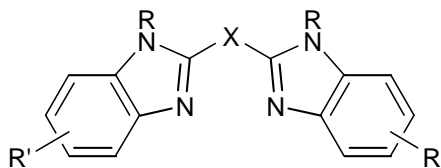


X: O; S; CH₂-O-CH₂; CH₂-S-CH₂; S-CH₂-CH₂-S.

Scheme 5.5: General structure of bis(benzimidazole)-based ligands containing an ether or thioether group in the linking chain where R and R' represent various substituents.

Alcohol Atoms in the Bridge

Only very few coordination compounds of bis(benzimidazole)-based ligands containing one, two or four alcohol groups in the linking chain have been reported ³⁰⁻³³. The chain length in such ligands can range from three to five carbon atoms, as shown in Scheme 5.6. It was this type of ligand, with alcohol groups present in the bridge, that were synthesised for our research. In Scheme 5.6, X = CH₂-CHOH for our ligands. In the complexes formed with these ligands, that is di- and tri- nuclear copper(II), nickel(II) and cobalt(II) complexes, the alcohol is deprotonated and can bridge two metal(II) atoms with each benzimidazole unit binding to a different metal(II) ion ³⁰.



X: CH₂-CHOH; (CHOH)₂; (CHOH)₄; CH₂-CHOH-CH₂; (CH₂)₂-CHOH-(CH₂)₂.

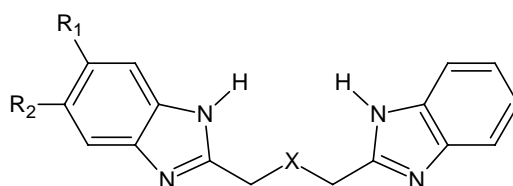
Scheme 5.6: General structure of bis(benzimidazole)-based ligands containing one, two or four alcohol groups in the linking chain where R and R' represent various substituents.

5.1.3.4 Substituted Variants

The structures given in the previous section all contained unspecified substituents denoted by R and R', therefore the type of substituents has not yet been introduced. If such features as the ring substituents are changed, and/or if there is a deviation in the bridging section as described in the previous section, the electron distribution and consequently the coordination ability of such derivatives are affected^{34, 35}. The N-R substituent in Scheme 5.6 represents, for our study, a proton. However, Broughton *et al*²⁸ carried out a study that varied the N-R substituent by introducing either a long octyl chain or a 3,5-(OMe)₂C₆H₃CH₂ component. It was observed that upon complexation with copper(II) a distorted tetrahedral character was favoured by the seven-membered chelate ring, rather than the square-planar or five-coordinate trigonal-bipyramidal, or square-based pyramidal structures that copper(II) tends to adopt with nitrogen ligands in the absence of bulky ligand substituents³⁶⁻³⁹. Comparison with other results in the literature, coupled with simple molecular mechanics calculations, suggested that the unexpected geometry might have been due to the fact that puckering was limited by the presence of two double bonds in the ring.

The aromatic protons have rarely been reported as substituted, though it is easy to introduce chloro, nitro, trifluoromethyl, methyl, or similar groups^{28, 32}. As part of this research a methyl group was substituted for a hydrogen atom on the benzene moiety. However, systematic studies showing the influence of substituents on electronic and steric properties of the complexes are still rare³². Lockhart *et al*²⁹ developed a synthetic route for bis(benzimidazole) ligands with built-in asymmetry, resulting from having different substituents on each benzimidazole moiety, such as a methyl group on only one

benzimidazole unit, as shown in Scheme 5.7. The resulting copper(II) complexes were found to be five coordinate, lying between perfect square-based-pyramidal and trigonal-bipyramidal extremes.



Scheme 5.7: Structure of bis(benzimidazole) ligand with in-built asymmetry, for example with R₁ and R₂ being methyl groups ²⁹.

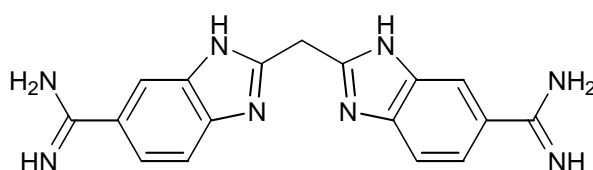
In each case the ligands acted as tridentate donors, coordinating through the imine nitrogens of the benzimidazole moieties and the ether donor atom of the linking bridge. Lockhart compared symmetrical bis(benzimidazole) complexes with the asymmetric complexes formed and demonstrated there was no significant change in the geometrical parameters around the copper(II) ion with the introduction of asymmetry and the subsequent change of pK_a within the bis(benzimidazole) fragment. Rather, Lockhart observed that the degree of hydrogen bonding, the solvent used for the crystallisation, and the nature of the anion had a greater impact on the geometrical parameters and coordination environment of the copper(II) ion. This observation supports the assumption in our study that comparable complexes should form with both **L1** and **L2**, with the only difference being the molecular mass of the ligands and subsequent complexes, provided the conditions of the experiment are constant.

5.1.3.5 Applications

The steady interest in bis(benzimidazole)-based chelating ligands over the last few years has led to many studies in the field of bioinorganic model chemistry based on the coordination compounds formed with such ligands, the aim being to mimic the active sites of metalloproteins ^{28, 40-42}. When the ligands coordinate to transition metals, it is believed that they react selectively towards certain biological substrates ⁴³. In the biological system the metal ions are anchored in the protein by at least one, but often two or three, histidyl

nitrogen atoms. The metal ions in the active sites often show unusual distorted coordination geometries which may be due to the steric constraints of the protein backbone ⁴⁴. Benzimidazole-based chelating ligands provide sufficient steric bulk and rigidity to impose similar unusual, distorted coordination geometries ^{27, 29}. Further, the possibility of π - π stacking interactions may be seen as another constraint favouring the unusual coordination geometries observed, and bis(benzimidazole) moieties enable significant π -stacking to occur between the ligands, which can further enable the formation of supramolecular structures. It has been shown that among the many possible intermolecular interactions, noncovalent interactions between aromatic rings are of particular importance in controlling the stacking of aromatic molecules as well as influencing the conformational preferences and development of supramolecular assemblies ⁴⁵⁻⁴⁸.

Bis(benzimidazole) ligands are also known and utilised for their biological activity. Ligands possessing a bis(benzimidazole) framework have been studied for their antitumor, antiproliferative, and antiviral activity ^{49, 50}, as well as for their cytotoxicity, antifungal and antimicrobial activity ⁵¹⁻⁵⁵. For example, the bis(benzimidazole) ligand bis(5-amidino-2-benzimidazolyl)methane, commonly named BABIM, constitutes a very important inhibitor of metalloproteases; the structure is depicted in Scheme 5.8. BABIM can bind to the zinc in the active site cleft by replacing a water ligand and thus inhibiting catalytic activity. Understanding the structural basis of the zinc-mediated inhibition has been led by Katz *et al* and Stevens *et al* ^{56, 57}.



Scheme 5.8: Structure of the metalloprotease inhibitor BABIM (bis(5-amidino-2-benzimidazolyl)methane).

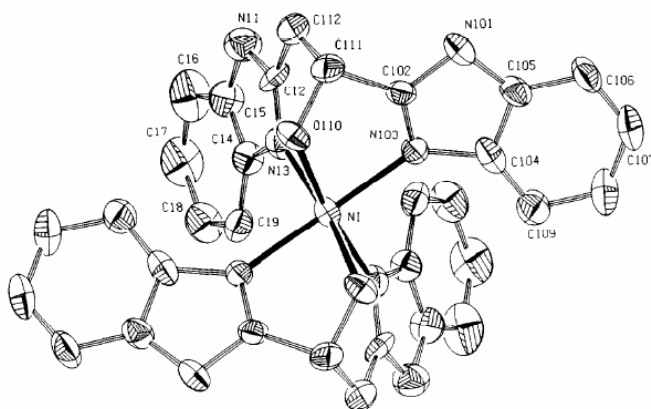
5.1.4 Stereoselectivity of ML_2 Complexes

5.1.4.1 Chirality

Complexes of the type ML_2 that have been formed from racemic mixtures of chiral ligands may exist as either the heterochiral complex $[M(R-L)(S-L)]$ or as a racemic mixture of the

homochiral complexes ($[M(R-L)_2]$ and $[M(S-L)_2]$)⁵⁸. The lability of a helical system may be conveniently measured by studying the rate of conversion between (*P*)- and (*M*)- helices formed by either *R* or *S* chiral ligands in solution⁵⁹. The stereoselectivity upon formation of such binary complexes of metal ions with optically active chelating agents has been the subject of numerous studies^{60, 61}. In this study the diastereoselectivity of ML_2 complex formation with the ligands **L1** and **L2** and the transition metals copper(II), nickel(II) and cobalt(II) were investigated. The stereochemistry of each metal complex was determined to be quite different. Additionally, it was also observed that changing the ligand from **L1** to **L2** altered the stereochemistry for some metals.

Previous research with the ligand **L1** by Van Albada and co-workers¹⁵ has demonstrated that the ligand **L1** can behave as a facially coordinating, tridentate ligand. **L1** was reported to form mononuclear complexes of the general form $M(L1)_2(anion)_2$ with metal ions such as copper(II), nickel(II), and zinc(II) and for a variety of anions. These complexes were described for the ligand in the (*R,S*) racemic form, but they also showed a few cases of metal complexes for the *S-L1* chiral form. Their research demonstrated that the deprotonated alcohol group coordinated to the metal centre; for example, with nickel(II) as the metal ion the ligand was observed to form an octahedral complex $[Ni(R-L1)_2]^{2+}$, shown in Figure 5.1. Interestingly, pure solid compounds of the chiral *S-L1* ligand could not be produced with nickel as the complexing ion. Hence, it was observed that the chiral species $Ni(S-L1)_2^{2+}$ may require a $Ni(R-L1)_2^{2+}$ to pack appropriately and enable the complex to crystallise.



Most complexes obtained were with the racemic mixture of the ligand as only a few complexes were reported to be isolated from the chiral isomeric ligand. The formation of a dinuclear species of the formula $[\text{CuCl}(\mathbf{L1})]_2(\text{H}_2\text{O})_2\text{Cl}_2$ were also described; it appeared to be formed with a bridging ligand and a bridging chloride anion, and was detailed for both the chiral (*S*) and racemic (*R,S*) forms of the ligand ¹⁵. Tetranuclear species were also reported with the formula $[\text{Cu}_4(\mathbf{L1})_4](\text{anion})_4(\text{EtOH})_x$, but only for copper nitrate and copper perchlorate. However, no solid compounds could be obtained for Co(II) and Mn(II) with either the racemic or chiral ligands ¹⁵.

The IR spectra of all compounds with the same stoichiometry were reported to be very similar, excluding the vibrational effects from the different anions that were present. It was found that the IR spectra for the *S* and *R,S* products hardly differed, supporting similar coordination modes for both ligands ¹⁵.

5.1.4.2 Theory

To determine the stereoselectivity of a helical compound the formation constants for the reaction $\text{M} + 2\text{L} \leftrightarrow \text{ML}_2$ are different for the optically pure ligand than for a racemic mixture. The most common technique employed to determine the stereoselectivity of complex formation is with acidimetric titration curves of 1:2 metal-ligand ratio mixtures. In this technique the titration of the optically pure ligand is compared to the titration with an equimolar mixture of both enantiomers ⁶¹. However, determination of stereoselectivity by means of this technique is limited by several restrictions, the most obvious being that the only suitable ligands are proton donors that must be used in stoichiometric amounts and in aqueous solutions. As the species of interest are determined indirectly by the proton activity, the sensitivity of the method is limited by the precision with which proton activity can be measured.

The acidimetric titration technique could not be applied to our studies to determine the stereoselectivity of the ML_2 complexes as the ligands **L1** and **L2** were insoluble in aqueous solutions. Bernauer and collaborators ⁶¹ have described another technique based instead on CD titrations. The technique involves studying the changing CD spectrum of complexes as the *R*- to *S*-ligand ratios are varied. This involves a continuous variation of the relative amounts of the two ligand enantiomers, with the total ligand concentration kept constant,

enabling a comparison of the CD intensity of the optically pure compounds relative to those of the mixtures. Thus, this enables the direct determination of the ratio of the stability constants and, therefore, of the diastereoselectivity, S , which is defined as a ratio of the formation constants, $K_{\text{meso}}/K_{\text{rac}}$. A value of S greater than one implies greater stability of the heterochiral *meso* form, and subsequently S less than one implies a preference for the formation of the homochiral species. Quantitative formation of the 1:2 species is ensured by using the ligand in sufficiently high excess. If the measurements are performed at wavelengths at which the free ligand shows no CD activity, the signal measured will be due only to $[\text{M}((R)\text{-L})_2]$ and $[\text{M}((S)\text{-L})_2]$ complexes, which have the same CD intensity but opposite sign. The concept is represented below in Equation (5.2).

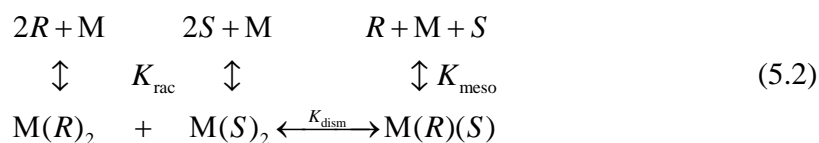


Figure 5.2 shows calculated curves of the changing relative CD intensities at three different stereoselectivity S values as a function of the concentration ratio $[(R)]/[(S)]$. For the case where $S = 1$, that is where there is no stereoselectivity, a straight line between the two extreme values for the two pure optically active enantiomers is obtained. Any deviation from this straight line indicates a nonstatistical distribution of the three complexed species, $\text{M}(R)_2$, $\text{M}(S)_2$, and $\text{M}(R)(S)$ and hence result in an observed CD signal. If the reaction is in favour of the mixed species, that is when $S > 1$, the deviation from linearity steadily increases with higher selectivity, but for reactions where $S < 1$ and there is higher stability of the optically pure species a limiting value is reached.

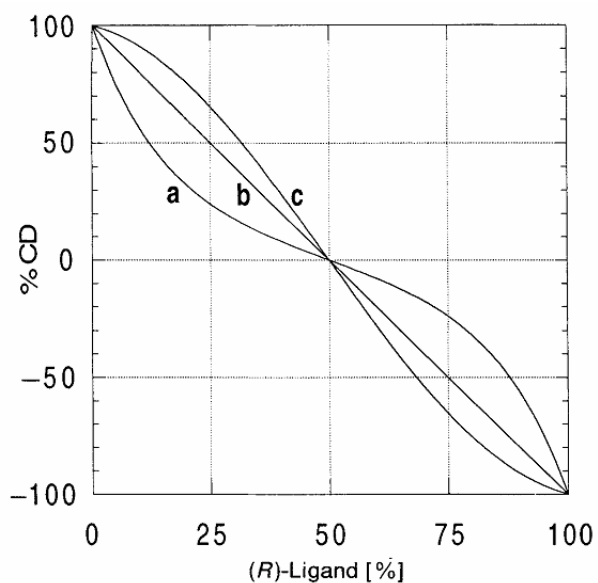


Figure 5.2: Calculated relative CD intensity as a function of the concentration ratio $[(R)]/[(S)]$ and the stereoselectivity S . $[M] = 5 \times 10^{-3}$ M, $[L]_{\text{tot}} = 5 \times 10^{-2}$ M, $K_{\text{meso}} = 109$. a) $S = 5$, b) $S = 1$, c) $S = 0.25$ ⁶¹.

Besides the stereoselectivity, the magnitude of the deviation from linearity depends on the ratio of the two enantiomers, $[(R)]/[(S)]$, and the excess of the ligand over the metal. As shown in Figure 5.3, for the salicylaldehyde derivative Bernauer and collaborators ⁶¹ investigated, it was determined that the best results were obtained for an enantiomeric ratio of 3 to 5 and a 10 to 100 fold excess of the ligand over the metal. However, this may not be the general case as such conditions are dependent on the equilibrium constant of the helicate formation as well as the concentrations of the metal and ligand in the reaction.

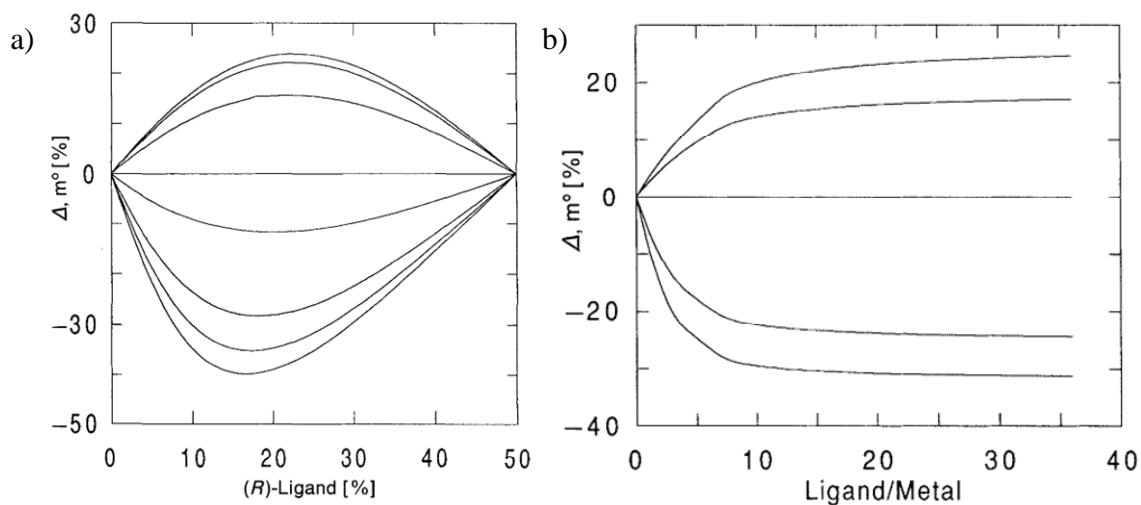
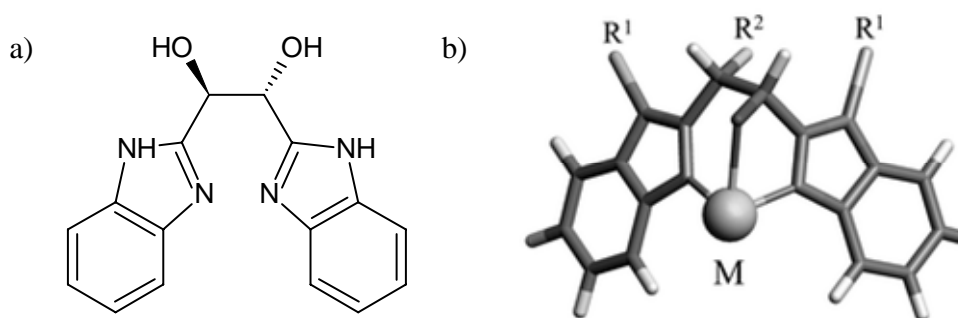


Figure 5.3: a) Deviation, % m°, from standard ($S = 1$) CD signal for various S . $[M] = 5 \times 10^{-3}$ M, $[L]_{\text{tot}} = 5 \times 10^{-2}$ M, $K_{\text{meso}} = 109$. Readings from the bottom upwards: $S = 10, 7.5, 5, 2, 1, 0.25, 0.05, 0.005$; b) Deviation % m°, from standard ($S = 1$) CD signal for $[(R)]/[(S)] = 30:70$ as a function of the ligand/metal ratio for various S . $[M] = 5 \times 10^{-3}$ M, $K_{\text{meso}} = 109$. Readings from the bottom upwards: $S = 10, 5, 1, 0.25, 0.05$ ⁶¹.

As the chemical properties of enantiomers of the free ligand are identical, the only chemical parameter changed for the different solutions in a series of measurements is the relative amount of the three complexes $[M(R-L)_2]$, $[M(S-L)_2]$ and $[M(R-L)(S-L)]$. Bernauer notes that, because the described method is based on a direct determination of the complexed species and can be easily applied to measurements in nonaqueous solutions, it can be extended to investigate the influence on stereoselectivity from secondary parameters such as temperature, ionic strength and so forth. However, the technique is limited to complexes where the CD spectra is due only to the optically active complexes, that is, there must be no CD signal for the free ligand at the wavelengths recorded, which was the case for our study.

5.1.5 Previous Studies

Isele *et al* ¹³ investigated the diastereoselectivity of the ligand represented in Scheme 5.9, which is an analogous ligand to the ligands investigated for our research, except there are two chiral carbons present in the bridging unit where ligands **L1** and **L2** have only one chiral centre.



Scheme 5.9: a) Structure of 1,2-bis(1H-benzimidazol-2-yl)-1,2-ethandiol; b) Model demonstrating the facial coordinating properties of 1,2-bis(1H-benzimidazol-2-yl) derivatives ¹³.

It was found that for this ligand a dramatic difference was evident between the diastereoselectivity of copper(II) and nickel(II) complexes. The variation of molar ellipticity with changing (S,S) / (R,R) ratio is shown in Figure 5.4. This difference was

presumed to be related to the different coordination geometries in the two cases. For the nickel complex Isele obtained a value of S of 0.44 in DMSO solution, implying a weak preference for the homochiral form. This homochiral complex was the form reported for the solid state, though it must be remembered that solid state and configurations in solution are not necessarily the same. In contrast to the nickel complex, a value of 0.01 was reported for the copper complex, showing instead virtually complete formation of the homochiral complex.

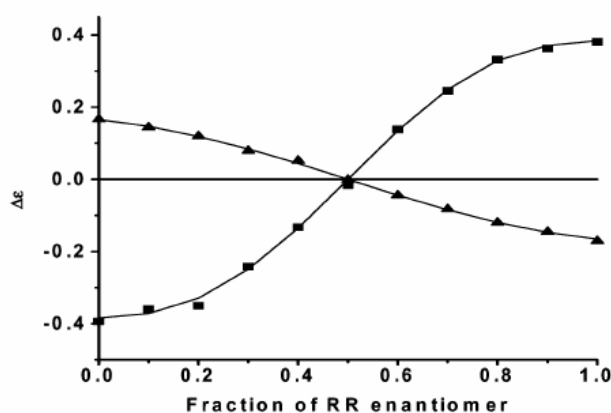


Figure 5.4: Variation in the molar ellipticity as a function of the $S,S/R,R$ ratio for the nickel(II) (▲) and copper(II) (■) complexes¹³.

5.2 Experimental

5.2.1 Instrumentation

NMR

^1H -NMR spectra for characterisation were recorded on a Varian Gemini at 300 MHz with tetramethylsilane (TMS) as the inner reference. Chemical shifts are given in parts per million (ppm), and abbreviations are as follows: s, singlet; d, doublet; t, triplet; q, quadruplet; m, multiplet; br, broad.

CD

CD spectra were recorded on a Jasco 710 spectrometer using thermostated quartz cells of path length 1.0 cm, a resolution of 0.5 nm, and at 25.0 °C.

ESMS

ESMS spectra were recorded on a Finnigan-Mat SSQ 7000 spectrometer at the Electrospray Mass Spectroscopy Laboratory at Geneva University.

UV/vis

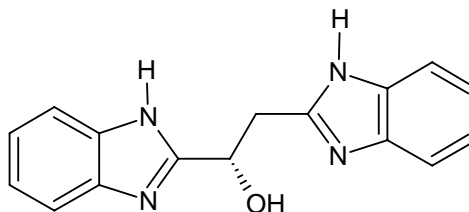
UV/vis spectra were recorded with a Perkin-Elmer Lambda 900 UV/vis/NIR machine at 25.0 °C.

5.2.2 Synthesis and Characterisation

Metal(II) perchlorate salts, L-malic acid, DL-malic acid, and 1,2-phenylenediamine were used as commercially available without further purification. *Safety note: Although no problems were experienced in handling perchlorate compounds, these salts when combined with organic ligands are potentially explosive and should be manipulated with care and used only in small quantities*⁶².

R-L1: (*R*)-1,2-di(1H-benzo[d]imidazol-2-yl)ethanol

The chiral ligand ***R-L1***, shown in Scheme 5.10, was synthesised from 1,2-phenylenediamine (7.25 g, 67 mmol) and L-malic acid (4.03 g, 30 mmol) which were dissolved in 6 M hydrochloric acid (50 mL). The solution was then heated to 120°C and refluxed for 24 hours. Upon cooling, green crystals of the chloride salt of the protonated ligand formed. The crystals were filtered and washed with ether then dissolved in 100 mL methanol, treated with activated charcoal and refluxed at 80°C for a minimum of 2 hours. The filtrate was then rotary evaporated to one-third of the original volume and on cooling a white precipitate formed. The precipitate was filtered, washed with ether and dried at 80°C under vacuum for 6 hours (6.13 g, 73.0 %). To obtain the neutral ligand, the solid was dissolved in water and excess NaOH added, which resulted in a white voluminous precipitate. The precipitate was filtered and washed with ether and dried overnight in a 60°C oven. The ***R-L1*** ligand was not soluble in water or methanol and ethanol. It dissolved easily in acetonitrile, DMSO and DMF.

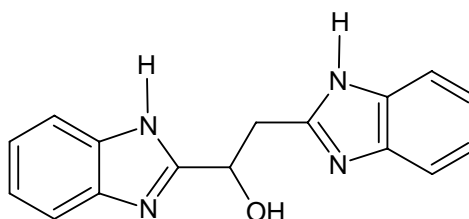


Scheme 5.10: Structure of the chiral ligand *R*-**L1** ((*R*)-1,2-di(1H-benzo[d]imidazol-2-yl)ethanol).

IR ν/cm^{-1} 3835w, 3736w, 3616w, 3524m, 2618br, 1809br(w), 1621w, 1588w, 1538m, 1486w, 1439s, 1318m, 1273s, 1223m, 1156m, 1073s, 1026s, 935m, 880m, 741s, 616m, 576m, 458w, 427m, 391w, 344w; **NMR** [DMF- d_6] δ_{H} (400MHz) 7.75(m, arom. H, 4H), 7.35(m, arom. H, 4H), 5.73(q, CH, 1H, $J = 4.4$ Hz), 3.92(d, CH_2 , 1H, $J = 4.4$ Hz), 3.89(d, CH_2 , 1H, $J = 4.4$ Hz); **ESMS** (DMSO) m/z 279.3(M^+), 257.0, 179.3, 174.4.

R,S-**L1**: (*R,S*)-1,2-di(1H-benzo[d]imidazol-2-yl)ethanol

The racemic ligand *R,S*-**L1**, shown in Scheme 5.11, was synthesised previously by Simon Verdan with a 74.2 % yield. The *R,S*-**L1** ligand was not soluble in water or methanol and ethanol. It was dissolved easily in acetonitrile, DMSO and DMF.



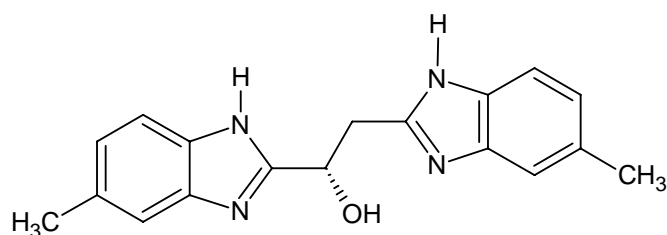
Scheme 5.11: Structure of the achiral ligand *R,S*-**L1** ((*R,S*)-1,2-di(1H-benzo[d]imidazol-2-yl)ethanol).

IR ν/cm^{-1} 3737w, 3602w, 3522m, 2617br, 1781br(w), 1621w, 1588w, 1538m, 1485w, 1433s, 1316m, 1272s, 1221m, 1156m, 1071s, 1026s, 933m, 880m, 741s, 616m, 577m, 457w, 426m, 384w, 353w; **NMR** [DMF- d_6] δ_{H} (400MHz) 7.74(m, arom. H, 4H), 7.34(m, arom. H, 4H), 5.73(q, CH, 1H, $J = 4.4$ Hz), 3.92(d, CH_2 , 1H, $J = 4.4$ Hz), 3.89(d, CH_2 , 1H, $J = 4.4$ Hz); **ESMS** (DMSO) m/z 279.3(M^+), 257.0, 179.4, 174.4.

R-**L2**: (*R*)-1,2-bis(6-methyl-1H-benzo[d]imidazol-2-yl)ethanol

The chiral ligand *R*-**L2**, shown in Scheme 5.12, was synthesised from 4-methylbenzene-1,2-diamine (7.32 g, 60 mmol) and L-malic acid (4.07 g, 30 mmol) which were dissolved in 6 M hydrochloric acid (50 mL). The solution was heated to 120°C and refluxed for 24 hours. Upon cooling, green crystals of the chloride salt of the protonated ligand formed. The crystals were filtered and washed with ether then dissolved in 100 ml ethanol, treated with activated charcoal and refluxed at 80°C for a minimum of 2 hours. The filtrate was

then rotary evaporated to approximately 10 mL volume, and on cooling a white precipitate formed. The precipitate was filtered, washed with ether and dried at 80°C under vacuum for 6 hours (3.0 g, 32.7 %). To obtain the neutral ligand, the solid was dissolved in water and excess NaOH added, which resulted in a white voluminous precipitate. The precipitate was filtered and washed with ether and dried overnight in a 60°C oven. The *R*-**L2** ligand was not soluble in water. It was partially soluble in methanol and ethanol, and dissolved easily in acetonitrile, DMSO and DMF.



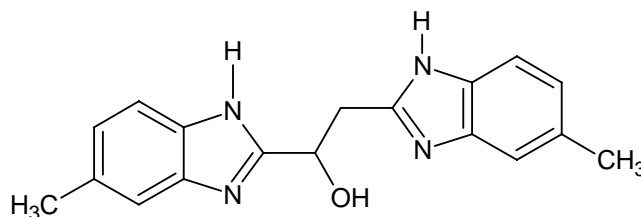
Scheme 5.12: Structure of the chiral ligand *R*-**L2** (*R*)-1,2-bis(6-methyl-1H-benzo[d]imidazol-2-yl)ethanol.

IR ν/cm^{-1} 3827w, 3737w, 3026br, 2108w, 1982w, 1868br(w), 1630m, 1595m, 1539m, 1445s, 1307s, 1279s, 1223m, 1184m, 1142m, 1089m, 1048s, 1021m, 943w, 854m, 794s, 599s, 563m, 429m, 400m; **NMR** [CD_3OD] δ_{H} (400MHz) 7.41(q, arom. H, 2H), 7.35(s, arom. H, H), 7.31(s, arom. H, H), 7.06(t, arom. H, 2H), 5.40(q, CH, 1H, $J = ?$ Hz), 3.57(d, CH_2 , 1H, $J = 4.4$ Hz), 3.54(d, CH_2 , 1H, $J = 4.4$ Hz), 2.49(s, CH_3 , 3H, $J = 4.4$ Hz); **ESMS** (DMSO) m/z 385.4, 308.4(M^+), 289.3, 179.1, 174.4.

***R,S*-L2:** (*R,S*)-1,2-bis(6-methyl-1H-benzo[d]imidazol-2-yl)ethanol

The racemic ligand *R,S*-**L2**, shown in Scheme 5.13, was synthesised from 4-methylbenzene-1,2-diamine (7.38 g, 60 mmol) and L,R-malic acid (4.06 g, 30 mmol) which were dissolved in 6 M hydrochloric acid (100 mL). The solution was then heated to 120°C and refluxed for 24 hours. Upon cooling, green crystals of the chloride salt of the protonated ligand formed. The crystals were filtered and washed with ether then dissolved in 100 mL ethanol, treated with activated charcoal and refluxed at 80°C for a minimum of 2 hours. The filtrate was then rotary evaporated to approximately 10 mL volume, and on cooling a white precipitate formed. The precipitate was filtered, washed with ether and dried at 80°C under vacuum for 6 hours. To obtain the neutral ligand, the solid was dissolved in water and excess NaOH added, which resulted in a white voluminous precipitate. The precipitate was filtered and washed with ether and dried overnight in a

60°C oven. The *R,S*-**L2** ligand was not soluble in water. It was partially soluble in methanol and ethanol, and dissolved easily in acetonitrile, DMSO and DMF.



Scheme 5.13: Structure of the achiral ligand *R,S*-**L2** (*R,S*)-1,2-bis(6-methyl-1H-benzo[d]imidazol-2-yl)ethanol.

IR ν/cm^{-1} 3836w, 3746w, 3616w, 3355m, 2917br, 2325m, 2074w, 1860br(w), 1631w, 1594w, 1531w, 1445s, 1416s, 1303s, 1820s, 1224m, 1173m, 1143m, 1070m, 1047m, 1015m, 943w, 858s, 797s, 597s, 550m, 433m 405m; **NMR** [CD_3OD] δ_{H} (400MHz) 7.42 (q, arom. H, 2H), 7.35(s, arom. H, H), 7.32(s, arom. H, H), 7.05(t, arom. H, 2H), 5.39(q, CH, 1H, $J = 4.4$ Hz), 3.58(d, CH_2 , 1H, $J = 4.4$ Hz), 3.54(d, CH_2 , 1H, $J = 4.4$ Hz), 2.49(s, CH_3 , 3H, $J = 4.4$ Hz); **ESMS** (DMSO) m/z 307.3(M^+), 257.0, 179.1, 174.1.

5.2.3 Coordination Compounds

Metal complexes with the ligands *R*-**L1**, *R,S*-**L1**, *R*-**L2**, and *R,S*-**L2** were prepared from respective ligand solutions and the required metal salt, either copper(II), nickel(II), or cobalt(II). The metal salts used were hexaqua perchlorate salts.

The coordination compounds were initially prepared in ethanol due to the poor solubility of all ligands in water. Both *R*-**L1** and *R,S*-**L1** were also poorly soluble in ethanol. To overcome this difficulty, the ligands were slurried in ethanol and then dissolved with the addition of the metal salt solution. The compounds **ML** and **ML**₂ were obtained for all ligands, along with numerous by-products, which are further discussed in Section 5.3.4. The concentration of metal and ligand used in the solutions were approximately 5×10^{-3} M, with a slight ligand excess. When carefully adding the metal salt mixtures to the ligand solutions or slurries, blue/purple solutions were obtained with copper(II), light green solutions with nickel(II), and bold purple with cobalt(II).

For crystallisation attempts, different ratios of metal and ligands, along with different solvent mixtures, for instance varying the ratio of ethanol to water, were prepared in 2 mL volumes and left to stand at room temperature to slowly evaporate. Unfortunately no crystals were collected as most solutions evaporated to dryness before any crystals were seen to form. In the few solutions where crystals were observed they were too fine to be collected. Repeated attempts to grow them in greater yields proved unsuccessful.

5.2.4 CD Spectra

The CD spectra of both the chiral and achiral forms of **L1** and **L2** with the transition metals copper(II), nickel(II) and cobalt(II) were measured. The achiral forms resulted in no CD spectra apart from noise, as could be expected for racemic complexes. The spectra for the chiral ligands showed significant signal for all complexes. The solutions prepared were 1:1 metal-ligand ratios of approximate concentrations 5×10^{-3} M with a slight ligand excess, using ethanol as the solvent. The CD spectra of the chiral ligands complexes have been discussed in Section 5.3.1.

5.2.5 CD Titrations with NaOH and HCl

The CD spectra for the ligand *R*-**L1** and copper(II) were measured with acid (HCl) added to determine if protonating the ligand affected the coordination properties of the ligand. Measurements were run with no acid present, one equivalent acid, and excess acid. The measurement with excess acid was repeated after 12 hours to ensure that no slow kinetic processes, such as rearrangement of the complex, were occurring. No significant change in the CD spectra was observed after the 12 hour period.

The deprotonation of the metal-ligand complexes was investigated for all ligand-metal complexes with NaOH used as the base. The investigations were followed using both CD and ESMS measurements. The CD investigations were performed with the chiral ligands *R*-**L1** and *R*-**L2** with the transition metals copper(II), nickel(II), and cobalt(II) with no base added, one equivalent base, and excess base. The metal-ligand ratio was approximately 1:1, with concentrations of 5×10^{-3} M with a slight ligand excess, using ethanol as the solvent.

5.2.6 CD Titration Technique for Determining Diastereoselectivity

The solutions for the enantiomerically pure (*R*) and racemic (*R,S*) CD titrations were prepared as 2 mL solutions with increasing amounts of the *R,S* ligand in each solution. For each investigation nine solutions were prepared with the ratios of *R*:*R,S* as shown in Table 5.1. The solutions were prepared by mixing set ratios of the enantiomeric pure solution and racemic solution so the overall metal-ligand ratio remained constant.

Sample	1	2	3	4	5	6	7	8	9
<i>R</i> (mL)	2.0	1.75	1.5	1.25	1.0	0.75	0.5	0.25	0
<i>R,S</i> (mL)	0	0.25	0.5	0.75	1.0	1.25	1.5	1.75	2.0

Table 5.1: Solution components for enantiomerically pure (*R*) and racemic (*R,S*) CD titrations.

The preliminary titrations for **L1** were run at 1:2 metal-ligand ratios. The solutions were prepared in ethanol at the concentrations detailed in Table 5.2, with an excess base concentration of 0.15 M (NaOH).

	[M] (mol/L)	[<i>R</i> - L1] (mol/L)	[M] (mol/L)	[<i>R,S</i> - L1] (mol/L)
Cu(ClO ₄) ₂ ·6H ₂ O	2.451×10^{-2}	4.971×10^{-2}	2.677×10^{-2}	4.904×10^{-2}
Ni(ClO ₄) ₂ ·6H ₂ O	2.494×10^{-2}	4.954×10^{-2}	2.464×10^{-2}	4.875×10^{-2}
Co(ClO ₄) ₂ ·6H ₂ O	2.530×10^{-2}	4.943×10^{-2}	2.505×10^{-2}	4.886×10^{-2}

Table 5.2: Concentrations for solutions prepared for diastereoselectivity CD measurements in ethanol and metal-ligand ratio 1:2 for the ligands *R*-**L1** and *R,S*-**L1**.

Further titrations for both **L1** and **L2** were run at a 20-fold ligand excess, and used DMSO as the solvent. The solutions Table 5.3 required sonification and heating in order to dissolve in the DMSO solvent.

The CD of each solution was measured in the wavelength range 250 – 850 nm at 0.5 nm intervals and then the appropriate sections of the spectra chosen for analysis. Each solution prepared was also sampled for the ESMS study (see Section 5.3.1) to determine the nuclearity of the species formed.

	[M] (mol/L)	[<i>R</i> - L1] (mol/L)	[M] (mol/L)	[<i>R,S</i> - L1] (mol/L)
Cu(ClO ₄) ₂ ·6H ₂ O	0.0100	0.1996	0.0113	0.1985
Ni(ClO ₄) ₂ ·6H ₂ O*	0.0099	0.2027	0.0105	0.2006

Co(ClO ₄) ₂ ·6H ₂ O	0.0106	0.2026	0.0103	0.2014
	[M] (mol/L)	[<i>R</i> - L2] (mol/L)	[M] (mol/L)	[<i>R,S</i> - L2] (mol/L)
Cu(ClO ₄) ₂ ·6H ₂ O	0.0102	0.1967	0.0104	0.2001
Ni(ClO ₄) ₂ ·6H ₂ O	0.0100	0.1991	0.0104	0.2011
Co(ClO ₄) ₂ ·6H ₂ O	0.0102	0.1994	0.0104	0.2006

Table 5.3: Concentrations for solutions prepared for diastereoselectivity CD measurements in DMSO and 20-fold ligand excess for the ligands *R*-**L1**, *R,S*-**L1**, *R*-**L2**, and *R,S*-**L2**. *The CD results of nickel(II) with *R*-**L1** and *R,S*-**L1** were unsatisfactory and the experiments were rerun with the addition of [OH⁻] = 0.1 M. Any greater addition of NaOH resulted in precipitation of the metal hydroxide.

5.2.7 ESMS Investigation of [M(L-H)]_n Compounds

The solutions for the ESMS study were prepared at varying metal-ligand ratios and with changing **L1** and **L2** concentrations with no base, one equivalent, and excess base added. The base used for the solutions was 1 M aqueous NaOH as this meant only small volumes were required to be added to the metal-ligand solutions. These investigations were performed using the racemic forms of the ligands, *R,S*-**L1** and *R,S*-**L2**, with approximate concentrations of [**L**] = 3.0×10^{-3} M and [M] = 1.5×10^{-3} M. The solution series was comprised of the following M:(**L1/L2**) ratios: 1:2**L1**, 1:1**L1**, 1:½**L1**:½**L2**, 1:1**L1**:1**L2**, 1:1**L2**, and 1:2**L2**.

5.3 Results and Discussion

5.3.1 Preliminary CD and ESMS Investigations of Metal Complexes

CD

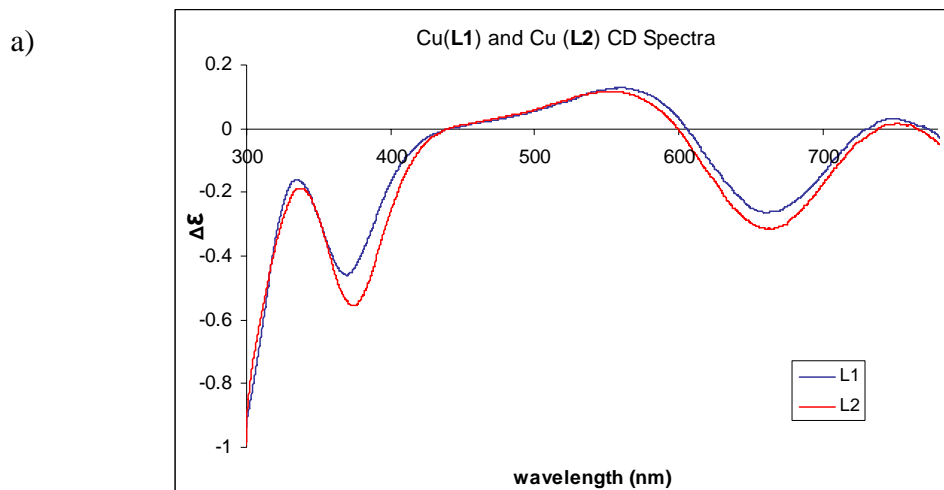
The CD spectra of both chiral ligands *R*-**L1** and *R*-**L2** were measured with the three transition metals: copper(II), nickel(II), and cobalt(II). The similarities and/or differences between the complexes formed with **L1** and **L2** can clearly be seen on the CD plots shown for each metal and both ligands in Figure 5.5.

There are clear similarities for the CD spectra with both ligands and copper(II), Figure 5.5a), which suggests that the coordination geometry and the dominant species formed are comparable for both **L1** and **L2**. This was further supported by the stereochemistry of the complexes, which was observed to be similar for both ligands, as discussed in Section 5.3.3.

The CD spectrum of **L1** and **L2** with nickel(II), Figure 5.5b), were also fairly similar with respect to both λ_{max} positions, although **L2** did have a higher peak intensity. This further supports the proposition that the substitution of a hydrogen for a methyl group on the benzimidazole moiety does not greatly influence the coordination geometry of the nickel(II) complex species and/or affect the dominant species that forms in solution. The species formed with **L1** and **L2** and nickel(II) were further investigated with ESMS studies as detailed in Section 5.3.4.

Cobalt(II), Figure 5.5c), also showed similar CD spectra for the ligands **L1** and **L2**. The CD spectra of the two ligands had λ_{max} positions at fairly similar wavelengths; however, there is a clear shoulder at 525 nm with **L1** that is not so evident with **L2**. Similar to the nickel(II) CD there are also deviations in signal strength between the two spectra. This may indicate that for the nickel(II) and cobalt(II) complexes the coordination geometry of **L1** and **L2** may slightly differ, or the major species formed may be different for each ligand.

These preliminary experiments with both ligands and the transition metals gave the primary indicators that generally similar coordination geometries were observed for the two very similar ligands, **L1** and **L2**.



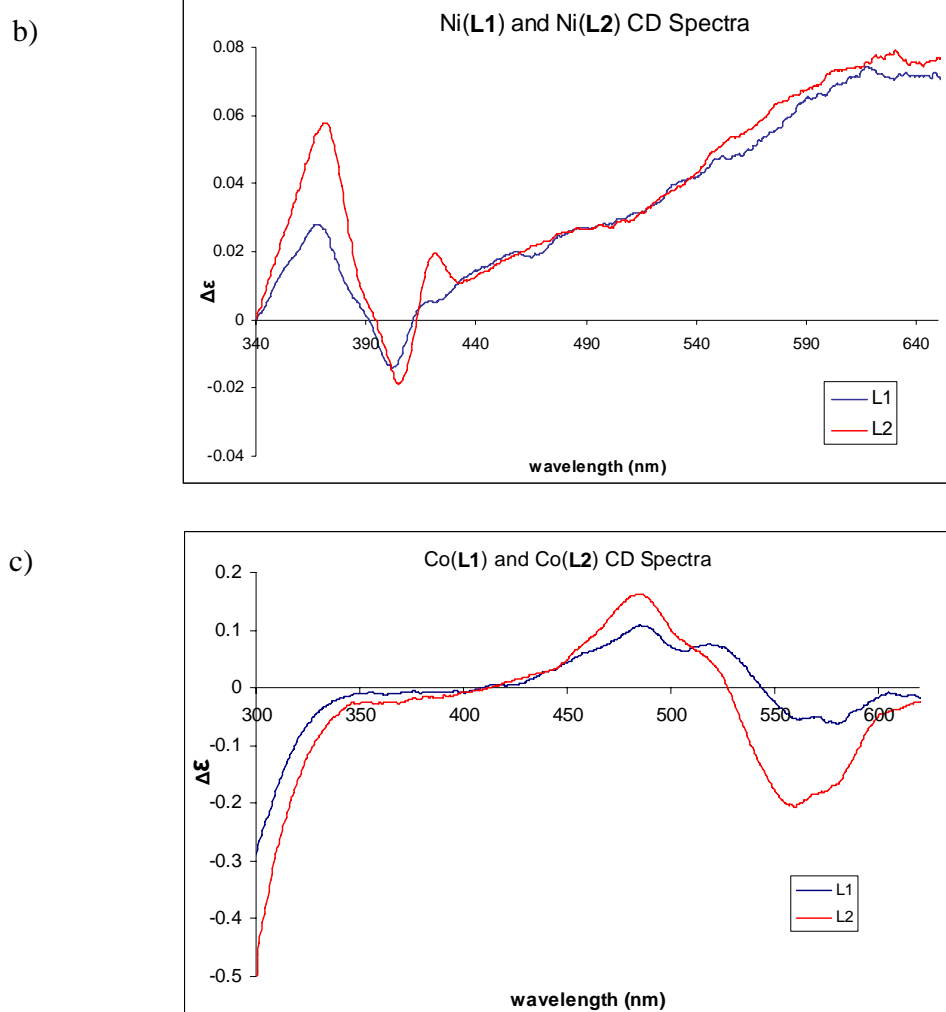


Figure 5.5: Plots showing the CD spectra of chiral ligands *R*-**L1** and *R*-**L2** when complexed with the transition metals in a 1:1 metal-ligand ratio: a) copper(II); b) nickel(II) and; c) cobalt(II).

ESMS

The ESMS investigations of the metal complexes were performed with both chiral and achiral forms of the ligands **L1** and **L2**. Comparable peaks were observed for the chiral and achiral forms of the ligands and studies showed no major changes in ESMS spectrum as the ratio of *R*-**L** to *R,S*-**L** was changed from 2*R*:0*R,S* → 0*R*:2*R,S*. Similarly, comparable species were observed to form for both **L1** and **L2**, with no new species identified when the ligand was changed from **L1** to **L2**. Hence, further discussions for ESMS results refer, for simplicity, only to **L**, which corresponds to the chiral and racemic forms of both ligands due to similar species being observed for both forms of both ligands.

Copper(II) ESMS investigations showed the major species present to be the dinuclear species $[\text{Cu}_2(\text{L-H})_2]^{2+}$, with smaller amounts of the species $[\text{Cu}_2(\text{L-2H})(\text{L-H})]^+$ present. However, the key species that was to be investigated for the diastereoselectivity study, $[\text{Cu}(\text{L-H})_2]^{2+}$, was present only in relatively small amounts. It was concluded that the solution conditions with only a 2-fold ligand excess were not optimal for the formation of the $[\text{Cu}(\text{L-H})_2]^{2+}$ species.

Similar to the copper(II) results, the ESMS study with nickel(II) initially used solutions of only 2-fold ligand excess. However, with nickel(II) the major species present, even at only 2-fold ligand excess, was identified to be $[\text{NiL}_2]^{2+}$, but numerous minor species were also observed, such as the trinuclear complex $[\text{Ni}_3(\text{L-H})_4]^{2+}$. The ESMS study with cobalt(II) showed the mononuclear $[\text{Co}(\text{L-H})\text{L}]^+$ to be the major species present, with the dinuclear $[\text{Co}_2(\text{L-H})_2\text{L}]^{2+}$ complex existing as a minor species.

To drive the speciation towards the desired 1:2 metal-ligand species, the experiments should be repeated with a 20-fold ligand excess. The solvent should also be changed to DMSO rather than ethanol due to the solubility of **L1** being too poor in ethanol at the concentrations required for a 20-fold ligand excess. Unfortunately the ESMS measurements at a 1:20 metal-ligand ratio were not performed due to technical problems, therefore it could not be confirmed that the major species present under 20-fold ligand excess conditions was in fact the $[\text{ML}_2]^{2+}$ species we wanted to investigate. As such, it was assumed from the method described in the literature⁶¹, and from previous research with analogous ligands under similar conditions,¹³ that the $[\text{ML}_2]^{2+}$ was the major species present with 20-fold excess of ligand.

5.3.2 CD Titrations

HCl

A titration with copper(II) and *R*-**L1** was performed in order to determine whether or not the coordination of the ligand changed, or if the complex would fall apart, as the acid concentration was increased and the nitrogen atoms on the ligand potentially became protonated. As is shown in Figure 5.6, changes in the CD spectra were observed, but it was noted that, under the conditions of an excess of protons, complexation was still present between copper(II) and *R*-**L1** as there was still significant CD spectra observed. Therefore

it could be inferred that the coordinate bonds between the ligand nitrogen atoms and the copper(II) ion were significantly strong so that even at a high acid excess the nitrogen atoms were still bound to the copper ion rather than being protonated. Alternatively, binding may also occur with the imine nitrogen, and protonation of the other nitrogen can be accommodated with dissociation of the complex. Even so, a clear change in the coordination geometry of the ligand may be inferred from the observed changes in the CD spectrum as acid was added to the complex. Rearrangement of the ligand around the metal ion has presumably occurred. For instance, the hydroxy group may in fact be protonated under excess acid conditions and hence not involved in complexation. Alternatively, as acid was added to the metal-ligand solution the speciation may have been altered; for example, an M_2L_3 species falling apart, but ML_2 remaining so that it becomes the dominant species present at high acid concentrations. The strength of the CD signal is not consistent with a shift to the monodentate coordination, hence chelation is evidently involved throughout.

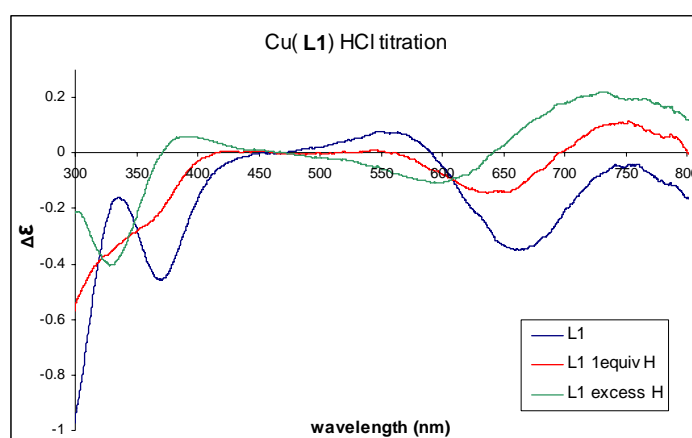


Figure 5.6: HCl titration with copper(II) and *R*-L1.

NaOH

Complexes of the ligands of the general form $[M_x(L-H_y)_z]^{n+}$ were investigated by NaOH titrations, as shown in Figure 5.7. The study involved increasing the concentration of base present in the complex solutions in order to deprotonate the hydroxy group and observe whether higher order species such as tetramers and helicates could form as the hydroxy group became involved in the bonding. The measurements aimed to determine the nuclearity of species present and also to observe the formation of new species as the base

concentration increased. Each CD measurement was also monitored by ESMS, so that changes in speciation could be supported by the appearance of new peaks in the mass spectrum. The measurements were performed for the metal-ligand solutions at a 1:1 ratio with no base, one equivalence added, and then $5 \times$ excess base added.

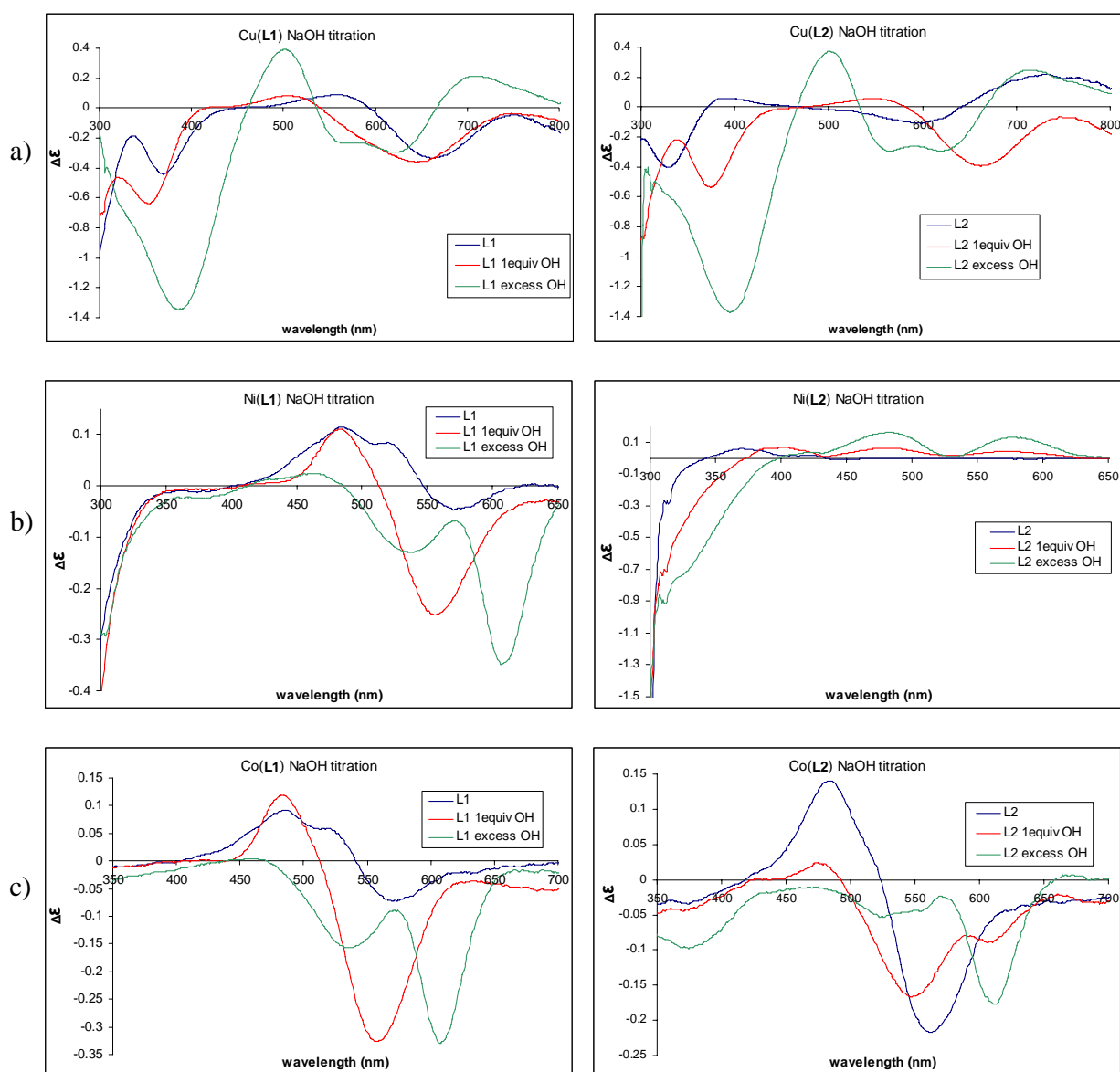


Figure 5.7: NaOH titrations with L1 (LHS) and L2 (RHS) and the transition metals in a 1:1 metal – ligand ratio: a) copper(II); b) nickel(II) and; c) cobalt(II).

The ESMS results for the study are shown in Table 5.4. The ESMS spectra were also measured at a 1:2 metal-ligand ratio with the same increasing base concentrations as

performed for the 1:1 investigations in order to determine whether the metal-ligand ratio affected the species that formed in solution. An example of the typical spectra obtained with the metal-ligand ESMS investigations has been provided in Figure 5.8.

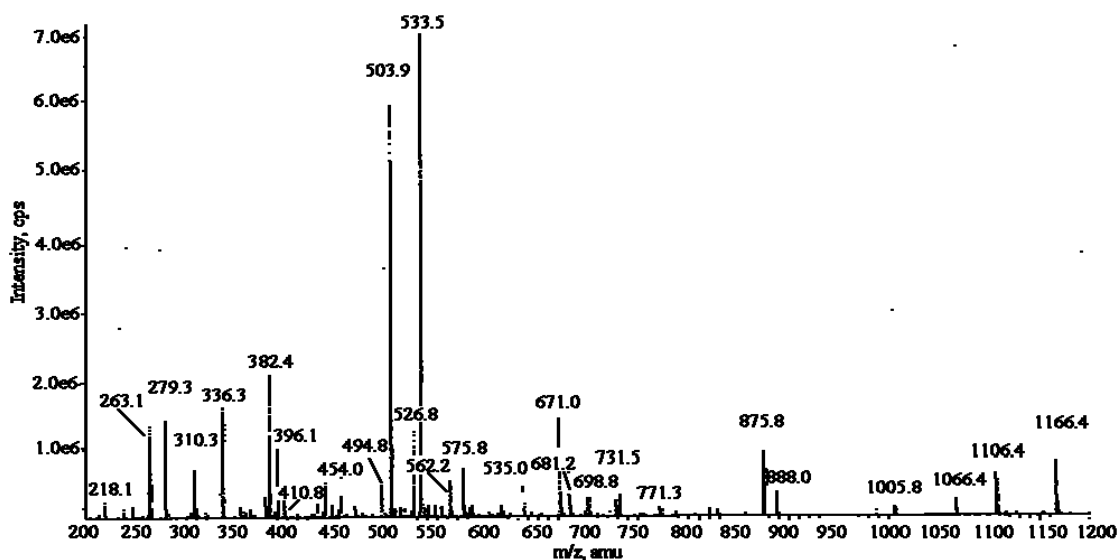


Figure 5.8: Example of a typical ESMS for the metal-ligand complexes: cobalt(II) and **L1** with no base present. The peak at 279.3 was identified as the free ligand, 503.9 as $[\text{Co}_3(\text{L1-H})_2(\text{L1-2H})]^{2+}$, and 533.5 as $[\text{Co}_4(\text{L1-2H})_3]^{2+}$.

In the ESMS study, no new species were observed to form as the base concentration was increased, but the relative concentrations of the species present did change and some species could no longer be observed in the ESMS spectrum. The same results were observed with the change in metal-ligand ratio; that is, there were no new species identified, but changes in the relative concentrations were again observed. Therefore it was concluded that the change in CD spectra seen with all metals, Figure 5.7, could be largely attributed to a change in the major species present in the solution rather than being due to the formation of new higher order complex species, as we were hoping to observe. Further, change in the oxygen-donor from a hydroxy group to a deprotonated oxygen atom may influence the way ligand chirality is induced in the metal centre, contributing to the change in CD with pH.

It can be seen from the cobalt(II) relative concentrations that as the pH was increased there was evidence of more clustering. The ESMS spectra with no base added had at least four species present as major peaks, whereas with excess base present the highly clustered M_4L_3

species is the only dominant species present. This trend was seen with both ligands **L1** and **L2** and would be expected due to their structural similarities. The general reduction in overall relative percentage of the metal complexes with increasing amount of base may be due the added base facilitating the formation of neutral species which cannot be detected by ESMS.

	ESMS m/z (% - free ligand)				
	$[\text{Cu}_2(\text{L1-H})_2]^{2+}$	$[\text{Cu}_2(\text{L1-H})(\text{L1-2H})]^+$	$[\text{Cu}_2(\text{L1-H})_2\text{ClO}_4]^+$		
no base	262%	107%	48%		
equivalent base	84%	20%	-		
excess base	48%	<10%	-		
	$[\text{Cu}_2(\text{L2-H})_2]^{2+}$	$[\text{Cu}_2(\text{L2-H})(\text{L2-2H})]^+$	$[\text{Cu}_2(\text{L2-H})_2\text{ClO}_4]^+$		
	$[\text{Cu}_2(\text{L2-H})_2]^{2+}$	$[\text{Cu}_2(\text{L2-H})(\text{L2-2H})]^+$	$[\text{Cu}_2(\text{L2-H})_2\text{ClO}_4]^+$		
no base	256%	183%	83%		
equivalent base	62%	12%	-		
excess base	79%	26%	-		
	$[\text{NiL1}]^{2+}$	$[\text{Ni}_2(\text{L1-H})_2]^{2+}$	$[\text{Ni}_4(\text{L1-2H})_3]^{2+}$	$[\text{Ni}_2(\text{L1-2H})(\text{L1-H})]^+$	$[\text{NiL1}_2\text{ClO}_4]^+ \cdot \text{H}_2\text{O}$
	$[\text{NiL1}]^{2+}$	$[\text{Ni}_2(\text{L1-H})_2]^{2+}$	$[\text{Ni}_4(\text{L1-2H})_3]^{2+}$	$[\text{Ni}_2(\text{L1-2H})(\text{L1-H})]^+$	$[\text{NiL1}_2\text{ClO}_4]^+ \cdot \text{H}_2\text{O}$
no base	63%	117%	83%	79%	42%
equivalent base	21%	<10%	<10%	24%	123%
excess base	-	-	24%	-	-
	$[\text{NiL2}]^{2+}$	$[\text{Ni}_2(\text{L2-H})_2]^{2+}$	$[\text{Ni}_4(\text{L2-2H})_3]^{2+}$	$[\text{Ni}_2(\text{L2-2H})(\text{L2-H})]^+$	$[\text{NiL2}_2\text{ClO}_4]^+ \cdot \text{H}_2\text{O}$
	$[\text{NiL2}]^{2+}$	$[\text{Ni}_2(\text{L2-H})_2]^{2+}$	$[\text{Ni}_4(\text{L2-2H})_3]^{2+}$	$[\text{Ni}_2(\text{L2-2H})(\text{L2-H})]^+$	$[\text{NiL2}_2\text{ClO}_4]^+ \cdot \text{H}_2\text{O}$
no base	34%	28%	-	49%	58%
equivalent base	-	-	-	13%	62%
excess base	62%	14%	-	22%	87%
	$[\text{Co}_2(\text{L1-H})_2]^{2+}$	$[\text{Co}_3(\text{L1-H})_2(\text{L1-2H})]^{2+}$	$[\text{Co}_4(\text{L1-2H})_3]^{2+}$	$[\text{Co}_2(\text{L1-2H})(\text{L1-H})]^+$	$[\text{CoL1}_2\text{ClO}_4]^+ \cdot \text{H}_2\text{O}$
	$[\text{Co}_2(\text{L1-H})_2]^{2+}$	$[\text{Co}_3(\text{L1-H})_2(\text{L1-2H})]^{2+}$	$[\text{Co}_4(\text{L1-2H})_3]^{2+}$	$[\text{Co}_2(\text{L1-2H})(\text{L1-H})]^+$	$[\text{CoL1}_2\text{ClO}_4]^+ \cdot \text{H}_2\text{O}$
no base	117%	417%	467%	100%	33%
equivalent base	-	30%	98%	8%	24%
excess base	-	-	32%	<10%	<10%
	$[\text{Co}_2(\text{L2-H})_2]^{2+}$	$[\text{Co}_3(\text{L2-H})_2(\text{L2-2H})]^{2+}$	$[\text{Co}_4(\text{L2-2H})_3]^{2+}$	$[\text{Co}_2(\text{L2-2H})(\text{L2-H})]^+$	$[\text{CoL2}_2\text{ClO}_4]^+ \cdot \text{H}_2\text{O}$
	$[\text{Co}_2(\text{L2-H})_2]^{2+}$	$[\text{Co}_3(\text{L2-H})_2(\text{L2-2H})]^{2+}$	$[\text{Co}_4(\text{L2-2H})_3]^{2+}$	$[\text{Co}_2(\text{L2-2H})(\text{L2-H})]^+$	$[\text{CoL2}_2\text{ClO}_4]^+ \cdot \text{H}_2\text{O}$
no base	51%	164%	247%	45%	-
equivalent base	-	12%	97%	<10%	37%

excess base	-	-	23%	<10%	-
-------------	---	---	-----	------	---

Table 5.4: Values showing the change in relative concentrations of complex species formed as the amount of base is increased. Percentages are given for each species signal compared to the signal height of the free ligand in the ESMS spectra, set at 100 %.

5.3.3 Determining Diastereoselectivity

The aim of this section of the project was to determine whether the ML_2 complexes formed with transition metals showed preference for the homochiral or mixed species, that is $[M(R-L)_2]$ or $[M(R,S-L)_2]$ respectively. The diastereoselectivity of complex formation for both ligands **L1** and **L2** was studied with the three transition metals copper(II), nickel(II), and cobalt(II), where the stereochemistry of complexation with each metal and ligand was observed to be quite different.

The CD titration technique described in the literature, and discussed in Section 5.2.6, that can be applied to determine the diastereoselectivity of a ML_2 complex was performed slightly differently in this study as the titrations were performed with $R-L$ and $R,S-L$, not $R-L$ and $S-L$. This is because the ligand $S-L$ was not synthesised as part of this project due to time constraints as once the experiments had been performed with $R-L$ and $R,S-L$ to ensure the technique was feasible there was not enough to continue on and synthesise $S-L$ and perform the required experiments. Clearly this could be done in the future to produce more complete data and results. Hence, this resulted in only 50% (R)-ligand being reached in the plot shown in Figure 5.2. However, the plot up to 50% provided sufficient information to determine the S value of the ML_2 complexes, as it can be seen that the three S values can be clearly distinguished from this first section of the graph. The actual S values were not calculated for the complexes, but the diastereoselectivity could still be easily identified from the curvature of each graph; that is, from the shape of the plot it could be determined whether S had a value greater than, equal to, or less than one and hence whether the complexes favoured homochiral or mixed formations.

1:2 Metal – Ligand Results

The experiments were performed as described in Section 5.2.4 and the results are shown in Figure 5.9. The 1:2 metal-ligand ratio used for this experiment was later proven from ESMS studies to not be a high enough ligand excess to ensure the dominant species present

to be the ML_2 species that was the target in an investigation of diastereoselectivity, therefore the change in CD spectra cannot be solely attributed to the change in diastereoselectivity of the ML_2 complex.

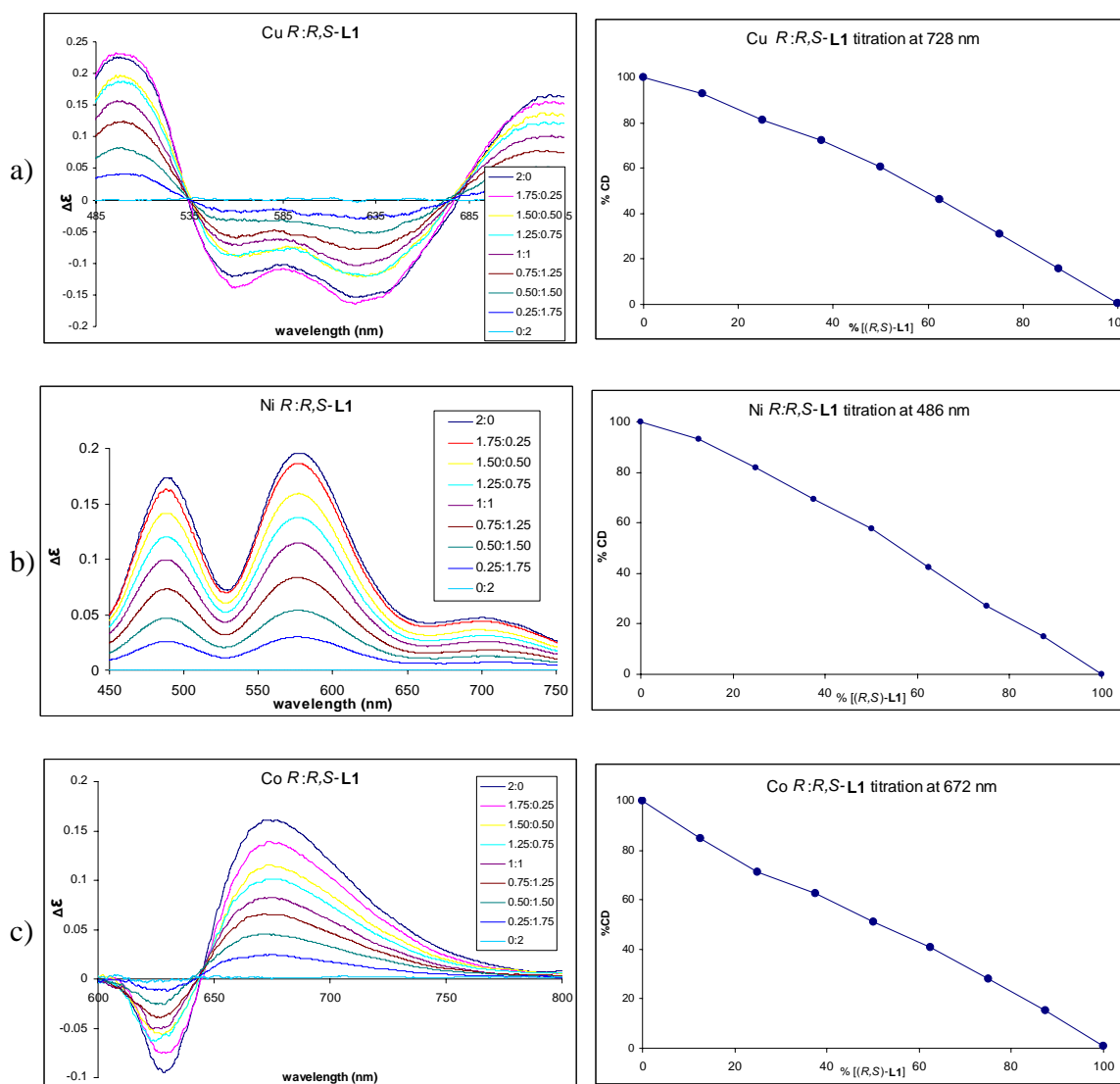


Figure 5.9: LHS: R -L1 series of increasing R,S -L1 ratio with the transition metals in a 1:2 metal-ligand ratio with ethanol as the solvent; RHS: Plots showing the calculated CD intensity as a function of the concentration ratio $[R-L1]/[R,S-L1]$ for a) copper(II); b) nickel(II) and; c) cobalt(II).

The CD spectrum with copper(II) showed a clear change in spectrum as the racemate ratio increased, with two zero points observed at 540 and 675 nm, Figure 5.9a(LHS). The change in CD% at one of the maximum wavelengths, 728 nm, showed an almost linear trend, Figure 5.9a(RHS). There is sufficient curvature, however, even in a situation where

ML₂ is not fully formed, to imply that a minor preference for the homochiral species exists. Quantification is not possible under conditions where there is not a single dominant species present and in any case, the effect is small. UV-Vis spectra of the solutions were also measured at each enantiometrically pure-racemic ratio, and these showed a slight increase in signal as the racemate ratio increased, but no change in shape or λ_{max} position.

For the nickel(II) *R*-L1 and *R,S*-L1 CD study no points with zero CD signal were observed, Figure 5.9b(LHS), but a clear change in the CD spectrum was still evident. The change in CD% at the maximum wavelength was also almost linear, as shown in Figure 5.9b(RHS), once again being indicative of no diastereoselectivity. The UV-Vis spectra showed a slight decrease in signal as the racemate ratio increased, but also showed no change in shape or λ_{max} position.

The cobalt(II) *R*-L1 and *R,S*-L1 CD study showed one zero point at 645 nm, Figure 5.9c(LHS), and also a fairly linear plot of the change in CD% at the maximum wavelength of 672 nm, shown in Figure 5.9c(RHS), once again indicating no ML₂ stereochemical preference. The UV-Vis spectra for Co(II) were not very useful as the absorbance was significantly greater than one in the wavelength range 450-650 nm, as could be expected for cobalt(II) complexes, and no change was observed in the spectra from 650-900 nm.

It could be concluded that, for the investigations represented in Figure 5.9, no significant preference for either the homochiral or the mixed ML₂ complex could be observed for any of the metals. As previously stated, this observation is compromised partly because experiments were performed at only a 1:2 metal-ligand ratio for which the ML₂ species was not excessively formed. Even though no stereoselectivity could be inferred, the preliminary experiments demonstrated that the CD titration technique should be a viable approach for determining the stereoselectivity, if the experimental conditions were optimised. Further, the results gave some indication that different preferences may exist for at least some transition metals, which should be more pronounced with further experimentations using increased ligand concentrations. This is shown below.

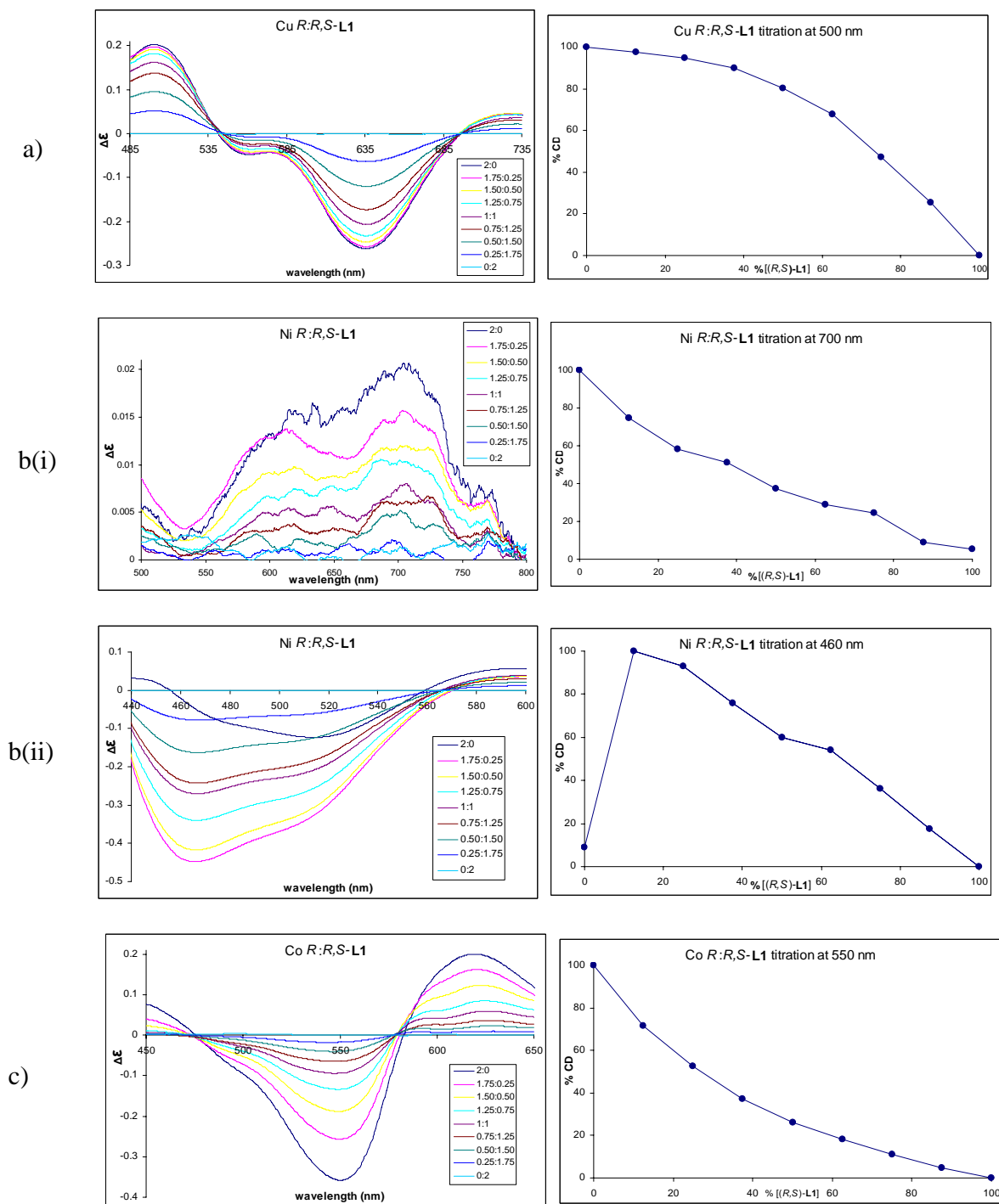


Figure 5.10: LHS: *R*-L1 series of increasing *R,S*-L1 ratio with the transition metals and a 20-fold ligand excess using DMSO as the solvent; RHS: Plots showing the calculated CD intensity as a function of the concentration ratio $[R-L1]/[R,S-L1]$ for a) copper(II); b(i) nickel(II); b(ii) nickel(II) with $\frac{1}{2}$ equivalence base (the first spectra at 2:0 *R*:*R,S* ratio appeared to be an outlier and as such it was not used in calculations), and; c) cobalt(II).

The experiments shown in Figure 5.10 were performed at a 20-fold ligand excess, with the ligands *R*-**L1** and *R,S*-**L1**, and in DMSO because of solubility considerations. The copper(II) CD spectrum had two zero points similar to the 1:2 ratio, that is at 540 and 690 nm. Compared to the previous experiment, the complexes formed showed clear stereochemical preferences. With the 20-fold ligand excess it could be seen that the ML₂ complex formed had a value of $S < 1$, indicating that the homochiral species was the preferred complex formed.

Unfortunately, the experiment with nickel resulted in a very small CD signal, hence a large amount of noise was present in the measurement. Even so, a small preference for the mixed ML₂ complex could be seen as S had a value slightly greater than one. The nickel(II) experiment was repeated to make sure that the poor CD signal was not due to experimental errors. However, the second experiment resulted in CD signals of the same magnitude and with considerable noise still present. The experiment was repeated a third time, Figure 5.10b(ii)(LHS), with half-equivalence of base added to the complex. The addition of base resulted in not only a clear increase in the signal strength, but also a very distinct change in the shape of the spectra. For this measurement one zero point was observed at 570 nm. The plot of CD% against the ratio of racemic ligand, Figure 5.10b(ii)(RHS), showed an almost linear plot, indicating no stereochemical preference for the nickel(II) ML₂ complex. To ensure that the addition of half-equivalence of base did not influence the speciation and consequently alter the CD spectra for the other metal-ligand complexes the experiments were also repeated with half-equivalence of base added. However, for these experiments, unlike for nickel(II) with **L1**, the CD spectra did not change with the addition of the base.

The cobalt(II) CD spectra showed two zero points at 475 and 575 nm and, in contrast to the copper(II) results, the cobalt(II) ML₂ complex had a clear preference for the mixed species as an S value greater than one could be seen. Therefore, each metal showed a different diastereoselectivity with **L1**. Copper(II) had a preference for the homochiral [M(*R*-**L**)₂] species, nickel(II) showed no clear preference for either species, and cobalt(II) showed a preference for the mixed species [M(*R,S*-**L**)₂]. This difference in the diastereoselectivity between the metal ion complexes could presumably be related to the different preferred coordination geometries of the three transition metals, or different

preferred metal-donor bond distances affecting the bite of the chelate and hence ring conformations and steric interactions. The results for copper(II) and nickel(II) were similar to what had been previously seen for the similar ligand investigated by Isele *et al*¹³. That is, nickel(II) showing only a slight preference for homochiral complex and copper(II) showing a clear selectivity for homochiral ML₂.

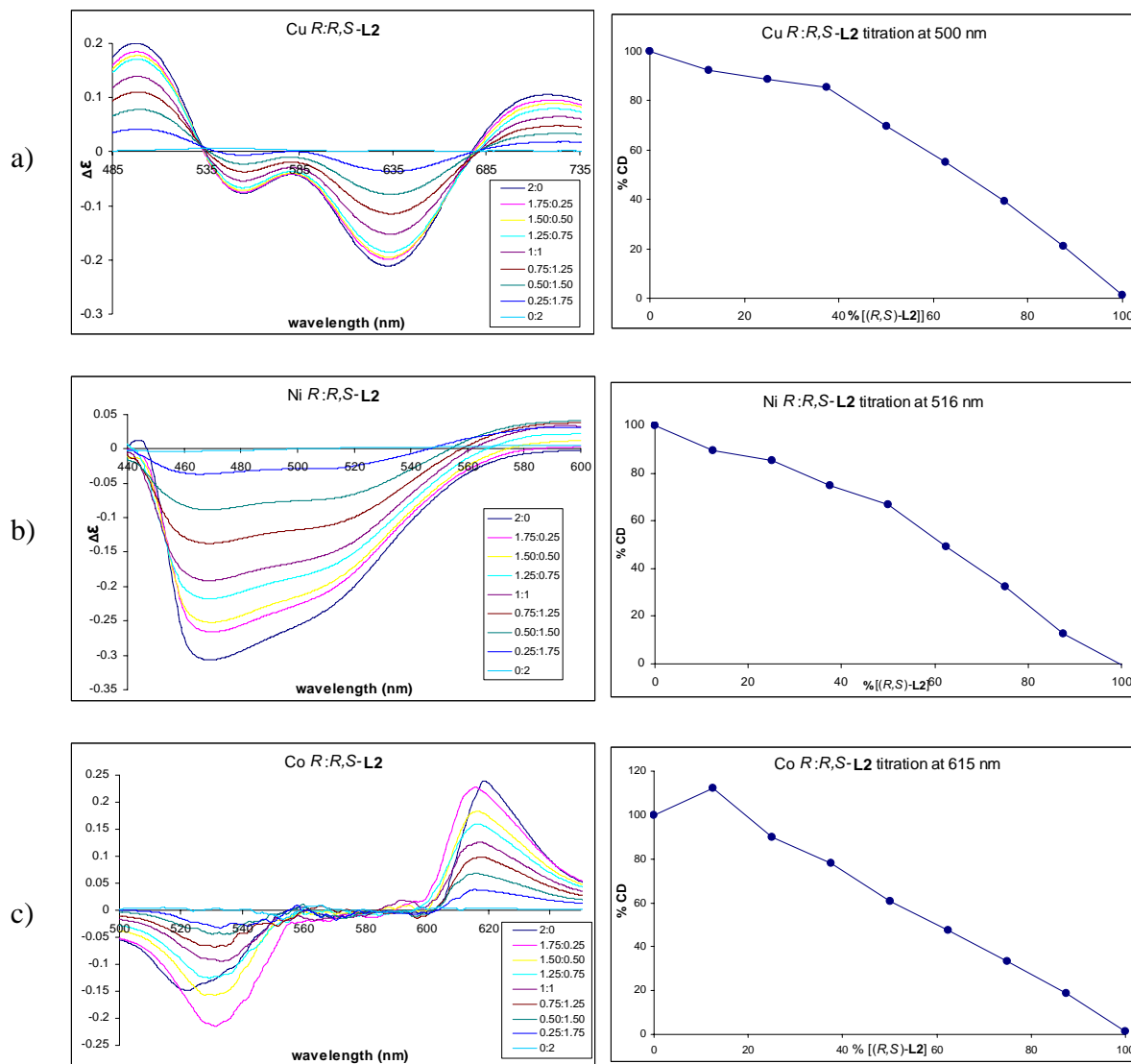


Figure 5.11: LHS: *R*-L2 series of increasing *R,S*-L2 ratio with the transition metals and a 20-fold ligand excess using DMSO as the solvent; RHS: Plots showing the calculated CD intensity as a function of the concentration ratio $[R-L2]/[R,S-L2]$ for a) copper(II); b) nickel(II) and; c) cobalt(II) (the second spectra recorded in the cobalt series, *R*:*R,S* ratio 1.75:0.25, appeared to be shifted and therefore considered an outlier and not used for calculations).

For copper(II) the results of the diastereoselective study were similar for both **L1** and **L2** ligands. This had been anticipated, as the substitution of a hydrogen for a methyl on the benzimidazole moiety was not expected to greatly affect the coordination properties of the ligands. The CD spectra with **L2** was similar to that of **L1**, with λ_{max} positions at comparable wavelengths and intensity as well as zero points being present at 540 and 675 nm. The ML_2 complex with **L2** also showed a preference for the homochiral species, with an S value clearly less than 1, Figure 5.11a(RHS).

The results with nickel(II) showed only small differences in the CD spectra when the ligand was changed from **L1** to **L2**; however the general shape of the spectra was quite similar. **L1** had shown an almost linear CD% plot whereas **L2** instead showed a slight preference for the homochiral ML_2 species as S was seen to be less than 1, although not to the same degree as with the copper(II) results. This small difference in stereochemical preference may be due to the substituted methyl groups having a more pronounced affect on the binding properties of the ligand with nickel(II) than seen with copper(II) as a result of subtle structural differences.

The most pronounced change in stereoselectivity was seen with the cobalt(II) ML_2 complex. **L1** had a clear preference for the mixed species, whereas **L2** instead had an S value slightly less than one indicating preference for the homochiral species, Figure 5.11c(RHS). Such a change in stereochemical preference is most likely due to the introduced methyl group on the benzimidazole moiety having a pronounced affect on the coordination geometry of the ligand about the cobalt(II) ion, as the conditions of the experiment for **L1** and **L2** were identical.

Overall, it proved interesting that changing the ligand from **L1** to **L2** did not affect the stereochemical preference of the copper(II) complex, only slightly changed the nickel(II), and completely reversed the preference of cobalt(II). This may be due to different binding modes or conformational differences for each metal ion. Previous reports with analogous bis(benzimidazole) ligands have noted that, for copper(II), the geometric constraints of such ligands impose a distorted coordination geometry. Further, if the ligands behave as tridentate ligands as expected, rather than bidentate, then a facial coordination mode must be adopted, as shown in Figure 5.12. This is because the expected Jahn-Teller distortion of

the copper(II) environment and further distortions caused by the tight geometric constraints of such ligands are apparent ⁶³.

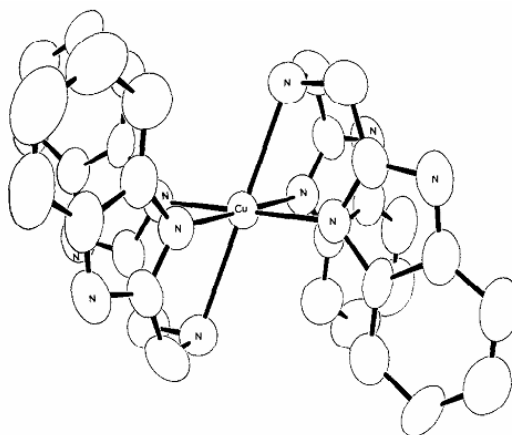


Figure 5.12: ORTEP structure of the complex $[\text{CuL}_2]^{2+}$, where L is a bis(benzimidazole) ligand with a sulfur present in the bridging unit. 50% thermal ellipsoids are shown ⁶³.

Pandiyan *et al* ⁶ noted that both copper(II) and nickel(II) have facial geometry with bis(benzimidazole) ligands when a sulfur atom is present in the bridging unit. They propose that the factors favouring facial coordination, as opposed to meridional, include the π -bonding ability of the benzimidazole at the termini of the tridentate ligand. In other tridentate ligands without the benzimidazole moieties, such as diethylenetriamine, the strong σ -donor ability of an amine at the termini instead facilitates the formation of meridional geometry.

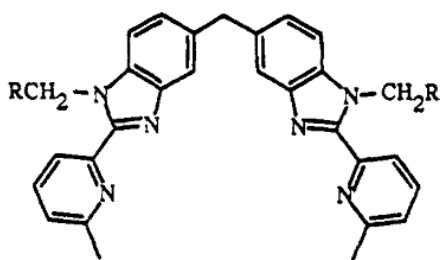
Further observations by Pandiyan suggest that the steric hindrance caused by the benzimidazole group at the terminus of the tridentate ligands also favours the facial coordination with nickel(II). This implies that the facial coordination appears to be facilitated when the terminal-donor sites in the tridentate ligand possess partial rigidity, thus reducing the π -donor as well as enhancing the π -bonding ability of benzimidazole.

We propose that the substitution of a hydrogen for a methyl group on the benzimidazole moiety may disrupt the π -bonding ability of the ligand in the cobalt(II) complexes, and perhaps to a lesser extent the nickel(II) complexes, resulting in a stereochemical preference for the homochiral species. In comparison, for the copper(II) the homochiral complex was always preferred, possibly due to the fact that copper(II) displays significant Jahn-Teller distortion in the complexes it forms compared with nickel(II) and cobalt(II) complexes.

Another consideration is the tridentate behaviour of the ligands. It has been reported that if bis(benzimidazole) ligands act as only bidentate ligands, that is binding with only the two nitrogen groups or one nitrogen group and the deprotonated hydroxy group, in which case a meridional geometry is adopted¹³. The substitution of a hydrogen for a methyl group may alter the binding nature of the ligand from tridentate to bidentate, therefore changing the overall geometry of the complex. This may also alter the diastereoselectivity of the ML_2 complex; for instance, with cobalt(II) such a change in geometry may result in the homochiral species being preferred when meridional geometry is adopted.

5.3.4 ESMS Study

Piguet *et al*⁶⁴ established in their research that the replacement of methyl substituents of the benzimidazole analogs by ethyl groups in ligands similar to the ligands investigated in this study (see Scheme 5.14) did not affect the formation of metal complexes, such as the triple helicates, they noted forming. In a similar fashion **L1** and **L2** are related in that an aromatic ring hydrogen was replaced by a methyl group. We made the assumption that, as was established in Piguet's research, the change of peripheral substituent would not significantly alter the species that formed and that only the molecular mass of the complexes would differ. The exchange of **L1** for **L2** in a complex therefore offers a means to accurately determine the configurations of the metal complexes formed, as ESMS can be applied to distinguish between ligands **L1** and **L2**, and the complexes formed with each, due to their molecular masses differences.



Scheme 5.14: Structure of the ligand used by Piguet *et al* for self-assembly studies ($R = H$ and $R = CH_3$)⁶⁴.

According to Charbonniere *et al*,⁶⁵ for ESMS to be applicable to the problem of identifying complexed species, the different peaks observed in the spectrum have to be unambiguously identifiable and their intensities related to the relative concentrations of the complexes.

Differences in m/z values observed in an ESMS spectra of complexes is dependant not only on the number of ligands involved in the complexation, but also the overall charge of the species. The charge can easily be altered by anions present in the complex and, as such for our ESMS studies, the perchlorate anion from the metal salts was considered as a possible fragment in the complexed species, along with ethanol and water, all of which affect the overall mass.

Charbonniere was able to monitor the kinetics of ligand exchange in the $[M_2L_3]^{4+}$ helical compound shown in Figure 5.13, the mass difference due to the methyl group being replaced with an ethyl group, **1_a** and **1_b**, respectively. The exchanged was followed using the ESMS technique shown in Figure 5.14. The technique proved successful in determining the path of substitution of one ligand with the other in the dynamic solution from the species that were identified to form during the exchange reaction. The species could be determined from the appearance of two new peaks in the spectrum resulting from the mass difference between the two ligands. Although peak intensity for identical concentrations will vary with molecular mass, the small mass differences in this study mean that this effect can be neglected as a close approximation, and therefore the peak intensities can be associated with the species concentrations.

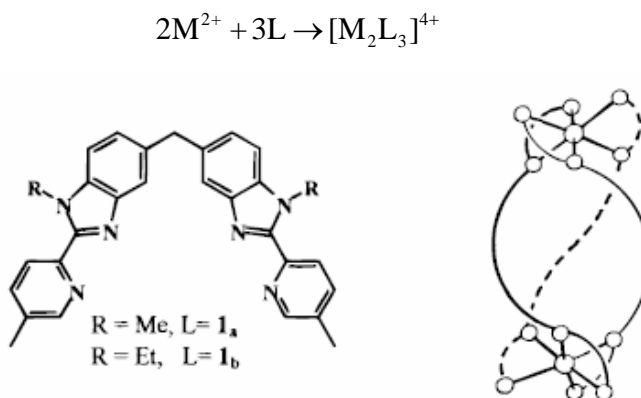


Figure 5.13: Charbonniere's strategy for the synthesis of triple-helical complexes using two octahedral metal cations. Ligand exchange between **1_a** and **1_b** enabled determination of the formation of the species using the ESMS technique ⁶⁵.

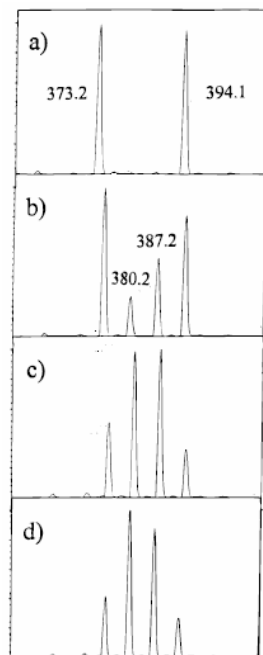


Figure 5.14: Scheme demonstrating how ESMS can be applied to monitor ligand exchange from the different species present due to the differences in molecular masses. ESMS spectrum of a mixture of equal volumes of $[\text{Co}_2(\text{L}_a)_3](\text{ClO}_4)_4$ (4.1×10^{-5} M) and $[\text{Co}_2(\text{L}_b)_3](\text{CF}_3\text{SO}_3)_4$ (3.1×10^{-5} M) in acetonitrile after a) 5, b) 67, c) 190, and d) 368 minutes⁶⁵.

This research was not a kinetic study; rather, the final products were analysed at different ratios of **L2** added to the **L1** metal complex solution, and the shift in peaks due to the mass difference of the two ligands used to determine the nuclearity of the species present in solution. The investigations were performed with the racemic forms of the ligands, as previous reports had shown that helical species seemed to form more readily with racemic ligand mixtures rather than with pure chiral species¹⁵. If the available instrumentation had enabled kinetic experiments these would have also been performed, as the results would have greatly aided in elucidating the reaction mechanisms for the complex species formed.

5.3.4.1 Mixed Ligand Species and Clear Resolution of Nuclearity

In order to precisely determine the nuclearity and speciation of the often numerous peaks resulting from ESMS investigations, **L1** and **L2** were exchanged in the complexes, therefore providing a means of studying the exchange of two practically identical ligands in the metal complexes formed. It was assumed that the replacement of a hydrogen atom on the benzimidazole moiety with a methyl group would not significantly alter the

coordination chemistry of the ligand, therefore similar species were expected to form with both **L1** and **L2** ligands.

Investigations of the series $\text{ML1} \rightarrow \text{M}(\text{L1L2})_{1/2} \rightarrow \text{ML2}$ were performed with the conditions described in Section 5.2.7 for the three transition metals copper(II), nickel(II) and cobalt(II). The mass difference introduced by the methyl groups on **L2**, along with the overall charge for each species in the mass spectrum, enabled determination of the number of ligands and metal ions in each complex. The major peaks in the ESMS spectrum were separated significantly, which enabled them to be unambiguously distinguished. Also, the most significant peaks could be easily identified. The intensities of the peaks in the different ESMS spectrums were approximately related to the relative concentrations of the complexes formed by comparing the signal height of the complex with the signal height of the free ligand, as the free ligand peaks were easily identifiable in each ESMS spectrum. This enabled the relative amounts of each complex formed to be compared in all measurements for each metal ion, as detailed in Table 5.5 to Table 5.7.

copper(II) species	M:L1	M:(L1L2) _{1/2}	M:L2
	ESMS <i>m/z</i>		
[Cu ₂ (L-H) ₂] ²⁺	341.0	341.3 (61%)	369.1
		355.0 (100%)	
		369.3 (81%)	
[Cu ₂ (L-H)(L-2H)] ⁺	679.3	678.8 (43%)	736.8
		709.0 (100%)	
		736.8 (60%)	
[Cu ₂ (L-H) ₂ ClO ₄] ⁺	780.8	780.7 (43%)	837.0
		809.0 (100%)	
		836.8 (60%)	

Table 5.5: ESMS values for copper(II)-ligand series $\text{ML1} \rightarrow \text{M}(\text{L1L2})_{1/2} \rightarrow \text{ML2}$. %-concentration values are provided for the mixed complex species to demonstrate the Pascal Triangle trend that was observed.

nickel(II) species	M:L1	M:(L1L2) _{1/2}	M:L2
		ESMS <i>m/z</i>	
[NiL ₂] ²⁺	307.5	307.5 (97%)	335.3
		321.5 (100%)	
		335.5 (109%)	
[Ni ₂ (L-H) ₂] ²⁺	335.4	307.5 (70%)	363.1
		321.5 (75%)	
		335.5 (100%)	
		350.5 (75%)	
[Ni ₄ (L-2H) ₃] ²⁺	533.5	363.4 (59%)	no peak
		531.8 (44%)	
		546.3 (100%)	
		561.3 (104%)	
[Ni ₂ (L-2H) (L-H)] ⁺	669.0	575.3 (60%)	726.8
		655.8 (67%)	
		669.8 (133%)	
		684.3 (100%)	
		698.7 (135%)	
		725.2 (75%)	

Table 5.6: ESMS values for nickel(II)-ligand series $ML1 \rightarrow M(L1L2)_{1/2} \rightarrow ML2$. %-concentration values are provided for the mixed complex species to demonstrate the Pascal Triangle trend that was observed.

cobalt(II) species	M:L1	M:(L1L2) _{1/2}	M:L2
		ESMS <i>m/z</i>	
[Co ₂ (L-H) ₂] ²⁺	336.3	335.6 (97%)	364.5
		370.6 (100%)	
		364.4 (147%)	
[Co ₃ (L-H) ₂ (L-2H)] ²⁺	503.9	503.9 (38%)	545.8
		517.8 (100%)	
		531.8 (72%)	
		546.0 (53%)	
[Co ₃ (L-H) ₂ (L-2H)] ²⁺ .EtOH	526.8	526.8 (33%)	568.8
		540.7 (100%)	
		554.7 (100%)	
		569.2 (50%)	
[Co ₄ (L-2H) ₃] ²⁺	533.5	533.8 (77%)	575.8
		547.3 (100%)	
		561.5 (100%)	
		575.8 (86%)	
[Co ₂ (L-2H)(L-H)] ⁺	671.0	671.2 (76.2%)	727.3
		699.2 (100%)	
		727.4 (75.9%)	
[Co ₂ L(L-H)(ClO ₄) ₂] ⁺	873.8	874.3 (39%)	944.5
		888.5 (57%)	
		902.0 (100%)	
		916.0 (102%)	
		930.3 (71%)	
		944.0 (37%)	

Table 5.7: ESMS values for cobalt(II)-ligand series **ML1** → **M(L1L2)_{1/2}** → **ML2**. %-concentration values are provided for the mixed complex species to demonstrate the Pascal Triangle trend that was observed.

The Pascal triangle phenomenon was noted for most of the mixed ligand spectra, **M(L1L2)_{1/2}**, as detailed in Figure 5.15, was clearly observed in the mass spectrum, which further aided the clear determination of the nuclearity of the species to be identified. Figure 5.16 demonstrates how the series **ML1** → **M(L1L2)_{1/2}** → **ML2** and the Pascal triangle enabled the progression of changing *m/z* peaks, due to the exchange of the complexed

ligand from **L1** to **L2**, to be used to calculate the nuclearity of three of the complex species present in the cobalt(II) ESMS spectrum.

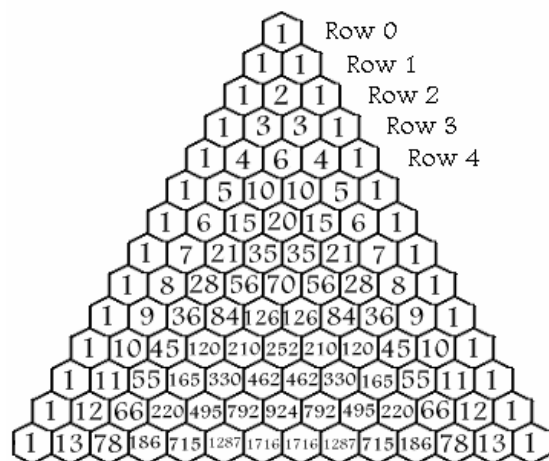


Figure 5.15: Pascal's Triangle ⁶⁶, the [1,3,3,1] sequence in Row 3 was observed in the ESMS spectrum for the $M(\mathbf{L1L2})_{1/2}$ experiment.

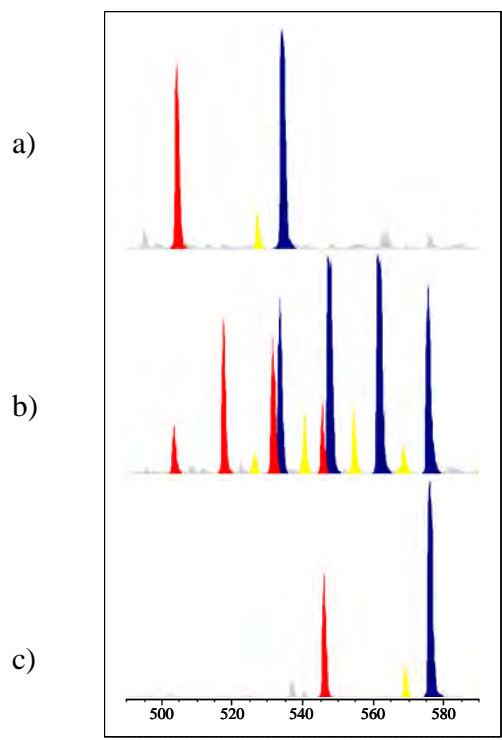


Figure 5.16: Key peaks of the ESMS spectrum for the series a) $\mathbf{ML1} \rightarrow$ b) $M(\mathbf{L1L2})_{1/2} \rightarrow$ c) $\mathbf{ML2}$ showing the complexes formed with cobalt(II). Each colour represents one species, the m/z changes are due to the substituted methyl group on the **L2** ligand; — $[\text{Co}_3(\mathbf{L-H})_2(\mathbf{L-2H})]^{2+}$, — $[\text{Co}_3(\mathbf{L-H})_2(\mathbf{L-2H})]^{2+} \cdot \text{EtOH}$, and — $[\text{Co}_4(\mathbf{L-2H})_3]^{2+}$.

Additionally, the $ML1 \rightarrow M(L1L2)_{1/2} \rightarrow ML2$ series were also investigated under the conditions with no base added, one equivalence, and excess base to determine if the deprotonation of the hydroxy group enabled the formation of new species. As previously seen in Section 5.3.2, the amount of base present only influenced the relative intensity of the peaks with no new species appearing to form, even with the hydroxy group being completely deprotonated.

An overall summary of the major species identified from all ESMS studies performed is provided in Table 5.8. It can be seen that some species are common for all metals, such as $[M_2(L-H)(L-2H)]^{1+}$, but that there are also significantly different species that form depending on the metal ion used for the complexation, even though all solutions were prepared under the same conditions. Not all the species identified were listed in the $ML1 \rightarrow M(L1L2)_{1/2} \rightarrow ML2$ study, detailed in Table 5.7, as some were formed only as minor species. Further, species identified are all low-charged entities, consistent with a tendency for ESMS to promote formation of low-charged species. Note that any neutral species will not be observed.

copper(II) species:	nickel(II) species:	cobalt(II) species:
$[M_2(L-H)_2]^{2+}$	$[ML_2]^{2+}$	$[M_2(L-H)_2]^{2+}$
$[M_2(L-H)_2(L-2H)]_2^-.EtOH$	$[M_2(L-H)_2]^{2+}$	$[M(L-H)]^+.EtOH$
$[M_3(L-H)_2(L-2H)]^{2+}.EtOH$	$[M_4(L-2H)_3]^{2+}$	$[M_3(L-H)_2(L-2H)]^{2+}$
$[M_2(L-H)(L-2H)]^+$	$[M_2(L-H)(L-2H)]^{1+}$	$[M_4(L-2H)_3]^{2+}$
$[M_2(L-H)_2ClO_4]^+$	$[ML_2ClO_4]^+.H_2O$	$[M_2(L-H)(L-2H)]^+$
		$[M_2L(L-H)(ClO_4)_2]^+$

Table 5.8: Species determined to exist in solution from ESMS studies of both **L1** and **L2** ligands. The concentrations for all the solutions prepared were of the order $10^{-5} - 10^{-6}$ M.

5.4 Conclusions

In general, the study showed that many species form with the complexation of **L1** and **L2** with the transition metal series. Interestingly, the chiral preferences of such complexes were seen to be different for each metal ion, highlighting the different coordination properties of each metal ion. It was also observed that, for cobalt(II), methylation of the benzene moiety unexpectedly changed the diastereoselectivity of the complex and it was

concluded that this change may be due to disruption of the π -stacking ability of the complexed ligand.

Further investigations with nickel(II) and **L1** were performed in order to form species of even higher nuclearity. Two equivalents of pyridine (py) were added to the 1:1 ratio **NiL1** to ascertain whether a bridging base would facilitate the formation of more complex species. Also, the addition of chloride ions along with NaOH was attempted, as the Cl^- is an anion reported to aid with the formation of larger complexes. However, with both techniques no higher nuclearity species were observed in the ESMS. Nonetheless, a $[\text{Ni}_2(\text{L-H})_2]^{2+}.\text{py}$ complex was successfully identified. Whether the oligomeric complexes identified in the ESMS experiments represent helical species is, of course, unable to be established from this technique. The ESMS technique used for the $\text{ML1} \rightarrow \text{M}(\text{L1L2})_{1/2} \rightarrow \text{ML2}$ study may also be applied to investigate the stereoselectivity of the ML_2 complexes if, for example, *R*-**L1** and *S*-**L2** are used as the ligands.

5.5 References

1. Baret, P.; Einhorn, J.; Gellon, G.; Pierre, J.-L., Synthesis of a Chiral Bis(bipyridine) Ligand of the Chiragen Family for the Self-Assembly of Enantiomerically Pure Helicates. *Synthesis* **1998**, 1998, 431-435.
2. Knof, U.; von Zelewsky, A., Predetermined Chirality at Metal Centers. *Angewandte Chemie - International Edition* **1999**, 38, 302-322.
3. Leigh, G. J., *Comprehensive Coordination Chemistry. II. From Biology to Nanotechnology*. Elsevier: Amsterdam, 2004; Vol. 3, p 2733-2742.
4. Mola, J.; Rodriguez, M.; Romero, I.; Llobet, A.; Parella, T.; Poater, A.; Duran, M.; Sola, M.; Benet-Buchholz, J., New Ru Complexes Containing the N-Tridentate bpea and Phosphine Ligands: Consequences of Meridional vs Facial Geometry. *Inorganic Chemistry* **2006**, 45, 10520-10529.
5. Bauer, P. D.; Mashuta, M. S.; O'Brien, R. J.; Richardson, J. F.; Buchanan, R. M., Synthesis, characterization and crystal structures of Nickel(II) complexes containing sterically hindering Benzimidazole ligands. *Journal of Coordination Chemistry* **2004**, 57, 361-372.
6. Pandiyan, T.; Salgado Barreiro, C. S.; Jayanthi, N., Facial Coordination Chemistry in Nickel(II) Compounds with Linear Tridentate Ligands: Synthesis, Spectra and Redox Behavior. *Journal of Coordination Chemistry* **2002**, 55, 1373-1383.
7. Subramaniam, V.; Hoggard, P. E., Amino acid coordination to chromium(III) with meridional geometry. *Journal of Coordination Chemistry* **1994**, 31, 157-65.
8. Addison, A. W.; Burke, P. J., Synthesis of some imidazole- and pyrazole-derived chelating agents. *Journal of Heterocyclic Chemistry* **1981**, 18, 803-5.
9. Addison, A. W.; Sinn, E., A stable bis(thiolate) of copper(II) with long axial copper-sulfur linkages: crystal and molecular structure of trans-[Cu(cyclam)(SC₆F₅)₂]. *Inorganic Chemistry* **1983**, 22, 1225-8.
10. Hendriks, H. M. J.; Birker, J. M. W. L.; Van Rijn, J.; Verschoor, G. C.; Reedijk, J., Synthesis and characterization of coordination compounds of chelating ligands containing imidazole groups. The crystal and molecular structures of the dinuclear copper(I) and copper(II) compounds. *Journal of the American Chemical Society* **1982**, 104, 3607-17.
11. Hendriks, H. M. J.; Ten Bokkel Huinink, W. O.; Reedijk, J., Synthesis, characterization and complex formation of N,N,N',N'-tetrakis(2-benzimidazolylmethyl)-1,2-ethanediamine, a new hexadentate ligand. *Recueil des Travaux Chimiques des Pays-Bas* **1979**, 98, 499-500.

12. Reedijk, J.; Driessen, W. L.; Van Rijn, J., Biological and Inorganic Copper Chemistry. In *Biological and Inorganic Copper Chemistry*, Karlin, K. D. Z., J., Ed. Adenine Press: New York, 1986; Vol. 2, p 143.
13. Isele, K.; Broughton, V.; Matthews, C. J.; Williams, A. F.; Bernardinelli, G.; Franz, P.; Decurtins, S., 1,2-Bis(2-benzimidazolyl)-1,2-ethanediol, a chiral, tridentate, facially coordinating ligand. *Journal of the Chemical Society, Dalton Transactions* **2002**, 3899-3905.
14. Van Albada, G. A.; Riggio, I.; Mutikainen, I.; Turpeinen, U.; Reedijk, J., Crystal structure and spectroscopy of bis[bis(2-benzimidazolyl)propane]copper(II) bis(triflate) monohydrate, a copper complex with a geometry intermediate between tetrahedral and square planar. *Journal of Chemical Crystallography* **2001**, 30, 793-797.
15. Van Albada, G. A.; Reedijk, J.; Hamalainen, R.; Turpeinen, U.; Spek, A. L., A novel type of tetranuclear cluster with the trinucleating ligand 1,2-bis(benzimidazol-2-yl)-1-hydroxyethane. Crystal and molecular structure of $\text{Ni}(\text{HRSL})_2(\text{CF}_3\text{SO}_3)_2$ and $[\text{Cu}_4(\text{SL})_4(\text{NO}_3)_2(\text{EtOH})](\text{NO}_3)_2(\text{EtOH})_3(\text{H}_2\text{O})_2$; spectroscopy and magnetism of these and related transition metal compounds. *Inorganica Chimica Acta* **1989**, 163, 213-22.
16. Viswanathan, R.; Palaniandavar, M.; Balasubramanian, T.; Muthiah, T. P., Functional Models for Catechol 1,2-Dioxygenase. Synthesis, Structure, Spectra, and Catalytic Activity of Certain Tripodal Iron(III) Complexes. *Inorganic Chemistry* **1998**, 37, 2943 - 2951.
17. Batra, G.; Mathur, P., Tetrahedrally distorted tetragonal copper complexes of a tridentate ligand. *Inorganic Chemistry* **1992**, 31, 1575-80.
18. Piguet, C.; Bünzli, J.-C. G.; Bernardinelli, G.; Hopfgartner, G.; Williams, A. F., Self-assembly of helical supramolecular lanthanide complexes. *Journal of Alloys and Compounds* **1995**, 225, 324-330.
19. Chen, X.-D.; Du, M.; Mak, T. C. W., Controlled generation of heterochiral or homochiral coordination polymer: helical conformational polymorphs and argentophilicity-induced spontaneous resolution. *Chemical Communications* **2005**, 4417-4419.
20. Greenwald, M.; Wessely, D.; Goldberg, I.; Cohen, Y., Bis(bipyridine)-phenanthroline double-stranded helicates of the metals: zinc(II), silver(I) and copper(I) helicates. *New Journal of Chemistry* **1999**, 23, 337-344.
21. Hou, L.; Li, D., A novel photoluminescent Ag-terpyridyl complex: one-dimensional linear metal string with double-helical structure. *Inorganic Chemistry Communications* **2005**, 8, (1), 128-130.
22. Birker, P. L.; Hendriks, H. M. J.; Reedijk, J.; Verschoor, G. C., Coordination compounds of chelating ligands containing imidazole groups. Synthesis and characterization of copper(I) and copper(II) complexes of N,N,N',N'-tetrakis[(2-benzimidazolyl)methyl]-1,2-

- ethanediamine and the x-ray structure of an [N,N,N',N'-tetrakis[(2-benzimidazolyl)methyl]-1,2-ethanediamine]copper(II) cation. *Inorganic Chemistry* **1981**, 20, 2408-2414.
23. Eulerling, B.; Schmidt, M.; Pinkernell, U.; Karst, U.; Krebs, B., An unsymmetrical dinuclear iron(III) complex with peroxidase properties. *Angewandte Chemie, International Edition* **1996**, 35, 1973-1974.
24. Holz, R. C.; Gobena, F. T., Synthesis, molecular structure and reactivity of a new dicopper(II) benzimidazole complex with non-identical copper(II) sites. *Polyhedron* **1996**, 15, 2179-85.
25. Kaim, W.; Schwederski, B., *Bioinorganic Chemistry: Inorganic Elements in the Chemistry of Life. An Introduction and Guide*. 1994; p 401.
26. Hommerich, B.; Schwoeppe, H.; Volkmer, D.; Krebs, B., Model complexes for ureases. A dinickel(II) complex with a novel asymmetric ligand and comparative kinetic studies on catalytically active zinc, cobalt, and nickel complexes. *Zeitschrift fuer Anorganische und Allgemeine Chemie* **1999**, 625, 75-82.
27. Berends, H. P.; Stephan, D. W., Copper(I) and copper(II) complexes of biologically relevant tridentate ligands. *Inorganica Chimica Acta* **1984**, 93, 173-8.
28. Broughton, V.; Bernardinelli, G.; Williams, A. F., Tetrahedral coordination by a seven-membered chelate ring. *Inorganica Chimica Acta* **1998**, 275-276, 279-288.
29. Matthews, C. J.; Leese, T. A.; Clegg, W.; Elsegood, M. R. J.; Horsburgh, L.; Lockhart, J. C., A Route to Bis(benzimidazole) Ligands with Built-in Asymmetry: Potential Models of Protein Binding Sites Having Histidines of Different Basicity. *Inorganic Chemistry* **1996**, 35, 7563-7571.
30. Hartmann, U.; Vahrenkamp, H., Pyrazolylborate-zinc complexes with drugs as ligands. *Chemische Berichte* **1994**, 127, 2381-5.
31. Kwak, B.; Woong Cho, K.; Pyo, M.; Soo Lah, M., Synthesis and characterization of a ferric complex of the tripodal ligand tris(2-benzimidazolylmethyl)amine-a superoxide dismutase mimic. *Inorganica Chimica Acta* **1999**, 290, 21-27.
32. Muller-Hartmann, A.; Vahrenkamp, H., Zinc complexes of condensed phosphates, 2. Diphosphate-zinc complexes with chelating coligands. *European Journal of Inorganic Chemistry* **2000**, 2355-2361.
33. Su, Y. S.; Cheng, K. L.; Jean, Y. C., Amplified potentiometric determination of pK00, pK0, pK1, and pK2 of hydrogen sulfides with Ag₂Se ISE. *Talanta* **1997**, 44, 1757-1763.
34. Dagdigian, J. V.; Reed, C. A., A new series of imidazole thioether chelating ligands for bioinorganic copper. *Inorganic Chemistry* **1979**, 18, 2623-6.

35. Dagdigian, J. V.; McKee, V.; Reed, C. A., Structural comparison of a redox pair of copper(I/II) complexes having benzimidazole thioether ligands. *Inorganic Chemistry* **1982**, 21, 1332 - 1342.
36. Cotton, F. A.; Wilkinson, G., *Advanced Inorganic Chemistry* Wiley: New York, 1988; Vol. 5th, p 766.
37. Csaszar, J.; Balog, J., The spectra, stereochemistry and electronic structures of copper(II) complexes. *Acta Physica et Chemica* **1977**, 23, 419-31.
38. Hathaway, B. J., Stereochemistry and electronic properties of complexes of the copper(II) ion. *Essays in Chemistry* **1971**, 2, 61-92.
39. Hathaway, B. J., A new look at the stereochemistry and electronic properties of complexes of the copper(II) ion. *Structure and Bonding* **1984**, 57, 55-118.
40. Burger, U.; Schmidlin, S. P.; Mareda, J.; Bernardinelli, G., A novel cycloaddition reaction of thermally generated sulfenes. *Chimia* **1992**, 46, 111-13.
41. Van Albada, G. A.; Lakin, M. T.; Veldman, N.; Spek, A. L.; Reedijk, J., Synthesis, Characterization, Spectroscopy, and Magnetism of Dinuclear Azido- and Alkoxo-Bridged Copper(II) Complexes of Bis(2-benzimidazolyl)alkanes. X-ray Structures of $[\text{Cu}_2(\text{tbz})_2(\text{CH}_3\text{O})_2](\text{ClO}_4)_2(\text{CH}_3\text{OH})_2$, $[\text{Cu}_2(\text{tbz})_2(\text{NO}_3)(\text{CH}_3\text{O})_2](\text{NO}_3)(\text{CH}_3\text{OH})_2$, and $[\text{Cu}(\text{tbz})(\text{N}_3)_2]_2(\text{CH}_3\text{OH})_2$ (tbz = Bis(2-benzimidazolyl)propane). *Inorganic Chemistry* **1995**, 34, 4910-17.
42. van Albada, G. A.; Mutikainen, I.; Riggio, I.; Turpeinen, U.; Reedijk, J., X-ray crystal structures, spectroscopic and magnetic measurements of dinuclear alkoxo-bridged copper(II) compounds with substituted bis(2-benzimidazolyl)alkane ligands. First X-ray structure of a copper(II) dinuclear propoxo-bridged compound. *Polyhedron* **2002**, 21, 141-146.
43. Sundberg, R. J.; Martin, R. B., Interactions of histidine and other imidazole derivatives with transition metal ions in chemical and biological systems. *Chemical Reviews* **1974**, 74, 471-517.
44. Ulkuseven, B.; Tavman, A.; Otuk, G., Synthesis, characterization and antimicrobial activity of d8-10 metal complexes of some 2-substituted-1H-benzimidazoles. *Metal-Based Drugs* **1999**, 6, 163-167.
45. Blake, A. J.; Champness, N. R.; Khlobystov, A. N.; Parsons, S.; Schroder, M., Controlled assembly of dinuclear metallacycles into a three-dimensional helical array. *Angewandte Chemie, International Edition* **2000**, 39, 2317-2320.

46. Childs, L. J.; Alcock, N. W.; Hannon, M. J., Assembly of nano-scale circular supramolecular arrays through p-p aggregation of arc-shaped helicate units. *Angewandte Chemie, International Edition* **2001**, 40, 1079-1081.
47. Jorgensen, W. L.; Severance, D. L., Aromatic-aromatic interactions: free energy profiles for the benzene dimer in water, chloroform, and liquid benzene. *Journal of the American Chemical Society* **1990**, 112, 4768-74.
48. Min, K. S.; Suh, M. P., Construction of various supramolecules by p-p interactions: self-assembly of nickel(II) macrocyclic complexes containing pyridine pendant arms with bidentate ligands. *European Journal of Inorganic Chemistry* **2001**, 449-455.
49. Roderick, W. R.; Nordeen, C. W.; Von Esch, A. M.; Appell, R. N., Bisbenzimidazoles. Potent inhibitors of rhinoviruses. *Journal of Medicinal Chemistry* **1972**, 15, 655 - 658.
50. Tavman, A., Bimetallic Cd(II) and Hg(II) complexes of 1,4-bis-(5-H/methyl/chloro-1H-benzimidazol-2-yl)-1,2,3,4-butane-tetraols. *Journal of the Serbian Chemical Society* **2005**, 70, 1067-1073.
51. Hay, R. W.; Clifford, T.; Lightfoot, P., Transition metal complexes of the tripodal ligand 4-(2'-pyridylmethyl)-4-azaheptane-1,7-diamine. Crystal structures of [CuLCl]ClO₄ and [NiL(MeCN)₂](ClO₄)₂. *Polyhedron* **1998**, 17, 4347-4352.
52. Tavman, A., 1,2-Bis-[(5-H/methyl/chloro/nitro)-2-1H-benzimidazolyl]-1,2-ethanediols and 1,4-Bis-[(5-H/methyl/chloro)-2-1H-benzimidazolyl]-1,2,3,4-butanetetraols complexes with AgNO₃. *Reviews in Inorganic Chemistry* **2002**, 22, 113-124.
53. Tavman, A.; Ulkuseven, B.; Agh-Atabay, N. M., 1,2-Bis-(2-benzimidazolyl)-1,2-ethanediol and 1,4-bis-(2-benzimidazolyl)-1,2,3,4-butanetetraol PdCl₂ complexes. *Transition Metal Chemistry* **2000**, 25, 324-328.
54. Wang, J.-L.; Li, A.-X.; Li, Y.-H.; Zhai, X.-H.; Miao, F.-M., Syntheses, biological activity and quantum chemical calculation of aromatic urea derivatives. *Huaxue Xuebao* **2001**, 59, 1490-1494.
55. Zippel, F.; Ahlers, F.; Werner, R.; Haase, W.; Nolting, H.-F.; Krebs, B., Structural and Functional Models for the Dinuclear Copper Active Site in Catechol Oxidases: Syntheses, X-ray Crystal Structures, Magnetic and Spectral Properties, and X-ray Absorption Spectroscopic Studies in Solid State and in Solution. *Inorganic Chemistry* **1996**, 35, 3409-19.
56. Palaniandavar, M.; Pandiyan, T.; Lakshminarayanan, M.; Manohar, H., Facial coordination in bis[bis(benzimidazol-2-ylmethyl)amine]copper(II) perchlorate dihydrate. Synthesis, structure, spectra and redox behavior. *Journal of the Chemical Society, Dalton Transactions: Inorganic Chemistry* **1995**, 455-61.

57. Pandiyan, T.; Bernes, S.; De Bazua, C. D., Structure, spectra and redox studies of nickel(II) bis(benzimidazole-2-ylmethyl)amines with coenzyme M reductase. *Polyhedron* **1997**, 16, 2819-2826.
58. Evans, D. A.; Kozlowski, M. C.; Murry, J. A.; Burgey, C. S.; Campos, K. R.; Connell, B. T.; Staples, R. J., C2-Symmetric Copper(II) Complexes as Chiral Lewis Acids. Scope and Mechanism of Catalytic Enantioselective Aldol Additions of Enolsilanes to (Benzyloxy)acetaldehyde. *Journal of the American Chemical Society* **1999**, 121, 669-685.
59. Zarges, W.; Hall, J.; Lehn, J.-M.; Bolm, C., Helicity induction in helicate self-organization from chiral tris(bipyridine) ligand strands. *Helvetica Chimica Acta* **1991**, 74, 1843-52.
60. Bernauer, K., Diastereoisomerism and diastereoselectivity in metal complexes. In *Theoretical Inorganic Chemistry II*, Springer: Berlin / Heidelberg, 1976; Vol. 65.
61. Bernauer, K.; Bourqui, S.; Hugi-Cleary, D.; Warmuth, R., Stereoselectivity in reactions of metal complexes. Part XIV. Use of circular dichroism to determine the stereoselective formation of [M(his)₂] and [M(PhEt-sal)₂] (M = nickel(II), copper(II), his = histidine, PhEt-sal = N-(1-phenylethyl)salicylaldimine). *Helvetica Chimica Acta* **1992**, 75, 1288-96.
62. Wosley, W. C., *Journal of Chemical Education* **1978**, 55, A355.
63. Berends, H. P.; Stephan, D. W., Copper(I) and copper(II) complexes of biologically relevant tridentate ligands. *Inorganica Chimica Acta* **1984**, 93, (4), 173-8.
64. Piguet, C.; Bernardinelli, G.; Bocquet, B.; Quattropiani, A.; Williams, A. F., Self-assembly of double and triple helices controlled by metal ion stereochemical preference. *Journal of the American Chemical Society* **1992**, 114, 7440-51.
65. Charbonniere, L. J.; Williams, A. F.; Frey, U.; Merbach, A. E.; Kamalaprija, P.; Schaad, O., A Comparison of the Lability of Mononuclear Octahedral and Dinuclear Triple-Helical Complexes of Cobalt(II). *Journal of the American Chemical Society* **1997**, 119, 2488-2496.
66. Pascal's Triangle. <http://ptr1.tripod.com/> (28/11/07),

Chapter 6

Combined Glass Electrode Calibration

6.1 Introduction

Potentiometric titrations with combined glass electrodes are an invaluable and widely used analytical technique for the experimental determination of hydrogen ion concentrations due to their convenience, affordable instrumentation and minimal time requirements ¹. Such determinations are important in many areas of chemistry as they enable the calculation of the concentrations of acids and bases and/or the determination of equilibrium constants. Authors go as far as to claim that glass electrode potentiometry is, with few exceptions such as spectrophotometric titrations, the only analytical technique capable of providing information about, and distinguishing between, the many chemical species that exist in solution when considering metal-ligand coordination reactions ². As such, it has been reported as being the most utilised technique for the determination of acid-base equilibrium constants ³⁻⁶. However, even though potentiometric titrations are now a matter of routine, the fundamentals governing them are still not widely agreed upon.

The combined glass electrode, commonly referred to as the pH electrode, was employed for the potentiometric research that was used for many areas of this study. In order to apply the potentiometric titration technique to determine accurate equilibrium constants precise calibration of the electrode was required. This is crucial as any error from the calibration becomes systematic error when interpreting the titration data, making internal consistency a prime requirement in order to guarantee comparability of readings and subsequent calculations and analyses.

However, it was brought to our attention that despite the many years of extensive effort that many researchers have directed towards obtaining unequivocal equilibrium constants using potentiometry, there are still many worrying uncertainties concerning the accurate calibration of the electrode ⁷. The calibration process is far from easy due to the interdependence of all the parameters involved and the changing experimental conditions. Hence, the following discussion is focused on describing the current techniques, concerns and applications related to the calibration of pH electrodes.

6.1.1 The Definition of pH

The term “pH” is an abbreviation for pondus hydrogenii and means the weight of hydrogen ⁸. It was proposed as a simple form for expressing low hydrogen ion concentration in very dilute acidic solutions. Since pH was defined at the beginning of last century it has perhaps been the most important and widely used parameter to describe aqueous systems. Properties of chemical, biological, and geological systems, emulsions and so forth are often very pH dependant and hence it is important to know the pH of a system.

In order to understand the current techniques used to measure pH the present IUPAC ⁹ definition and subsequent recommendations for pH electrode calibration must be described. According to the IUPAC guidelines, pH measurements are based on the definition proposed by Sørensen and Linderstrøm-Lang in 1924, where pH is defined as the negative logarithm of hydrogen ion activity as described in Equation (6.1), in which $\{H^+\}$ is the relative activity, m is molality, γ is activity coefficient and m^0 is standard molality (1 mol kg⁻¹) ¹⁰.

$$pH = -\log\{H^+\} = -\log \frac{m_H \gamma_H}{m^0} \quad (6.1)$$

A commonly overlooked fact is that a pH measurement determines the activity of the hydrogen ions in solution, and not the hydrogen ion concentration. Therefore, pH as strictly defined above is more troublesome than it looks as single ion activities, or activity coefficients, are immeasurable quantities. pH can therefore only be measured relative to other solutions where the pH has been defined in some other way. This is discussed further in Section 6.2.

6.1.2 pH Electrode Mechanism

Understanding the basic process involved when taking measurements with a pH electrode it is a key factor for appreciating what the electrode is responding to, as well as how to perform an accurate and appropriate calibration. As a rule, the pH electrode is a system that consists of two components, the working solution and the electrode. The system can be schematised as follows, where \mid denotes the liquid junction ¹¹.

reference electrode \mid KCl (3M) \mid solution \mid glass electrode

The potential difference that the electrode measures is comprised of a number of contributions ¹². Two of them are due to the external and internal reference electrodes,

which have a constant value, opposite sign and are usually comparable in magnitude. There are also potential differences due to the liquid junction, E_j , the glass membrane, which is dependant on the activity of the hydrogen ion on both sides of the membrane, and the asymmetry potential, E_{as} . Hence, the potential measured, E_{meas} , by the pH electrode is comprised from many influences, as shown in Equation (6.2) where $\{H^+\}_{int}$ and $\{H^+\}_{ext}$ are the activities of hydrogen ions in the internal and external sides of the glass membrane, respectively.

$$E_{meas} = E_{as} + E_j - s \log\{H^+\}_{int} + s \log\{H^+\}_{ext} \quad (6.2)$$

It can be seen that the fundamental linear correlation between the potential reading of an electrode and a pH value can be applied to the above equation as all components on the right hand side are considered constant except for the variable $\{H^+\}_{ext}$. Therefore, the measured potential follows a linear relationship with the logarithm of the activity of the hydrogen ion, $\{H^+\}_{ext}$. In Equation (6.2) s is the Nernst factor, $2.3RT/nF$, which is equal to 59.16 mV/pH in pure water at 25 °C, and describes the slope of the linear correlation line.

The general equation for relating the measured potential and hydrogen ion activity can be described by Equation (6.3).

$$E_{meas} = E_{const} + s \log\{H^+\}_{ext} \quad (6.3)$$

In the above equation E_{const} comprises of the constant potential differences of the electrode as shown below in Equation (6.4).

$$E_{const} = E_{as} + E_j - s \log\{H^+\}_{int} \quad (6.4)$$

Further, substituting the logarithm of hydrogen ion activity for pH according to Equation (6.1) results in Equation (6.5), where E_{const} is the intercept and s is the slope of the linear calibration line that can be experimentally determined.

$$E_{meas} = E_{const} + s \text{ pH} \quad (6.5)$$

Although the Nernst factor is widely accepted to accurately describe the theoretical mechanism of the electrode response, the experimental slope obtained usually departs from the given Nernstian value because glass electrodes exhibit a sub-Nernstian response³, which is a thermodynamic consequence of the mechanism of the electrodes functioning¹³. Therefore, the slope of the calibration line should be experimentally

determined, that is a practical slope calculated, rather than using the theoretical value of 59.16 mV/pH. Also, the intercept of the calibration line, E_{const} , varies with each electrode and from measurement to measurement, as it is dependant on the potential difference parameters pertinent to each experimental condition, and also to the internal parameters of the electrode's composition, such as the glass potential. Therefore, ideally, E_{const} should also be experimentally determined for each measurement performed.

6.2 Hydrogen Ion Activity Calibration Methods

When performing measurements to determine equilibrium constants the calibration of the electrode is one of the most influential steps. The accuracy of the measured pH value relies on precise calibration in order for the response of the electrode to correspond directly to the free hydrogen ions present, that is to be directly related to $\log\{H^+\}$.

6.2.1 IUPAC Recommended Methods

Using a solution of known activity for a given ion entails measuring the exact activity of that individual ionic species. Such a task is fundamentally impossible because ions never occur alone. According to the principle of electroneutrality, cations and anions are always present simultaneously, and together they make up the ionic strength of a solution. Since pH is defined in terms of a quantity that cannot be measured by a thermodynamically valid method, Equation (6.1) can only be a notional definition of pH. In order to strictly measure pH using the activity scale activity coefficients must be assigned on the basis of non-thermodynamic assumptions.

It is not possible to determine the activity coefficient of the hydrogen ion, γ_{H^+} , exactly as evaluation of the activity of single ionic species cannot be done without certain assumptions and approximations. As such, it is necessary to use approximations that are related to measurable quantities. The approximations introduced by the Debye-Hückel model provide an accurate evaluation of the ionic strength which is fundamental to the calculation of activity coefficients and hence the pH¹⁴. Therefore, according to IUPAC guidelines¹⁵, such assumptions are inherent to pH calculations and hence the activity of the hydrogen can only be experimentally verified along with the appropriate stated uncertainties. The Debye-Hückel approximation is shown in Equation (6.6) where z is the valence of each ion, a is its effective radius which includes closely bound

solvent molecules, μ is the ionic strength and A and B are constants with values of respectively 0.51 and 0.33 at 25 °C in water.

$$\log(\gamma) = -\frac{Az\sqrt{\mu}}{1 + Ba\sqrt{\mu}} \quad (6.6)$$

Calibration of the pH electrode is commonly performing by using the commercially available National Bureau of Standards (NBS), now known as National Institute of Standards and Technology (NIST), reference solutions or other similar standards. Such standards are usually made of acid/base systems with high buffer capabilities, and hence referred to as buffers. The use of such buffers has become the most common technique for calibration of the pH electrode. The purpose of buffer calibrations are to enable the response of the electrode in each buffer solution to be compared with the electrode response in samples as the pH of unknown solutions can be determined through comparison, using verified calibration procedures, with the conventionally assigned pH of standard reference buffer solutions.

The pH of buffer solutions has been defined by IUPAC in two levels of precision ¹⁶, the first being primary standard buffer solutions, pH(PS), and the second being secondary standard buffer solutions, pH(SS). The unifying principle for the measurement of pH in an unknown solution, as outlined by IUPAC ¹⁷, follows the simple path: method combined with the quality of materials → standard with known uncertainty; standard combined with suitable calibration procedure → measurement of unknown pH with stated uncertainty. This procedure can be generalised and represented by the traceability chain, where the measurement of the pH of an unknown solution is denoted by pH(X); pH(X) → pH(SS) → pH(PS) → pH as defined in Equation (6.1). Each step in the chain has stated uncertainties. Traceability is thus the governing metrological principle in pH measurements. The two standard buffer solutions, primary and secondary, are discussed in more detail in the following sections.

6.2.1.1 Primary Standard Buffer Solutions

A primary standard can be understood to mean without reference to other standards of the same quantity. Since pH, as defined by Equation (6.1), is immeasurable as it involves a single ion quantity, that is the activity of the hydrogen ion, the pH(PS) of primary standard solutions thus approaches the definition of pH as closely as present electrolyte theory permits, but is not necessarily identical to it. Primary standard buffer

solutions are assigned a pH(PS) value determined from electrochemical data from measurements carried out in a Harned cell¹⁸ which has no transference, that is no liquid junction, and has been defined as a primary method of measurement as the determined values have good reducibility and low uncertainty.

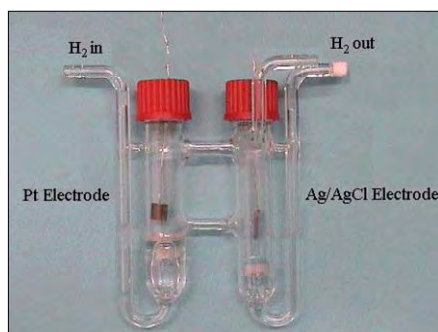
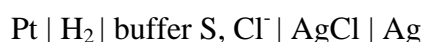


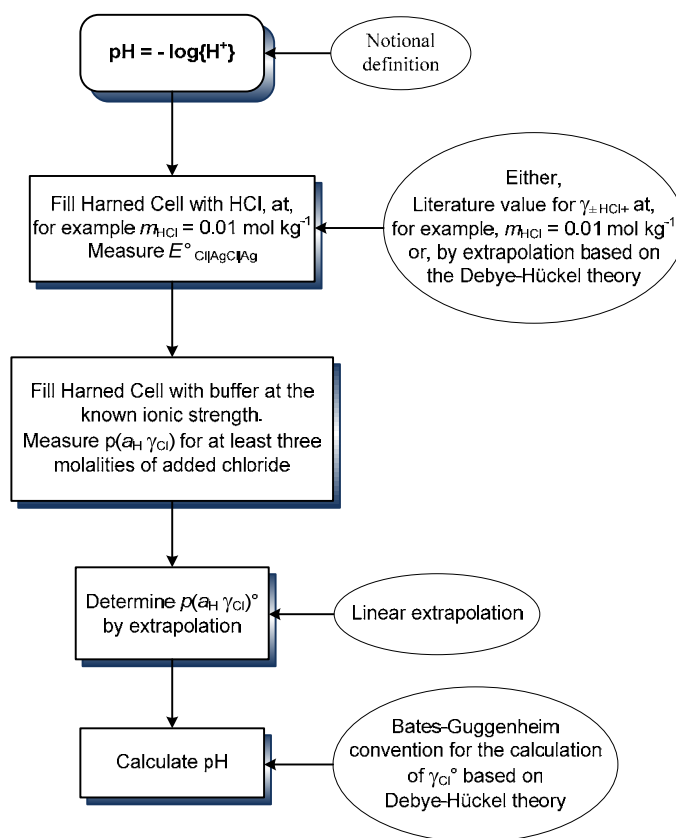
Figure 6.1: Diagram of a Harned cell.

The potentials of the Pt | H₂ and the Ag | AgCl electrode obey the Nernst equation and correctly indicate the activity of the hydrogen and chloride ions, and because the cell is without transference there are no complications from liquid junction potentials.



The effect of the buffer solution, which contains a small concentration of chloride ions, is eliminated by using at least three buffer solutions of varying chloride concentrations followed by extrapolation to zero added chloride ion concentration in order to remove the uncertainty of the effect of the chloride ion.

The Bates-Guggenheim convention is used in order to define the pH(PS) value, according to which the *Ba* term in the Debye-Hückel equation is taken to be $1.5 (\text{mol kg}^{-1})^{1/2}$ at all temperatures and for all compositions of the solutions. Hence, pH(PS) is a conventional quantity. Consideration of the uncertainty of the Bates-Guggenheim convention permits the determination of pH to be incorporated into the internationally accepted SI system of measurement as it enables measured values to be experimentally verified with appropriate stated uncertainties.



Scheme 1: Operation of the Harned cell as a primary method for the measurement of absolute pH ¹⁶.

In order for a particular buffer solution to be considered a primary standard buffer solution, it must be of the ‘highest metrological’ quality ¹⁹ in accordance with the definition of a primary standard. IUPAC recommends ¹⁶ that primary standards have the following attributes: high buffer value in the range 0.015-0.07 (mol OH⁻)/pH; small dilution value at half concentration, that is the change in pH with change in buffer concentration to be in the range 0.01-0.20; small dependence of pH on temperature less than $\pm 0.01 \text{ K}^{-1}$; low residual liquid junction potential (RLJP) < 0.01 in pH; ionic strength $\leq 0.1 \text{ mol kg}^{-1}$ to permit applicability of the Bates-Guggenheim convention; National Metrological Institutes (NMI) certificate for specific batch; reproducible purity of preparation with lot-to-lot differences of $|\Delta\text{pH(PS)}| < 0.003$; and long-term stability of the stored solid material.

Indication of the extent of possible systematic uncertainties for primary standard buffers arises from three sources. Firstly, experimental uncertainties such as variations in chemical purity of the primary buffer materials or variations in the preparation of the solutions. Secondly, error may arise from variation in the residual liquid junction potential between primary buffer solutions, and thirdly inconsistencies may result from

the application of the Bates-Guggenheim convention to chemically different buffer solutions that have an ionic strength less than 0.1 M.

primary standards (PS)	pH value at 25 °C
saturated potassium hydrogen tartrate	3.557
0.05 mol kg ⁻¹ potassium dihydrogen citrate	3.776
0.05 mol kg ⁻¹ potassium hydrogen phthalate	4.005
0.025 mol kg ⁻¹ disodium hydrogen phosphate + 0.025 mol kg ⁻¹ potassium dihydrogen phosphate	6.865
0.03043 mol kg ⁻¹ disodium hydrogen phosphate + 0.008695 mol kg ⁻¹ potassium dihydrogen phosphate	7.413
0.01 mol kg ⁻¹ disodium tetraborate	9.180
0.025 mol kg ⁻¹ sodium hydrogen carbonate + 0.025 mol kg ⁻¹ sodium carbonate	10.012

Table 1: Typical values of pH(PS) for primary standards at 25 °C .

Substances that do not fulfil all the criteria for primary standards, but to which pH values can be assigned using a Harned cell are considered to be secondary standards. Some reasons for a material to be excluded as a primary standard include difficulties in achieving consistent suitable chemical quality, for example acetic acid is a liquid, high liquid junction potential or inappropriateness of the Bates-Guggenheim convention as is the case for charge-type buffers. In most cases the use of high accuracy primary standards for the measurement of pH is not justified if a traceable secondary standard of sufficient accuracy is available.

6.2.1.2 Secondary Standard Buffer Solutions

Buffer solutions which do not meet the stringent requirements of primary standards are called secondary standards. The pH(SS) values are assigned by comparison with a primary standard of the same quantity. Comparison of pH(PS) values in recommended cells with transference yields secondary standards, whose pH(SS) can be traced back to pH(PS) and consequently to the definition of pH given in Equation (6.1). Since such measurements must be carried out in cells with liquid junction, secondary standard pH(SS) values have necessarily larger uncertainties than pH(PS) values from which they are derived.

secondary standards (SS)	pH value at 25 °C
0.05 mol kg ⁻¹ potassium tetroxalate	1.68
0.05 mol kg ⁻¹ sodium hydrogen diglycolate	3.49
0.1 mol dm ⁻³ acetic acid + 0.1 mol dm ⁻³ sodium acetate	4.65
0.02 mol kg ⁻¹ piperazine phosphate	6.29
0.05 mol kg ⁻¹ tris hydrochloride + 0.01667 mol kg ⁻¹ 2-amino-2-(hydroxymethyl)-1,3 propanediol	7.70
0.05 mol kg ⁻¹ disodium tetraborate	9.19
saturated calcium hydroxide	12.25

Table 2: Typical values of pH(SS) for some secondary standards at 25 °C .

6.2.1.3 Calibration Using Buffer Solutions

The traceability chain is continued by practical cells with transference for the measurement of unknown pH values, pH(X). Practical pH measurements are necessarily carried out in cells with liquid junction. Such electrodes which are commonly used for pH measurements employ a single glass and a single reference electrode, or consist of a combined electrode as detailed below.

reference electrode | KCl (3M) | solution pH(S) or pH(X) | glass electrode

When using an electrode, such as a combined glass electrode, various random and systematic effects must be considered. Firstly, as previously discussed, glass electrodes exhibit a sub-Nernstian response. Therefore, when performing measurements with combined glass electrodes application of the practical slope factor is mandatory because of the sub-Nernstian behaviour and other effects of the glass electrode in addition to the presence of residual liquid junction potentials.

$$\frac{dE}{dpH} = k' < \frac{RT}{F(\ln 10)} \quad (6.7)$$

Additionally, the response of electrode may vary with time and history of use. The potential of the glass, the reference electrode and the liquid junction potential also all have different temperature coefficients, hence calibration and measurements are recommended to be carried out under temperature controlled conditions. The liquid junction potential of an electrode depends on the composition of the solutions forming the junction and thus change when one solution, for example, when a buffer solution is

exchanged for an unknown. Since these effects are unknown in magnitude the electrode must be calibrated by suitable methods when unknown pH values are to be measured.

Three calibration procedures have been recommended by IUPAC¹⁶ for the calibration of a glass electrode using buffer solutions, either primary or secondary, depending on the quality of the standard buffer used.

One-point Calibration

The one-point calibration method is the least accurate of the calibration methods described by IUPAC because a single electrode reading is insufficient to determine both slope and intercept of the electrode response axis, E_{const} , as defined in Equation (6.5). A theoretical slope may be assumed, but the practical slope may be up to 5% lower than the theoretically determined value. Alternatively, a predetermined value by the manufacturer for the practical slope can be assumed. The one-point calibration, therefore, yields only an estimate pH value as the uncertainty is high and is strongly dependant on the difference, ΔpH , between the unknown solution and the standard buffer solution used for the calibration, that is, the greater the difference between the $\text{pH}(\text{S})$ value of the standard buffer and the measured $\text{pH}(\text{X})$ value of the unknown, the greater the uncertainty in the $\text{pH}(\text{X})$ value.

The equation used to determine unknown pH values from a one-point calibration is shown in Equation (6.8), where the pH of the unknown solution is denoted by $\text{pH}(\text{X})$, $\text{pH}(\text{S})$ is the pH value of the standard buffer, and $E(\text{X})$ and $E(\text{S})$ are the pH electrode potential readings in the unknown and standard buffer, respectively.

$$\text{pH}(\text{X}) = \text{pH}(\text{S}) - [E(\text{X}) - E(\text{S})] \quad (6.8)$$

Two-point Calibration (Bracketing)

In the majority of practical applications pH electrodes are calibrated by a two-point calibration, otherwise known as a bracketing procedure, using two standard buffer solutions where the pH of the two standards bracket the expected pH range of the measurement or samples. The bracketing technique involves the pH electrode being placed in a standard buffer equal to a pH of 7.00, and the meter adjusted accordingly until the reading is such, then subsequently placing the electrode in a second standard buffer solution of pH 4.01, and adjusting the meter again. The process is repeated until the electrode reads the correct pH value in each respective standard buffer. If

measurements involve high pH values than a buffer of pH value 10.00 is substituted for the 4.01 buffer. For potentiometric titrations pH 4.01 and 7.00 rarely bracket the required pH range, and neither do the 7.00 and 10.00 pH standards. Therefore, the electrode is not usually adequately calibrated when using such two-point techniques for titration experiments.

Using the two calibration points, linearity between the known pH of each standard buffer solution and the measured potential is assumed, and a straight calibration line is calculated therefore enabling the pH of an unknown solution to be related to the electrode response. The calculation of the slope of the calibration line is represented in Equation (6.9), and subsequent determination of the pH of an unknown, pH(X), is shown in Equation (6.10), where pH(S₁) and pH(S₂) are the pH values of the two bracketing standards, E(S₁) and E(S₂) are the pH electrode potential readings in each standard buffer respectively, and E(X) is the potential reading in the unknown solution.

$$s = \frac{E(S_1) - E(S_2)}{\text{pH}(S_2) - \text{pH}(S_1)} \quad (6.9)$$

$$\text{pH}(X) = \text{pH}(S) - \frac{E(X) - E(S)}{s} \quad (6.10)$$

However, calibration using a bracketing technique with standard buffers has drawbacks and inconsistencies. The two-point calibration technique as described above cannot identify any systematic offsets caused by one or both buffer solutions, for instance due to changing liquid junction potentials, nor can the procedure detect any outlying observations since the two calibration points will always define a straight line.

Multi-point Calibration

The introduction of multi-point calibration, in which up to five buffer solutions are used, resolves the aforementioned concerns with the bracketing calibration procedure. Even so, multi-point calibrations are still not common practise among researchers. Using this technique the five calibration points result in the calibration function shown below.

$$E(S) = E_{const} - s \cdot \text{pH}(S) \quad (6.11)$$

The intercept corresponds to the standard potential, E_{const} , and s is the experimentally determined slope. Both parameters can be determined by the linear regression of

Equation (6.11)²⁰. This enables the unknown pH(X) to be calculated from the potential measured in the unknown solution, $E(X)$, by application of Equation (6.12) as shown where E_{const} and s values have previously been determined from the multi-point calibration procedure.

$$\text{pH}(X) = E_{\text{const}} - \frac{E(X)}{s} \quad (6.12)$$

The uncertainty range for determining the pH of an unknown solution using the three techniques described by IUPAC have been provided in Table 3¹⁶. These values show that the one-point calibration has approximately ten times greater uncertainty than the bracketing or multi-point calibration procedures. The uncertainty for bracketing and multi-point calibrations are similar, however multi-point calibration methods are clearly superior as they enable the identification of outliers or systematic inconsistencies.

Electrode Calibration	
one-point calibration ($\Delta\text{pH}^* = 3$ and assumed slope)	0.3
two-point calibration (bracketing)	0.02-0.03
multi-point calibration	0.01-0.03

Table 3: Summary of the uncertainties for the three electrode calibration methods recommended by IUPAC¹⁶; $\Delta\text{pH} = |\text{pH}(X) - \text{pH}(S)|$.

Standards have to be prepared with appropriate care in order to be able to exploit the high reliability of their pH values. However, there are always differences between the ionic compositions of the reference and test solutions and this means that the buffer and test solutions can be expected to differ in activity coefficients and hence, as highlighted by Irving *et al*²¹, the pH measured under such circumstances cannot be expected to coincide precisely with $-\log\{\text{H}^+\}$ values as defined in Equation (6.1).

6.3 Calculating Equilibrium Constants

As previously detailed in Equation (6.1), pH is fundamentally defined in terms of the activity of the hydrogen ion. If the electrode has been calibrated by reference to standard solutions of known activity then the measured pH value corresponds as closely as experimentally possible to the activity of the hydrogen ion. When such values are applied to the calculation of equilibrium constants they result in ‘mixed’ constants, also

known as Brønsted constants, as represented below for the protonation of a ligand ²². Such constants are neither the theoretical thermodynamic constants gained from activity measurements, nor the experimentally preferred stoichiometric constants gained from concentrations, as they involve both activity and concentration quantities.

$$\text{LH} \leftrightarrow \text{L} + \text{H} \quad pK = -\log_{10}\left(\frac{[\text{L}]\{\text{H}\}}{[\text{LH}]}\right) \quad (6.13)$$

Although calibration for the activity of the hydrogen ion with standard buffer solutions remains valid in work where only a relative scale of acidity is required, it is an unsatisfactory technique for performing equilibrium studies for many reasons as well as the problem of determining mixed constants. For instance, equilibrium constants of the mixed constant type lack physical significance since the standard buffer solutions used to calibrate the electrode are by definition dilute solutions, whereas equilibrium constants are usually determined using solutions of high ionic strength ^{12, 23, 24}. While there are plenty of low ionic strength standard buffers available, standards with high ionic strength are not. Therefore the differences from ionic strength inconsistencies result in uncertainty due to differing liquid junction potentials as these are dependant on the composition of the solutions forming the junction and therefore change when the standard buffer and test solutions are exchanged. In order for the comparison of the pH of a standard buffer with the unknown pH to be valid, the standard buffer solutions need to be treated, in all respects, as similar as possible to the samples.

Due to these complications and inconsistencies researchers who employ potentiometric methods to measure equilibrium constants have long used solutions of known hydrogen ion concentration instead of standard buffer solutions to calibrate the electrode ²⁵. Calibration with solutions of known hydrogen ion concentration is the technique most commonly used by researchers as such solutions are more readily prepared than activity standard buffers, since there are no complications with knowing the activities of each individual ion, and therefore no need to estimate the activities. The most common calibration method preferred by researchers for analytical potentiometric investigations are that of a strong acid/strong base titration where the hydrogen ion concentration is accurately known.

6.4 Hydrogen Ion Concentration Calibration Methods

Although the pH electrode responds to hydrogen ion activity, the hydrogen ion concentration in a solution can also be determined provided that the electrode is accordingly calibrated. The majority of researchers usually prefer to measure the concentrations of ions rather than activities as then stoichiometric constants can be accurately determined rather than the calculation of mixed constants which cannot be easily compared and lack physical meaning.

The electrode can be calibrated to measure hydrogen ion concentration from application of the definition of activity, $\{H^+\} = \gamma \times [H^+]$, and substituting this for the $\{H^+\}_{\text{ext}}$ term in Equation (6.3). The equation can then be rewritten as shown below.

$$E_{\text{meas}} = E_{\text{const}} + s \log \gamma_{H^+} + s' \log [H^+]_{\text{ext}} \quad (6.14)$$

In order to measure the concentration of the hydrogen ion the ionic strength of the solution must be known as this directly affects the activity of the hydrogen ion. The calculations required to determine the hydrogen ion concentration in a measurement of non-constant ionic strength is a new development in the area of analytical chemistry and is still not common practise amongst chemists. This technique will be described later in this chapter in Section 6.7. The common practise is to instead perform measurements at constant ionic strength as it is known that if the ionic strength of the medium is kept constant the activity coefficient of the hydrogen ion is constant as well. Therefore, the $s \log \gamma_H$ term can be encompassed to be part of the standard potential E_{const} , as shown in Equation (6.15). Therefore, it can be seen that pH can be ultimately associated with the hydrogen ion concentration²⁶.

$$E_{\text{meas}} = E_{\text{const}} + s \log [H^+] \quad (6.15)$$

where

$$E_{\text{const}} = E_{\text{as}} + E_j - s \log \{H^+\}_{\text{int}} + s' \log \gamma_{H^+} \quad (6.16)$$

6.4.1 Strong Acid / Strong Base Titration Calibration

Calibration of the electrode to measure hydrogen ion concentrations using the titration method has many advantages compared with standard buffers. Concentration calibration performed using a strong acid/strong base titration can be done at varying ionic strengths, which removes any dilution restrictions associated with using standard

buffer solutions. However, its main advantage is that fact the stoichiometric pH, that is pH defined by hydrogen ion concentration, is a well-defined, transparent quantity unlike the conventional pH as defined by activity²⁷.

The calibration process of a strong acid/strong base titration involves the potential reading at each point in the titration being plotted against the corresponding volume of base added. The hydrogen ion concentration can be accurately calculated at each point on the titration curve using Equations (6.17) and (6.18), where $[H^+]$ denotes the free hydrogen ion concentration, c_a and c_b are the initial concentrations of the acid and base solutions respectively, V_0 is the initial titrant volume, v is the added titrate volume, and K_s is the ionisation constant of the solvent.

$$[H^+] = \frac{c_a V_0 - c_b v}{V_0 + v} \quad (6.17)$$

$$[H^+] = \frac{K_s}{[OH^-]} = \frac{K_s (V_0 - v)}{(c_b v + c_a V_0)} \quad (6.18)$$

This calculation enables the potential reading at each point to be plotted against the corresponding calculated values of $\log [H^+]$, and hence the linear relationship between the electrode potential readings and free hydrogen ion concentration can be determined. The calibration equation obtained from a strong acid/strong base titration is similar to multi-point standard buffer calibration, which was discussed in Section 6.2.1.3, and is shown in Equation (6.11). Instead of the pH value from the standard buffer solutions being related to the potential readings, the hydrogen ion concentration is logarithmically related as shown in Equation (6.19). In concentration calibration the pH range from 2 – 4 is used to define the linear parameters E_{const} and s , and the range from 10 – 12 defines s as well as the ionisation constant of the solvent, pK_s . The pK_s constant of a solvent critically affects the calculation of acid concentration in the final stage of the titration as the pK_s value is very highly correlated with the concentration of base in the burette. That is, a small error in the concentration of the base will cause significant deviation in the slope s of the electrode response as the pK_s is used to convert the hydroxide ion excess into free hydrogen ion concentration, as previously shown in Equation (6.18).

A strong acid/strong base titration adequately covers both these regions and can therefore be used for accurate and reliable calibration.

$$E_{\text{meas}} = E_{\text{const}} + s \log[\text{H}^+] \quad (6.19)$$

Using the calibration equation the potential readings in an unknown solution can be directly related to the free hydrogen ion concentration, whose value can then be used to calculate the pH, according to Equation (6.20).

$$\text{pH} = -\log[\text{H}^+] \quad (6.20)$$

For such a calculation to be valid the ionic strength of the solution must be constant to ensure that the hydrogen ion activity coefficient is constant as discussed previously and shown in Equation (6.14). The process of calibration using known hydrogen ion concentration is illustrated in Figure 6.2 where a) shows the potential readings at each point of added base in the titration, b) shows the calculated $-\log [\text{H}^+]$ values for each potential reading, c) shows the addition of the linear calibration line, and d) demonstrates how the calibration line can be used to calculate the pH at each volume of added base, resulting in the recognisable strong acid/strong base titration curve.

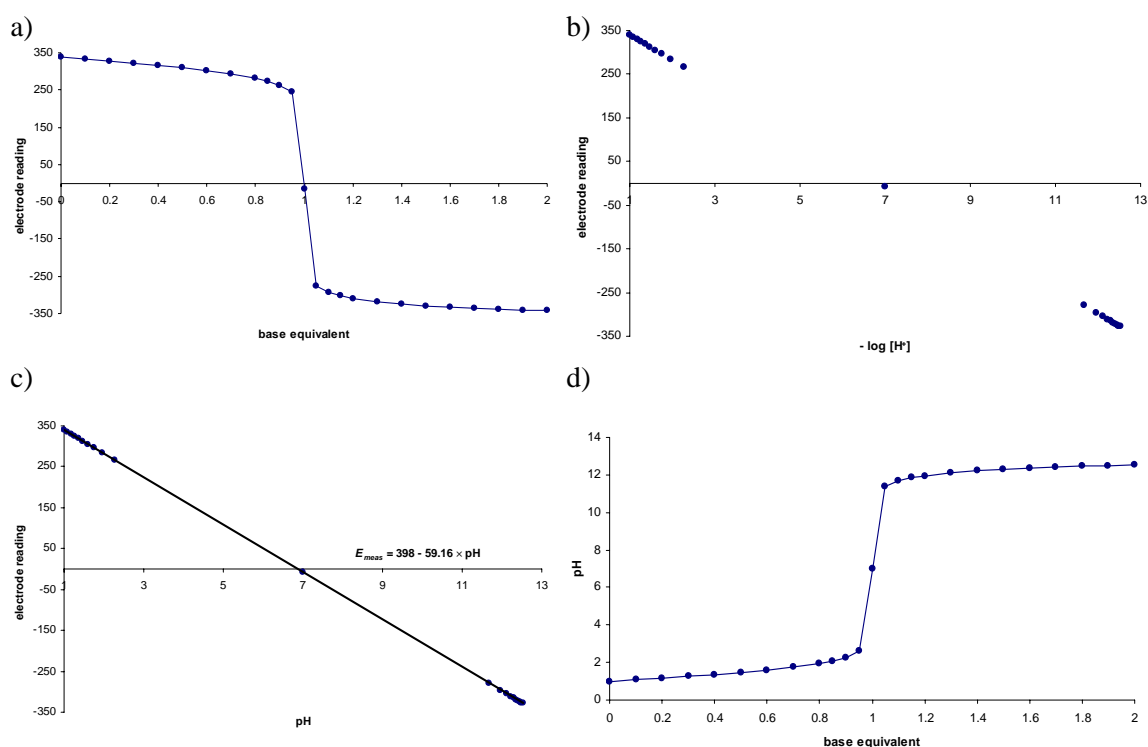


Figure 6.2: Sequence detailing the calibration process of an electrode using a strong acid/strong base titration to calculate the calibration parameters E_{const} and s .

6.5 Mixed and Non-aqueous Solvent Measurements

It is crucial to recognise that ‘... a pH measurement is definitely not just a matter of switching on a pH meter, plunging the electrodes into the test solution and taking the

meter reading’²⁸. This statement is especially true when the test solution is not an aqueous mixture, but instead a mixed solvent or non-aqueous solution. This was the case for the majority of our investigations as the ligands for our studies were insoluble in pure aqueous solvents. Instead 50/50 (v/v) ethanol/water solutions were used to investigate the protonation constants of the ligands as well as to determine the equilibrium constants when combined with metal ions. As such, it was an important consideration to calibrate the electrode properly in a mixed solvent composition.

In aqueous solutions potentiometry is known to be a relatively simple, quick, accurate and reliable technique for the determination of acid-base equilibrium constants, but only provided that the substance is sufficiently soluble in aqueous solutions²⁹. However, many new substances of interest are very poorly soluble in water and therefore a mixed solvent or non-aqueous approach needs to be applied. Titrations in such solvents have not been widely reported, particularly in cases where metal ions are involved as part of the reaction^{30, 31}. The pH electrode is still the electrode of choice when performing measurements in mixed or non-aqueous solvents as the medium does not require a minimum water content in order for the electrode to function³². However, determination of pH in mixed and non-aqueous solvents has traditionally been difficult due to the lack of a way to relate the electrode potential readings to absolute pH because of complications that arise with calibrating the electrode for such investigations³³.

6.5.1 Standard Buffer Calibration

The common calibration procedure using standard buffer solutions should not be employed when calibrating the electrode for measurements in mixed or non-aqueous solvents because the calibration will not be valid as standard buffer solutions are commonly made in pure aqueous solutions. The calibration parameters determined using standard buffers are dependant on the electrode, the ionic strength of the solution, the liquid junction potential between the two systems, and the activity coefficient of hydrogen ion^{21, 34}. These factors will all be affected if the medium for the measurement is changed. Consider, as an example, measurements in alcohol-water solvent mediums. In order to accurately determine the pK values of ligands and metal-ligand equilibrium constants the pH measured must accurately be determining the hydrogen ion activity in the solvent mixture. Obviously, due to differences such as dielectric constants and the bonding capabilities of different solvents, the effective hydrogen ion activity will differ greatly depending on the solvent, therefore also necessarily changing the parameters of

the electrode with each new solvent system. Therefore, calibration parameters determined using aqueous standard buffer solutions are not valid for measurements in mixed or non-aqueous solvents as the parameters can change significantly with the changing solvent conditions.

However, some researchers have determined pH values for standard buffers in mixed solvents and these can be used to calibrate the electrode for such solvent systems. Barbosa *et al*³⁵ determined the standard pH values, pH(PS), for seven primary standard buffer solutions in 0, 10, 30, 40, 50, 70 and 100% (w/w) acetonitrile-water mixed solvents at 25° C according to the criteria recently endorsed by IUPAC. They examined the influence of the variation in the solvent composition on the pH(PS) values in order to obtain correlations that could be used to determine the pH(PS) values in any acetonitrile-water mixture up to 70% (w/w) acetonitrile. The equations obtained from the correlation enabled the calibration of electrodes in such acetonitrile-water solvent mixtures. Even so, it remains that calibration in standard buffers result in calibration of the electrode for hydrogen ion activity not concentration, hence the calculation of so-called mixed equilibrium constants will still result.

6.5.2 Alternative Calibration Techniques

There are other techniques that have been developed to determine equilibrium constants in mixed and non-aqueous solvent investigations. These techniques were not applied during this research, but they are worthwhile discussing as researchers use them in order to compensate for the problems associated with mixed and non-aqueous solvents.

6.5.2.1 Extrapolation

Takács-Novák *et al*³⁶ used strong acid/strong base titrations in order to perform a four-parameter electrode calibration in order to investigate pK_a values in methanol/water mixtures of varying methanol content. For the procedure HCl solutions of known concentration, containing 0-75 wt% methanol were titrated with standardised NaOH at $25.0 \pm 0.1^\circ\text{C}$, $I = 0.10\text{ M}$, under N_2 atmosphere, in the pH interval 2-12. The operational pH readings were related to the concentration pH values, which were denoted as $p_c\text{H}$, by the multiparametric equation shown below.

$$\text{pH} = \alpha + Sp_cH + j_{\text{H}}[\text{H}^+] + j_{\text{OH}} \frac{K_w}{[\text{H}^+]} \quad (6.21)$$

The intercept parameter α in aqueous solution mainly corresponds to the negative logarithm of the activity coefficient of the hydrogen ion at the working temperature and ionic strength. The j_H term corrects pH readings for the nonlinear pH response due to liquid junction and asymmetry potentials in moderately acidic solutions, while the j_{OH} term corrects for high-pH nonlinear effect and for the different ionisation values of each solvent composition. Factor S accounts for the fact that a particular electrode may not have 100% Nernstian slope, and K_w is the ionisation constant of water. For this method each of the four calibration parameters had to be determined for every methanol/water mixture used in the investigation, the results of which are shown in Table 4.

R (wt%)	α	S	j_H	j_{OH}
0	-0.007	1.0037	1.8	-0.8
7.5	0.002	1.0031	1.6	-0.7
15.1	0.019	1.0005	1.6	0.1
23.1	0.055	0.9972	0.5	-1.3
31.1	0.073	0.9970	1.4	-1.0
39.3	0.128	0.9972	1.3	-1.6
47.9	0.17	0.9950	1.6	-0.8
57.4	0.167	1.0021	2.4	-2.8

Table 4: The four calibration parameters of an electrode shown for increasing methanol/water wt%, where R is the wt% of methanol in solvent mixtures.

Therefore, depending on the % methanol content chosen the corresponding calibration parameters were applied to calculate what Takács-Novák have termed p_cH , which represents the pH value calculated using hydrogen ion concentration, not activity. An advantage of this technique, even though it is very time consuming and impractical, is that if equilibrium values are determined at multiple % methanol contents the determined values can then be extrapolated to zero methanol content in order to determine the corresponding equilibrium values for the reaction in pure aqueous solutions.

6.5.2.2 Correction Coefficients

Previously, measurements of pH in mixed solvents have been performed using equations of the type $pH^* = pH[R] - \delta$, where pH^* is the corrected value and $pH[R]$ is the pH-meter reading obtained in the solvent mixture. The correction values of δ correspond to each different solvent mixture and can be obtained from literature such as published by Douheret in 1967³⁷. According to Bates³⁸ the correction constant is related to the electrode junction potential, E_j , between the two solvents and the primary

medium effect for the solvent, that is the hydrogen ion activity coefficient on transfer from water to the organic solvent and water mixture, m°/H , by the equation $\delta = E_j - \log m^{\circ}/H$. This quantity has been shown to be substantially constant for a medium of given composition ³⁹.

Gibson *et al* ³³ performed potentiometric titrations in pure alcohol solvents. To overcome the problem of relating the electrode potential readings to absolute pH, a similar correction constant was applied to the pH readings determined in the alcohol solvents. The correction coefficient Gibson applied in alcohol solutions was determined independently many years ago by two researchers Bates *et al* ⁴⁰ and Grunwald *et al* ^{41, 42}. For the designation of pH in the nonaqueous alcohol solvents Gibson *et al* applied the technique based on the recommendations of the IUPAC ⁴³ with the correction value defined previously. For measurements in methanol and ethanol the correction value has been calculated to be $\delta = -2.24$ and -2.54 respectively, and this value is then added to the pH value measured in each alcohol solution, in order to determine what the absolute pH would be if the measurement had have been in an aqueous solution.

6.5.3 Titration Calibration

As previously stated, calibration of the electrode for hydrogen ion concentration is usually performed using a strong acid/strong base titration, which can be performed using mixed or non-aqueous solvents. Sigel, Zuberbühler and Yamuchi ³⁴ used strong acids and bases of known concentration to calibrate the electrode in solutions of mixed solvents as such a method of calibration does not rely upon the solvent composition. The calibration technique that was developed involved making a number of measurements of the potential in the flat acid region of the pH curve, pH 3-4, and also in the flat base region, pH 10-11 ⁴⁴. When the solvent composition is changed, for example from pure water to a 50/50 (v/v) ethanol/water solvent mixture, the determined calibration line is subsequently affected. Calibration parameter values of 59.16 mV/pH and 400.0 mV for s and E_{const} respectively are commonly quoted for pure aqueous solutions. However, in a 50/50 (v/v) ethanol/water solvent mixture the calibration parameters are generally 59.86 mV/pH and 385.3 mV. Such a change in calibration parameters can result in significant differences for the calibrated pH value of an unknown solution.

Even with the well-established titration calibration technique complications arise with using mixed or non-aqueous solvents. For example, the ionisation constant of many mixed or non-aqueous solvents, pK_s , are unknown, especially if the temperature is changed from the commonly used 25° C. The accurate value of pK_s for each solvent is required as this constant defines the pH value above 7 and if temperature changes or different solvent compositions are not taken into account then the pH values measured above a pH of 7 will be systematically incorrect.

The problem of unknown ionisation constants of mixed solvents can be resolved by applying an iterative method to alter the pK_s of the solvent in order to obtain the best fit of the measured and calculated data. The correlation coefficient and graphical examination of the calibration points, both of which indicate the goodness of fit, serve as a guide to the suitability of the calibration. Such a calibration should be rejected on the basis of poorly correlated points in a linear least squares fit of the calibration values or an unreasonable value of pK_s .

Taking into account that the ionisation constant of the solvent can be determined from a strong acid/strong base calibration titration, and that such a titration results in the calibration of the electrode to read hydrogen ion concentration, and hence enables the calculation of stoichiometric equilibrium constants, there are still many drawbacks with using such a method for calibration. This is because there are several other factors that affect the accuracy of potential readings for example, the potential of the glass electrode being strongly temperature dependant, as are the liquid junction and reference potentials, and to a lesser extent stirring, aging of the reference electrode, changing liquid junction potentials from calibration titration to measurement, sensitivity limits, suspension effects and interferences, stability and the limits of the electrode all have differing effects on the electrode and its response ⁴⁵.

Further complications arise with the liquid junction potential as this factor varies with the composition of the solutions forming the junction, and as such this should be accounted for by the calibration procedure. This is often difficult to achieve as the strong acid and strong base solutions used for calibration can differ greatly from the composition of solutions used for the measurement. It is also well known that the standard potential of the glass membrane varies from day to day due to asymmetry effects, therefore making it difficult to reproduce liquid junction potentials with adequate precision. These factors all affect the linear parameters, s and E_{const} , that are

used to calibrate the electrode response⁴⁶. Therefore, calibrations that are titration based must be performed regularly in order to reduce the effect of all the variable factors and to accurately determine the linear parameters. Although many cannot be adequately dealt with researchers either make an attempt to minimise their influences or chose to ignore them altogether.

Thus the titration calibration technique is not only time consuming, but also has drawbacks, such as the need to re-calibrate the electrode regularly to ensure that the linear relationship between the electrode response and hydrogen ion concentration is as consistent and valid as possible. In order to effectively reduce these concerns, and to enable measurements to be accurately performed in mixed or non-aqueous solvents an internal calibration of the pH electrode, performed in the test solution itself, is a highly desirable procedure.

6.5.4 Internal Concentration Calibration

A few researchers have developed internal calibration techniques that enable the electrode calibration parameters, that is s and E_{const} as defined in Equation (6.19), to be determined as part of the titration of the test solution. For example, if an unknown ligand solution is titrated in order to determine the respective protonation constants, the electrode can be calibrated as part of the analysis of that measurement rather than performing a calibration titration prior to experimentation. In principle the concept is simple. A strong acid/strong base titration was previously used to determine the calibration parameters as it adequately covered the two pH ranges, 2 – 4 and 10 – 12, that are required. However, any titration that adequately covers these two pH ranges carries sufficient information in order to calibrate the electrode.

The procedure becomes more complex with the determination of the hydrogen ion concentration at each point on the titration curve. Such a task was trivial for the strong acid/strong base titration as the concentration was directly related to the initial concentrations of the acid and base solutions, the initial volume and the amount of titrant added, as detailed in Equation (6.17). However, for more complex titrations the calculation of the hydrogen ion concentrations are not as trivial, often involving complicated protonation and metal-ligand equilibria. Therefore, internal calibration techniques require fairly sophisticated optimisation programs in order for the internal calibration concept to be successfully implemented.

As mentioned earlier, researchers who investigate equilibrium constants generally use the concentration technique for calibration, and then use the titration of the species being investigated measuring the hydrogen ion concentration at each value of added base in order to calculate equilibrium constants. Hence, the same computational programs that researchers used to optimise equilibrium constants using hydrogen ion concentration values, could also be extended to calculate the electrode calibration parameters simultaneously with the equilibrium constants and, depending on the depth of the program, also determine other pertinent titration parameters such as the analytical concentrations^{7, 46}.

In fact, such optimisation is, in essence, critical as the most pronounced influence on the determination of equilibrium constants stems from experimental errors in titration parameters such as the electrode calibration parameters, known analytical concentrations, and any ‘fixed’ constants, especially protonation constants and the ionisation constant of the solvent. Besides from the inconsistencies with electrode parameter calculations it is also often assumed that in aqueous solvents the pK_s is equal to 10^{-14} . However, this is only true for neutral pure water and not for all pH ranges. Deviations from the theoretical value for the ionisation of water may result in solutions that are not neutral and contain electrolytes, which is essentially every solution for equilibrium investigations. Also, if there are any variations in temperature the pK_s alters accordingly. For instance, if the temperature increases the dissociation of hydrogen and hydroxide ions also increases, and subsequently the pH reading decreases, even though the water is still charge neutral. Therefore, the pH value of a solution at a particular temperature is reliant on the relationship between the dissociation constant of the solvent and the temperature⁸. The matter is further complicated if the study involves the use of mixed or non-organic solvents as the ionisation of the solvent is not equal to pK_w and often may not be known.

If the pK_s is incorrect or unknown then complications arise with calibrating the electrode as this factor is used to define the hydrogen ion concentration at pH values greater than a pH of approximately 7.

$$[H^+] = \frac{K_s}{[OH^-]} \quad (6.22)$$

Therefore, if an incorrect value is used, for example 10^{-14} in a mixed solvent, then the calculation of the calibration line will not be accurate and hence all conversions of

electrode response to pH values will also be systematically incorrect. Due to these considerations it is clear to see that great errors can occur in the calculation of equilibrium constants if the pK_s is considered to be equal to 10^{-14} and not accurately determined for each solvent system and for each temperature range. The refinement of the ionisation constant of the solvent as part of the calibration calculation removes the concern with pK_s not being 10^{-14} and also enables calibration in mixed or non-aqueous solvents where the solvent ionisation value is not equal to that of pure water, and often unknown.

Internal calibration, that is the refinement of all relevant experimental parameters simultaneously from one titration, greatly reduces the influences discussed above and is key to reliable and accurate analysis of titration data ⁷. The concept of simultaneous refinement of the titration parameters along with the equilibrium constants has been proven to be generally advantageous providing the chemical species in the analysed solution are well established, for examples of analysis see references [12, 47-52]. For instance, Fiol *et al* ⁵³ noted that systematic errors in the analytical concentrations can have different effects on the electrode response depending on the specific form of the calibration equation, therefore, if the concentrations of the components are included as part of the refinement of the calibration parameters, this concern is removed. The limitation of species not forming to high enough concentrations is discussed later in Section 6.6.

6.5.5 Internal Concentration Computer Programs

There are some researchers who have developed sophisticated programs in order to simultaneously refine titration parameters. A basic example of a computer program that was designed is the program GLEE (GLass Electrode Evaluation) ⁵⁴, which was developed as part of the Hyperquad ⁵⁵ suite of programs for stability constant determination. The program provides an estimate of the carbonate contamination of the base, the pseudo-Nernstian standard potential, E_{const} , and slope s of the electrode and, optionally, the concentration of the base and pK_s .

May *et al* ¹² also designed a computer program capable of internal calibration called MAGEC (Multiple Analysis of titration data for Glass Electrode Calibration) that could optimise simultaneously any or all of the titration parameters pertinent to the calibration of pH electrodes. For instance, the hydrogen ionisation constants of a ligand and the

glass electrode parameters could be optimised simultaneously from a given single set of titration data.

Brandariz *et al*¹ is another researcher who applied the internal calibration approach in order to overcome the hindrance and errors associated with calibration. He noted that one clear advantage of this method of calibration was that the electrode has been calibrated in very specific pH range, that is the pH range used for calibration is identical to the pH range of the measurement.

Baeza *et al*⁵⁶ stated that better results were reported for the analysis of hydrogen ionisation constants if the ionisation constant of the solvent and some electrode calibration parameters, such as the standard potential E_{const} , the slope, which he has termed the sensitivity factor g , and the liquid junction potentials j_h and j_{oh} , were determined simultaneously with the equilibrium constants. The program Baeza developed is known as PHCONST and it was developed to carry out the simultaneous determination of a maximum of twelve parameters. It could compute up to six hydrogen ionisation constants, four electrode calibration parameters (E_{const} , g , j_h , j_{oh}), the ionisation constant of the solvent (pK_s) as well as the titrant concentration.

The program ACBA (Acid-Base titrations), developed in 1979 by Arena *et al*⁵⁷, is very similar to the program that was developed at the University of Newcastle, discussed in-depth in the following section. The program was developed in order to increase the possibilities of analysing potentiometric titration curves in acid-base titrations. It is a non-linear least-squares computer program that is able to refine any parameter of an acid-base titration, even in the case of mixtures. Moreover, parameters common to several titrations, and parameters which have different values from titration to titration, can be simultaneously refined with this program. The particular points of the operation of the program are (i) the parameters to be refined are divided into common parameters, those that are common to all titrations being analysed, and titration parameters, those that are relevant to only a single titration; (ii) the shifts are obtained and used to calculate new parameters; (iii) the program then performs the convergence controls. However, the limitations of this program are that it only applies to acid-base titrations and not to complex ligand titrations or ligand-metal interactions. It is also restricted to a maximum of nine common parameters and two titration parameters.

6.6 Our Global Internal Calibration Program

Unfortunately, limitations still do exist for potentiometric analysis even with the internal calibration development. There are instances when it is not possible to have a complete titration, that is one that adequately covers the two required pH ranges, due to complications with the test sample. For example, the ligand may precipitate at pH values above 9 or the lowest pH attainable may only be a pH of 5, therefore making the internal calibration procedure unusable as the required pH ranges have not been adequately covered by the measurement. Also, internal calibration programs can be hampered by limitations arising from badly defined parameters, for instance if individual species are not formed to a high enough concentrations, or if correlations exist between two or more parameters ⁷.

In order to overcome these concerns and still use internal calibration as an effective technique of calibration, one can apply the methodology that has been termed 'global' analysis, which is where two or more measurements are analysed together in the one process. The 'global' analysis concept has been previously discussed in greater detail in Chapter 2. To our knowledge, currently there are no published accounts of global analysis being used as part of the optimisation procedure for an internal calibration technique.

Essentially, global analysis enables the researcher to perform multiple titrations, under different conditions such as different initial concentrations, in order to cover the required pH range and properly define all relevant parameters. For example, if a metal forms a hydroxide species and precipitates at high pH values due to the ligand being too labile, then a second titration that covers the pH range up to 12 can be performed with, for instance, the ligand only. These titrations can then be combined as together they cover the required range for electrode calibration. Additionally, it enables the researcher to perform titrations at varying initial concentrations in order to ensure that all species are formed to a suitable concentration in at least one of the titrations in the set. Then the titrations can be analysed together as one set in the global analysis and because the required pH range is covered, and all species are well established, the internal calibration procedure can be applied.

6.6.1 Defining Parameters

The procedure aims to obtain a linear calibration curve for the electrode system while simultaneously optimising all other relevant parameters of the experiment. The computer program is a non-linear least-squares optimisation that has been written for the refinement of the multiple parameters that define a potentiometric titration.

The core of the program has been previously explained in detail in Chapter 2, Section 2.3. Essentially the program optimises all parameters by applying them to a defined model of the experiment in order to determine the calculated data. The measured and calculated data are then compared and the difference between each pair of measured and calculated data is determined, this difference is commonly termed the residual and defined as shown in Equation (6.23), where R is the residual, D_{meas} is the measured data, and D_{calc} is the calculated data.

$$R = D_{\text{meas}} - D_{\text{calc}} \quad (6.23)$$

Obviously the less difference between the two sets of data, that is the smaller the residuals, the better the parameter values. The non-linear least-squares optimisation calculates parameter values until a minimum over the sum of all squares of residuals has been determined.

Each parameter value that is optimised by the program is defined by different sections of the experimental titration curve providing that the correlations between parameters are not significantly high. To demonstrate how each parameter is defined by a titration an example of a ligand with three protonated nitrogen atoms titrated with NaOH is given. The protonation constants of the ligand were determined to be $\log K(\text{LH}_3) = 2.01$, $\log K(\text{LH}_2) = 7.66$, and $\log K(\text{LH}) = 8.86$ and the titration is shown below in Figure 6.3.

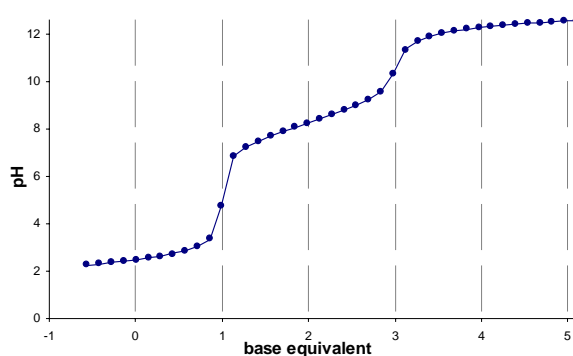
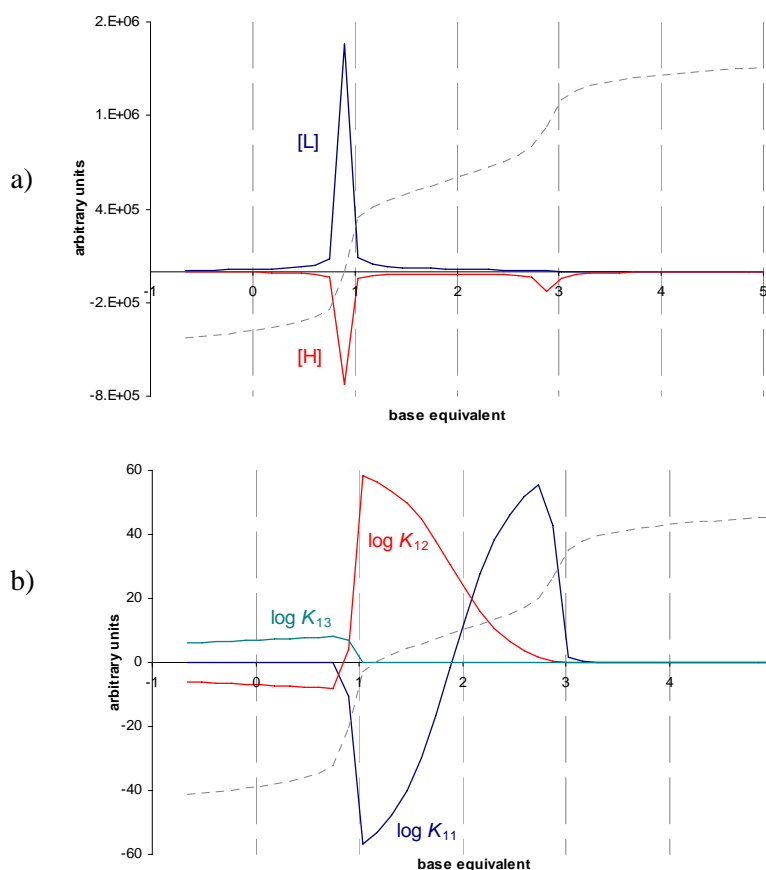


Figure 6.3: Titration of a ligand with three protonated nitrogen atoms.

A visual way to describe the dependence of each parameter on the titration is to depict the Jacobian plots after optimisation of the parameters has been completed. The Jacobian, \mathbf{J} has been previously discussed in Chapter 2, Section 2.3.4 and its formula is shown below. It can be defined as the calculation of the derivatives of the residuals \mathbf{R} with respect to the parameters \mathbf{p} of the measurement.

$$\mathbf{J} = \frac{\delta \mathbf{R}}{\delta \mathbf{p}} \quad (6.24)$$

The relevant Jacobian plots for the above titration are shown Figure 6.4. They illustrate the dependence of each parameter on different sections of the complete titration curve in order to be defined. For example, it can be seen from Figure 6.4a) how the initial component concentrations of the reaction are defined. The ligand concentration is defined by the first equivalent point, that is, where one equivalent of base has been added. If the concentration of ligand were to change then this first equivalence point would adjust accordingly. However, a change in acid concentration would affect the position of both equivalent points as can be seen by the presence of two peaks in the plot. For example, an increase in acid concentration would shift the entire titration curve to the right as more base would need to be added to reach the end points.



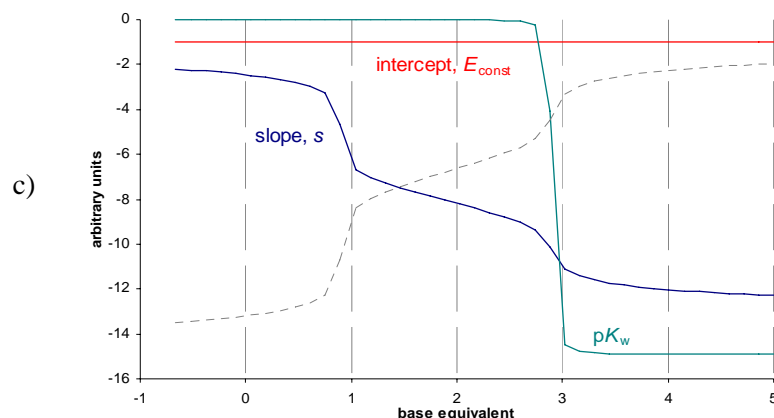


Figure 6.4: Jacobian plots showing the influence each parameter has on the calculated residuals throughout the titration of a protonated ligand. The actual titration is shown as a dashed line in the background.

Figure 6.4b) illustrates which parts of the titration curve, that is at what equivalent of base added, each equilibrium constant is defined. The loss of the first proton, $\log \beta_{13}$, is completely defined by the position of the first end point. The loss of the second proton, $\log \beta_{12}$, is also partly defined by the equivalent of base required to reach the first end point, but more so by the equivalent moles of base required to move from the first to the second end point in the titration. The third deprotonation, $\log \beta_{11}$, is defined only by the equivalent amount of base required to move from the first end point to the second. This demonstrates how equilibrium constants are defined by different sections of a titration.

Consideration of Figure 6.4c) highlights the need for a complete titration in order to determine the linear calibration parameters of the electrode. The E_{const} linear parameter is defined by the first reading of the electrode as it is the intercept of the calibration line and hence is, by definition, constant throughout the titration. The slope parameter, s , is defined by the entire titration, but it is the relationship between s and the ionisation constant of the solvent, pK_s , that requires both pH ranges in order to fully define both parameters as they are somewhat inter-dependant. It is clear to see that pK_s is only defined at high pH values, that is after the second end point in the example which occurs at an approximate pH of 10. If the titration were to end before this pH then the pK_s parameter would not be defined and therefore could not be optimised because of the correlation it has with the ionisation constant of the solvent.

Table 5 shows the correlation coefficients for all parameters to one another. A value of zero indicates complete independence and -1 or +1 indicates complete correlation. The correlation coefficient of 0.831 between the slope parameter s and pK_s is fairly high, and

even though it does not indicate complete dependence it does demonstrate that if one of the parameters is not adequately defined then the other will also not be definite. It can also be seen that the ligand and hydrogen ion concentrations are highly dependant, with a value of -0.982. However, this is to be expected as the protonation of the ligand is directly related to the concentration of hydrogen ions in solution.

	$\log \beta_{11}$	$\log \beta_{12}$	$\log \beta_{13}$	pK_s	[L]	[H]	slope, s	int, E_{const}
$\log \beta_{11}$	1.000	-0.544	-0.020	-0.026	-0.108	0.029	-0.082	-0.023
$\log \beta_{12}$	-0.544	1.000	-0.175	0.000	0.082	-0.105	-0.366	-0.365
$\log \beta_{13}$	-0.020	-0.175	1.000	0.000	0.334	-0.325	-0.169	-0.539
pK_s	-0.026	0.000	0.000	1.000	0.000	0.059	0.831	0.615
[L]	-0.108	0.082	0.334	0.000	1.000	-0.982	-0.118	-0.214
[H]	0.029	-0.105	-0.325	0.059	-0.982	1.000	0.211	0.292
slope, s	-0.082	-0.366	-0.169	0.831	-0.118	0.211	1.000	0.904
int, E_{const}	-0.023	-0.365	-0.539	0.615	-0.214	0.292	0.904	1.000

Table 5: Values of the normalised curvature matrix showing the correlation coefficients of each optimised parameter.

For instances where one titration does not cover the required pH range for calibration, it is still possible to determine the calibration parameters along with the highly correlation ionisation constant of the solvent, if the previously described global analysis technique is applied. That is, if two or more titrations are performed that together cover the required pH range, then the titrations are analysed together globally, the calibration parameters and ionisation constant will be fully defined and can therefore be optimised along with the other relevant titration parameters. Thus, it can be seen that the globalisation technique we developed is clearly superior to other available techniques as all parameters can be optimised in one analysis, even if not all of the titrations contain the necessary information to fully define each parameter.

To illustrate this point consider the titration of piperazine shown below in Figure 6.5a). It can be seen that the titration clearly does not cover the required pH range as it ends at a pH before 10. Therefore, the calibration of the electrode will not be adequate as pK_s will not be defined. Analysis with the incomplete titration results in a pK_s of -42.651, with error estimates for the measurement being infinity because of the uncertainty in the calculation. By performing another titration under different conditions, for this example that is continuing the titration till a pH of approximately 12

has been reached, and then combining both titrations in a global analysis, both titrations can be adequately analysed as the second titration defines the pK_s as -13.585 ± 0.019 .

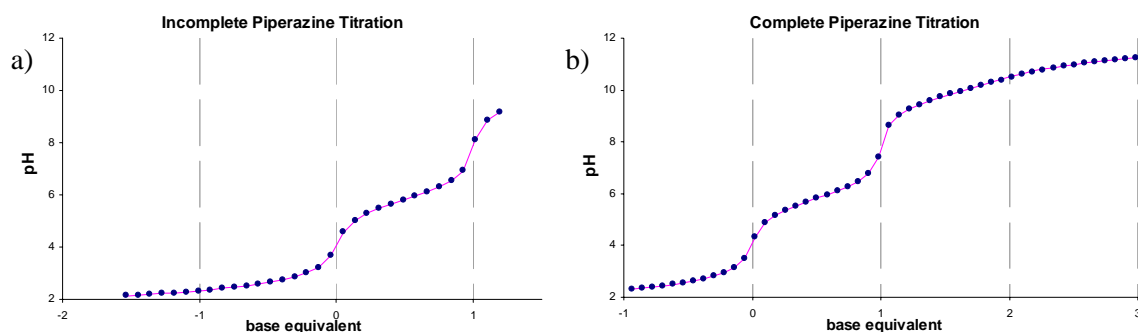


Figure 6.5: a) Incomplete titration of piperazine; b) complete titration of piperazine adequately covering the required pH range for calibration of the electrode. Global analysis enables both titrations to be analysed in the one procedure with all parameters adequately defined.

6.7 Activity Approximations

The computations performed for the analytical process described in Section 6.6 are only strictly valid for ideal situations. Experimental conditions are usually specifically chosen to minimise the adverse effects of various assumptions such as constant ionic strength that have to be made for the analysis of the data. In particular, very high concentrations of background electrolytes have been employed to obviate such difficulties as the characterisation of activity and liquid junction potential changes that are associated with non-constant ionic strength conditions⁵⁸. If conditions are non-ideal then the approximations, such as concentration being directly related to the activity of the hydrogen ion, can no longer be considered valid.

Non-constant ionic strength is a non-ideal difficulty that is traditionally circumvented by the addition of an excess concentration of an inert salt to the reaction solutions. The excess inert salt reduces the fluctuations of the ionic strength, but large excesses are required to maintain almost constant ionic strength and the inert ions have the potential to interfere in undesirable ways with the process. The addition of excess salt can also be problematic if the ideal situation cannot be maintained, for example even though it is routine procedure to add inert salts in academic research, such methods are not feasible for industrial situations. Also, for many common applications, it is inappropriate to measure equilibrium constants under constant ionic strength conditions. For instance, many biological solutions such as natural waters, for example, rivers, lakes and soil solutions, as well as physiological fluids, such as plant xylem sap and blood plasma,

have much lower ionic strengths. Therefore, the relevant measurements ought to be performed in concentrations that are indicative of the natural systems they are meant to mimic. Under these conditions, the assumption of constant ionic strength is less valid and can lead to significant errors ⁷.

Therefore some experiments need to be performed under non-ideal conditions. Being able to perform experiments at non-constant ionic strength is also beneficial in a laboratory as it makes measurements easier and also removes the uncertainty of whether or not the added salt is interfering in the reaction in some manner.

Recent developments in analytical processes attempt to model inconsistencies such as the problems associated with non-constant ionic strength, therefore enabling the application of analysis techniques to non-ideal data sets that may be encountered in industrial situations, where conditions are usually far from ideal, and in academic research where ionic strength has not been held constant. In simple terms the computational remedy is to replace concentrations with the activities of the species for all calculations that previously involved using concentrations.

En-route to calculating the activity coefficients, and hence activities to replace concentrations, other concepts need to be defined. The first is to define ionic strength (μ), which is shown in the equation below where c_i is the molar concentration and z_i is the valence of each ion.

$$\mu = \frac{1}{2} \sum_i c_i z_i^2 \quad (6.25)$$

The ionic strength is simply a measure of the number of ions present in solution. It is important to note that the ionic strength is dependant on all ions in solution, not just the ion of interest, which in our case is the hydrogen ion. Activity coefficients are mainly influenced by on the ionic strength of the solution.

There are several equations that approximately calculate activity coefficients as a function of ionic strength. At low concentrations, and subsequent low ionic strength, the approximations are simple and relatively accurate, however at high concentrations the approximations are poor even if more complex equations are used for the approximation. The standard Debye-Hückel equation was used for the approximations and was shown previously in Equation (6.6). Such an approximation is useable up to ionic strengths and concentrations of approximately 1 M.

In general, the development of modern analytical software is attempting to incorporate non-ideal situations into the computations, thus avoiding external control of factors such as the ionic strength as discussed here. While this is useful in academic investigations as it simplifies experimentation, it is essential for industrial processes where additions of inert salts are not possible. Most of the non-ideal correction factors are based on approximations and are therefore not perfect, however the approximate calculations are usually preferable to either ignoring the ionic strength changes altogether or to the complicated calculations associated with the experimental difficulties encountered with external control of the ionic strength.

Incorporating approximations for non-constant ionic strength also enables the calculation of pH as defined by the hydrogen ion activity, as given in the IUPAC guidelines in Equation (6.1). This means that the true pH, $\log\{H^+\}$, of a solution can now be determined. That is, rather than measuring the concentration of the hydrogen ion, pH measurements can be based on the hydrogen ion activity. In addition, such approximations enable the determination of the activities of all species in solutions, rather than concentrations, meaning that using pH as defined in Equation (6.1) will not result in the calculation of mixed equilibrium constants. Therefore, the theoretically preferred thermodynamic equilibrium constants can be determined, rather than the experimental stoichiometric constants that are commonly calculated using pH values defined by hydrogen ion concentrations.

6.8 Complex Solution Calibration Applications

As previously described in Section 6.6, internal calibration of the electrode is clearly the leading technique for precise and accurate pH measurements. The important understanding is that any titration contains the necessary information for calibration as long as the two pH ranges, 2 – 4 and 10 – 12, are adequately covered and providing the hydrogen ion concentration can be accurately determined at each electrode reading of the titration.

The internal calibration technique can be developed further to enable more than the accurate determination of equilibrium constants in any desired solvent. There are much broader applications possible such as the precise calibration and measurement of pH in complex samples where current methods can only provide approximate readings. Many industrial practices that require pH measurements in complex samples calibrate the electrode using the popular standard buffer solutions, refer to Section 6.2.1.3, then take

a subsequent pH reading and incorrectly assume that the pH value is a reflection of the hydrogen ion concentration in the sample.

The current, widespread calibration techniques, that is standard buffer solutions and also strong acid/strong base titrations, cannot accurately calibrate the electrode because the sample mixture is very different in composition from the solutions used for the calibration process. This has many effects on the potential measured by the electrode as the electrode reading is highly influenced by the many changing parameters from calibration to measurement. For instance, the liquid junction potential will change, the ionic strength of the solutions will be different, in industry temperature inconsistencies are common, and there will also be accentuated fluctuations in the standard potential of the glass electrode. These variable parameters not only affect the potential reading of the electrode, they also result in different hydrogen ion activity coefficients which means the calibration no longer accurately relates the potential to free hydrogen ion concentration, and hence the pH.

6.8.1 pH Measurements in Beverages

One such industry where pH measurements are vital, yet not accurately performed, is with wine and fruit juice samples. We modified the previously described internal calibration technique for calibrating the pH electrode in order to obtain accurate free hydrogen ion concentrations, pH values, in such samples.

In beverages, such as wine and fruit juice, there are various kinds of organic acids present, for example tartaric, malic, succinic, and citric acid. Acid content differs depending on the particular origin and growth conditions of the original fruits and also changes during the manufacturing process. The total acid content in beverages is termed “total acid” or “total acidity” and serves as an indication of the taste, aroma and quality of beverage ⁵⁹.

The determination of the total acidity is an essential gauge in process and quality control. The official analytical method currently applied is to use a NaOH titration with phenolphthalein as an indicator ⁵⁹. However, even though a titration method is being used, problems exist because the ‘endpoint’ is arbitrary and any pH could be defined as the ‘end’, therefore the method does not always produce satisfactory results. There are also further ambiguities due to the vagueness of the indicator colour change. This ambiguity is particularly evident in the case of red or pink wines and non-transparent or

highly coloured fruit juice samples. Hence, potentiometric titrations would be a viable alternative method to the use of indicators to detect the concentrations via the pK_a 's of the acids present. However, popular calibration techniques for the electrode are somewhat unsatisfactory for such measurements due to the aforementioned complications.

It would seem straightforward to apply the previously described internal calibration technique where the unknown calibration parameters of the electrode are simply optimised with the other parameters of the titration. However, the difficulties arise not from determining the calibration parameters, but because it is impossible to know exactly which acids are present and in what concentrations in a natural sample. Even if the acids and their concentrations were determined for a sample every beverage differs, naturally having varying acids and acid concentrations present. It is therefore not feasible to determine each acid and its concentration for every individual sample that needs to be measured. Consequently, due to this uncertainty, the hydrogen ion concentration cannot be accurately determined at each potential reading. This is required to determine the linear calibration line that defines the relationship between electrode reading and pH.

6.8.1.1 Secondary Calibration

Process Description

In order to overcome the restriction of not knowing the acids that are present in the varying beverage samples, which therefore prevents the application of the standard internal calibration techniques, we applied a modified calibration technique. The basic idea was to determine the titration curve of a particular acid in the beverage. To describe the process required for this secondary calibration method we will initially only consider two particular points on a titration curve, that is two specific pH readings in the titration of the sample. The method is represented by the series of graphs in Figure 6.6. In order to make the following process and graphs easier to interpret instead of plotting the potential readings from the electrode the measured potential value has been converted into a pH value using the standard calibration parameters that have been determined from calibration of the electrode in pure water. These pH values are shown are obviously not the precise pH, only an approximation that we have used in order to aid with interpretation.

The first step in the process is to add a set amount of acid to the sample which will consequently lower the pH value, as shown in Figure 6.6a). It is important to note that the addition of acid not only lowers the pH, but also changes any acid/base equilibria that exist in the complex sample. Consider a sample orange juice. In such a beverage there are obviously complex combinations of acids present due the naturally occurring acids such as citric, ascorbic, tartaric and malic acids, all being present in varying concentrations. The acid/base equilibria of all these acids interact according to Le Chatelier's principle, and therefore the change in acid concentration from the added acid will also alter all of the equilibria positions and species concentrations. However, as we will demonstrate, this unknown change in equilibria does not affect the calibration technique.

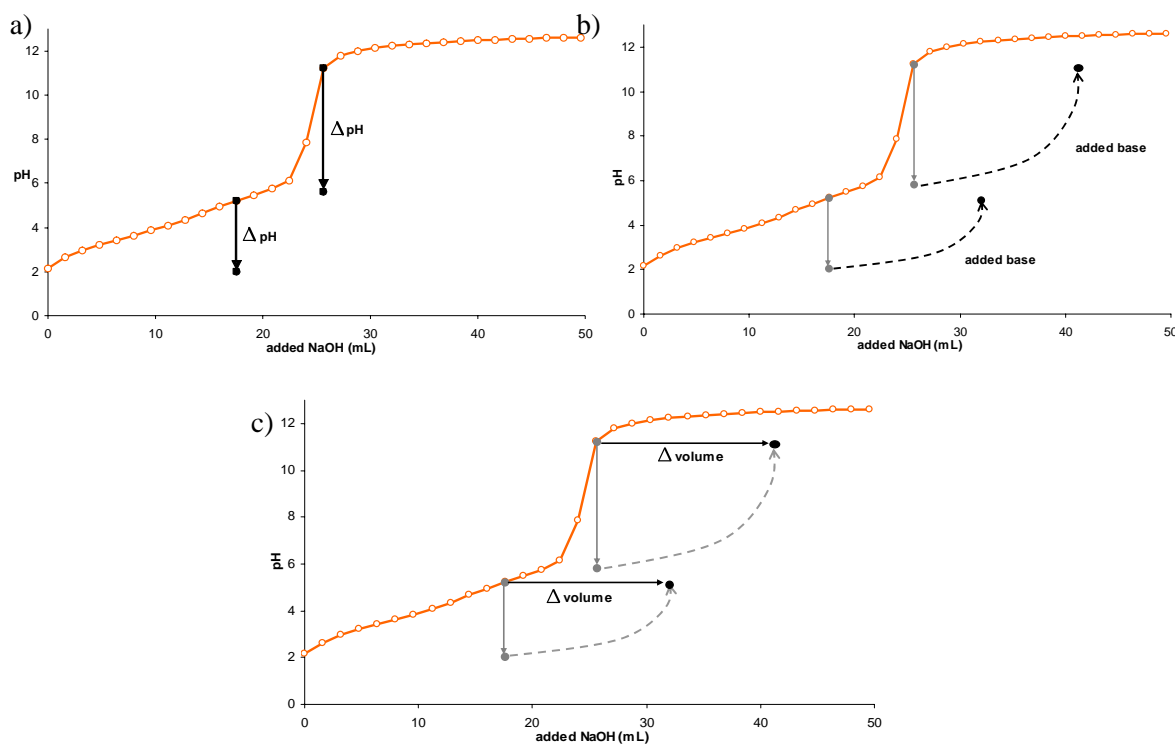


Figure 6.6: Graphs showing a) the addition of acid at two pH values in an orange juice titration; b) the subsequent lowering of pH and re-establishment of the original pH value by the addition of base; c) the calculated volume of base required to re-establish the original pH value.

After the pH has been lowered from the addition of acid, sufficient base is then added at each point in order to return the pH back to its original value, this step is depicted in Figure 6.6b). Due to the complicated nature of samples the path here is unknown. Nevertheless, the amount of base required to re-establish the pH value is a direct measure of the free hydrogen ion concentration present due to the added acid. The calculation of the volume of base required to re-establish the original pH value is

graphically shown in Figure 6.6c). It is important to note that when the pH value has been re-established the complicated and unknown equilibria in the system are also re-established.

For both pH points on the titration curve the same set amount of acid was added, however the subsequent change in pH was not necessarily equal for both changes due to the acid/base equilibria in the system. Hence, the amount of free hydrogen ions will also differ at each pH value, the amount of free hydrogen ions at each value being determined by the required quantity of base needed in order to re-establish the original pH value.

The measurement that is important in this secondary calibration technique is actually not the set amount of acid added at each pH value, as the consequent change in pH is strongly influenced by the complex equilibria in the sample. Rather, it is the measure of base required to re-establish the original pH value, as this volume is independent of the complex equilibria and is therefore a direct measurement of the excess free acid in the solution.

Titration Method

The technique as described above details a very tedious method that requires the addition of a set amount of acid, followed by the addition of the subsequent required volume of base, at each pH measurement in a titration. This is not a feasible technique as titrations can often range upwards of fifty data points. However, in practise the calibration technique is much simpler and in fact requires only two titrations. For the previous example of orange juice the first step is a simple titration of the sample in the normal manner; a base, typically NaOH, is titrated against the naturally acidic orange juice solution. The electrode reading is taken after each addition of base as is done in a normal titration with the resultant titration curve depicted in Figure 6.7.

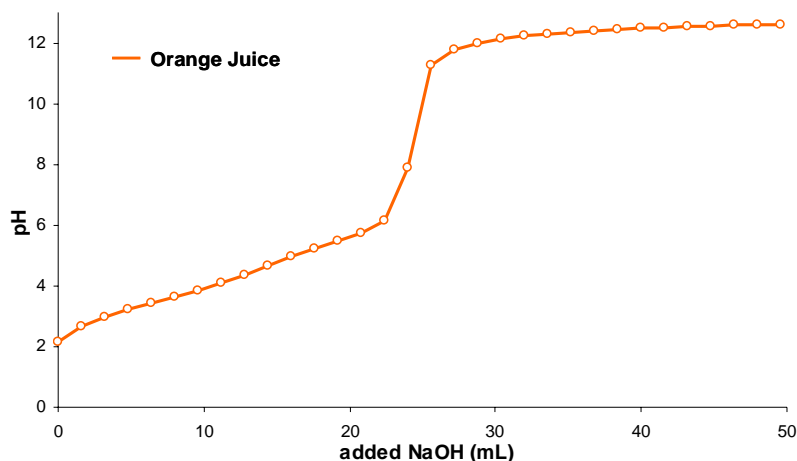


Figure 6.7: Titration curve of orange juice with added NaOH.

The second step involves the addition of a known concentration of acid, for example HCl. The acid is added to the original orange juice sample, then this acidified orange juice solution is titrated in the same manner as before. It is important that the volume of acid added to the sample is small comparative to the sample size, for example 0.5 mL in a 50 mL sample, in order to minimise disturbances to the sample matrix. If the amount of acid added is greater than approximately one percent the properties of the orange juice may substantially change. For instance, acid is usually prepared in aqueous medium, therefore if 25 mL of acid was added to a 50 mL sample then the solvent composition of the orange juice would be significantly altered and the two titrations of orange juice could not be accurately compared with one another. It is essential for this calibration technique that the only significant difference between the two orange juice titrations is the concentration of acid that present, all other factors need to be held as constant as possible.

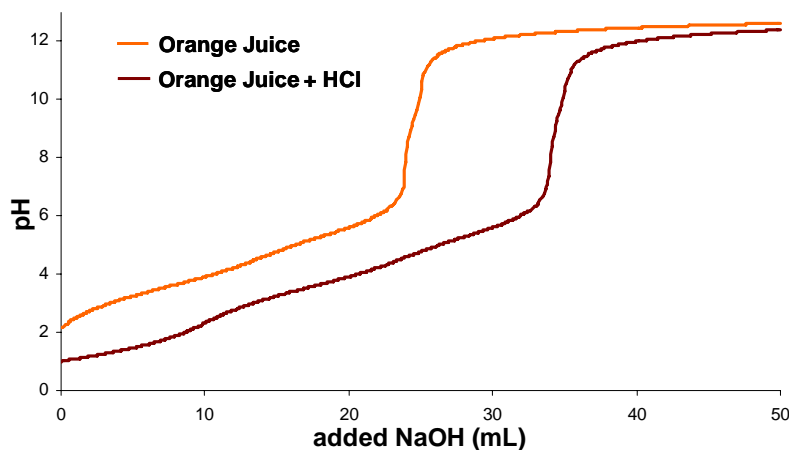


Figure 6.8: Titration curves of plain orange juice — and acidified orange juice —.

The two titrations of orange juice are depicted in Figure 6.8. It can be seen that there is a clear difference between the two titrations. This shift is obviously due to the addition of acid before the second titration and is directly related to the different volume of base required in order for the pH to be the same value in both the natural and acidified orange juice titration curves. Using computational techniques the volume of added base required to re-establish the pH in the original orange juice titration can be calculated. This calculation can easily be made at every pH point on the orange juice titration curve. However, it must be remembered that the pH values measured in the natural orange juice titration do not coincide exactly with the pH values measured in the acidified sample, as is demonstrated in Figure 6.9a) at the equivalence point. Therefore the second titration must be interpolated to enable the exact pH values to be calculated so the same pH readings are known for the natural and acidified titration, therefore enabling the exact volume difference between two pH values to be calculated.

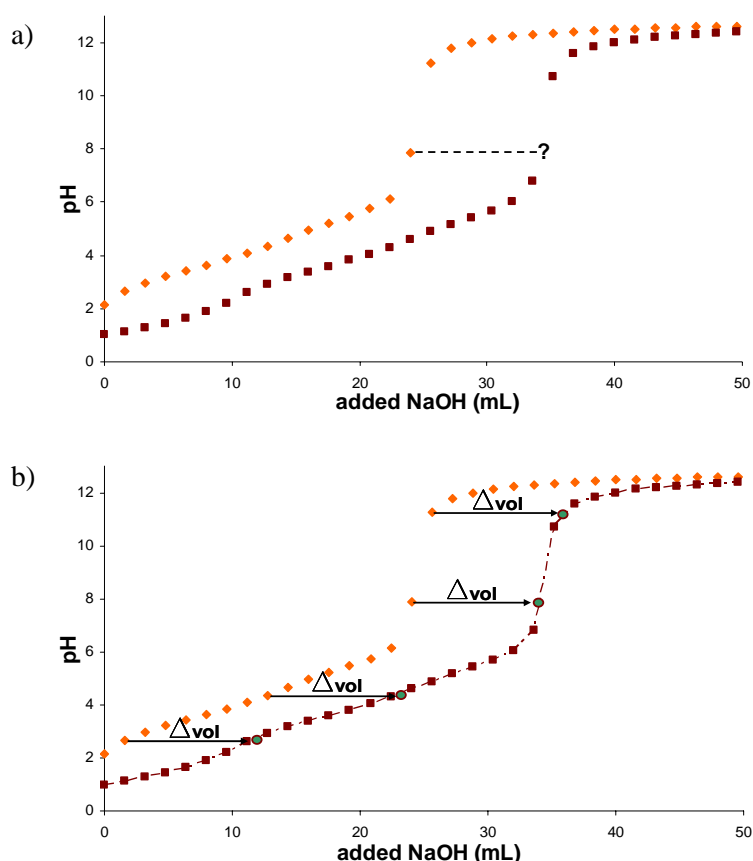


Figure 6.9: a) Points on the two titration curves of orange juice demonstrating that pH values do not coincide with each other for both curves; b) To enable the volume difference between two identical pH points on both titrations the titration curve of orange juice and acid is interpolated so the exact volume difference between the same pH value on each titration can be calculated.

Calculation of this volume difference at each pH value, as depicted in Figure 6.9b), results in the titration curve corresponding to the titration of the added acid, this is shown in Figure 6.10. Importantly, the calculated titration curve is a strong acid/strong base titration, and can therefore be used in the same manner as a standard acid/base titration to calibrate the electrode. Calibration using acid/base titrations has been previously described in Section 6.5.3.

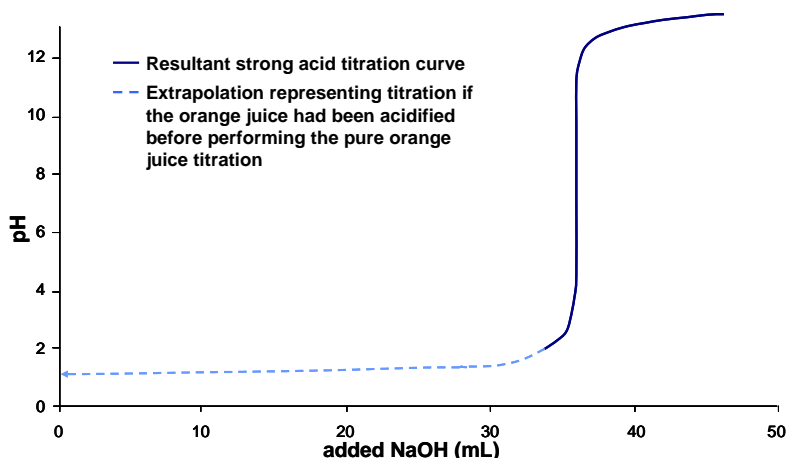


Figure 6.10: The resultant calculated titration curve of the added acid. The — line is the suggested curve if the orange juice had been lowered to a pH of 1 before beginning the standard addition process.

The titration of the orange juice sample begins at an approximate pH of 2 due to the acids that naturally occur in the juice. However, in order to better define the beginning of the calibration titration the initial pH of the orange juice sample should be lowered before performing the first titration of the process. If the orange juice titration is instead started at a pH of 1 then the beginning of the calculated calibration titration will be better defined, as shown by the dashed line in Figure 6.10. Nevertheless, even using the orange juice titration curve beginning at a pH of 2 the electrode calibration can adequately be performed as the required pH ranges are still covered.

Now that we have a strong acid/strong base titration the next step is to calculate the calibration parameters of the electrode. The same calibration line can be plotted as was previously detailed in Figure 6.2 from the calibration using a standard strong acid/strong base titration. The resulting electrode parameter values, slope s and intercept E_{const} , calculated using Equation (6.19) are, as one would expect, slightly different from the calibration constants generally determined for titrations in aqueous solvents. Therefore, it can be demonstrated that if the pH value for the orange juice sample had been determined using an electrode calibrated in water, where s equals -59.16 and E_{const}

equals 398, a potential reading of 200 mV would correspond to a pH value of 3.35. However, using the electrode parameters determined from the secondary calibration procedure in the orange juice sample, where s was calculated to equal -61.94 and E_{const} to be equal to 362.34, the pH can instead accurately be calculated as a value of 2.62. This difference corresponds to a value of 0.73 pH units, which is a significant difference as it must be remembered that pH is a logarithmic scale. The difference in pH determined from the two different sets of calibration parameters has been represented graphically in Figure 6.11.

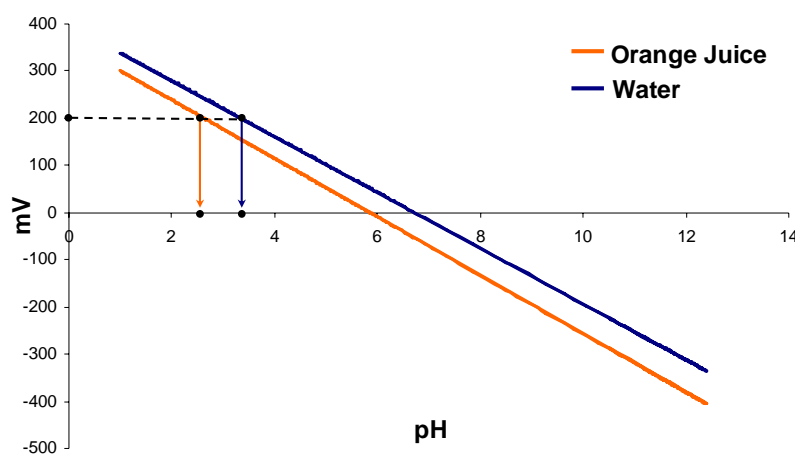


Figure 6.11: Graph showing the different calibration lines calculated from strong acid/strong base titrations in water — and in orange juice —, and the different pH values each calibration results in.

The outcome of calculating the calibration curve from two titrations in orange juice is that the electrode parameters that are generally affected by this significant change in the experimental conditions between calibration and measurement are now constant as the calibration and measurement are performed in the same complex solvent matrix. Changes in the liquid junction potential have been minimised, there are reduced ionic strength changes, and any fluctuations in standard glass potential of the electrode have been lessened. The potential readings from the electrode have now been calibrated to directly read the free hydrogen ion concentration in an orange juice sample and hence accurate pH reading of samples can be performed.

Standard Addition Similarities

The basic idea of adding acid to each pH value in an orange juice titration and calculating the subsequent strong acid titration curve can be compared with the well established technique of standard addition. This technique is probably most known best in atomic absorption spectroscopy (AAS), and the basic principle is shown in Figure

6.12. A solution of the sample is analysed for a specific analyte, for this example the absorbance reading, then subsequent readings are taken of the same sample with added standard amounts of the specific analyte. The resulting calibration line is then extrapolated back and the unknown concentration of the analyte in the sample is determined.

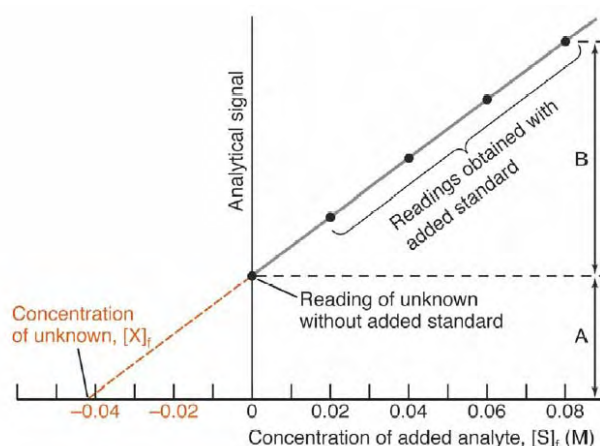


Figure 6.12: Diagram detailing the technique of standard addition in order to determine the concentration of an unknown quantity.

The clear benefit of the standard addition calibration technique is that calibration is performed under the same conditions as the sample measurements, therefore minimising any matrix effects and compatibility problems. This minimisation of negative effects for calibrations that was well known from the standard addition technique was the basis for the development of the secondary calibration technique.

6.8.1.2 Extended Applications

The basic principle that can be applied from the above example of secondary calibration in an orange juice sample is that a method has been developed which enables the calibration of an electrode in any complex solution, therefore enabling accurate determination of pH in samples such as wines and other fruit juices.

This method can also be applied to other research areas where the concentration of hydrogen ions is also an extremely important indicator and control parameter for chemical reactions, especially biochemical systems. For example, complex biological samples, such as blood, where the solution matrix is unknown, but accurate pH determinations are needed. This form of in situ calibration can be used to internally calibrate the electrode in order to achieve accurate pH readings in any complex sample

and therefore has the potential for very broad applications depending on the researchers needs.

A drawback to this calibration method is that the addition of acid for the calibration titration may damage some component of the sample, such as the orange juice or blood. This would result in wrong interpretations for the calculated electrode constants and subsequent pH values. Therefore, before the technique can be applied to a new system it should be ensured that the addition of acid does not alter the composition of the sample in a significant way.

6.8.2 Determination of the Purity of Room-Temperature Ionic Liquids

Interest in the production of 'Room Temperature Ionic Liquids', RTILs, has increased rapidly, as attested by the number of recent publications in the area. This has been especially due to their label as 'green solvents'. Depending on the process, the use of RTILs as a reaction media can offer decisive advantages, especially in the area of safety due to their low volatility and flammability⁶⁰. RTILs not only have the potential to increase chemical reactivity and thus lead to more efficient processes, but they are also non-flammable and less toxic than conventional solvents due to their aforementioned low vapour pressure. Moreover, there are specific solvents available for the most disparate types of applications.

In any synthetic process determining the purity of product is a key step. However, monitoring the synthetic process of RTILs to ascertain when the reaction is complete, or when all side-products have been removed, is not trivial as RTILs cannot be recrystallised, distilled or sublimed. Consequently, thorough investigations into quantifying RTILs purity, stability, biodegradability, and toxicity have lagged behind the pace of other research in the area⁶¹.

The preparation of RTILs is varied as they can be synthesised using a variety of different methods. Each technique gives rise to different impurity profiles, however there are four main categories of impurities generally prevalent in RTILs. These include such species as halides, water and other protic species such as hydrochloric acid, organics, and unreacted inorganic salts. The physicochemical properties of RTILs have been shown to be dramatically affected by the presence of impurities such as water and halides⁶², it is obvious that the presence of such impurities can be detrimental for their numerous applications. For example certain chemical applications of ionic liquids

such as electrochemical, spectroscopic, and catalytic applications require utmost purity ⁶¹.

In particular, the presence of unreacted starting material in an RTIL from incomplete alkylation can pose potential downstream problems such as catalyst poisoning and introduction of protic impurities. Unreacted starting materials have especially proven difficult to remove at later stages in the synthetic process ⁶³. If RTILs are to become commonplace solvents in synthetic chemistry it is imperative that the physicochemical properties are accurately, if not precisely, detailed in the literature. If any new RTIL is to have its physicochemical properties properly characterised then it is imperative that all impurities be absent. Thus, RTILs of highest purity must be prepared so such data can be obtained.

In order to obtain a pure final product the presence of unreacted starting material must be monitored. Current procedures to determine the presence of unreacted starting material include ¹H NMR spectroscopy, where the reactions can be monitored at regular intervals until starting material is no longer detected ⁶⁰, or colorimetric methods ^{63, 64}. These techniques for determining the purity of the RTIL product are a key step in the process, nevertheless they are complicated and cumbersome to perform, often not resulting in reliable qualitative data ^{65, 66}.

Potentiometric titrations, based on the global internal calibration technique described in Section 6.6 was developed as a novel technique to monitor the synthetic process during the production of RTILs, and to also determine the final purity of RTIL product. Analysis of the potentiometric data recorded from titrations of samples from the RTIL synthesis enables the identification of all pH-active species present throughout the synthetic process from each species pK_a value(s), as well as providing quantitative information about the concentration of each species identified.

A general overview of the method requires samples of the reaction mixture being taken at successive stages during synthesis. Potentiometric titrations of the RTIL at varying stages of the reaction can be analysed to qualitatively describe the progress of the reaction, and a final titration at the completion of synthesis can assess the purity of the RTIL product. All titrations can be analysed together using the previously described global analysis program. Such analysis of the complete series of titrations from the synthesis is a robust method enabling the progress of the reaction to be quantitatively followed. The data analysis fits, for all titrations together, the calculated pH data to the

measured data and determines such parameters as the pK_a values of pH-active species and their corresponding concentrations in each titration, even if they are only present in small quantities, as well as importantly determining the calibration parameters of the electrode for each measurement.

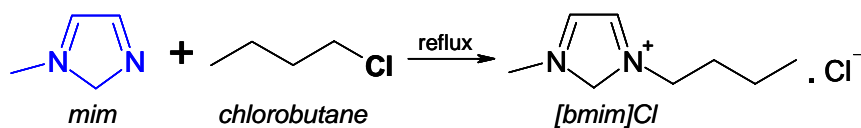
6.8.2.1 Synthetic Process

RTILs are typically comprised of an organic cation and a weakly coordinating inorganic anion, such as a halogenated alkane⁶⁷. The general synthetic procedure for an RTIL almost always involves the alkylation of an organic amine. The alkylation step usually involves the reaction of a nucleophilic, Lewis-basic heteroatom in the starting material with an alkyl halide. The resulting organic salt contains an anionic component, a halide ion, which can then be metathesised with another ion, for example BF_4 or PF_6^- , to produce a different RTIL. In such cases an amount of residual halide invariably remains⁶¹.

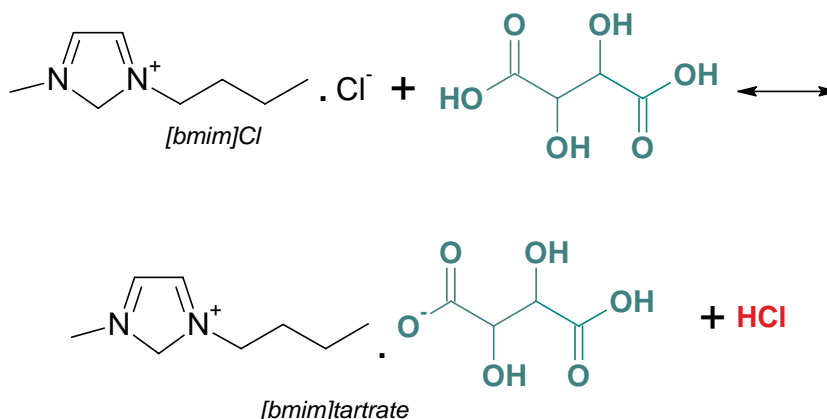
For the given example in Scheme 2 1-methylimidazolium (mim) and chlorobutane were refluxed to produce the intermediate RTIL, 1-butyl-3-methylimidazolium ([bmim]Cl). Step One of the formation of the RTIL was performed using two techniques. The first technique was the traditional method, which involved refluxing the mixture for a period of 72 hours, after which time it was determined that starting materials were still present in small quantities. The second synthetic process was the modern microwave synthesis in which the starting materials were reacted together for a comparatively small amount of time at high temperatures. Similarly to the traditional method, this synthetic procedure also had remaining starting material present at the conclusion of the synthesis. In both methods any unreacted chlorobutane was easily removed by heating the product under vacuum, however removing unreacted mim is not easily done.

Step Two involved the exchange of the anion with the addition of an aqueous tartaric acid solution to the intermediate RTIL, [bmim]Cl. The mixture was then rotary evaporated for five hours to remove water introduced from the aqueous tartaric acid and to also remove the hydrochloric acid product and produce the final product, [bmim]tartrate. As a final step the reaction mixture was heated under high vacuum to remove any trace water and acid from the RTIL.

Step One:



Step Two:



Scheme 2: Reaction scheme for the synthesis of an ionic liquid (pH-active species are shown in colour): Step One shows the synthetic procedure for [bmim]Cl (ionic liquid intermediate); Step Two shows synthetic procedure for the replacement of the halide with an acid to form [bmim]tartrate.

6.8.2.2 Global Analysis Method

The progress of the synthesis of an RTIL can be monitored by observation of the disappearance of the pH-active base, as seen in the first step of Scheme 2 where the disappearance of mim can be monitored. The RTIL product is not pH-active, however the percentage yield can be monitored indirectly using molar ratio calculations because the product exactly equals the concentration of the starting base which has reacted.

In order to analyse Step One of the synthesis described in Scheme 2 by the traditional reflux procedure the reaction mixture was sampled at regular intervals during the reflux. The reaction was not stopped for sampling, and sample size was minimal compared to the total reaction volume. Reproducibility was checked by triplicate sampling at 4, 24, 48 and 72 hour stages. Each sample was acidified with a set amount of acid and titrated with NaOH using the fully automated titration procedure previously described in Chapter 2, Section 2.2.3.4. The small variability in data from these samples, less than 5%, showed the procedure to be within acceptable error limits and the sampling procedure to be reproducible.

The progression of the first step of the synthetic procedure is shown in Figure 6.13 in which the consumption of the starting material, mim, can be clearly seen as the end point disappears as the reaction progresses over the 72 hour reaction period. The concentration of chlorobutane was calculated using the initial mass of chlorobutane in the reaction and the 1:1 molar ratio of chlorobutane to mim. Global analysis of these titrations from the first step enabled the concentration of the formation of the ionic liquid [bmim]Cl to be calculated.

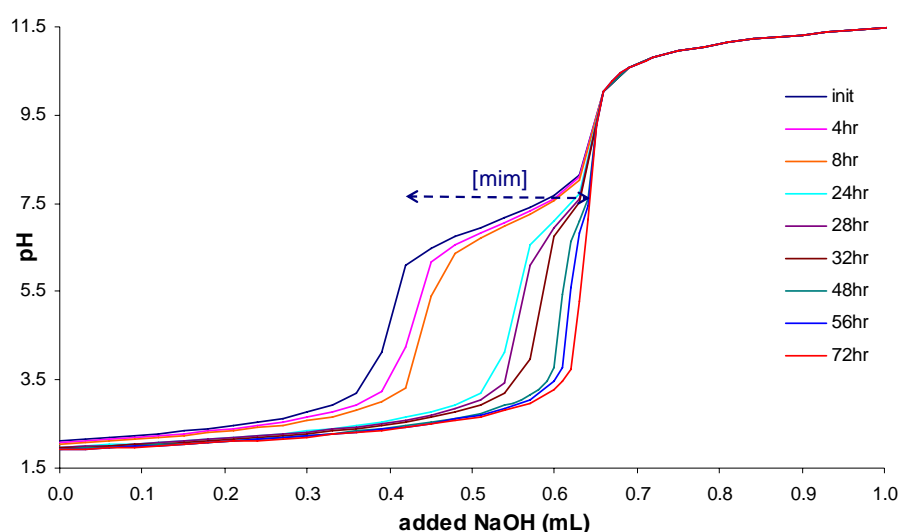


Figure 6.13: Plot showing the global analysis of the complete series of titrations for the first stage of the synthetic procedure using reflux technique (0 – 72 hours).

Theoretically, a second order reaction should be able to define the formation of the [bmim]Cl, however, due to sampling procedures and uncertainty in the initial component concentrations for each sample, such a rate law could not be applied to the experiment. Instead an exponential was fitted to the experiment over time in order to estimate the approximate time needed for 100% yield since the reaction was incomplete. This trend of formation is shown in Figure 6.14.

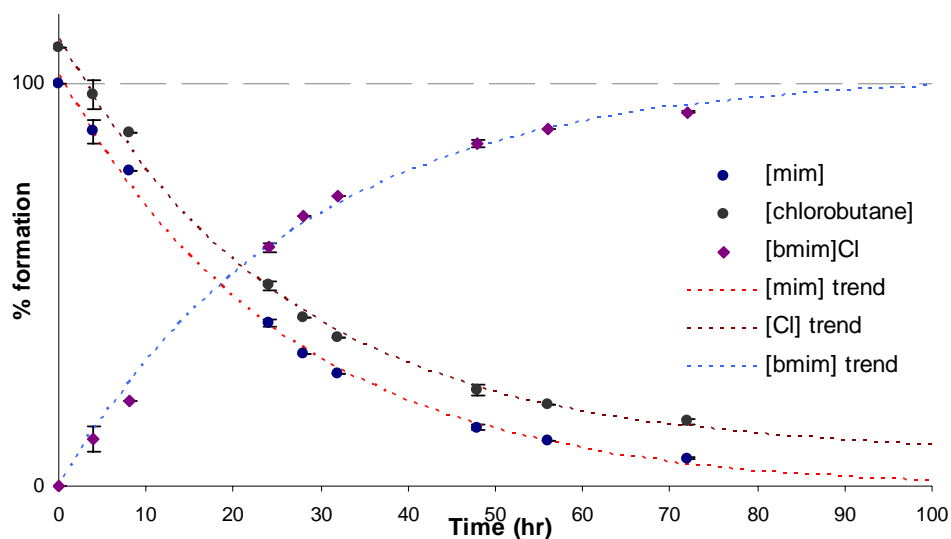


Figure 6.14: Plot showing the production of the intermediate ionic liquid [bmim]Cl and the predicted 100% yield time (100 hrs) using reflux synthesis. Error estimates from triplicate sampling are shown at the 4, 24, 48 and 72 hour points.

The first step in the synthesis was also repeated using the modern technique of microwave technology the starting materials were reacted together over a time frame of 45 minutes. For this experiment the sampling of the reaction mixture was not performed at progressive time intervals as this would require the microwave to be stopped, the reaction mixture to be cooled and sampled, and then the reaction continued until the next time interval. This process would result in losses of reactant due to low boiling points and high vapour pressure and also lead to inaccurate time measurements as the microwave required time to reheat the reaction mixture to the 150 °C at which the reaction is performed, and this time is not included as part of the overall reaction time. To prevent these complications and improve the accuracy of the analysis the reaction was run several times, each at increasing lengths of reaction time, in order to monitor the progress of the reaction. The reactants for each repeat were sampled from a standard mixture of the two starting materials to ensure the same ratios of starting material were used for each reaction.

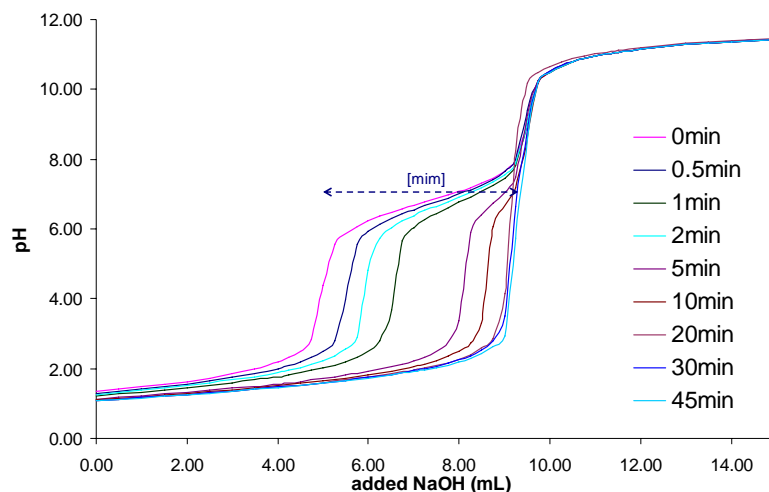


Figure 6.15: Plot showing the global analysis of the complete series of titrations for the first stage of the synthetic procedure using the microwave technique (0 – 45 minutes).

The conditions of the microwave experiment were; temperature of 150 °C, power set at 150 W, and the pressure was set at a limit of 200 psi. Each solution was prepared using approximately 1 g of the starting stock solution, which was prepared by mixing 1-methylimidazole and 1-chlorobutane in a 1:1.2 molar ratio as excess 1-chlorobutane can be easily removed by evaporation after the synthesis. Each 1 g sample was reacted for increasing time periods, as shown in Figure 6.15. After each reaction period the sample was acidified and made up to 50 mL with water before being titrated in the same manner as for the traditional reflux measurements. From these titrations the progress of the reaction over time could again be monitored and the percentage formation calculated. A second order rate curve was successfully fitted to the data points resulting in a rate constant $k = 6.0 \text{ M}^{-1} \text{ min}^{-1}$, and an estimated 100% yield time of 60 minutes.

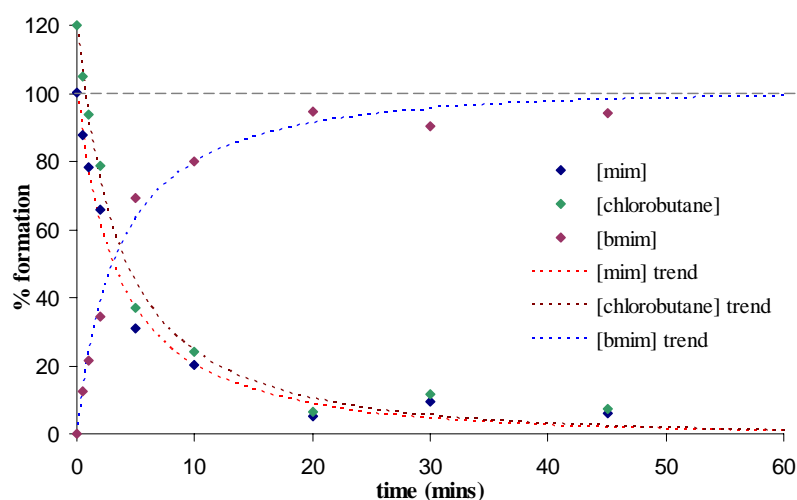


Figure 6.16: Plot showing the production of the intermediate ionic liquid [bmim]Cl and the predicted 100% yield time (60 mins) using microwave synthesis.

Subsequent reactions with [bmim]Cl can also be monitored in a similar fashion. Often the halide is replaced with another more interesting ion, such as a stereo-active acid, as shown by the substitution of the chloride ion for tartaric acid in step two of Scheme 2. The acid is naturally pH-active, therefore enabling the substitution process to also be monitored via potentiometric titrations. Figure 6.17 shows a simulation of what the titration curve would look like if a sample was taken part-way through step two in the synthesis where the ionic liquid [bmim]Cl from the first step had not been properly purified before the second stage in the reaction, resulting in unreacted mim being present. The titration curve clearly shows how the pH-active species and their concentrations can be identified. Using fixed ratios and mass-balance equations the concentration of non-pH-active species can also be subsequently determined from the titration. Figure 6.18 illustrates the concentration of each species for the titration shown below, the pK_a values can be identified for each pH-active species present.

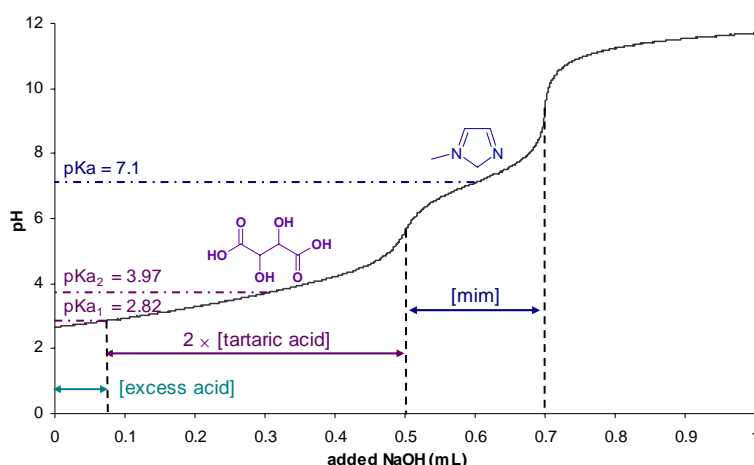


Figure 6.17: Plot showing an example of the titration of a sample taken from the reaction mixture where starting material, side-products, tartaric acid and ionic liquid product are all present.

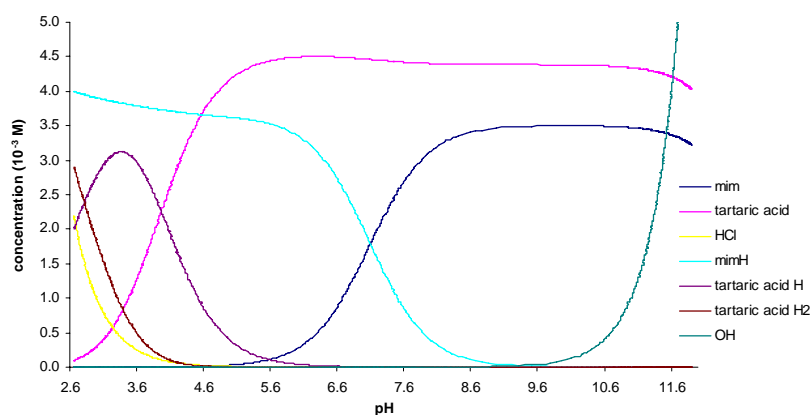


Figure 6.18: Plot of the species concentrations from the titration shown in Figure 6.17 where starting material, side-products, tartaric acid and ionic liquid product are all present.

For the second step of the synthesis it has been reported that, in order to drive the reaction forward, the reaction mixture is rotary evaporated and heated under high vacuum conditions in order to remove the HCl through evaporation⁶⁸. Thus, the process of the reaction should be able to be monitored by determining the loss of HCl as the amount of HCl produced is obviously equal to the amount of [bmim]tartrate formed. The synthetic procedure assumed that nearly all the HCl was removed from rotary evaporation and final heating under high vacuum, however analysis of the samples taken during the second step of the synthesis showed that in fact no HCl was removed from this process. The majority of mass lost from process was determined in fact to be due to the removal of water from the aqueous tartaric acid.

The titrations of each sample, taken hourly during the rotary evaporation and also after the high vacuum, are depicted in Figure 6.19. It can be seen that over the process of rotary evaporation and high vacuum treatment the acid concentration increases because as the water is removed the reaction mixture becomes more concentrated. The titrations shown in the left-hand side of Figure 6.19 show that the majority of water was removed in the first two hours of rotary evaporation, with significantly smaller amounts removed over the next three hours. The titration also show that the final heating under high vacuum succeeded in removing more water even after the rotary evaporation showed no more change in concentration. The appearance of the end point at a pH of 7.1 is due to the presence of the starting material from Step One, mim, which becomes more pronounced as the concentration is increased with the removal of water. Hence, the titration also showed that the pure ionic liquid [bmim]Cl still contained some starting material.

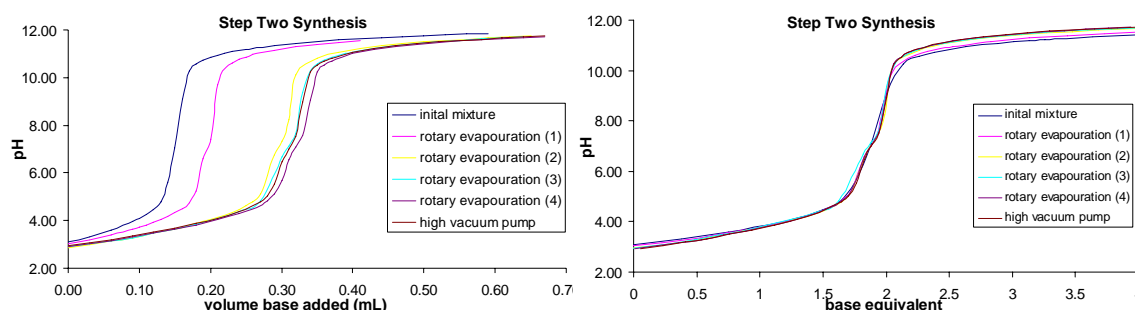


Figure 6.19: (LHS) Plot showing the titrations of samples from the Step Two synthetic process; (RHS) Same titration plots but plotted as the base equivalent added for the tartaric acid present, clearly showing that the acid concentration is constant throughout the synthesis.

The removal of HCl can easily be monitored as it is equal to the difference between double the tartrate ion concentration and the calculated hydrogen ion concentration. In the initial reaction mixture the acid concentration is exactly equal to double the tartrate ion concentration as tartaric acid is diprotic. Therefore, any reduction in the acid concentration comparative to double the tartaric acid concentration will be due to the removal of HCl. However, even in the final solution after the high vacuum pump, the hydrogen ion concentration is double the tartrate ion concentration, within the error limits of the titration, as shown in Figure 6.20. This means that no HCl was removed from the synthesis, even under the high vacuum conditions, as was assumed to occur.

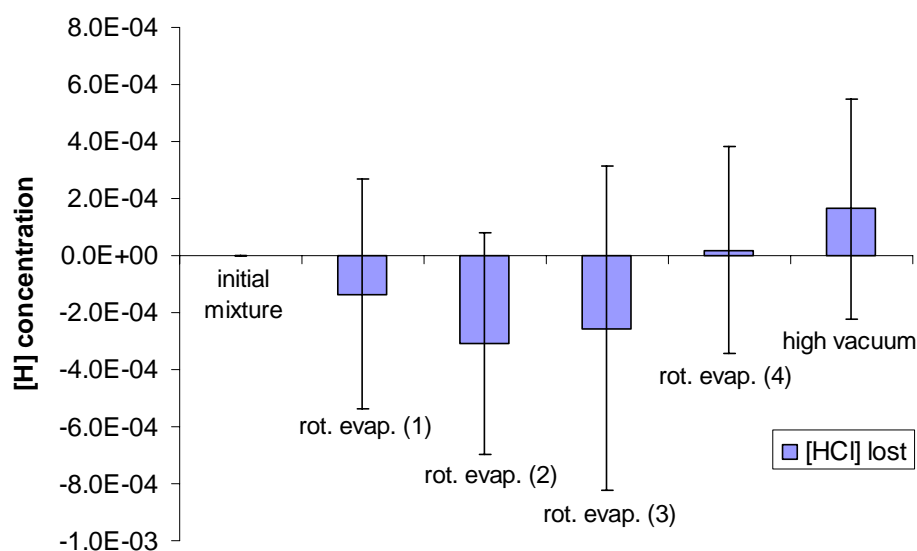


Figure 6.20: Graph showing the calculated HCl removed for each step of the reaction. Within the error limits each step shows that no HCl is being removed.

6.8.2.3 Summary of Analytical Process

The global analysis technique that we applied for the determination of purity of RTILs required the analysis of multiple samples throughout the synthetic procedure. For individual titrations where minor species are present, or where species exist in only small concentrations, the corresponding equilibrium constants were naturally poorly defined. By analysing the complete set of measurements for all samples taken from each step in the synthesis, all species were adequately defined and the analysis was significantly more robust, with the statistics of the parameters being greatly improved, compared to if individual analysis has been performed on each sample titration.

Analysing titration data using this global technique results in one analysis process give quantitative results for the entire synthetic procedure. This affords a fast and efficient method for monitoring the process and determining the purity and yield of an RTIL. The proposed method for analysing the potentiometric titration data from RTILs has the advantages of graphic representation, internal pH electrode calibration, and high accuracy.

From our measurements we were able to demonstrate that the popular microwave synthesis of RTILs, due to its speed of reaction and ease of set-up, does not actually result in the 100% yield of ionic liquid expected. Further, it was shown that for the reflux procedure, samples that had been refluxed for the recommended period of time at the appropriate temperature, still contained a small concentration of the starting material mim. For the microwave synthesis after 15 minutes of reaction the solution appeared homogenous to the naked eye, and yet the titration of the sample showed significant quantities of starting material still present. This remaining starting material may in fact contribute to the liquid properties of many RTILs.

The secondary reaction with RTILs, as shown in Step Two of Scheme 2, was shown to not proceed as was thought as no HCl was removed from the reaction mixture, only water. Therefore, any properties determined with such impurities present will not be indicative of the true RTIL properties. Hence, it is imperative that researchers determine the purity of their products before reported their properties and before using such RTILs in further reactions. It is clear that potentiometry provides a quick and robust method for such determinations and the technique described here is an advantageous one to use for these studies.

6.9 Conclusions

This research proposed a methodology to overcome the uncertainties and limitations associated with current calibration techniques by introducing a global internal calibration technique. Further, a new secondary calibration technique that can enable pH measurements to be accurately made in complex samples was proposed along with a technique demonstrating how the methodology can be implemented for processes such as determining the purity of synthetic processes. The example provided in the work involved the determination of the purity of RTIL synthesis.

To establish the procedure we generalised the principle that essentially any titration carries enough information for complete calibration of the pH electrode provided there are sufficient titration points and the titration covers a large enough pH range. Internal calibration is designed in such a way that the calibration of the electrode is performed as part of the analysis of the potentiometric titration data. This enables the simultaneous determination of the parameters required to calibrate the combined glass electrode, that is the slope, s and intercept, E_{const} . Calibration using such programs are of added benefit as they can easily be applied to mixed solvent studies and also to electrodes other than combined glass electrodes as the specific electrode parameters are determined internally and for every individual measurement.

Along with determining the calibration parameters other experimental parameters such as the ionisation constant of the solvent, pK_s , the equilibrium constants, and accurate initial component concentrations, for example the metal ion, ligand and hydrogen ion concentrations, can also be optimised. This not only removes the need to run a calibration separately from the measurement, but also enables numerous other parameters to be accurately determined as well in the one analytical process.

Meinrath *et al* ⁶⁹ proposed the tree diagram depicted in Figure 6.21 detailing all the possible areas from which errors can be introduced in a pH measurement. Using the global internal calibration program detailed in this chapter the errors introduced from such branches as the analyte concentration and the titration parameters will be minimal compared with other available analytical techniques. Obviously good experimental practises are still required in order to produce quality titration data that can be analysed, however the global internal calibration technique does reduce many of the concerns with accurate pH determinations and measurements. Many of these concerns are completely correlated, for example the concentration of an acid and base in a titration. Other parameters can be determined from analysis, such as the slope and the dissociation constant of the solvent. Analysing information such as the Jacobian plots previously detailed in Figure 6.4 enables the determination of what parameters can be analysed and what cannot be accurately defined from the analytical procedure.

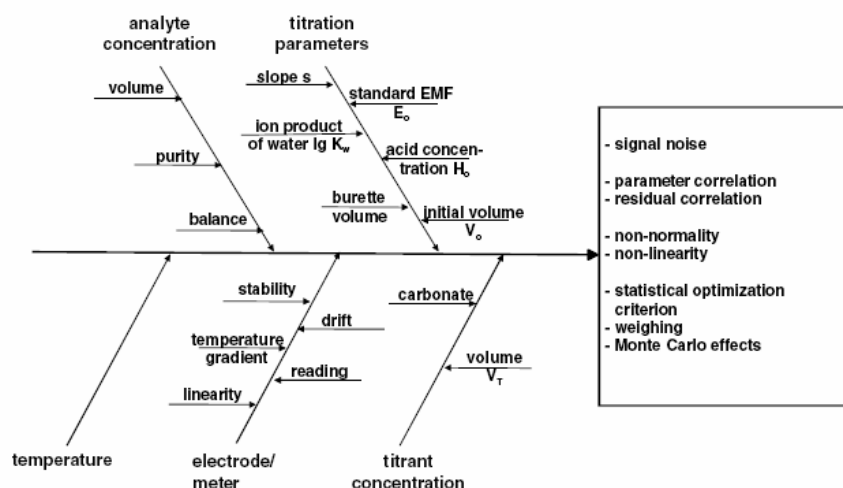


Figure 6.21: Cause-and-effect diagram for glass electrode potentiometric determination of acidity constants. The contributions given in the box are intertwined with the experimental data ⁶⁹.

Performing an internal electrode calibration means that the conditions of the calibration and experiment are identical, therefore previous uncertainties and limitations concerned with other calibration procedures are overcome as internal consistency is a prime requirement in order to guarantee comparability of readings ²⁶. The internal calibration technique results in ionic strength conditions that are identical for both calibration and measurement, as there is also no difference in liquid junction potentials, because the measurement is the calibration. Any fluctuations and degradation of the electrode that may have previously affected the accuracy of a measurement are now compensated for as they are easily detectable from the calibration parameters that are obtained along with the titration analysis. An important benefit is also that internal calibration removes time consuming calibration procedures and this means that there is no time lag between calibration and measurement, so the maximum accuracy in results can be achieved.

In conclusion, the amount of information that can be drawn from a potentiometric titration using the analysis method developed using internal calibration, and the possibility of global parameters is far superior to that obtained by many other available methods.

6.10 References

1. Brandariz, I.; Barriada, J. L.; Vilarino, T.; Sastre de Vicente, M. E., Comparison of Several Calibration Procedures for Glass Electrodes in Proton Concentration. *Monatshefte fuer Chemie* **2004**, 135, 1475-1488.
2. Filella, M.; May, P. M., Reflections on the calculation and publication of potentiometrically-determined formation constants. *Talanta* **2005**, 65, 1221-1225.
3. Bates, R. G., *Determination of pH; theory and practice*. Wiley: New York, 1973.
4. Harned, H. S.; Owen, B. B., *The Physical Chemistry of Electrolytic Solutions*. 3rd ed. Am. Chem. Soc. Monograph No. 137. 1958; p 803.
5. Robinson, R. A.; Stokes, R. H., *Electrolyte Solutions* 2nd ed. Dover Publications; 1959; p 572.
6. Serjeant, E. P., *Potentiometry and Potentiometric Titrations*. Wiley: New York, 1984.
7. May, P. M.; Murray, K.; Williams, D. R., The use of glass electrodes for the determination of formation constants. III. Optimisation of Titration Data: The ESTA Library of Computer Programs. *Talanta* **1988**, 35, 825-830.
8. pH, Babylon, <http://www.babylon.com/definition/pH/All> (25/05/07).
9. IUPAC http://www.iupac.org/index_to.html (25/5/07),
10. Sorensen, S. P. L.; Linderstrom-Lang, K., The determination and value of pH in electrometric measurements of hydrogen-ion concentrations. *Compt. rend. trav. ab.* **1924**, 15, 40.
11. Buck, R. P.; Lindner, E., Recommendations for nomenclature of ion-selective electrodes. *Pure and Applied Chemistry* **1994**, 66, 2527-36.
12. May, P. M.; Williams, D. R.; Linder, P. W.; Torrington, R. G., The use of glass electrodes for the determination of formation constants. I. A definitive method for calibration. *Talanta* **1982**, 29, 249-56.
13. Baucke, F. G. K., Thermodynamic Origin of the Sub-Nernstian Response of Glass Electrodes. *Analytical Chemistry* **1994**, 66, 4519-24.
14. Guimar, M. J.; Lito, H. M.; Filomena, M.; Camoes, G. F. C., Reassessment of pH reference values with improved methodology for the evaluation of ionic strength. *Analytica Chimica Acta* **2005**, 531, 141-146.
15. Baucke, F. G. K., New IUPAC recommendations on the measurement of pH - background and essentials. *Analytical and Bioanalytical Chemistry* **2002**, 374, 772-777.

16. Buck, R. P.; Rondinini, S.; Covington, A. K.; Baucke, F. G. K.; Brett, C. M. A.; Camoes, M. F.; Milton, M. J. T.; Mussini, T.; Naumann, R.; Pratt, K. W.; Spitzer, P.; Wilson, G. S., Measurement of pH. Definition, standards, and procedures: (IUPAC Recommendations 2002). *Pure and Applied Chemistry* **2002**, 74, 2169-2200.
17. Rondinini, S. Measurement of pH. Definition, standards, and procedures. http://www.iupac.org/reports/provisional/abstract01/rondinini_310102.html (24/08),
18. Harned, H. S.; Owen, B. B., *The Physical Chemistry of Electrolytic Solutions*. 3rd ed. Am. Chem. Soc. Monograph No. 137. 1958; p 803 pp.
19. Verlag, B., *International Vocabulary of Basic and General Terms in Metrology (VIM)*. 2nd ed.; Berlin, 1994.
20. Naumann, R.; Baucke, F. G. K.; Spitzer, P. *Traceability of pH measurements to standard pH values and calibration of pH meter-electrode assemblies. Recommended procedures and definitions*; Merck K.-G.a.A., Darmstadt, Germany.: 1997; pp 38-56.
21. Irving, H. M. N. H.; Miles, M. G.; Pettit, L. D., A study of some problems in determining the stoichiometric proton dissociation constants of complexes by potentiometric titrations using a glass electrode. *Analytica Chimica Acta* **1967**, 38, 475-88.
22. Harrison, R. M., *Understanding Our Environment: An Introduction to Environmental Chemistry*. The Royal Society of Chemistry: Cambridge, 1999.
23. Martell, A. E.; Motekaitis, R. J., *The determination and use of stability constants*. VCH Publishers: Weinheim, New York, 1988.
24. McBryde, W. A. E., pH-Meter as a hydrogen-ion concentration probe. *Analyst* **1969**, 94, 337-46.
25. Williams, D. R., In *Proc. Summer School on Stability Constants*, Paoletti, P. B., R.; Fabbri, L., Ed. Bivigliano: Florence, Italy, 1974; p 125.
26. Lito, M. J.; M., G. H.; Camoes, M.; C., F. G. F., Reassessment of pH reference values with improved methodology for the evaluation of ionic strength. *Analytica Chimica Acta* **2005**, 531, 141-146.
27. Tomisic, V.; Gopurenko, T.; Majorinc, K.; Simeon, V., Calibration of Glass Electrode in Terms of H^+ Concentration by Titration of Weak Acid in Cells with and without Liquid Junction. *Croatica Chimica Acta* **2006**, 79, 613-618.
28. Linder, P. W.; Torrington, R. G.; Williams, D. R., *Analysis Using Glass Electrodes*. Open University Press: Milton Keynes, 1984.
29. Avdeef, A.; Comer, J. E. A.; Thomson, S. J., pH-Metric log P. 3. Glass electrode calibration in methanol-water, applied to pKa determination of water-insoluble substances. *Analytical Chemistry* **1993**, 65, 42-9.

-
30. Moeller, T.; Martin, D. F.; Thompson, L. C.; Ferrus, R.; Fiestel, G. R.; Randall, W. J., The coordination chemistry of yttrium and the rare earth metal ions. *Chemical Reviews* **1965**, 65, 1-50.
 31. Burgess, J., *Metal ions in solution*. Ellis Horwood: Chichester, 1978.
 32. Galster, H., *pH Measurement: Fundamentals, Methods, Applications, Instrumentation*. VCH: New York, 1991; p 356.
 33. Gibson, G. T. T.; Mohamed, M. F.; Neverov, A. A.; Brown, R. S., Potentiometric Titration of Metal Ions in Ethanol. *Inorganic Chemistry* **2006**, 45, 7891-7902.
 34. Sigel, H.; Zuberbuehler, A. D.; Yamauchi, O., Comments on potentiometric pH titrations and the relationship between pH-meter reading and hydrogen ion concentration. *Analytica Chimica Acta* **1991**, 255, 63-72.
 35. Barbosa, J.; Sanz-Nebot, V., Assignment of reference pH-values to primary standard buffer solutions for standardization of potentiometric sensors in acetonitrile-water mixtures. *Fresenius' Journal of Analytical Chemistry* **1995**, 353, 148-55.
 36. Takacs-Novak, K.; Box, K. J.; Avdeef, A., Potentiometric pKa determination of water-insoluble compounds: validation study in methanol/water mixtures. *International Journal of Pharmaceutics* **1997**, 151, 235-248.
 37. Douheret, G., Dissociation of organic compounds in aqueous organic media. I. Determination of the liquid junction potential and the effect of the medium on the hydrogen ion in these systems, and the study of the dissociation of some acid-base couples. *Bulletin de la Societe Chimique de France* **1967**, 1412-19.
 38. Bates, R. G., *Determination of pH-Theory and Practice*. 1964; p 435.
 39. El-Gahami, M. A.; Ibrahim, S. A.; Fouad, D. M.; Hammam, A. M., Medium Effect on the Acid Dissociation Constants of 2,2',6',2''-Terpyridine. *Journal of Chemical and Engineering Data* **2003**, 48, 29-31.
 40. Bates, R. G.; Paabo, M.; Robinson, R. A., Interpretation of pH measurements in alcohol-water solvents. *Journal of Physical Chemistry* **1963**, 67, 1833-8.
 41. Gutbezahl, B.; Grunwald, E., The acidity and basicity scale in the system ethanol-water. The evaluation of degenerate activity coefficients for single ions. *Journal of the American Chemical Society* **1953**, 75, 565-74.
 42. Grunwald, E.; Berkowitz, B. J., The measurement and correlation of acid dissociation constants for carboxylic acids in the system ethanol-water. Activity coefficients and empirical activity functions. *Journal of the American Chemical Society* **1951**, 73, 4939-44.
 43. IUPAC, *Compendium of Analytical Nomenclature. Definitive Rules 1997*. 3rd ed.; Blackwell: Oxford, UK, 1998.

44. Martell, A. E. M., R.J., *Determination and Use of Stability Constants*. VCH: Weinheim, 1988.
45. Cheng, K. L., Recent development of non-faradaic potentiometry. *Microchemical Journal* **2002**, 72, 269-276.
46. Cheng, K. L., Explanation of Misleading Nernst Slope by Boltzmann Equation. *Microchemical Journal* **1998**, 59, 437.
47. Filella, M.; Casassas, E.; Williams, D. R., The binding of metal ions by mercaptoacids. II. Formation constants for the complexes of mercaptosuccinate with cadmium(II) and computer simulation of its ability to mobilize the low molecular weight fraction of cadmium(II) in blood plasma. *Inorganica Chimica Acta* **1987**, 136, 177-83.
48. Filella, M.; Izquierdo, A.; Casassas, E., The binding of metal ions by mercaptoacids. I. Formation constants for the complexes of mercaptosuccinate with zinc(II), nickel(II) and hydrogen ions. *Journal of Inorganic Biochemistry* **1986**, 28, 1-12.
49. Filella, M.; Town, R. M.; Bugarin, M. G., Cadmium Succinate and Cadmium Malate Stability Constants Revisited. *Journal of Chemical and Engineering Data* **1999**, 44, 1009-1019.
50. Filella, M.; Williams, D. R., Speciation of N-(2-mercaptopropionyl)glycine zinc, nickel, cadmium and lead complexes in aqueous solution. *Inorganica Chimica Acta* **1985**, 106, 49-57.
51. Bugarin, M. G.; Filella, M., The formation constants of dimethylthallium (III)-glutathione complexes in aqueous solution. *Journal of Inorganic Biochemistry* **1999**, 73, 17-29.
52. Garcia Bugarin, M.; Casas, J. S.; Sordo, J.; Filella, M., Thallium(I) interactions in biological fluids: a potentiometric investigation of thallium(I) complex equilibria with some sulfur-containing amino acids. *Journal of Inorganic Biochemistry* **1989**, 35, 95-105.
53. Fiol, S.; Arce, F.; Armesto, X. L.; Penedo, F.; Sastre de Vicente, M., Analysis of systematic errors in calibrating glass electrodes with hydrogen-ion as a concentration probe. *Fresenius' Journal of Analytical Chemistry* **1992**, 343, 469-72.
54. Gans, P.; O'Sullivan, B., GLEE, a new computer program for glass electrode calibration. *Talanta* **2000**, 51, 33-37.
55. Gans, P.; Sabatini, A.; Vacca, A., Investigation of equilibria in solution. Determination of equilibrium constants with HYPERQUAD suite of programs. *Talanta* **1996**, 43, 1739-1753.
56. Baeza, J. J.; Ramis, G.; Mongay, C., A program for the simultaneous potentiometric determination of protonation constants and electrode calibration parameters. *Journal of Chemometrics* **1988**, 3, 223-9.

-
57. Arena, G.; Rizzarelli, E.; Sammartano, S.; Rigano, C., A nonlinear least-squares approach to the refinement of all parameters involved in acid-base titrations. *Talanta* **1979**, 26, 1-14.
58. Biedermann, G., The hydrolysis of metal ions. V. The hydrolysis of the thallium(III) ion. *Arkiv. Kemi* **1953**, 5, 441-55.
59. Takamura, K.; Ohtsuki, S.; Kusu, F., Development of a New Amperometric Sensor for Probing the Total Acid of Beverages. *Analytical Sciences* **2001**, 17, 737-740.
60. Deetlefs, M.; Seddon, K. R., Improved preparations of ionic liquids using microwave irradiation. *Green Chemistry* **2003**, 5, 181-186.
61. Scammells, P. J.; Scott, J. L.; Singer, R. D., Ionic Liquids: The Neglected Issues. *Australian Journal Of Chemistry* **2005**, 58, 155-169.
62. Seddon, K. R.; Stark, A.; Torres, M.-J., Influence of chloride, water, and organic solvents on the physical properties of ionic liquids. *Pure and Applied Chemistry* **2000**, 72, 2275-2287.
63. Holbrey, J. D.; Seddon, K. R.; Wareing, R., A simple colorimetric method for the quality control of 1-alkyl-3-methylimidazolium ionic liquid precursors. *Green Chemistry* **2001**, 3, 33-36.
64. Beyersdorff, T.; Gonsior, M.; Schubert, T. J. S., Ion chromatography: A valuable method for the quality control of ionic liquids. *Abstracts of Papers, 232nd ACS National Meeting, San Francisco, CA, United States, Sept. 10-14, 2006* **2006**, 526.
65. Deetlefs, M. S., K. R. , *Green Chemistry* **2003**, 5, 181-186.
66. Holbrey, J. D. S., K. R.; Wareing, R. , *Green Chemistry* **2001**, 3, 33-36.
67. Room Temperature Ionic Liquids.
<http://www.chem.binghamton.edu/HANDY/greenpage.htm> (10/12/07),
68. Whitehead, J. A.; Lawrance, G. A.; McCluskey, A., Analysis of Gold in Solutions Containing Ionic Liquids by Inductively Coupled Plasma Atomic Emission Spectrometry. *Australian Journal of Chemistry* **2004**, 57, (2), 151-155.
69. Meinrath, G.; Kufelnicki, A.; Swiatek, M., Approach to accuracy assessment of the glass-electrode potentiometric determination of acid-base properties. *Accreditation and Quality Assurance* **2006**, 10, 494-500.